MATHEMATICAL MODELING OF PHOTOCHEMICAL AIR POLLUTION

Thesis by

Steven Diggs Reynolds

In Partial Fulfillment of the Requirements

for the Degree of

Doctor of Philosophy

California Institute of Technology

Pasadena, California

1974

(Submitted March 19, 1974)

ACKNOWLEDGMENTS

I would like to take this opportunity to express my sincere appreciation to several institutions and individuals that have made my stay at Caltech both possible and rewarding. First, the John A. McCarthy Foundation, National Science Foundation, and Union Oil Company have generously provided financial support. Second, my gratitude is extended to P. M. Roth and M. K. Liu for their numerous conversations and significant contributions to the material presented in this report. Finally, I wish to thank Professor J. H. Seinfeld for his interest, support, and assistance in this work.

ABSTRACT

A model is presented for predicting the dynamic behavior of both inert and chemically reacting air pollutants in an urban atmosphere. Pollutants of interest include carbon monoxide, nitric oxide, nitrogen dioxide, ozone, and high and low reactivity hydrocarbons. The model is developed for a general urban area and then applied to the Los Angeles airshed. To evaluate the model, six smoggy days occurring in Los Angeles in 1969 are simulated followed by a comparison of the predictions with the numerous air quality measurements reported by the local air pollution control agencies. In addition, since evaluation of emission control strategies is an important potential use of the model, simulation results are also given demonstrating the possible impact on air quality in the Los Angeles area resulting from implementation of the U. S. Environmental Protection Agency's control strategy for the South Coast Air Basin proposed in July of 1973.

The governing equations of the model are based on the general mass conservation relationships for a chemically reactive species in a three-dimensional, turbulent atmospheric boundary layer. These equations are solved independently of the coupled Navier-Stokes and energy equations; meteorological parameters in the model are estimated from measured wind and mixing depth data. Reaction rate expressions for the reacting species are derived from a concise, fifteen step kinetic mechanism describing the important chemical reactions that take place in the atmosphere. A detailed discussion is

included of the treatment of the winds and temperature inversion in the Los Angeles area.

Since pollutant emissions are an essential input to the model, a general model and comprehensive inventory of contaminant emissions for Los Angeles is presented. Considered in this study are the spatial and temporal distribution of emissions from motor vehicles, aircraft, and fixed sources (including power plants, refineries, etc.).

Because of the nonlinear nature of the chemical kinetics, the governing equations themselves are nonlinear. Thus, a finite-difference scheme based on the method of fractional steps is developed to solve the equations. A detailed exposition of all difference equations and their manner of solution is given.

As mentioned previously, an evaluation study of the model is performed by making extensive comparisons of predictions and measurements for Los Angeles. It is found that local pollutant sources near monitoring stations can hamper the comparison of spatially averaged predictions with point measurements. In an effort to account for sub-grid scale effects, a "microscale" model is developed to predict the concentration elevation observed at a monitoring site caused by local sources, such as traffic on nearby streets and freeways. In general, it is found that the model predicts pollutant concentrations reasonably well considering the complexity of the problem and the uncertainty in many of the parameters in the model.

Finally, possible future applications of the model are discussed, including the short range forecast of pollutant concentrations

(say up to a few days in the future) and the evaluation of the impact of regional planning decisions and emission control strategies on air quality. To gain experience in applying the model to evaluate emission control strategies, simulations of the Los Angeles region are performed using an emission inventory based on control measures proposed by EPA for the region in 1977. The model results indicate that ozone concentrations will be reduced substantially from 1969 levels; however, definitive statements with regard to air quality in 1977 must await further refinement of the model and better understanding of the effects of the various proposed control strategies on pollutant emissions.

TABLE OF CONTENTS

Table of Contents (Cont'd)

Table of Contents (Cont'd)

CHAPTER 1

FORMULATION OF THE MODEL

1.1 Introduction

Urban airshed models are mathematical representations of atmospheric transport and chemical reaction processes which, when combined with a source emissions inventory and pertinent meteorological data, may be used to predict pollutant concentrations as a function of time and location in the airshed. Models capable of accurate prediction over a range of meteorological and source emission conditions will serve as an important aid in urban and regional planning, including use in:

1. Simulating the effects of alternative emission control strategies on pollutant concentrations in the airshed;
2. Real-time prediction in an alert warning system; and
3. Examining the air pollution impact of new sources, such as freeways and power plants.

A dynamic airshed simulation model that is to be generally useful in urban planning studies must meet several requirements. First, it should be capable of predicting accurately the ground level concentrations of inert pollutants, as well as those formed in the atmosphere by chemical reactions. Second, the model should have a spatial and temporal resolution appropriate for the analysis of concentration variations which occur in a city throughout the course of a day. For a typical large urban area, the horizontal spatial resolution may be of the order of a mile, and the temporal

resolution, of the order of an hour. The resolution of the model will, of course, be influenced by the availability of data of similar resolution. Third, the complexity of the model, and thus the computing time and computer storage requirements, should be such that the model can be operated at a reasonable cost using computers of general availability.

The objective of this study is to develop and validate an airshed simulation model for photochemical air pollution. The focus of this work is the prediction of carbon monoxide (CO), nitric oxide (NO), nitrogen dioxide (NO_2), hydrocarbon, and ozone (O_3) concentrations and their variations in space and time. Also of interest, although not pursued in the present study, is the estimation of sulfur dioxide (SO_2) and aerosol concentrations.

The Los Angeles airshed was chosen as the region for initial application of the model. This choice was made for three reasons. First, the meteorological and pollutant data base in Los Angeles is one of the richest available for any major urban center. A network of nearly three dozen wind speed and direction sensors and twelve air quality monitoring stations dot the Basin. In addition, during the summer of 1969, the Scott Research Laboratories (1970) carried out an extensive data gathering program in Los Angeles. Particularly valuable were the vertical temperature profile data they gathered over three sites in the Basin, thereby permitting much more accurate specification of the depth of the mixing layer than is normally possible. Second, Los Angeles smog represents the most serious and persistent incidence of photochemical air pollution in

the United States. Third, because of its lack of proximity to other large urban areas, Los Angeles has an air pollution problem which is entirely locally generated. Thus, there is no need to account for the influx of significant amounts of pollutants from upwind areas.

The model development and validation program is presented in the first four Chapters:

1. FORMULATION OF THE MODEL
2. A MODEL AND INVENTORY OF POLLUTANT EMISSIONS
3. NUMERICAL INTEGRATION OF THE GOVERNING EQUATIONS
4. EVALUATION OF THE MODEL

In addition, the model has been employed to examine the impact on air quality of a control strategy recently proposed for the Basin. The study of this proposal is the subject of the fifth Chapter:

5. EVALUATION OF THE 1977 ENVIRONMENTAL PROTECTION AGENCY IMPLEMENTATION PLAN FOR LOS ANGELES

The first part of this Chapter is devoted to a presentation of the basic equations constituting the model. Next, the nature and extent of the region to be modeled is specified. Then a brief description is given of the required inputs to the model, including the source emissions inventory, the kinetic mechanism for the atmospheric chemical reactions, and maps of wind speed, wind direction, the height of the inversion base as a function of time and location. Because of the detail involved in the presentation of the source

emissions inventory, it will be the subject of Chapter 2. The latter portion of the present Chapter will be devoted to the treatment of meteorological variables and the chemical kinetic mechanism. A comprehensive discussion of the numerical integration of the governing partial differential equations of the model is given in Chapter 3. The subject of Chapter 4 is the validation of the model, that is, the comparison of the model's predictions with pollutant monitoring data collected by the Los Angeles and Orange County Air Pollution Control Districts. Six days in 1969, each exhibiting somewhat different meteorological conditions and smog severity, were chosen for the model validation.

1.2 The General Theory of Urban Air Pollution Modeling

The simulation of photochemical air pollution is essentially the problem of describing the behavior of a number of chemically reactive species in the turbulent atmospheric boundary layer. Consider N chemically reactive species in a fluid. The concentration $c_\ell(x, y, z, t)$ of each constituent must satisfy the continuity equation,*

$$\frac{\partial c_\ell}{\partial t} + \frac{\partial}{\partial x}(uc_\ell) + \frac{\partial}{\partial y}(vc_\ell) + \frac{\partial}{\partial z}(wc_\ell) = \frac{\partial}{\partial x}\left(D_\ell \frac{\partial c_\ell}{\partial x}\right) + \frac{\partial}{\partial y}\left(D_\ell \frac{\partial c_\ell}{\partial y}\right) + \frac{\partial}{\partial z}\left(D_\ell \frac{\partial c_\ell}{\partial z}\right) + R_\ell(C_1, \ldots, C_N, T) + S_\ell(x, y, z, t) \quad \ell = 1, 2, \ldots, N \tag{1.1}$$

where u, v, and w are the components of the wind velocity, D_ℓ is the molecular diffusivity of species ℓ in air, R_ℓ is the rate of formation of species ℓ by chemical reaction, T is the temperature, and S_ℓ is the rate of emission of species ℓ from sources. In most fluid dynamics problems involving chemical reaction, it is necessary to carry

*(Footnote to page 4) In writing the continuity relationship for species ℓ, it is customary to treat sources of the contaminant in the boundary conditions rather than in the partial differential equation itself. While all "ground level" emissions may be injected into the "bottom" of the modeling region and included in the boundary conditions, additional consideration must be given to the treatment of pollutants emitted from tall stacks. Perhaps the best way of handling this situation would be to define the lower boundary of the region as illustrated below:

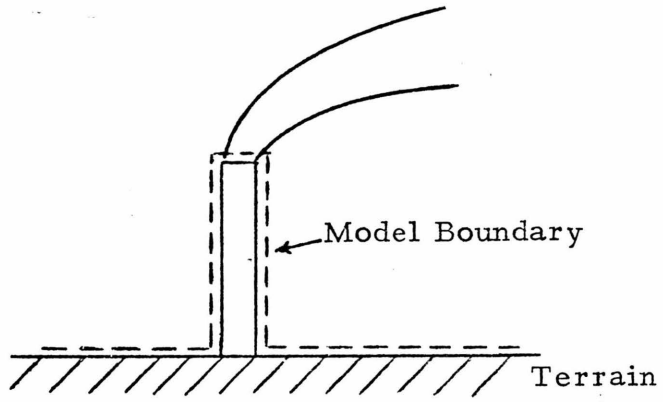

Thus, the mass flux from the stack may be treated in the boundary conditions in a straightforward manner. In actual application, however, the modeling region is partitioned into a network of grid cells. Then the continuity relationship is spatially averaged over each cell and subsequently solved for the average concentration. Since the grid cells typically have horizontal and vertical dimensions of several kilometers and a few tens of meters, respectively, emissions from a stack are best represented by a source term in the appropriate grid cell aloft. Thus, the term S_ℓ will be introduced in equation (1.1) at this time to facilitate the later treatment of emissions injected into the atmosphere from tall stacks.

out the simultaneous solution of the coupled equations of mass, momentum, and energy to account properly for the changes in c_ℓ, u, v, w, and T and the effects of the changes in each of these variables on each other. In considering air pollution, however, it is often quite reasonable to assume that the presence of pollutants in the atmosphere does not affect the meteorology to any detectable extent. An important exception is the attenuation of incoming radiation by photochemically-generated haze, a common occurrence, for example, in the Los Angeles area during the summer and autumn months. While the variation in pollutant concentrations may, in this way, alter the energy input to the system, and thus affect both the energy and momentum equations, it is possible to incorporate this effect in the equations of continuity alone (by treating measured intentities as data) if it is not of interest to predict temperature and velocity. Thus, the equations of continuity (1.1) can be solved independently of the coupled Navier-Stokes and energy equations.

Since atmospheric flows are turbulent, it is customary to represent the wind velocity components as the sum of a deterministic and stochastic component, e.g. $u = \overline{u} + u'$. Substituting $u = \overline{u} + u'$, etc., into equation (1.1), taking the expected value of the equation, and assuming that molecular diffusion is negligible when compared with turbulent dispersion yields the following equation governing the mean concentration $\langle c_\ell \rangle$,*

---

* A different notation is employed for the mean wind components, $\overline{u}$, $\overline{v}$, and $\overline{w}$ and the mean concentrations $\langle c_\ell \rangle$, since the former represent time average quantities, whereas the latter represent ensemble averaged quantities.

$$\frac{\partial \langle c_\ell \rangle}{\partial t} + \frac{\partial}{\partial x}(\bar{u}\langle c_\ell \rangle) + \frac{\partial}{\partial y}(\bar{v}\langle c_\ell \rangle) + \frac{\partial}{\partial z}(\bar{w}\langle c_\ell \rangle)$$

$$+ \frac{\partial}{\partial x}\langle u'c'_\ell \rangle + \frac{\partial}{\partial y}\langle v'c'_\ell \rangle + \frac{\partial}{\partial z}\langle w'c'_\ell \rangle \qquad (1.2)$$

$$= \langle R_\ell(\langle c_1 \rangle + c'_1, \ldots, \langle c_N \rangle + c'_N, T) \rangle + S_\ell(x, y, z, t)$$

where $c_\ell = \langle c_\ell \rangle + c'_\ell$, $\langle c'_\ell \rangle = 0$, and turbulent fluctuations of the temperature have been neglected. This is the basic equation for the mean concentration of a reactive pollutant species in the atmosphere. Its direct solution is precluded by the appearance of the new dependent variables, $\langle u'c'_\ell \rangle$, $\langle v'c'_\ell \rangle$, $\langle w'c'_\ell \rangle$, as well as any variables of the form $\langle c'_\ell c'_j \rangle$ which arise from $\langle R_\ell \rangle$. There has been considerable study of means of approximating the variables $\langle u'c'_\ell \rangle$, $\langle v'c'_\ell \rangle$, and $\langle w'c'_\ell \rangle$ [see, for example, Kraichnan (1962), Saffman (1969), and Monin and Yaglom (1971).] The simplest and most popular means of representing terms of the form $\langle u'c'_\ell \rangle$ is by the so-called K-theory (Calder, 1949; Pasquill, 1962; Monin and Yaglom, 1971) in which one sets

$$\langle u'c'_\ell \rangle = -K_{xx}\frac{\partial \langle c_\ell \rangle}{\partial x} \qquad \langle v'c'_\ell \rangle = -K_{yy}\frac{\partial \langle c_\ell \rangle}{\partial y} \qquad \langle w'c'_\ell \rangle = -K_{zz}\frac{\partial \langle c_\ell \rangle}{\partial z} \qquad (1.3)$$

It is well known that in the proper general form of the K-theory, the set of quantities K_{xx}, K_{xy}, etc. constitute the components of a second order tensor $\underset{\approx}{K}$. In most reported applications of the K-theory, off-diagonal terms of the form K_{xy}, etc. are set equal to zero. For the diagonal form of $\underset{\approx}{K}$ to be valid at all points of the region, it is necessary for the tensor to have the coordinate axes as principal axes at

all points of space. Such a situation can occur in the surface layers of the atmosphere, where the mean wind vector can be regarded as everywhere parallel to a given vertical plane (Calder, 1965). In a large airshed this is clearly not the case. If it is possible to assume merely that the mean velocity is parallel to the ground, with components $u \neq 0$, $v \neq 0$, $w = 0$, then the only valid form of the K-theory as given by equation (1.3) can be that in which $K_{xx} = K_{yy}$. Henceforth, $K_{xx} = K_{yy}$ and are denoted as K_H, and K_{zz} is denoted as K_V.

While there has been considerable study of means of relating the variables $\langle u'c'_\ell \rangle$, $\langle v'c'_\ell \rangle$, and $\langle w'c'_\ell \rangle$ to the mean concentrations, there has been comparatively little examination of approximations for terms of the form $\langle c'_\ell c'_j \rangle$ which arise when chemical reactions take place in turbulence. This lack of study is primarily a result of both the enormous theoretical difficulties associated with the description of turbulent chemical reactions and the lack of experimental data against which to compare the predictions of the turbulence theories which have been developed.* Consequently, for simplicity, one final assumption is made relative to equation (1.2), namely that the mean rate of reaction can be approximated by the rate based on the mean concentrations, i.e.

$$\langle R_\ell(\langle c_1 \rangle + c'_1, \ldots, \langle c_N \rangle + c'_N, T) \rangle \cong R_\ell(\langle c_1 \rangle, \ldots, \langle c_N \rangle, T) \qquad (1.4)$$

---

* The reader is referred to Corrsin (1958), Lee (1966), and O'Brien (1966, 1968ab, 1969, 1971) for further information concerning initial studies of means for approximating joint moments of the form $\langle c'_\ell c'_j \rangle$. In spite of these studies, it is still not possible to assess the importance of the contribution of fluctuating terms of the form $\langle c'_\ell c'_j \rangle$ to the mean rate of reaction $\langle R_\ell \rangle$ in atmospheric chemical reactions, although an initial effort along these lines has been made by Donaldson and Hilst (1972).

Since definitive data on the temperature dependence of photochemical reaction rates are not generally available, it will be assumed for the purposes of this study that R_ℓ is independent of T.

Substituting equations (1.3) and (1.4) into (1.2) yields

$$\frac{\partial \langle c_\ell \rangle}{\partial t} + \frac{\partial}{\partial x}(\bar{u}\langle c_\ell \rangle) + \frac{\partial}{\partial y}(\bar{v}\langle c_\ell \rangle) + \frac{\partial}{\partial z}(\bar{w}\langle c_\ell \rangle) =$$

$$\frac{\partial}{\partial x}\left(K_H \frac{\partial \langle c_\ell \rangle}{\partial x}\right) + \frac{\partial}{\partial y}\left(K_H \frac{\partial \langle c_\ell \rangle}{\partial y}\right) + \frac{\partial}{\partial z}\left(K_V \frac{\partial \langle c_\ell \rangle}{\partial z}\right) \qquad (1.5)$$

$$+ R_\ell(\langle c_1 \rangle, \ldots, \langle c_N \rangle) + S_\ell(x, y, z, t)$$

Contrary to the impression conveyed in a number of earlier air pollution modeling studies, equation (1.5) is <u>not</u> the fundamental equation governing the dynamic behavior of air pollutants in the atmosphere; rather, by virtue of equations (1.3) and (1.4) it is an approximate equation, valid only under certain circumstances. Equation (1.5) is employed as the basic model in this study. However, before doing so, it is necessary to consider the limitations inherent in equation (1.5) that restrict its applicability in describing the transport and reactions of air pollutants in the atmosphere.

Assessing the validity of equation (1.5) for modeling air pollutant dynamics has been the subject of two recent studies (Lamb, 1973; Lamb and Seinfeld, 1973). It has been shown in these studies that equation (1.5) is a valid representation of atmospheric transport and chemical reaction provided that the:

1. Time resolution Δt* is large compared with the Lagrangian time scale of the turbulence;
2. Characteristic temporal and spatial scales for gradients in the mean velocity field are large compared with the time resolution Δt and the average distance that a fluid particle travels in Δt;
3. Characteristic temporal and spatial scales for gradients in the turbulent velocity correlations are large compared with the time resolution Δt and the average distance that a fluid particle travels in Δt;
4. Characteristic temporal and spatial scales for gradients in the source emission functions S_ℓ are large compared with Δt and the distance a particle travels in Δt;
5. Characteristic temporal scale for changes in the rate of generation or depletion of species by chemical reaction, R_ℓ, is large compared with Δt.

These conditions may be expressed more precisely. In particular, conditions 2 and 3 imply that each of the fluid velocity components should satisfy the requirements:**

---

* Δt refers to a measure of the time scale for the most rapid changes which equation (1.5) is capable of resolving. Δt does not necessarily coincide with the time step used in the ultimate numerical solution of equation (1.5), as discussed in Chapter 3.

** For convenience in stating these conditions, the notation u_1, u_2, u_3 and x_1, x_2, x_3 is employed in place of u, v, w and x, y, z respectively.

$$\frac{1}{\bar{u}_i}\ \frac{\partial \bar{u}_i}{\partial t} \ll \frac{1}{\Delta t} \qquad i = 1, 2, 3$$

$$\frac{1}{\bar{u}_i}\ \frac{\partial \bar{u}_i}{\partial x_k} \ll \left[(R_{kk} + \bar{u}_k^2\ \Delta t)\Delta t\right]^{-\frac{1}{2}}$$

$$\frac{1}{\langle u_i' u_j' \rangle}\ \frac{\partial \langle u_i' u_j' \rangle}{\partial t} \ll \frac{1}{\Delta t} \qquad i, j = 1, 2, 3$$

$$\frac{1}{\langle u_i' u_j' \rangle}\ \frac{\partial \langle u_i' u_j' \rangle}{\partial x_k} \ll \left[(R_{kk} + \bar{u}_k^2\ \Delta t)\Delta t\right]^{-\frac{1}{2}}$$

where $R_{kk}(\underset{\sim}{x}, t)$ is the Lagrangian time correlation function,

$$R_{kk}(\underset{\sim}{x}, t) = \int_0^\infty \langle \nu_k(\underset{\sim}{x}, t)\nu_k(\underset{\sim}{x}, t+\tau)\rangle\ d\tau \qquad k = 1, 2, 3$$

and $\nu_k(\underset{\sim}{x}, t)$ is the Lagrangian particle velocity at position $\underset{\sim}{x}$ at time t. Conditions 4 and 5 can be written as:

$$\frac{1}{S_\ell}\ \frac{\partial S_\ell}{\partial t} \ll \frac{1}{\Delta t} \qquad \ell = 1, 2, \ldots, N$$

$$\frac{1}{S_\ell}\ \frac{\partial S_\ell}{\partial x_k} \ll \left[(R_{kk} + \bar{u}_k^2\ \Delta t)\Delta t\right]^{-\frac{1}{2}}$$

$$\frac{1}{R_\ell}\ \frac{\partial R_\ell}{\partial t} \ll \frac{1}{\Delta t}$$

These conditions, of course, impose restrictions on Δt and on the temporal and spatial resolution of the velocity field and the source emission functions that are to be used in equation (1.5). Therefore, the extent to which these restrictions apply for conditions typically observed in the Los Angeles Basin must be determined. Only then can the appropriate spatial and temporal scales for the model be

specified.

In the Los Angeles airshed there are roughly three dozen wind monitoring stations, with an average spacing between them of roughly five miles. At most stations the wind speed and direction data are averaged over a one hour period. From these hourly-averaged values the mean surface wind field $\bar{u}(x, y, t)$ and $\bar{v}(x, y, t)$ can be constructed. Subtracting the mean values from the instantaneous readings at each station and averaging over time yields the Eulerian correlations $\langle u'_i u'_j \rangle$, $i, j = 1, 2, 3$. An Eulerian time scale for the turbulence,

$$T_E = \max_{i, j, \underset{\sim}{x}, t} \left\{ \frac{1}{\langle u'_i(\underset{\sim}{x}, t) u'_j(\underset{\sim}{x}, t) \rangle} \int_0^\infty \langle u'_i(\underset{\sim}{x}, t) u'_j(\underset{\sim}{x}, t+\tau) \rangle d\tau \right\}$$

can be estimated from these correlations. Although the precise relation between the Eulerian and Lagrangian time scales, T_E and T_L, where

$$T_L = \max_{i, j, \underset{\sim}{x}, t} \left\{ \frac{1}{\langle u'_i(\underset{\sim}{x}, t) u'_j(\underset{\sim}{x}, t) \rangle} \int_0^\infty \langle v_i(\underset{\sim}{x}, t) v_j(\underset{\sim}{x}, t+\tau) \rangle d\tau \right\}$$

is unknown, a convenient estimate is that $T_L \cong 4T_E$ (Hay and Pasquill, 1959). Having then estimated T_L from the wind station data, from the condition that $\Delta t >> T_L$, a lower limit can be placed on Δt, such as $5T_L$. Using a $\Delta t >> T_L$ insures that the four conditions pertaining to the fluid velocity components will be satisfied.

Once Δt has been selected, the spatial and temporal resolutions for S_ℓ and the temporal resolution for R_ℓ that satisfy the final three conditions must be specified. These conditions will determine

the degree of detail required for the source emissions inventory and the chemical reaction mechanism, one which is commensurate with that of the meteorological data.

Unfortunately, data of the type needed to estimate the Eulerian time scale of the turbulence in the Los Angeles Basin are not generally available. In an effort to gather data of this type, Lamb and Neiburger (1970) measured the turbulent structure of the atmosphere at a height of 20 meters in West Los Angeles. The wind velocities were averaged over a period of 0.3 hour. From these data, T_E was estimated to be 50 seconds. Assuming that $T_L = 4T_E$, T_L equals 200 seconds. Therefore, it is estimated that $\Delta t \geq 10^3$ seconds, on the basis of $\Delta t \geq 5T_L$. The Lagrangian correlation functions were estimated to be: $R_{11} \cong 100\ m^2 sec^{-1}$, $R_{22} \cong 100\ m^2 sec^{-1}$, and $R_{33} \cong 10\ m^2 sec^{-1}$. With $\Delta t = 10^3$ seconds and these values of the R_{kk}, the conditions limiting the validity of equation (1.5) assume the quantitative values shown in Table 1.1. Since the conditions in Table 1.1 are based on data for which the averaging time was 0.3 hour, they are somewhat less stringent than those based on data for which the averaging time is one hour.

The maximum temporal and horizontal spatial resolution in the source emission function must be 10^3 seconds and 2000 meters, respectively. Thus, the averaging time and distance for source emissions should be at least, say, twice these values. Note that, in spite of the fact that many major pollutant sources are point and line sources, emissions must be averaged over relatively large distances to conform with the resolution of equation (1.5). In the

Table 1.1 Conditions Limiting Equation (1.5) Based on the Measurements of Wind Turbulence of Lamb and Neiburger (1970)

1.	Source emission function	$\frac{1}{S_\ell}\frac{\partial S_\ell}{\partial t} \ll 10^{-3}\ \text{sec}^{-1}$
		$\frac{1}{S_\ell}\frac{\partial S_\ell}{\partial x_k} \ll \frac{1}{2000}\ \text{meter}^{-1},\ k = 1, 2$
2.	Chemical reaction rate	$\frac{1}{R_\ell}\frac{\partial R_\ell}{\partial t} \ll 10^{-3}\ \text{sec}^{-1}$
3.	Mean velocity components	$\frac{1}{\bar{u}_i}\frac{\partial \bar{u}_i}{\partial t} \ll 10^{-3}\ \text{sec}^{-1}$
		$\frac{1}{\bar{u}_i}\frac{\partial \bar{u}_i}{\partial x_k} \ll \frac{1}{2000}\ \text{meter}^{-1},\ k = 1, 2$
		$\ll \frac{1}{100}\ \text{meter}^{-1},\ k = 3$
4.	Turbulent velocity components	$\frac{1}{\langle u_i' u_j' \rangle}\frac{\partial \langle u_i' u_j' \rangle}{\partial t} \ll 10^{-3}\ \text{sec}^{-1}$
		$\frac{1}{\langle u_i' u_j' \rangle}\frac{\partial \langle u_i' u_j' \rangle}{\partial x_k} \ll \frac{1}{2000}\ \text{meter}^{-1},\ k=1, 2$
		$\ll \frac{1}{100}\ \text{meter}^{-1},\ k = 3$

source emissions inventory to be described in Chapter 2, source emissions have been spatially and temporally averaged over two miles (approximately 3000 meters) and one hour, respectively.* Thus, the spatial averaging employed is somewhat finer than that suggested by the conditions in Table 1.1. The condition on R_ℓ states that the characteristic time scale for changes in the concentrations as a result of chemical reaction should be greater than 10^3 seconds, say, perhaps, one hour. This condition is discussed further in Section 1.5, where the reaction mechanism employed in the study is presented. Finally, Lamb and Neiburger (1970) estimated that the minimum vertical resolution of concentration changes is the order of 20 meters or more. The minimum vertical mesh spacing employed is roughly 20 meters.

In summary, equation (1.5) is applicable in resolving only those perturbations in the concentration field which have horizontal scales greater than 2 kilometers, vertical scales greater than 20 meters, and temporal scales greater than 10^3 seconds. These conditions serve as a guide to the choice of grid size and averaging time to be used in the solution of equation (1.5).

1.3 The Model Developed in This Study

The model developed is based on the solution of the N coupled partial differential equations (1.5) defined on the region, $x_W \le x \le x_E$, $y_S \le y \le y_N$, and $h(x,y) \le z \le H(x,y,t)$ for $t \ge t_o$, where x_W, x_E, y_S, y_N are the

* In the early morning, in order to account for the nonuniform distribution of trip starts, motor vehicle emissions are temporally averaged over 15 minute periods for the first hour (6-7 A.M.).

west, east, south, and north boundaries of the airshed, h(x, y) is the ground elevation above sea level at (x, y), and H(x, y, t) is the elevation above sea level of an assumed upper limit for vertical mixing or transport. The initial condition on equations (1.5) is that the mean concentration be specified at all locations,

$$c_\ell(x, y, z, t_o) = f_\ell(x, y, z) \tag{1.6}$$

(At this point and henceforth, for convenience, the brackets on the concentrations and overbars on the velocities will be omitted. However, all concentrations and velocities continue to be mean and time-averaged quantities, respectively.)

The vertical boundary conditions are:

$$1. \quad z = h(x, y) \qquad -\underset{\approx}{K} \cdot \underset{\sim}{\nabla} c_\ell \cdot \underset{\sim}{n}_h = Q_\ell(x, y, t) \tag{1.7}$$

where $\underset{\approx}{K}$ is the eddy diffusivity tensor,

$$\underset{\approx}{K} = \begin{bmatrix} K_H & & \\ & K_H & \\ & & K_V \end{bmatrix}$$

$\underset{\sim}{n}_h$ is the unit vector normal to the terrain directed into the atmosphere, and Q_ℓ is the mass flux of species ℓ at the surface.

$$2. \quad z = H(x, y, t)$$

$$\begin{aligned} (\underset{\sim}{V} c_\ell - \underset{\approx}{K} \cdot \underset{\sim}{\nabla} c_\ell) \cdot \underset{\sim}{n}_H &= [\underset{\sim}{V} g_\ell(x, y, z, t)] \cdot \underset{\sim}{n}_H \quad \text{if } \underset{\sim}{V} \cdot \underset{\sim}{n}_H \leq 0 \\ -\underset{\approx}{K} \cdot \underset{\sim}{\nabla} c_\ell \cdot \underset{\sim}{n}_H &= 0 \qquad\qquad\qquad\qquad \text{if } \underset{\sim}{V} \cdot \underset{\sim}{n}_H > 0 \end{aligned} \tag{1.8}$$

where $\underset{\sim}{V}$ is the advective velocity of pollutants relative to the moving inversion base and is given by

$$\underset{\sim}{V} = u\underset{\sim}{i} + v\underset{\sim}{j} + \left(w - \frac{\partial H}{\partial t}\right)\underset{\sim}{k} \tag{1.9}$$

$\underset{\sim}{n}_H$ is the outwardly directed unit vector normal to the surface defined by the inversion base, and g_ℓ is the mean concentration of species ℓ aloft (just above the inversion base).

The condition $\underset{\sim}{V}\cdot\underset{\sim}{n}_H \leq 0$ in equation (1.8) applies when material is transported into the modeling region from above the inversion base. The boundary condition simply states that the normal component of the mass flux is continuous across the upper boundary. The condition $\underset{\sim}{V}\cdot\underset{\sim}{n}_H > 0$ applies when pollutants are transported through the inversion base. Because of the abrupt stability change associated with an inversion layer, it is reasonable to assume that the turbulent diffusive flux across the boundary is zero, thereby attributing any pollutant transport into the inversion layer to vertical advection alone. The second boundary condition in equation (1.8) expresses the negligible turbulent diffusive flux at the inversion base.

The horizontal boundary conditions are:

$$\begin{aligned} (\underset{\sim}{U}c_\ell - \underset{\approx}{K}\cdot\nabla c_\ell)\cdot\underset{\sim}{n} &= \underset{\sim}{U}g_\ell(x, y, z, t)\cdot\underset{\sim}{n} \quad \text{if } \underset{\sim}{U}\cdot\underset{\sim}{n} \leq 0 \\ -\underset{\approx}{K}\cdot\nabla c_\ell &= 0 \qquad\qquad\qquad \text{if } \underset{\sim}{U}\cdot\underset{\sim}{n} > 0 \end{aligned} \tag{1.10}$$

where $\underset{\sim}{U} = u\underset{\sim}{i} + v\underset{\sim}{j}$, $\underset{\sim}{n}$ is the outwardly directed unit vector normal to the horizontal boundary, and g_ℓ is the mean concentration of species ℓ just outside the airshed boundary. The first condition is, as before, a statement of the continuity of mass flux across the boundary

when the flow is directed into the airshed. The second condition specifies that the diffusive component of the total mass flux is set equal to zero when the wind is directed out of the airshed. This condition is equivalent to that conventionally employed at the exit of a tubular chemical reactor (Wehner and Wilhelm, 1956) although the conditions prevailing at the boundary of the region are not precisely the same as those at the exit of such a reactor. Since the horizontal advective component of the mass flux generally dominates the horizontal diffusive component, the error incurred due to this approximation is generally small.

In this study, equations (1.5)-(1.10) are applied to the prediction of pollutant concentrations over a fifty mile square area that includes virtually all centers of population in the Los Angeles Basin.* The region was divided into a grid of 625 2 mi. x2 mi. squares, 198 of which lie over ocean or mountainous terrain having no pollutant sources. These "source-free" grid squares were not included in the region actually modeled, which is shown in Figure 1.1. Source emissions and meteorological variables are distributed in conformance with this grid, i.e., two miles is the resolution of the model, or the spatial dimension over which all quantities are averaged. Furthermore, the grid actually used in the solution of equations

---

* The modeling region is the 50 mile x 50 mile area having the following lines of longitude and latitude as its boundaries:

Longitude west	118°	38'	15"
east	117°	46'	3"
Latitude north	34°	17'	30"
south	33°	34'	2"

Figure 1.1 The Modeling Region. Locations of Monitoring Stations and Major Contaminant Sources in the Los Angeles Basin.

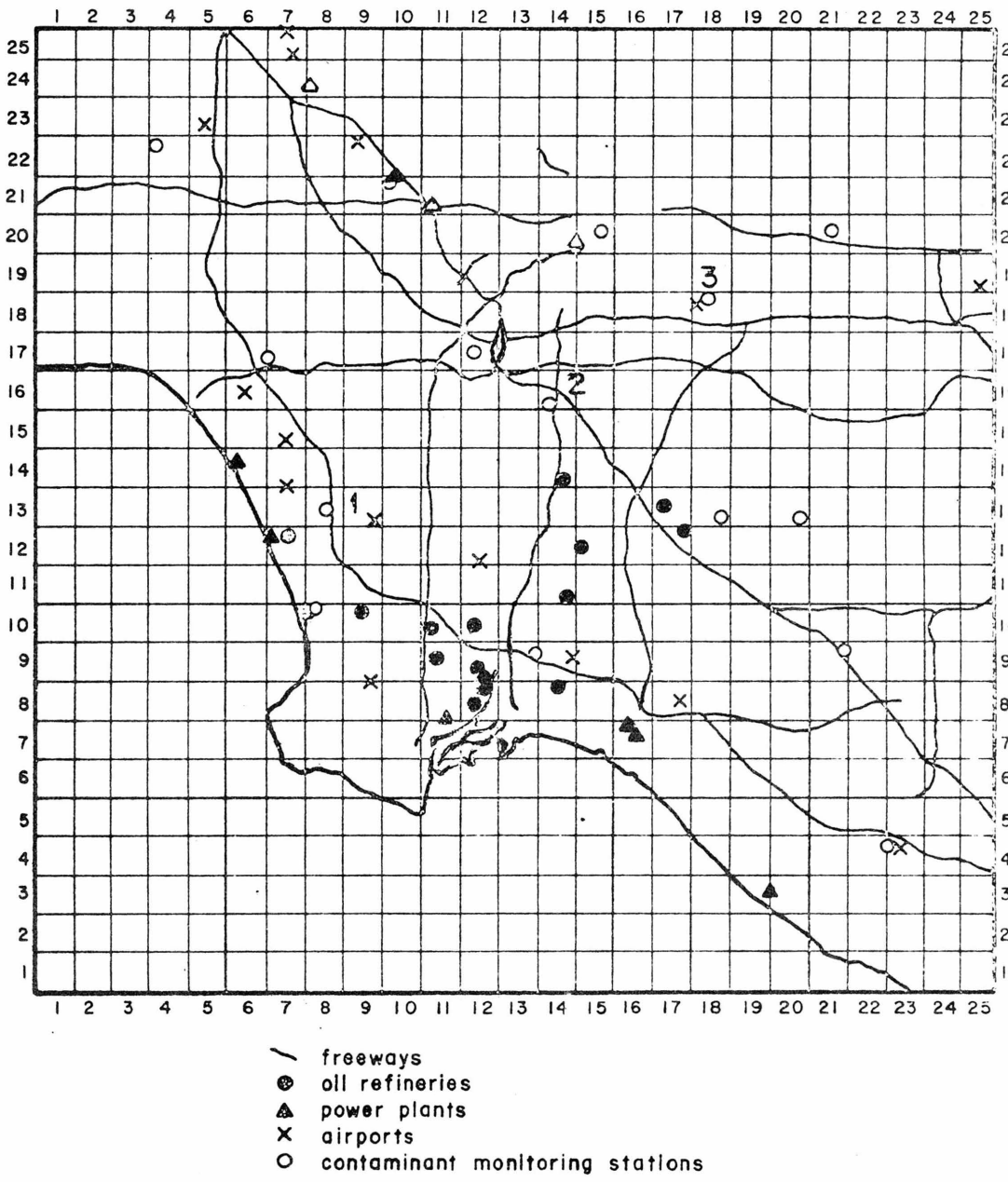

(1.5) is a three-dimensional array of five layers of cells occupying the space between the ground and the base of the inversion and lying directly over the area shown in Figure 1.1. Thus, each cell has a base two miles square and a height of (H-h)/5. The center of each cell, or node, is the point to which values of all variables are assigned or referenced. Unfortunately, due to variations in both H and h with x and y and, in the case of H, with t, the three-dimensional modeling region has an irregular "roof" and "floor." To eliminate these irregularities, which hamper the solution of the equations, the following change of variables is performed:

$$\tau = t \qquad \xi = x \qquad \eta = y \qquad \rho = \frac{z - h(x, y)}{H(x, y, t) - h(x, y)}$$

With these changes, equation (1.5) becomes

$$\frac{\partial}{\partial \tau}(\Delta H c_\ell) + \frac{\partial}{\partial \xi}(u \Delta H c_\ell) + \frac{\partial}{\partial \eta}(v \Delta H c_\ell) + \frac{\partial}{\partial \rho}(W c_\ell) =$$

$$\frac{\partial}{\partial \xi}\left\{K_H \Delta H \frac{\partial c_\ell}{\partial \xi} - K_H\left(\frac{\partial h}{\partial \xi} + \rho \frac{\partial \Delta H}{\partial \xi}\right)\frac{\partial c_\ell}{\partial \rho}\right\}$$

$$+ \frac{\partial}{\partial \eta}\left\{K_H \Delta H \frac{\partial c_\ell}{\partial \eta} - K_H\left(\frac{\partial h}{\partial \eta} + \rho \frac{\partial \Delta H}{\partial \eta}\right)\frac{\partial c_\ell}{\partial \rho}\right\}$$

$$+ \frac{\partial}{\partial \rho}\left\{- K_H\left(\frac{\partial h}{\partial \xi} + \rho \frac{\partial \Delta H}{\partial \xi}\right)\frac{\partial c_\ell}{\partial \xi} - K_H\left(\frac{\partial h}{\partial \eta} + \rho \frac{\partial \Delta H}{\partial \eta}\right)\frac{\partial c_\ell}{\partial \eta}\right.$$

$$\left. + \left(\frac{K_H}{\Delta H}\left(\frac{\partial h}{\partial \xi} + \rho \frac{\partial \Delta H}{\partial \xi}\right)^2 + \frac{K_H}{\Delta H}\left(\frac{\partial h}{\partial \eta} + \rho \frac{\partial \Delta H}{\partial \eta}\right)^2 + \frac{K_V}{\Delta H}\right)\frac{\partial c_\ell}{\partial \rho}\right\}$$

$$+ R_\ell \Delta H + S_\ell \Delta H \qquad (1.11)$$

where

$$\Delta H = H(x, y, t) - h(x, y)$$

and

$$W = w - u\left(\frac{\partial h}{\partial \xi} + \rho \frac{\partial \Delta H}{\partial \xi}\right) - v\left(\frac{\partial h}{\partial \eta} + \rho \frac{\partial \Delta H}{\partial \eta}\right) - \rho \frac{\partial \Delta H}{\partial \tau}$$

The initial and boundary conditions now become:

$$c_\ell(\xi, \eta, \rho, \tau_o) = f_\ell(\xi, \eta, \rho) \tag{1.12}$$

1. $\rho = 0$ $\quad Q_\ell(\xi, \eta, \tau) = -\left(\frac{K_H}{\Delta H}\left(\frac{\partial h}{\partial \xi}\right)^2 + \frac{K_H}{\Delta H}\left(\frac{\partial h}{\partial \eta}\right)^2 + \frac{K_V}{\Delta H}\right)\frac{\partial c_\ell}{\partial \rho}$

$$+ K_H\left(\frac{\partial h}{\partial \xi}\right)\frac{\partial c_\ell}{\partial \xi} + K_H\left(\frac{\partial h}{\partial \eta}\right)\frac{\partial c_\ell}{\partial \eta} \tag{1.13}$$

2. $\rho = 1$ $\quad Wc_\ell + K_H\left(\frac{\partial H}{\partial \xi}\right)\frac{\partial c_\ell}{\partial \xi} + K_H\left(\frac{\partial H}{\partial \eta}\right)\frac{\partial c_\ell}{\partial \eta}$

$$-\left(\frac{K_H}{\Delta H}\left(\frac{\partial H}{\partial \xi}\right)^2 + \frac{K_H}{\Delta H}\left(\frac{\partial H}{\partial \eta}\right)^2 + \frac{K_V}{\Delta H}\right)\frac{\partial c_\ell}{\partial \rho} = Wg_\ell(\xi, \eta, 1, \tau) \text{ if } W \le 0$$

$$K_H\left(\frac{\partial H}{\partial \xi}\right)\frac{\partial c_\ell}{\partial \xi} + K_H\left(\frac{\partial H}{\partial \eta}\right)\frac{\partial c_\ell}{\partial \eta} - \left(\frac{K_H}{\Delta H}\left(\frac{\partial H}{\partial \xi}\right)^2 + \frac{K_H}{\Delta H}\left(\frac{\partial H}{\partial \eta}\right)^2 + \frac{K_V}{\Delta H}\right)\frac{\partial c_\ell}{\partial \rho} = 0 \quad \text{if } W > 0 \tag{1.14}$$

3. $\xi = \xi_W$ or ξ_E

$$uc_\ell - K_H\left(\frac{\partial c_\ell}{\partial \xi} - \frac{1}{\Delta H}\left(\frac{\partial h}{\partial \xi} + \rho \frac{\partial \Delta H}{\partial \xi}\right)\frac{\partial c_\ell}{\partial \rho}\right) = ug_\ell \quad \text{if } \underset{\sim}{U} \cdot \underset{\sim}{n} \le 0$$

$$- K_H\left(\frac{\partial c_\ell}{\partial \xi} - \frac{1}{\Delta H}\left(\frac{\partial h}{\partial \xi} + \rho \frac{\partial \Delta H}{\partial \xi}\right)\frac{\partial c_\ell}{\partial \rho}\right) = 0 \quad \text{if } \underset{\sim}{U} \cdot \underset{\sim}{n} > 0 \tag{1.15}$$

4. $\eta = \eta_S$ or η_N

$$vc_\ell - K_H\left(\frac{\partial c_\ell}{\partial \eta} - \frac{1}{\Delta H}\left(\frac{\partial h}{\partial \eta} + \rho \frac{\partial \Delta H}{\partial \eta}\right)\frac{\partial c_\ell}{\partial \rho}\right) = vg_\ell \quad \text{if } \underset{\sim}{U} \cdot \underset{\sim}{n} \le 0$$

$$- K_H\left(\frac{\partial c_\ell}{\partial \eta} - \frac{1}{\Delta H}\left(\frac{\partial h}{\partial \eta} + \rho \frac{\partial \Delta H}{\partial \eta}\right)\frac{\partial c_\ell}{\partial \rho}\right) = 0 \quad \text{if } \underset{\sim}{U} \cdot \underset{\sim}{n} > 0 \tag{1.16}$$

Equations (1.11)-(1.16) are the transformed form of equations (1.5)-(1.10). Fortunately, several of the terms appearing in the above equations are small when compared with other terms, and can thus be neglected. For example, in the Los Angeles Basin the changes in ground elevation and inversion height with location are generally sufficiently gradual that the derivatives, $\partial h/\partial \xi$, $\partial h/\partial \eta$, $\partial \Delta H/\partial \xi$, and $\partial \Delta H/\partial \eta$ are considerably smaller than one. With the assumption that terms in equation (1.11) containing these derivatives can be neglected, equation (1.11) becomes

$$\frac{\partial}{\partial \tau}(\Delta H c_\ell) + \frac{\partial}{\partial \xi}(u \Delta H c_\ell) + \frac{\partial}{\partial \eta}(v \Delta H c_\ell) + \frac{\partial}{\partial \rho}(W c_\ell) =$$

$$\frac{\partial}{\partial \xi}\left(K_H \Delta H \frac{\partial c_\ell}{\partial \xi}\right) + \frac{\partial}{\partial \eta}\left(K_H \Delta H \frac{\partial c_\ell}{\partial \eta}\right) + \frac{\partial}{\partial \rho}\left(\frac{K_V}{\Delta H}\frac{\partial c_\ell}{\partial \rho}\right) \qquad (1.17)$$

$$+ R_\ell \Delta H + S_\ell \Delta H$$

Whereas the assumption that the derivatives $\partial h/\partial \xi$, etc. are small is generally satisfied in the flat portions of the Los Angeles airshed, it is violated in the mountainous areas, such as the Palos Verdes Hills and the Santa Monica Mountains. However, since the terms omitted in equation (1.11) involve horizontal diffusion, which is generally less important than horizontal advection, significant errors in using equation (1.17) are not expected to be incurred even in these regions.

Under the assumptions invoked in obtaining equation (1.17) the boundary conditions (1.13)-(1.16) become:

1. $\rho = 0$ $$Q_\ell(\xi, \eta, \tau) = - \frac{K_V}{\Delta H} \frac{\partial c_\ell}{\partial \rho} \tag{1.18}$$

2. $\rho = 1$ $$Wc_\ell - \frac{K_V}{\Delta H} \frac{\partial c_\ell}{\partial \rho} = Wg_\ell(\xi, \eta, 1, \tau) \quad \text{if} \quad W \le 0$$

$$- \frac{K_V}{\Delta H} \frac{\partial c_\ell}{\partial \rho} = 0 \qquad \text{if} \quad W > 0 \tag{1.19}$$

3. $\xi = \xi_W$ or ξ_E

$$uc_\ell - K_H \frac{\partial c_\ell}{\partial \xi} = ug_\ell \qquad \text{if} \quad \underset{\sim}{U} \cdot \underset{\sim}{n} \le 0$$

$$- K_H \frac{\partial c_\ell}{\partial \xi} = 0 \qquad \text{if} \quad \underset{\sim}{U} \cdot \underset{\sim}{n} > 0 \tag{1.20}$$

4. $\eta = \eta_S$ or η_N

$$vc_\ell - K_H \frac{\partial c_\ell}{\partial \eta} = vg_\ell \qquad \text{if} \quad \underset{\sim}{U} \cdot \underset{\sim}{n} \le 0$$

$$- K_H \frac{\partial c_\ell}{\partial \eta} = 0 \qquad \text{if} \quad \underset{\sim}{U} \cdot \underset{\sim}{n} > 0 \tag{1.21}$$

The entire airshed is thus transformed into a rectangular parallelopiped in the (ξ, η, ρ) space. The actual model is then based on the solution of equations (1.17)-(1.21) and (1.12) over a region comprised of 427 X 5 cells.

Having specified the governing equations, attention is now turned to solution of these equations and the validation of the model, i.e., comparison of predicted concentrations with those measured at local air quality monitoring stations. In order to carry out a solution, all components of the model must be satisfactorily developed and accurately specified. In particular, attention must be given to the following tasks:

1. The development of a means for including in the model the meteorological parameters $u(\xi, \eta, \rho, \tau)$, $w(\xi, \eta, \rho, \tau)$, $H(\xi, \eta, \tau)$, $K_H(\xi, \eta, \rho, \tau)$ and $K_V(\xi, \eta, \rho, \tau)$;
2. The development of a kinetic mechanism capable of describing the rates of chemical reactions occurring in the atmosphere, and the adaptation of this mechanism for inclusion in the airshed model, i.e., specification of the functional form of the terms $R_\ell(c_1, \ldots, c_N)$;
3. The development of a contaminant emissions inventory for the modeling region, i.e., specification of the functions $S_\ell(\xi, \eta, \rho, \tau)$ for elevated sources and $Q_\ell(\xi, \eta, \tau)$ for ground-level sources;
4. The selection and adaptation of a numerical method suitable for the solution of equations (1.17)-(1.21).

As noted earlier, items 3 and 4 are the subjects of Chapters 2 and 3, respectively, while items 1 and 2 will be discussed in this Chapter.

Validation of the model is undertaken upon completion of the four tasks outlined and is comprised of two parts, to be carried out in sequence:

1. Validation for carbon monoxide. The main purpose of this part is to provide a test of the meteorological facets of the model. If the model can be validated for CO, then confidence may be placed in the treatment of the winds and the inversion. Validation for CO, of course, also constitutes a test of the numerical integration technique and of portions of the source emissions inventory.

2. Validation for hydrocarbons, nitrogen oxides, and ozone. This consists of two parts, namely validation of the kinetic mechanism both in the absence and presence of transport processes. The first part refers to the comparison of the predictions of the kinetic mechanism with laboratory smog chamber data, whereas the second refers to the comparison of the predictions of the full airshed model to monitoring data.

Each of these facets of model validation will be discussed in detail in Chapter 4.

1.4 The Treatment of Meteorological Variables

Atmospheric transport and dispersion processes find expression in the overall airshed model in a number of ways: wind speed and wind direction enter through the component variables u, v, and w, the height of the inversion base H appears in the boundary conditions, while the turbulent diffusivities K_H and K_V enter into both the continuity equations and the boundary conditions.

The wind velocities u, v, and w must be specified as a function of location and time over the entire modeling region. Since equations (1.17)-(1.21) are integrated numerically, it is necessary to create a three-dimensional network of cells having nodes at their centers. Thus, the components u, v, and w must be specified at each node (at the surface and aloft) for each time step. To represent the surface winds, maps of wind speed and wind direction for hourly time intervals were constructed using data gathered at the

network of ground-based monitoring stations. Unfortunately, no measurements are made of the winds aloft. (Of particular interest is the wind field up to an elevation of about 1000 meters above terrain.) Thus, in order to specify the wind field above the surface layer of cells, it is necessary to construct or calculate wind speed and direction for all horizontal layers (except, of course, the lowest) at regular intervals of time. Two principles guide the construction--similarity to the surface winds and adherence to the requirement that conservation of mass for both air and pollutant species be satisfied. Finally, spatial and temporal variations in the height of the inversion base must also be entered as data--427 values of H for each hourly interval.

In much of the remainder of this section the discussion will focus on the preparation of contour maps of surface wind speed and direction (isotachs and streamlines, respectively) and of the height of the inversion base - in each case hourly representations. It will become apparent that methods of generating, manipulating, and transferring meteorological data are needed that are more sophisticated than manual drafting and translation of hand-drawn maps to punched cards. An initial effort aimed at the development of methods and models for organizing, codifying, and transferring meteorological data has recently been discussed by Liu et al. (1973).

1.4.1 The Inversion Layer Over Los Angeles

During the summer months the North Pacific anticyclone, a major high pressure area, maintains a virtually stationary position several hundred miles off the coast of California. Air emanating

from this "high" moves in a southeasterly direction along the Pacific Coast. Subsidence occurs during this horizontal movement, heating the upper layers through adiabatic compression. The air within the planetary boundary layer, as it spirals about the Pacific subtropical anticyclone, tends to move along sea surface isothermal areas. Finally, the air mass encounters cold subsurface waters that have welled-up at the coast. Turbulent mixing within the lowest layers results in the entrainment of moisture and the establishment of the "marine layer," a layer several hundred meters deep. The lowest layers are thus cooled from below, tending to form an elevated inversion layer.

Thus, air arriving over the Los Angeles Basin during the summer months undergoes a series of transport and energy transfer processes that tend to create an elevated inversion lying over a well-mixed marine layer. These processes occur over a spatial scale of the order of 1,000 km., but it is necessary to examine a much smaller scale, of the order of 10 to 100 km., to understand the behavior of the inversion over Los Angeles. Such an examination is necessary because, unlike inversions of approximately constant depth that lie over urban areas situated inland, the depth of the well-mixed layer over Los Angeles varies substantially from place to place at any instant in time. For example, during the early afternoon it is not unusual for the height of the inversion base over terrain at the coast to be one-fourth the height of the inversion base at a point twenty miles inland.

Edinger (1959) has studied the behavior of the marine layer over the Los Angeles Basin. Based on extensive observations, Edinger made the following generalizations regarding the depth of the marine layer during daylight hours: 1) the depth inland is greater than at the coast; 2) the depth increases early in the day and then decreases during the afternoon; and 3) the time at which the depth reaches a maximum occurs earlier near the coast and later inland.

Variations in the depth of the mixing layer as a function of both location and time can be explained in terms of three atmospheric phenomena: 1) convergence or divergence of the horizontal wind within the layer; 2) dilution of the marine layer from above by the mixing of air from within the elevated inversion layer with the marine air; and 3) advection of deeper or shallower layers of marine air into the area. These three phenomena form the basis of a semi-quantitative model developed by Edinger (1959) for representing the changes in depth of the marine layer as a function of time and location over the Basin. This model, in turn, provided the basis for the development of a set of guidelines which were used in the estimation of hourly values of the mixing depth at each location. In the discussion that follows a description is given of both the nature of available mixing depth data and the guidelines used to construct maps of mixing depth from these data.

Two sources of data exist for determining the structure of the marine layer for the modeling region. First, radiosonde measurements were made at approximately 6 A. M. and 10 A. M. PST at Los Angeles International Airport, and second, Scott Research

Laboratories (1970) flew several aircraft flights in the Basin measuring the vertical temperature profiles over three locations. The three locations, Hawthorne, Commerce, and El Monte, indicated by points 1, 2, and 3, respectively, in Figure 1.1, all lie within the Basin and are colinear, with the line connecting the points being approximately perpendicular to the coastline. The temperature data gathered during spiral ascents and descents above the specified locations were analyzed to determine the height of the inversion base locally. A summary of this analysis for September 29 and 30, 1969, is presented in Table 1.2.

Table 1.2 Height of the Inversion Base, as Taken From Vertical Temperature Soundings over Four Locations in the Los Angeles Basin

Location	29 September 1969		30 September 1969	
	Time (PST)	Height of the Inversion Base, H (meters above mean sea level)	Time (PST)	Height of the Inversion Base, H (meters above mean sea level)
Commerce	0815	182		
	0910	258	0750	243
	1206	395	1235	516
	1257	304		
El Monte	0756	137	0730	152
	0924	250	0855	243
	1156	516	1330	880
	1312	a		
Hawthorne	0826	197	0820	225
	1228	213		
Los Angeles International Airport	0600	167	0600	152
	1000	228	1000	164

a) Inversion breaks up; a height of 850 meters assigned.

Measured vertical temperature profiles, along with the guidelines based on the findings of Edinger and other investigators, formed the strategic basis for the preparation of maps of mixing depth. First, procedures for constructing mixing depth contours for the Los Angeles Basin (that portion of the modeling region south of the Santa Monica Mountains) are discussed. One of the observations made by Edinger is that contours of the inversion base over the Basin roughly parallel the curvature of the local coastline. Since the three points at which aircraft soundings were made lie on a line roughly perpendicular to the coast, the following strategy was adopted:

1. Interpolate in time between any two soundings made at each of the four measurement sites to estimate hourly values of the inversion base height at each of these locations. Extrapolate prior to and after the first and last measurements. Interpolation and extrapolation rules may be inferred from observed variations in mean height of the inversion base and observed variations of these height/time profiles with distance from the coast (Edinger, 1959).
2. Plot contours of the height of the inversion base on hourly maps, the contours being roughly parallel to the coast. Contours passing through points 1, 2, and 3 in Figure 1.1 assume the observed values at the measuring sites.

3. Interpolate in space along the line connecting points 1 and 3. Assign interpolated inversion heights to all contours not passing through a measurement location.

In this way, the height of the inversion base may be estimated throughout the Los Angeles Basin during the daylight hours. This procedure, unfortunately, may only be used for the Basin; other rules are needed to estimate variations in the height of the inversion base over the San Fernando Valley and over mountainous areas. Thus:

4. For the San Fernando Valley, the assigned mixing depth (height of inversion base less terrain height) is equal to that over El Monte at the same time. This rule was adopted as the residence time over land of air over the Valley, and thus the time available for convective heating of the air, is about equal to that of air over El Monte during the daylight hours. As a result, the lapse rate profiles are expected to be similar at both locations.
5. Inland mountainous areas are treated as follows. A mixing depth of 15 meters is assumed for early morning hours, increasing thereafter. In accordance with observations made in other regions, the maximum morning mixing depth over mountains is assumed to be 185 meters. In the afternoon, depths over mountains can increase beyond 185 meters.

Finally, the following general rules were adopted:

6. In the absence of specific data and at points removed from regions were interpolation is reliable, it was

assumed that the inversion height increases during the morning hours (after sunrise) at a rate of about 60 m. per hour in the absence of advection (an increase of about 90 m. per hour due to surface heating and a decrease of 30 m. per hour due to convergence-divergence effects. See Edinger (1959) for details). In the presence of advection, the rate of rise was assumed to be the sum of 1) a surface heating effect--a rise of 90 m. per hour times the time (in hours) of residence of the air parcel over land, and 2) a convergence-divergence effect--a sinking of 30 m. per hour from 8 A.M. to noon, or a maximum decrease in height of 120 m.

7. Subsequent to interpolation, certain checks were made:
   a. Time at which peak height occurs is checked with Edinger's observations.
   b. Variations in height of the inversion base with time, at any location, should correspond grossly with contours reported by Edinger.
8. A mixing height of 930 m. was assigned to those regions over which the inversion did break up, an exception being the high mountain region north and east of El Monte, where a height of 1500 m. was assigned.
9. Linear interpolation was used to arrive at magnitudes of mixing depths at locations between measurement points.

10. Minor changes in terrain height were ignored in the preparation of mixing depth maps.

Upon completion of maps constructed according to these rules, a final step is necessary:

11. Smooth maps of mixing depth, $\Delta H(x, y, t)$, then reconstruct $H(x, y, t)$. Nearly all previous steps in the procedure are based only on the estimation of $H(x, y, t)$, since both Edinger's model and collected data are reported for this variable.

By following these rules, a map such as that shown in Figure 1.2 can be extended to the entire modeling region and then converted to digital form by assigning values of mixing depth to each of the 625 2 mile X 2 mile grid squares. The procedure outlined above was used to construct ten hourly maps for each of the six validation days.

The procedure adopted for estimating mixing depths is based on a very limited amount of data (three or four soundings taken twice a day) and on a semi-quantitative model derived from a comprehensive measurement program. The accuracy of the procedure is probably quite adequate for those regions for which heights of the inversion base were derived through interpolation. Inversion heights for the period before 8 A.M. and after 2 P.M. PST and for the San Fernando Valley and mountain and ocean regions are certainly less accurate. The accuracy of these maps, however, probably compares quite favorably with the accuracy of the estimated wind fields.

Figure 1.2 Contours of Constant Inversion Height, in Feet Above Sea Level, at 12:00 A.M. PST on September 30, 1969

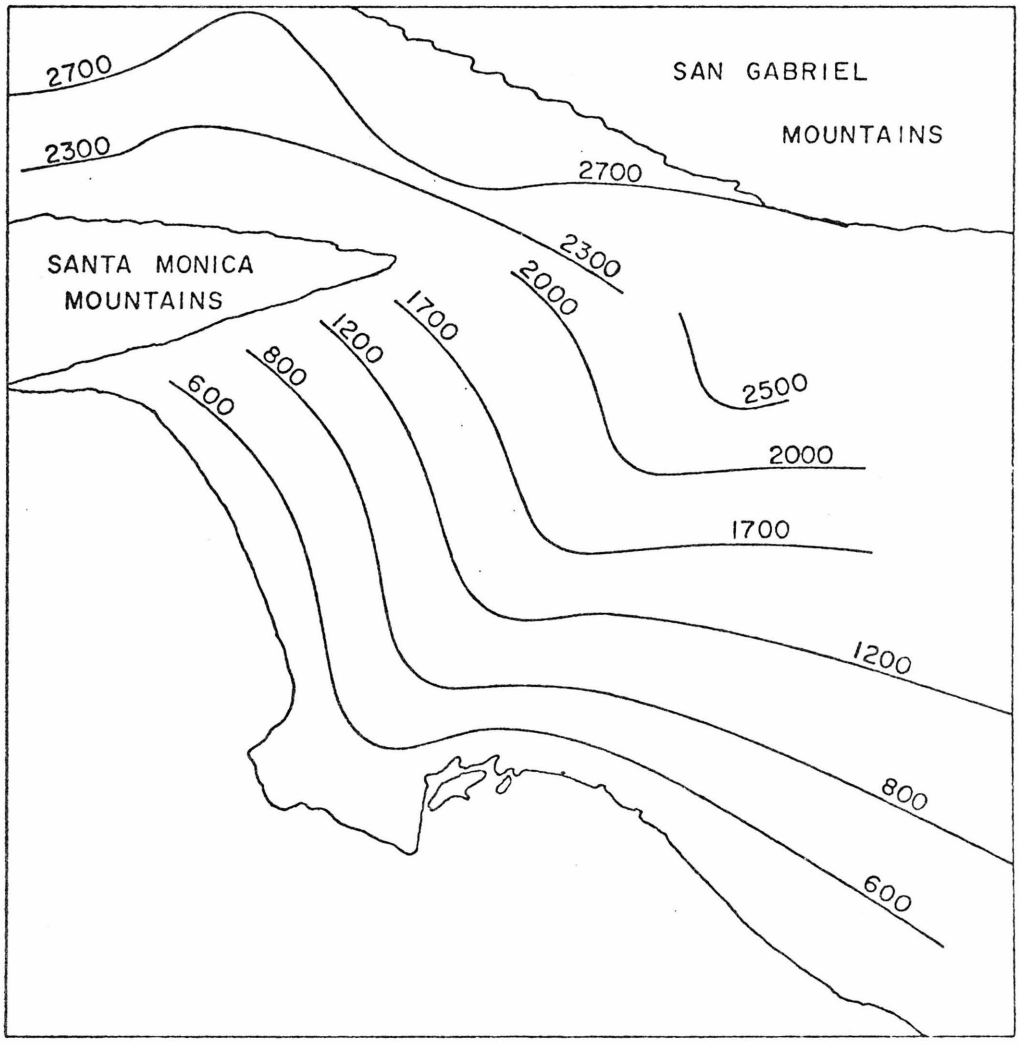

The major problem that is faced in the construction of the maps is that a substantial amount of labor is involved in manual preparation and conversion to digital form. If the airshed model is to be employed conveniently, the development and use of automated procedures for the generation of mixing depths is mandatory. The reader is referred to the work of Liu et al. (1973) for a discussion of automated input procedures.

1.4.2 The Wind Field

As indicated earlier, the North Pacific anticyclone exerts the dominant influence over air movements along the Southern California Coast during the summer and autumn months. In general, daytime winds over Los Angeles move from the ocean to the land in an easterly direction with an average speed of about five to seven miles per hour. At night, there is a reversal in the direction of flow, and winds are typically light. The movement of air near the ground is heavily influenced, however, by the hills and mountains that surround the Basin--notably the Santa Monica, San Gabriel, and Santa Ana Mountains, and the Palos Verdes and Puente Hills. The effects of these terrain features--in channeling and re-routing flows, in inducing flow up inclined, heated surfaces during the day and down along these same, cooled surfaces during the night, and in creating regions of convergence and divergence--are paramount in determining the complex flow patterns that characterize air movements in the Basin. The heating (or cooling) that an air mass undergoes in flowing from sea to land (or from land to sea) also influences flow patterns, as do the unique roughness features of the city. While many studies

have been carried out in an attempt to better understand the movements of air masses in the Basin [see, for example, Neiburger and Edinger (1954), Neiburger et al. (1956), and Bell (1969)], it remains virtually impossible to predict local surface wind behavior.

Surface wind speed and direction measurements were available at 34 sites in the Basin. Unfortunately, frequency of measurement and averaging period vary among the stations. Wind speed and direction averages are reported for periods of one hour, ten minutes, and one minute, depending on the particular measurement station. In general, the measurement apparatus for both wind speed and direction have thresholds of one to two miles per hour. Thus, these quantities are poorly determined during periods of low winds, which occur primarily during the night and early morning hours.

Two possible means for the construction of surface level wind fields were considered - manual preparation and development of an interpolation scheme through which wind speed and direction are computed automatically, given an array of measurements for the day in question. The obvious advantages of an interpolation scheme, when compared with manual procedures, were ease of use and savings in time. However, for this initial study the surface wind maps were prepared manually. The magnitudes of predicted pollutant concentrations were expected to be quite sensitive to the magnitude and direction of the wind vector, and thus it was desired not only to minimize inaccuracies, but also to be aware of their sources. Thus, while realizing the need for an automated computational procedure, the development of an appropriate algorithm was postponed.

Figures (1.3)-(1.5) show manually prepared surface wind maps for September 29, 1969 for 6:30-7:30 A.M., 9:30-10:30 A.M., and 12:30-1:30 P.M. PST, respectively. A complete listing of the meteorological data for September 29, 1969 is included in Appendix B.

One of the assumptions upon which the model is based is that the turbulent atmospheric flow is incompressible, i.e.,

$$\frac{\partial u}{\partial x} + \frac{\partial v}{\partial y} + \frac{\partial w}{\partial z} = 0 \tag{1.22}$$

or, in (ξ, η, ρ) coordinates,

$$\frac{\partial}{\partial \xi}(\Delta H u) + \frac{\partial}{\partial \eta}(\Delta H v) + \frac{\partial \overline{W}}{\partial \rho} = 0 \tag{1.23}$$

where

$$\overline{W} = w - u\left(\frac{\partial h}{\partial \xi} + \rho \frac{\partial \Delta H}{\partial \xi}\right) - v\left(\frac{\partial h}{\partial \eta} + \rho \frac{\partial \Delta H}{\partial \eta}\right)$$

Unfortunately, the surface wind field generally does not satisfy equation (1.22) with $w = 0$ since terrain and the convergence and divergence properties in the surface wind field will force w to assume nonzero values. However, if the three-dimensional wind field is not rendered divergence-free, artificial elevations or depressions in predicted concentrations will occur in areas where equation (1.22) is not satisfied.

Having discussed the construction of the surface wind field, attention is now turned to the specification of the wind field aloft. Aside from several tetroon flights on September 29 and 30 carried out by Angell et al. (1972), there are virtually no measurements available of winds aloft on the six validation days. In the absence of such data, therefore, the surface values of u and v are applied to

all levels between the ground and the inversion base. Thus, $u = u(\xi, \eta, \tau)$ and $v = v(\xi, \eta, \tau)$. Having specified u and v, one need only use equation (1.23) to calculate $\overline{W}$, and the resultant wind field will satisfy mass conservation. Equation (1.23) can be written in finite difference form for cell (i, j, k) as

$$\frac{(u\Delta H)_{i+\frac{1}{2},j,k} - (u\Delta H)_{i-\frac{1}{2},j,k}}{\Delta\xi} + \frac{(v\Delta H)_{i,j+\frac{1}{2},k} - (v\Delta H)_{i,j-\frac{1}{2},k}}{\Delta\eta}$$

$$+ \frac{\overline{W}_{i,j,k+\frac{1}{2}} - \overline{W}_{i,j,k-\frac{1}{2}}}{\Delta\rho} = 0 \qquad k = 1, 2, \ldots, 5 \qquad (1.24)$$

where $\overline{W}_{i,j,\frac{1}{2}} = 0$ (which constrains the wind to flow parallel to the terrain at ground level). As u and v are known for each horizontal level, equation (1.24) may be written as five linear equations for the five unknowns, $\overline{W}_{k,j,k+\frac{1}{2}}$, $k = 1, 2, \ldots, 5$.

Note that the vertical velocity W appearing in equation (1.17) is related to $\overline{W}$ through the following relationship:

$$W = \overline{W} - \rho \frac{\partial \Delta H}{\partial \tau}$$

It is appropriate to close this section with a few comments pertaining to the wind data itself. The existing measurement network of thirty-two stations scattered throughout the modeling region seems sufficiently dense to permit adequate representation of the wind field. However, the variation among stations in the mode of reporting data--in length of the averaging periods, in duration of measurement, and in initial time of averaging period--creates an

obvious problem in dealing with the data, a problem that could easily be eliminated by the adoption of a standard format (or formats). Finally, as alluded to earlier, the relative inaccuracy of wind data collected during periods of low wind speed, largely due to the high thresholds characteristic of the monitoring equipment, can create serious difficulties in modeling. Monitoring equipment that is responsive to low speed air movements is badly needed.

1.4.3 Turbulent Diffusivities

Horizontal and vertical turbulent diffusivities, K_H and K_V, are two of the most difficult quantities to estimate. They are difficult to establish through direct measurement and, therefore, are usually calculated from observed data. Furthermore, on the days of interest there was very little data taken aloft from which to estimate K_H and K_V. Thus, the accurate estimation of these parameters was virtually impossible.

Some useful qualitative observations can be made, however, regarding the turbulent diffusivity. K_V is a function of local velocity, shear field, and lapse rate; unfortunately, the functional relationship between K_V and these variables is largely unknown. In general, K_V increases approximately linearly with z near the ground. In the presence of an elevated inversion, however, K_V is expected to decrease with increasing z in the upper portions of the surface layer due to suppression of vertical buoyant fluctuations near the inversion base. Finally, values of K_V vary from about 30 m^2/minute under stable conditions to about 6000 m^2/minute under unstable conditions.

Figure 1.3 Surface Wind Map for the Los Angeles Basin

September 29, 1969

Averaging Period: 6:30 - 7:30 A.M. PST

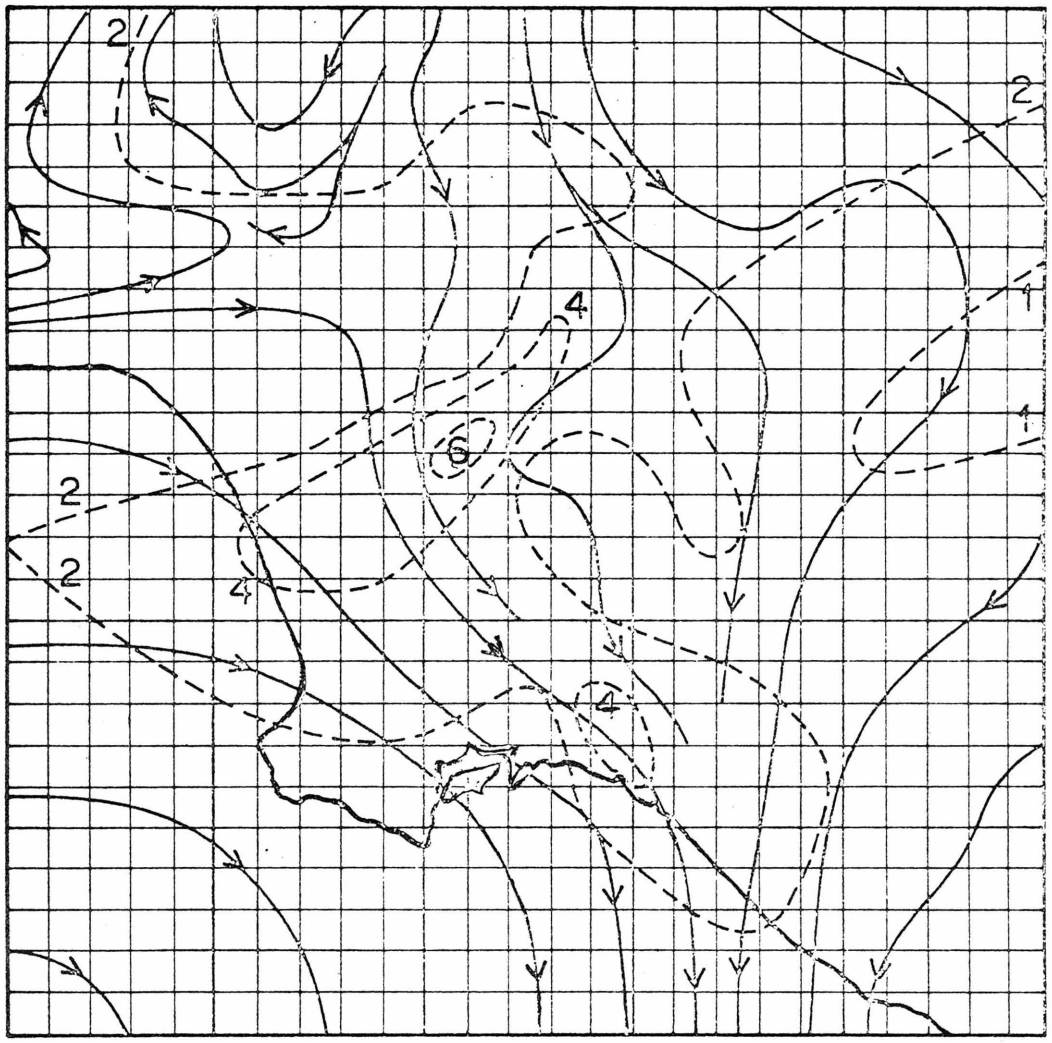

Figure 1.4 Surface Wind Map for the Los Angeles Basin

September 29, 1969

Averaging Period: 9:30 - 10:30 A.M. PST

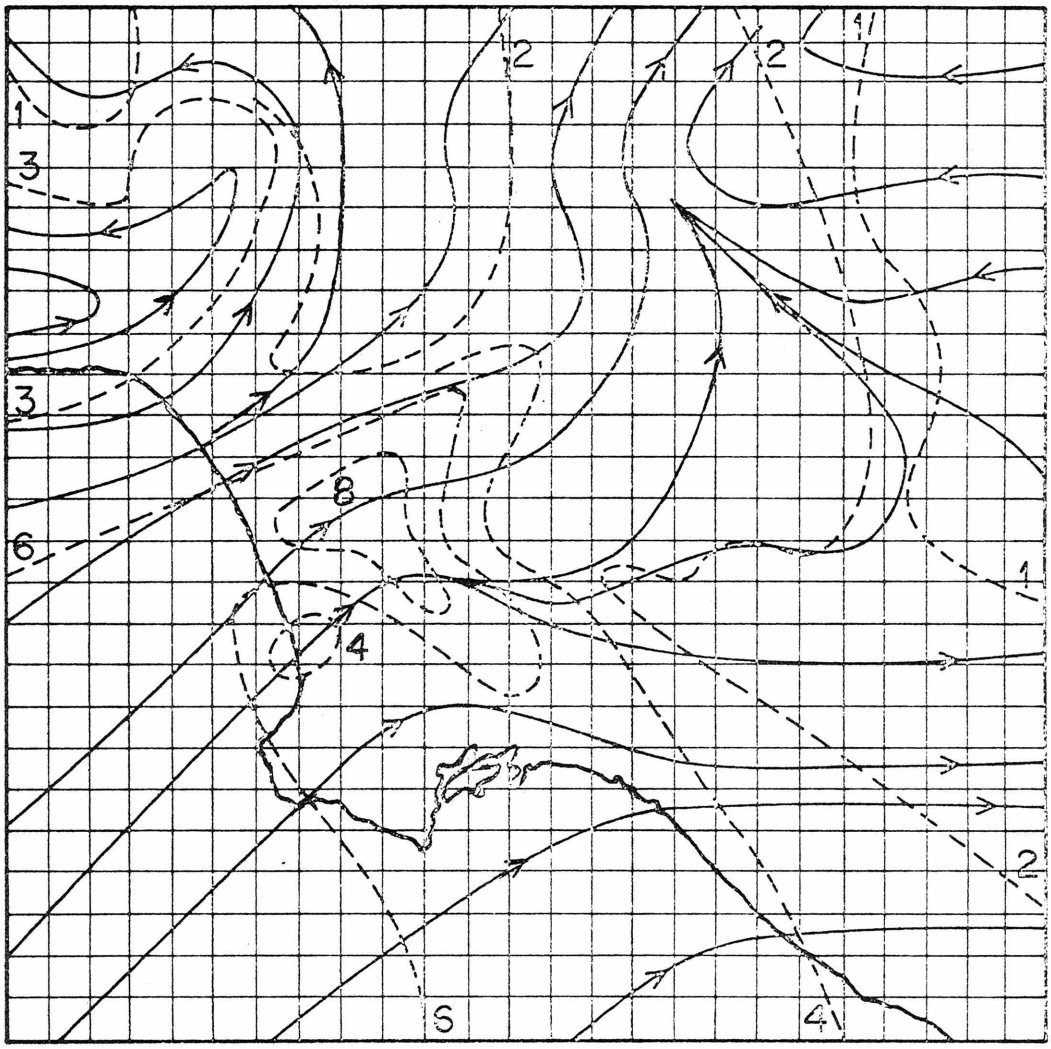

Streamlines

Isotachs (wind speeds given in miles per hour)

Figure 1.5 Surface Wind Map for the Los Angeles Basin

September 29, 1969

Averaging Period: 12:30 - 1:30 P.M. PST

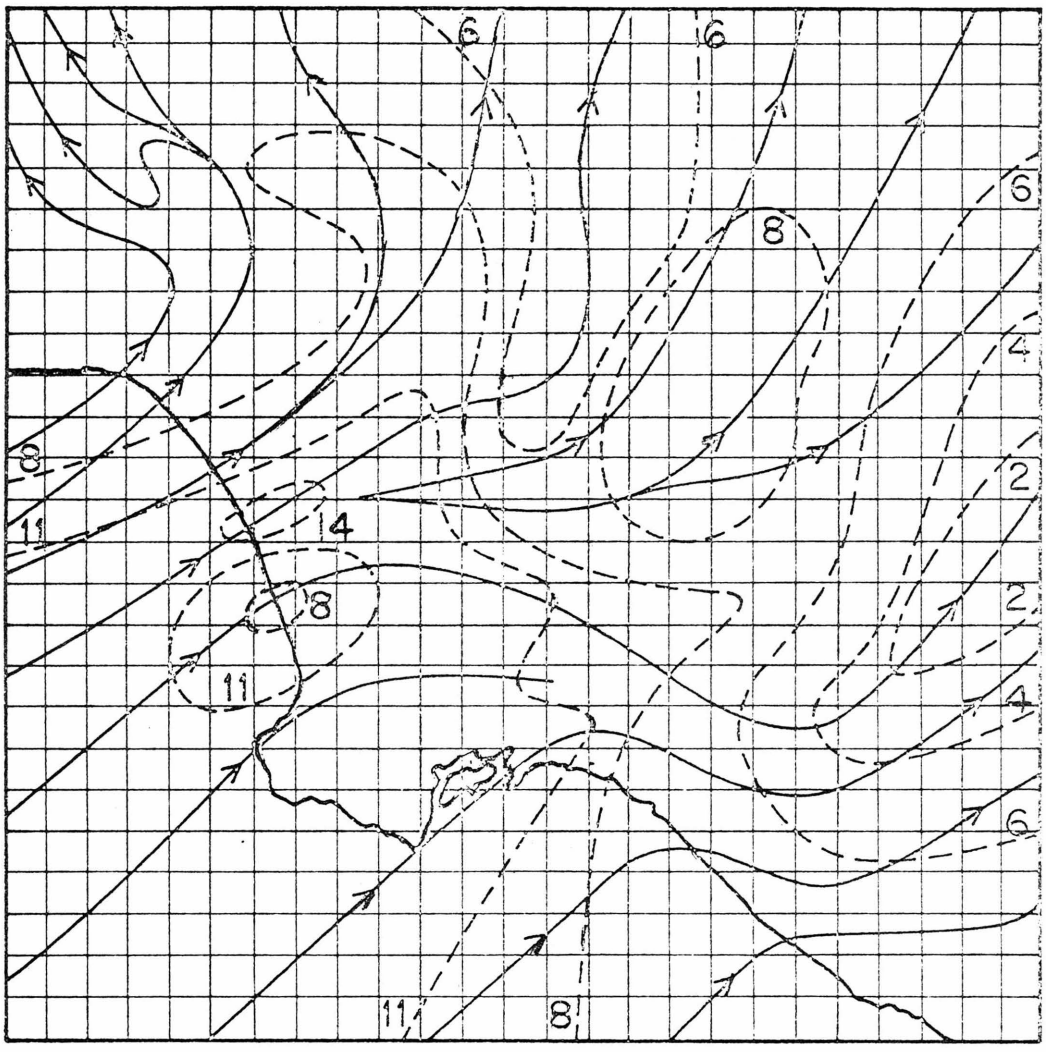

Eschenroeder and Martinez (1969) reviewed the literature pertaining to measurements of the turbulent diffusivity in the atmosphere. As a part of their study, they developed a simple model to account for the vertical variation of K_V. Using their work as a guide, the following relationship for K_V was adopted:

$$K_V = \begin{cases} [2.5\ q(\xi, \eta, \tau) - 77.3]\rho + 30.9 & 0 \le \rho < 0.4 \\ q(\xi, \eta, \tau) & 0.4 \le \rho < 0.8 \\ 5[30.9 - q(\xi, \eta, \tau)]\rho + 5q(\xi, \eta, \tau) - 123.6 & 0.8 \le \rho \le 1 \end{cases} \quad (1.25)$$

where

$$q(\xi, \eta, \tau) = 0.85 \sqrt{u^2 + v^2} + 232$$

K_V and $q(\xi, \eta, \tau)$ both have the units of $m^2\ min^{-1}$, and u and v are the horizontal wind components ($m\ min^{-1}$). Note that this relationship expresses the variation of K_V with ρ through the assumed form of the distribution and with ξ, η, and τ through variations in the horizontal wind components. However, the effects of wind shear and vertical temperature structure are not considered in the formulation.

The horizontal diffusivity K_H was treated as a constant over the airshed, equal to 2980 $m^2\ min^{-1}$.

1.5 A Kinetic Mechanism for Photochemical Smog

The basic kinetic mechanism incorporated in the airshed model is given in Table 1.3. The mechanism, discussed in detail in Appendix B of Roth et al. (1971), Hecht and Seinfeld (1972), and Appendix B of Reynolds et al. (1973), consists of 15 reactions

involving 10 chemical species. The mathematical representation includes four differential equations to permit prediction of the change of concentration with time of NO, NO_2, O_3, and reactive hydrocarbons (RHC). Five of the species, all radicals, are assumed to be in pseudo-steady state. These species are O, OH, HO_2, RO_2, and NO_3. The tenth species, HNO_2, has been treated as if the steady state approximation were valid for it, although this is known not to be the case. The basis for this assumption will be discussed shortly. The concentration of H_2O is prescribed based on the measured relative humidity. Thus, the right hand sides of the four differential equations for NO, NO_2, O_3, and RHC comprise the four functions R_{NO}, R_{NO_2}, R_{O_3} and R_{RHC}. Since the mechanism has been reported elsewhere, the discussion given in this section will be devoted to a summary of the pertinent developmental and validation work presented in the references cited above.

1.5.1 The Treatment of HNO_2

The original formulation of the kinetic mechanism (Hecht and Seinfeld, 1972) included a differential equation to describe the variation in HNO_2 concentration with time. This species, however, is not of major importance in the urban airshed model, is not measured in the atmosphere, and is not, in fact, listed among those pollutants for which air quality standards have been written. The urban airshed model, as formulated, requires the integration of the coupled, time-dependent, partial differential equations of conservation of mass for NO, NO_2, ozone, and reactive hydrocarbon. Inclusion of a fifth equation for HNO_2 would increase computing time by 20 to 25%

and would also increase computer storage requirements. Therefore, it appeared worthwhile to explore the possibility of introducing the artifact of a steady-state approximation in describing the concentration of HNO_2, achieving the necessary scaling by suitably modifying the reaction rate constant. Two questions immediately arise: 1) Is such an assumption justifiable? and 2) If it is justifiable, is it warranted?

The justifiability of the assumption can be argued on two grounds. First, the term R_{HNO_2} is quite sensitive to changes in the magnitude of k_6 and water concentration in reaction 6 (Table 1.3) and to k_7 in reaction 7 (Table 1.3). k_6 has not yet been accurately determined, k_7, which depends on light intensity, is not well known, and water concentrations were not controlled with care during the experimental programs which furnish the validation data. Thus, R_{HNO_2} can be determined only with considerable uncertainty. (This does not, however, imply that its magnitude is negligible.) Second, there are no available measurements of HNO_2 either in smog chambers or the atmosphere; thus, there is no way to verify predicted values of HNO_2 concentration.

In light of these considerations and due to the need to avoid the inclusion of an additional partial differential equation in the airshed model, an investigation was carried out to determine the effects of invoking the steady-state assumption for HNO_2. In particular:

1. If the assumption were made, what effect would it have on predicted concentration/time behavior for NO, NO_2, ozone, and reactive hydrocarbon?

2. Assuming the effect were small, what modifications, if any, in the value of k_6 would be needed? Would it be possible to establish a value, $\zeta = (\tilde{k}_6/k_6)$, where $\tilde{k}_6$ is the pseudo rate constant that yields HNO_2 vs. time profiles under the steady-state assumption that closely match the profiles computed when the differential equation for HNO_2 was included in the formulation?

If the NO, NO_2, O_3, and reactive hydrocarbon concentration/time profiles could be duplicated, or nearly duplicated, under the steady-state assumption by adopting a rate constant, $\tilde{k}_6 = \zeta k_6$, which was invariant, or nearly so, for the various reaction systems of interest, then it may be concluded that the steady-state assumption was both justifiable and warranted.

To investigate the appropriateness of the steady-state approximation, validation runs were carried out at different initial HC/NO_x ratios for the reactants, n-butane and n-butane/toluene. These validation runs consisted of comparing the predictions of the kinetic mechanism to laboratory smog chamber data. (The experimental smog chamber data against which the mechanism was validated will be presented in Chapter 4.) Two runs were carried out for each reactant system, one including the differential equation for HNO_2 with $k_6 = 0.004$ ppm^{-1} min^{-1}, and one assuming HNO_2 to be in steady-state, with $\tilde{k}_6 = k_6/8$. Virtually identical profiles were obtained in the two calculations over the six hour integration for each reactant. In view of these results, the steady-state artifact was introduced into the formulation of the mechanism in the interest of easing the

the computational burden associated with the full airshed model. It is believed, however, that the inclusion of a differential equation for HNO_2 may eventually be desirable.

Table 1.3 The Generalized Photochemical Kinetic Mechanism

The Basic 15-Step Mechanism

$$NO_2 + h\nu \xrightarrow{1} NO + O$$

$$O + O_2 + M \xrightarrow{2} O_3 + M$$

$$O_3 + NO \xrightarrow{3} NO_2 + O_2$$

$$O_3 + NO_2 \xrightarrow{4} NO_3 + O_2$$

$$NO_3 + NO_2 \xrightarrow[H_2O]{5} 2\ HNO_3$$

$$NO + NO_2 \xrightarrow[H_2O]{6} 2\ HNO_2$$

$$HNO_2 + h\nu \xrightarrow{7} OH + NO$$

$$CO + OH \xrightarrow[O_2]{8} CO_2 + HO_2$$

$$HO_2 + NO \xrightarrow{9} OH + NO_2$$

$$HO_2 + NO_2 \xrightarrow{10} HNO_2 + O_2$$

$$RHC + O \xrightarrow{11} \alpha RO_2$$

$$RHC + OH \xrightarrow{12} \beta RO_2$$

$$RHC + O_3 \xrightarrow{13} \gamma RO_2$$

$$RO_2 + NO \xrightarrow{14} NO_2 + \epsilon OH$$

$$RO_2 + NO_2 \xrightarrow{15} PAN$$

Table 1.3 The Generalized Photochemical Kinetic Mechanism (Continued)

Additional Reactions Considered for Smog Chamber Validation Studies

$$RHC_2 + O \xrightarrow{16} \alpha_2 RO_2$$

$$RHC_2 + OH \xrightarrow{17} \beta_2 RO_2$$

$$RHC_2 + O_3 \xrightarrow{18} \gamma_2 RO_2$$

$$NO_2 + PARTICLE \xrightarrow{19} NITRATE$$

1.5.2 Hydrocarbon Mixtures

During validation of the kinetic mechanism with smog chamber data, to better account for the wide range in reactivity of hydrocarbon mixtures, the basic 15 step mechanism was modified as illustrated in Table 1.3. The hydrocarbon mixture is represented by two lumped hydrocarbon species, a low reactivity hydrocarbon (RHC) and a high reactivity hydrocarbon (RHC_2). The inclusion of RHC_2 creates the need for the three additional reactions 16-18 in Table 1.3 and a fifth differential equation. RHC_2 includes all olefins, while RHC is comprised of aromatics (other than benzene), acetylenes (other than C_2H_2), and paraffins with four or more carbon atoms. C_1 to C_3-paraffins, acetylene, and benzene are taken to be unreactive. The representation of hydrocarbons in this way enhances the accuracy of the mechanism, especially with respect to the NO oxidation and hydrocarbon consumption rates. The division of hydrocarbons by class and the assignment of rate constants and

stoichiometric coefficients are discussed in Chapter 4.

1.5.3 Reactions Involving Particles

Aerosols may have a significant influence on atmospheric chemical processes (Wilson, 1972) Unfortunately, little is known about chemical interactions between photochemical smog and particulate matter. However, it has been found that a loss of NO_X occurs in smog chambers prior to the NO_2 peak when particles are present in the chamber. To account for such removal mechanisms reaction 19 has been included in the mechanism, although this reaction has not been used in the airshed simulations to be reported in Chapters 4 and 5.

1.5.4 Validity of the Kinetic Mechanism

Before its incorporation into the full airshed model, the mechanism must be tested thoroughly by comparing its predictions to smog chamber data for a variety of reactive systems, including single hydrocarbons, binary mixtures, and auto exhaust. Rules must be established for choosing the values of the stoichiometric coefficients and those rate constants associated with lumped hydrocarbon reactions. If validation were judged "successful," the mechanism could then be considered for incorporation into the full airshed model. The results of the validation of the mechanism will be reported in Chapter 4.

The final point to be considered relative to the kinetic mechanism in Table 1.3 is whether the rate equations derived from the mechanism satisfy the time scale requirements of Table 1.1, namely condition 2. Since the R_ℓ are complicated, nonlinear functions of

all the concentrations, it is difficult to ascertain if condition 2 of Table 1.1 is satisfied. However, Lamb and Seinfeld (1973) proposed an alternative criterion, namely that the eigenvalues λ_ℓ of the reaction rate equations satisfy the condition,

$$|\lambda_\ell| \ll \frac{1}{\Delta t}$$

From Table 1.1, note that $|\lambda_\ell| \ll 10^{-3}$ seconds^{-1}. Lamb and Seinfeld (1973) found that for the mechanism in Table 1.3, the dominant eigenvalue has a magnitude of about 10^{-3} seconds^{-1}. Therefore, the mechanism has a level of detail which is somewhat finer than that in the meteorological portion of the model. In spite of this discrepancy, the mechanism in Table 1.3 is employed since it already represents a bare minimum with respect to the desirable degree of chemical detail in such a mechanism.

1.6 Summary

In this Chapter a model for the prediction of the dynamic behavior of photochemical air pollutants in an urban airshed is presented. The derivation of the governing equations, the treatment of the meteorological variables, and the treatment of the chemical reactions that take place in the urban atmosphere are discussed in detail. The two remaining important components of the basic model, the source emissions model and inventory for Los Angeles and the numerical integration technique will be the subjects of Chapters 2 and 3, respectively. The model evaluation study, performed by comparing model predictions with actual air quality data, will be presented in Chapter 4.

CHAPTER 2

A MODEL AND INVENTORY OF POLLUTANT EMISSIONS

2.1 Introduction

A mathematical model capable of describing the dynamic behavior of air pollutants requires the following components: 1) meteorological data, including wind speed and direction, inversion height, and atmospheric stability; 2) a kinetic mechanism for atmospheric chemical reactions among pollutant species (if reactions take place); and 3) a source emission inventory. The first two components of a model that is applicable in the Los Angeles airshed were described in Chapter 1. In this Chapter the discussion will focus on the third component, the treatment of emissions. In particular, a description is given of a general approach to the formulation of an emissions model for an urban area that may be included in an airshed model having relatively fine spatial and temporal resolution. Then a model and inventory for representing emissions in the Los Angeles airshed is presented.

The compilation of a complete contaminant emissions inventory is perhaps the most tedious and mundane aspect of urban airshed modeling. Yet, such an inventory is a sine qua non in model validation, and, if done properly, the emissions estimates probably constitute the most precise segment of the requisite input data. Furthermore, an emissions inventory need be established but once to serve as an adequate data base for validation purposes when the days of interest all occur within the span of a few months. Meteorological data, however, must be collected for each validation day.

Thus, it is wise to devote considerable effort to the establishment of an accurate emissions inventory for the region to be modeled. The material presented in this Chapter is based largely on work carried out at Systems Applications, Incorporated and reported in Appendix A of Roth et al. (1971) and Appendix A of Reynolds et al. (1973).

Particular emphasis must be placed on developing a detailed representation of the spatial and temporal distribution of motor vehicle emissions, as these account for approximately 99% of CO, 71% of reactive hydrocarbon, and 58% of NO_x emissions in the Los Angeles area. Attention must also be given to those sources which, while responsible for only a small proportion of the total emissions on a regional basis, contribute substantially to pollutant levels in their own locale-airports, power plants, and refineries. The locations of these major fixed sources, as well as those of all freeways and air quality monitoring stations, are shown in Figure 1.1.

Before proceeding with a discussion of the work, recall that pollutant emissions are introduced into the model through the source terms $S_\ell(\xi, \eta, \rho, \tau)$ and $Q_\ell(\xi, \eta, \tau)$ in equations (1.17) and (1.18), respectively. In practice the region of interest is subdivided into an array of three dimensional cells. The term S_ℓ [ppm/min.] accounts for the emissions from elevated sources into each cell. Emissions from ground level sources are treated as surface fluxes defined at the base of each ground level cell and thus enter through Q_ℓ [ppm-meters/min.] in the boundary conditions. The source emissions inventory provides values of these inputs as mass of pollutant ℓ per unit time. The conversion to the appropriate units is carried

out in the following manner:

$$S_{\ell} = \frac{10^6 M_{e\ell} \bar{V}_{\ell}}{\Delta\xi \Delta\eta \Delta\rho \Delta H}$$

$$Q_{\ell} = \frac{10^6 M_{g\ell} \bar{V}_{\ell}}{\Delta\xi \Delta\eta}$$

where

$M_{e\ell}$ = rate of emission of species ℓ from elevated sources [kg/min]

$M_{g\ell}$ = rate of emission of species ℓ from ground level sources [kg/min]

$\bar{V}_{\ell}$ = specific volume of species ℓ [m^3/kg]

$\Delta\xi$, $\Delta\eta$ = horizontal dimensions of the grid cell [m]

$\Delta\rho$ = dimensionless vertical grid spacing

ΔH = mixing depth [m]

The remainder of this Chapter is divided into three major sections:

2.2 Automotive Emissions

2.3 Aircraft Emissions

2.4 Fixed Source Emissions

At the beginning of each section a general model for computing pollutant emissions is presented which may be applied to any urban area. Then the general model is employed to estimate emissions rates of CO, total hydrocarbons (HC) and NO_x($NO + NO_2$) in the Los Angeles airshed in Autumn 1969. Results obtained from the airshed

model using the emissions inventory described in this Chapter are discussed in Chapter 4.

2.2 Automotive Emissions

The magnitude of contaminant emissions from a motor vehicle is a variable in time and is a function of the percentage of time the vehicle is operated in each driving mode (accelerate, cruise, decelerate, and idle). The modal split is in turn dependent on the habits of the driver, the type of street on which the vehicle is operated, and the degree of congestion on that street. Also affecting emissions are the presence or absence of a smog control device, the condition of the car, its size, and other factors. The distribution of vehicles in an urban area at any time is similarly governed by a number of factors--commuting routes, distribution of centers of employment, shopping centers, residential and recreational areas, topography, the occurrence of special events, etc. Thus, precise calculation of the magnitude of emissions as a function of location and time is clearly not possible.

A number of studies have been conducted in recent years having as their objective the development of a vehicle emissions inventory for a particular urban area. In a study published in 1955, Larson et al. describe an inventory undertaken for the County of Los Angeles. In this effort, emission rates were measured for a number of vehicles, and traffic count data were used to obtain the geographical and temporal distribution of vehicles in the area. Ozolins and Smith (1966) discuss a procedure based on gasoline sales

figures, traffic flow maps, and average emission rates to obtain total daily vehicle emissions and an approximate measure of their spatial variation over an area. Rehmann (1968) performed an inventory for Gary, Indiana, using for emissions data the results of a study reported by Rose et al. (1965). [Vehicle emissions rates reported by Rose (and obtained from tests of 1955-1963 automobiles) are presented as a function of average route speed.] Rehmann assumed in his study that emissions from a vehicle are a function only of its average speed. He used traffic counts and traffic flow maps, along with estimates of average speeds on different classes of streets, to obtain the spatial variation of automobile emissions in the city. Lamb (1968) compiled an inventory for the Los Angeles Basin in a manner similar to that of Rehmann. Lamb, as Rehmann, adopted the emissions figures published by Rose. He also applied an average temporal distribution of traffic flow to obtain the variation of emissions through the day, although he did not present the geographical distribution of traffic which he derived.

An attempt has been made to develop an emissions model and inventory which possess a degree of detail that is concomitant with the level of accuracy desired in the predicted concentrations to be derived using the urban airshed model. To this end, the following tasks have been emphasized:

1. Estimating the spatial and temporal distribution of traffic with acceptable accuracy;
2. Estimating average vehicle emission rates applicable for traffic in the area;

3. Appropriately treating certain aspects of vehicular emissions behavior that may be of importance at specific times of the day, such as the large fraction of cold-running vehicles that are operative during the morning rush hours, as compared with other times of the day, and the relatively large variation in vehicle speed (and thus emission rates) with time of day during the rush hour periods.

Also note that, in general, the emission characteristics of motor vehicles operated on surface streets are different from those operated on freeways. Thus, it is convenient to treat emissions from surface and freeway traffic separately.

Emissions are attributable to the following three sources in an uncontrolled automobile:

1. Exhaust emissions account for approximately 65% of hydrocarbons and 100% of nitrogen oxides and carbon monoxide;
2. Crankcase leakage (or blow-by) accounts for approximately 20% of hydrocarbons;
3. Evaporation from the fuel tank and carburetor accounts for approximately 15% of hydrocarbons.

As a result of vehicle modifications and changing legislation for automobile emissions through the 1960's, the magnitudes and relative contributions of these three sources vary with vehicle model year. Thus, in developing an emissions inventory, one must do so for a particular time, usually a period of one year or less. An

inventory developed for 1969, for example, will not be applicable in 1973.

The first part of this section is devoted to a presentation of a model for each of the three sources of automotive emissions cited. Then the results obtained by applying the model to the Los Angeles airshed are summarized. Emission rates are expressed in grams/mile for exhaust and blow-by, and grams/day for evaporation. The rate at which CO, HC, and NO_x are emitted into each ground level grid cell from exhaust and blow-by is obtained by summing the product of the appropriate emission rate and the number of miles driven per minute for both surface and freeway traffic. The total daily evaporative loss from all vehicles in the airshed is estimated, and is distributed in proportion to the daily non-freeway vehicle mileage driven in each cell.

2.2.1 Exhaust Emissions

The rate (in grams/min.) at which species ℓ is injected into a given ground level cell from engine exhaust, $E_\ell(t)$, may be expressed as the sum of the mass (in grams) of species ℓ emitted per minute from freeways and surface streets, $E_\ell^f(t)$ and E_ℓ^s, respectively, that is

$$E_\ell(t) = E_\ell^f(t) + E_\ell^s(t) \qquad (2.1)$$

In this section models for the computation of E_ℓ^f and E_ℓ^s are given.

To develop models for freeway and surface street emission rates, the following assumptions are made:

1. Freeway emission rates are a function of average vehicle speed. All vehicles on freeways are assumed to be "hot-running," that is, the engine has reached a steady operating temperature.
2. Surface street emission rates are determined from data based on a "driving cycle" which is representative of a typical trip in the urban area.

For a particular grid cell, the freeway emissions rate for species ℓ may be expressed, as a function of time and average driving speed, by

$$E_{\ell}^{f}(t) = \frac{1}{60}\left\{n_f(t)\alpha_{\ell}[\bar{v}_f(t)] + n_s(t)\alpha_{\ell}[\bar{v}_s(t)]\right\} \qquad (2.2)$$

where $\bar{v}_f$, $\bar{v}_s$ = average speed (mph) in the fast and slow* directions, respectively, at time t.

n_f, n_s = number of vehicle miles driven per hour in the fast and slow directions, respectively.

$\alpha_{\ell}[\bar{v}]$ = emission rate of species ℓ in grams per vehicle mile at an average vehicle speed of $\bar{v}$.

Values of α_{ℓ} are computed from the following correlations, based on the work of Rose et al. (1965) and modified as described later in the test:

$$\alpha_{\ell} = a_{\ell}(\bar{v})^{b_{\ell}} \qquad (2.3)$$

---

* "Fast" and "slow" refer to an assignment of names to the two directions of flow on a freeway.

where

ℓ	a_ℓ^*	b_ℓ^*
CO	295	-0.49
HC	34.8	-0.40
NO_x (as NO_2)	4.16	0

n_f and n_s are calculated from

$$n_f = \frac{N_p^f}{1+x} \qquad n_s = \frac{N_p^f x}{1+x} \tag{2.4}$$

where

$$N_p^f = d_p^f M^f \tag{2.5}$$

and

d_p^f = fraction of daily (24-hour) freeway traffic counts assignable to hourly period p†

M^f = freeway vehicle mileage per day for the grid cell

x = n_s/n_f, as computed from freeway traffic counts

N_p^f = total freeway miles driven during hourly period p in the grid cell.

With the exception of the parameters appearing in equation (2.3), the quantities required to compute $E_\ell^f(t)$ come from traffic counts on the freeways in the region. The formulation of the temporal distribution, d_p^f, is explained subsequently. The parameters

* The values of a_ℓ and b_ℓ given in this table have been estimated for motor vehicles operating in the Los Angeles Basin during the summer of 1969.

† The appropriate hourly period, p, is determined by the value of t.

M^f and x are computed from freeway traffic count data and presented on hourly grid maps for use in equations (2.4) and (2.5).

The total emissions rate of species ℓ (grams/min) from automobiles operating on surface streets in a particular grid cell at time t is given by

$$E^s_\ell(t) = \frac{1}{60} Q^s_\ell(t) d^s_p M^s \beta_\ell(t) \qquad (2.6)$$

where

$Q^s_\ell(t)$ = emission rate of species ℓ in grams per vehicle mile for an average vehicle at time t

d^s_p = fraction of daily (24-hour) surface street traffic counts assignable to hourly period p

M^s = surface street vehicle mileage per day for the grid cell

$\beta_\ell(t)$ = a factor to account for variations in the average emission rates that occur when the total number of "cold-started" cars in operation changes rapidly, such as during the morning rush hours. (The calculation of $\beta_\ell(t)$ is discussed in more detail in Section 2.2.4.3.)

The value of $Q^s_\ell(t)$ is calculated as a weighted sum of the emissions from vehicles which are cold and hot-running at time t:

$$Q^s_\ell(t) = y(t)Q^c_\ell + [1 - y(t)]Q^h_\ell \qquad (2.7)$$

where

$y(t)$ = fraction of cars in operation at time t that were cold-started

Q_ℓ^c, Q_ℓ^h = emissions rate of species ℓ (grams/mile) from an "average vehicle," as determined from driving cycle tests in which the vehicle is cold and hot-started, respectively. (The calculation of the average emission rate will be discussed shortly.)

The total daily freeway and surface street vehicle mileages in a particular grid cell are computed from

$$M^f = \sum_{k=1}^{s^f} \nu_k^f M_k^f \qquad M^s = \sum_{k=1}^{s^s} \nu_k^s M_k^s \tag{2.8}$$

where

ν_k^f, ν_k^s = number of vehicles per day traveling on freeway and surface street segment k, respectively (available from traffic count data).

M_k^f, M_k^s = number of miles associated with freeway and surface street segment k, respectively.

s^f, s^s = total number of freeway and surface street segments in the grid cell.

Given the distribution of vehicles by age and make, the annual mileage accumulated by each vehicle, and the exhaust emission rates for each type of vehicle (as measured over a driving cycle test), the emission rate of each species from an "average motor vehicle" is computed as the appropriately weighted sum of the individual emission rates from all the types of vehicles. Specifically, the emission rate of species ℓ from the exhaust of an average vehicle, in grams per mile, may be computed as follows:

$$Q_{\ell} = \frac{\sum_{i=1}^{N^c} u_i \sum_{j=1}^{N^y} x_{ij} m_{ij} e_{\ell ij}}{\sum_{i=1}^{N^c} u_i \sum_{j=1}^{N^y} x_{ij} m_{ij}} \qquad (2.9)$$

where the subscripts i and j denote the vehicle class and model year, respectively, and

N^c = number of vehicle classes. (In this study two vehicle classes were considered, including light and heavy-duty vehicles.)

N^y = number of model years

u_i = fraction of the vehicle population belonging to class i.

x_{ij} = fraction of class i vehicles manufactured in model year j

m_{ij} = annual mileage accumulated by class i, model year j vehicles.

$e_{\ell ij}$ = average exhaust emission rate of pollutant ℓ from class i, model year j vehicles, where

ℓ = 1 CO

2 HC (total hydrocarbons)

3 NO_x (as NO_2)

The key parameter in the computation of Q_{ℓ}^h or Q_{ℓ}^c from equation (2.9) is the exhaust emission rate, $e_{\ell ij}$. Several test procedures for measuring exhaust emissions have been proposed in recent years. These procedures have as their common aim the simulation of emissions in a stationary test of a vehicle being operated

in traffic. All that have been proposed thus far are based on the concept of simulating an average "downtown-to-near-suburbs" commute trip. It is hoped that the trip will in some way be representative of the driving habits of the airshed population. The trip, usually termed a driving cycle, is composed of a series of driving modes (idle, accelerate, cruise, and decelerate) in which a pre-determined length of time is spent in each mode. Such a cycle is formulated by "tagging" a large number of vehicles on a particular day and analyzing the trips made with them, including the time spent in each mode. A recent study of this type has been reported by Smith and Manos (1972). The emissions from a large population of automobiles are measured as the vehicles are run through the cycle on a chassis dynamometer, and the resulting average yields a set of figures for each automobile type--the grams of pollutant ℓ emitted per mile. Averaging over the total vehicle population yields Q_ℓ, the grams of species ℓ emitted per mile by the "average vehicle" when driven over the "average cycle." There is currently considerable debate concerning the degree to which the various test procedures are representative of actual vehicular operations, or, indeed, if it is possible to simulate the operations of a vehicle by any single test procedure. European control agencies, for example, are considering the combined use of three driving cycles to represent city driving characteristics. A choice must also be made between the use of a hot-start and a cold-start procedure.

A method which has enjoyed widespread use in recent years, including adoption as the Federal testing procedure up to 1971, is the

California Driving Cycle (CDC). This is a seven-mode test procedure and is based on a Los Angeles commuter run [see State of California Air Resources Board (1968)]. Recently, however, the representativeness of the CDC has been questioned, and a new method, the 1972 Federal Driving Cycle (FDC), has been proposed. This procedure employs a cold-start and a driving cycle derived from a Los Angeles driving route during heavy traffic periods. Actual mass emissions are monitored over the entire driving cycle, in contrast to the CDC, in which concentrations are measured. Note that emission rates may be measured over a cycle which includes the start of the car from a cold engine condition (a cold-start test) or over a cycle which includes only the hot-running emissions (a hot-running test). The FDC, which is adopted in this study as a basis for the estimation of emission factors, includes a cold-start in its sequence of driving modes. Hot-running emission rates for the FDC are best obtained from the appropriate measurements; however, these emission rates may also be estimated if the ratio of hot to cold-start emission rates is known. (These ratios as well as FDC emission rates will be presented in Section 2.2.4.)

2.2.2 Crankcase Emissions

Positive Crankcase Ventilation (PCV) devices have been installed on automobiles in recent years to prevent the loss of hydrocarbons to the atmosphere resulting from leakage between the piston and cylinder during the compression stroke. As these devices recycle crankcase fumes through the carburetor air intake, blow-by losses from properly equipped vehicles have been virtually eliminated.

California law requires the PCV devices be fitted to all autos of

1. domestic manufacture of model year 1963 and later
2. domestic manufacture of 1955-1962 vintage upon change of ownership
3. foreign manufacture of model year 1965 and later.

However, these devices were installed on new domestic cars sold in California as early as 1961, and the law concerning 1955 to 1962 model years became effective in 1964.

Since it is estimated that 85% of all automobiles in 1969 were equipped with PCV valves, crankcase losses contribute but a small fraction of total emitted hydrocarbons. The estimated figure for blow-by losses (see Section 2.2.4.4 for details) is 0.7 grams/mile for the average vehicle in the Los Angeles Basin in 1969.

2.2.3 Evaporative Emissions

Evaporative losses occur at the fuel tank and the carburetor and involve only hydrocarbons. While tank losses occur primarily during vehicle operation and carburetor losses during the periods after a hot engine is stopped, elevated daytime temperatures and exposure to the sun serve to enhance evaporation rates. In the absence of definitive data, the daily evaporative losses are distributed evenly throughout the daylight hours, assuming nighttime evaporative losses to be small.

2.2.4 Application to the Los Angeles Airshed

In describing the application of the automotive emissions model to Los Angeles, the following discussion is segmented into

five parts. In the first two parts, the means by which the spatial and temporal distributions of traffic were constructed are described. In the third part, the treatment of exhaust emissions is discussed. Particular attention is given to the temporal distribution of the fraction of hot-running (vs. cold-running) vehicles in operation, the influence on emission rates of suddenly introducing a large population of cold-running vehicles into the system, and the effect of average vehicle speed on average emission rates. In the concluding two parts, the discussion will focus on crankcase and evaporative emissions, respectively.

2.2.4.1 Spatial Distribution of Traffic

The spatial distribution of traffic in the modeling region (the 427 2 mi. X 2 mi. grid squares shown in Figure 1.1), was determined from existing traffic count data. These data were obtained from nearly 100 municipalities and are very extensive, with counts being available for all but minor residential streets. Using the traffic count data, estimates were made of the total daily vehicle miles driven in each grid square. The temporal distribution of traffic over the area, represented as hourly variations in vehicular flow, was also computed from these traffic count data. Freeways and surface streets were treated separately in the derivation of both the temporal and spatial distributions.

In determining the spatial distribution of traffic, a key question involved the level of detail to incorporate, that is, to include traffic counts only for freeways and major and minor arteries, ignoring residential and side streets, or to include all streets. Since this

effort was to be undertaken only once, the inventory was made as complete as possible. However, as there exists a dearth of data for the smaller streets, the policy adopted was comprised of using all available counts and estimating traffic flow on the remaining streets from the local traffic data in the area, the type of neighborhood, and reference to counts on similar streets.

Figures 2.1 and 2.2 show the estimated spatial distribution of freeway and non-freeway traffic in the Los Angeles area in thousands of vehicle miles per day for late 1969 in the modeling region.

2.2.4.2 Temporal Distribution of Traffic

It is commonly accepted that the hourly variation in weekday traffic flow may be represented over a 24-hour period by a bimodal distribution having peaks at the morning and afternoon rush hours and a high plateau between these peaks. However, the parameters needed to describe this distribution--the height of each peak, the height of the plateau, the time interval encompassing each peak--vary from street to street. Shopping areas have a high frequency of traffic between peak hours. Streets in lower middle class neighborhoods experience earlier morning and afternoon peaks than do streets in upper middle class neighborhoods. Downtown streets carry light traffic following the afternoon peak, whereas suburban and residential arterials have higher traffic loads at this time. Ideally then, one would like to classify streets in accordance with a workable identification scheme, applying an appropriate distribution for each class.

Classification was more easily postulated as theory than applied in practice. Various street classifications were examined

Figure 2.1 Spatial Distribution of Freeway Traffic (thousand vehicle miles per day) in Los Angeles in 1969

Source: Appendix A of Roth et al. (1971)

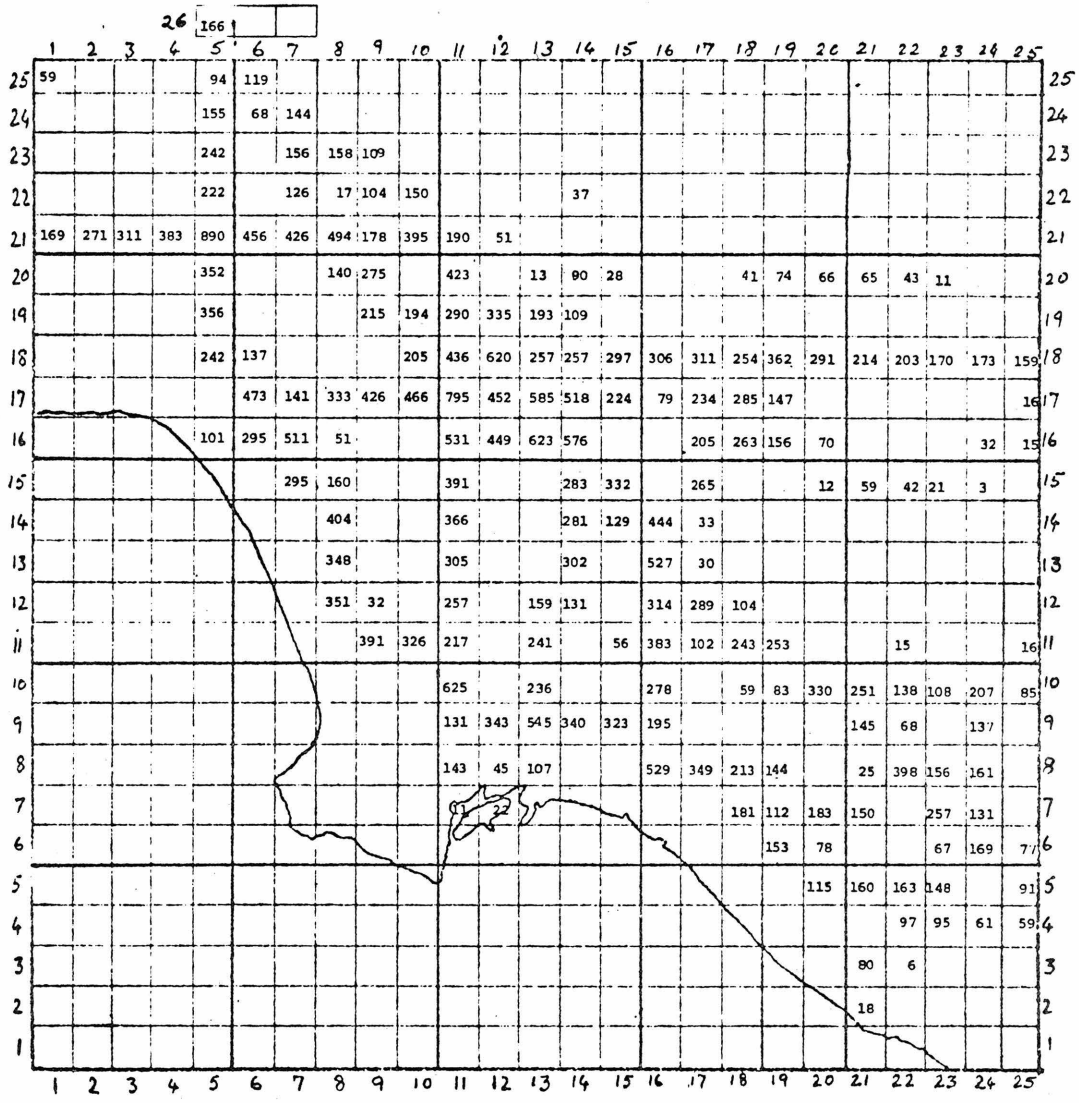

Figure 2.2 Spatial Distribution of Non-Freeway Traffic (thousand vehicle miles per day) in Los Angeles in 1969

Source: Appendix A of Roth et al. (1971)

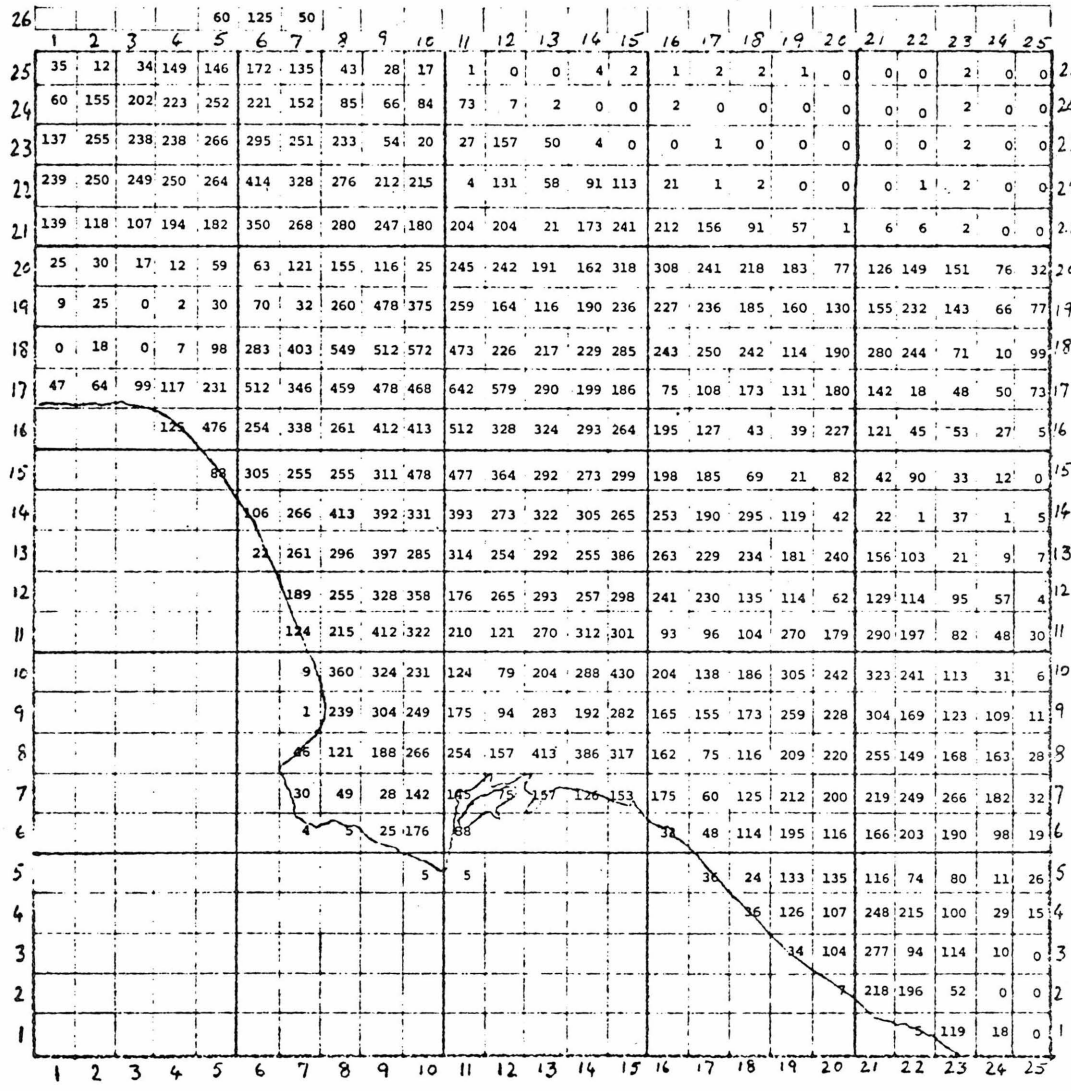

according to geographical area, type of street (business, residential, warehouse, etc.), and distance from major working centers, all with a notable lack of success. The first and third classification schemes were probably unsuccessful because of the large number of employment centers in Los Angeles. Most large cities experience morning flows into vs. out of town (and afternoon flows out vs. into town) in ratios of between 2 and 3 to 1. In Los Angeles the ratio is more nearly 1 to 1. The second scheme suggested proved most difficult to implement, as the effort of classification is so large.

Prior to examining classification schemes, however, a test was made of the hypothesis that the traffic counts on 25 randomly selected streets (stratified with respect to the magnitude of daily traffic flow) represent draws from a common population--the "grand" distribution.* As might be inferred from the need to examine classification schemes, the variability among the distributions of traffic on the various streets was sufficiently great that, on statistical grounds, traffic flows could not be represented by a "grand" distribution. However, it was soon realized that the 2 mi. x 2 mi. grid squares, the smallest spatial unit under consideration, commonly contained streets of many classifications. Thus, an attempt was made to develop a "grand" distribution which, if not statistically justified from street to street, was applicable to groupings of streets defined by the grid system.

---

* Data were taken from the 24-hour traffic count sheets of the City of Los Angeles Department of Traffic. Counts were summarized as number of vehicles passing over a pneumatic tube for each 15-minute interval throughout the day. For the analysis performed, these statistics were lumped into hourly intervals.

In order to develop this grand distribution, an hourly distribution of vehicle counts (i.e., the fraction of daily traffic assignable to each of 24 hourly periods) was derived based on an average of 52 randomly selected city streets (again, the sample being stratified according to the magnitude of daily traffic flow), the counts on individual streets being weighted in proportion to the magnitude of traffic flow on the street. The resulting distribution was then multiplied by total vehicle mileage per day for a particular grid square. These calculated hourly vehicle mileages were then compared with hourly vehicle mileages for the same grid square, determined using actual hourly traffic counts. The calculated discrepancies in vehicle mileage for each time period for the prototype grid square are given in Table 2.1.

Table 2.1
Calculated Discrepancies in Vehicle Mileage for a Prototype Grid Square (in the Wilshire/LaBrea area) Using the Grand Temporal Distribution

Time Period*	Discrepancy	Approximate Percentage of Daily Traffic Flow
6-7 a.m.**	-10.5%	3
7-9 a.m.	0.3	13
9-11 a.m.	- 7.0	10
11 a.m. -4 p.m.	4.0	30
4-6 p.m.	- 6.0	16
6-8 p.m.	- 3.1	11

* Local time. PDT when daylight savings time is in force, PST at other times.

** Hourly traffic counts remain approximately constant within the time intervals listed.

(Note: Traffic flows for the 6-7 a.m. period are highly variable. While the 10.5% discrepancy is somewhat large, its net effect will be small due to the low traffic flow characteristic of that time of the day.)

The temporal distribution for freeways, not considered as a part of the analysis just described, was more easily treated. 15 minute count data were acquired for a 24-hour period at 30 locations scattered throughout the Basin. As counts were available for 7 to 14 day periods, an average figure was computed for the Monday to Thursday period. These averages exhibited only minor variations when compared to an overall computed average temporal distribution. Thus, this overall distribution was taken as representative of temporal variations in traffic flow on the freeways. The temporal distributions for both freeways and non-freeways are shown in Table 2.2.

Finally, the temporal distributions for traffic were shifted one hour later in time for three grid squares in the downtown Los Angeles area [those having the following column and row numbers: (12, 17), (11, 17), and (12, 16) (see Figure 1.1)]. For example, the fraction of daily surface traffic assignable to the period 6 a.m. to 7 a.m. throughout the airshed is applied to the period 7 a.m. to 8 a.m. for these three grid squares. This shift provides a simple means to account for the fact that these squares contain few residences and thus, in the net, receive vehicles rather than discharge them during the morning hours.

2.2.4.3 Exhaust Emissions

As noted, the Federal Driving Cycle (FDC) was adopted as the basis for computing exhaust emission factors. The emission rates used have been estimated by the Environmental Protection Agency (Sigworth, 1971). (Thus, it was not necessary in this instance

Table 2.2

Temporal Distribution of Traffic in the Los Angeles Airshed

Hourly Period* (local time)	Fraction of Daily Traffic
Freeways	
12-5 a.m.	.0388
5-6	.0178
6-7	.0591
7-8	.0768
8-9	.0648
9-10	.0536
10 a.m.-2 p.m.	.1977
2-3	.0569
3-6	.2238
6-7	.0598
7-12	.1511
Surface Streets	
12-6 a.m.	.0407
6-7	.0293
7-9	.1302
9-11	.1004
11 a.m.-4 p.m.	.3044
4-6	.1639
6-8	.1081
8-12	.1231

* Distributions are approximately uniform for the daylight time periods indicated. However, traffic is not uniformly distributed within the periods 7 p.m. to 5 a.m. for freeways and 8 p.m. to 5 a.m. for surface streets. These groupings are included only for completeness.

to carry out the calculations required for evaluating equation (2.9). They had already been done.) In the vehicle emissions model outlined above, freeways and non-freeways (surface streets, including major and minor arterials and residential streets) are treated separately. "Hot-start" emission factors are used to calculate freeway

emission rates; a weighted average of hot and cold-start factors form the basis for calculating surface street emission rates. The cold-start emission factors are those reported by Sigworth (1971). Hot-running emission factors (with the exception of NO_x*) were estimated through the following equation:

$$Q_\ell^h = Q_\ell^c \frac{\gamma P_\ell^h + (1-\gamma)T_\ell}{\gamma P_\ell^c + (1-\gamma)T_\ell} \qquad \ell = CO,\ HC \qquad (2.10)$$

where

γ = fraction of automobile registration (assumed equal to vehicle mileage attributable to automobile traffic) = 0.87

P_ℓ^h, P_ℓ^c = hot and cold-start emission rates for automobiles, as reported by Martinez et al. (1971, p. 9, Table 5). (While the cold-start rates given in this report are less recent, and probably less representative, estimates than those of Sigworth (1971), they do permit estimation of the ratio of hot-running to cold-start emission rates. Note that these figures were used to estimate only this ratio.)

T_ℓ = emission rates from trucks and buses (grams/mile),

T_{CO} = 150 grams/mile

T_{HC} = 11 grams/mile

---

* At the time when these emission factors were computed, some available data indicated that NO_x emission rates increase as the car warms up; other data indicated that they decrease. Because of the uncertainty in the data, NO_x emissions were assumed to be invariant with engine operating temperature.

$$T_{NO_x} = 7 \text{ grams/mile (as } NO_2)$$

based on the data of Springer (1969).

and the values of P_ℓ^h, P_ℓ^c and T_ℓ for CO and HC are given in Table 2.3.

Table 2.3

Hot and Cold-Start Emission Rates (Martinez et al., 1971)

	CO	HC
P_ℓ^h	82.49 gm/mi	16.81 gm/mi
P_ℓ^c	116.60	18.25
T_ℓ	150	11

Estimated average hot and cold-start emission factors for 1969 are given in Table 2.4.

Table 2.4

Exhaust Emission Rates for the 1969 Vehicle Population in Los Angeles Based on the Federal Driving Cycle (Grams/Mile)

Species	Q_ℓ^h	Q_ℓ^c
CO	68.6	91.0
HC (exhaust and blow-by only)[a]	10.8	11.7
NO_x, as NO_2[b, c]	4.16	4.16
as NO[c]	2.71	2.71

[a] For hydrocarbons (Papa, 1967; Kircher, 1972)
molecular weight (reactive species) 47.8
molecular weight (unreactive species) 21.1
fraction reactive (mol %) 67.4
fraction unreactive (mol %) 32.6
where it is assumed that methane, ethane, propane, benzene, and acetylene are unreactive. All other hydrocarbons are assumed to be reactive.

[b] The values presented are based on those measured in vehicle surveillance studies in Los Angeles in December 1971, for model years 1957 through 1971. Using these data, the average NO_x emission rate, as of September 1969, was calculated to be 4.16 grams/mile (as NO_2). The fact that these measurements were made in 1971, and not in 1969, biases the result. However, no attempt was made to account for this.

[c] The two values, 4.16 and 2.71, represent grams/mile emissions on the basis of the exhaust NO_x and NO, respectively. As shall be seen later, the actual split for automobile exhaust is taken to be 99% NO and 1% NO_2. This split represents the actual input to the model.

Both Q_ℓ^h and Q_ℓ^c are based on the FDC, which is defined to simulate a trip having an average speed of about 19.6 miles/hour. It is assumed that vehicles on surface streets travel at approximately this average speed throughout the day (and throughout the airshed).

However, freeway emissions are treated as a function of average speed, which varies both spatially and temporally. Attention is now turned to the treatment of freeway and non-freeway automotive emissions.

A. Freeway Emissions - the emissions rate/average speed correlation

In the original formulation of the vehicle emissions model (Appendix A of Roth et al., 1971), it is assumed that emission rates from freeways may be treated as constants, independent of driving conditions and route speeds. A major weakness of this formulation is that it fails to account for both the high emission rates that occur during the rush hour congestion and the reduced emission rates associated with higher average speeds. Rose et al. (1965) have shown that, while variations in emission rates are attributable to factors such as route conditions and the percentage of time in accelerate, decelerate, idle, and cruise modes (these factors being reflected in traffic volume, average route speed, and the nature of the local terrain), average emission rates for Los Angeles correlate well with average route speed alone. Furthermore, this single index is sufficient to provide estimates of emission rates. Their correlations are based on a linear relationship between the logarithm of average emission rates and the logarithm of average route speed. These findings form the basis for the correlations derived in this study.

The following information was required to develop the emissions rate/average speed correlation presented in equation (2.3):

1. The slopes of emissions rate/average speed curves for CO, hydrocarbons, and nitrogen oxides. However, as these values are estimated from tests of vehicles of 1955 to 1963 manufacture, a_ℓ and b_ℓ have been modified in a manner to be described.
2. Average emission rates for hot-running conditions at a known average speed. These rates, given in Table 2.4, were estimated as described in the preceding section.
3. Average freeway speed as a function of time for both directions on all freeways in the Los Angeles Basin. These data were obtained from the State Division of Highways (Arcineaux, 1971).
4. Average vehicle flow as a function of time for both directions on all freeways. Individual flows were estimated from the data base discussed in Sections 2.2.4.1 and 2.2.4.2. Values of x (equal to n_s/n_f) were computed using these data.

The data for items 1 and 2 were needed to estimate the emission rate as a function of average speed, the data under 3 and 4, average speed as a function of location and time. Values of $\overline{v}_s$, $\overline{v}_f$, and x are given in Appendix C.

Unfortunately, emissions/average speed data were very scarce at the time when this inventory was prepared. Thus, while Rose's data were somewhat out of date (less than 50% of the vehicles on the road in September 1969 were represented by this test group), they represented the best available data that pertained to the period

of interest. However, when correlations based on these data were used to estimate average emission rates at high speeds under hot-running conditions, the estimates were judged to be rather low. For example, while the values of 91 and 68.6 grams/mile represent FDC-based average CO emission rates under cold and hot-running conditions, respectively, an average rate of only 26.5 grams/mile at 65 mph is predicted using a correlation based on Rose's slope (b_{CO} = -.89). Thus, it was decided to modify Rose's values for use in the present work.

The modifications cited are based on the premise that, since the California and the Federal Driving Cycles have been the standard for testing new emissions control systems, automobile manufacturers design their systems with the expectation that they will be tested at low average speeds (22.2 mph and 19.6 mph, respectively for the two test cycles). Thus, contrasting 1963 (the last year of manufacture for Rose's test vehicles, a time during which vehicles were uncontrolled) with the present, it may be expected that average emission rates at low average speeds have decreased more rapidly, from model year to model year, than average emission rates at high average speeds. The net effect would be that the b_ℓ values that were estimated for CO and hydrocarbons at the time of Rose's study would increase with each engine or exhaust system modification, becoming less negative with each succeeding year.

Unfortunately, no data were available on which to base an estimate of a revised slope. In the absence of appropriate information, the slopes b_ℓ reported earlier were estimated using two points, the

hot-running emission rates at 19.6 mph, and the rates at 60 mph, the latter computed from

$$Q_\ell^h(60) + 1/3\left[Q_\ell^h(19.6) - Q_\ell^h(60)\right]$$

where $Q_\ell^h(19.6)$ are FDC values, modified for hot-running conditions, and $Q_\ell^h(60)$ are the rates computed using Rose's correlation equation and his estimates of the slopes. The factor of 1/3 is an estimate of the relative decrease in emission rates at high average speeds. It must be made clear that this factor might be anywhere between 0.1 and 0.5; the value of 1/3 is merely a guess and is certainly subject to revision as data become available.

B. Non-freeway emissions

Average emission rates for vehicles operating on surface streets are computed from equations (2.6) and (2.7). Values of y(t) appropriate for Los Angeles are presented in Table 2.5.

Table 2.5

Fraction of Cars Started During Given Time Periods that are Cold-Started

Time period	y
0:00 - 6:00	0.90
6:00 - 9:00	0.85
9:00 - 11:30	0.25
11:30 - 13:30	0.30
13:30 - 16:30	0.20
16:30 - 18:30	0.50
18:30 - 21:00	0.15
21:00 - 24:00	0.20

A factor $\beta_{\ell}(t)$ was introduced in equation (2.3) to account for the effect on average emission rates of sudden variations in the number of vehicle starts. The need for this modification is best illustrated through a simple example.

Assume that all vehicles on the road are operated as prescribed by the FDC, namely that they are run for 23 minutes, and that steady-state engine temperature is attained about 8-1/2 minutes after start-up. Emissions from an individual vehicle, as a function of time, might thus be described as shown in Figure 2.3. If it is further assumed that 1) trip starts are distributed uniformly in time, and 2) all vehicles on the road were "cold" when started, then, at any time, about 100 (8.5/23)%, or 37%, of the vehicles on the road have not yet achieved steady-state operating temperature. Under these conditions the average emissions for all vehicles is given by the horizontal dotted line in Figure 2.3.

Suppose now that 10,000 vehicles are currently in operation, under the circumstances cited above, in some region of interest. Suppose further that an additional 5000 vehicles are started in the next three minutes (all cold-started). The immediate effect of adding these additional vehicles to the pool of autos in use, each emitting at relatively high rates owing to their "cold" operation, would be to temporarily increase the average emissions of all 15,000 vehicles in operation to a value in excess of that given by the dotted line.

Suppose, however, that vehicle starts are maintained at the increased rate of 5000 starts every three minutes for the next several hours. After about 20 minutes (i.e., 23 minutes less 3 minutes), it

would be found that trips are terminated at the same rate that they are initiated, and that, as before, 37% of vehicles on the road are still in the "warm-up" period. The average emissions rate for all vehicles is once again given by the dotted line despite the fact that the total number of cars in operation has increased dramatically.

Thus, the effect of suddenly increasing the rate of vehicle starts, and maintaining that rate at a constant level thereafter, is to temporarily increase the fraction of cars in warm-up to a value greater than 0.37. Since vehicles in warm-up emit carbon monoxide and hydrocarbons at a higher rate than do hot-running vehicles, the average emission rate of all cars in operation increases. After sufficient time passes to equalize the rate of start-ups and trip terminations (23 minutes), the original value of the average emission rate again applies.

The phenomenon that this example illustrates, the inducement of variations in the average emission rate due to variations in the rate of vehicle start-ups, is best exemplified during the morning rush hours. The rapidly increasing rate of vehicle starts in the early morning has the effect of increasing average emission rates until some time when the rate of starts begins to taper off. Soon, more trips will be terminated than initiated, and the average emission rate will drop, not only returning to its original level, but falling below that given by the dotted line in Figure 2.3. Eventually, however, an approximately steady rate of vehicle starts will be attained (immediately following the "rush" period), and the average "dotted line" rate will again apply.

The effects of variations in the rate of vehicle starts is accounted for through the correction function, $\beta_{\ell}(t)$, that appears in equation (2.6). The curves shown in Figure 2.4 describe the variation in $\beta_{\ell}(t)$ with time for carbon monoxide and hydrocarbons. The derivation of these functions is discussed in Appendix D. Three points may be noted about these functions. First, since the hot and cold-running emission rates for NO_x are assumed to be equal, $\beta_{NO}(t) = 1$ for all t. Second, even though the rate of trip starts varies throughout the day (as may be seen in Figure 2.5), the effect of these variations is considered only for the period 6 a.m. to 9:23 a.m. The effect on $\beta_{\ell}(t)$ of the "midday bump" in Figure 2.5 is not included, as the majority of vehicles operating during that period are hot-started* and the bump is small compared with the rush-hour bumps. In addition, the effect of the "evening bump" is also not included since validation of the model is not planned for that time period. Third, it should be evident that, in order to properly evaluate $\beta_{\ell}(t)$, large quantities of data are needed. Pertinent data include those involving driving patterns in the Los Angeles area, trip length, average speed, time between trips, etc. Also needed are emissions data as functions of time for both cold and hot-starts. As such data are, for the most part, unavailable, the model is based on what data could be obtained. In the absence of full information, reasonable simplifying assumptions were made in order to derive $\beta_{\ell}(t)$.

---

* Note that if all vehicles are hot-running and there is a sudden increase in vehicle starts (all "hot"), then there will be no effect on the average emission rate. For the effect to be noticeable, a reasonable percentage of vehicle starts must be "cold."

Figure 2.3 Estimated Variation in Carbon Monoxide Exhaust Emission Rate as a Function of Time.
W = Assumed warmup time (8.5 minutes)
T = Length of Federal Driving Cycle (23 minutes)
(The dashed line is the average cold-start emissions rate. The solid line is an estimate of the actual emissions over the 23 minute test assuming an 8.5 minute warmup.)

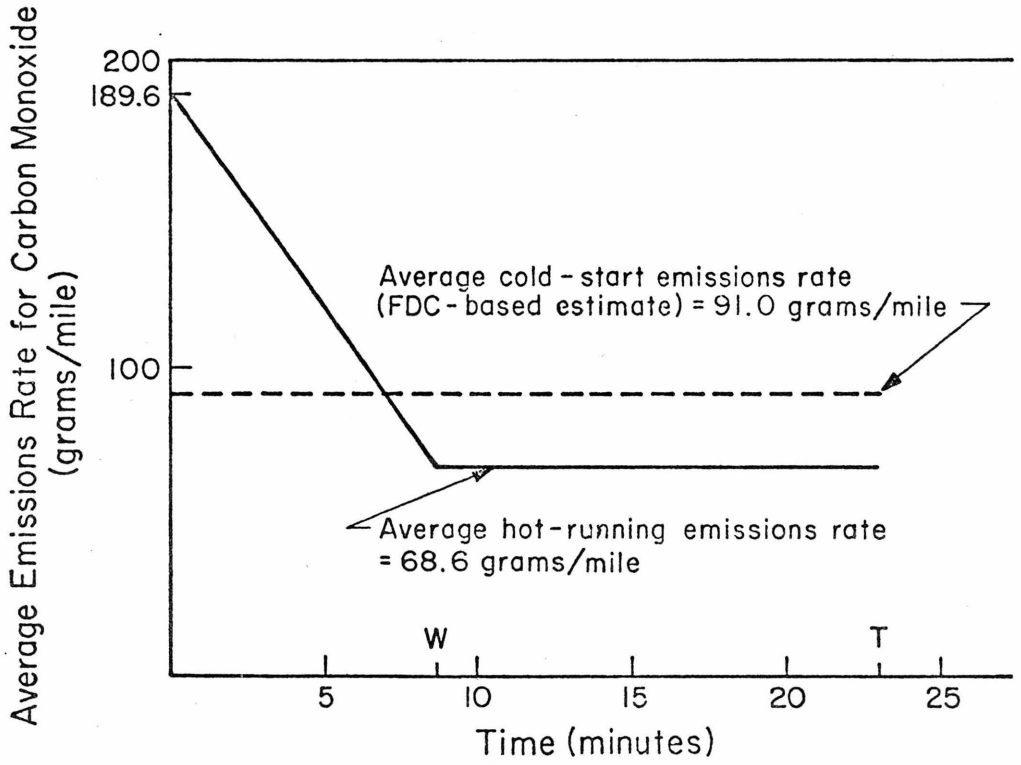

Figure 2.4 Correction Factor $\beta_{\ell}(t)$ for Carbon Monoxide and Hydrocarbon Motor Vehicle Emissions

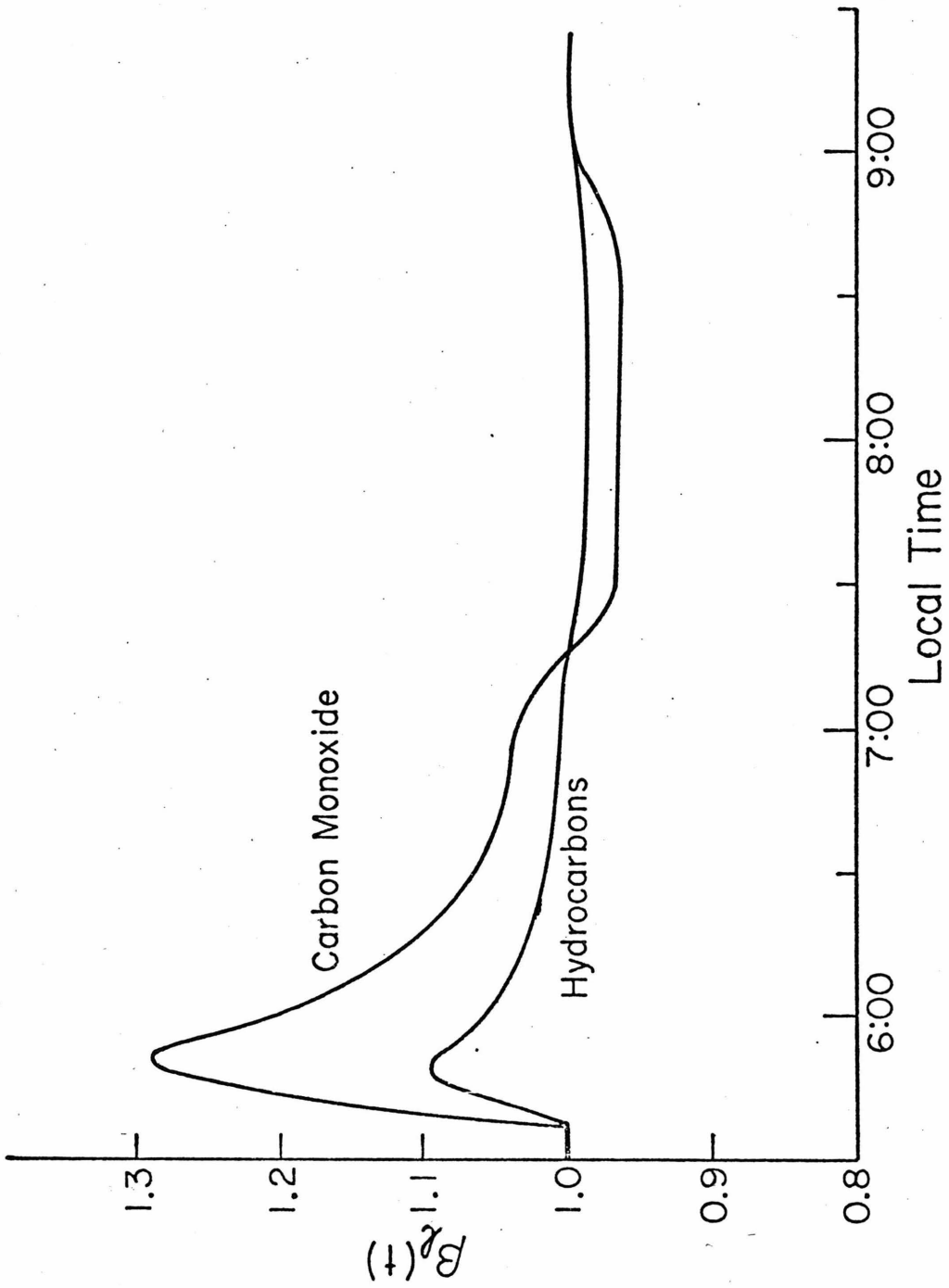

Figure 2.5 Distribution of Weekday Trip Start Times in Los Angeles (Kearin et al., 1971)

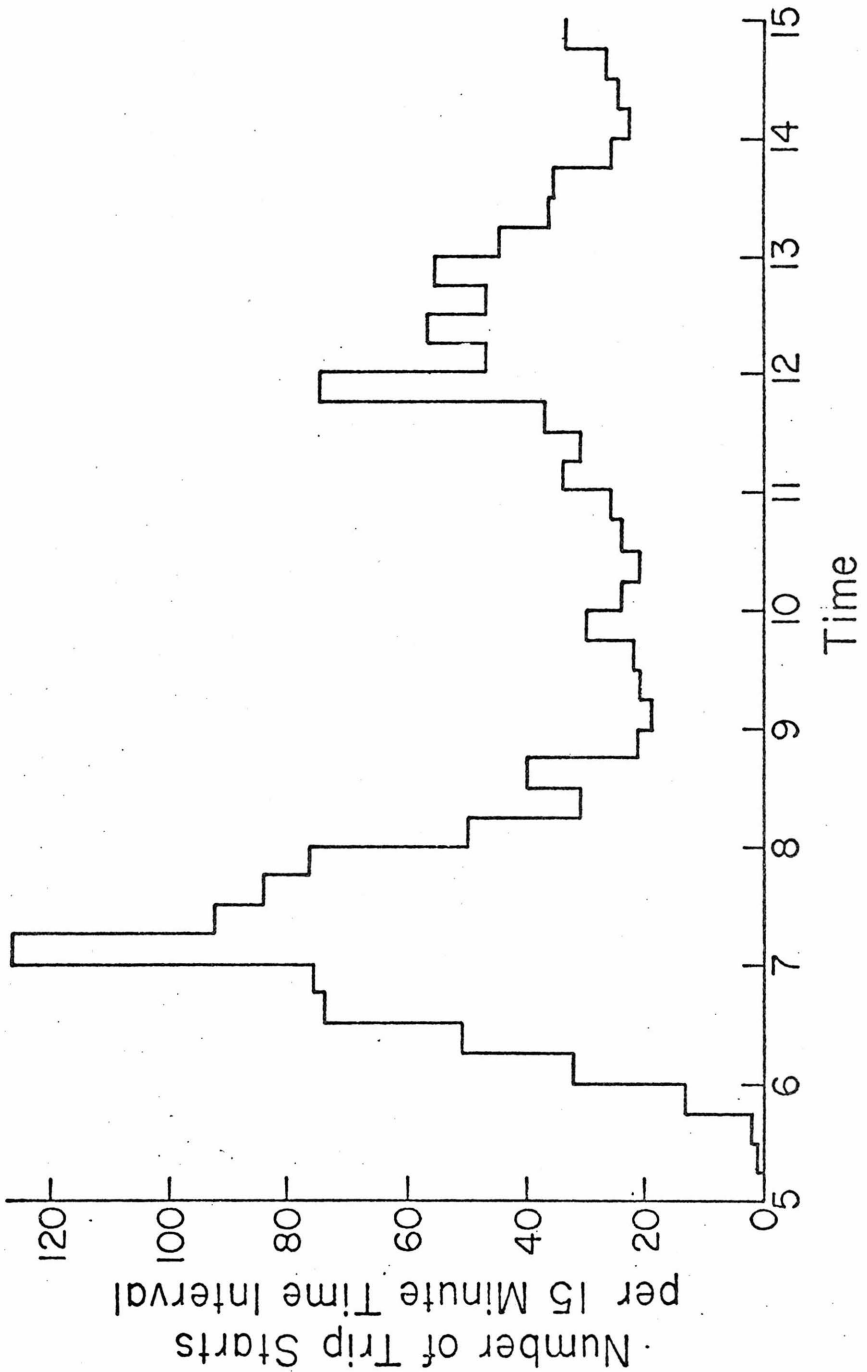

C. Summary

A summary of the assumptions made in the treatment of freeway and non-freeway automotive emissions is given in Table 2.6.

Table 2.6

Summary of Assumptions Relating to Automotive Emissions

	Freeways	Non-freeways
Average emission factors*	Hot-running factors	Weighted average of cold-start and hot-running factors
Correction for nonuniform distribution included	No	Yes
Emissions/speed modification included	Yes	No

* Average emission rate based on the FDC.

2.2.4.4 Crankcase Emissions

Estimates of the blow-by emissions rate have been made by EPA (Sigworth, 1971). Their estimate for the blow-by rate from an uncontrolled automobile (pre-1961 domestic or pre-1965 import) is 4.1 grams/mile. The PCV devices on 1961, 1962, and 1963 domestic vehicles are assumed to be about 80% effective in controlling blow-by; emissions from these vehicles are thus about 0.8 grams/mile. The PCV devices on 1964 and later cars are assumed to be 100% effective, and hence there are no blow-by emissions from these vehicles.

Unfortunately, there appears to be no way of finding the number of 1955-1962 domestic autos which have been resold between 1964 and 1969, thus necessitating the installation of a PCV valve.

The number of pre-1961 domestic autos fitted with PCV valves is estimated to be 60% of the total. Using the vehicle age distribution, pre-1961, 1961 to 1963 domestic, and pre-1965 imported automobiles are estimated to comprise approximately 19%, 20%, and 7%, respectively, of the total automobile registration. Hence, blow-by emissions from the average vehicle in the Los Angeles Basin (automobiles comprise 87% of all vehicles) in 1969 were:

$$0.87\ (0.4 \times 0.19 \times 4.1 + 0.07 \times 4.1 + 0.20 \times 0.8) = 0.7 \text{ grams/mile}$$

2.2.4.5 Evaporative Emissions

Evaporative losses from autos are very difficult to measure and are subject to wide variations in magnitude resulting from different auto operating conditions, weather conditions, and automobile. design. The subject is discussed by Hurn (1968, page 62). Using Hurn's figures, the total daily evaporative loss per vehicle is about 72 grams/day.

In order to distribute the evaporative emissions, it was assumed that these losses occur mainly during the hours 7 a.m. - 7 p.m. PDT and that they are evenly distributed over this period. Hence, the evaporative emissions rate from the 4,135,000 automobiles registered in Los Angeles and Orange Counties in 1969 was 4,135,000 x 72 (grams/vehicle/day) or 4,135,000 x 6 (grams/hour).

The evaporative emissions in each square are assumed to be proportional to the number of non-freeway vehicles miles in that square. Non-freeway vehicle mileage was chosen as being more representative of driving conditions leading to high evaporative

emissions than any other available parameter. In particular, the spatial distribution of non-freeway mileage should correspond reasonably well with the spatial distributions of both parked cars and cars in stop-and-go driving conditions. The total non-freeway vehicle mileage in the Los Angeles airshed in 1969 was 72, 367, 000 miles. Thus the evaporative emissions for grid cell (i, j), in kg/hr, are

$$m_{ij} \times \frac{4,135,000}{72,367} \times 6 \times 10^{-3} = 0.343\ m_{ij}$$

where m_{ij} = thousands of non-freeway vehicle miles per day driven in grid cell (i, j), as given in Figure 2.2.

2.3 Aircraft Emissions

Aircraft operating from the fifteen airports in the Los Angeles Basin contribute approximately 0.1% of nitrogen oxides, 0.6% of organic gases and 1% of carbon monoxide from all sources in the Basin (See Table 2.15). Whereas the contribution of aircraft emissions to the total contaminant load in the Basin is small, the percentages of pollutants in the local environs that are attributable to aircraft operations is quite significant. Furthermore, several of the contaminant monitoring stations are located in the vicinity of airports. Thus, it was necessary to devise a special model to account properly for the local impact of aircraft emissions. In addition, there is currently some interest in the modeling of pollutant behavior in the vicinity of airports. The model presented in this section should be helpful to those undertaking such a task.

The aircraft emissions model consists of two major components: a ground operations and airborne operations model. Emissions from ground operations are treated as surface fluxes, while emissions from airborne operations are treated as elevated volume sources. The first part of this section is devoted to a description of the emissions model, and the second part consists primarily of relevant data.

Aircraft operations are classified as ground operations and airborne operations. Ground operations consist of three distinct modes: 1) taxi mode (taxi between runway and satellite and idle at satellite), 2) landing mode, and 3) takeoff mode. Airborne operations are comprised of two modes: 1) approach mode (descent from inversion height). A flight, whether for fixed wing aircraft or rotocraft, is defined as consisting of the five modes cited.

In the formulation of an aircraft emissions model, the following assumptions are made with regard to the treatment of aircraft operations:

1. For every aircraft arrival, there is one departure. Furthermore, arrival and departure rates are equal within a given time period. (Pertinent time periods are shown in Table 2.11.)
2. Aircraft follow straight line flight paths from inversion height to touchdown and from lift-off to inversion height.*

* Since the modeling region is bounded aloft by the base of the elevated inversion (or some assigned mixing depth), only that portion of the flight path under the inversion need be considered in the present formulation of the airshed model.

(Many light aircraft never reach the inversion height and, in fact, do not follow straight line paths above 250 meters. However, information concerning these departures from linear flight paths is not available.)

3. The angles of ascent and descent of all aircraft at a particular airport are assumed to be fixed and equal to those angles associated with the class of craft (e.g., medium-range jet transport, business jet, etc.) having the highest fraction of total operations at that facility. [This assumption is reasonable for twelve of the fifteen Los Angeles Basin airports, since at these facilities the fraction of total operations assignable to a particular class of aircraft exceeds 0.81. (See Table 2.10.) The exceptions are Los Angeles International LAX), Hollywood/Burbank (LK), and Culver City (CC) Airports. At LAX Class 1 and Class 2 aircraft, transports having similar flight paths comprise 63% of total daily flights and contribute by far the greatest fraction of contaminants. Class 6 aircraft represent 68% of air traffic at LK, while at CC total daily traffic is very light.]
4. Flight paths originate and terminate at the most frequently used runway at each airport.
5. The proportion of aircraft of a given class that arrive and depart from each airport is invariant with time. (Aircraft classes are defined in Section 2.3.1.)

6. The temporal distribution of airborne operations at a Basin airport, if not known, may be represented by the temporal distribution measured at an airport at which the mix of aircraft, by class, most closely resembles the mix of aircraft at the airport in question. [Temporal distributions are available for the following airports: Los Angeles International (Class 1 aircraft predominate), Van Nuys (Class 6), and Hollywood/Burbank (Class 6). Of the remaining twelve airports, ten are predominantly Class 6 (the exceptions being Los Alamitos and Culver City), and the Van Nuys distribution is assumed to be representative of flight operations at these airports.]

It should be noted that emissions along flight paths contained within, but originating from airports lying just outside of, the airshed boundary are ignored (e.g., Ontario International, El Toro Marine Base, etc.)

Turning now to aircraft emissions, the model is based on the following assumptions:

1. For each class of aircraft, pollutants are emitted at a uniform rate during each of the five operating modes. Thus, for airborne operations, the amount of contaminants injected into a cell is proportional to the length of the flight path occupying that cell.
2. Emissions from aircraft can be treated as continuous releases, emitted at a uniform rate and averaged over a one-hour time period, one hour being the resolution of

the temporal distribution of airport traffic.

2.3.1 Ground Operations Model

The amount of contaminant species ℓ emitted into a surface grid cell during ground operations is equal to the summed products of average emissions rate and residence times in each of three modes--taxi, landing, and take-off. The rate of emissions, in kg/min, from grid square (i, j) due to ground operations for the hourly period p is given by:

$$B^{g}_{\ell p} = \frac{1}{60}\left\{d^{a}_{p}\,\theta_{ij}\sum_{u=1}^{7}\bar{n}_{u}\bar{N}_{u}\sum_{v=1}^{3}f^{\ell}_{vu}\,C_{vu}\right\} \qquad (2.11)$$

where

v is an index denoting the ground operation modes

1 taxi

2 landing

3 take-off

u is an index denoting aircraft class

1 long-range jet transport

2 medium-range jet transport

3 business jet

4 turboprop transport

5 piston engine transport

6 piston engine utility

7 turbine engine helicopter

and

d^{a}_{p} = fraction of total daily flights assigned to hourly period p

θ_{ij} = fraction of airport area assignable to grid square (i,j)

$\bar{n}_u$ = number of flights per day of class u aircraft

$\bar{N}_u$ = average number of engines per class u aircraft

f_{vu}^{ℓ} = kilograms of pollutant ℓ emitted per kilogram of fuel consumed by class u aircraft operating in mode v

C_{vu} = kilograms of fuel consumed per engine for class u aircraft operating im mode v.

2.3.2 Flight Operations Model

The mass of species ℓ emitted into grid cell (i, j, k) during the approach mode is assumed to be proportional to the length of the flight path occupying that cell. The corresponding rate of emissions (kg/min) is given by:

$$B_{\ell p}^{f} = \frac{1}{60}\left\{d_p^a L_{ijk} \sum_{u=1}^{7} \bar{n}_u \bar{N}_u f_u^{\ell} C_u \frac{t_u}{t'_u}\right\} \qquad (2.12)$$

where

t_u = time spent in descent from inversion height to touchdown by class u aircraft

t'_u = time spent in descent from 915 meters* above ground elevation to touchdown by class u aircraft (see Table 2.7)

f_u^{ℓ} = kilograms of pollutant ℓ emitted by aircraft of class u per kilogram of fuel consumed during descent (see Table 2.8)

---

* An elevation of 915 meters is used to conform to the data reported by Northern Research (1968) on aircraft emission characteristics during approach and climb-out.

C_u = kilograms of fuel consumed per engine on class u aircraft during descent from 915 meters above ground elevation (see Table 2.9).

L_{ijk} = fraction of the length of the flight path assignable to cell (i, j, k).

The mass of species ℓ emitted into cell (i, j, k) during climb-out is also given by equation (2.12), where t_u and f_u^{ℓ} now apply to an aircraft ascending from lift-off to inversion height, and t_u and C_u to an aircraft ascending to 915 meters above ground elevation.

In general, it can be shown that, for an airshed model of the type described in this report, ground operations make a significant contribution to the contaminant concentrations in the immediate vicinity of the source, whereas flight operations make a negligible contribution. In application to Los Angeles, for example, only the ground operations model was included. There may be instances, however, in which airborne operations should be considered; therefore, this portion of the model is also included in the preceding discussion.

2.3.3 Emissions and Airport Data

Required data may be classified as information pertaining to 1) aircraft location, and 2) aircraft emissions. Included in the former category are airport location and, for each airport, flight paths and runway and taxi-way coordinates. Major aircraft emission studies have been reported by Lemke et al. (1965), Hochheiser and Lozano (1968), Lozano et al. (1968), Northern Research and Engineering Corporation (1968), Bastress and Fletcher (1969), and

Scott Research Laboratories (1970). The Northern Research and Engineering (NREC) study is the most recent and comprehensive of the reports cited. The emissions statistics of NREC as well as those of Scott (1970), including pertinent emissions data and aircraft performance characteristics for flight operations, take-off, and landing provide the basic inputs to the aircraft emissions model. These characteristics include, for each class of craft, the average distance over which the operation is performed, the time required, and, for approach and climb-out, the angles of descent and ascent. These data are summarized in Tables 2.7-2.9.

The average number of flight operations occurring per day at each of the 15 Los Angeles airports is tabulated, by class of aircraft, in Table 2.10. The distribution of daily operations by hour, for the three major airports, is given in Table 2.11. The primary flight paths for each airport, are given in Appendix B of Roth et al. (1971). Finally, it is assumed, for lack of better information, that aircraft exhaust has approximately the same hydrocarbon composition as automobile exhaust, and thus the same molecular weights for the reactive and unreactive groupings.

Table 2.7

Aircraft Performance Characteristics During Approach and Climb-out Operations (Northern Research, 1968)

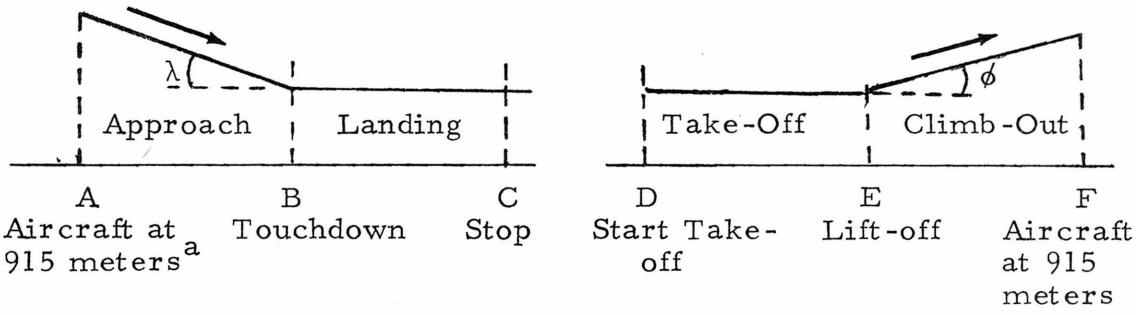

T_{AB} Time to travel A to B T_{EF} Time to travel E to F

λ Angle of Descent ϕ Angle of Ascent

Aircraft Class	T_{AB} (Minutes)	λ (Degrees)	T_{EF} (Minutes)	ϕ (Degrees)
1	3.6	3.46	2.2	4.01
2	3.0	3.61	1.9	5.00
3	1.6	5.41	0.5	8.08
4	4.5	3.16	3.6	3.07
5	4.6	3.61	5.0	2.20
6	3.8	6.48	2.5	5.15
7	6.5	2.17	6.5	2.17

[a] above ground elevation

Table 2.8

Fuel Consumption During Landing and Take-Off Operations for Representative Engines (Northern Research, 1968)

Aircraft Class	Representative Engine	Fuel Consumed, C_{vu} and C_u (kilograms per engine)						
		Taxi	Idle	Landing Run	Take-Off Run	Approach[a]	Climb-out	Total LTO-Cycle
1	Pratt & Whitney JT3D	98.7	8.2	16.5	72.0	135.4	126.7	457.5
2	Pratt & Whitney JT8D	83.5	6.9	7.3	47.0	64.2	89.3	298.2
3	Pratt & Whitney JT12	49.0	4.1	5.9	10.1	21.4	10.1	100.7
4	Allison 501-D13	53.9	3.9	2.2	9.3	30.4	44.4	144.1
5	Pratt & Whitney R-2800	32.7	1.2	2.4	9.5	16.7	63.6	126.1
6	Continental 10-520-A	2.5	0.2	0.0	0.4	1.2	2.1	6.5
7	General Electric	16.8	1.4	0.0	0.0	27.0	35.0	80.1

[a] Between ground elevation and 915 meters.

Table 2.9

Emission Factors, f_{vu}^{ℓ} and f_{u}^{ℓ} (Northern Research, 1968)

Aircraft Class	Operating Mode	Emission factors, f_{vu}^{ℓ} and f_{u}^{ℓ} (kilograms/1000 kilograms of fuel) CO	Organics	NO_x (as NO_2)
u = 1	Idle & Taxi	174	75	2.0
	Approach	8.7	16	2.7
	LTC[a]	0.7	0.1	4.3
2	Idle & Taxi	50	9.6	2.0
	Approach	6.6	1.4	2.7
	LTC	1.2	0.6	4.3
3	Idle & Taxi	118	11.5	2.0
	Approach	11	0.6	2.7
	LTC	4	0.3	4.3
4	Idle & Taxi	24.8	8.1	3.7
	Approach	1.6	0	2.9
	LTC	2.3	3.2	3.1
5	Idle	896	32	7
	Taxi	910	43	2
	Approach	825	104	3
	LTC	1050	110	1
6	Idle	896	32	7
	Taxi	910	43	2
	Approach	825	104	3
	LTC	1050	110	1
7	Idle & Taxi	118	11.5	2.0
	Approach	11	0.6	2.7
	Climb-out	4	0.3	4.3

[a]Land, Take-Off, and Climb-Out

Table 2.10

Average Number of Daily Flights at Los Angeles Basin Airports

Airport	Aircraft Class 1	2	3	4	5	6	7
Brackett	0	0	6	0	0	288	10
Compton	0	0	0	0	0	191	0
Culver City	0	0	12	0	0	21	20
El Monte	0	0	0	0	0	700	0
Hawthorne	0	0	0	0	0	428	0
Hollywood/Burbank	0	47	19	4	25	225	10
Long Beach	0	0	2	0	67	591	25
Los Alamitos	0	0	50	0	50	0	0
Los Angeles Int'l.	264	249	9	57	21	159	58
Orange County	0	12	0	0	0	850	0
San Fernando	0	0	0	0	0	100	0
Santa Monica	0	0	0	0	0	525	25
Torrance	0	0	0	0	0	500	0
Van Nuys	0	0	0	0	14	720	125
Whiteman	0	0	0	0	0	200	0

Table 2.11

Temporal Distribution of Daily Flights at Los Angeles Basin Airports

Los Angeles Int'l.		Van Nuys		Hollywood/Burbank	
Time Period	Fraction of Daily Traffic	Time Period	Fraction of Daily Traffic	Time Period	Fraction of Daily Traffic
11 pm-1 am	.048	10 pm-8 am	.017	11 pm-1 am	.026
1-7	.051	8-9	.014	1-7	.021
7-8	.043	9-10	.056	7-9	.063
8 am-6 pm	.629	10- 12 noon	.156	9-12 noon	.193
6-8	.109	12-4	.511	12-1	.087
8-9	.048	4-5	.078	1-4	.164
9-11	.072	5-7	.103	4-8	.314
		7-8	.036	8-9	.062
		8-9	.021	9-11	.070
		9-10	.008		

2.4 Fixed Source Emissions

Whereas the emission rates from a motor vehicle population may be specified with reasonable precision - the primary difficulty being the determination of a representative driving cycle-emissions data for individual fixed sources are often poorly known. Information relating to the emissions of various pollutants as a function of the quantity of fuel burned in power plants or of the process throughout of a refinery or factory is often difficult to obtain. Thus, general models, such as those for motor vehicle emissions, are inappropriate for fixed sources; rather, all that is required is accurate information on mass emissions from each important fixed source in the area. Therefore, the fixed source emissions inventory discussed in this section is only applicable in in the Los Angeles airshed.

The eleven power plants situated in the Los Angeles airshed accounted for approximately 23% of the total daily NO_x emitted into the airshed in 1969. The fifteen oil refineries contributed 7% of the NO_x and 2% of the organic gas emissions (see Section 2.5). Although emissions from these large point sources can result in elevated ground concentrations in their immediate vicinity, the appropriate calculations have not been incorporated in the present grid model to account for this effect. However, because of the high emission rates from these sources and their special emission characteristics, it is unrealistic to treat them simply as area sources. This section is devoted to a discussion of the methods for incorporating the emissions into the overall grid model and a summary of pertinent data relating

to emissions from power plants, refineries, and other miscellaneous fixed sources.

2.4.1 Power Plant Emissions

High emission rates from point sources can result in substantial local ground-level concentrations. For power plants of the size found in the Los Angeles Basin and under typical meteorological conditions, maximum ground-level concentrations occur about two miles downwind of the plant. In treating power plants simply as area sources, it is not possible to predict these high concentrations and the locations of their occurrence using a grid of two-mile resolution. However, a separate sub-grid scale treatment of the power plant plume may be necessary in model validation when the air quality data with which predictions are to be compared are collected at monitoring stations in the immediate vicinity of a power plant. However, since none of the air quality measurements used for the model validation were likely to be influenced by the presence of power plants, plume dispersion calculations were not included in the model for the current validation studies.

While power plant emissions are not treated as plumes in the model, it is inappropriate simply to consider them as well mixed in the cell into which they are injected. Instead, these emissions are distributed as volume sources downwind of the plant, in cells where the plume width has grown to be of the order of the cell size. The allocation procedure is outlined in this section. In contrast, refinery emissions are treated as area sources; they are discussed in Section 2.4.2.

A Gaussian dispersion model was used to evaluate the possibility of treating point source emissions as volume sources centered in grid squares downwind of the square in which the point source is located. Pollutant concentrations are assumed to be normally distributed in the horizontal and vertical planes with dispersion parameters σ_y and σ_z, respectively. The half-width, b, of the plume is defined as 2.15 σ_y and is the horizontal distance from the plume centerline. The parameters σ_y and σ_z are functions both of downwind distance and of atmospheric stability. Correlations of σ_y and σ_z with these variables are given by Turner (1969).

Having defined the half-width, b, an estimate of the plume spread as function of downwind distance may be obtained using the plume dispersion model. The result of this calculation indicates that the plume width for Pasquill stability class B (the most prevalent during daytime hours) is about two miles at 3.75 miles downwind. It is therefore reasonable to treat emissions as volume sources in adjacent 2x2 mile grid squares downwind of the plant. Furthermore, typical values of σ_z suggest that at this distance the plume is well mixed up to the inversion base (assumed to be located at a maximum elevation of 800 meters). The volume sources are therefore distributed evenly in the column of cells up to the inversion base.

Emissions from a point source located in the ground cell (i, j, 1) may be distributed using the following simple algorithm. A straight line is drawn starting at the source location parallel to and in the direction of the wind in that square. This line extends to the farthest edge of that square either touching or immediately diagonal

to the square containing the source. The emissions from the point source are then apportioned as volume sources in the two or three columns of cells through which this line passes. The strength of the volume source in each cell is proportional to the length of the line contained in that cell, with the sum of the volume sources being equal to the strength of the point source.

While in many circumstances the model, as stated, is acceptable, it displays a major flaw under low wind conditions. At wind speeds of one to two mph, emissions are advected too far and too quickly by the model, thus providing estimates that are too low near the source and too high downwind. To alleviate this problem, the following constraints are added to the model formulation. The fraction, $r_i/(r_1 + r_2 + r_3)$ of power plant emissions is allocated to each of the three downwind grid squares in such a way that

$$r_1 + r_2 + r_3 \leq 3.5 \text{ miles}$$

and

$$r_1 + r_2 + r_3 \leq (60 \text{ min.}) \times (\text{wind speed in meters/min.})$$

are satisfied (see Figure 2.6a). If the situation depicted in Figure 2.6b occurs, the segment r_4 is ignored and apportionment is carried out in proportion to the lengths r_1, r_2, and r_3. Note that both inequalities above must apply.

Of the eleven power plants in the Los Angeles Basin, four are operated by the Southern California Edison Company, four by the Los Angeles Department of Water and Power, and one each by the cities of Pasadena, Burbank, and Glendale. Data relating to plant

location, electric capacity, and emissions are given in Table 2.12. Data on the diurnal variation of power plant emissions are available in Tables 2.13a and 2.13b.

2.4.2 Refinery Emissions

Pollutants emitted by oil refineries are released from an array of stacks which are usually distributed over a large area. For this reason, and because individual refinery emissions data are not available, refinery emissions are treated as surface sources in the cell into which they are injected. The daily emissions are distributed uniformly over 24 hours in proportion to the crude capacity of each refinery (see Table 2.14). The spatial distribution of refinery emissions is illustrated in Figures 2.7-2.9.

2.4.3 Distributed Fixed Source Emissions

Distributed fixed sources (defined as all fixed sources, with the exception of power plants and oil refineries) account for approximately 11% of NO_x and 34% of organic gas emissions from all sources in the Los Angeles airshed. Pollutants emitted from these sources are treated as surface fluxes into the appropriate ground level grid cell. Locations and emissions data for distributed fixed sources for 1969 are available in Profile of Air Pollution Control in Los Angeles County (Los Angeles County Air Pollution Control District, 1969) and Emissions Inventory-1969 (County of Orange Air Pollution Control District, 1970). The estimated spatial distributions of RHC, URHC, and NO_x emissions from these sources are given in Figures 2.10-2.12. The total quantities of emissions from distributed fixed sources are summarized in Table 2.15.

Figure 2.6 Apportionment of Power Plant Emissions in Downwind Grid Cells

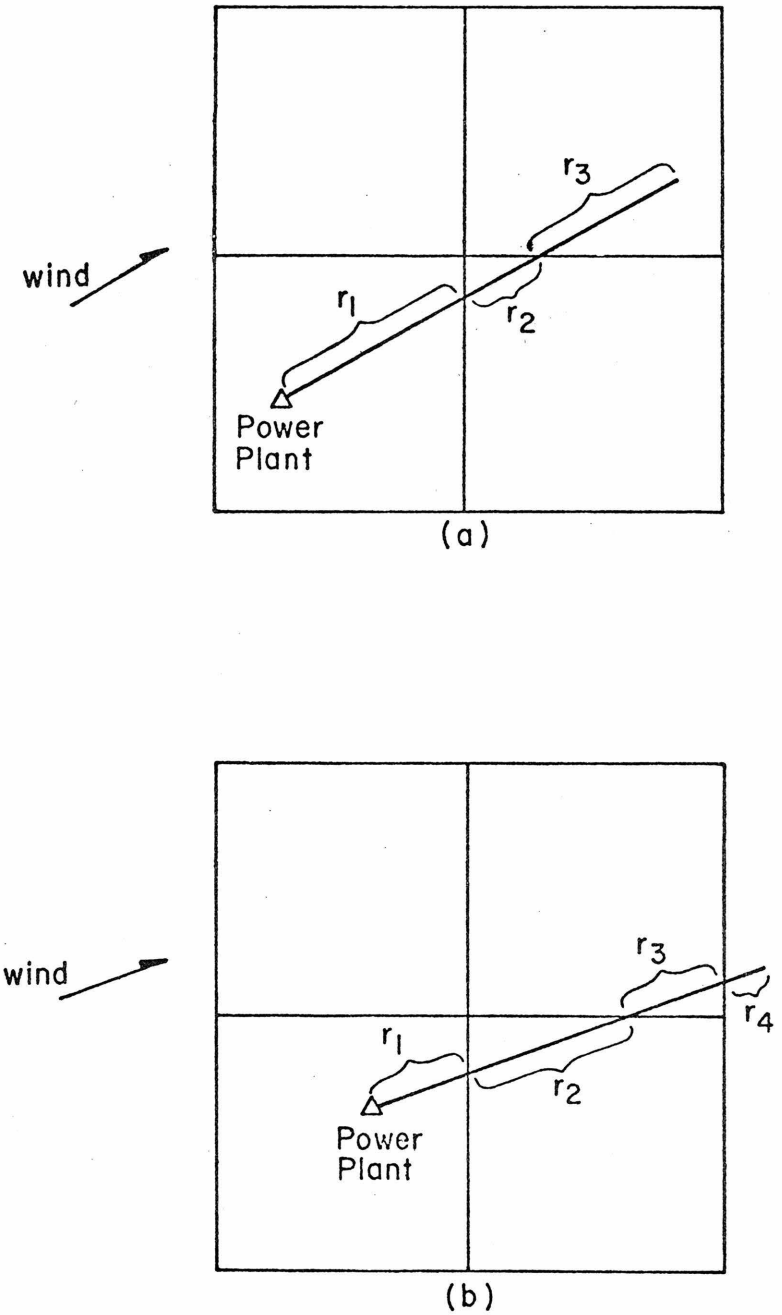

Table 2.12

Summary of Los Angeles Basin Power Plant Data for 1969

Name	Coordinates of Plant Location[a]	Electric Capacity (megawatts)	Average Total NO_x Emissions Rate (as NO_2) (kg/hour)
Southern California Edison			
Los Alamitos	15.90, 7.45	1950	2085
El Segundo	6.60, 12.35	1020	995
Redondo Beach	7.50, 10.25	1530	2008
Huntington Beach	19.40, 3.20	880	1226
Los Angeles Department of Water and Power			
Harbor	11.20, 7.50	355	334
Haynes	16.05, 7.20	1580	609
Scattergood	5.95, 14.15	312	78
Valley	7.55, 23.85	512	186
City of Pasadena			
Broadway & Glenarm[b]	14.55, 19.75	230	31
City of Burbank			
Magnolia & Olive[b]	9.80, 21.55	174	211
City of Glendale			
San Fernando & Highland[b]	10.85, 20.75	153	60

[a] In Figure 1.1, the center of the grid square in column I and row J is considered to have the coordinate I, J.

[b] Street locations, rather than name.

Table 2.13a Temporal Distribution of Power Plant Emissions Between 1 A.M. and 12 A.M. [a]

TIME (LOCAL) A.M.	1	2	3	4	5	6	7	8	9	10	11	12	Remarks
Southern Cal. Edison													
Los Alamitos	59.8	55.3	50.8	49.9	44.3	48.9	43.7	59.7	78.9	71.3	86.9	100.8	b
El Segundo	53.2	51.4	50.5	50.5	51.4	56.8	52.3	63.2	82.7	79.5	84.1	75.9	b
Redondo Beach	69.6	63.9	51.3	53.0	65.2	77.3	65.6	85.4	94.4	90.8	93.9	90.3	b
Huntington Beach	39.4	38.9	38.9	38.9	38.9	38.9	74.4	82.2	100.0	98.3	98.3	98.3	b
L.A. Dept. of Water	59.1	59.1	59.1	59.1	59.1	60.5	69.6	81.9	91.3	96.8	100.4	100.8	c
and Power	55.1	55.1	55.1	55.1	55.1	62.7	71.0	81.6	85.5	87.0	86.3	86.3	d
City of Pasadena	33.9	33.9	33.9	33.9	33.9	33.9	34.8	40.9	51.3	61.3	67.0	70.4	c
	25.7	25.7	25.7	25.7	25.7	22.2	29.6	35.7	42.2	47.0	47.8	47.0	d
City of Burbank	44.8	44.8	44.8	44.8	44.8	46.6	56.9	70.1	77.6	83.9	88.5	90.2	c
	41.4	41.4	41.4	41.4	41.4	47.1	58.0	69.0	71.3	71.8	71.8	69.0	d
City of Glendale	35.9	35.9	35.9	35.9	35.9	37.3	42.5	51.0	60.1	68.6	74.5	78.4	c
	32.0	32.0	32.0	32.0	32.0	35.9	46.4	55.6	59.5	62.1	62.1	62.1	d

[a] Note that the entries in this Table are percentages of the average emission rates given in Table 2.12.

[b] Entries estimated from actual data reported on September 30, 1969.

[c] Entries represent summer averages.

[d] Entries represent winter averages.

Table 2.13b Temporal Distribution of Power Plant Emissions Between 1 P.M. and 12 P.M.[a]

TIME (LOCAL) P.M.	1	2	3	4	5	6	7	8	9	10	11	12	Remarks
Southern Cal. Edison													
Los Alamitos	113.0	121.3	123.9	121.7	116.0	110.0	123.0	112.0	110.0	102.0	91.7	87.6	b
El Segundo	96.8	105.9	110.5	108.2	98.2	82.3	89.1	90.0	80.9	61.8	56.4	54.5	b
Redondo Beach	97.5	102.0	106.5	104.3	98.3	90.0	98.3	92.6	90.9	89.2	83.3	81.3	b
Huntington Beach	102.2	102.2	104.4	104.4	104.0	98.3	102.0	100.0	98.3	76.4	60.0	50.8	b
L.A. Dept. of Water	104.0	104.4	105.1	103.7	101.0	97.5	92.7	93.8	97.1	90.2	79.3	68.4	c
and Power	87.4	87.4	85.9	84.1	84.4	95.3	100.0	94.5	89.8	82.2	72.7	63.6	d
City of Pasadena	72.2	74.8	76.5	76.1	74.8	73.0	69.6	67.4	62.6	55.6	48.6	41.7	c
	46.5	46.5	46.1	45.7	46.0	52.2	56.5	55.7	52.2	47.8	43.5	34.8	d
City of Burbank	96.6	97.7	100.6	98.3	97.7	92.0	92.0	92.0	86.2	80.5	69.0	57.5	c
	70.0	70.7	67.0	65.5	68.4	71.8	69.0	69.0	69.0	63.2	57.5	51.7	d
City of Glendale	81.0	86.3	89.5	91.5	92.8	92.2	91.5	91.5	91.5	91.5	75.2	55.6	c
	60.1	60.1	58.8	57.5	60.1	71.9	71.9	71.9	71.9	71.9	58.8	45.8	d

a. Note that the entries in this Table are percentages of the average emission rates given in Table 2.12.

b. Entries estimated from actual data reported on September 30, 1969.

c. Entries represent summer averages.

d. Entries represent winter averages.

Table 2.14 Summary of Los Angeles Basin Oil Refinery Data in 1969

Name	Location		Crude Capacity (barrels/stream day)	NO_x (as NO_2)	Emission Rates (Kg/hour) reactive HC	unreactive HC
Atlantic Richfield Co.	12.10,	9.65	173,000	458	176	192
Douglas Oil Co. of California	14.60,	11.95	26,000	69	27	29
Edgington Oil Refineries, Inc.	14.15,	10.95	16,000	42	16	18
Fletcher Oil & Refining Co.	10.80,	9.10	13,000	34	13	14
Carson Oil Co., Inc.	9.65,	9.90	10,000	26	10	11
Gulf Oil Corporation	17.35,	12.35	51,000	135	52	57
Lunday-Thagard Oil Co.	14.05,	13.75	3,000	8	3	3
MacMillan Ring-Free Oil Co.	15.00,	8.20	10,000	26	10	11
Mobil Oil Corporation	9.05,	10.35	130,000	344	132	144
Powerine Oil Co.	16.85,	13.15	30,000	80	31	33
Shell Oil Company	11.95,	10.00	44,000	117	45	49
Shell Oil Company	11.80	8.90	44,000	117	45	49
Standard Oil of California	7.00	12.30	210,000	556	214	233
Texaco, Inc.	12.05,	8.15	61,000	162	62	68
Union Oil Co. of California	11.85,	7.80	107,000	284	109	119

Figure 2.7 Reactive Organic Gas Emissions (kilograms/hour) from Oil Refineries

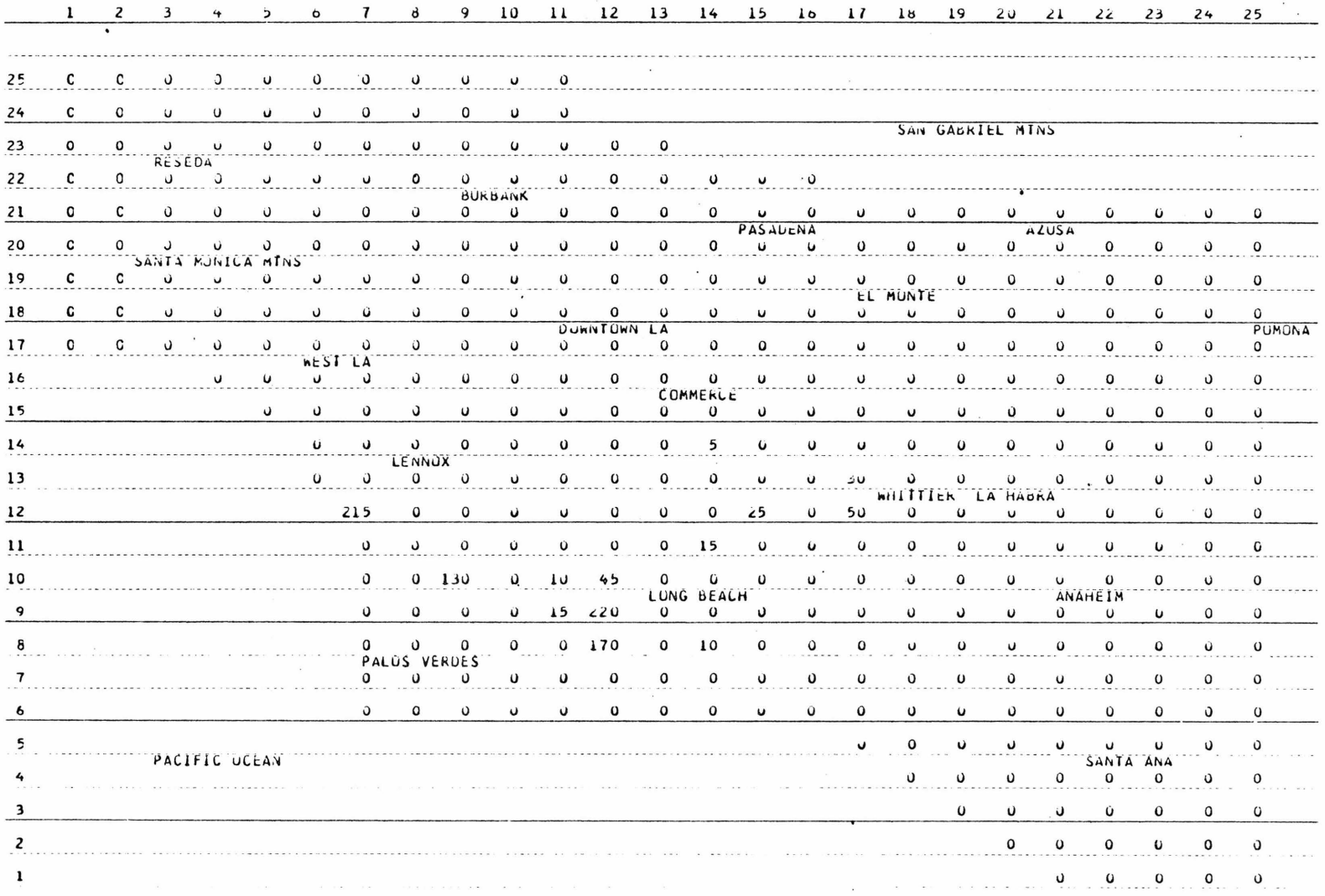

Figure 2.8 Unreactive Organic Gas Emissions (kilograms/hour) From Oil Refineries

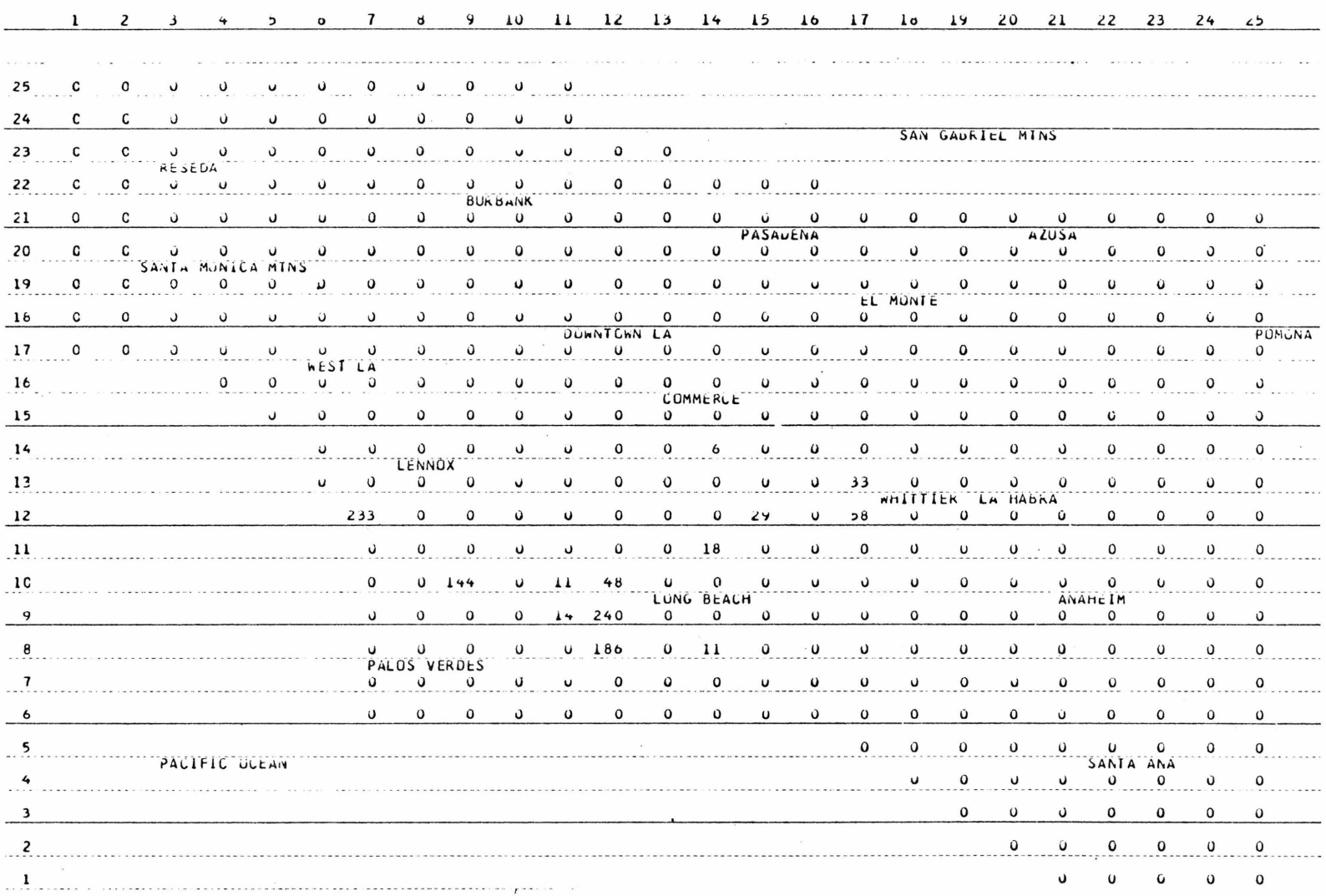

Figure 2.9 NO_x Emissions (kilograms/hour) from Oil Refineries (as NO_2)

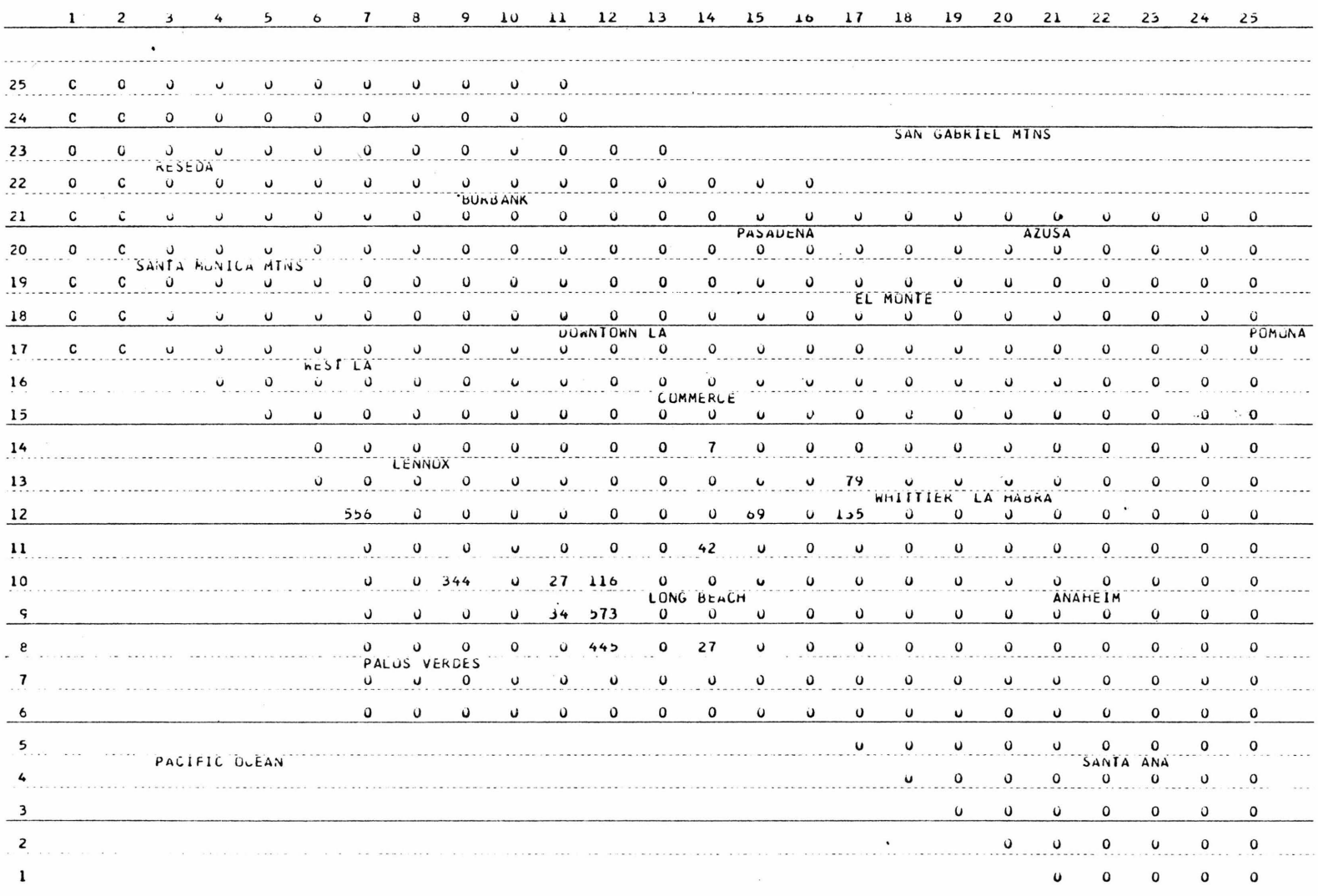

Figure 2.10 Reactive Organic Gas Emissions (kilograms/hour) from Petroleum Marketing and Organic Solvent Users

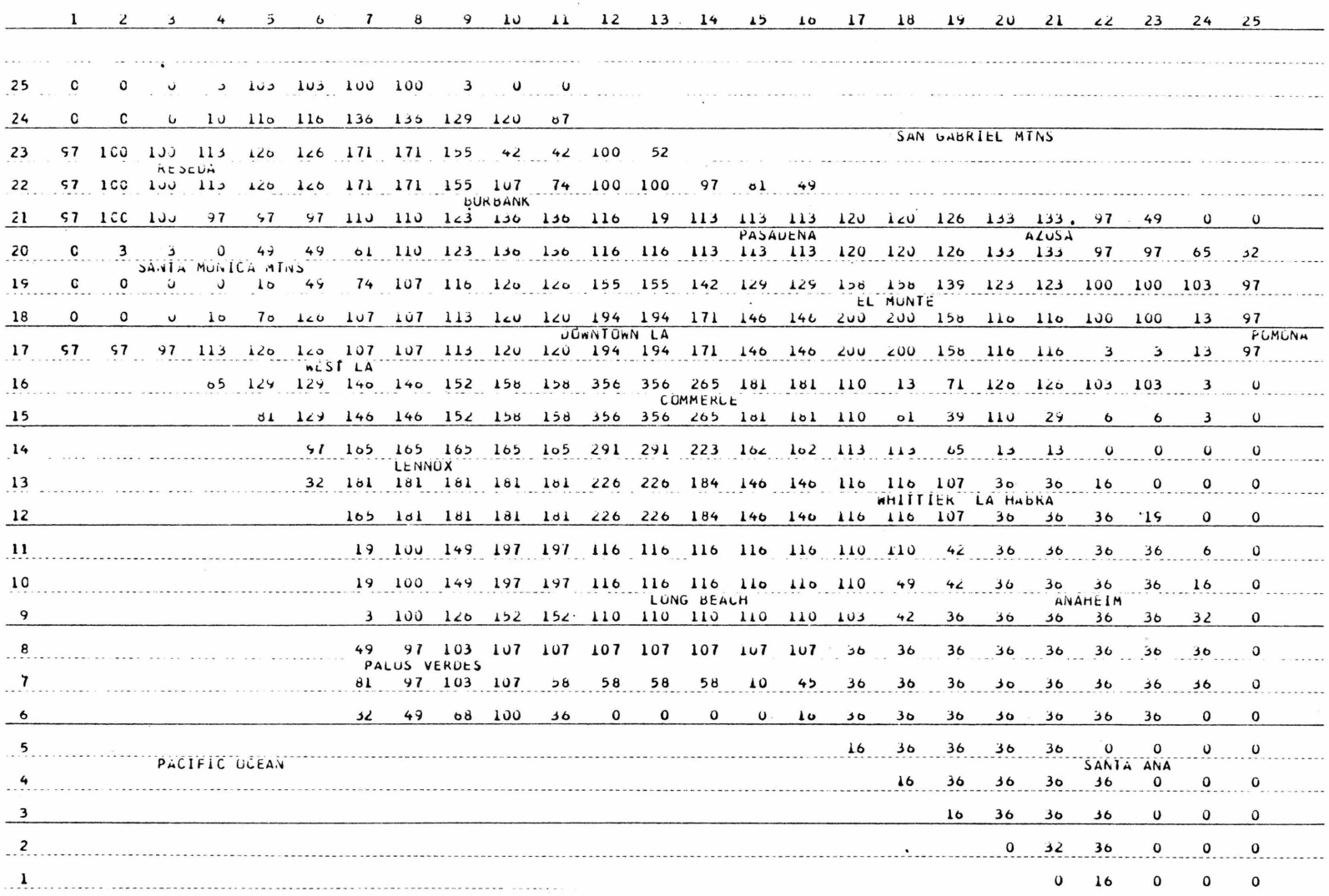

Figure 2.11 Unreactive Organic Gas Emissions (kilograms/hour) from Petroleum Marketing, Organic Solvent Users, Petroleum Production

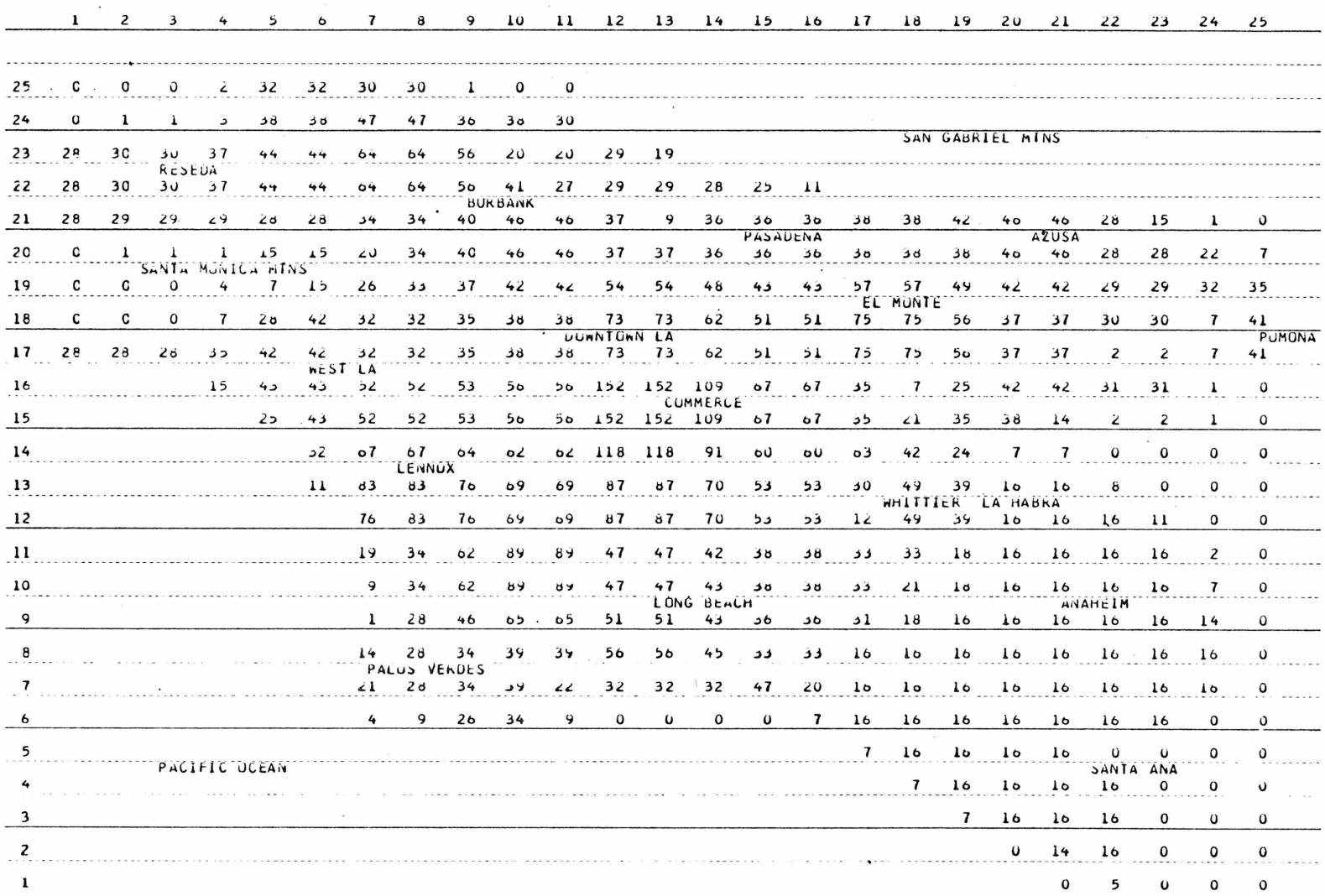

Figure 2.12 NO_x (as NO_2) Emissions (kilograms/hour) from Petroleum Marketing, Domestic, Ships and Railroads, Incinerators, Minerals, Metals, Petroleum Production, and "Other Industries"

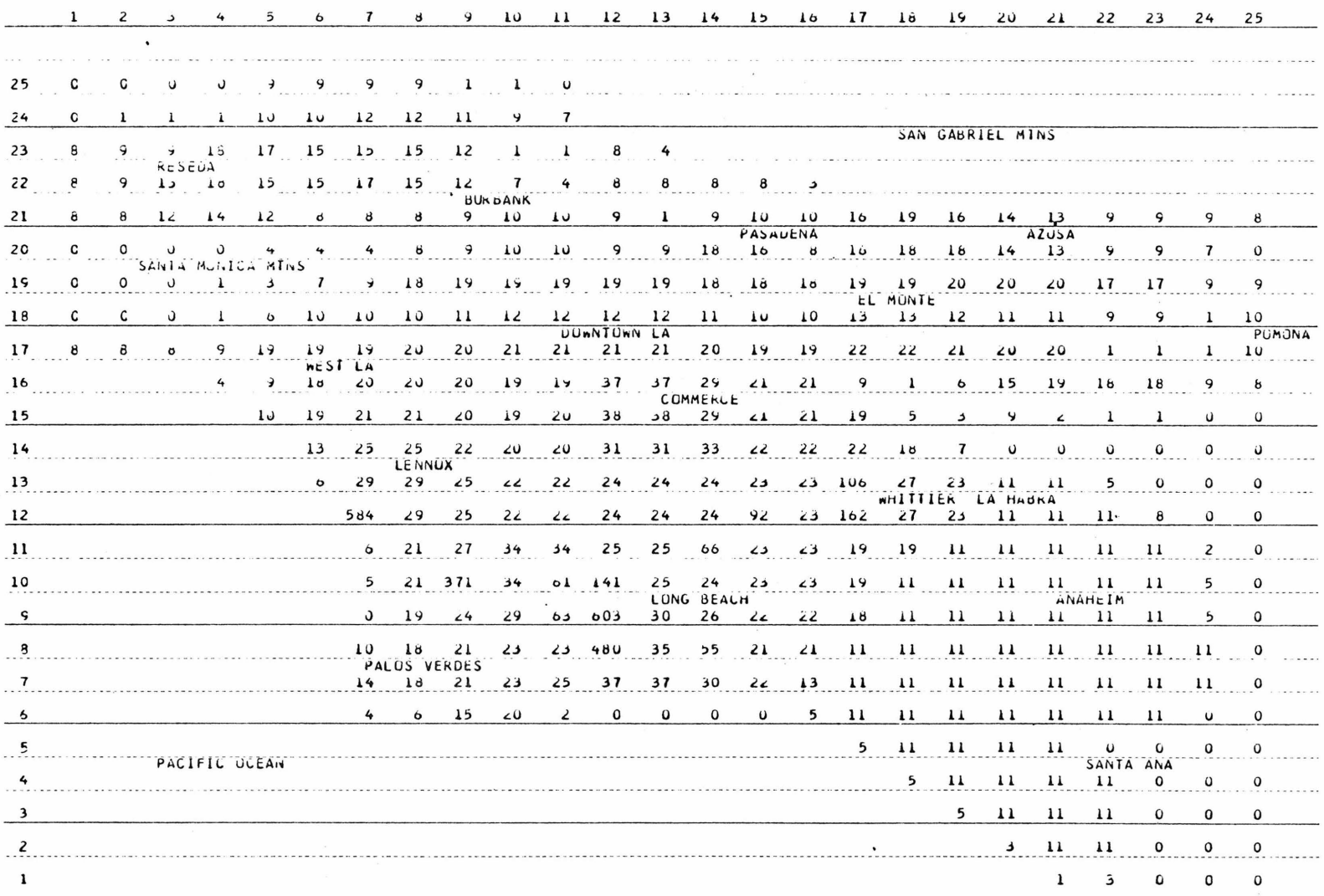

2.5 Contaminant Emissions Inventory of the Los Angeles Airshed in 1969

In this section a summary is given of the approximate magnitudes of the different emissions sources operating in the Los Angeles airshed during 1969. Average daily emission rates of NO_x, organic gases, and CO are shown in Table 2.15. These data, with the exception of automotive, aircraft, and power plant emissions, were obtained from the appropriate County Air Pollution District. Automotive emissions were computed from the product of the vehicle mileage in the parts of each county within the modeling area and the average emissions rate per vehicle mile. The power plant data were determined as discussed in Section 2.4.1. Emissions from aircraft were specified by using equation (2.11) and Tables 2.8-2.10.

To use this inventory in conjunction with an airshed model, it is necessary to specify the fraction of total NO_x emissions from each class of sources that is NO_2. As the measurement of the individual oxides is rarely made, the magnitude of the NO/NO_2 split can only be estimated. The following figures were employed in the validation study to be reported in Chapter 4 (Sawyer, 1972):

	% NO_2
Automobiles	1
Power Plants	5
Aircraft	1
Other fixed sources	2

In previous tables and figures (Tables 2.4, 2.9, 2.12, 2.14, 2.15 and Figures 2.9 and 2.12) NO_x emission rates are specified as NO_2,

that is, as if the emissions were 100% NO_2. For actual input to the model, the NO_x mass emission rates consist of both NO and NO_2, computed according to the NO/NO_2 split above.

Table 2.15 Emissions of NO_x, Organic Gases, and CO in the Los Angeles Airshed (tons/day) in 1969

Emission Source	NO_x[a]	Organic Gases		CO
		Reactive	Unreactive	
Motor Vehicles	520	1331	214	8127
Aircraft[c]	1	12	2	81
Petroleum				
Refining	25	25	25	30
Production	10		60	
Marketing	10	122		
Power Plants	171		4	
Oil Refineries	40		4	1
Other Industries	29		2	
Domestic[b]	41			
Incineration	1		1	1
Ships and Railroads	3		1	4
Metals	3			3
Minerals	6		1	
Organic Solvent Usage		394	138	
TOTAL	860	1884	452	8247

[a] As NO_2. The split between NO and NO_2 must be considered when these values are used as the actual input to the model calculations.

[b] Domestic, commercial, and industrial facilities on firm natural gas schedules.

[c] Ground operations only.

2.6 Discussion of the Model and Inventory

A necessary step in the development of any model is an assessment of the levels of uncertainty in each of the input variables and the effect of these uncertainties on the predictions of the model. Thus, the objective of this section is to estimate the levels of accuracy with which the source emissions inputs to an urban airshed model can be determined and to enumerate, thereby, those emission factors which can be expected to lead to the most uncertainty in the predictions of the model. A discussion will be given relating to the expected level of accuracy in the most important components of the Los Angeles emissions inventory, namely automotive and fixed source emissions.

2.6.1 Automotive Emissions

For a given grid square the vehicle miles per day, M^f and M^s, travelled on all roads in the square can be computed from equation (2.8). It is estimated that M^f and M^s for each grid square are accurate to 5-10%. Thus, a figure of 400,000 vehicle miles/day, for example, should be interpreted as $400,000 \pm 40,000$ if the accuracy were $\pm$ 10%. Based on discussions in Section 2.2.4.2, the estimated uncertainties in the grand temporal distributions are:

$$d_p^f: \ 2\text{-}4\% \qquad d_p^s: \ 5\text{-}7\%$$

The matter of determining a driving cycle representative of a particular urban area is discussed in Section 2.2.1. To illustrate the importance of the choice of driving cycle, the differences among emissions as measured by hot-start and cold-start CDC and FDC are illustrated in Table 2.16. It is apparent from Table 2.16 that measured emission rates are strongly dependent on the testing procedure employed.

Table 2.16

Comparison of Automobile Emission Rates Using the Hot and Cold-Start CDC and Cold-Start FDC

	Approximate increase in emission rates when measured by cold-start CDC, as compared with hot-start CDC (all vehicles).	Approximate increase in emission rates when measured by 1972 Federal procedure as compared with cold-start CDC.	
		Pre-1966 vehicles	1966-1969 vehicles
HC	+ 30%	+ 40%	+ 90%
CO	+ 0-10%	+ 60%	+100%
NO_x	- 5%	+ 60%	+ 30%

	Values of Q_ℓ (Grams/Mile)		
Species	CDC Hot-Start	FDC Hot-Start	FDC Cold-Start
CO	63.9	68.6	91.0
HC (exhaust + blowby)	9.0	10.8	11.7
NO_x (as NO)	2.9	2.7	2.7

It is believed that by far the greatest uncertainty in the calculation of motor vehicle emissions is the representativeness of a driving cycle in a particular locale. Recently the FDC has replaced the CDC as the standard emissions test procedure. Nevertheless, the representativeness of the FDC or any other cycle has yet to be demonstrated. It is recommended that studies such as those reported by Smith and Manos (1972) be undertaken for cities for which urban airshed models are to be developed. Consideration should also be given to using a series of test cycles, rather than any particular cycle, to represent driving patterns in a metropolitan area.

2.6.2 Fixed Source Emissions - Power Plants and Refineries

The principal problem associated with fixed source emissions is a lack of data. Few measurements of effluent concentrations are made, and there are virtually no data available that reflect the effect of process variations on emission rates. In addition, temporal variations, particularly in the operation of power plants, are often considerable, yet unpredictable, since they frequently depend on such unreliable and capricious factors as the weather.

In general, highly simplified assumptions are made in estimating emission rates from large "point sources" in an urban area. For example, emission rates from refineries are usually assumed to be directly proportional to the crude throughput rate. This rate is not only assumed uniform over a day (uniform temporal distribution), but usually represents an average taken over a period of one month to a year. Data related to emissions from power plants are generally easier to obtain and are often fairly complete. However, measurements

made for one day are generally assumed to apply for all days, corrected for daily temporal distribution and season (summer vs. winter); the validity of this assumption remains in question.

The following types of data are needed to estimate emission rates from power plants:

1. electric capacity of plant (megawatts)
2. mass flow of flue gas (kg/hr)
3. volume flow of flue gas (m^3/min.)
4. effluent temperature
5. volume concentration of NO_x and SO_2 (ppm)
6. temporal distribution of operation

Similar data are needed to estimate emissions from refinery process units, although temporal variations (on a daily basis) are likely to be unimportant. In addition, emissions and evaporative losses of both reactive and unreactive organic gases must be estimated, the latter being particularly difficult to determine.

In general, then, emissions data from power plants, while of variable quality (from quite good to rather poor), are generally available. Refinery emissions data are usually unavailable, and thus estimates of emissions from this class of sources are highly uncertain (perhaps up to ± 100% or more). Inaccuracies in emission rates from large, concentrated or point sources can have a noticeable impact on model prediction, particularly in the case of NO_x.

CHAPTER 3

NUMERICAL INTEGRATION OF THE GOVERNING EQUATIONS

3.1 Introduction

The simulation model for estimating ground level concentrations of photochemical pollutants is based on the equations of continuity for a turbulent fluid in which chemical reactions occur. The basic form of these equations, with initial and boundary conditions, is given by equations (1.5) - (1.9). Since the three-dimensional modeling region is bounded vertically by the terrain and the base of the elevated temperature inversion, the vertical coordinate, z, is scaled by the mixing depth, ΔH, to transform the region into a rectangular parallelopiped. The final forms of the transformed continuity equations and initial and boundary conditions are given by equations (1.12) and (1.17) - (1.21). These equations are coupled since they share a common argument in the chemical reaction rate expressions $R_\ell(c_1, c_2, \ldots, c_N)$. In general, one is faced with the task of solving N coupled, nonlinear partial differential equations in three spatial dimensions. Because the partial differential equations are nonlinear, the solution must be obtained numerically, rather than analytically. Thus, the objective of this Chapter is to present and discuss the numerical integration technique employed in this study to solve the governing equations of the model.

In the present version of the model, the dynamic behavior of six chemical species is followed, including reactive (RHC) and unreactive (URHC) hydrocarbons, NO, NO_2, O_3, and CO. The extent

to which "unreactive" hydrocarbon and CO participate in chemical reactions is generally small, and hence the reaction rate term, R_ℓ, is set equal to zero for these two species. Consequently, the governing equations reduce to a system of four coupled, nonlinear partial differential equations for RHC, NO, NO_2, and O_3, and two systems of uncoupled, linear partial differential equations for CO and URHC.

Many methods have been reported in the literature for the solution of parabolic partial differential equations. Five classes of methods to be considered are:

1. Finite-difference methods (Richtmyer and Morton, 1967);
2. Particle-in-cell methods (Sklarew et al., 1971);
3. Method of Egan and Mahoney (1972);
4. Finite-element methods (Guymon, 1970; Guymon et al., 1970; Shum, 1971); and
5. Galerkin-type methods (Price et al., 1968; Douglas and Dupont, 1970; Culham and Varga, 1971).

Although each of the methods cited have been employed to solve the advection-diffusion equation without photochemistry in one and, in some instances, two spatial dimensions, only recently has experience been reported in the use of one of the methods (the particle-in-cell method) for solving the complete three-dimensional airshed equations with photochemistry. Finite-difference methods were selected for use in this study because 1) at the time a method had to be chosen there was a dearth of reported experience in the application of the other methods for the solution of large systems of coupled, nonlinear equations in three spatial dimensions; 2) special methods for treating

multidimensional problems had been developed for finite-difference methods; and 3) finite-difference methods had enjoyed widespread use in the numerical solution of fluid flow and diffusion problems. It should be noted, however, that there is currently substantial interest in the application of the other four classes of methods since they may provide a means for obtaining more accurate numerical solutions utilizing comparable amounts of computing time.

The remainder of this Chapter is divided into four sections. In Section 3.2, considerations pertinent to the selection of a specific finite-difference method are discussed. A detailed exposition of all finite-difference equations employed is given in Section 3.3. Since systems of linear equations arise from the use of implicit difference schemes, the algorithms employed to solve these systems of equations are presented in Section 3.4. In the final section, the discussion will focus on the experience gained in the application and testing of finite-difference methods for use in photochemical simulations.

3.2 Selection of a Finite-Difference Technique

Many finite-difference methods have been developed for the solution of parabolic partial differential equations. In evaluating available methods, one must consider the following characteristics of each: 1) stability, 2) accuracy, 3) computer storage requirements, 4) computing time requirements--expressible as the ratio of computing time to simulation time, and 5) adaptability of the method to the solution of the governing equations. In addition to specifying finite-difference approximations for each term in the governing

equations, one must also consider the treatment of the multidimensional nature of the equations.

Finite-difference techniques are often classified as explicit or implicit, depending on whether each succeeding integration step is direct (explicit) or based on the simultaneous solution of difference equations (implicit). While implicit techniques are generally computationally more burdensome than explicit methods, in many instances they offer the advantage of being stable over larger ranges in spatial and temporal step sizes. Other finite-difference methods exist which are difficult to classify in this way. Typically, these techniques may have some characteristics of implicit methods yet, because of some unique aspect of the particular technique, involve less burdensome calculations than are normally expected with an implicit method. Two such techniques were considered for use in solving the governing equations, the method of alternating directions and the method of fractional steps.

The basic procedure that was ultimately adopted for treating the three-dimensional nature of the governing equations was selected by elimination. Considering the five criteria cited above, the reasoning was as follows:

1. Use of classical implicit methods would involve the solution of extraordinarily large systems of linear and nonlinear equations. For the Los Angeles simulation, two systems of over 2000 linear equations and one system of over 8000 nonlinear equations would have to be solved at each integration step. This method was

eliminated based on the expectation that computation times would be excessive.

2. Explicit schemes were ruled out because of the highly nonlinear nature of the reaction rate terms which are more suitably treated implicitly. In addition, during the early morning hours the mixing depth is characteristically only a few hundred feet deep. Thus, the vertical grid spacing is small, and a prohibitively small time step would be required for stability.

3. The alternating direction method was attractive since it possesses the stability characteristics of implicit techniques and yet involves the solution of only relatively small systems of equations. A major simplification and savings in computation times is thereby realized, when compared with classical implicit methods (see Richtmyer and Morton (1967) for further details). Unfortunately, knowledge of the concentration distribution (over 2000 values for each pollutant) at three levels of time (current and two previous) are required. In order to store this information, use of external memory would be required, resulting in a more complicated computer code, extended computation times, and increased costs.

4. The method of fractional steps involves the fragmentation of an n-dimensional partial differential equation (with time as a variable) into n-1 two-dimensional partial differential equations. The fragment involving vertical

transport may be treated implicitly to eliminate stability problems associated with an explicit formulation coupled with a small vertical grid spacing in the early morning hours. As each fragment is two-dimensional, implicit difference formulations result in only relatively small systems of simultaneous equations. Another convenient feature of the method is that the concentration distribution at only one time level need be stored; thus, computer storage requirements are minimized.

The method of fractional steps thus appears to be preferable to the other classes of techniques for the particular problem under consideration. The method is discussed in detail by Yanenko (1971).

One of the primary considerations regarding the use of finite-difference methods to solve the governing equations is the manner in which the advection terms are to be approximated. Since vertical transport is generally dominated by turbulent diffusion and since horizontal transport is dominated by advection, of particular interest is the finite-difference approximation employed for the terms $\frac{\partial u \Delta Hc_\ell}{\partial \xi}$ and $\frac{\partial v \Delta Hc_\ell}{\partial \eta}$ in equation (1.17). These terms are commonly approximated by first-order finite-difference expressions; however, it is well known that the truncation error for a low-order method has the characteristics of a diffusion process (Bella and Grenney, 1970; Lantz, 1971). This additional diffusion, often termed numerical or artificial diffusion, may in some instances be larger than the actual turbulent diffusion. To minimize these truncation error effects, high-order finite-difference approximations must be employed.

In order to obtain a quantitative estimate of the relative merits of high-order advective schemes, two numerical advection experiments were performed using representative first, second, and fourth-order finite-difference approximations. In the first experiment, assuming that:

1. horizontal diffusion may be neglected;
2. pollutants are well mixed vertically;
3. all source and chemical reaction rate terms are equal to zero; and
4. the mixing depth, ΔH, is a constant;

equation (1.17) may be written as

$$\frac{\partial c_\ell}{\partial \tau} + \frac{\partial uc_\ell}{\partial \xi} + \frac{\partial vc_\ell}{\partial \eta} = 0 \qquad (3.1)$$

which is the so-called advection equation. The method of fractional steps was applied to the solution of equation (3.1), as discussed by Crowley (1968), employing the second and fourth-order difference schemes described by Crowley (1968) and Fromm (1969), respectively.

The first experiment consisted of advecting a conical concentration distribution across the Basin using a uniform windfield. The initial concentration distribution and the location of the pollutants after five hours is illustrated in Figure (3.1). The following conditions were applied to the test:

Wind: Uniform, $6\sqrt{2}$ mph, from the southwest (moving northeast at 45°); thus u = 6 mph, v = 6 mph

Grid Spacing: $\Delta\xi = \Delta\eta = 2$ miles

Initial Concentration Distribution:	Right circular cone with concentration of 2 ppm at apex, 1 ppm at base, and 1 ppm at all other points (see Figure 3.1)
Time Step:	10 minutes

The combination of wind speed and direction and size of the time step are such as to move the concentration distribution exactly one-half a grid spacing per time step in both the ξ and η directions. The errors in the peak concentration that accumulate over a five-hour period, the time required to traverse 60% of the Basin, are indicated in Table 3.1. Note that the fourth-order method proved to be substantially more accurate in predicting peak concentrations than the second-order scheme. Furthermore, using the fourth-order approximation, after one hour all other predicted concentrations were accurate to within 2%, and after five hours, to within 4%. Although the first-order scheme was not tested, the errors in the peak concentrations would be greater than those reported in Table 3.1 for the second-order method. The reader is referred to the results of a similar experiment employing both first and fourth-order techniques reported by Sklarew et al. (1971). In general, these test results are in agreement with similar numerical experiments using high-order methods carried out by Molenkamp (1968), Crowley (1968), and Sklarew et al. (1971).

Figure 3.1 Test Distribution and its Path of Transport

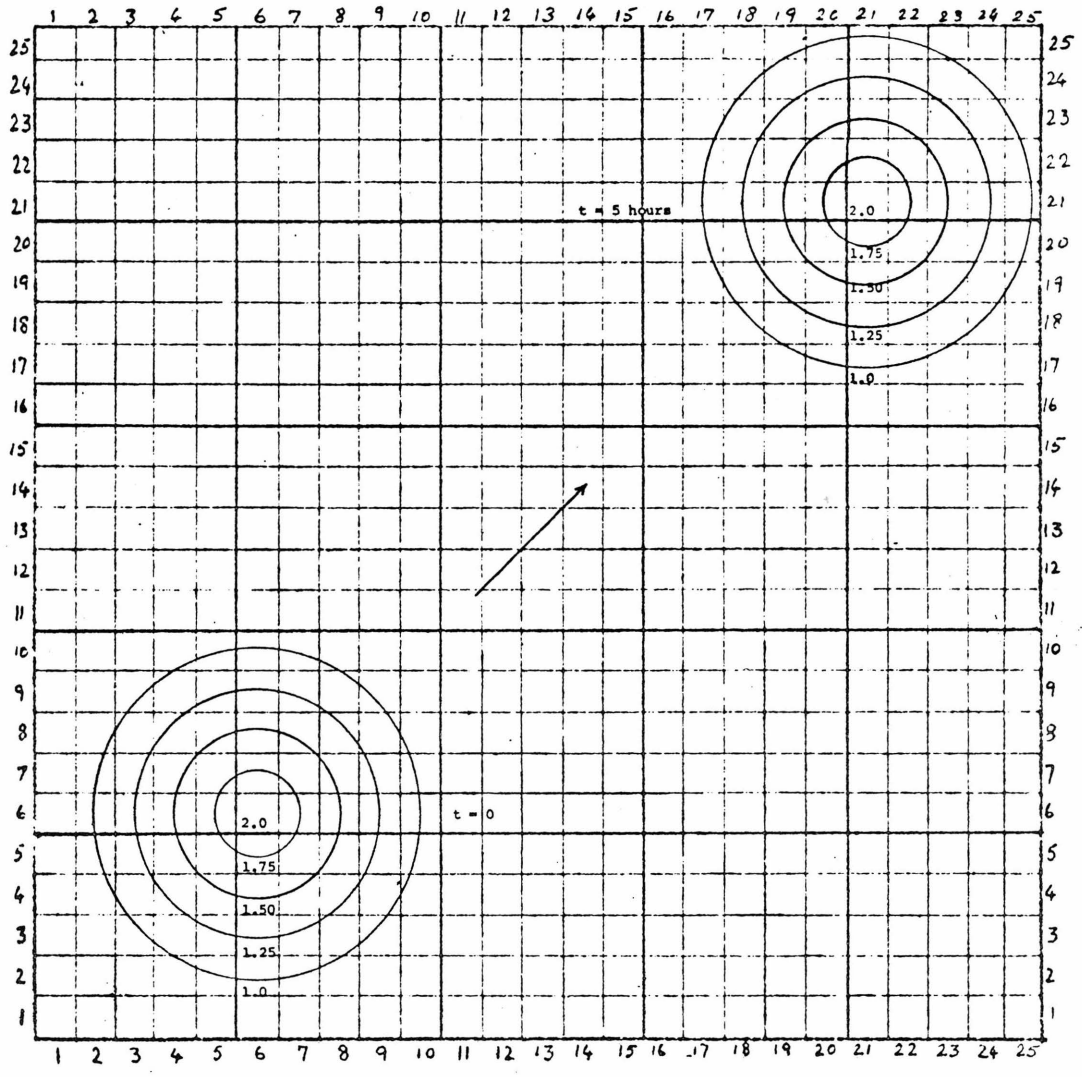

TABLE 3.1

RESULTS OF TESTS OF HIGH-ORDER NUMERICAL TECHNIQUES

	Second-Order		Fourth-Order	
Time (hr)	Peak Conc. (ppm)	Error (ppm)	Peak Conc.	Error
0	2.0	0.0	2.0	0.0
1	1.83	-0.17	1.87	-0.13
2	1.78	-0.22	1.86	-0.14
3	1.74	-0.26	1.86	-0.14
4	1.68	-0.32	1.85	-0.15
5	1.69	-0.31	1.84	-0.16

The second numerical experiment was designed to demonstrate to what extent the choice of a high or low-order horizontal advective difference scheme would affect predicted concentrations in an actual airshed simulation. To carry out this test, two six hour CO simulations were performed using both first and fourth-order difference approximations for the horizontal advective terms. Initial and boundary conditions, emissions, and meteorological inputs were typical of those employed in the 1969 validation studies. In addition, the full three-dimensional model was used. The results from the two simulations may be summarized as follows:

1. The maximum difference in hourly-averaged predicted concentrations was observed in one grid cell to be 6 ppm. The predictions in this cell using the first and fourth-order schemes were 18 and 12 ppm, respectively.

This discrepancy occurred between 0600 and 0700 PST; the simulation was started at 0500 PST.

2. The majority of predicted hourly-averaged concentrations differed by 2 ppm or less.
3. After six hours of simulation, the maximum difference in predicted concentrations, averaged between 10 A.M. and 11 A.M. PST, was found to be 3 ppm. This difference was observed in two ground level grid cells.

Since substantial differences in predicted concentrations were observed in a few locations, high-order advective difference schemes may be required to minimize the maximum numerical error at any location on the grid. Low-order difference approximations may be sufficient if relatively large numerical errors can be tolerated in some areas on the grid.

To assess the impact of low and high-order advection schemes on photochemical calculations, simulations similar to those described above for CO were carried out for RHC, NO, NO_2 and O_3. Although no integration difficulties were encountered using the first-order advection scheme, complete simulations could not be performed employing either the second or fourth-order schemes given by Crowley (1968) and Fromm (1969), respectively. During the course of the simulations using these high-order methods, negative NO concentrations were predicted in grid cells located offshore, adjacent to coastal grid cells containing power plants. Due to the combination of substantial NO emissions in these coastal cells and low NO background concentrations over the ocean, relatively large gradients in

the NO concentration field occur in these areas on the grid. Negative concentrations may be predicted when the calculated net transport of pollutant out of a cell is greater than the amount of pollutant originally in the cell. This unfortunate behavior of high-order methods often occurs in the vicinity of steep concentration gradients and has been observed by Roberts and Weiss (1966) and Sklarew et al. (1971). When negative concentrations occurred, the Newton iterative technique employed in the integration procedure (to be described more fully in the next section) failed to converge.

Since the centered second and fourth-order approximations cited above proved unsatisfactory for use in this study, an uncentered second-order difference scheme given by Price et al. (1966) was tested. It was found that using this method, no difficulties were encountered in performing photochemical simulations. That is, the method was capable of predicting positive concentrations in the vicinity of the coastal power plants. Although the uncentered method is somewhat less accurate than the centered second-order approximation given by Crowley (1968), and although use of the fourth-order scheme would be preferable to minimize numerical errors, the uncentered second-order method was adopted for use in this study as a compromise between achieving accuracy on the one hand, and avoiding the possible calculation of negative concentrations on the other. The possibility of employing the fourth-order method in conjunction with an imposed lower bound on any predicted concentration was dismissed since this alternative would have the effect of adding additional "sources" of pollutant to the model.

3.3 The Method of Fractional Steps Applied to the Integration of the Governing Equations

In this section a detailed discussion is given of the numerical solution of equations (1.17), six partial differential equations in three spatial dimensions and time. The problem is complicated by the fact that four of the equations are coupled and nonlinear due to the appearance of the chemical reaction term R_ℓ. To apply the method of fractional steps, the original four-dimensional equation (ξ, η, ρ, τ) is fragmented into three two-dimensional equations in (ξ, τ), (η, τ) and (ρ, τ), respectively. The chemical reaction and source terms, R_ℓ and S_ℓ, are included in the (ρ, τ) fragment. The solution of the (ξ, τ) and (η, τ) fragments is explicit, while the solution of the (ρ, τ) fragment is implicit. To compute an integration time step, the equations representative of the (ξ, τ), (η, τ), and (ρ, τ) fragments are solved successively. Before presenting the details of the finite-difference equations, however, a brief description is given of the grid network and the nomenclature employed in this section.

3.3.1 The Computational Grid

Originally, a 25 X 25 X 5 grid network was adopted for the Los Angeles simulation study, where $\Delta\xi = \Delta\eta = 2$ miles, and $\Delta\rho = 0.2$ (ξ and η can be scaled by the length of the airshed, but this only introduces additional arithmetic operations into the finite-difference equations). Upon examining the 25 X 25 horizontal grid layout, it was found that 198 of the 625 grid squares were over the Pacific Ocean

and the San Gabriel Mountains--two areas having no emissions sources. Consequently, these grid squares were eliminated from the original grid to form the region over which the actual computations were performed. This amounted to a savings of approximately 30% in the required computing time. The ground-level grid layout is illustrated in Figure 1.1. Thus the computational grid consists of 2135 grid cells (427 horizontal grid squares X 5 vertical levels). Each grid cell is addressed by the integer triple (i, j, k), where i, j, and k correspond to the ξ, η and ρ coordinate directions, respectively.

3.3.2 Nomenclature

The exposition of finite-difference schemes generally requires the use of subscripts and superscripts to denote spatial and temporal aspects of a particular variable. This application is no exception and, in fact, is somewhat more complicated than most. The concentration distribution on the grid shall be denoted by

$$ {}^{m}_{\ell}C^{n}_{i,j,k} $$

where ℓ is an index denoting chemical species, $1 \leq \ell \leq 6$, and

$\ell = 1$ RHC

2 NO

3 O_3

4 NO_2

5 CO

6 URHC

i, j, k are indices designating the grid cell location in the ξ-η-ρ coordinate system

$$I_W \leq i \leq I_E$$

$$J_S \leq j \leq J_N$$

$$1 \leq k \leq K$$

where I_W, I_E, J_S, and J_N indicate the column or row number of cells adjacent to the west, east, south, or north borders, and K is the number of vertical levels.

n is an index in time, $n \geq 0$

m refers to the iteration number, $m \geq 0$

Subscripts and superscripts are used on other variables in an analogous manner.

3.3.3 Finite-Difference Equations

The method of fractional steps is applied to the solution of equations (1.12) and (1.17) - (1.21) as follows. First, equation (1.17) is split into three two-dimensional equations in (ξ, τ), (η, τ), and (ρ, τ). The three equations are given by:

$$\text{Step I:} \quad \frac{\partial}{\partial \tau}(\Delta H c_\ell) + \frac{\partial}{\partial \xi}(u \Delta H c_\ell) = \frac{\partial}{\partial \xi}\left(K_H \Delta H \frac{\partial c_\ell}{\partial \xi}\right) \tag{3.1}$$

$$\text{Step II:} \quad \frac{\partial}{\partial \tau}(\Delta H c_\ell) + \frac{\partial}{\partial \eta}(v \Delta H c_\ell) = \frac{\partial}{\partial \eta}\left(K_H \Delta H \frac{\partial c_\ell}{\partial \eta}\right) \tag{3.2}$$

$$\text{Step III:} \quad \frac{\partial}{\partial \tau}(\Delta H c_\ell) + \frac{\partial}{\partial \rho}(W c_\ell) = \frac{\partial}{\partial \rho}\left(\frac{K_V}{\Delta H} \frac{\partial c_\ell}{\partial \rho}\right) + R_\ell \Delta H + S_\ell \Delta H \tag{3.3}$$

The calculation of ${}_\ell C^{n+1}_{i,j,k}$ given values of ${}_\ell C^{n}_{i,j,k}$ requires three steps:

Step I: Integration in the ξ direction

Step II: Integration in the η direction

Step III: Integration in the ρ direction

The actual finite-difference expressions employed in the three-step integration procedure are given below.

STEP I: Integration in the ξ Direction

The concentration distribution at the n^{th} time level, ${}_{\ell}C^{n}_{i,j,k}$, is advanced to the first intermediate time level, ${}_{\ell}C^{*}_{i,j,k}$, by integrating equation (3.1) over the time interval $\Delta\tau$. The explicit, second-order finite-difference expressions adopted for the spatial derivatives are based on those described by Price et al. (1966).

$$ {}_{\ell}C^{*}_{i,j,k} = {}_{\ell}C^{n}_{i,j,k} + \frac{\Delta\tau}{\Delta\xi \Delta H^{n}_{i,j}} \left({}_{\ell}F^{n}_{i-\frac{1}{2},j,k} - {}_{\ell}F^{n}_{i+\frac{1}{2},j,k} \right) \qquad (3.4) $$

where

$$ \frac{\Delta\tau}{\Delta\xi} {}_{\ell}F^{n}_{i-\frac{1}{2},j,k} = \frac{\alpha^{n}_{i-\frac{1}{2},j,k}}{2} \left(3\, {}_{\ell}C^{n}_{i-1,j,k} - {}_{\ell}C^{n}_{i-2,j,k} \right) $$

$$ + \gamma^{n}_{i-\frac{1}{2},j,k} \left({}_{\ell}C^{n}_{i-1,j,k} - {}_{\ell}C^{n}_{i,j,k} \right) \text{ if } \alpha^{n}_{i-\frac{1}{2},j,k} \geq 0 $$

or

$$ \frac{\Delta\tau}{\Delta\xi} {}_{\ell}F^{n}_{i-\frac{1}{2},j,k} = \frac{\alpha^{n}_{i-\frac{1}{2},j,k}}{2} \left(3\, {}_{\ell}C^{n}_{i,j,k} - {}_{\ell}C^{n}_{i+1,j,k} \right) $$

$$ + \gamma^{n}_{i-\frac{1}{2},j,k} \left({}_{\ell}C^{n}_{i-1,j,k} - {}_{\ell}C^{n}_{i,j,k} \right) \text{ if } \alpha^{n}_{i-\frac{1}{2},j,k} < 0 $$

and

$$ \alpha^{n}_{i-\frac{1}{2},j,k} = \frac{u^{n}_{i-\frac{1}{2},j,k} \, \Delta H^{n}_{i-\frac{1}{2},j} \, \Delta\tau}{\Delta\xi} $$

$$ \gamma^{n}_{i-\frac{1}{2},j,k} = \frac{K^{n}_{H_{i-\frac{1}{2},j,k}} \, \Delta H^{n}_{i-\frac{1}{2},j} \, \Delta\tau}{\Delta\xi^{2}} $$

In equation (3.4) the following assumption is made with regard to the evaluation of ΔH at the first intermediate time level:

$$\Delta H^{*}_{i,j} = \Delta H^{n}_{i,j}$$

Since the effects of temporal mixing depth changes on pollutant concentrations are best treated in Step III, the movement of the inversion is deferred to that point in the computational scheme.

When applying equation (3.4) in grid cells adjacent to the western or eastern borders (ξ_W or ξ_E), the expressions for the boundary conditions given in equation (1.20) are employed. Thus, grid cells adjacent to the western border (ξ_W) are treated as follows:

$$\ell C^{*}_{I_w,j,k} = \ell C^{n}_{I_w,j,k} + \frac{\Delta\tau}{\Delta\xi \Delta H^{n}_{I_w,j}} \left(\ell F^{n}_{I_w-\frac{1}{2},j,k} - \ell F^{n}_{I_w+\frac{1}{2},j,k} \right)$$

where

$$\frac{\Delta\tau}{\Delta\xi} \ell F^{n}_{I_w-\frac{1}{2},j,k} = \left(\alpha^{n}_{I_w-\frac{1}{2},j,k} \right) \ell g^{n}_{I_w-\frac{1}{2},j,k} \qquad \text{if } \alpha^{n}_{I_w-\frac{1}{2},j,k} \geq 0$$

$$\frac{\Delta\tau}{\Delta\xi} \ell F^{n}_{I_w-\frac{1}{2},j,k} = \frac{\alpha^{n}_{I_w-\frac{1}{2},j,k}}{2} \left(3\,\ell C^{n}_{I_w,j,k} - \ell C^{n}_{I_w+1,j,k} \right)$$

$$\text{if } \alpha^{n}_{I_w-\frac{1}{2},j,k} < 0$$

and

$$\frac{\Delta\tau}{\Delta\xi} \ell F^{n}_{I_w+\frac{1}{2},j,k} = \frac{\alpha^{n}_{I_w+\frac{1}{2},j,k}}{2} \left(3\,\ell C^{n}_{I_w,j,k} - \ell g^{n}_{I_w-\frac{1}{2},j,k} \right) \qquad (3.5)$$

$$+ \gamma^{n}_{I_w+\frac{1}{2},j,k} \left(\ell C^{n}_{I_w,j,k} - \ell C^{n}_{I_w+1,j,k} \right)$$

$$\text{if } \alpha^{n}_{I_w+\frac{1}{2},j,k} \geq 0$$

$$\frac{\Delta\tau}{\Delta\xi}\,{}^{\ell}F^{n}_{I_w+\frac{1}{2},j,k} = \frac{\alpha^{n}_{I_w+\frac{1}{2},j,k}}{2}\left(3\,{}^{\ell}C^{n}_{I_w+1,j,k} - {}^{\ell}C^{n}_{I_w+2,j,k}\right)$$

$$+\,\gamma^{n}_{I_w+\frac{1}{2},j,k}\left({}^{\ell}C^{n}_{I_w,j,k} - {}^{\ell}C^{n}_{I_w+1,j,k}\right)$$

$$\text{if } \alpha_{I_w+\frac{1}{2},j,k} < 0$$

In equation (3.5) the original term ${}^{\ell}C^{n}_{I_w-1,j,k}$ is replaced by ${}^{\ell}g^{n}_{I_w-\frac{1}{2},j,k}$, the value of the concentration outside the modeling region. The treatment at the eastern border (ξ_E) is analogous to that given for the western border above. It should be noted that in moving from grid cell to grid cell in the ξ direction, one need only compute

$$\frac{\Delta\tau}{\Delta\xi}\,{}^{\ell}F^{n}_{i+\frac{1}{2},j,k}$$

for grid cell (i, j, k) since

$$\frac{\Delta\tau}{\Delta\xi}\,{}^{\ell}F^{n}_{i-\frac{1}{2},j,k}$$

is available from the calculations performed in grid cell (i-1, j, k).

STEP II: Integration in the η Direction

In this step, the first level intermediate concentrations ${}^{\ell}C^{*}_{i,j,k}$ are advanced to the second level intermediate concentrations ${}^{\ell}C^{**}_{i,j,k}$ by the finite-difference analog of equation (3.2). These equations are the η direction counterparts of those given for Step I.

$${}^{\ell}C^{**}_{i,j,k} = {}^{\ell}C^{*}_{i,j,k} + \frac{\Delta\tau}{\Delta\eta\Delta H^{n}_{i,j}}\left({}^{\ell}F^{*}_{i,j-\frac{1}{2},k} - {}^{\ell}F^{*}_{i,j+\frac{1}{2},k}\right) \quad (3.6)$$

where

$$\frac{\Delta\tau}{\Delta\eta}\,{}^{\ell}F^{*}_{i,\,j-\frac{1}{2},\,k} = \frac{\beta^{n}_{i,\,j-\frac{1}{2},\,k}}{2}\left(3\,{}^{\ell}C^{*}_{i,\,j-1,\,k} - {}^{\ell}C^{*}_{i,\,j-2,\,k}\right)$$

$$+\,\delta^{n}_{i,\,j-\frac{1}{2},\,k}\left({}^{\ell}C^{*}_{i,\,j-1,\,k} - {}^{\ell}C^{*}_{i,\,j,\,k}\right)$$

$$\text{if } \beta^{n}_{i,\,j-\frac{1}{2},\,k} \geq 0$$

$$\frac{\Delta\tau}{\Delta\eta}\,{}^{\ell}F^{*}_{i,\,j-\frac{1}{2},\,k} = \frac{\beta^{n}_{i,\,j-\frac{1}{2},\,k}}{2}\left(3\,{}^{\ell}C^{*}_{i,\,j,k} - {}^{\ell}C^{*}_{i,\,j+1,\,k}\right)$$

$$+\,\delta^{n}_{i,\,j-\frac{1}{2},\,k}\left({}^{\ell}C^{*}_{i,\,j-1,\,k} - {}^{\ell}C^{*}_{i,\,j,\,k}\right)$$

$$\text{if } \beta^{n}_{i,\,j-\frac{1}{2},\,k} < 0$$

and

$$\beta^{n}_{i,\,j-\frac{1}{2},\,k} = \frac{v^{n}_{i,\,j-\frac{1}{2},\,k}\,\Delta H^{n}_{i,\,j-\frac{1}{2}}\,\Delta\tau}{\Delta\eta}$$

$$\delta^{n}_{i,\,j-\frac{1}{2},\,k} = \frac{K^{n}_{H_{i,\,j-\frac{1}{2},\,k}}\,\Delta H^{n}_{i,\,j-\frac{1}{2}}\,\Delta\tau}{\Delta\eta^{2}}$$

Using the expressions for the boundary conditions as given in equation (1.21), grid cells adjacent to the southern border (η_S) are treated as follows:

$${}^{\ell}C^{**}_{i,\,J_s,\,k} = {}^{\ell}C^{*}_{i,\,J_s,\,k} + \frac{\Delta\tau}{\Delta\eta\Delta H^{n}_{i,\,J_s}}\left({}^{\ell}F^{*}_{i,\,J_s-\frac{1}{2},\,k} - {}^{\ell}F^{*}_{i,\,J_s+\frac{1}{2},\,k}\right)$$

where

$$\frac{\Delta\tau}{\Delta\eta}\,{}^{\ell}F^{*}_{i,\,J_s-\frac{1}{2},\,k} = \left(\beta^{n}_{i,\,J_s-\frac{1}{2},\,k}\right){}^{\ell}g^{n}_{i,\,J_s-\frac{1}{2},\,k} \quad \text{if } \beta^{n}_{i,\,J_s-\frac{1}{2},\,k} \geq 0$$

$$\frac{\Delta\tau}{\Delta\eta}\,{}_{\ell}F^{*}_{i,\,J_s-\frac{1}{2},\,k} = \frac{\beta^{n}_{i,\,J_s-\frac{1}{2},\,k}}{2}\left(3\,{}_{\ell}C^{*}_{i,\,J_s,\,k} - {}_{\ell}C^{*}_{i,\,J_s+1,\,k}\right)$$

$$\text{if } \beta^{n}_{i,\,J_s-\frac{1}{2},\,k} < 0$$

$$\frac{\Delta\tau}{\Delta\eta}\,{}_{\ell}F^{*}_{i,\,J_s+\frac{1}{2},\,k} = \frac{\beta^{n}_{i,\,J_s+\frac{1}{2},\,k}}{2}\left(3\,{}_{\ell}C^{*}_{i,\,J_s,\,k} - {}_{\ell}g^{n}_{i,\,J_s-\frac{1}{2},\,k}\right)$$

$$+\,\delta^{n}_{i,\,J_s+\frac{1}{2},\,k}\left({}_{\ell}C^{*}_{i,\,J_s,\,k} - {}_{\ell}C^{*}_{i,\,J_s+1,\,k}\right)$$

$$\text{if } \beta^{n}_{i,\,J_s+\frac{1}{2},\,k} \geq 0$$

$$\frac{\Delta\tau}{\Delta\eta}\,{}_{\ell}F^{*}_{i,\,J_s+\frac{1}{2},\,k} = \frac{\beta^{n}_{i,\,J_s+\frac{1}{2},\,k}}{2}\left(3\,{}_{\ell}C^{*}_{i,\,J_s+1,\,k} - {}_{\ell}C^{*}_{i,\,J_s+2,\,k}\right)$$

$$+\,\delta^{n}_{i,\,J_s+\frac{1}{2},\,k}\left({}_{\ell}C^{*}_{i,\,J_s,\,k} - {}_{\ell}C^{*}_{i,\,J_s+1,\,k}\right)$$

$$\text{if } \beta^{n}_{i,\,J_s+\frac{1}{2},\,k} < 0$$

The treatment of grid cells adjacent to the northern border (η_N) is analogous to that given for the southern border above.

STEP III: Integration in the ρ Direction

Having established values of ${}_{\ell}C^{**}_{i,\,j,\,k}$ from Step II, the integration sequence is completed by solving a finite-difference approximation of equation (3.3). These equations have been formulated in an implicit (Crank-Nicolson) manner to avert stability problems that might arise in the treatment of the diffusion term when the mixing depth is shallow. In addition, the implicit formulation is also more suitable for treating the nonlinear chemical reaction terms.

$$
{}_{\ell}C^{n+1}_{i,j,k} = {}_{\ell}C^{**}_{i,j,k}\,\frac{\Delta H^{n}_{i,j}}{\Delta H^{n+1}_{i,j}} + \frac{\Delta\tau}{2\Delta\rho\Delta H^{n+1}_{i,j}}\left({}_{\ell}F^{n+1}_{i,j,k-\frac{1}{2}} + {}_{\ell}F^{**}_{i,j,k-\frac{1}{2}}\right.
$$

$$
\left. - {}_{\ell}F^{n+1}_{i,j,k+\frac{1}{2}} - {}_{\ell}F^{**}_{i,j,k+\frac{1}{2}}\right) + \frac{\Delta\tau}{2\Delta H^{n+1}_{i,j}}\left({}_{\ell}R^{n+1}_{i,j,k}\,\Delta H^{n+1}_{i,j}\right.
$$

$$
\left. + {}_{\ell}R^{**}_{i,j,k}\,\Delta H^{n}_{i,j}\right) + \frac{\Delta\tau}{2\Delta H^{n+1}_{i,j}}\left({}_{\ell}S^{n+1}_{i,j,k}\,\Delta H^{n+1}_{i,j} + {}_{\ell}S^{n}_{i,j,k}\,\Delta H^{n}_{i,j}\right) \tag{3.7}
$$

where

$$
\frac{\Delta\tau}{\Delta\rho}\,{}_{\ell}F^{n+1}_{i,j,k-\frac{1}{2}} = \frac{\phi^{n+1}_{i,j,k-\frac{1}{2}}}{2}\left({}_{\ell}C^{n+1}_{i,j,k-1} + {}_{\ell}C^{n+1}_{i,j,k}\right)
$$

$$
+ \mu^{n+1}_{i,j,k-\frac{1}{2}}\left({}_{\ell}C^{n+1}_{i,j,k-1} - {}_{\ell}C^{n+1}_{i,j,k}\right) \qquad k = 2, 3, \ldots, K
$$

$$
\frac{\Delta\tau}{\Delta\rho}\,{}_{\ell}F^{**}_{i,j,k-\frac{1}{2}} = \frac{\phi^{n}_{i,j,k-\frac{1}{2}}}{2}\left({}_{\ell}C^{**}_{i,j,k-1} + {}_{\ell}C^{**}_{i,j,k}\right)
$$

$$
+ \mu^{n}_{i,j,k-\frac{1}{2}}\left({}_{\ell}C^{**}_{i,j,k-1} - {}_{\ell}C^{**}_{i,j,k}\right) \qquad k = 2, 3, \ldots, K
$$

and

$$
\phi^{n}_{i,j,k-\frac{1}{2}} = \frac{W^{n}_{i,j,k-\frac{1}{2}}\,\Delta\tau}{\Delta\rho}
$$

$$
\mu^{n}_{i,j,k-\frac{1}{2}} = \frac{K^{n}V_{i,j,k-\frac{1}{2}}\,\Delta\tau}{\Delta H^{n}_{i,j}\,\Delta\rho^{2}}
$$

From equation (1.18), the boundary conditions at the ground are:

(1) $\rho = 0$

$$
\frac{\Delta\tau}{\Delta\rho}\,{}_{\ell}F^{n+1}_{i,j,\frac{1}{2}} = \frac{\Delta\tau}{\Delta\rho}\,{}_{\ell}Q^{n+1}_{i,j}
$$

$$
\frac{\Delta\tau}{\Delta\rho}\,{}_{\ell}F^{**}_{i,j,\frac{1}{2}} = \frac{\Delta\tau}{\Delta\rho}\,{}_{\ell}Q^{n}_{i,j}
$$

where $k = \frac{1}{2}$ is equivalent to $\rho = 0$. The boundary conditions aloft are given in equation (1.19) and may be expressed in finite-difference form as follows:

$$\frac{\Delta\tau}{\Delta\rho} F^{n+1}_{i,j,K+\frac{1}{2}} = \left(\phi^{n+1}_{i,j,K+\frac{1}{2}}\right) {}_{\ell}g^{n+1}_{i,j,K+\frac{1}{2}} \quad \text{if} \quad \phi^{n+1}_{i,j,K+\frac{1}{2}} \leq 0$$

$$\frac{\Delta\tau}{\Delta\rho} {}_{\ell}F^{n+1}_{i,j,K+\frac{1}{2}} = \left(\phi^{n+1}_{i,j,K+\frac{1}{2}}\right) {}_{\ell}C^{n+1}_{i,j,K} \quad \text{if} \quad \phi^{n+1}_{i,j,K+\frac{1}{2}} > 0$$

$$\frac{\Delta\tau}{\Delta\rho} {}_{\ell}F^{**}_{i,j,K+\frac{1}{2}} = \left(\phi^{n}_{i,j,K+\frac{1}{2}}\right) {}_{\ell}g^{n}_{i,j,K+\frac{1}{2}} \quad \text{if} \quad \phi^{n}_{i,j,K+\frac{1}{2}} \leq 0$$

$$\frac{\Delta\tau}{\Delta\rho} {}_{\ell}F^{**}_{i,j,K+\frac{1}{2}} = \left(\phi^{n}_{i,j,K+\frac{1}{2}}\right) {}_{\ell}C^{**}_{i,j,K} \quad \text{if} \quad \phi^{n}_{i,j,K+\frac{1}{2}} > 0$$

where $k = K+\frac{1}{2}$ is equivalent to $\rho = 1$.

Note that the values of $W^{n}_{i,j,k}$ are obtained from equation (1.24).

At this point the following two topics require further discussion:

A. Step III applied to inert species

B. Step III applied to chemically reactive species

A. The Treatment of Inert Species

For those species which are treated as being chemically inert, the rate terms ${}_{\ell}R^{n}_{i,j,k}$ are set equal to zero. The difference equations for Step III reduce to a system of linear equations involving the values of ${}_{\ell}C^{n+1}_{i,j,k}$, for $1 \leq k \leq K$. The linear system for species ℓ can be written as follows:

$$\begin{bmatrix} b_1 & c_1 & & & & \\ a_2 & b_2 & c_2 & & & \\ & \ddots & \ddots & \ddots & & \\ & & a_{K-1} & b_{K-1} & c_{K-1} & \\ & & & a_K & b_K \end{bmatrix} \begin{bmatrix} {}^{n+1}_{\ell}C_{i,j,1} \\ {}^{n+1}_{\ell}C_{i,j,2} \\ \vdots \\ {}^{n+1}_{\ell}C_{i,j,K-1} \\ {}^{n+1}_{\ell}C_{i,j,K} \end{bmatrix} = \begin{bmatrix} y_1 \\ y_2 \\ \vdots \\ y_{K-1} \\ y_K \end{bmatrix}$$

where the elements of the matrix and the column vector on the right-hand side of the equation can easily be determined using the finite-difference expressions given in Step III. The algorithm used to solve this tridagonal system of linear equations is described in Section 3.4.

B. The Treatment of Chemically Reactive Species

The computation of vertical transport coupled with chemical reaction is the most complicated step in the numerical procedure, and thus this aspect of Step III will be discussed in more detail. Recall that reactive hydrocarbon (RHC), NO, NO_2, and O_3 are all coupled through the chemical reaction terms. Therefore, one is confronted with solving a system of nonlinear algebraic equations in 4K unknowns, where K is the number of vertical levels. In the present simulation effort, five vertical levels are employed, and so twenty nonlinear equations in twenty unknowns must be solved, where the

unknowns are the values of ${}_{\ell}C^{n+1}_{i,j,k}$, $1 \le k \le 5$, for RHC, NO, NO_2, and O_3.

To solve the system of nonlinear equations, a Newton iterative procedure is used. To begin, one introduces the iterates, ${}^{m}_{\ell}C^{n+1}_{i,j,k}$. Using equation (3.3), the initial values of the iterates, ${}^{o}_{\ell}C^{n+1}_{i,j,k}$, are given by the following slightly modified Taylor series expansion

$$
\begin{aligned}
{}^{o}_{\ell}C^{n+1}_{i,j,k} = {}_{\ell}C^{**}_{i,j,k} \frac{\Delta H^{n}_{i,j}}{\Delta H^{n+1}_{i,j}} + \frac{\Delta\tau}{\Delta\rho\ \Delta H^{n+1}_{i,j}} \left({}_{\ell}F^{**}_{i,j,k-\frac{1}{2}} - {}_{\ell}F^{**}_{i,j,k+\frac{1}{2}} \right) \\
+ \frac{\Delta\tau}{\Delta H^{n+1}_{i,j}} \left({}_{\ell}R^{**}_{i,j,k}\ \Delta H^{n}_{i,j} \right) + \frac{\Delta\tau}{2\Delta H^{n+1}_{i,j}} \left({}_{\ell}S^{n+1}_{i,j,k}\ \Delta H^{n+1}_{i,j} \right. \\
\left. + {}_{\ell}S^{n}_{i,j,k}\ \Delta H^{n}_{i,j} \right) \qquad (3.8)
\end{aligned}
$$

The difference expressions for the terms in equation (3.8) are given in the discussion of Step III above. Higher iterates are obtained by setting

$$
{}^{m+1}_{\ell}C^{n+1}_{i,j,k} = {}^{m}_{\ell}C^{n+1}_{i,j,k} + {}^{m}_{\ell}\delta C^{n+1}_{i,j,k} \qquad (3.9)
$$

Next, the right-hand side of equation (3.9) is substituted into the difference equations for Step III in place of ${}_{\ell}C^{n+1}_{i,j,k}$, and all quadratic terms involving ${}^{m}_{\ell}\delta\, C^{n+1}_{i,j,k}$ are neglected. The resulting system of linear equations can be written in the following form:

$$\begin{bmatrix} {}^{m}B_1 & E_1 & & & \\ A_2 & {}^{m}B_2 & E_2 & & \\ & \ddots & \ddots & \ddots & \\ & & A_{K-1} & {}^{m}B_{K-1} & E_{K-1} \\ & & & A_K & {}^{m}B_K \end{bmatrix} \begin{bmatrix} {}^{m}\delta X_1 \\ {}^{m}\delta X_2 \\ \vdots \\ {}^{m}\delta X_{K-1} \\ {}^{m}\delta X_K \end{bmatrix} = \begin{bmatrix} {}^{m}P_1 \\ {}^{m}P_2 \\ \vdots \\ {}^{m}P_{K-1} \\ {}^{m}P_K \end{bmatrix} \qquad (3.10)$$

where A_K, ${}^{m}B_k$, and E_k are 4 x 4 matrices, and ${}^{m}\delta X_k$ and ${}^{m}P_k$ are column vectors. The coefficient matrix is block-tridiagonal, and systems of equations in this form can be solved efficiently. The chemical reaction rate expressions are readily derived from the mechanism given in Table 1.3. The elements of each matrix and column vector in equation (3.10) are defined below.

$$A_k = a_k I \qquad k = 2, 3, \ldots, K$$

where

$$a_k = -\frac{1}{2\Delta H_{i,j}^{n+1}} \left(\frac{\phi_{i,j,k-\frac{1}{2}}^{n+1}}{2} + \mu_{i,j,k-\frac{1}{2}}^{n+1} \right)$$

and I is the 4 x 4 identity matrix.

$$E_K = e_k I \qquad k = 1, 2, \ldots, K-1$$

where

$$e_k = \frac{1}{2\Delta H^{n+1}_{i,j}} \left(\frac{\phi^{n+1}_{i,j,k+\frac{1}{2}}}{2} - \mu^{n+1}_{i,j,k+\frac{1}{2}} \right)$$

$$m_{B_k} = b_k \, I + \frac{\Delta\tau}{2} \, m_{D_k} \tag{3.11}$$

where

$$b_k = \begin{cases} 1 + \dfrac{1}{2\Delta H^{n+1}_{i,j}} \left(\dfrac{\phi^{n+1}_{i,j,k+\frac{1}{2}}}{2} + \mu^{n+1}_{i,j,k+\frac{1}{2}} \right) & k = 1 \\ 1 + \dfrac{1}{2\Delta H^{n+1}_{i,j}} \left(\dfrac{\phi^{n+1}_{i,j,k+\frac{1}{2}} - \phi^{n+1}_{i,j,k-\frac{1}{2}}}{2} + \mu^{n+1}_{i,j,k-\frac{1}{2}} + \mu^{n+1}_{i,j,k+\frac{1}{2}} \right) & k = 2, 3, \ldots, K-1 \\ 1 + \dfrac{1}{2\Delta H^{n+1}_{i,j}} \left(\dfrac{2\phi^{n+1}_{i,j,K+\frac{1}{2}} - \phi^{n+1}_{i,j,K-\frac{1}{2}}}{2} + \mu^{n+1}_{i,j,K-\frac{1}{2}} \right) & k = K, \; W^{n+1}_{i,j,K+\frac{1}{2}} > 0 \\ 1 + \dfrac{1}{2\Delta H^{n+1}_{i,j}} \left(- \dfrac{\phi^{n+1}_{i,j,K-\frac{1}{2}}}{2} + \mu^{n+1}_{k,j,K-\frac{1}{2}} \right) & k = K, \; W^{n+1}_{i,j,K+\frac{1}{2}} \leq 0 \end{cases}$$

$$m_{D_k} = \begin{bmatrix} d_{11} & d_{12} & d_{13} & d_{14} \\ d_{21} & d_{22} & d_{23} & d_{24} \\ d_{31} & d_{32} & d_{33} & d_{34} \\ d_{41} & d_{42} & d_{43} & d_{44} \end{bmatrix}$$

where

$$d_{11} = k_{11}O + k_{12}OH + k_{13}O_3$$

$$d_{12} = d_{21} = d_{14} = d_{41} = 0$$

$$d_{13} = k_{13}RHC$$

$$d_{22} = k_3O_3 + k_6NO_2 + k_9HO_2 + k_{14}RO_2$$

$$d_{23} = k_3NO$$

$$d_{24} = k_6NO - k_1$$

$$d_{31} = k_{13}O_3$$

$$d_{32} = k_3O_3$$

$$d_{33} = k_3NO + k_4NO_2 + k_{13}RHC$$

$$d_{34} = k_4O_3$$

$$d_{42} = k_6NO_2 - k_3O_3 - k_9HO_2 - k_{14}RO_2$$

$$d_{43} = k_4NO_2 - k_3NO$$

$$d_{44} = k_1 + k_4O_3 + k_5NO_3 + k_6NO + k_{10}HO_2 + k_{15}RO_2$$

and

$$RHC = {}^{m}_{1}C^{n+1}_{i,j,k}$$

$$NO = {}^{m}_{2}C^{n+1}_{i,j,k}$$

$$O_3 = {}^{m}_{3}C^{n+1}_{i,j,k}$$

$$NO_2 = {}^{m}_{4}C^{n+1}_{i,j,k}$$

The expressions for the steady-state species O, OH, HO_2, RO_2, and NO_3 appearing in the matrices ${}^{m}D_k$ are evaluated using the values of ${}^{m}_{\ell}C^{n+1}_{i,j,k}$. See Appendix B of Reynolds et al. (1973) for the expressions relating the concentrations of the steady-state

species to the concentrations of RHC, NO, NO_2 and O_3. The remaining terms in equation (3.10) are defined by:

$$ {}^{m}\delta X_k = \begin{bmatrix} {}^{m}_{1}\delta C^{n+1}_{i,j,k} \\ {}^{m}_{2}\delta C^{n+1}_{i,j,k} \\ {}^{m}_{3}\delta C^{n+1}_{i,j,k} \\ {}^{m}_{4}\delta C^{n+1}_{i,j,k} \end{bmatrix} $$

$$ {}^{m}P_k = P_k + {}^{m}\bar{P}_k \qquad (3.12) $$

where

$$ P_k = \begin{bmatrix} {}_{1}P_k \\ {}_{2}P_k \\ {}_{3}P_k \\ {}_{4}P_k \end{bmatrix} \quad \text{and} \quad {}^{m}\bar{P}_k = \begin{bmatrix} {}^{m}_{1}\bar{P}_k \\ {}^{m}_{2}\bar{P}_k \\ {}^{m}_{3}\bar{P}_k \\ {}^{m}_{4}\bar{P}_k \end{bmatrix} $$

and

$$ \ell P_k = \ell C^{**}_{i,j,k} \frac{\Delta H^{n}_{i,j}}{\Delta H^{n+1}_{i,j}} + \frac{\Delta\tau}{2\Delta\rho\Delta H^{n+1}_{i,j}} \left(\ell F^{**}_{i,j,k-\frac{1}{2}} - \ell F^{**}_{i,j,k+\frac{1}{2}} \right) $$

$$ + \frac{\Delta\tau}{2\Delta H^{n+1}_{i,j}} \left(\ell R^{**}_{i,j,k} \Delta H^{n}_{i,j} + \ell S^{n+1}_{i,j,k} \Delta H^{n+1}_{i,j} + \ell S^{n}_{i,j,k} \Delta H^{n}_{i,j} \right) $$

$$\overline{{}^{m}_{\ell}P}_{k} = - {}^{m}_{\ell}C^{n+1}_{i,j,k} + \frac{\Delta\tau}{2\Delta\rho\Delta H^{n+1}_{i,j}} \left({}^{m}_{\ell}F^{n+1}_{i,j,k-\frac{1}{2}} - {}^{m}_{\ell}F^{n+1}_{i,j,k+\frac{1}{2}} \right)$$

$$+ \frac{\Delta\tau}{2\Delta H^{n+1}_{i,j}} \left({}^{m}_{\ell}R^{n+1}_{i,j,k} \Delta H^{n+1}_{i,j} \right)$$

Note that each iteration involving the solution of equation (3.10) requires only the additional evaluation of ${}^{m}D_{k}$ and ${}^{m}\overline{P}_{k}$ before the system can be solved, since all other terms are invariant from one iteration to the next. Thus, the matrices A_{k}, $b_{k}I$, and E_{k} and the column vectors P_{k} are established once per integration time step. To perform an iteration, ${}^{m}D_{k}$ and ${}^{m}\overline{P}_{k}$ are evaluated, and using equations (3.11) and (3.12), the definition of the linear system given by equation (3.10) is completed. The method used to solve this block-tridiagonal system of linear equations is described in Section 3.4.

Upon solving equation (3.10) for values of ${}^{m}_{\ell}\delta C^{n+1}_{i,j,k}$, equation (3.9) is used to obtain an improved estimate of ${}^{m}_{\ell}C^{n+1}_{i,j,k}$. The iterative process is terminated when

$$\left| \frac{{}^{m}_{\ell}\delta C^{n+1}_{i,j,k}}{{}^{m}_{\ell}C^{n+1}_{i,j,k}} \right| \leq \epsilon$$

for all ℓ and k in each column of grid cells. For the present simulation study, $\epsilon = 0.01$.

This completes the presentation of Step III of the numerical integration procedure. Attention is now focused on stability characteristics of the difference equations. The basic statement that can be made with regard to stability is that if each step is stable, then

the entire procedure is stable. Thus, each step is examined individually to determine the conditions for stability. Step I is analyzed first. To facilitate the analysis, the values of u, ΔH, and K_H are assumed constants, and using the stability criteria given by Price et al. (1966), the following expression is obtained:

$$\frac{u\Delta\tau}{\Delta\xi} + \frac{K_H\Delta\tau}{\Delta\xi^2} \leq \frac{1}{2}$$

A similar expression for Step II is obtained after making the analogous assumptions

$$\frac{v\Delta\tau}{\Delta\eta} + \frac{K_H\Delta\tau}{\Delta\eta^2} \leq \frac{1}{2}$$

Typically, the left-hand sides of these expressions are less than 0.3 for a grid spacing of two miles and a time step of four minutes (values of the spatial and temporal step sizes employed in this study).

Step III is more difficult to analyze since the equations are both coupled and nonlinear. One can, however, state the conditions for stability when the equations are linear, that is, when $R_\ell = 0$. Since the Crank-Nicolson treatment is employed in this step, the solution is stable for all values of $\Delta\tau$. One must rely on numerical experimentation and experience to ascertain if the treatment of the full nonlinear set of equations is stable. As of this writing, no evidence of instability has ever been observed in over a dozen photochemical simulations.

The final aspect of the finite-difference solution technique worthy of further consideration is the error introduced by using discrete difference approximations for the various spatial and temporal

partial derivatives in the governing equations. As noted previously, particular attention must be given to the treatment of the horizontal transport terms. While a complete truncation error analysis of the method would be a substantial algebraic undertaking, the following abbreviated analysis gives a reasonable estimate of the nature and magnitude of the numerical errors. Consider the difference approximation in Step I for the advection term $\frac{\partial u\, c_\ell}{\partial \xi}$, where for simplicity it is assumed that ΔH is a constant and thus cancels from all terms involving horizontal transport in the governing equations. The horizontal advection approximation may be written as follows:

$$\left.\frac{\partial u\, c_\ell}{\partial \xi}\right|^{n}_{i,j,k} \cong \frac{u^{n}_{i+\frac{1}{2},j,k}}{2\Delta\xi}\left(3_\ell c^{n}_{i,j,k} - {}_\ell c^{n}_{i-1,j,k}\right) - \frac{u^{n}_{i-\frac{1}{2},j,k}}{2\Delta\xi}\left(3_\ell c^{n}_{i-1,j,k} - {}_\ell c^{n}_{i-2,j,k}\right)$$

Expanding each term in the right hand side of the above approximation and combining terms results in the following expression:

$$\frac{\partial u\, c_\ell}{\partial \xi} + \Delta\xi^2\left(\frac{1}{24}\frac{\partial^3 u}{\partial \xi^3} c_\ell + \frac{1}{8}\frac{\partial^2 u}{\partial \xi^2} - \frac{1}{4}\frac{\partial u}{\partial \xi}\frac{\partial^2 c_\ell}{\partial \xi^2} + \frac{1}{6}\, u\frac{\partial^3 c_\ell}{\partial \xi^3}\right) + O(\Delta\xi^3)$$

Paying particular attention to those terms not involving the third derivative of either c_ℓ or u, the truncation term can be rewritten as:

$$\frac{\partial\left(u + \frac{\Delta\xi^2}{8}\frac{\partial^2 u}{\partial \xi^2}\right)c_\ell}{\partial \xi} - \left(\frac{\Delta\xi^2}{4}\frac{\partial u}{\partial \xi}\right)\frac{\partial^2 c_\ell}{\partial \xi^2} + O(\Delta\xi^2)$$

where the terms included in $O(\Delta\xi^2)$ do not have any physical significance. Note that the difference scheme causes advection velocity errors on the order of $\frac{\Delta\xi^2}{8}\frac{\partial^2 u}{\partial\xi^2}$, and also note that the numerical, or artificial, diffusivity is given by $\frac{\Delta\xi^2}{4}\frac{\partial u}{\partial\xi}$. If a similar analysis were performed on the first-order finite-difference representation of the advection term, it would be found that the velocity error is $-\frac{\Delta\xi}{2}\frac{\partial u}{\partial\xi}$, and the numerical diffusivity is $\frac{\Delta\xi}{2}u$. Thus, it is apparent that the effect of using a higher-order advection technique is to cause the errors with physical significance to be functions of higher derivatives of the wind velocity.

To obtain an estimate of the magnitude of the errors in the transport velocity and dispersion, typical values for $\frac{\partial u}{\partial\xi}$ and $\frac{\partial^2 u}{\partial\xi^2}$ may be substituted in the error expressions cited above. Approximating the order of magnitude of the derivatives of u by the following expressions:

$$\frac{\partial u}{\partial\xi} \cong \frac{\Delta u}{\Delta\xi}$$

$$\frac{\partial^2 u}{\partial\xi^2} \cong \frac{\Delta u}{\Delta\xi^2}$$

and assuming that Δu is 2 mph over a grid spacing of 2 miles, the velocity error and numerical diffusivity are given by

$$\frac{\Delta\xi^2}{8}\frac{\partial^2 u}{\partial\xi^2} \cong \frac{\Delta u}{8} = .25 \text{ mph}$$

$$\frac{\Delta\xi^2}{4}\frac{\partial u}{\partial\xi} \cong \frac{\Delta u \Delta_\xi}{4} = 720 \frac{m^2}{sec}$$

From these estimates it is apparent that the error in the transport velocity is certainly comparable, if not less, than the inherent

uncertainty in the wind data itself. Unfortunately, the numerical diffusivity is much larger than the assumed value of 50 m^2/sec employed in this study. However, the numerical diffusivity cited above is comparable to value of 500 m^2/sec employed by Shir and Shieh (1973) and Eschenroeder (1973), and the value of 800 m^2/sec employed by Lamb (1972). While the true magnitude of the horizontal turbulent diffusivity is somewhat in doubt, it is clear that further improvements in the numerical method must be made if the horizontal diffusion process is to be treated accurately. Recall, however, that the primary mechanism for horizontal transport is advection, and considering the uncertainties in the meteorological and emission inputs to the model, the numerical method described in this section should be sufficiently accurate for this initial formulation of the model.

3.4 Methods for Solving the Linear Systems of Equations

In Step III of the numerical integration procedure, two systems of linear equations must be solved, each of the form

$$Ax = y$$

where the characteristics of the matrix A distinguish the first system from the second. The two forms assumed by matrix A are tridiagonal and block-tragonal, respectively. A tridiagonal matrix of order n can be written in the following manner:

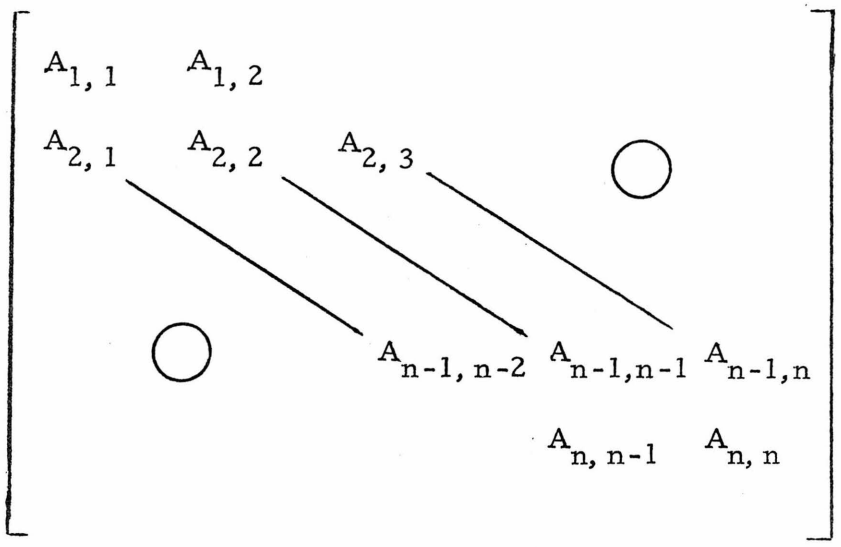

The block-tridiagonal matrix assumes the same form, but the distinguishing feature is that each element, $A_{i,j}$, is itself an m x m matrix. Thus the order of the matrix in this case is n•m. Note that the tridiagonal matrix is actually a block-tridiagonal matrix with m = 1. The algorithm employed to solve the block-tridiagonal system is equivalent to that used to solve the tridiagonal system, but each shall be treated separately for two reasons. First, the recursion formulas for the tridiagonal system are particularly simple to formulate; whereas, the recursion formulas for the block-tridiagonal system involve matrix inversions which need to be discussed in further detail. Second, it is desirable to formulate the algorithms using notation similar to that found in the computer codes described in Reynolds (1973).

3.4.1 The Algorithm for the Tridiagonal System

As the algorithm adopted for the solution of a tridiagonal system of linear equations is described in detail by Conte (1965),

only a summary of the recursive formulas is given here. To solve the following system of linear equations:

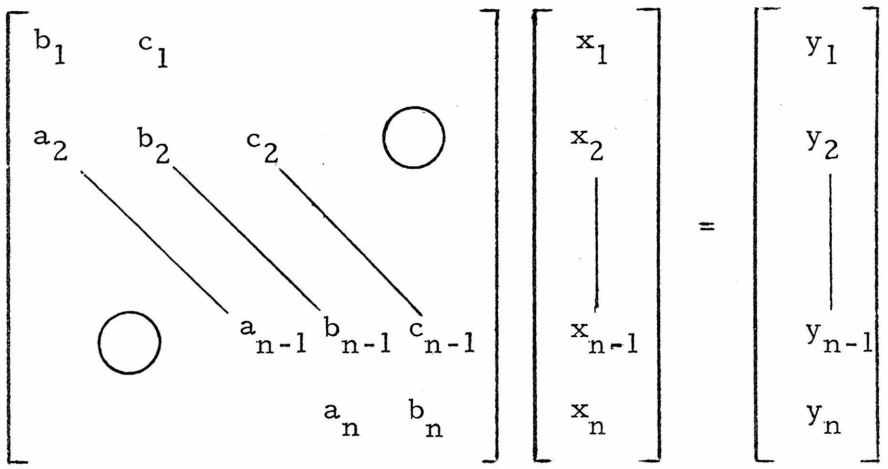

the solution vector x is obtained from the following four-step procedure:

(1) $\omega_1 = b_1$

$z_1 = y_1/\omega_1$

(2) Compute ω_i and z_i from

$$\omega_i = b_i - a_i c_{i-1}/\omega_{i-1}$$

$$i = 2, 3, \ldots, n-1$$

$$z_i = (y_i - a_i z_{i-1})/\omega_i$$

(3) Set: $\omega_n = b_n - a_n c_{n-1}/\omega_{n-1}$

(4) Solve for the solution vector

$$x_n = (y_n - a_n z_{n-1})/\omega_n$$

$$x_{n-i} = z_{n-i} - c_{n-i} x_{n-i+1}/\omega_{n-i} \qquad i = 1, 2, \ldots, n-1$$

3.4.2 The Algorithm for the Block-Tridiagonal System

The algorithm described in this section is fashioned after that given by Isaacson and Keller (1966). Consider the following block-tridiagonal system of linear equations:

$$Ax = f \tag{3.13}$$

is written as:

$$\begin{bmatrix} B_1 & C_1 & & & \\ A_2 & B_2 & C_2 & & \\ & \ddots & \ddots & \ddots & \\ & & A_{n-1} & B_{n-1} & C_{n-1} \\ & & & A_n & B_n \end{bmatrix} \begin{bmatrix} x_1 \\ x_2 \\ \vdots \\ x_{n-1} \\ x_n \end{bmatrix} = \begin{bmatrix} f_1 \\ f_2 \\ \vdots \\ f_{n-1} \\ f_n \end{bmatrix}$$

A_i, B_i, and C_i are m x m matrices, and x_i and f_i are m-component column vectors. The coefficient matrix is written as the product of lower and upper triangular matrices in the following manner:

$$A = LU = \begin{bmatrix} D_1 & & & \\ A_2 & D_2 & & \\ & \ddots & \ddots & \\ & & A_n & D_n \end{bmatrix} \begin{bmatrix} I & \Gamma_1 & & \\ & I & \ddots & \\ & & \ddots & \Gamma_{n-1} \\ & & & I \end{bmatrix}$$

If each element in A is equated with each element in the matrix formed by the produce LU, the following identities can be written:

$$D_1 = B_1$$
$$\Gamma_1 = D_1^{-1} C_1 \tag{3.14}$$

$$D_i = B_i - A_i \Gamma_{i-1} \qquad i = 2, 3, \ldots, n$$
$$\Gamma_i = D_i^{-1} C_i \qquad i = 2, 3, \ldots, n-1 \tag{3.15}$$

Defining a new vector y, note that equation (3.13) is equivalent to

$$Ly = f \tag{3.16}$$
$$Ux = y \tag{3.17}$$

One proceeds by solving equation (3.16) for y, and then solving equation (3.17) for x, which is the desired solution. The first step can be written as:

$$y_1 = D_1^{-1} f_1 \tag{3.18}$$

$$y_i = D_i^{-1} (f_i - A_i y_{i-1}) \qquad i = 2, 3, \ldots, n \tag{3.19}$$

and the second step is given by:

$$x_n = y_n$$

$$x_{n-i} = y_{n-i} - \Gamma_{n-i} x_{n-i+1} \qquad i = 1, 2, \ldots, n-1$$

The algorithm given above is formally correct, but it can be improved upon computationally in the following way. The following equivalent expressions are written for equations (3.14) and (3.18), and equations (3.15) and (3.19):

$$D_1 \left(\Gamma_1 \vdots y_1 \right) = \left(C_1 \vdots f_1 \right)$$

$$D_i \left(\Gamma_i \vdots y_i \right) = \left(C_i \vdots f_i - A_i y_{i-1} \right) \qquad i = 2, 3, \ldots, n$$

where the parentheses and dotted line indicate a partitioned matrix.*

The algorithm is now summarized in its final form.

(1) Set $D_1 = B_1$

(2) Solve for Γ_1 and y_1

$$D_1 \left(\Gamma_1 \vdots y_1 \right) = \left(C_1 \vdots f_1 \right)$$

(3) Set $D_i = B_i - A_i \Gamma_{i-1}$

$$i = 2, 3, \ldots, n$$

$$\overline{f}_i = f_i - A_i y_{i-1}$$

(4) Solve for Γ_i and y_i

$$D_i \left(\Gamma_i \vdots y_i \right) = \left(C_i \vdots \overline{f}_i \right) \qquad i = 2, 3, \ldots, n$$

(5) Set $x_n = y_n$

$$x_{n-i} = y_{n-i} - \Gamma_{n-i} x_{n-i+1} \qquad i = 1, 2, \ldots, n-1$$

The m+1 linear systems in steps (2) and (4) are solved by Gaussian elimination.

---

* The partitioned matrix $(\Gamma_1 \vdots y_1)$ is formed by combining the m x m matrix Γ_1 with the m x 1 matrix y_1 to form a m x (m + 1) matrix.

3.5 Discussion of the Numerical Method

In the preceding sections a comprehensive description of the computational procedures used to solve the governing equations has been given. This section is devoted to a summary of the pertinent experience gained in the formulation, testing, and application of the finite-difference technique, as these experiences have had a direct bearing on the final numerical procedure adopted for use in this study. A summary of tests conducted with various high and low-order advection difference formulations has already been discussed in Section 3.2. It was found that a second-order advection scheme described by Price et al. (1966) proved to be the most satisfactory of those methods considered. In selecting a difference scheme for use in photochemical calculations, one must be concerned not only with the accuracy of the method but also with the fact that the method must not predict negative concentrations, which, of course, lead to physically erroneous results. It should also be noted that while some difficulty has been encountered in the treatment of horizontal transport, similar difficulties have not occurred in the calculation of vertical advection and diffusion. Since the vertical concentration distribution is relatively smooth, and since turbulent diffusion is the primary mechanism for vertical transport, no problems have arisen from using finite-difference methods to approximate the equations in Step III. For convenience, a centered, second-order approximation is employed to represent the advection term $\frac{\partial W c_\ell}{\partial \rho}$.

In addition to studying advection approximations for use in Steps I and II, tests were also conducted of the finite-difference

formulation used in Step III. The primary objective of this test was to evaluate the numerical treatment of the nonlinear chemical reaction terms. First, all wind velocities and surface emissions fluxes were set equal to zero in a particular column of grid cells. Then a uniform distribution of each pollutant was established in the column of cells, followed by the integration of the governing equations. Note that the governing equations reduce to the following form:

$$\frac{\partial c_\ell}{\partial t} = R_\ell \qquad \ell = 1, 2, \ldots, N \tag{3.20}$$

which may be recognized as the ordinary differential equations employed in simulating smog chamber experiments. Equations (3.20) were solved using the method developed by Gear (1971). The Gear routine is employed to provide an accurate set of predicted concentrations with which to compare analogous results obtained from the difference scheme used in Step III. Using the following initial conditions:

$$\begin{aligned} \text{RHC} &= 40 \text{ pphm} \\ \text{NO} &= 20 \text{ pphm} \\ \text{O}_3 &= 0.5 \text{ pphm} \\ \text{NO}_2 &= 5 \text{ pphm} \\ \text{CO} &= 10 \text{ ppm} \end{aligned}$$

and rate constants typical of those used in simulation studies of the Los Angeles airshed, it was found that, after two hours, paired sets of results agreed to within 2% for all species. The finite-difference results were obtained using a four-minute time step and a relative error tolerance of 1%, while the results from the Gear routine were obtained using a one-minute time step.

To determine the effect that the size of the integration time step has on the predicted concentrations, two simulations were performed, identical in all respects except for the size of the time step. The time period 11 A.M. to 1 P.M. PST was chosen since the photolysis rate constants are largest at this time of day. A normal simulation starting at 5 A.M. PST was performed and terminated at 11 A.M. The results obtained at 11 A.M. were then used as the initial conditions for the test. The two integrations were performed using one-minute and four-minute time steps. For purposes of comparison, the percentage difference between the two results in each grid cell was calculated at 1 P.M. using the following relationship:

$$\% \text{ Difference} = \left| \frac{C(1)-C(4)}{C(1)} \right| \times 100\ \%$$

where

C(1) = result using a 1-minute time step

C(4) = result using a 4-minute time step.

Both the average and maximum percentage differences were computed for each species, and the results are presented below:

Species	Average % Difference	Largest % Difference
RHC	0.9	3.1
NO	2.2	6.9
O_3	1.8	6.3
NO_2	1.4	2.1
CO	0.8	4.9
URHC	0.6	2.9

These results indicate that a four-fold increase in the computational effort was accompanied by only a marginal change in the predicted concentrations.

Based on the results presented above, a four-minute maximum time step was adopted for this study. In some instances, however, it is necessary to reduce the size of the time step. For example, if a negative concentration is ever predicted, then the size of the time step is decreased, and the integration sequence is reinitiated. Note that negative numbers may be predicted by the horizontal advection scheme if the time step is too large. The time step size is also reduced whenever the iterative procedure in Step III fails to converge in a reasonable number of iterations (say 20). The relative error tolerance was chosen as 0.01 to insure that the Newton iterative process had converged, or at least that the concentrations were not changing by more than one percent.

The final observation to be made with regard to the numerical scheme deals with the order in which equations (3.1) - (3.3) are processed computationally. Note that there is no particular reason to integrate in the ξ direction first; in fact, it is just as reasonable to integrate in the η direction first. To reduce the possibility of introducing a bias into the predictions that might result from employing a fixed integration sequence, the following rule is applied regarding the order in which equations (3.1)-(3.3) are integrated:

	Computational Order		
	Step I	Step II	Step III
odd-numbered time steps:	ξ-direction	η-direction	ρ-direction
even-numbered time steps:	η-direction	ξ-direction	ρ-direction

Thus the integration sequence is ξ-η-ρ, η-ξ-ρ, ξ-η-ρ, etc. In Section 3.3, the algorithm for the ξ-η-ρ sequence is given. The algorithm for the η-ξ-ρ sequence differs from the ξ-η-ρ sequence only in that values of

$$_{\ell}C^{*}_{i,j,k}$$

are determined from the finite-difference representation of equation (3.2), and values of

$$_{\ell}C^{**}_{i,j,k}$$

are determined from the finite-difference approximation of equation (3.1).

CHAPTER 4

EVALUATION OF THE MODEL

4.1 Introduction

A general model for the prediction of the three-dimensional, time-dependent behavior of photochemical air pollutants in an urban airshed was formulated in Chapter 1. The Los Angeles airshed was chosen as the region for initial application and validation of the model primarily because of the existence of an extensive meteorological and air quality monitoring network in the area. The treatment of the wind and inversion behavior in the Los Angeles airshed was presented in Chapter 1, together with a kinetic mechanism describing the chemical reactions that take place in the atmosphere. The other major component of the model, the source emissions inventory, and the numerical integration procedure, were the subjects of Chapters 2 and 3, respectively. The objective of this Chapter is to present the results obtained using the model to predict concentrations of CO, hydrocarbons, NO, NO_2, and O_3 on six different days in 1969, and to compare the predictions with actual air monitoring data.

The purpose of model validation is to determine to what degree confidence may be placed in the predictions obtained from the model. To make this determination, the airshed model is used to recreate the temporal and spatial distribution of air pollutants in the region of interest, preferably on several typical days. Then comparisons of the predictions with available measurements are made and conclusions are drawn as to the success or failure of the validation effort.

A discussion of the meteorological inputs is given in Chapter 1 and the source emissions inventory is presented in Chapter 2. In addition, a kinetic mechanism for the atmospheric chemical reactions was given in Chapter 1. However, rate constants and stoichiometric coefficients appropriate for the atmosphere must be determined. Therefore, the determination of these parameters through comparison of the predictions of the kinetic mechanism with laboratory smog chamber data is discussed in Section 4.2. Of particular importance is the estimation of rate constants and stoichiometric coefficients for the reactions involving different classes of hydrocarbons, such as paraffins, olefins, and aromatics.

In initial airshed validation studies for CO, it was frequently observed that the atmospheric measurements were substantially higher than the model predictions, especially during the peak traffic hours in the morning. This discrepancy was soon recognized, in many instances, to be attributable to the fact that many of the monitoring stations are situated near heavily-travelled streets and thus tend to record elevated CO concentrations. Since the full airshed model has a maximum spatial resolution equivalent to the grid spacing used in the numerical solution of the partial differential equations (in the present case, two miles), the model is incapable of resolving these local effects. Nevertheless, the performance of the model is to be judged by comparing its predictions for the average concentrations in each four square mile area that contains a monitoring station with the data from that station. To account for these subgrid scale effects, a microscale model is employed in conjunction with the

airshed model, as discussed in Section 4.3. The microscale model is used to predict "local corrections" for model predictions for several grid squares in which the monitoring station is located in the vicinity of a busy roadway.

The validation of the full airshed model is carried out in two steps. First, the model is evaluated for CO in order to test the treatment of meteorological variables, portions of the numerical integration technique, and the source emissions inventory. Then validation studies are carried out for hydrocarbons, NO, NO_2, and O_3. Section 4.4 is devoted to a detailed description of the validation procedure and the results obtained.

4.2 Validation of the Kinetic Mechanism

The kinetic mechanism, discussed in Chapter 1, is a concise representation of the chemical reactions that take place in photochemical air pollution. For the mechanism to be useful in airshed modeling, values of all rate constants and stoichiometric coefficients must be determined. The most convenient means for estimating these parameters is through the controlled validation of the mechanism using concentration-time histories measured in laboratory smog chamber experiments. To insure that the mechanism is accurate over a wide range of conditions, validation studies must be carried out for different types of hydrocarbons and hydrocarbon mixtures as well as for various initial reactant ratios and light intensities. The discussion given in this section is a summary of the extensive validation work presented in Appendix B of Reynolds et al. (1973). Before presenting

validation results, a brief description is given of the data base employed.

4.2.1 The Data Base

The significance of the validation results for a kinetic mechanism is, to a large degree, dependent upon the diversity and reliability of the experimental data base. Experimental data for this study involving both high and low reactivity hydrocarbons, as well as simple mixtures and auto exhaust, were supplied by the Division of Chemistry and Physics of the Environmental Protection Agency. The data were comprised of the following four hydrocarbon-NO_x systems:

1. Toluene - NO_x at five different initial reactant ratios;
2. Toluene-n-butane-NO_x at three different initial reactant ratios;
3. Propylene-ethane-NO_x at four different initial reactant ratios; and
4. Auto exhaust at two different initial reactant ratios.

All chamber runs were made between June 1966 and March 1967 by the staff of the Chemical and Physical Research and Development Program at the National Center for Air Pollution Control (Altshuller et al., 1967ab, 1969, 1970).

The experiments are best specified by a statement of initial conditions, as given in Table 4.1. Duplicate experiments were carried out for all but two sets of initial conditions, both for the propylene-ethane-NO_x system. In general, the experimental run in each replicate pair having the smoother concentration-time profiles and the

smaller loss of NO_x prior to the NO_2 maximum were selected for model validation. Other aspects of the experimental studies, including the determination of light intensity and water concentration, wall effects, and the accuracy of the analytical measurements are discussed in detail in Appendix B of Reynolds et al. (1973).

It appears that in general, the data are reproducible, were carefully taken, and are as suitable as any currently available for validation purposes. Probably the most serious weakness in the chamber data with regard to their use in validation is the lack of precise knowledge of the light intensity. As will be shown in Section 4.2.2, the magnitude of light intensity has a substantial effect on the speed of the overall reaction process, as evidenced by the time at which the NO_2 maximum occurs.

4.2.2 Validation Procedure

Validation of the kinetic mechanism consists of:

1. Obtaining estimates of the various parameters in the mechanism -- the reaction rate constants and the generalized stoichiometric coefficients -- and establishing, when appropriate, how these parameters vary with changes in the species and composition of hydrocarbons in the reactant mixture;
2. Carrying out sensitivity studies for these parameters, i.e., establishing the effect of controlled variations in the magnitudes of the various parameters on the concentration/time profiles for NO, NO_2, O_3, and hydrocarbon;

3. Generating concentration/time profiles for the various reactant mixtures using specified initial conditions. These predictions are then compared with experimental results to assess the "goodness of fit."

In the next sections, the discussion will focus on the basis for selection of some of the more uncertain parameters, notably the rate constants for the hydrocarbon oxidation reactions (with O, O_3, and OH) and the generalized stoichiometric coefficients α, β, γ, and ϵ. (See Table 1.3 for a statement of the mechanism.)

4.2.2.1 Estimation of Rate Constants

While the kinetic mechanism is both general and compact, it is formulated in such a way that the majority of rate constants may be taken from the literature dealing with the study of individual reaction steps. However, due to the generalized nature of the model, some rate constants, of necessity, are artifacts, notably those specified for reactions 6, 11, 12, 13, and 15. All other rate constants have been estimated from the results of experiments reported in the literature; their magnitudes are given in Table 4.2.

The rate constant for reaction 6 was selected such that a model based on four differential equations, with HNO_2 at steady state, gives predictions comparable with those of a model in which a differential equation for HNO_2 is included. The rationale for this decision was discussed in Section 1.5.

The results of early validation runs indicated that the literature values of k_{11} (O+ RHC), as given by Johnston et al. (1970), are too low to account for the observed oxidation rate of hydrocarbons and

Table 4.1 Initial Conditions Associated with Experimental Chamber Data

EPA No.	HC Type	Initial Concentrations, ppm $[NO_2]_o$	$[NO]_o$	$[HC]_o$
300	Toluene	.02	1.25	3.22
258	Toluene	.05	.35	2.88
250	Toluene	.04	1.17	1.53
272	Toluene	.04	.55	1.67
271	Toluene	.05	.32	1.20
251	n-Butane-toluene	.07	1.10	4.62†
253	n-Butane-toluene	.08	.53	4.91†
257	n-Butane-toluene	.07	.27	4.26†
318	Propylene-ethane	.06	1.12	.51‡
325	Propylene-ethane	.04	.35	.45‡
321	Propylene-ethane	.10	1.31	.275‡
329	Propylene-ethane	.05	.26	.24‡
222	Auto Exhaust	.12	1.95	2.21*
231	Auto Exhaust	.23	2.80	.61*

† combined total of n-butane and toluene

‡ propylene only (the ethane was virtually unreactive)

* combined total of all hydrocarbons in the auto exhaust

Table 4.2 Base Values of Reaction Rate Constants

$k_1 = 0.266\ min^{-1}$	$k_6 = 5 \times 10^{-4}\ ppm^{-1} min^{-1}$
$k_2 = 2.76 \times 10^{6}\ min^{-1}$*	$k_7 = 5 \times 10^{-3} min^{-1}$
$k_3 = 21.8\ ppm^{-1} min^{-1}$	$k_8 = 1.8 \times 10^{3}\ ppm^{-1} min^{-1}$
$k_4 = 0.006\ ppm^{-1} min^{-1}$	$k_9 = 1.8 \times 10^{3}\ ppm^{-1} min^{-1}$
$k_5 = 0.1\ ppm^{-1} min^{-1}$	$k_{10} = 10\ ppm^{-1} min^{-1}$
$k_{14} = 1.8 \times 10^{3}\ ppm^{-1} min^{-1}$	

* Pseudo-first order

Note: Rate constants for reactions 11, 12, 13, 15, and 16-18 are given subsequently in Table 4.4. For values of k_{19} see Appendix B of Reynolds et al. (1973). Studies upon which the above values are based have been summarized by Johnston et al. (1970).

the oxidation of NO to NO_2 when employed in the general mechanism given in Chapter 1. Oxidation of hydrocarbons by O atoms is most important early in the photo-oxidation process. A number of other reactions, for example, the oxidation of hydrocarbons by oxygen-containing free radicals, have been excluded from the mechanism for the sake of compactness. These reactions, although not thought to be particularly rapid, may play an important role early in the smog forming process by competing with O atom attack on hydrocarbons. Consequently, values of k_{11} higher than those reported in the literature have been adopted to account for the early loss rate of hydrocarbon observed experimentally. Note, however, that the influence of other reactions, such as the OH-hydrocarbon reaction become relatively

greater as the smog reactions proceed. The contribution of reaction 11 to the overall hydrocarbon loss rate thus becomes less significant with time.

In general, it was possible to use literature values for k_{12} and k_{13}, the rate constants for the OH and O_3-hydrocarbon reactions, for the validation runs [see Johnston et al. (1970)]. In cases where O_3 does not react directly with the hydrocarbon, a small residual value of k_{13} has been assigned to account for the reaction of ozone with hydrocarbon oxidation products. For example, in the case of n-butane, it is possible that various butenes form subsequent to O or OH attack on the hydrocarbon. The reaction of these butenes with O_3 is accounted for through the artificial increase in k_{13}.

Finally, the value of k_{15} was selected so that, on a qualitative basis, the predicted concentration/time profiles of organic nitrates and pernitrates formed as reaction products conformed with expected behavior. The observed rate of loss of NO_2 after the NO_2 peak was also taken into account in estimating the magnitude of this constant.

4.2.2.2 Estimation of Generalized Stoichiometric Coefficients

Stoichiometric coefficients are those parameters introduced into each individual reaction step to satisfy the requirement of conservation of mass. While these coefficients, in general, are easily established by carrying out a mass balance for all elements appearing in the reaction expression, a problem arises in the treatment of vaguely defined species such as the generalized hydrocarbon, RHC. The exact number of atoms that comprise this fictitious species cannot be specified, and thus it is impossible to derive or compute

appropriate coefficients. To skirt this problem, flexible parameters, termed "generalized" stoichiometric coefficients are introduced (such as in the reaction, $HC + O \xrightarrow{11} \alpha RO_2$). These generalized coefficients must be established through deductive procedures such as "chemical" arguments and trial and error calculations. In the discussion that follows, the rationale for selecting the generalized coefficients α, β, γ, and ϵ introduced in the mechanism is presented.

Consider the selection of a value of α, the number of radicals formed in the reaction of hydrocarbons and atomic oxygen. This choice is of prime importance, as α strongly governs the chain length of the reaction, and the hydrocarbon-atomic oxygen reaction itself is critical in determining the rate of oxidation of NO to NO_2. Values of α used in validation were established by comparison of predicted and observed concentrations of NO and hydrocarbon.

The stoichiometric coefficient γ is determined by comparing predicted and observed concentrations of a reaction system in which an olefin is the principal reacting hydrocarbon. The magnitude of the coefficient is selected so as to minimize discrepancies between the predicted and observed hydrocarbon loss rate after the NO_2 peak and between the maximum predicted and observed ozone levels ultimately attained. Because most C_3 and greater hydrocarbons can form olefins as degradation products, the value of γ is the same for all hydrocarbon systems.

The stoichiometric coefficient β in reaction 12 is analogous to α and γ, in that it governs the number of RO_2 radicals formed due to reaction of hydrocarbons -- in this instance, with hydroxyl radicals.

As in the case of the other generalized stoichiometric coefficients, β is treated as a constant for a given hydrocarbon system. In general β will be about one since likely products of the HC-OH reaction are one free radical and an aldehyde (in the case of olefins) or water (in the case of paraffins).

The stoichiometric coefficient ϵ, the number of moles of OH formed per mole of RO_2 that reacts with NO, provides a means of accounting for the fact that a certain fraction of the RO_2 chains result in the regeneration of an OH radical. While ϵ is basically an empirical parameter, its value, along with that of β, can be determined from experimental data for reaction systems in which the initial charge of CO varies from zero to some substantial concentration. The product of β and ϵ will determine the amount by which the time to the NO_2 maximum is shortened for a given increase in CO concentration. In addition to making these qualitative observations, quantitative limits for the product $\beta\epsilon$ can also be specified. In particular, in order for CO to exert an accelerating influence on the reaction system, it is necessary that that the product $\beta\epsilon$ be less than one. (This condition can be verified by inspection of the rate equation for NO concentration.) In general, observed reductions in time to the NO_2 peak are greatest in the presence of CO when the hydrocarbon components of the system are of low reactivity and least when reactant systems consist primarily of highly reactive olefins (Dodge and Bufalini, 1972). Also note that at the levels found in urban atmospheres, CO cannot be expected to exert a significant influence on the smog forming reactions.

4.2.2.3 Sensitivity of the Mechanism to Variations in the Magnitudes of Parameters

An important facet in a program of parameter estimation and model evaluation is the performance of a sensitivity analysis. The main purpose of such analyses is to determine the effect of changes in the magnitude of each parameter in the model on the magnitude of the predicted response (in this case, concentrations). Sensitivity studies are of interest for two reasons: 1) they are quite useful in establishing a rank-ordering of parameters in terms of the importance of accurately determining each, and 2) they are helpful in relating the variation (or lack of precision in determination) of each parameter to the uncertainty in predictions of the model. Preliminary evaluation of the experimental data base revealed that several parameters in the mechanism were not known with desirable accuracy, namely, the light intensity, the water concentration, and the initial NO_2 concentration. Consequently, a limited investigation of model sensitivity was carried out for four parameters: k_1 (light intensity), k_6 (water concentration), k_7 (light intensity), and $[NO_2]_o$. The response followed was the predicted time to the NO_2 maximum, T. The parameters selected for study had been identified in earlier work as being those whose variations would probably have a substantial influence on predictions. The variable T was selected as the decision variable because it had been observed previously that it is particularly sensitive to variations in the parameters cited, because other key variables such as time to the onset of O_3 formation are closely linked to it, and because it can be conveniently expressed as a scalar.

The sensitivity calculations were performed for the toluene-n-butane system for various initial concentrations. The four parameters were varied within the limits of their estimated uncertainty bounds, and the effects of these changes on T were noted. Typical results are presented in Table 4.3. The mechanism is clearly quite sensitive to variations in the NO_2 photolysis rate and initial NO_2 concentrations, but is insensitive to variations in HNO_2 production and photolysis rates.* Unfortunately, both k_1 and $[NO_2]_o$ were subject to considerable experimental uncertainty.

In carrying out the validation runs that are discussed in the following section, concentration-time profiles were calculated using, first, base values of all parameters and second, base values of the parameters with k_1 and $[NO_2]_o$ varied within their limits of uncertainty so as to minimize the discrepancy between prediction and experiment. In this way one can compare the paired results and ascertain the degree of variation (really, improvement) in predicted values to be expected as a result of parameter variation for the limited, yet perhaps highly indicative, case of varying two "sensitive" parameters. Viewed another way, a demonstration is given of how lack of accuracy in certain measurements, in this case initial NO_2 concentration and light intensity, can affect predictions, and thus one's ability to properly assess the validity of the mechanism.

---

* Upon applying the steady state assumption to HNO_2, it can be shown that the concentrations of RHC, NO, NO_2, and O_3 are all independent of the value of k_7. This accounts for the "insensitivity" of the mechanism to variations in k_7.

Table 4.3 Sensitivity of the Kinetic Mechanism to Light Intensity, Water Concentration, and Initial NO_2 Concentration

Base Values of Parameters:*

$[NO_2]_o$ = 0.07 ppm k_1 = 0.266 min^{-1}

$[NO]_o$ = 1.10 ppm k_6 = $5x10^{-4}$ $ppm^{-1}min^{-1}$

$[HC]_o$ = 4.62 ppm (toluene + n-butane) k_7 = $5x10^{-3}$ min^{-1}

Parameter	Variation	Resultant Change in time to NO_2 maximum (minutes)
k_1	-0.10	+57
	+0.10	-28
k_6	-25%	+4
	+25%	-4
k_7	-50%	0
	+50%	0
$[NO_2]_o$	-50%	+21
	+50%	-12

* NO_2 maximum occurs at 112 minutes for these settings of the base parameters.

4.2.3 The Validation Results

The validation results consist of the comparison of experimental and predicted concentration vs. time histories for hydrocarbons, NO, NO_2, and O_3 for each of the systems listed in Table 4.1. As mentioned previously, for each set of data validations were carried out using base values of the parameters and base values of all parameters

in the mechanism except for k_1 and $[NO_2]_o$, which were varied within their limits of uncertainties to obtain improved (but not necessarily optimal) predictions.

The basic problem in adapting a kinetic mechanism for use in an atmospheric model is achieving proper representation of the complex hydrocarbon mixture in the atmosphere. This mixture is represented in the mechanism by the two fictitious species RHC and RHC_2. As noted in Section 1.5, RHC represents C_4^+ paraffins and aromatics, excluding benzene, while RHC_2 includes all olefins. C_1 to C_3 paraffins, benzene, and acetylene were considered to be unreactive, and therefore are not included in either RHC or RHC_2. The primary importance of carrying out validation studies for the toluene-NO_x, toluene-n-butane-NO_x, and propylene-ethane systems is that rate constants and stoichiometric coefficients for simple hydrocarbon mixtures can be established as an initial basis for the atmospheric system.

Space limitations preclude the presentation of validation results on the 14 sets of experimental data. Thus, only one example of validation results is presented for each of the four systems listed in Table 4.1. Figures 4.1a, 4.1b, and 4.1c illustrate typical validation results for the toluene, toluene-n-butane, and propylene systems, respectively. In each of these three systems only a single lumped species need be used: in the case of toluene and toluene-n-butane, RHC, and in the case of propylene, RHC_2. The base values of the rate constants and stoichiometric coefficients used are given in Table 4.4. When more than one hydrocarbon in the same reactivity class is

present, the rate constants and stoichiometric coefficients for the lumped species are determined by a weighting procedure similar to that given below in the discussion of the auto exhaust system.

The simulation of an auto exhaust system will serve as a basis for establishing the extent to which the mechanism is applicable in the atmosphere. As seen in Table 4.1, two sets of auto exhaust irradiation data were available, one based on the exhaust of a Chevelle equipped with controls, the second from an uncontrolled Chevelle.

One notable difference between the irradiation results for the auto exhaust gases and those for the "pure" system such as toluene-NO_x was that in the exhaust runs a substantial amount of NO_x was lost before the NO_2 peak. Because exhaust contains a large amount of particulate matter, it has been suggested that nitrate formation might occur on particle surfaces. This is consistent with the results of Lee et al. (1971), who found that the nitrate content of particulate matter in exhaust that had been irradiated through the region of sharp decrease in NO and increase in NO_2 was 175 times that of the particulate matter in unirradiated exhaust. Other chamber studies of synthetic auto exhaust (Wilson, 1972) have shown that the loss of NO_x prior to the NO_2 peak is not observed in the absence of particulate matter. Consequently, an additional reaction is

$$NO_2 + \text{PARTICLE} \xrightarrow{19} \text{NITRATE}$$

While the exact chemical details of early NO_x loss are not yet known, inclusion of this type of reaction aids in accounting for the effect observed.

For the purpose of validating the exhaust data, the two hydrocarbon classes, RHC and RHC_2, are employed. In doing so, the reactivities of C_4^+ paraffins are assumed equal to that of n-butane, and the reactivities of all olefins are assumed equal to that of propylene. Although these assumptions obviously are subject to some question, they allow estimates of group reactivities to be based on values established in validation runs performed previously. Moreover, the uncertainties in the hydrocarbon data do not justify a further refinement in the rate constants and stoichiometric coefficients at this time.

In order to carry out the validation runs, the rate constants and stoichiometric coefficients corresponding to RHC_2 were taken to be those of propylene. For RHC, on the other hand, the lumped rate constants and stoichiometric coefficients were calculated as the weighted average of the parameter values for pure toluene and pure n-butane according to the initial concentrations of paraffins and aromatics present in the exhaust. The formulas used to calculate the various parameters for RHC are as follows:

$$\bar{k}_j = \frac{\sum_\ell k_{\ell,j} c_\ell}{\sum_\ell c_\ell} \tag{4.1}$$

$$\bar{\alpha} = \frac{\sum_\ell \alpha_\ell k_{\ell,11} c_\ell}{\bar{k}_{11} \sum_\ell c_\ell} \tag{4.2}$$

$$\bar{\epsilon} = \frac{\sum_\ell \epsilon_\ell c_\ell}{\sum_\ell c_\ell} \tag{4.3}$$

$$\bar{\beta} = \frac{\sum_{\ell} \beta_{\ell} k_{\ell, 12} c_{\ell}}{\bar{k}_{12} \sum_{\ell} c_{\ell}} \qquad (4.4)$$

where c_{ℓ} refers to the initial concentration of species ℓ and

$$\ell = \begin{cases} 1 & \text{paraffins} \\ 2 & \text{aromatics} \end{cases}$$

and j = 11, 12, 13, 15 (j refers to the reaction number in Table 1.3. The base values of the rate constants and stoichiometric coefficients for use in equations (4.1)-(4.4) are summarized in Table 4.4. The validation results obtained for EPA experiment #222 are given in Figure 4.2.).

To conclude, it is believed that the reported validation results indicate that the mechanism provides an adequate, perhaps good, description of smog chamber kinetics. In particular, the model appears capable of predicting the concentration/time behavior of a variety of reactant systems over a wide range of initial conditions. The few auto exhaust simulations performed indicate that the mechanism displays promise for describing the complex mixtures that exist in the atmosphere. The guidelines established for estimating rate constants and stoichiometric coefficients also have proven to be quite adequate. Nevertheless, the kinetic mechanism employed has a number of fundamental shortcomings, most notably the need for semi-empirical stoichiometric coefficients. A new kinetic mechanism for photochemical smog has recently been formulated (Hecht and Seinfeld, 1973) which eliminates the weaknesses inherent in the mechanism employed here. In particular, the mechanism describes

Table 4.4

Values of Base Parameters Used to Calculate Rate Constants and Stoichiometric Coefficients for Complex Hydrocarbon Mixtures*

ℓ	Species	$k_{\ell,11}$	$k_{\ell,12}$	$k_{\ell,13}$	$k_{\ell,15}$	α_ℓ	β_ℓ	γ_ℓ	ϵ_ℓ
1	C_4^+ Paraffins	1920	5720	.0001125	9	5	1.2	4	.61
2	Aromatics (excluding benzene)	6420	15000	.000075	30	6	1.2	4	.61
3	Ethylene	7720	2500	.00287	3	16	.2	4	.22
4	Other Olefins	40000	25000	.0165	3	16	.2	4	.22

* Reaction rate constants are given in $ppm^{-1} min^{-1}$

the important inorganic chemistry in detail, yet minimizes the overall number of reactions by taking advantage of the general behavior of specific groupings of similar hydrocarbons and free radicals. Most importantly, the mechanism is free of arbitrarily assignable stoichiometric coefficients. Extensive validation exercises have shown that this new mechanism is capable of reproducing a variety of experimental data using literature rate constants. Future airshed modeling studies may be carried out with this new mechanism when hydrocarbon emissions data with the same level of detail become available.

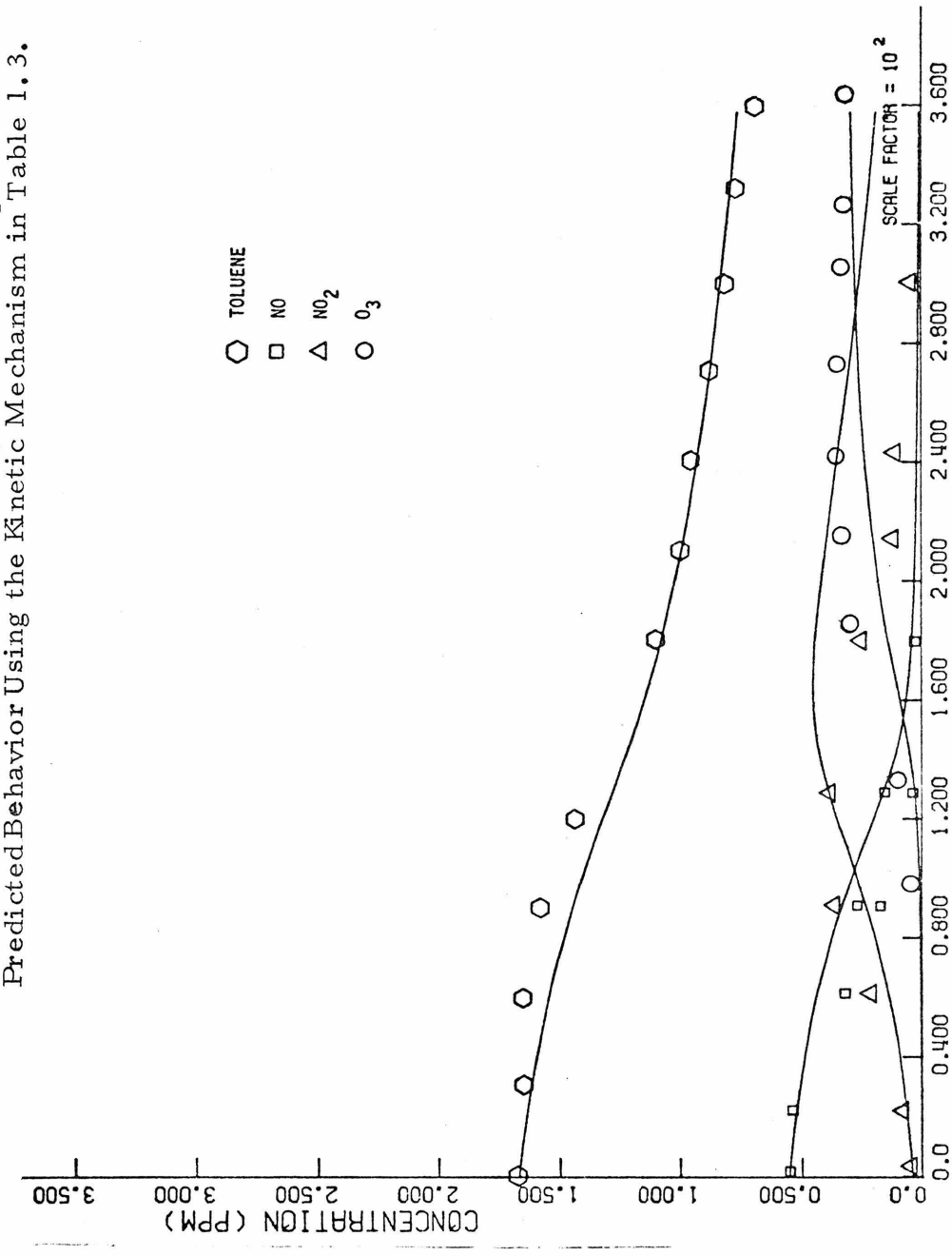

Figure 4.1a Concentration/time Behavior in an Irradiated System of Toluene, NO_x and Air. Data Points Refer to EPA Experiment #272. Lines Represent the Predicted Behavior Using the Kinetic Mechanism in Table 1.3.

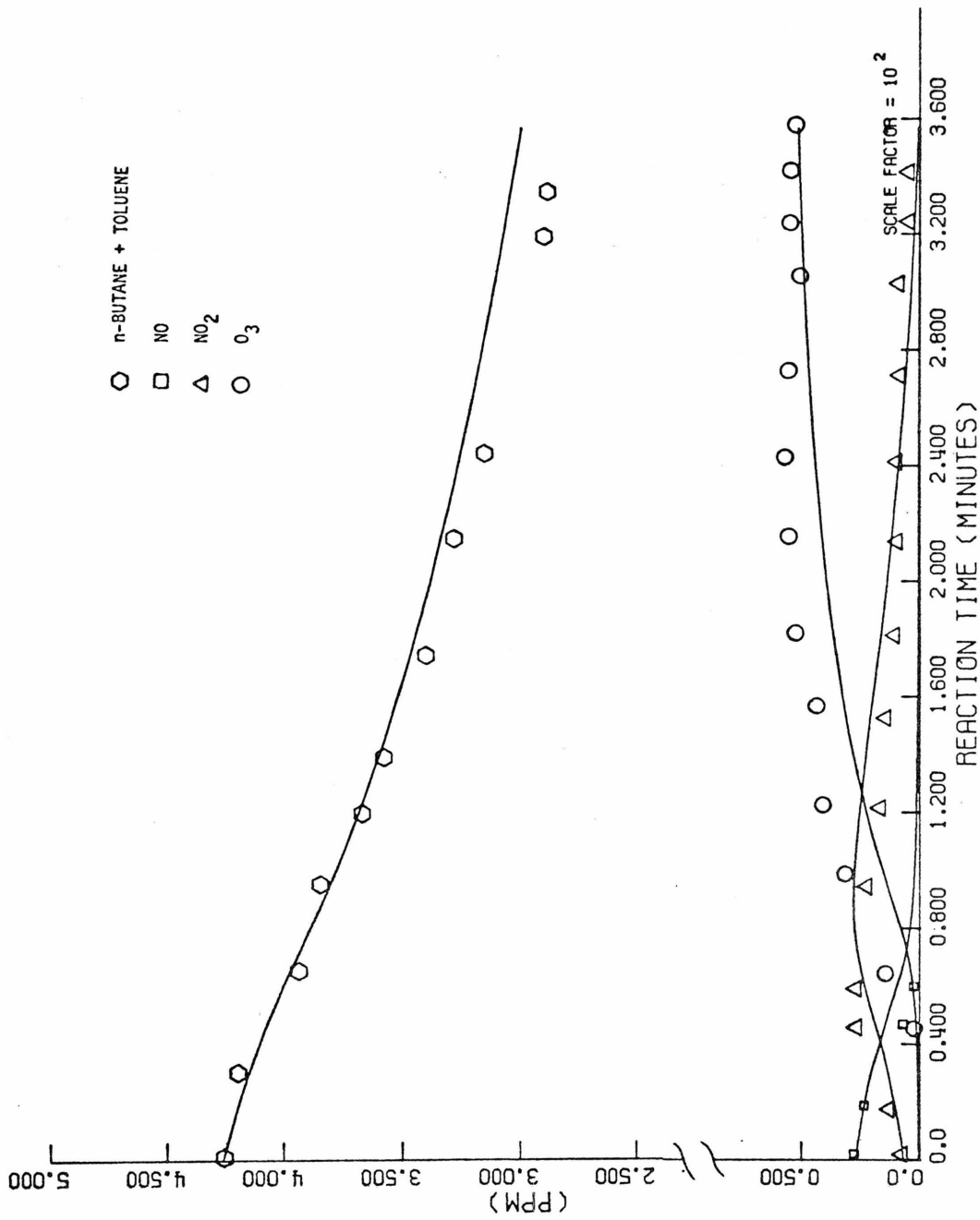

Figure 4.1b Concentration/time Behavior in an Irradiated System of n-Butane, Toluene, NO_x and Air. Data Points Refer to EPA Experiment #257.

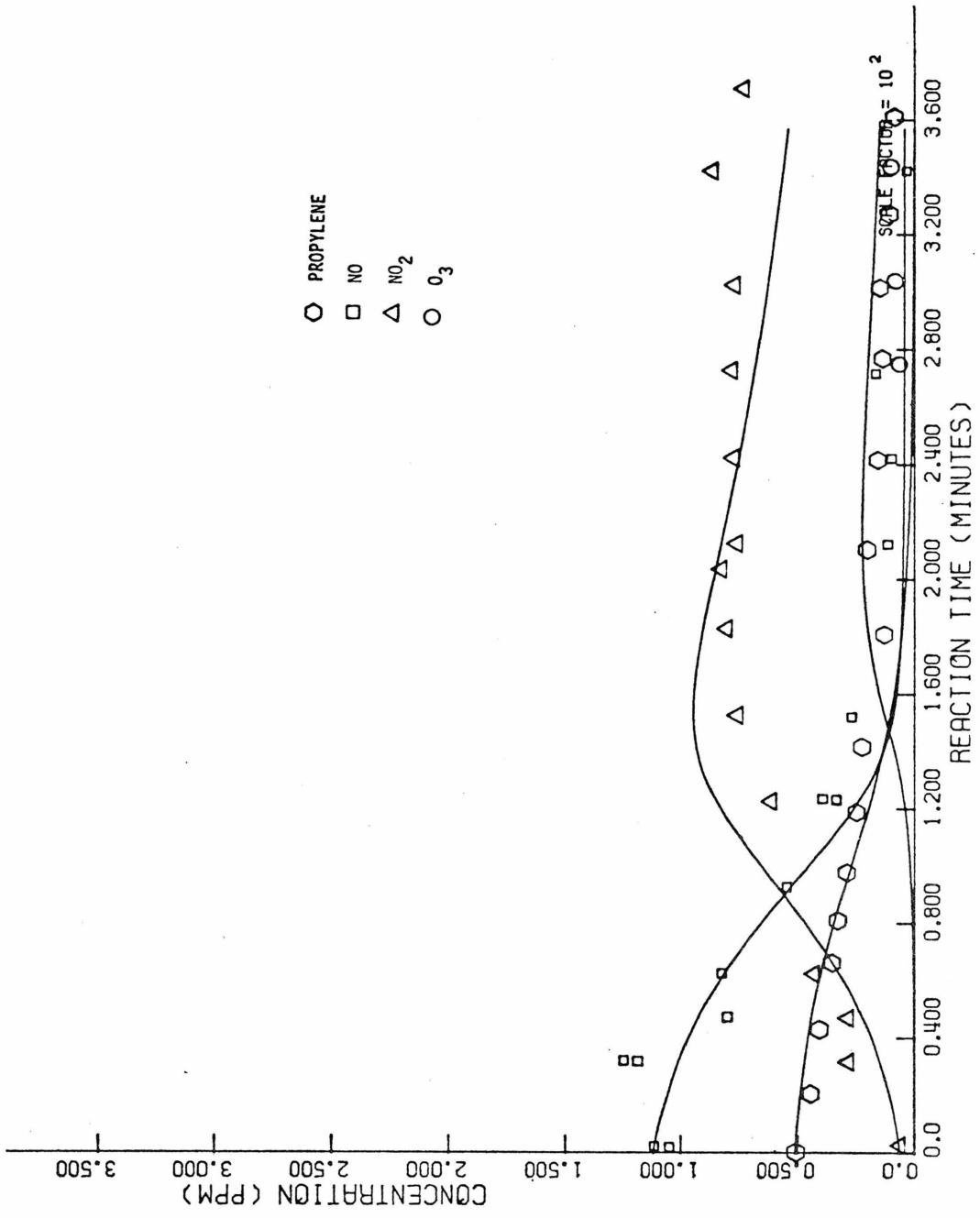

Figure 4.1c Concentration/time Behavior in an Irradiated System of Propylene, and Air. Data Points Refer to EPA Experiment #318.

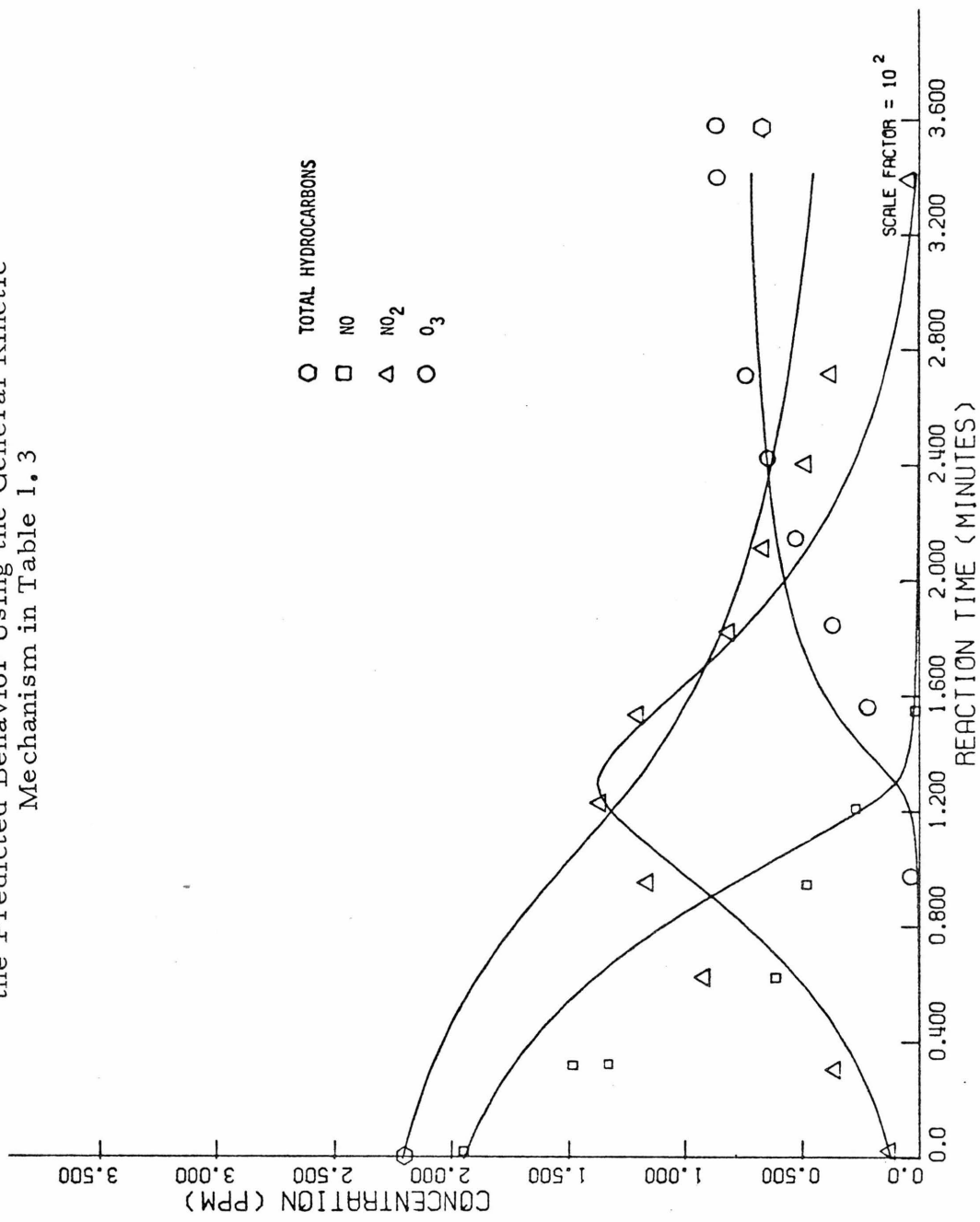

Figure 4.2 Concentration/time Behavior in an Irradiated System of Auto Exhaust, NO, NO_2 and Air. Data Points Refer to EPA Experiment #222. Lines Represent the Predicted Behavior Using the General Kinetic Mechanism in Table 1.3

4.3 The Microscale Model

One of the most important considerations in the development of an urban airshed model is the selection of an appropriate spatial scale. The choice of scale is influenced by a number of factors which were discussed in Section 1.2. A survey of available meteorological data indicated that a spatial resolution of two miles was appropriate for the Los Angeles study. When the spatial scale is of this size, the model is unable to account for the effects of sub-grid scale effects, such as variations in contaminant concentrations that occur in the vicinity of major roadways and strong point sources. Buildings and elevated or depressed freeway structures alter local wind patterns and turbulence levels, which contribute to the establishment of local concentration levels. Similarly, the presence of high-rise buildings along the street borders, the so-called "street canyon," can reduce considerably the influence of "main stream" convective transport processes on the dilution of street level emissions. Effects such as these occur on a scale that is small compared with that typically adopted in urban modeling. The inability of an airshed model to resolve these sub-grid scale effects is of particular concern when validating the model by comparing its predictions with point measurements of pollutant concentrations.

Consider the validation of an urban airshed model, where CO is the pollutant of concern. As noted previously, the model is based on the assumption that emissions are uniformly distributed in space and time (over an hourly interval) over each 2 x 2 mile cell and that meteorological conditions are also invariant over this scale. The

direct result of these assumptions is that the predicted pollutant concentrations are uniform within each grid cell. The observed values of CO, however, typically are representative only of the CO concentrations in the immediate vicinity of the monitoring station. Of the nine monitoring stations operated by the Los Angeles County APCD, seven are located within 30 meters of a roadway having a daily traffic count in excess of 15,000 vehicles. Ott (1971) has shown that CO concentrations measured at a monitoring station situated along a busy city street are approximately twice the background level (100 meters or more away from the street) and slightly more than half that measured at the sidewalk located between the street and the station. While a properly formulated urban scale model will predict spatially averaged concentrations with reasonable accuracy, there may be little justification for comparing these predictions directly with local point observations. Some basis for comparison is required, however, if the validity of the model is to be established. Either spatially averaged observations must be made, or an additional model must be employed that is capable of predicting concentrations at a point that are affected by local sources. The microscale model used in this study was originally formulated in Appendix C of Reynolds et al. (1973); the discussion given in this section will be a summary of that report.

As noted previously, the main source of CO emissions in the vicinity of Los Angeles County air pollution monitoring stations is the automobile. Thus, to establish a basis for validation, a sub-grid, or microscale, model is needed. The model must be capable of

predicting the elevation in concentration at the monitoring station, above background levels, that is contributed by local automotive emissions. The sum of this predicted concentration and the background concentration predicted using the urban scale model can then be compared with observed concentrations for the purpose of validation.

While the main purpose of developing a microscale model was to provide a realistic basis for validating an urban scale model, the microscale model (or "micromodel") may well be useful in other contexts. The coarse resolution of the urban scale model does not suggest its use in the prediction of dosage in areas of substantial local variation in concentrations, such as along the sidewalk, in street canyons, and in areas of public access at airports. The micromodel may be of considerable value in estimating dosages in such situations, when used in concert with the urban scale model. The micromodel may also be of value in establishing a basis for formulating air quality standards. As concentrations can vary substantially in the vicinity of strong sources, perhaps air quality standards should be based on obtaining measurements at locations of greatest exposure--along sidewalks, within the automobile, inside the school yard. To properly establish such standards, based on historical measurements, one must rely on a model capable of describing local variations.

4.3.1 Survey of Previous Studies

Because emissions from automobiles constitute a major contribution to the total atmospheric pollutant load in urban areas, a number of studies have been undertaken in recent years that have been concerned with the dispersion of air contaminants in the vicinity of

city streets. The important findings of these investigations are summarized in this section.

Carbon monoxide concentrations at "curbside" locations were measured by McCormick and Xintaras (1962) in Nashville, Tennessee and Cincinnati, Ohio. They found that the temporal variation in CO concentration at both sites were correlated with hourly traffic counts made at the street along which the concentrations were measured, thus confirming the conclusions of an earlier study by Brief (1960). Furthermore, they noted that meteorological conditions, such as wind speed, wind direction, turbulence level, and atmospheric stability, also played an important role in determining the level of CO concentrations.

An extensive investigation was later carried out in Germany by Georgii et al. (1967) and Georgii (1969). Carbon monoxide concentrations, traffic density, and pertinent meteorological variables were measured at three sites located near three major streets in downtown Frankfurt/Main. (Traffic counts on the streets ranged between 1200 and 1800 cars per hour during peak hours.) Good correlation was established between the diurnal CO concentration and the temporal variation in traffic density. They found that one of two distinct local flow regimes will be established within a street canyon (see Figure 4.3). Which regime persists is dependent upon whether the rooftop wind speed is less than, or is greater than 2 m/sec. The results of Georgii et al. are generally confirmed by Schnelle et al. (1969) and Johnson et al. (1971).

In general, the studies cited above have involved attempts to establish empirical relationships between concentrations in the vicinity of a roadway and meteorological, emissions, and spatial variables. Several investigators have proposed numerical models based on the use of the atmospheric diffusion equation (Chang et al., 1971; Djuric et al., 1971; Hotchkiss, 1971). The next section is devoted to a description of such a model.

4.3.2 Governing Equations of the Microscale Model

No single model will suffice for describing transport and dispersion phenomena in the vicinity of a street, largely because distinctly different flow patterns can occur above the roadway surface. Thus, in order to describe the dispersion of pollutants in the vicinity of roadways and buildings, a distinction must be made between the two flow patterns that generally exist in such an environment, as illustrated in Figure 4.3.

1. Free Flow Regime: air at street level is directly ventilated by the prevailing wind at the rooftop. This case may be characterized by the fact that directions of the street-level wind and rooftop wind are the same.
2. Circulatory Flow Regime: air at street level does not have direct access to the prevailing wind. Instead, a vortex of opposite sense relative to the rooftop wind will be generated.

In Appendix C of Reynolds et al. (1973), a simple methodology is presented which may be used to determine which regime exists under a given set of meteorological conditions. With the exception of the downtown station in Los Angeles, only the free flow regime needs to be

Figure 4.3 Typical Flow Patterns in an Urban Boundary Layer Characterized by Large Surface Irregularity

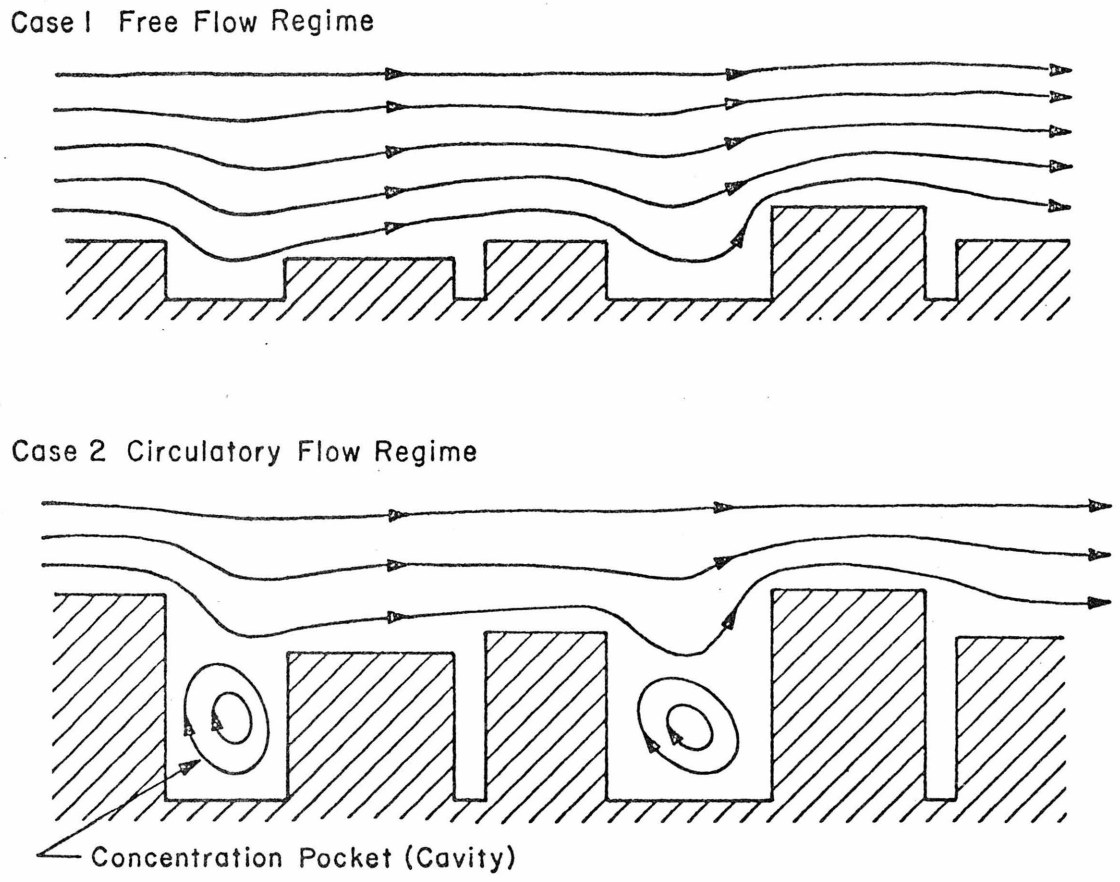

considered in the vicinity of air quality monitoring stations of interest. Thus, the efforts of this study are restricted to the development of a model for this regime.

Assume that steady state conditions prevail with a constant wind speed U directed at a right angle to the roadway. The streamlines of flow are as illustrated in case 1 in Figure 4.3. x is taken to be a coordinate measured from the centerline of the roadway (x = 0) along the wind streamlines, as shown in Figure 4.4 where the location of a possible monitoring station is indicated. The vertical direction z is then normal to the streamlines at each point. It is assumed that K-theory is applicable with horizontal and vertical diffusivities constant and equal.

With the above assumptions, the equation for the mean concentration of an inert species is

$$U \frac{\partial c}{\partial x} = K\left[\frac{\partial^2 c}{\partial x^2} + \frac{\partial^2 c}{\partial z^2}\right] \tag{4.5}$$

The boundary conditions are:

$$\begin{aligned} &c(x, 0) = \delta(x) && z = 0 \\ &K \frac{\partial c}{\partial z}\bigg|_{z=0} = 0 && z = 0,\ x \neq 0 \\ &c(x, z) \to 0 && x \to \pm\infty \\ &c(x, z) \to 0 && z \to \infty \\ &\int_{-\infty}^{\infty} - K \frac{\partial c}{\partial z}\, dx = Q \end{aligned} \tag{4.6}$$

where U is the wind speed, K is the turbulent eddy diffusivity, and

Figure 4.4 Coordinate System Employed for the Micromodel

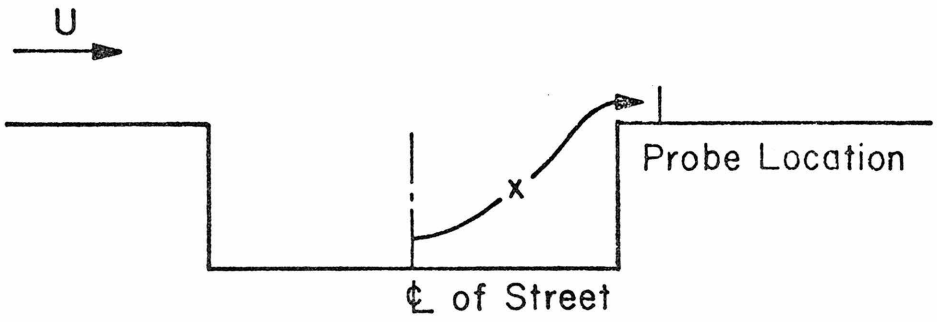

Figure 4.5 Temporal Variation of the Eddy Diffusivity K in the Micromodel

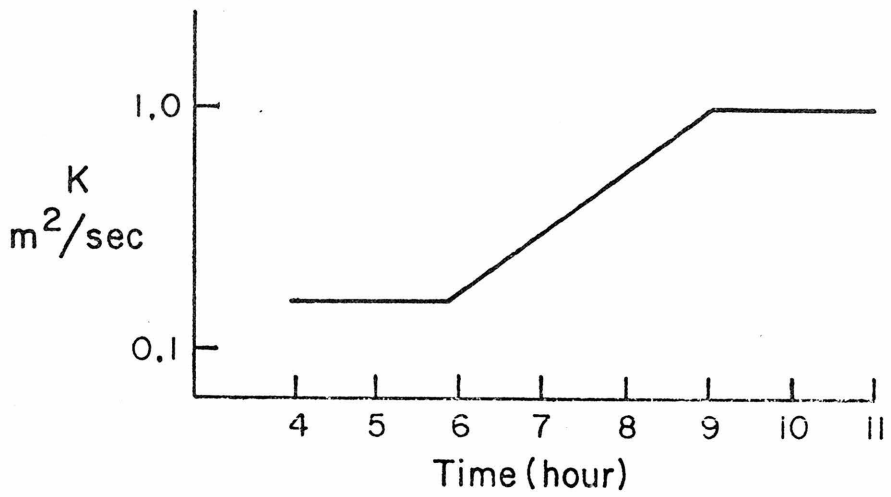

Q is the emission rate of pollutant per unit length of roadway in gm/m - min, assumed to be concentrated at the centerline of the roadway.

The solution of equation (4.5) subject to equations (4.6) can be shown to be

$$c(x, z) = \frac{Q}{\pi K} e^{\xi} K_o\left[\frac{U(x^2+z^2)^{\frac{1}{2}}}{2K}\right] \tag{4.7}$$

where $\xi = Ux/2K$, and K_o is the modified Bessel function of the second kind of order zero. The ground-level concentration ($z = 0$) is given by

$$c(x, 0) = \frac{Q}{\pi K} e^{\xi} K_o \quad (|\xi|) \tag{4.8}$$

As noted, the solution of equation (4.5) is based on the assumption of a constant vertical diffusivity, invariant with height. Because the region adjacent to the surface is very shallow and because mixing is vigorous due to the flow, this assumption is probably fairly good. However, during the period over which the change in surface temperature with time is large--the morning hours following sunrise--the changes in diffusivity with time may also be substantial. To account for these changes, it is assumed that K changes with time in a manner shown in Figure 4.5. The functional relationship, as well as the magnitude of K (note that the plot is semilogarithmic), is based on the results of Staley (1956). While the values of K are subject to considerable uncertainty, the relationship shown also corresponds with the findings of other investigations, for example, Jehn and Gerhardt (1950). Note that both U and K may vary from hour to hour to correspond with the time resolution of the measured wind and concentration

data. The situation in which the horizontal and vertical eddy diffusivities vary linearly with z has been considered by Walters (1969).

In solving equation (4.5) the emissions are assumed to be concentrated along the centerline of the street, in effect treating the street as a source of infinitesimal width. In reality, typical distances of interest from centerline to sampling port are of the order of 10 to 40 meters. Street widths are of the magnitude of these transport distances, varying from 8 to 30 meters. In order to assess the effect of the line source assumption on predicted concentrations, the solution of equation (4.5) is compared to that for emissions from a street of finite width. The only change in the governing equation in the latter case, when compared with equation (4.5), is in the boundary conditions, wherein the source strength is specified by q, the mass emission of pollutant per unit area of roadway,

$$q = \begin{cases} Q/2\ell \text{ at } z = 0 \text{ for } |x| < \ell \\ 0 \quad \text{at } z = 0 \text{ for } |x| > \ell \end{cases} \tag{4.9}$$

The remaining boundary conditions are unchanged.

The solution of equation (4.5) for the ground-level concentration in the finite width case is

$$c(x, 0) = \frac{2q}{\pi U} \int_{\frac{U(x-\ell)}{2K}}^{\frac{U(x+\ell)}{2K}} e^{\xi} K_o(\xi)\, d\xi \qquad |x| \geq \ell \tag{4.10}$$

To assess the effect of the finite street width, the two solutions, equations (4.8) and (4.10) were compared for the case in which the traffic flow is 1000 vehicles/hour, $K = 1\ m^2/sec$, and $U = 1\ m/sec$. The results indicate that at a distance of 15 meters, the minimum from

street center line to any of the Los Angeles monitoring stations considered in this study, the discrepancy in predicted concentrations is 0.025 ppm at an average level of 0.72 ppm, or about 3.5%. This discrepancy decreases as the distance from centerline increases, becoming zero at distances in excess of 50 meters. Based on this comparison, it appears that the assumption of emissions emanating from a source of infinitesimal width is justified.

4.3.3 Results of Micromodel Usage

As discussed earlier, the main purpose of this limited modeling effort was to investigate the feasibility of developing a simple model capable of describing local or sub-grid scale emissions and transport processes and thus their contributions to measured air quality levels. Since the scope of the effort was quite restricted, there were necessarily a number of considerations of practical importance that were not addressed. In particular, application was limited to

1. roadway sources
2. inert pollutants, in this case carbon monoxide
3. the free flow regime
4. a selected group of monitoring sites
5. times of day when corrections are likely to be significant. The primary period of interest is between 5 A.M. and 10 A.M., when heavy traffic and light winds are common.

Fifteen monitoring stations were operative during the six "validation days" in 1969--11, 29, and 30 September, 29 and 30 October, and 4 November. Ten were operated by the LA APCD, three by the Orange County APCD, and two by Scott Research Laboratories.

Of these the Orange County stations and the Pasadena station were not considered for this feasibility study because they were inoperative on several of the validation days. The mobile Scott stations were not considered because their locations with respect to neighboring streets were unknown. Of the remaining nine stations, two (at Reseda and Azusa) are located on streets having little or no traffic, one (downtown Los Angeles) is situated along a street canyon, one (Burbank) is located in a region of complex and rapidly varying wind patterns, and one (Pomona) is located one mile outside of the modeling region. The remaining four stations--Lennox, West Los Angeles, Whittier, and Long Beach--were selected for application of the micromodel.

Hourly averaged CO concentrations attributable to local roadway sources were estimated for the period 5 A.M. to 10 A.M. (local time) for each of the six validation days using the diffusivity vs. time curve of Figure 4.5. Typical estimated increases in CO concentration above background are given in Figure 4.6. Traffic counts used in these calculations were taken from average traffic statistics made available by the traffic department of the municipality in which the station is located. Wind speed and direction were measured continuously at each monitoring station, with the exception of Lennox; however, the recorder sheets were unavailable.* Thus, hourly-averaged wind statistics were used.

In evaluating the results, comparisons can only be made between measured concentrations and the sum of predicted concentrations

*Readings taken at the three nearest stations served as the basis for estimating wind parameters at Lennox.

Figure 4.6 Predicted CO Concentrations

with Micromodel Corrections

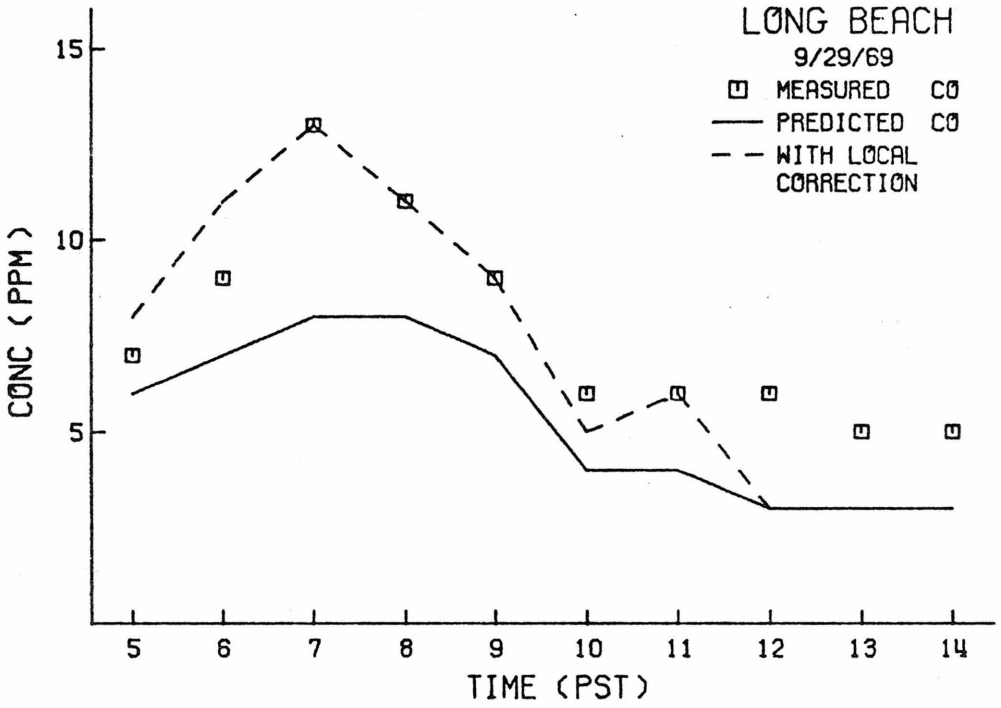

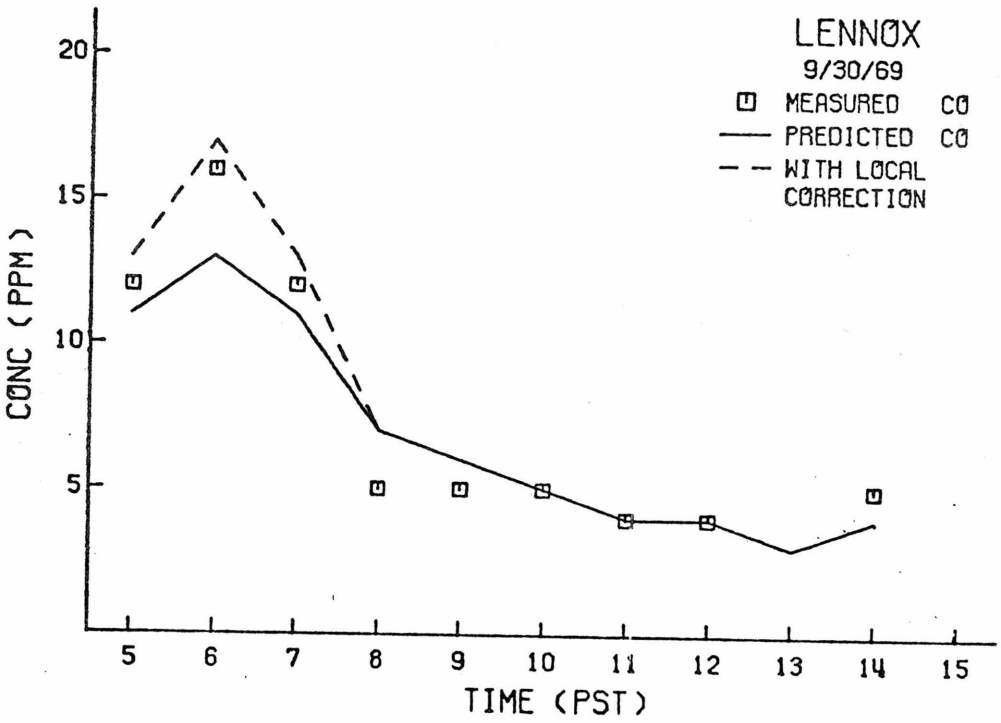

calculated using both the microscale model and the full airshed model. For this reason, evaluation of the results is presented in Section 4.4. It should suffice here to say that the results appear to be quite promising, given the restricted nature of the data. However, a full and fair evaluation must await the acquisition of a more complete data base, more suited to the temporal and spatial resolution of the microscale model.

To properly validate a local model, it is most important to have available a data base collected for the specific purpose of filling this role. In order to distinguish between local and background contributions to air quality at a particular location, pollutant concentrations should be measured on a temporary basis upwind of the monitoring or test site. In addition, continuous recordings of wind speed and direction and pollutant concentrations should also be made available. The data could then be averaged over varying periods of time--say from one minute to one hour-- and the model tested in order to establish both appropriate averaging periods and the effects of selecting long averaging periods. Finally, turbulence measurements would be most helpful in obtaining improved estimates of K and its variation in time during the morning hours following sunrise.

For more details involving the applications of the model, and for more complete discussion of the model and its limitations, the reader is referred to Appendix C of Reynolds et al. (1973).

4.4 Evaluation of the Airshed Model

Validation of the urban airshed model consists of integrating the governing equations and comparing predicted concentrations with

those measured at local air quality monitoring stations. Validations were carried out in the following sequence for each of six days in 1969, days for which a rich data base was available: 1) validation for carbon monoxide, and 2) validation for hydrocarbons, nitrogen oxides, and ozone. Exercise of the model for an inert species, such as CO, provides a basis for evaluating the treatment of meteorological variables. Validation for CO, of course, also constitutes a test of most aspects of the numerical integration technique and portions of the source emissions inventory. Upon successful completion of the first task, and upon incorporating the modifications suggested by the results of the CO validation, the validation for reactive species may proceed.

The treatment of hydrocarbons in the airshed model requires some comment. Because most available air monitoring data are reported only in terms of total organic carbon, and because of the computational requirements associated with simulating the behavior of two reactive species (such as RHC and RHC_2), the atmospheric hydrocarbon mix is represented in the present study by two hydrocarbon species only, RHC and URHC. The species URHC represents all unreactive hydrocarbons, including C_1-C_3 paraffins, acetylene and benzene. In the model calculations, URHC is treated, therefore, as an inert species. The species RHC represents all other hydrocarbons present in the atmosphere. Thus, RHC includes both species RHC and RHC_2 in the kinetic mechanism. As noted shortly, the rate constants and stoichiometric coefficients corresponding to RHC are determined by equations (4.1)-(4.4). RHC is therefore a lumped

composite of RHC and RHC_2.

It is the purpose of this section to describe the validation procedure, to present the results of the validation effort, and to examine and evaluate these results.

4.4.1 The Evaluation Procedure

The evaluation procedure for a particular "validation day" consists of the following four steps:

Step I. Preparation of meteorological and emissions data. Hourly wind speed, wind direction, and mixing depth maps are prepared for each validation day, as described in Section 1.4. As it is assumed that the emissions inventory is applicable for all weekdays in 1969, and as all validation days are weekdays, the inventory is used as reported in Chapter 2 without alteration.

Step II. Preparation of other inputs to the model specific to the validation day. These include:

1. Initial conditions. Initial concentrations are specified in each ground level grid cell by interpolation using the data collected at monitoring stations during the hour at which solution is initiated. Maps are needed for CO, NO, NO_2, and reactive and unreactive hydrocarbon (RHC and URHC). Initial ozone concentrations are calculated assuming that the net reaction rate of ozone is equal to zero. From the mechanism given in Table 1.3, the following expression may be written for the steady state ozone concentrations (considering only reactions 1-15):

$$[O_3] = \frac{k_2[O]}{k_3[NO]+k_4[NO_2]+k_{13}[RHC]} \qquad (4.11)$$

where

$$[O] = \frac{k_1[NO_2]}{k_2 + k_{11}[RHC]} \qquad (4.12)$$

and $[NO]$, $[NO_2]$, $[RHC]$ refer to the initial NO, NO_2, and reactive hydrocarbon concentrations in a particular ground-level grid cell. Initial concentrations in cells aloft are set equal to the concentration in the ground level cell.

2. Boundary conditions. The boundary conditions for the air-shed model are given by equations (1.18)-(1.21). The emissions model and inventory is used to specify the surface pollutant flux, equation (1.18). Of particular concern on the horizontal and upper boundaries of the modeling region is the specification of the pollutant flux when species are transported into the modeling region. This may be accomplished by defining the function g_ℓ given in equations (1.19)-(1.21). Note that g_ℓ is simply the concentration of species ℓ at a point just outside the boundary. Values of g_ℓ are allowed to vary both temporally and spatially. The horizontal boundary conditions (east, west, north, and south boundaries, where winds enter the modeling region) are established by using the concentrations measured at the nearest monitoring station as a guide. Variations in concentrations with x and y along the boundary at a given time in regions remote from monitoring stations are

estimated solely on a judgemental basis. It is assumed that the boundary concentration is invariant with z for a given x, y, and t. Boundary concentrations for O_3 are calculated assuming O_3 to be at steady state, i.e. from equation (4.11).

In order to specify the concentration of pollutants that enter the modeling region as the inversion rises, one must, in the absence of concentration data aloft, make some assumption as to the nature of the vertical concentration distribution. Thus, at the beginning of a simulation, the concentration distribution shown in Figure 4.7 is established over each grid square. In the profile shown in Figure 4.7, $\overline{AB}$ denotes the initial condition, and $\overline{BCD}$ denotes the assumed concentration profile aloft (above the inversion base). As the base of the inversion rises, the concentration of pollutant in the air engulfed is given by the location of the height of the inversion base and the corresponding concentration on the segment $\overline{BCD}$. A profile is constructed for all species except ozone. In the case of this pollutant, the concentration at the boundary is calculated through use of the steady-state approximation involving RHC, NO, and NO_2.

3. Radiation intensity data. Actual measurements of radiation intensity at the ground as a function of time were made by Scott Research Laboratories (1970) at El Monte and Commerce on each of the validation days. Averages

Figure 4.7 Initial Vertical Concentration Distribution

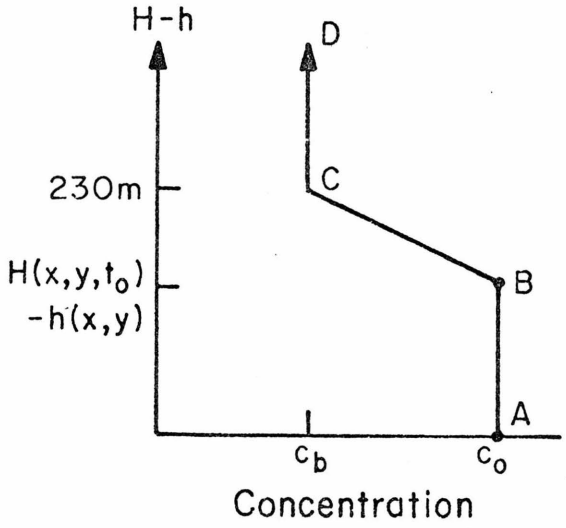

c_o = initial concentration in the column of grid cells above a particular grid square.

c_b = assumed background concentration aloft above the grid square.

$H(x, y, t_o)$ = height of the inversion base at t_o and location (x, y).

$h(x, y)$ = terrain elevation at (x, y).

of the normalized, solar zenith angle corrected intensity measurements made at the two stations were related to the NO_2 photolysis rate constant, k_1, through a relationship given by Eschenroeder and Martinez (1970). As an illustration of the form of the results, Figure 4.8 shows k_1 as a function of time on 30 September 1969 as derived directly from intensity measurements. The k_1 values derived from the intensity measurements at Commerce and El Monte are shown in Figure 4.8. The solid curve in Figure 4.8 represents the k_1 values used in the validation studies for 30 September 1969. Values of the photolysis rate constant for HNO_2, k_7, were calculated by multiplying the values of k_1 by k_7/k_1, as given in Table 4.2.

4. Rate constants and stoichiometric coefficients for hydrocarbon reactions. Referring to the kinetic mechanism presented in Section 1.5, the following rate constants and stoichiometric coefficients must be established for the hydrocarbon reactions: k_{11}, k_{12}, k_{13}, k_{15}, α, β, γ, and ϵ. Recall that in the airshed model only reactive and unreactive hydrocarbon species are considered. Thus, only reactions 1-15 of the mechanism presented in Table 4.3 are used.

The rate constants and stoichiometric coefficients cited above were calculated for each validation day using detailed hydrocarbon measurements taken in the

Figure 4.8 Photolysis Rate Constant for NO_2 Decay in Los Angeles on September 30, 1969

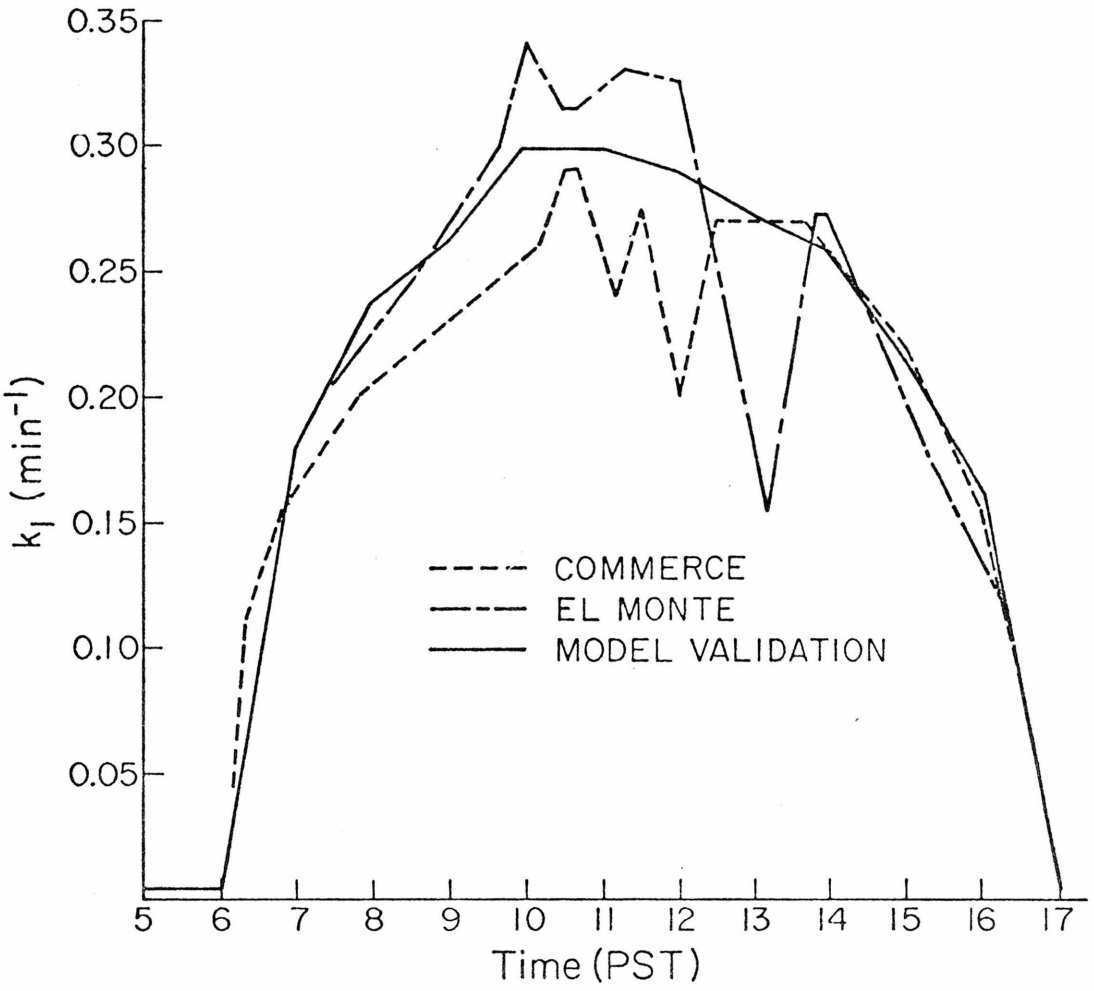

atmosphere and a weighted-average procedure similar to that described in Section 4.2. Gas chromatographic data collected by Scott Research Laboratories (1970) at Commerce and El Monte on the validation days were used in determining the averaged parameters. In applying equations (4.1)-(4.4) with Table 4.4, the subscript ℓ is defined as follows:

$$\ell = \begin{cases} 1 & \text{paraffins} \\ 2 & \text{aromatics} \\ 3 & \text{ethylene} \\ 4 & \text{olefins} \end{cases}$$

Since little temporal variation in calculated values of the constants was obtained for any particular day, daily average values of the parameters were used in the simulations. The values of the constants calculated for 29 September 1969 are presented in Table 4.5. Constants for the other validation days are given by Reynolds et al. (1973). The rate constants for the inorganic reactions are given in Table 4.2.

Table 4.5 Computed Values of Hydrocarbon Rate Constants and Stoichiometric Coefficients for 29 September 1969

$\bar{k}_{11} = 7300$ ppm^{-1}min^{-1}	$\bar{\alpha} = 12$
$\bar{k}_{12} = 9500$ ppm^{-1}min^{-1}	$\bar{\beta} = 0.95$
$\bar{k}_{13} = 1.9\text{x}10^{-3}$ ppm^{-1}min^{-1}	$\bar{\gamma} = 4$
$\bar{k}_{15} = 13.8$	$\bar{\epsilon} = 0.51$

Step III. Validation for carbon monoxide. The airshed model is exercised from 5 A.M. to 3 P.M. PST for each of the validation days. Predicted elevations in concentration in the vicinity of four monitoring stations due to local emissions are added to the airshed model predictions. Alterations were made in the 29 September and 30 September wind fields after initial simulations were carried out for these days. No other changes in input data to the model were made for these days, nor were any changes made for the four additional days upon examining the CO results. Hourly-averaged predicted ground level concentrations were calculated for each ground level cell, and hourly-averaged predicted concentrations applicable at each monitoring station were also calculated.

Step IV. Validation for nitrogen oxides, hydrocarbons, and ozone. Upon satisfactory completion of the carbon monoxide simulation for a particular day, validation was carried out for the reactive species. All procedures are as described for CO.

Comparison of predictions with measured values are made at the sites shown in Figure 1.1. Since monitoring stations are not, in general, situated near the center of a ground level grid cell, an interpolation procedure is employed to calculate the predicted station concentration. The computations involved in the interpolation procedure are illustrated in Figure 4.9.

4.4.2 Validation Results

Validation was carried out for carbon monoxide (CO), nitric oxide (NO), nitrogen dioxide (NO_2), reactive plus unreactive (or total) hydrocarbon (HC), and ozone (O_3) for the ten hour period 5 A.M. to

Figure 4.9 Interpolation Procedure for Calculating the Predicted Concentration at a Monitoring Station

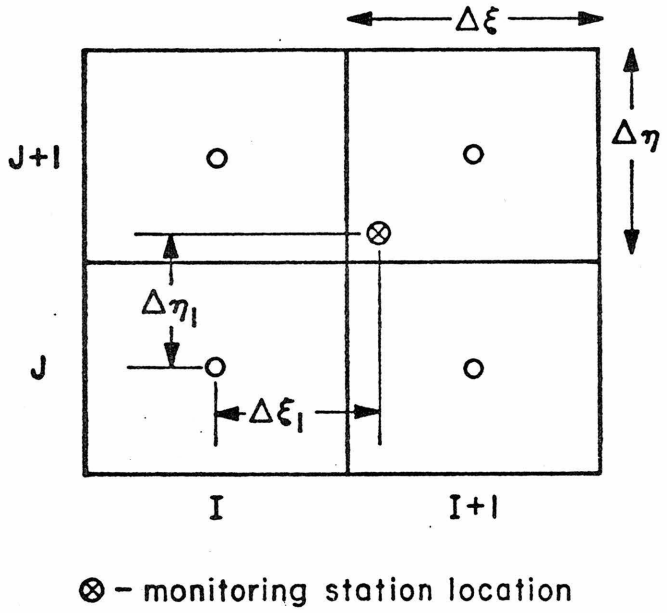

$$C_{station} = [C_{I,J}(1-\alpha) + C_{I+1,J}\alpha](1-\beta) + [C_{I,J+1}(1-\alpha) + C_{I+1,J+1}\alpha]\beta$$

where

$$\alpha = \frac{\Delta\xi_1}{\Delta\xi}$$

$$\beta = \frac{\Delta\eta_1}{\Delta\eta}$$

$C_{I,J}$ = predicted ground level concentration above grid square (I, J)

$C_{station}$ = predicted concentration at the monitoring station

3 P.M. for the following days in 1969:

11 September	29 October
29 September	30 October
30 September	4 November

Air quality data for 29 September and 30 September are described in detail in Appendix E of Roth et al. (1971). Data for the remaining four days were supplied by EPA. Most of the air quality data were collected by the Los Angeles and Orange County Air Pollution Control Districts which together operate a total of thirteen monitoring stations in the modeling region. However, as mentioned earlier, Scott Research Laboratories collected air quality data at two additional sites during this period. The reader is referred to their report, "Atmospheric Reaction Studies in the Los Angeles Basin," Vol. I-IV (1970), describing the data collection program.

The air quality measurement techniques employed by the APCD have been reviewed with regard to accuracy, specificity, and reliability, and the following observations can be made. First, accuracies are, in general, no better than ± 10% in the determination of pollutant concentrations (for any pollutant), and degree of specificity and reliability varies greatly, depending upon the measurement. Second, corrections to measurements must be made for certain pollutants. These are as follows:

CO No correction needed.

NO The oxidation of NO to NO_2 prior to colorimetric measurement of the product NO_2 is 70 to 85% efficient. Thus, reported NO concentrations must be increased by about 25% for use in

validation.

NO_2 — PAN interferes with measurement of NO_2. Accuracy of measurement is ±10 to 20%. No correction is recommended, however, due to lack of information--knowledge of PAN concentration and other sources of uncertainty.

oxidant — Presence of NO_2 increases oxidant readings by 10 to 20% of the NO_2 concentration; SO_2 decreases readings by an amount approximately equal to the SO_2 concentration. In Los Angeles, NO_2 will be the most significant interferent, although SO_2 will have a substantial effect in the southwest portion of the Basin. These interferences are corrected for when they are significant.

total hydrocarbons — Flame ionization (FIA) is specific for carbon, recording oxygenated hydrocarbons as well as hydrocarbons. Readings are difficult to interpret because

1. Calibration is carried out using a specific hydrocarbon (APCD uses methane), whereas the hydrocarbons measured are a complex mixture. While it is assumed that response is proportional to the number of carbon atoms, significant deviation from this assumption may occur.
2. Methane is by far the dominant constituent, making determination of nonmethane constituents by difference a highly uncertain matter. In fact, the determination of nonmethane hydrocarbon concentrations from the difference of total hydrocarbon and methane

measurements is of little value since nonmethane hydrocarbon consists of both reactive and unreactive species. It is thus concluded that these measurements are too uncertain to be of much value.

In summary, CO and NO_2 concentrations are used as reported, whereas NO and oxidant are "corrected" in the manner indicated. Total hydrocarbon measurements are considered to be of little value.

In applying these corrections, the following exceptions were made:

1. At Commerce and El Monte, the NO and O_3 measurements made by Scott were not corrected since they were made using procedures that do not require a correction.
2. At Long Beach, oxidant measurements were not corrected for SO_2 or NO_2 interference due to the uncertainty inherent in applying the correction when the interferents are present in high concentrations relative to the species being measured.

Due to discrepancies in the units used to represent measured and predicted hydrocarbon concentrations, special attention must be given to the comparative presentation of hydrocarbon concentrations. Total hydrocarbon measurements were made on a regular basis at four locations in the Basin--Downtown L. A., Azusa, Pasadena, and Anaheim. Methane is monitored at three of these stations, the exception being Anaheim. In addition, Scott measured hydrocarbons using both flame ionization and gas chromatographic methods at El Monte and Commerce. As unreactive (U) and reactive (R)

hydrocarbons are treated separately, measured and predicted concentrations must be placed on the same basis for the purpose of comparison.

As most data are reported as ppm carbon (ppm C), predicted hydrocarbon concentrations (ppm) for both reactive and unreactive groupings have been converted to ppm C in the following manner. From the Scott GC measurements, the average number of carbon atoms per molecule for both unreactive and reactive classes of hydrocarbons (NC_U and NC_R, respectively) were computed using the following two expressions:

$$NC_U = \frac{\sum_\ell C_\ell (NC_U)_\ell}{\sum_\ell C_\ell}$$

and

$$NC_R = \frac{\sum_\ell C_\ell (NC_R)_\ell}{\sum_\ell C_\ell}$$

For total hydrocarbons (in ppm carbon), as measured by the Los Angeles and Orange County APCD's and by Scott, available data are compared with the quantity

$$(NC_R)\,[RHC] + (NC_U)[URHC]$$

where [RHC] and [URHC] are predicted hydrocarbon concentrations (ppm). For 29 September 1969, NC_R and NC_U were found to be 4.76 and 1.08, respectively. These values represent the average of all determinations of the respective parameters over the period 5 A.M. to 3 P.M. PST.

Results of the evaluation studies are available in two forms. First, hourly-averaged concentrations predicted at each station are presented as computer-drawn plots. Typical examples of these plots are given in Figure 4.6 and Appendix E, and indicate to what extent the measured and predicted concentrations agree. The dashed lines in Figure 4.6 represent the result of adding the local corrections from the microscale model to the predictions from the airshed model. To indicate the spatial variation of pollutant concentrations, hourly-averaged ground level concentration maps have been prepared for each species. Examples are shown in Figures 4.10-4.15. The reader is referred to Appendix E for a complete presentation of the validation results for all six days.

4.4.3 Discussion of the Results

Dealing with such a large volume of validation results presents obvious problems in analysis. Diagnosing the causes of observed discrepancies between comparative plots is particularly difficult, owing to the complexity of the model and the many facets of the modeling problem in general. The remarks in this section are confined largely to statements of observation, in effect, summarizing the results. In some instances it is possible to either explain, or at least speculate about, the causes of observed behavior. Subjecting the model to a complete sensitivity analysis would, of course, provide a better level of understanding of the limitations of the model, and thus, of areas of concentration for future work.

The most notable observation that can be made, perhaps, is in regard to the overall consistency of the predictions. In general, the

Figure 4.10 Predicted Hourly-Averaged (1 - 2 P.M.) RHC Ground-Level Concentrations (PPHM) on September 29, 1969

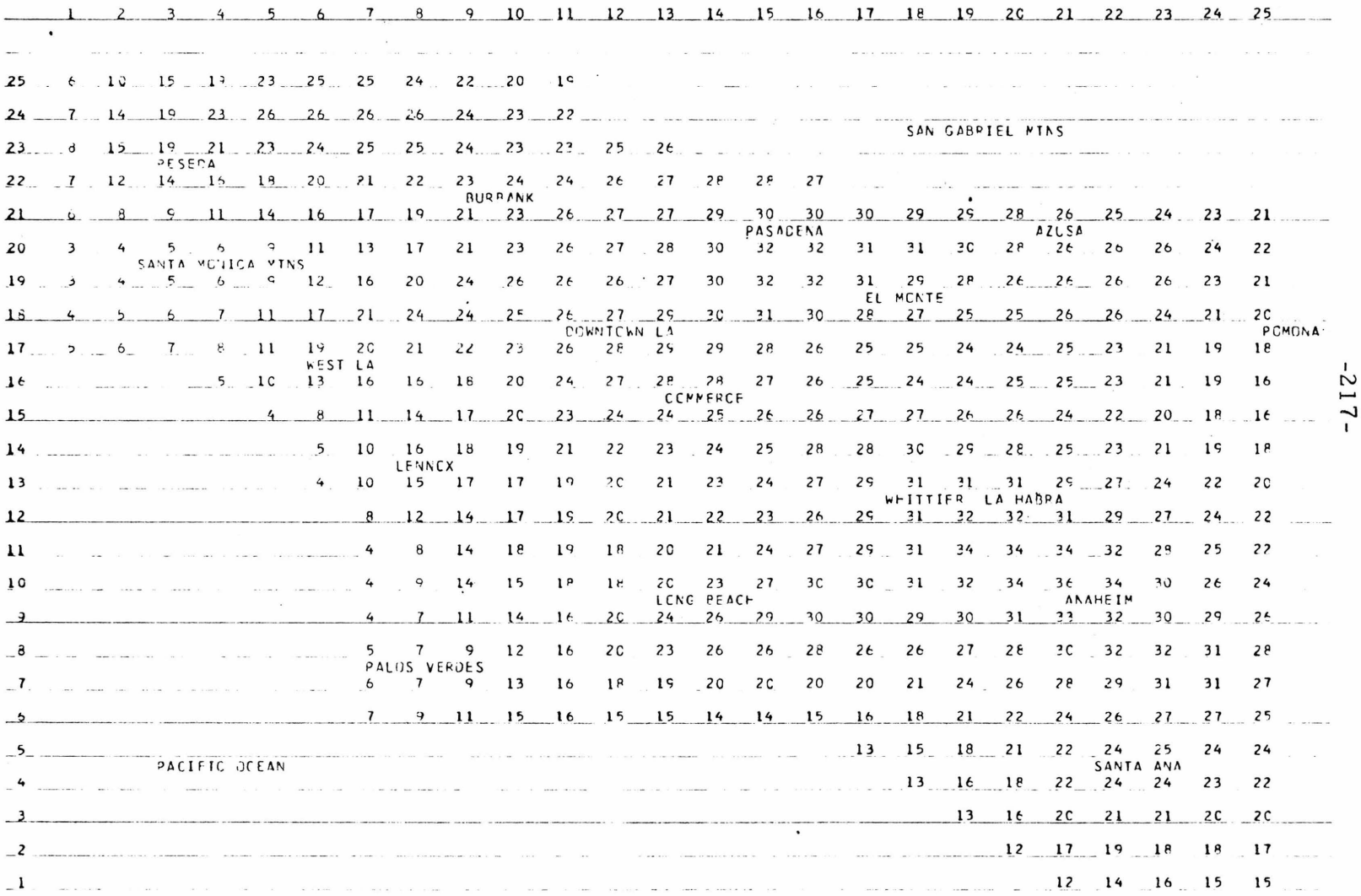

Figure 4.11 Predicted Hourly-Averaged (1 - 2 P.M.) NO Ground-Level Concentrations (PPHM) on September 29, 1969

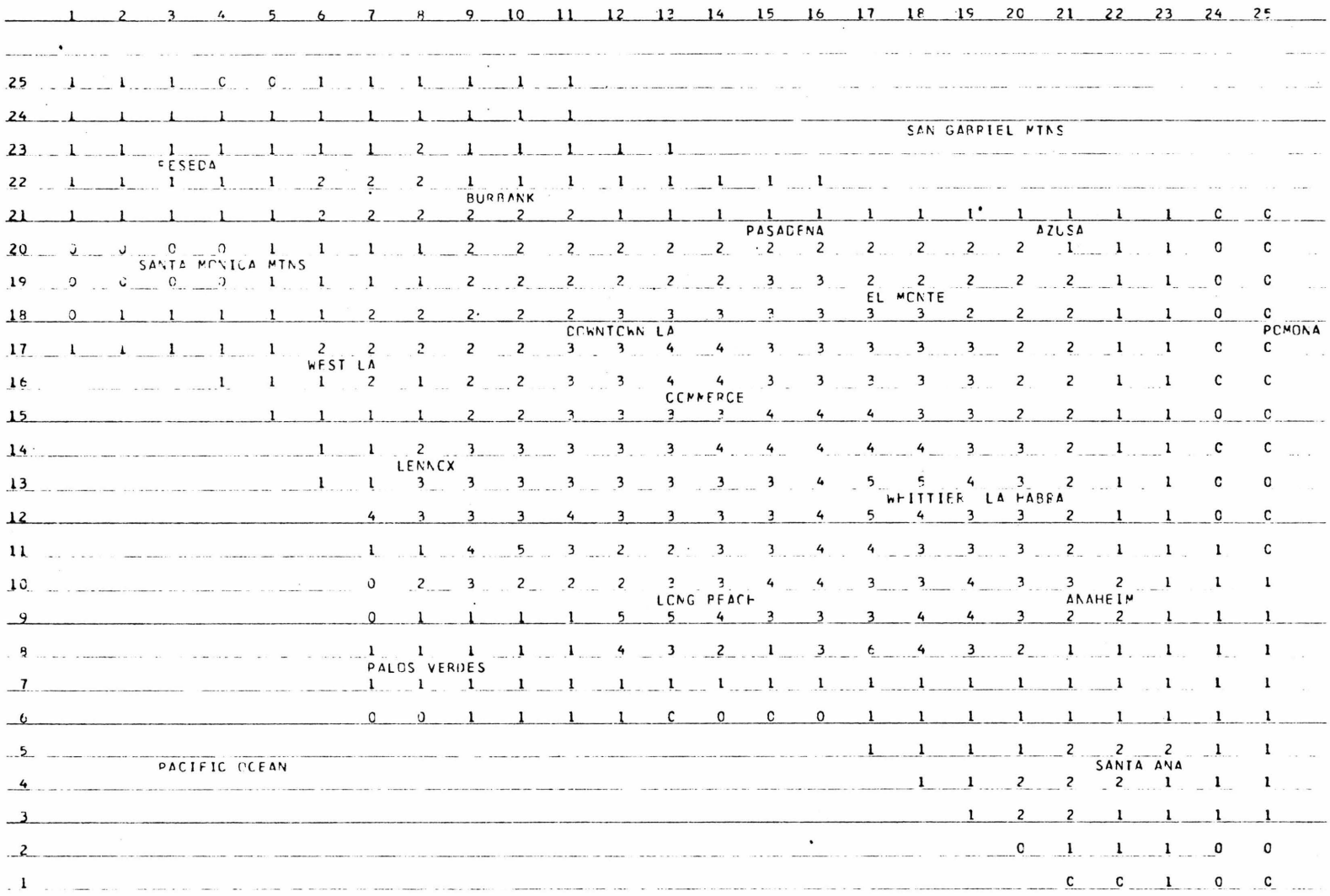

Figure 4.12 Predicted Hourly-Averaged (1 - 2 P.M.) O_3 Ground-Level Concentrations (PPHM) on September 29, 1969

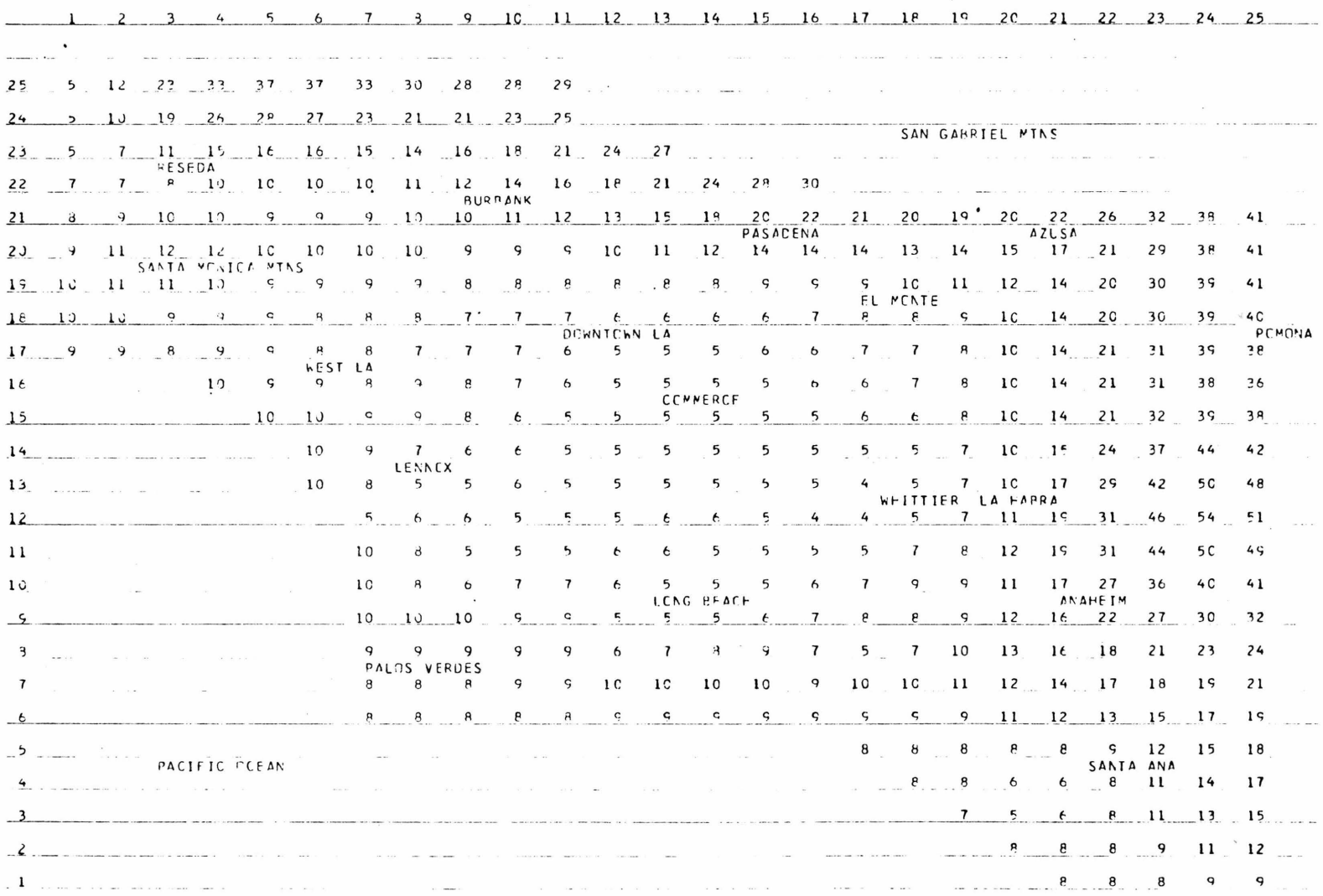

Figure 4.13 Predicted Hourly-Averaged (1 - 2 P.M.) NO_2 Ground-Level Concentrations (PPHM) on September 29, 1969

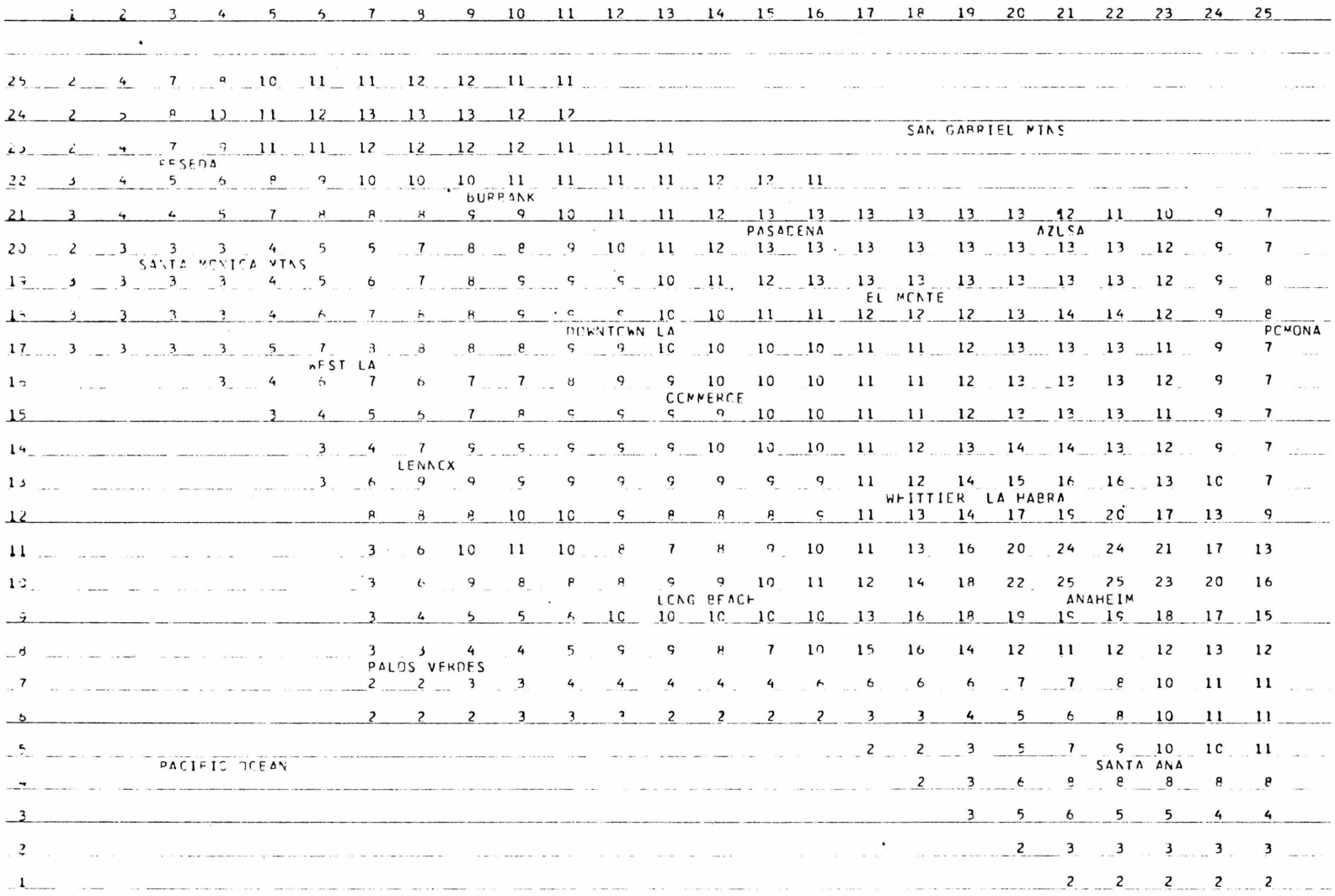

Figure 4.14 Predicted Hourly-Averaged (1 - 2 P.M.) CO Ground-Level Concentrations (PPM) on September 29, 1969

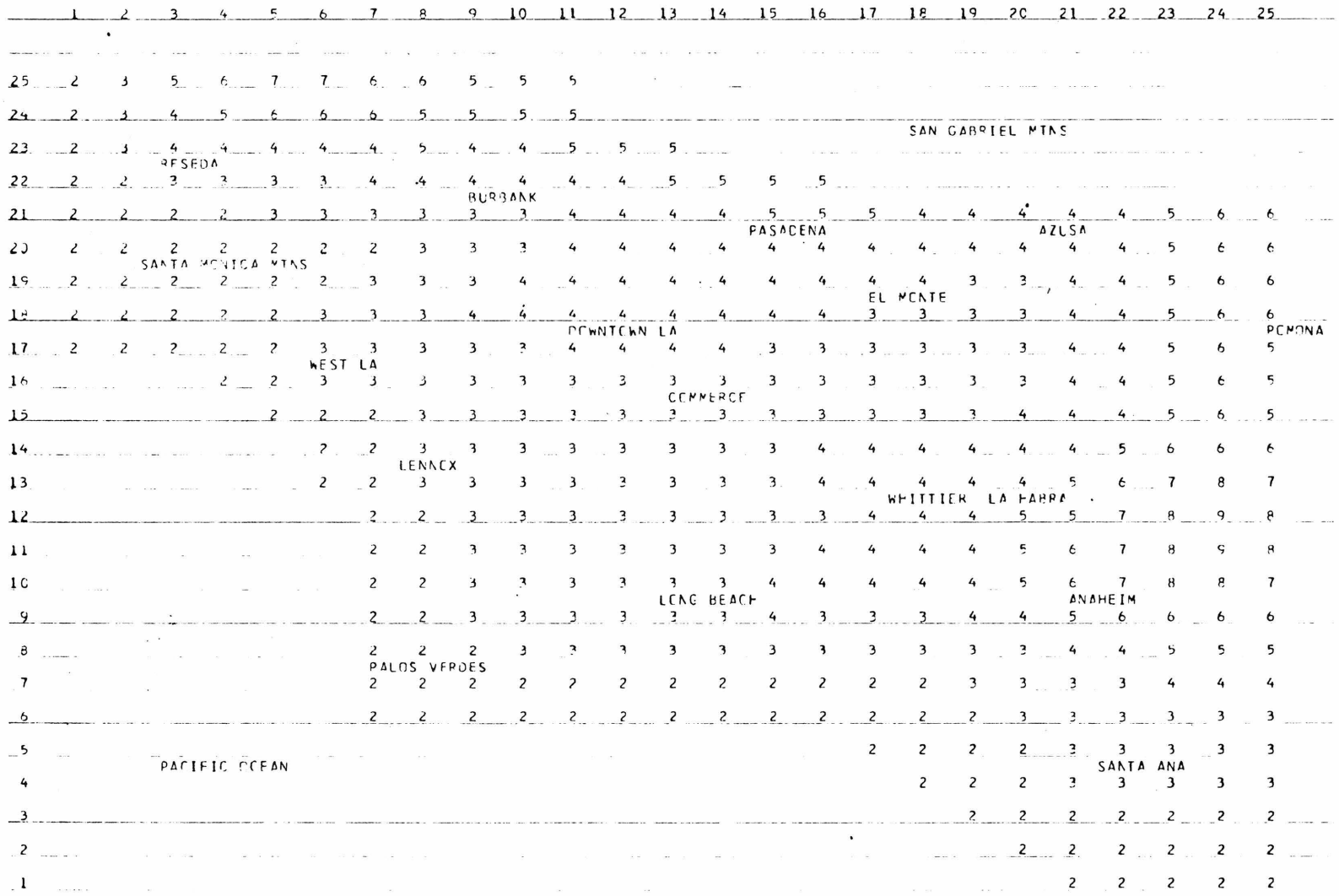

Figure 4.15 Predicted Hourly-Averaged (1 - 2 P.M.) URHC Ground-Level Concentrations (PPTM) on September 29, 1969

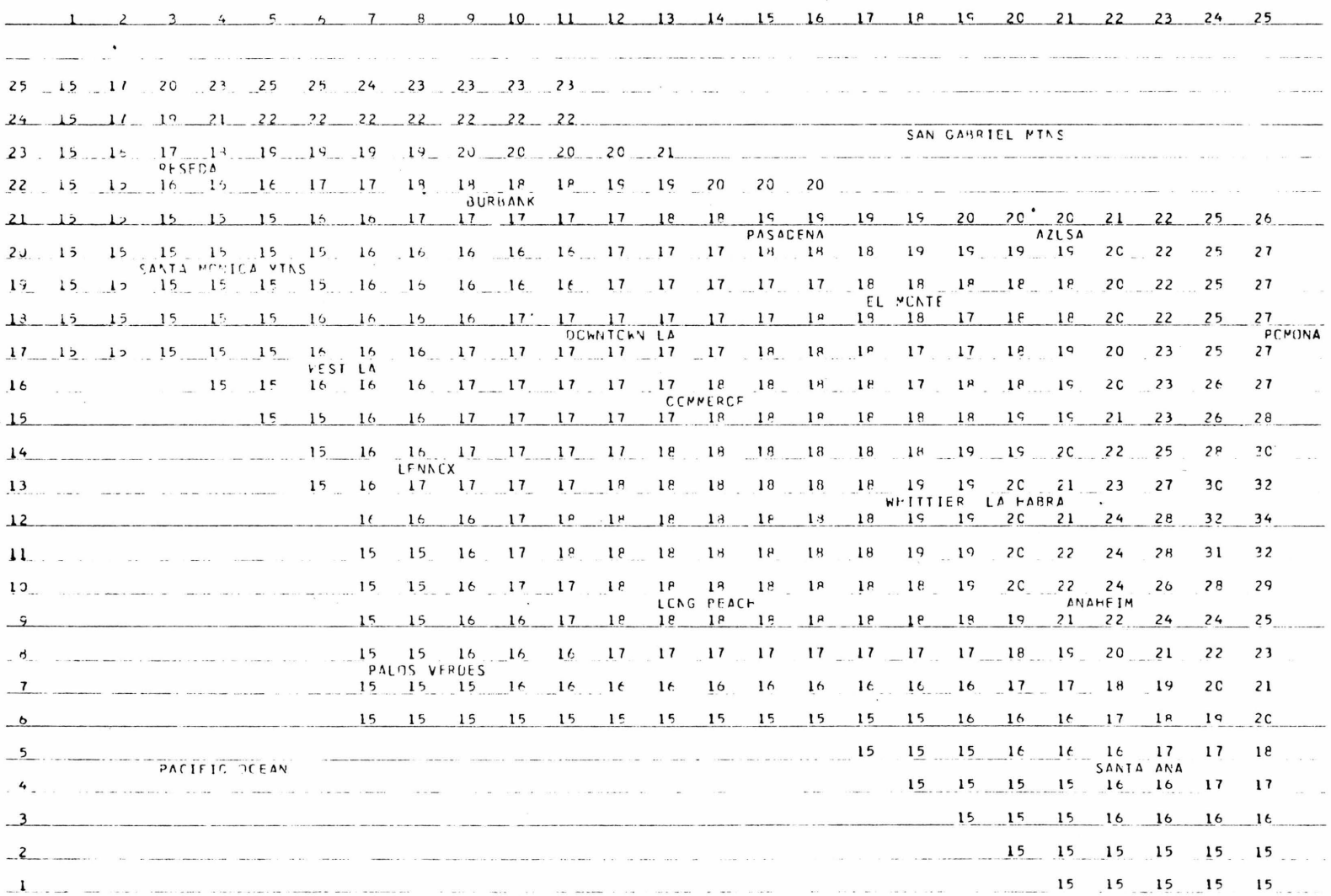

results for any one day are of the same quality as those for any other day. Thus, while the quality of station-to-station comparisons may vary between days, the number of "good," "fair," and "poor" comparisons for each day is fairly uniform. However, while overall consistency is observed, there seems to be an absence of systematically errant (or for that matter, "good") behavior. The only specific phenomenon observed is the repeatedly low ozone predictions in downtown Los Angeles.

Discussion of the results is facilitated if the following groupings are considered separately:

CO and NO	in the morning
O_3 and NO	in the late morning
O_3 and NO_2	midday and afternoon
hydrocarbon	throughout the day

Carbon monoxide, nitric oxide, and hydrocarbons are emitted by automobiles, the major source of these pollutants in Los Angeles. [NO_x emissions from tall stacks (primarily power plants and refineries) is also an important source, but emissions are elevated and generally somewhat farther removed from monitoring station sites.] As a result, morning peaks are observed for all three contaminants. The hydrocarbon peaks, however, are less sharp (or spread over a broader time span), due most likely to the high background levels of this pollutant relative to the other two. In any event, all three pollutants behave as inert species during the morning hours (until 8 o'clock or so), and observed CO and NO concentrations tend to have a similar pattern of variation during this period. As ozone forms during the

late morning hours, NO tends to decrease, and thus, during the period 9 A.M. to midday, the concentration patterns of these two pollutants are expected to be related. Finally, during the midday to afternoon period, the model should predict the buildup of the secondary pollutants, NO_2 and ozone.

Considering first CO and NO, predictions agree fairly well with the measurements, an important exception being at times (and locations) of sharp peaks during the morning rush hours. Specifically the following observations may be made with regard to the prediction of CO and NO concentrations:

1. Correlation between CO and NO concentrations during the morning hours is high. Moreover, patterns of prediction are consistent between days, both relative to the individual pollutant and relative to each other.
2. During the "peaking period," generally 6 to 8 A.M., the two pollutants, behaving to some extent as inert species, have essentially the same pattern of variation and error in prediction. When peaks are sharp, predicted profiles are generally flatter and lie well below the peak; when peaks are less pronounced, discrepancies are frequently more than proportionately reduced. But predictions are always less the observed concentrations during this period.
3. The local correction for CO often reduces the magnitude of discrepancies between prediction and observation, sometimes fully, sometimes only partially. On occasion, however, the correction fails to account for the discrepancy.

In some instances the reasons for observed discrepancies can be explained; in others only speculation will suffice at the present time. The reduced "peakedness" of the predictions relative to observations is probably due in large part to the problem of disparate scales discussed earlier. While the resolution of the model is two miles, measurements are heavily influenced by local emissions phenomena. The model, in effect, "averages" these local variations, thus flattening the peaks. Local corrections, as predicted by the microscale model described earlier, often, but not always, account fully or in part for the observed discrepancies. It thus appears that a model capable of describing sub-grid scale processes may be a useful tool for resolving difficulties that are due to mismatches in scale.

Inaccuracies in input variables may also contribute substantively to the morning discrepancies in CO and NO predictions. Estimates of the magnitude of local emissions rates are based on a driving cycle that may or may not represent actual driving behavior, either Basin-wide or in the vicinity of a monitoring station. Furthermore, driving characteristics during the rush hours vary considerably from those that typify a full day. An attempt was made to account for this (the β correction for surface streets and treatment of emissions as a function of vehicle speed on freeways), actual variations in emissions with time of day are undoubtedly not fully taken into account. Uncertainties in meteorological variables--wind speed, wind direction, and mixing depth--can also influence the results. Uncertainties in wind parameters are highest during periods of low wind, which tend to prevail during the morning hours. Errors in wind direction of 30

to 60° at these times can have a serious impact over periods of one hour or longer. Moreover, periods of low winds, as were observed on the morning of 30 September, can lead to pronounced morning peaks. While it is an easy matter to list additional possible causes of the observed discrepancies, one can only speculate at this point as to their relative importance. Extensive sensitivity studies are needed to better establish the effect of variations in each of the variables cited on the magnitude of predicted concentrations. Unfortunately, such studies have not as yet been initiated. Yet, despite the focus on shortcomings of the model in this discussion, it should be stressed that predicted CO and NO concentrations compare fairly well with observation, particularly when disparities in the scales of compared quantities are taken into account.

Turning now to a consideration of NO_2 concentration behavior, consider the following observations. In general, measured NO_2 concentrations peak around 8 A. M. to 9 A. M., decreasing thereafter. In qualitatively comparing predicted and measured profiles, approximately 50% matched well. In about 25% of the cases predictions tended to be high (although not necessarily bad), in about 15% predictions were low (although, again, not necessarily bad). In the remaining cases (about 10%) predictions were poor. Overall, then, comparisons were reasonably good and displayed little bias.

In examining NO_2 profiles after the midmorning peak, however, a pattern of bias does emerge. In general, predicted NO_2 concentrations exceeded those measured after the observed NO_2 peak, i. e., during the late morning and early afternoon hours. This effect may

be seen by examining the validation results. A notable exception to this general pattern was observed, however, for the Long Beach station. In this case measured NO_2 concentrations exceeded predicted on five of the six validation days. This anomaly may be attributable to the fact that there exist strong NO_2 sources in the vicinity which have not been properly accounted for. Included among the possible NO_2 sources are the accelerated production of the pollutant as a consequence of high local concentrations of NO and RHC (which may be due to a substantial number of large point sources in the vicinity).

In considering the general pattern of prediction exceeding measurement after the time of the measured NO_2 peak, one inevitably must note that this behavior is consistent with the fact that only a limited number of "sinks" are included in the model. Conversion of NO_2 to products other than nitric acid and PAN, formation of aerosol, and adsorption of NO_2 by vegetation have simply been ignored in the present version of the model. A second, less likely causative factor is the assumption of an excessive NO_x flux into the Basin. While this question has not been examined in any detail, it appears, however, that if the NO_x flux used is high, it is only by a factor of 10 to 30%.

Analysis of the measured data confirms an expectation that O_3 buildup will usually occur after the NO_2 peak, and that the observed NO_2 and O_3 concentration-time curves will be out of phase (i.e., have slopes that are opposite in sign for most of the period of interest). In examining the predictions, however, the times of the NO_2 and O_3 peaks are generally quite close together, with the NO_2 peak preceding the O_3 peak usually by no more than one hour. No explanation for

this unexpected pattern can be offered at present.

Observations show that the onset of O_3 formation generally occurs as NO disappears (i.e., NO is less than 0.1 ppm). In contrast to the disappointing performance of the model with regard to the NO_2 - O_3 phasing, predicted behavior is quite similar to observed behavior in the case of the NO - O_3 phasing. Unfortunately, prediction of the time and magnitude of the ozone peak leaves much to be desired. In only 2/3 of the cases (87 profiles in all) was the observed time of the peak predicted to be within one hour of the measured time, and in only 1/3 of the cases was the magnitude of the observed maximum predicted to be within 20% of that measured. There are a number of possible causes for this pattern of deviation, as predicted O_3 level is influenced by virtually every variable of consequence that is treated in the model. Well planned sensitivity studies, aimed at examining the effects of variations in k_1, in NO_x emissions rates, etc. offer the only feasible means of diagnosing the problem in any meaningful way.

Finally, consider hydrocarbons. In general, comparison between prediction and measurement is quite favorable. In about 3/4 of the profiles, comparisons are excellent (generally, 0 to 1 ppmC discrepancy throughout the day). Unfortunately, relatively little value is placed on these results, despite their generally good quality, because of the high levels of uncertainty in the total hydrocarbon measurements. Only the GC measurements made at El Monte and Commerce are of sufficient accuracy to provide useful comparisons. However, they were not made often enough to provide a suitable

data base for validation.

4.5 Conclusion

In the first four chapters of this report, an urban scale mathematical model of photochemical air pollution has been formulated which may be used to predict ground level concentrations of nitrogen oxides, hydrocarbons, carbon monoxide, and ozone. Because of the existence of a rich data base for use in defining inputs and validating the model, the Los Angeles Basin was chosen as the initial region for application of the model. The treatment of all important components of the model have been described, including meteorology, emissions, atmospheric chemistry, the numerical solution of the governing equations, and the microscale model.

In general, the validation studies have provided encouraging results. Overall, the results have usually been at least qualitatively in agreement with observations, and in many instances, good quantitative agreement has also been achieved. The experimental data base is rich, and the validation results are extensive. Many opportunities for worthwhile analysis therefore exist. But it must be emphasized that there is an equal, if not greater need to carry out a full and well planned sensitivity analysis. The model, as it stands, is complex; it contains facets of varying detail and importance. Moreover, as sensitivities of predictions to variations in parameters are uncovered, the number of possible causative factors that may explain a type of discrepancy between prediction and experiment may be reduced, thus simplifying the search for causative relationships and means for improving the model's predictions.

CHAPTER 5

EVALUATION OF THE ENVIRONMENTAL PROTECTION AGENCY IMPLEMENTATION PLAN FOR LOS ANGELES

5.1 Introduction

In Chapters 1-4 a mathematical model of photochemical air pollution has been developed and initial validation results have been presented for Los Angeles. Although models of this type must be evaluated by comparing their predictions with past episodes, their real utility lies in their use as means for assessing the impact on air quality of future urban and regional planning decisions. As mentioned previously, the significant applications of airshed models include:

1. Real-time prediction in an alert warning system;
2. Examination of the air pollution impact of new sources; and
3. Simulation of the effects of alternative emission control strategies on pollutant concentrations in the airshed.

Real-time prediction capabilities may be utilized in two ways. First, short-term pollutant concentration forecasts may be generated to determine if air quality standards will be violated in the region. Upon prediction of an alert situation, appropriate emergency control measures may be ordered and their expected effects forecasted [see, for example, Kyan and Seinfeld (1973)]. Second, a mathematical air pollution model can be an aid in monitoring pollutant concentrations. Presently, air pollution control agencies must evaluate the air quality

of a region from measurements taken at a limited number of fixed monitoring stations. In the region considered in Chapters 1-4, for example, there are 15 measuring sites over a 1712 sq. mi. area, that is one station per 114 sq. mi. of populated area. If the concentrations measured at each station are representative of, say, those in a one sq. mi. area surrounding the station, then only about 1% of the populated area is actually subject to air quality surveillance. The most important consequence of this potential lack of information is that high pollutant concentrations may remain undetected in the airshed.

To improve the pollutant surveillance capabilities of local governmental agencies, urban air pollution models, once validated, can be operated on a real-time basis. The model predictions at the existing monitoring sites may be compared with the actual measurements to verify the accuracy of prediction. If violations of air quality standards are predicted in areas where no measurements are available, appropriate short-term emission control strategies may be instituted. Interfacing a meteorological data gathering program with numerical predictions will be the primary developmental work required for this application.

The assessment of the impact of new emission sources on air quality in the airshed is perhaps a more immediate application of air pollution modeling in its present state of development. To illustrate the manner in which a model may be used for this purpose, suppose a new freeway is to be constructed. First, employing typical meteorological conditions, a simulation is carried out to determine

the nominal pollutant concentrations in the absence of the freeway. Then a new emissions inventory is prepared, including all effects of the proposed freeway on emissions, such as altered population growth rates and the resulting change in vehicle miles travelled (VMT). Based on the new inventory, a second simulation is performed, and the pollutant levels under the two conditions are compared. If air quality standard violations are predicted, then plans for the proposed freeway can be modified to whatever extent is necessary.

While real-time prediction and examination of the air pollution impact of new sources are significant future uses of urban air pollution models, presently the most important potential use of such models is simulation of the effects of alternative emission control strategies on air quality. Under the provisions of the 1970 Clean Air Act, local, state, and Federal authorities are charged with the responsibility of implementing necessary control measures to insure that Federal air quality standards will not be exceeded. As a result, the Environmental Protection Agency (EPA) has proposed control strategy implementation plans for those urban areas that are presently in violation of the standards.

Since mathematical models relating emission levels of oxides of nitrogen and hydrocarbons to air quality in terms of nitrogen dioxide and oxidants were essentially undeveloped at the time when control strategies were first promulgated, the so-called rollback method was used to relate reactive hydrocarbon (RHC) and NO_x emission reductions to improvements in oxidant and NO_2 air quality (Barth, 1970). Barth employed the rollback approach to determine

motor vehicle emission goals for CO, RHC, and NO_x. The approach is based on first calculating the fractional reduction α in ambient concentrations necessary to achieve desired air quality. If c_{max} is the present maximum pollutant concentration, c_{des} is the desired pollutant concentration, c_b is the background pollutant concentration, and g is the emission growth factor, then α is computed by

$$\alpha = \frac{gc_{max} - c_{des}}{gc_{max} - c_b}$$

It is then assumed that emission rates must be fractionally reduced by α. The key assumption made is that there exists a linear relationship between air quality and emissions.

In applying rollback to propose and evaluate control strategies, α is calculated from the following relationship

$$\alpha = \frac{c_{mb} - c_{des}}{c_{mb} - c_b}$$

where c_{mb} is the maximum concentration of a pollutant of interest observed in the airshed during a specified yearly period, termed the base year. The allowable total daily emissions in the airshed, E_{da}, (in tons per day) consistent with the desired air quality level is given by

$$E_{da} = (1-\alpha) E_{db}$$

where E_{db} is the daily emissions estimate (in tons per day) for the airshed during the base year. Before any control strategies are proposed, a projected, or baseline, emissions inventory for some future year of interest must be assembled, considering all factors that will

affect emissions. Given the daily emissions for the baseline inventory, sufficient control measures must be proposed which will reduce emissions in the future year to the allowable level, E_{da}, calculated above.

Use of rollback to establish a control strategy for an airshed is a direct process, as illustrated in the block diagram in Figure 5. 1. In contrast, the effort involved in determining a final control policy employing the airshed model is somewhat more involved since the strategy is the result of an iterative procedure, as shown in Figure 5.2. Note that in addition to the usual inputs to the model (i. e., meteorology and initial and boundary conditions), an initial control strategy must be proposed in order to establish the emission inputs. The initial strategy could be generated, for example, using the rollback approach. Upon examining the air quality predictions from the model, appropriate changes are made in the control strategy until the model predicts acceptable air quality levels.

The rollback technique provides a simple means of relating emission reductions to air quality improvements. In the case of photochemical smog the most obvious deficiency of the method is that maximum oxidant concentrations are usually assumed to be completely independent of NO_x emissions, and similarly, maximum NO_2 concentrations are assumed to be independent of RHC emissions. An examination of the chemistry of photochemical smog reveals that these two assumptions are not valid. In addition, the spatial distribution of sources and the extent to which each source contributes to the maximum pollutant concentrations are also not considered in the rollback calculation.

Figure 5.1 Block Diagram Illustrating the Specification of an Emission Control Strategy Using Rollback

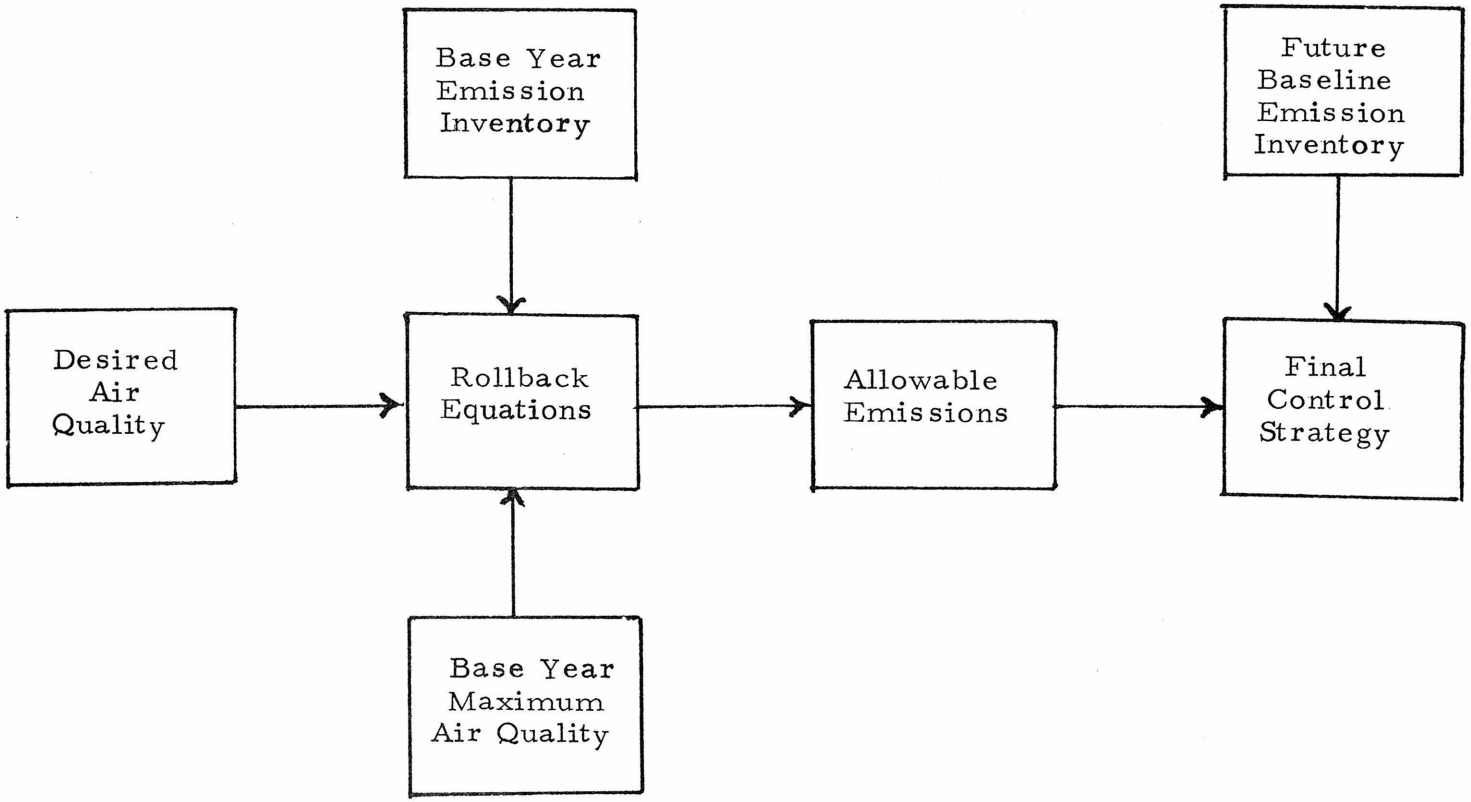

Figure 5.2 Block Diagram Illustrating the Specification of an Emission Control Strategy Using the Airshed Model

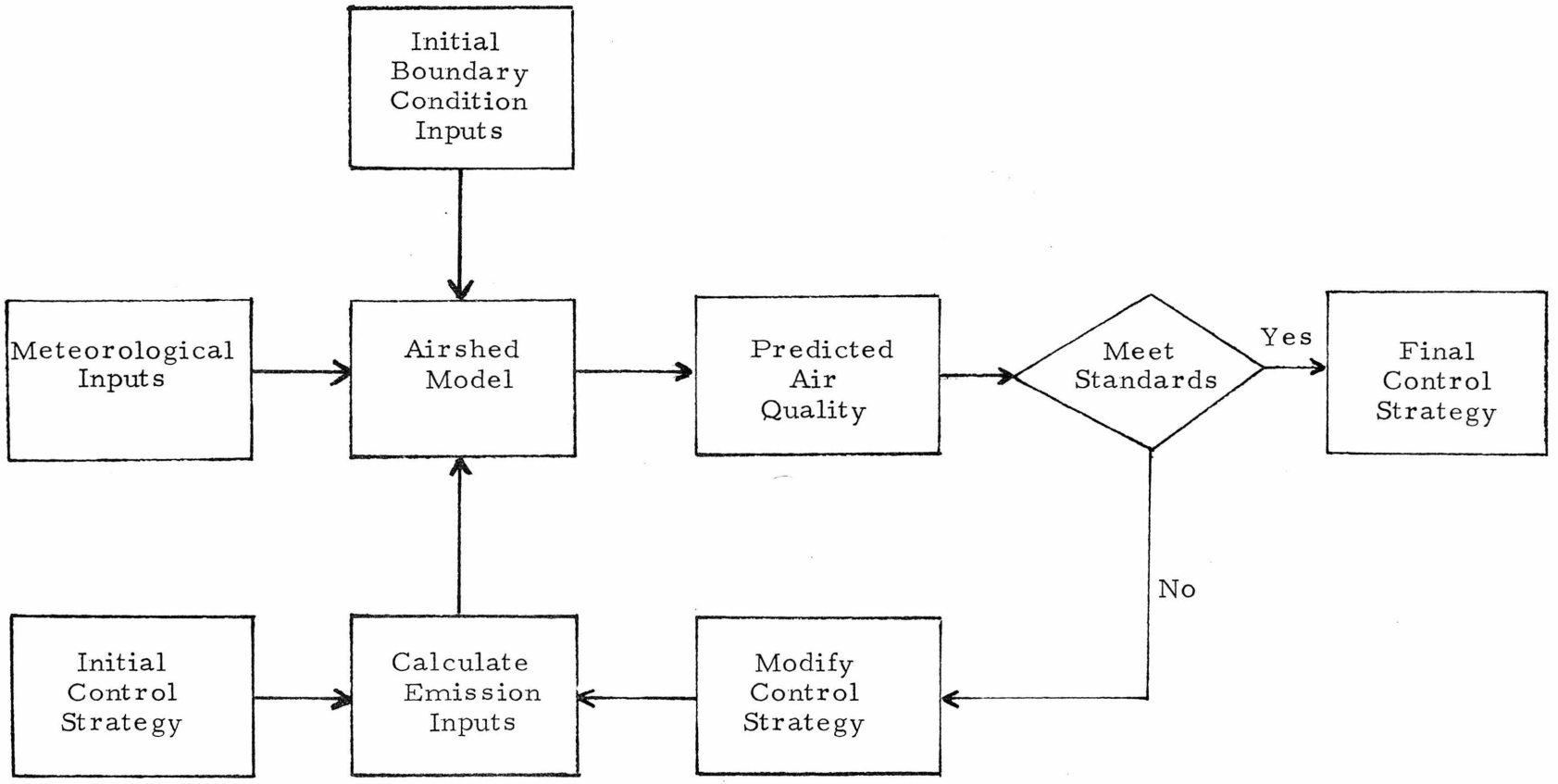

Control measures which have the greatest impact on emissions in areas upwind of those in which the highest pollutant concentrations are experienced will be the most effective. For example, the Los Alamitos, Haynes, and Huntington Beach power plants in the Los Angeles modeling region have a more profound influence on the high NO_x concentrations in Orange County than do the other power plants located in Los Angeles County. Thus, when control strategies are planned, it is essential to control those sources that are directly responsible for the maximum pollutant concentrations observed in the airshed.

Another difficulty associated with rollback calculations is that the choice of the base year may have a substantial influence on the calculated allowable emissions in some future year. For example, a base year which is "good" meteorologically (that is one in which the maximum pollutant concentrations were not high due to favorable meteorological conditions) will lead one to the conclusion that allowable emissions in a future year may be greater than those calculated from a base year that is "bad" meteorologically. In rollback calculations carried out by the Bay Area APCD in which two different base years were selected to determine allowable RHC emissions in that area in 1977, it was found that using 1971 as the base year, a substantial VMT reduction would be required in the Bay Area in 1977 to meet the air quality standards, whereas the second calculation employing 1970 as the base year indicated that only a small VMT reduction would be required in 1977 (Levaggi, 1973). Clearly, these results and the previous discussion point to possible serious

weaknesses in the use of rollback calculations for setting long-term control strategies. In fact, in his 1970 paper Barth stated, "Clearly what is needed is to fully relate all these effects to emissions and to predict future events in growth and required control using a comprehensive simulation model complete with modules reflecting all input variables, meteorological variables including air transport parameters, and ... the chemical kinetics describing the multiplicity of reactions which occur."

The remainder of this chapter is devoted to a discussion of the application of the mathematical model of photochemical air pollution to evaluate emission control strategies. The objectives of this work are: 1) to illustrate the treatment of all model inputs through the use of a specific example, 2) to compare results obtained using rollback with those obtained on the basis of the simulation model for 1977 Los Angeles control strategies, and 3) to determine the major difficulties to be encountered in using the model to evaluate emission control strategies.

Emission control strategies aimed at reducing oxidant and NO_2 levels in the Los Angeles area have been proposed by various groups, including the State of California Air Resources Board (1972), the California Institute of Technology Environmental Quality Laboratory (Lees et al., 1972), and the EPA (1973g). Because the EPA plan, as described in the July 2, 1973 issue of the Federal Register, appears to be the most probable strategy to be adopted at this time, the evaluation study presented here will focus on this strategy.

The EPA control plan for Los Angeles consists of several actions to reduce both vehicular and fixed source emissions. The plan consists of the following elements:

1. Limitation of annual gasoline sales in years subsequent to 1973 to that amount sold between July 1, 1972 and June 30, 1973;
2. Mandatory periodic vehicle inspection and maintenance of all light-duty vehicles beginning March 1, 1974;
3. Establishment of exclusive bus and carpool lanes on freeways and major streets during the morning and evening peak traffic hours;
4. Immediate ban on the construction of all new parking facilities in the Los Angeles area;
5. Reduction of existing parking spaces by 20% beginning January 31, 1974;
6. Restricted registration of all motorcycles to 1973 levels beginning in 1974, and restriction of the operation of two-stroke motorcycles during daylight hours in the months from May through October, beginning May 1, 1974;
7. Installation of vacuum spark advance disconnect (VSAD) retrofit devices on pre-1971 light-duty motor vehicles, and installation of oxidizing catalyst retrofit devices on 1966-74 light-duty motor vehicles;

8. Additional control of fixed sources;* and

9. Additional limitations on gasoline sales, beyond the 1972-73 sales level cited above, to insure that air quality standards will not be violated.

Although it is not clear precisely how these measures were arrived at, it appears that these represent a group of technologically feasible steps which would serve to reduce total mass emissions of RHC and NO_x by percentages which, by means of a rollback calculation, would reduce pollutant levels to those closely approaching the air quality standards. As noted previously, the rollback concept affords a means of computing necessary emission levels directly from current air quality levels, desired air quality levels, and estimated growth factors. The use of a dynamic mathematical model necessitates that the emission levels first be postulated, then all model inputs (meteorological data, reaction rate constants, radiation intensities, initial and boundary conditions) be chosen, perhaps as representative of those of typical days, with the resulting air quality finally predicted. If the air quality does not meet the standards, then the emission level can be adjusted and the simulation repeated. The values of some

---

* While specific control measures for fixed sources were not included in the EPA (1973g) plan, EPA is considering such measures as substitution of unreactive solvents for reactive solvents and use of vapor recycle systems. Liu (1973) has recently compiled a fixed source inventory for the Basin in 1977 assuming implementation of control measures similar to those considered by EPA. This work has been adopted for use in this study. The strategy employed by Liu (1973) includes controls on refinery heaters and internal combustion engines, substitution of 1, 1, 1-trichloroethane for 1, 1, 1-trichloroethylene by organic solvent users and use of vapor recycle systems in petroleum marketing operations.

inputs, particularly the initial and boundary conditions, may themselves be related to the emissions inventory, since pollutant levels in early morning will be governed to some extent by the overnight emission ratio. The model simulation has the advantage of providing estimates not only of the maximum pollutant concentrations which will occur* but also of the pollutant dosages to the population in different areas of the airshed.

In the study to be described, the meteorological condition of September 29, 1969, a day on which high oxidant and NO_2 concentrations were experienced in Los Angeles, will be used as a basis for evaluating the EPA implementation plan for Los Angeles. Since only one set of meteorological conditions will be used, no definitive conclusions can be drawn with respect to the maximum pollutant levels that can be expected in 1977. Nevertheless, comparison of the predictions for the 1969 and 1977 emission inventories should provide a good indication of the general improvement in air quality to be expected if the EPA plan is followed.

The evaluation of the EPA implementation plan will be carried out in the following manner. First, essentially as a base case, one simulation is performed in which only currently legislated control measures are assumed to be applied in 1977. The second simulation will then include all control measures proposed by EPA except additional gasoline sales limitations beyond the 1972-3 limit mentioned above. (Additional simulations based on further limitations on

---

* Current regulations specify that the Federal air quality standard of 0.08 ppm oxidant and the California standard of 0.25 ppm NO_2 for one-hour may only be exceeded once a year.

gasoline sales could be carried out if predictions indicate that air quality standards will be violated in 1977 at the 1972-3 sales level.)

In the sections that follow, the discussion will focus first on each of the model inputs: emissions (Section 5.2) and meteorology, reaction rate constants, and initial and boundary conditions (Section 5.3). Section 5.4 is devoted to a discussion of the simulation results obtained for the Basin in 1977. In addition, the predictions from the airshed model for 1977 are compared with those obtained from a roll-back calculation. The conclusions from this study are summarized in Section 5.5.

5.2 Projected Emissions for the Los Angeles Basin in 1977

Although the estimation of emissions from each source in the region of interest is basically a straightforward process, the prediction of emission levels in future years is subject not only to the usual problems in compiling an inventory (see Chapter 2) but also with those associated with forecasting changes in emission rates in the future. Growth rates must be properly taken into account and emission levels and the degree of effectiveness of control devices must be estimated. Clearly, these aspects introduce degrees of uncertainty that do not exist for past years. In this section, a source inventory is developed for Los Angeles in 1977. In particular, detailed emission inventories for two 1977 cases (the baseline case and the EPA implementation plan) are presented. In addition, guidelines are given which may be used to estimate emissions if gasoline sales are limited beyond the 1972-73 sales level.

5.2.1 1977 Baseline Inventory for Los Angeles

Emissions in the baseline inventory are intended to be representative of those expected in the Los Angeles modeling region in 1977 if no additional control measures other than scheduled motor vehicle exhaust emission controls on 1975-77 model vehicles are implemented.

5.2.1.1 Motor Vehicle Emissions

As outlined in Chapter 2, motor vehicle emissions are determined by specifying the pollutant emission rate from an "average" vehicle (in grams/mile) and from the number of daily miles driven. Hot and cold-start emission rates, as well as the emission/driving speed correlation parameters (see Section 2.2.1) for the "average" vehicle in the Basin in 1977 are summarized in Tables 5.1 and 5.2, respectively. These factors, discussed in detail in Appendix A, were derived from reported and estimated emission rates for light and heavy-duty vehicles and motorcycles.

The daily VMT for both freeways and surface streets in 1969 are given in Figures 2.1 and 2.2. Since the population in several areas of the modeling region is expected to grow, the VMT in these areas is also expected to show a similar increase. Liu (1973) has estimated that the VMT in the Basin will increase by about 17% between 1969 and 1977. The VMT increase in each grid square can then be computed by apportioning the 17% increase in total mileage according to projected population growth in each square. The daily VMT increases for freeways and surface streets over the 1969 levels for 1977 are illustrated in Figures 5.3 and 5.4, respectively.

Table 5.1

Estimated Hot and Cold-Start Emission Rates (grams/mi.) for the 1977 Baseline Motor Vehicle Population in Los Angeles

	HC	CO	NO_x (as NO_2)
Hot-start	2.14	21.5	2.60
Cold-start	3.20	35.0	2.58

Table 5.2

Estimated Emission/Driving Speed Correlation Parameters for the 1977 Baseline Motor Vehicle Population in Los Angeles

Species	Driving Speed range (mph)	a_ℓ	b_ℓ
HC	15-30	7.253	-0.544
HC	30-60	2.746	-0.259
CO	15-45	428.8	-1.080
CO	45-60	1.498	0.406
NO_x	15-60	2.094	1.846

The temporal distributions of surface street and freeway traffic in 1977 are assumed to be identical to those derived for 1969. Similarly, the fraction of cold-starts to total starts and the correction for the nonuniform distribution of cold-starts are also taken as unchanged from the 1969 values. To calculate the total daily emissions from

Figure 5.3 Estimated Nominal Increase in Freeway Mileage for Los Angeles Between 1969 and 1977 (thousands of miles per day). Source: Liu (1973)

	1	2	3	4	5	6	7	8	9	10	11	12	13	14	15	16	17	18	19	20	21	22	23	24	25
25	17.8	0.0	0.0	0.0	53.4	53.4	0.0	0.0	0.0	0.0	0.0														
24	0.0	0.0	0.0	0.0	53.4	35.6	53.4	0.0	0.0	0.0	0.0														
																			SAN GABRIEL MTNS						
23	0.0	0.0	0.0	0.0	53.4	0.0	53.4	35.6	35.6	0.0	0.0	0.0	0.0												
			RESEDA																						
22	0.0	0.0	0.0	0.0	53.4	0.0	35.6	0.0	35.6	35.6	0.0	0.0	0.0	53.4	0.0	0.0									
									BURBANK																
21	53.4	53.4	53.4	53.4	53.4	53.4	53.4	53.4	53.4	35.6	17.8	8.9	0.0	0.0	0.0	0.0	0.0	0.0	0.0	0.0	0.0	0.0	0.0	0.0	0.0
															PASADENA						AZUSA				
20	0.0	0.0	0.0	0.0	35.6	0.0	0.0	35.6	53.4	0.0	17.8	0.0	0.0	26.7	7.1	0.0	0.0	53.4	53.4	53.4	53.4	53.4	53.4	0.0	0.0
			SANTA MONICA MTNS																						
19	0.0	0.0	0.0	0.0	35.6	0.0	0.0	0.0	35.6	17.8	17.8	35.6	17.8	17.8	0.0	0.0	0.0	0.0	0.0	0.0	0.0	0.0	0.0	0.0	0.0
																	EL MONTE								
18	0.0	0.0	0.0	0.0	35.6	35.6	0.0	0.0	0.0	17.8	17.8	17.8	17.8	17.8	17.8	17.8	35.6	35.6	35.6	35.6	35.6	35.6	53.4	53.4	53.4
											DOWNTOWN LA														POMONA
17	0.0	0.0	0.0	0.0	0.0	35.6	35.6	35.6	35.6	17.8	17.8	17.8	17.8	17.8	17.8	5.3	35.6	35.6	35.6	0.0	0.0	0.0	0.0	0.0	53.4
						WEST LA																			
16				0.0	53.4	53.4	35.6	3.6	0.0	0.0	17.8	17.8	17.8	17.8	0.0	0.0	35.6	35.6	35.6	53.4	0.0	0.0	0.0	53.4	53.4
													COMMERCE												
15					0.0	0.0	35.6	35.6	0.0	0.0	35.6	0.0	0.0	35.6	35.6	0.0	35.6	0.0	0.0	53.4	53.4	53.4	53.4	53.4	0.0
14						0.0	0.0	35.6	0.0	0.0	35.6	0.0	0.0	35.6	35.6	35.6	3.6	0.0	0.0	0.0	0.0	0.0	0.0	0.0	0.0
								LENNOX																	
13						0.0	0.0	53.4	0.0	0.0	35.6	0.0	0.0	35.6	0.0	35.6	3.6	0.0	0.0	0.0	0.0	0.0	0.0	0.0	0.0
																		WHITTIER		LA HABRA					
12							0.0	53.4	3.6	0.0	35.6	0.0	35.6	35.6	0.0	35.6	35.6	35.6	0.0	0.0	0.0	0.0	0.0	0.0	0.0
11							0.0	0.0	53.4	53.4	35.6	0.0	35.6	0.0	5.3	35.6	35.6	35.6	35.6	0.0	0.0	1.8	0.0	0.0	1.8
10							0.0	0.0	0.0	0.0	35.6	0.0	35.6	0.0	0.0	35.6	0.0	5.3	8.9	53.4	53.4	53.4	53.4	53.4	53.4
													LONG BEACH								ANAHEIM				
9							0.0	0.0	0.0	0.0	35.6	35.6	35.6	35.6	35.6	35.6	0.0	0.0	0.0	0.0	53.4	17.8	0.0	53.4	0.0
8							0.0	0.0	0.0	0.0	35.6	7.1	35.6	0.0	0.0	35.6	35.6	53.4	53.4	0.0	1.8	53.4	53.4	53.4	0.0
								PALOS VERDES																	
7							0.0	0.0	0.0	0.0	1.8	1.8	0.0	0.0	0.0	0.0	0.0	53.4	53.4	53.4	53.4	0.0	53.4	53.4	0.0
6							0.0	0.0	0.0	0.0	0.0	0.0	0.0	0.0	0.0	0.0	0.0	0.0	53.4	26.7	0.0	0.0	53.4	53.4	53.4
5																	0.0	0.0	0.0	53.4	53.4	53.4	53.4	0.0	53.4
			PACIFIC OCEAN																			SANTA ANA			
4																		0.0	0.0	0.0	0.0	53.4	53.4	53.4	53.4
3																			0.0	0.0	53.4	17.8	0.0	0.0	0.0
2																				0.0	35.6	0.0	0.0	0.0	0.0
1																					0.0	0.0	0.0	0.0	0.0

Figure 5.4 Estimated Nominal Increase in Surface Street Mileage for Los Angeles Between 1969 and 1977 (thousands of miles per day). Source: Liu (1973)

	1	2	3	4	5	6	7	8	9	10	11	12	13	14	15	16	17	18	19	20	21	22	23	24	25
25	14.1	28.2	28.2	28.2	28.2	42.3	42.3	28.2	14.1	14.1	0.0														
24	28.2	42.3	42.3	42.3	42.3	42.3	42.3	14.1	14.1	14.1	14.1									SAN GABRIEL MTNS					
23	28.2	42.3	42.3	42.3	42.3	42.3	42.3	42.3	14.1	0.0	14.1	14.1	14.1												
			RESEDA																						
22	42.3	42.3	42.3	42.3	42.3	42.3	28.2	28.2	14.1	14.1	14.1	14.1	14.1	14.1	14.1	14.1									
									BURBANK																
21	42.3	28.2	28.2	28.2	28.2	42.3	42.3	42.3	42.3	42.3	42.3	14.1	14.1	14.1	14.1	0.0	0.0	0.0	0.0	0.0	0.0	0.0	0.0	0.0	0.0
															PASADENA						AZUSA				
20	0.0	0.0	0.0	0.0	28.2	28.2	42.3	42.3	42.3	0.0	42.3	42.3	14.1	14.1	14.1	14.1	14.1	14.1	14.1	14.1	14.1	42.3	14.1	28.2	28.2
			SANTA MONICA MTNS																						
19	0.0	0.0	0.0	0.0	0.0	0.0	0.0	14.1	14.1	28.2	28.2	28.2	28.2	28.2	28.2	28.2	28.2	28.2	28.2	28.2	42.3	42.3	42.3	28.2	42.3
																		EL MONTE							
18	0.0	0.0	0.0	0.0	0.0	0.0	42.3	28.2	28.2	28.2	14.1	14.1	14.1	28.2	28.2	28.2	28.2	28.2	28.2	28.2	42.3	42.3	28.2	14.1	14.1
											DOWNTOWN LA														POMONA
17	14.1	14.1	14.1	14.1	14.1	28.2	42.3	28.2	28.2	28.2	14.1	14.1	14.1	14.1	28.2	28.2	28.2	28.2	28.2	28.2	42.3	42.3	28.2	28.2	42.3
						WEST LA																			
16				14.1	28.2	28.2	42.3	28.2	28.2	28.2	28.2	28.2	28.2	28.2	28.2	14.1	28.2	28.2	28.2	28.2	42.3	42.3	42.3	42.3	42.3
														COMMERCE											
15					14.1	42.3	28.2	28.2	28.2	28.2	28.2	14.1	14.1	14.1	14.1	14.1	28.2	28.2	28.2	28.2	42.3	42.3	42.3	42.3	14.1
14						28.2	28.2	28.2	28.2	28.2	28.2	28.2	28.2	28.2	28.2	28.2	28.2	28.2	28.2	28.2	28.2	28.2	28.2	28.2	0.0
								LENNOX																	
13						14.1	28.2	28.2	28.2	42.3	28.2	28.2	28.2	28.2	28.2	28.2	28.2	42.3	42.3	42.3	28.2	42.3	42.3	42.3	28.2
																		WHITTIER		LA HABRA					
12							28.2	28.2	28.2	42.3	28.2	28.2	28.2	28.2	28.2	28.2	28.2	42.3	42.3	42.3	42.3	42.3	42.3	42.3	42.3
11							14.1	28.2	42.3	42.3	28.2	28.2	28.2	28.2	28.2	28.2	28.2	14.1	42.3	42.3	42.3	42.3	42.3	42.3	42.3
10							0.0	42.3	28.2	42.3	42.3	28.2	28.2	28.2	28.2	42.3	42.3	42.3	42.3	42.3	42.3	42.3	42.3	42.3	42.3
														LONG BEACH							ANAHEIM				
9							0.0	42.3	28.2	28.2	42.3	28.2	28.2	28.2	28.2	42.3	42.3	42.3	42.3	42.3	42.3	42.3	42.3	42.3	42.3
8							14.1	42.3	28.2	28.2	28.2	28.2	14.1	14.1	14.1	42.3	42.3	42.3	42.3	42.3	42.3	42.3	42.3	42.3	42.3
							PALOS VERDES																		
7							28.2	42.3	42.3	14.1	14.1	14.1	14.1	14.1	14.1	42.3	42.3	42.3	42.3	42.3	42.3	42.3	42.3	42.3	42.3
6							14.1	14.1	28.2	42.3	0.0	0.0	0.0	0.0	0.0	28.2	42.3	42.3	42.3	42.3	42.3	42.3	42.3	42.3	42.3
5																	28.2	42.3	42.3	42.3	42.3	42.3	42.3	42.3	42.3
			PACIFIC OCEAN																			SANTA ANA			
4																		28.2	42.3	42.3	42.3	42.3	42.3	42.3	42.3
3																			28.2	42.3	42.3	42.3	42.3	42.3	42.3
2																				14.1	42.3	42.3	42.3	42.3	42.3
1																					14.1	14.1	42.3	42.3	42.3

vehicles operated on freeways, the emissions/driving speed correlation is used in conjunction with the total daily freeway mileage driven on the grid, assuming an average speed of 50 mph.

Evaporative controls on 1972 and newer cars will reduce emissions substantially, although about 50% of the vehicle population will be uncontrolled in 1977. Evaporative emissions from 1957-71 light-duty vehicles can be estimated from tests of 125 automobiles performed by Automotive Environmental Systems, Inc. (AESi, 1973). The evaporative test procedure employed by AESi was comprised of two steps to determine both the carburetor and fuel tank losses from each vehicle tested. After operating a motor vehicle on the Federal Driving Cycle, the engine was turned off, and evaporative emissions from the carburetor were collected for one hour. The diurnal losses from the fuel tank were estimated by attaching a heating element to the tank, heating the tank in such a manner that the gasoline temperature increases from 60°F to 84°F over a one hour period, and measuring the hydrocarbon emissions over the one hour heating period. These measurements of carburetor and fuel tank losses are used in this study to estimate the carburetor emissions associated with each trip made by a motor vehicle and the daily fuel tank evaporative emissions. Average emission factors for fuel tank and carburetor losses are summarized in Table 5.3.

Total daily evaporative losses from each vehicle may be estimated by combining the tank and carburetor losses in the following manner. Total daily carburetor losses are obtained by multiplying the carburetor emissions by the number of daily hot-soaks. From

Table 5.3

Fuel Tank and Carburetor Evaporative Losses from 1957-71 Light-Duty Vehicles*

Model Year	Evaporative Losses (grams per test) Tank	Carburetor
1957-69	25.8	14.6
70-71	16.1	11.0

* Source: AESi (1973)

Table D.1 in Appendix D, the average vehicle makes 4.66 trips per day, and of these, two are cold-started. Assuming that only half of the hot-soak carburetor losses occur when a vehicle is restarted during a hot-start, then the total daily carburetor losses are obtained by multiplying the test results in Table 5.3 by 3.33 (i.e., 2+0.5x2.66). Total daily evaporative emissions from each vehicle are obtained by adding the fuel tank losses to the total carburetor losses. The results of this calculation are summarized in Table 5.4. Note that the value of 74.4 grams/day for pre-1970 light-duty vehicles agrees closely with the value of 72 grams/day used in the 1969 validation study (see Chapter 2).

Table 5.4

Total Daily Motor Vehicle Evaporative Emissions (grams/day)

Model Year	Light-Duty*	Heavy-Duty*
pre-1970	74.4	74.4
1970-71	52.7	74.4
1972	2.0	74.4
post-1972	2.0	2.0

* gasoline powered vehicles

Evaporative emissions for 1973 motor vehicles (EPA, 1973d) appear to be quite small, and thus, post-1972 light and heavy-duty vehicle emissions are assumed to be 2 grams/day, and pre-1973 heavy-duty truck emissions are assumed equal to those of uncontrolled light-duty vehicles. Motorcycle losses are calculated from EPA (1973b) emission estimates, assuming that each motorcycle travels 3900 miles per year, using the following relationship:

$$\frac{0.36(\text{grams/mile}) \times 3900(\text{miles/year})}{365\ (\text{days/year})} = 3.8\ (\text{grams/day})$$

Emissions from heavy-duty diesel vehicles are assumed to be negligible.

To obtain the total daily evaporative emissions emitted into the airshed, the emission rates given in Table 5.4 must be multiplied by the total number of vehicles of each class and model year. Using 1972 vehicle registration statistics (County Supervisors Association of California, 1972) and projected registration growth (TRW, 1973), it is estimated that there will be 4,919,700 automobiles, 688,800 trucks, and 210,000 motorcycles in the modeling region in 1977. The total number of vehicles in a particular class and model year grouping is obtained from the projected number of vehicles cited above and from the distribution of motor vehicles, both by class and model year, given in Appendix A. Total daily evaporative emissions in 1977 are estimated to be 204 tons of hydrocarbons per day. The treatment of the temporal and spatial distribution of evaporative emissions is discussed in Chapter 2.

5.2.1.2 Aircraft Emissions

To estimate aircraft emissions in 1977, three changes have been made in the 1969 aircraft inventory, including the addition of another class of aircraft, the revision of jet aircraft emission factors, and the projection of the number of daily aircraft operations at each airport in 1977. Since wide body jets, such as the Boeing 747, Lockheed L-1011, and Douglas DC-10, will be operating at LAX in 1977, an eighth class of aircraft, characterized by the JT9D engine, has been added to the inventory presented in Chapter 2.

Jet aircraft emission factors have been revised for several reasons. First, JT3D engines on class 2 medium-range jet aircraft will be retrofitted with smoke control devices by 1977. Second, EPA has recently published general guidelines for estimating jet aircraft emissions which, used in conjunction with aircraft time-in-mode data for LAX reported by the Los Angeles County APCD, should allow LAX jet aircraft emissions to be determined with greater accuracy than was heretofore possible. Emissions from a particular segment of a complete LTO cycle, such as taxi, idle, and take-off, are estimated by forming the product of the pollutant emission rate (kilograms/minute) and the time-in-mode (minutes). Emission rates for class 1, 2, and 8 aircraft for each ground operation mode are given in Table 5.5, and the mode times for each class are summarized in Table 5.6. Since guidelines for class 3 aircraft emissions were not included in the EPA (1973b) report, no change in the emission factors given in Chapter 2 was made. In addition, emission factors for class 4-7 aircraft were also unchanged.

Table 5.5

Jet Engine Emission Rates as a Function of Operating Mode*
(kilograms/minute)

Class	Engine	Mode	HC	CO	NO_x (as NO_2)
1	JT3D	Taxi-Idle	.745	.823	.011
1	JT3D	Takeoff	.035	.093	1.118
1	JT3D	Approach	.059	.300	.165
2	JT8D	Taxi-Idle	.062	.253	.022
2	JT8D	Takeoff	.006	.057	1.497
2	JT8D	Approach	.013	.138	.233
8	JT9D	Taxi-Idle	.207	.772	.046
8	JT9D	Takeoff	.023	.063	5.45
8	JT9D	Approach	.023	.247	.408

* Source: EPA (1973b)

Table 5.6

Mode Times at LAX* (minutes)

Class	Taxi-Idle	Takeoff Run	Landing Run
1	20.8	1.0	0.4
2	20.8	0.8	0.3
8	20.8	0.7	0.4

* Sources: Los Angeles County APCD (1971b), EPA (1973b), and Chapter 2.

The projected number of total daily aircraft operations at each airport is expected to increase each year between 1969 and 1977. However, the exact increase or decrease in the total operations of each class of aircraft at a particular airport is difficult to estimate. Total aircraft operations at each airport in 1977 were estimated in the following manner. First, from Los Angeles County APCD (1971a) data, the total number of operations for each class of aircraft at each

airport in 1970 was determined. From conversations with several managers of small airports throughout the Basin, it is estimated that total operations will increase at an annual rate of about 2.5%. Thus, the estimated daily operations of each aircraft class at all airports, except LAX and Hollywood/Burbank, were increased by 2.5% compounded over 7 years. FAA projections (Hubert, 1973) of total annual operations at LAX and Hollywood/Burbank in 1975, 1976, and 1984 were used to scale the 1970 operations at these airports for use in 1977. The estimated daily operations at each airport in the Basin in 1977 are summarized in Table 5.7.

Table 5.7

Projected Daily Aircraft Operations in 1977
at Los Angeles and Orange County Airports

Airport/Class	1	2	3	4	5	6	7	8
Brackett	0	0	0	0	0	396	2	0
Compton	0	0	0	0	0	267	1	0
Culver City	0	0	14	0	0	25	24	0
El Monte	0	0	0	0	0	449	0	0
Hawthorne	0	0	0	0	0	416	2	0
Hollywood/Burbank	0	54	22	3	8	437	16	0
Long Beach	0	0	7	0	2	847	42	0
Los Alamitos	0	0	357	0	59	0	0	0
LAX	401	378	14	33	29	258	44	26
Orange County	0	14	0	0	0	1011	0	0
San Fernando	0	0	0	0	0	144	5	0
Santa Monica	0	0	1	0	0	546	24	0
Torrance	0	0	0	0	0	682	4	0
Van Nuys	0	0	8	0	1	1010	89	0
Whiteman	0	0	0	0	0	208	0	0

5.2.1.3 Fixed Source Emissions

Although the contribution of fixed sources to the total emissions inventory in 1969 was relatively small, as increasingly stringent Federal standards cause motor vehicle emissions to decline in the future, fixed sources, unless controlled to the same extent as motor vehicles, will make larger relative contributions to total emissions in subsequent years. Since few guidelines are available for estimating future fixed source emissions directly, projections made in this study are based on indirect relationships, such as the assumption that increased motor vehicle fuel consumption will cause refinery emissions to increase proportionately. The three types of stationary sources to be considered in this section are power plants, oil refineries, and other miscellaneous fixed sources.

Power plant emissions are affected by the demand for electricity and the type of fuel burned. However, information with regard to future electrical demand and fuel usage at each power plant are generally not available. Fortunately, projected NO_x emissions in 1977 at each of the power plants to be operated by the Southern California Edison Company and the Los Angeles Department of Water and Power were furnished by the respective power companies (Felgar, 1973; Sonderling, 1973). Emissions from power plants operated by the Cities of Pasadena, Burbank, and Glendale were estimated by increasing the reported emissions as of April 1973 (Los Angeles County APCD, 1973) by 38% as suggested by Nevitt (1973). The daily NO_x emissions projected for each power plant in 1977 are summarized in Table 5.8.

Table 5.8

Projected Power Plant Emissions in 1977 (tons/day)

Power Plant	NO_x (as NO_2)
Alamitos	27.0
El Segundo	12.2
Redondo Beach	18.0
Huntington Beach	15.9
Long Beach	4.1
Harbor	6.1
Haynes	37.6
Scattergood	18.7
Valley	9.4
Pasadena	2.6
Burbank	3.6
Glendale	3.7

The temporal distribution of power plant emissions for 1977 is taken to be the same as that employed in 1969.

The major sources of uncertainty in the power plant emissions are 1) the electrical demand, and 2) the type of fuel that will be available. Since there is some question as to the amount of natural gas and the type of fuel oil that will be available in 1977, the emission figures cited in Table 5.8 will be subject to revision at such time when fuel supply schedules are finalized.

Since the construction of no new oil refineries in the Basin is expected by 1977, only changes in emissions from existing refineries are considered in this study. Due to the lack of guidelines for estimating future refinery emissions, it is assumed that emissions will increase in proportion to increases in gasoline fuel consumption. Assuming a 4.5% annual growth of gasoline consumption (EPA, 1973h), refinery emissions are estimated to increase by about 36% from the

corresponding 1969 values cited in Chapter 2. Because all emissions are assumed to increase by the same percentage, no attempt was made to alter the relative spatial distribution of emissions. Note that all refinery emissions, including RHC, URHC, and NO_x, will increase by 36%.

Emissions from all fixed sources other than power plants and refineries have been estimated by Liu (1973). These sources include industrial and domestic boilers, petroleum marketing operations, and organic solvent usage. Using the work of Trijonis (1972) as a guide, and assuming that emissions resulting from petroleum marketing operations are proportional to fuel consumption, the 1969 RHC and NO_x emissions given in Chapter 2 are estimated to increase by 23.9% and 28.6%, respectively. URHC emissions are also assumed to increase by 23.9%.

5.2.1.4 Total Inventory Summary - 1977 Baseline

A complete summary of the total estimated daily emissions for 1977 in the modeling region is given in Table 5.9. As an aid in comparing the 1977 baseline inventory with that for 1969, the percentage change of the total emissions for each pollutant is also included.

Table 5.9 Total Daily Projected Emissions in the Los Angeles Modeling Region in 1977 (tons/day)

Source	NO_x (as NO_2)	RHC	URHC	CO
Motor Vehicles	406	444	52	2882
Aircraft	6	26	6	79
Power Plants	159			
Oil Refineries	88	34	37	
Misc. Stat. Sources	134	640	246	
Total Emissions	793	1144	341	2961
% change from 1969	-8%	-39%	-25%	-64%

Thus, while significant reductions of RHC and CO emissions are projected for 1977 subject only to existing legislation as of 1973, only an 8% decrease in NO_x emissions is expected.

5.2.2 1977 EPA Control Strategy - Phase 1 Emissions Inventory

Phase I of the 1977 EPA control strategy includes those measures listed in Section 5.1, with the exception of further gasoline sales limitations beyond the 1972-73 levels. In this section the projected emissions inventory achievable with this plan is presented.

5.2.2.1 Motor Vehicle Emissions

Due to the extensive control measures proposed for motor vehicles, all aspects of the 1977 baseline motor vehicle emissions inventory given in Section 5.2.1 must be revised.

A major difficulty in estimating motor vehicle emissions is that retrofit device emission reduction factors have not been reported for all types of driving conditions (that is, reductions based on hot-start, cold-start, and steady cruise tests). For lack of better information, it is assumed here that reported emission reductions for a particular device apply to all driving modes.* The effectiveness of parking limitations and exclusive bus/carpool lanes on reducing VMT is also largely unknown. Thus, the emission reductions estimated here are, at best, speculative and subject to revision as better information becomes available.

The procedure for calculating "average" hot-start, cold-start, and steady cruise emission rates for use in the present inventory is

* This assumption is obviously questionable for those devices that employ catalysts because of the temperature dependence of the catalyst efficiency.

the same as that given in Appendix A. However, the emission rates of certain vehicle classes will be different than the 1977 baseline case due to the required installation of retrofit devices. For those motor vehicles affected, the uncontrolled emission rates in Appendix A must be reduced by the combined effectiveness of the VSAD, the oxidizing catalyst, and the inspection/maintenance programs. Each of these programs is now discussed.

VSAD Retrofit

On October 30, 1973 the State of California ARB voted to implement the VSAD retrofit program. The VSAD device is scheduled for installation on all 1957-65 light-duty vehicles with engines larger than 140 cu. in. upon change of ownership and on all 1966-70 light-duty vehicles. (Since foreign automobiles and trucks tend to have small engines, it is assumed that all 1957-65 foreign light-duty vehicles have engines smaller than 140 cu. in.) The percentage emission reductions employed in this study are summarized in Table 5.10. Assuming that 80% of the 1957-65 vehicles will have changed ownership by 1977 (EPA, 1973a), the overall percentage reduction in emissions from 1957-65 domestic vehicles is obtained by multiplying the approximate values in Table 5.10 by 0.8.

Oxidizing Catalyst Retrofit

To reduce HC and CO emissions, the installation of oxidizing catalyst retrofit devices will be required on those 1966-74 light-duty vehicles capable of running on lead free gasoline. Holmes et al. (1973) have estimated that 20% of the pre-1971 and 75% of the 1971-74

Table 5.10

Percentage VSAD Emission Reductions
for Domestic and Foreign Light-Duty Vehicles

Model Year	HC		CO		NO_x	
	Dom.	For.	Dom.	For.	Dom.	For.
1957-65	25†	0	9†	0	23†	0
1966-70	23*	3**	6*	3**	44*	42**

* Source: Lees et al. (1972)

† Source: Horowitz (1973b); emission reductions also subject to change of ownership factor (see text).

** Source: State of California ARB (1973)

model year vehicles will be eligible for these devices. HC and CO reductions average 50%, while NO_x emissions are unaffected (TRW, 1973).

Mandatory Inspection/Maintenance

In an effort to reduce emissions from pre-1975 vehicles caused by mechanical malfunctioning and to insure that the sophisticated post-1974 emission control systems are operating properly, a mandatory inspection/maintenance program is proposed for the Basin. Although the exact nature of the inspection has not yet been specified, it will probably be similar to either the idle or key mode tests (Horowitz, 1973a). In tests comprised of subjecting a fleet of vehicles to mandatory inspection/maintenance procedures, it was found that HC, CO, and NO_x emissions were reduced by 12%, 10%, and 0%, respectively (TRW, 1973).

Motorcycle Registration Limitation and Operation Ban

Hydrocarbon emissions from motorcycles, especially two-stroke motorcycles (16 grams/mi; EPA, 1973b) are greater than those from post-1970 light-duty automobiles and trucks. In order to discourage a significant shift to motorcycles upon institution of gasoline sales limitations, EPA has proposed to limit the total number of motorcycles in the Basin to the total number registered in 1973. On the basis of past vehicle growth data, this limitation can be expected to reduce the total number of motorcycles by about 9% from that which would otherwise have been present in 1977. In addition, it is proposed that operation of two-stroke motorcycles not be allowed between the hours of 6 A.M. and 8 P.M. from May to October. Thus, two-stroke motorcycles were assumed to be inoperative during the 5 A.M. to 3 P.M. PST simulation performed in this study.

Exclusive Bus/Carpool Lanes

To discourage use of low occupancy motor vehicles during peak traffic hours, one lane on all three-lane freeways and two lanes on all four-lane freeways would be reserved for exclusive use of buses and carpools (vehicles containing three or more persons) between the hours of 6:30 A.M. and 9:30 A.M., and 3:30 P.M. and 6:30 P.M. In addition, one lane on all three-lane surface streets will also be reserved for buses and carpools during these hours.

Assessing the impact of bus/carpool lanes is difficult.*

The following assumptions have been employed in this study to estimate the VMT reduction associated with exclusive bus/carpool lanes. First, the VMT associated with freeway traffic travelling in the "slow" direction is assumed to be reduced by 20% during the hours 6:30 A.M. to 9:30 A.M. and 3:30 P.M. to 6:30 P.M. This percentage reduction could be accomplished if 1) one-third of the people travelling in the slow direction form carpools, or 2) 15% of the people originally travelling in the slow direction take buses and 10% form carpools. Case 1) simply states that everyone travelling in one lane of a three-lane freeway forms a carpool. The traffic congestion in the two regular lanes would be no greater than that which would normally occur. Congestion in the exclusive lane would be less than usual, resulting in faster driving speeds. Since freeway driving speeds in the "fast" direction are generally high (see Appendix C), the exclusive lanes are assumed to have no effect on the VMT associated with freeway travel in the "fast" direction.

The formation of exclusive lanes on surface streets is assumed to have a negligible effect on surface street VMT. However, surface street VMT would be reduced to some extent by those people causing

---

* With freeways already congested, removal of one or two available freeway lanes would stimulate an increase in carpooling and public transit usage. Work schedules could be revised to spread the traffic volume over a larger time interval. The ceiling on gasoline sales (to be discussed subsequently) is estimated to reduce VMT by 15%. Those persons that can reduce their individual daily VMT 15% by carpooling or using public transportation will not be forced to reduce the VMT associated with other activities. Thus, the limited supply of gasoline may also encourage carpooling and transit use.

the assumed 20 % VMT reduction on freeways cited above. The estimated VMT reduction on surface streets between 6:30 A. M. and 9:30 A. M. is 10 %. This reduction was calculated by first computing total freeway VMT reduced during this time period. For an average home to work trip, the ratio of surface street miles to freeway miles is 1.75 (TRW, 1973). If no VMT were required to form the carpools or get people to the buses, then the total surface street VMT savings would be computed by multiplying the number of freeway miles not driven by 1.75. To account for some VMT due to carpool formation, the surface street mileage reduction calculated above is multiplied by 0.75. This savings in surface street VMT is found to be 10 % of the original 6:30 A. M. to 9:30 A. M. mileage.

Regulation of Off-Street Parking

To further encourage carpooling and transit ridership, EPA has proposed to reduce existing publicly owned off-street parking spaces by 20 %. In addition, anyone wishing to construct new or additional parking facilities must show that such construction will not cause a large VMT increase and subsequent violation of air quality standards. Since the 20 % reduction cited above does not apply to private parking facilities, the Basinwide parking reduction will be less than 20 %. It is assumed in this study that the regulation of off-street parking will cause no additional reductions in VMT; that is, this strategy will only strengthen the plausibility of the VMT reductions associated with exclusive bus/carpool lanes and gasoline sales limitations.

Gasoline Sales Limitation at 1972-73 Levels.

The most effective means for reducing the Basinwide VMT is the limitation of gasoline sales. For Phase I of the EPA strategy, annual gasoline sales will not be allowed to exceed the total amount sold between July 1, 1972 and June 30, 1973. To compute the percentage reduction in VMT, note that gasoline consumption is increasing by 4.5 % each year and that the projected total Basinwide VMT increase is 17 % between 1969 and 1977. Assuming that the total VMT is proportional to gasoline consumption, the result of the gasoline sales limitation will be to reduce VMT by 15 %.

Due to the "essential" nature of home to work trips that take place between 6:30 A. M. and 9:30 A. M., it is assumed that the only VMT reduction during this three hour period is caused by the implementation of exclusive bus/carpool lanes. After treating the "essential" work to home trips during the evening in an analogous manner, the remaining Basinwide VMT must be reduced by 17.5 % in order to obtain an overall 15 % daily VMT reduction.

The contributions from gasoline and diesel powered vehicles to the "average" hot and cold-start emission factors are given in Table 5.11. Diesel vehicle emissions are calculated by multiplying the factors in Table 5.11 by the 1977 baseline surface mileage in each grid square; gasoline vehicle emissions are calculated by multiplying the factors in Table 5.11 by the adjusted 1977 baseline mileages (i.e., modified to reflect the percentage VMT reductions from the exclusive lane and gasoline sales limitation strategies). This treatment insures that diesel emissions will not be affected by

strategies aimed at reducing VMT associated with gasoline powered vehicles.

Table 5.11

Hot and Cold-Start Emission Factors Estimated for the 1977 EPA Phase I Strategy (grams/mile)

	HC		CO		NO_x (as NO_2)	
	Gas	Diesel	Gas	Diesel	Gas	Diesel
Cold-Start	2.09	.03	25.4	.2	1.95	.35
Hot-Start	1.39	.03	16.1	.2	1.96	.35

* The figures given in this Table are the relative contributions from gasoline and diesel powered vehicles to the "average" motor vehicle emission rate obtained from equation (A.1) in Appendix A.

Freeway emissions are treated analogously; the emissions/driving speed correlation parameters for both gasoline and diesel vehicles are summarized in Table 5.12.

Table 5.12

Emission/Driving Speed Correlation Parameters Estimated for the 1977 EPA Phase I Strategy*

Pollutant	Driving Speed Range (mph)	a_ℓ		b_ℓ	
		Gas	Diesel	Gas	Diesel
HC	15-30	5.206	9.823×10^{-2}	-.587	-.553
HC	30-60	1.821	4.484×10^{-2}	-.278	-.322
CO	15-45	2.205×10^{2}	6.691	-.980	-1.266
CO	45-60	1.279	4.645×10^{-3}	.372	.644
NO_x	15-60	1.523×10^{-3}	2.761×10^{-4}	1.868	1.855

* The figures in this Table are for use in calculating the relative contributions of gasoline and diesel powered vehicles to the "average" freeway emission rates.

Daily evaporative losses from motor vehicles are estimated as follows. Emissions from the fuel tank are assumed to be unaffected by the control strategies, but carburetor losses are to be reduced by 15%, corresponding to the Basinwide VMT reduction. This is analogous to assuming that the total daily trips, and hence carburetor losses, are also reduced by 15%. The total evaporative emissions are estimated to be 184 tons per day.

5.2.2.2 Aircraft Emissions

The EPA control strategy will affect neither the aircraft emission factors nor the flight operation data presented in Section 5.2.1.2.

5.2.2.3 Fixed Source Emissions

Although specific control measures for fixed sources were not proposed in the June 15, 1973 implementation plan, EPA is currently considering such measures as installation of vapor collection and disposal systems and substitution of non-reactive solvents for the reactive solvents presently employed by organic solvent users. Employing the work of Trijonis (1972) as a guide, Liu (1973) has estimated that implementation of the EPA control strategy will reduce RHC and NO_x emissions from oil refineries by 58% and 61%, respectively, and that RHC and NO_x emissions from other fixed sources will be reduced by 81% and 54%, respectively. These percentage reductions are with respect to the 1977 baseline inventory discussed in Section 5.2.1.3. Power plant emissions will not be affected by the EPA strategies.

5.2.2.4 Total Inventory Summary

The total daily emissions from sources in the modeling region are listed in Table 5.13. As an aid in assessing the impact of the EPA control plan, the percentage change in emissions, both from the 1969 and 1977 baseline inventories, are also included in Table 5.13.

Table 5.13

Total Daily Projected Emissions Resulting from Implementation of Phase I of the EPA Control Strategy (tons/day)

Source	NO_x	RHC	URHC	CO
Motor Vehicles	314	322	28	1831
Aircraft	6	26	6	79
Power Plants	159			
Oil Refineries	34	14		
Misc. Stat. Sources	62	115	246	
Total Emissions	575	477	311	1910
% Change from the 1977 Baseline Inventory	-28%	-58%	-9%	-35%
% Change from the 1969 Inventory	-33%	-75%	-31%	-77%

5.2.3 1977 EPA Control Strategy - Phase II Emissions Inventory

Phase II of the EPA control strategy consists of further limitations on gasoline sales to whatever extent is necessary to insure that the Federal air quality standards are not violated. Because present mass transit facilities in the Basin are quite limited, it is doubtful that a VMT reduction greater than 30% could be achieved without a significant expansion in mass transit facilities. However, as a means for reducing VMT in the Basin, the gasoline sales

limitation strategy would be very effective. The following discussion indicates those sources which would be affected by this strategy.

In order to prepare an inventory based on a given percentage reduction in gasoline sales, the following changes must be made in the Phase I inventory discussed in Section 5.2.2. First, the total daily VMT must be reduced to that level which is compatible with the gasoline supply. Second, evaporative emissions from both motor vehicles and gasoline marketing sources must also be reduced accordingly. Liu (1973) has estimated that 20% of the RHC emissions from miscellaneous stationary sources and over 90% of the RHC and NO_x emissions from oil refineries are proportional to gasoline sales.

After evaluating Phase I of the EPA control strategy (to be discussed in Section 5.4), it was decided that simulations employing additional gasoline sales limitations would not be undertaken in this study. Thus, the discussion given in this section is included primarily for completeness, and may serve as a basis for preparing a Phase II emissions inventory in future simulation studies.

5.3 Meteorological and Chemical Input Parameters for the 1977 Simulations

As mentioned previously, the simulations to be performed for the 1977 emission levels are to be based on a day with the meteorology of September 29, 1969. Thus, wind speed and direction, mixing depth, turbulent diffusivity, and solar radiation intensity inputs are identical to those used in the model evaluation studies for this day. The remaining inputs to be specified are reaction rate constants and

initial and boundary concentrations.

The only reaction rate constants possibly requiring revision are those associated with reactive hydrocarbons, particularly if changes occur in the types of hydrocarbons emitted from sources. Unfortunately, detailed information with regard to the hydrocarbon composition of new and future automobile, aircraft, or fixed source emissions has not been reported. Thus, it will be assumed for this study that the relative amounts of each reactive hydrocarbon species are unchanged from those found in measurements taken on September 29, 1969, and therefore that all rate constants and stoichiometric coefficients for reactions involving RHC are the same as those used in the 1969 evaluation studies.

The initial and boundary concentrations employed for the 1977 simulation were obtained by modifying those used in the September 29, 1969 validation. Since CO and URHC are essentially inert, it is assumed that initial and boundary concentrations of these two species are reduced from the 1969 values in direct proportion to the reduction in total emissions of CO and URHC in 1977. Lacking better guidelines, it is also assumed that RHC and total NO_x (i.e., $NO + NO_2$) concentrations appearing in the initial and boundary conditions are reduced from their 1969 values in proportion to the 1977 emission reductions. The key problem is estimating the ratio of the concentrations of NO to NO_2 and the ozone concentration in the initial and boundary conditions for the 1977 studies.

Since the initial and boundary NO/NO_2 ratio and ozone concentration prove to have an important effect on predicted concentrations

throughout the day, two cases were studied that reflect the limits that these concentrations might be expected to obey. Recall that ozone initial and boundary concentrations have been calculated from the ozone steady state relationship (see Chapter 4), so that, if this relationship is assumed to hold, specifying the ratio of NO_2 to NO fixes the ozone concentration.

Case 1. The first method of calculation is based on the assumption that NO and NO_2 concentrations at sunrise and at the boundaries of the airshed will be reduced from the 1969 values in direct proportion to the reduction in total NO_x emissions in the Basin, i.e.,

$$[NO]_{77} = \phi_{NO_x} [NO]_{69} \tag{5.1}$$

$$[NO_2]_{77} = \phi_{NO_x} [NO_2]_{69} \tag{5.2}$$

where the subscripts 69 and 77 refer to the initial or boundary concentrations in 1969 and 1977, and ϕ_{NO_x} is the ratio of the total daily NO_x emissions in 1977 to those in 1969. Recall that if a steady-state relationship is assumed to exist among NO, NO_2, and O_3, the ozone concentration may be approximately computed from*

$$[O_3]_{ss} \cong \frac{k_1 [NO_2]}{k_3 [NO]} \tag{5.3}$$

From equations (5.1) and (5.2), it is seen that the ratio of $[NO_2]$ to [NO] does not change from 1969 to 1977 in this case, and consequently that the initial and boundary ozone concentrations will be virtually

* In the exact expression there is a small dependence of $[O_3]_{ss}$ on [RHC].

unchanged from 1969 to 1977 (except for the small dependence of $[O_3]_{ss}$ on [RHC]). Thus, this method of calculation does not lead to lower ozone concentrations at sunrise or outside the airshed in 1977 in spite of the reductions in NO_x and RHC emissions. This method of calculation provides an upper limit on the estimated initial and boundary ozone concentrations in 1977.

Case 2. The second approach for specifying the NO, NO_2, and O_3 initial and boundary conditions is suggested by the rollback concept, in which ozone concentrations are assumed to be proportional to RHC emissions. If the total NO_x concentrations, either initially or at the boundary, are assumed to be proportional to NO_x emissions, then the following two expressions may be written for $[NO]_{77}$ and $[NO_2]_{77}$ (again assuming that ozone obeys the steady-state relation):

$$\frac{[NO]_{77} + [NO_2]_{77}}{[NO]_{69} + [NO_2]_{69}} = \phi_{NO_x} \tag{5.4}$$

$$\frac{[NO_2]_{77}/[NO]_{77}}{[NO_2]_{69}/[NO]_{69}} = \phi_{RHC} \tag{5.5}$$

where ϕ_{RHC} is the fractional reduction in RHC emissions in 1977 from 1969.

Typical NO, NO_2, and O_3 concentrations predicted in Cases 1 and 2 are presented in Table 5.14. Case 1 predicts a ratio of $[NO_2]$ to [NO] four times as large as Case 2, and consequently an ozone concentration four times as large as Case 2. Clearly, the initial and boundary concentrations that will occur in 1977 are the result of very complex processes, such as the previous day's conditions and

the meteorology at night. These two simple methods of estimation certainly do not take these factors into account. It is to be stressed that the basic object of these two cases is to illustrate the range of values that can be obtained using "reasonable" assumptions. In both cases the weakest point is the reliance on the steady-state relationship for calculating ozone concentrations. The O_3 concentration depends directly on the light intensity through the rate constant for NO_2 photolysis, k_1. At sunrise k_1 is changing rapidly (recall Figure 4.8) and the choice of the proper value of k_1 to use in equation (5.3) is difficult even assuming the relation is valid. In the next section simulation results will be presented corresponding to both Cases 1 and 2. These simulations indicate the level of sensitivity of the computed concentrations to the initial and boundary conditions.

Table 5.14

Typical NO, NO_2, and O_3 Concentrations (ppm) Predicted Along the Palos Verdes Coastline at 12 A.M. by Cases 1 and 2

	$[NO]_{77}$	$[NO_2]_{77}$	$[NO_2]_{77}/[NO]_{77}$	$[O_3]_{77}$
Case 1	0.0034	0.0207	6.0	0.1228
Case 2	0.0097	0.0146	1.5	0.0304

Note: Concentrations in this Table were derived for the 1977 EPA Phase I inventory. From Table 5.13,

$$\phi_{RHC} = 0.25$$

$$\phi_{NO_x} = 0.69$$

Values for the rate constants used were:

$$k_1 = 0.44 \text{ min}^{-1}$$

$$k_3 = 21.8 \text{ ppm}^{-1}\text{min}^{-1}$$

5.4 Simulation of the 1977 Baseline and EPA-Phase I Cases

Combining the various meteorological, emissions, and chemical inputs described in the previous sections, simulations were carried out for the 5 A.M. - 3 P.M. PST period for each of the two emission inventories discussed in Sections 5.2.1 and 5.2.2 and for each of the two cases of initial and boundary concentrations. Computer-generated plots of predicted hourly-averaged CO concentrations at Reseda and Downtown Los Angeles are presented in Figure 5.5. On Figure 5.5 and subsequent plots the letters A, B, and C designate predictions employing the 1969, 1977 baseline, and 1977 EPA-Phase I emissions inventories, respectively. Predictions of NO, NO_2, and O_3 concentrations are given in Figures 5.6a - 5.10b. In each set, the figures labeled "a" and "b" denote the use of Cases 1 and 2, respectively, for the initial/boundary condition computation. Predicted hourly-averaged ground-level concentration maps for O_3 and NO_2 are shown in Figures 5.11 - 5.16b; the use of the letters "a" and "b" is the same as in Figures 5.6a-5.10b. The emission inventory associated with each map is given in Table 5.15.

Table 5.15
Emission Inventories Associated with Figures 5.11 - 5.16b

Figure Number	Emission Inventory
5.11	1969
5.12a-b	1977 Baseline
5.13a-b	1977 EPA-Phase I
5.14	1969
5.15a-b	1977 Baseline
5.16a-b	1977 EPA-Phase I

First, it is of interest to examine the magnitude of any discrepancy that may exist between concentrations predicted by the mathematical model and those predicted by the simple rollback methodology. For example, the maximum hourly-averaged CO concentration predicted in 1969 was 17 ppm. From Table 5.9, CO emissions for the 1977 baseline inventory are only 36% of the 1969 emissions. Therefore, assuming the maximum CO prediction in 1969 to be reduced by 64%, the rollback estimate for the maximum 1977 baseline CO concentration is 6 ppm. Maximum hourly-averaged ground-level CO, NO_2, and O_3 concentrations predicted over the region are presented in Table 5.16 together with those predicted by reducing the 1969 levels by the percentage reduction in emissions of CO, NO_x, and RHC, respectively. Because CO is essentially inert, good agreement between the model and rollback predictions is to be expected. For the reactive species, NO_2 and O_3, however, the concentrations predicted on the basis of simple rollback are generally higher than those predicted by the airshed model.

Although the NO_2 predictions for the 1977 baseline inventory are in close agreement with those calculated on the basis of rollback, the same statement is not applicable to the NO_2 results for the 1977 EPA-Phase I strategy; predictions from the airshed model are about one-half of those obtained from rollback. These results indicate the importance of considering the impact of RHC emission reductions on NO_2 concentrations. As RHC emissions are reduced, the time required for the oxidation of NO to NO_2 increases, thus retarding the photochemical processes.

Table 5.16

Comparison of the Maximum Hourly-Averaged Ground-Level CO, NO_2, and O_3 Concentrations Predicted by Rollback and the Airshed Model*

	1969	1977 Baseline			1977 EPA-Phase I		
	AM	Rb	AM1	AM2	Rb	AM1	AM2
CO							
Max. Conc. (PPM)	17	6	6	6	4	4	4
% Reduction from 1969		65%	65%	65%	76%	76%	76%
NO_2							
Max. Conc. (PPM)	.38	.35	.36	.35	.25	.15	.09
% Reduction from 1969		8%	5%	8%	34%	60%	76%
O_3							
Max. Conc. (PPM)	.54	.33	.19	.16	.14	.14	.04
% Reduction from 1969		39%	65%	70%	74%	74%	96%

* Results under the Rb column are based on the rollback assumptions; results under the AM1 and AM2 columns are based on predictions from the airshed model using the first and second NO_x IC/BC algorithms, respectively, discussed in Section 5.3. The percentage reductions for rollback entries may vary slightly from the corresponding reductions in emissions as a result of round-off errors in the maximum concentration calculations.

With the exception of the EPA-Phase I inventory using the Case 1 IC/BC algorithm, the O_3 predictions from the airshed model are in most cases considerably lower than the corresponding rollback predictions. The agreement in that one case is coincidental since the maximum O_3 concentration of 0.14 ppm occurred adjacent to the boundary near the coast and is a direct result of the boundary

condition used. In fact, Figures 5.11, 5.12a and 5.13a reveal that O_3 concentrations near the coast are relatively independent of the emission inventory, a result of the use of the Case 1 IC/BC algorithm. The extent to which this result is an accurate reflection of the 1977 situation would, of course, depend on overnight and background conditions, effects which have not been accounted for here.

Based on the results presented in Table 5.16, the rollback method seems to provide a conservative estimate of the percentage reduction of the maximum NO_2 and O_3 concentrations in the airshed, at least for two projected emission inventories in which RHC emissions are subject to more control than NO_x emissions. If these results are accurate, control measures adopted from rollback calculations may be unnecessarily stringent. To reduce the maximum O_3 concentration of .54 ppm in 1969 to .08 ppm in 1977 using rollback, an 85% reduction in the 1969 RHC emissions would be required (100% - .08/.54 x 100%). From the inventory summaries given in Tables 5.9 and 5.13, this required reduction in emissions may be accomplished by employing the EPA-Phase I strategy with an additional 75% reduction in RHC emissions from motor vehicles. If fuel tank evaporative emissions are assumed to be unaffected by limitations on gasoline sales, then an 88% reduction in gasoline sales will be required to reduce motor vehicle RHC emissions by 75% (i.e., an 88% reduction in the amount of gasoline allowable for sale under the EPA-Phase I control strategy in 1977). Thus, the 1977 baseline VMT must be reduced by 90% (i.e., 100% - (1-.88)(1-.15) x 100%). Of course, a smaller VMT reduction would be required if

further controls were imposed on aircraft and fixed source RHC emissions.

In contrast to this result, note from Table 5.16 that the maximum O_3 concentrations predicted for the EPA-Phase I strategy model ranged between .04 and .14 ppm, depending on the algorithm used to compute the NO_x initial and boundary concentrations. Upon examination of the spatial distribution of ground-level O_3 concentrations for the 1977 EPA-Phase I strategy given in Figures 5.13a and 5.13b, it will be noted that all O_3 concentrations except those adjacent to the coast in Figure 5.13a, are within the Federal standards (0.08 ppm). If the true behavior of the airshed lies somewhere between the two sets of results presented in Figures 5.13a and 5.13b, then implementation of the EPA-Phase I plan may be sufficient to bring O_3 concentrations in the Basin into compliance with the Federal standards.

A complete listing of current California and Federal air quality standards for CO, NMHC (non-methane hydrocarbon), NO_2, and O_3 are given in Table 5.17. In addition, the maximum predicted ground-level concentrations, averaged over the appropriate time intervals, for each simulation performed in this study are also included in Table 5.17. These results indicate that at least one of the standards for each pollutant was violated in 1969. For the 1977 baseline inventory, CO is the only pollutant predicted to meet the standards. All predictions from the 1977 EPA-Phase I control strategy simulations fall below the standards, with the possible exception of the annual NO_2 concentration and the hourly O_3 concentration.

Table 5.17 Comparison of State and Federal Air Quality Standards with Corresponding Maximum Airshed Model Predictions‡

Pollutant	Standard	Time Period	Standard (ppm)	1969 AM (ppm)	1977 Baseline AM1† (ppm)	1977 Baseline AM2† (ppm)	1977 EPA-Phase I AM1† (ppm)	1977 EPA-Phase I AM2† (ppm
CO	Calif.	1 hr.	40	17	6	6	4	4
CO	Federal	1 hr.	40	17	6	6	4	4
CO	Federal	8 hr.	9	12	4	4	3	3
CO	Calif.	12 hr.	10	10*	4*	4*	3*	3*
NMHC	Federal	3 hr. (6-9 A.M.)	.24	.87**	.55**	.55**	.20**	.20**
NO_2	Calif.	1 hr.	.25	.38	.36	.35	.15	.09
NO_2	Federal	1 year	.05	.19*	.16*	.14*	.10*	.06
O_3	Calif.	1 hr.	.10	.54	.19	.16	.14	.04
O_3	Federal	1 hr.	.08	.54	.19	.16	.14	.04

* Entry based on the maximum 10 hour average predicted concentration

** Non-methane hydrocarbon entries are approximated by RHC averages. Since non-methane hydrocarbon includes RHC, ethane, propane, benzene, and acetylene, the airshed model predictions will be somewhat low.

† AM1 and AM2 refer to use of the first and second NO_x IC/BC algorithms, respectively.

‡ California and Federal air quality standards were obtained from the State of California ARB (1972) and EPA (1971), respectively. These standards are not to be exceeded more than once each year.

It must be emphasized that the evaluation of the EPA-Phase I strategy given above is based on the assumption that the airshed model developed in this report accurately represents the emissions, transport, and chemical reaction processes that take place in the atmosphere. Although it is clear that in principle the use of such a model is preferred to that of simple rollback calculations, the results presented here must be considered a preliminary evaluation of the EPA-Phase I control plan and will be subject to revision as improvements are made in the model.

5.5 Conclusions

This chapter has been devoted to an illustration of the potential use of the mathematical model developed and evaluated in Chapters 1-4 through a study of the 1977 EPA implementation plan for Los Angeles. In addition, the treatment of and sources of uncertainty in the model inputs and the assessment of the proportional rollback methodology currently used to relate emission reductions to air quality improvements were considered.

The major sources of uncertainty in performing a simulation of future emission levels were identified as:

1. Uncertainties in emissions
    a. Future vehicle emission rates
    b. Effectiveness of retrofit control devices
    c. Composition of hydrocarbon emissions
    d. Number and distribution of vehicles in the Basin
    e. Impact of exclusive bus/carpool lanes and parking limitations

f. Quantity of fixed source emissions

2. Uncertainties in initial and boundary concentrations.

As control strategies are implemented and the effects on emissions observed, projected emissions may be more precisely specified. The uncertainties in the specification of initial and boundary concentrations can be reduced by choosing the size of the region modeled large enough so that only background concentrations may be needed. The influence of initial conditions may be diminished by performing multi-day simulations.

A preliminary evaluation of the 1977 EPA implementation plan has been made. Based on a limited number of simulation results, it appears that pollutant concentrations in the Los Angeles Basin in 1977 may be reduced sufficiently to meet the California and Federal air quality standards for CO, hydrocarbons, NO_2 and O_3 if the basic EPA control strategy is adopted (i.e. all measured proposed by EPA except further gasoline sales limitations beyond the 1972-73 limit). It must be emphasized, however, that because of uncertainties in emission predictions, the adequacy of the kinetic mechanism, and the overall validity of the airshed model, any statements made at this time as to the future air quality in the Los Angeles Basin must be regarded as speculative. Further evaluation of the airshed model is required before it can be systematically used in control policy decision-making.

Figure 5.5

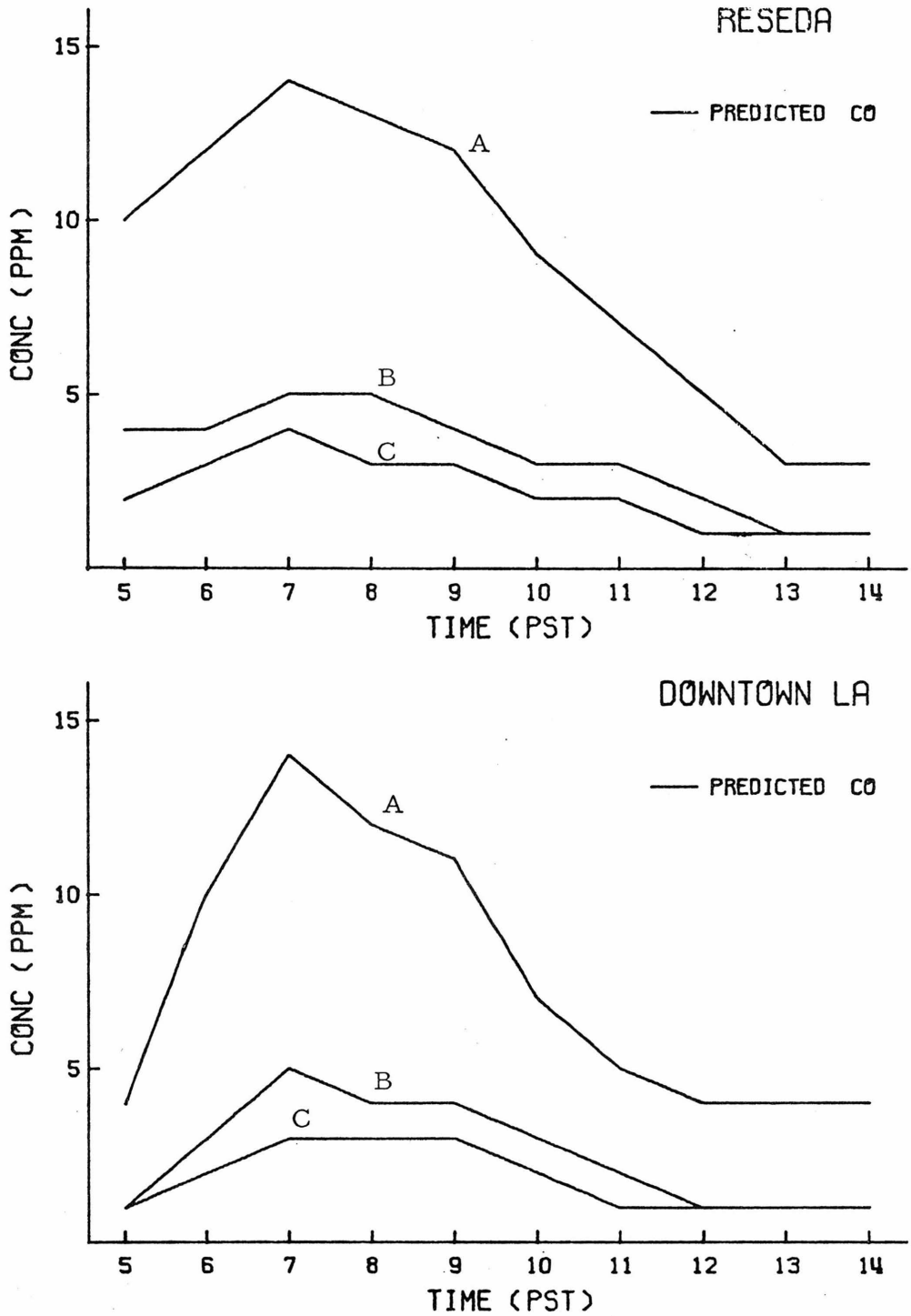
RESEDA
PREDICTED CO
A
B
C
CONC (PPM)
15
10
5
5 6 7 8 9 10 11 12 13 14
TIME (PST)
DOWNTOWN LA
PREDICTED CO
A
B
C
CONC (PPM)
15
10
5
5 6 7 8 9 10 11 12 13 14
TIME (PST)

Figure 5.6a

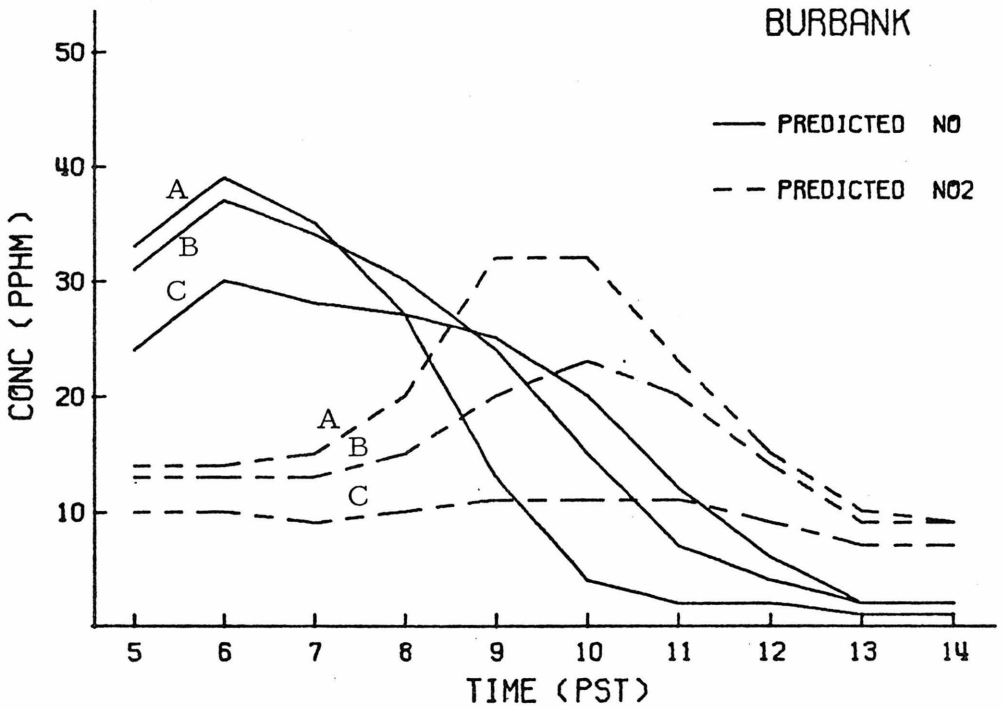
BURBANK
PREDICTED NO
PREDICTED NO2
CONC (PPHM)
TIME (PST)
A
B
C
50
40
30
20
10
5
6
7
8
9
10
11
12
13
14

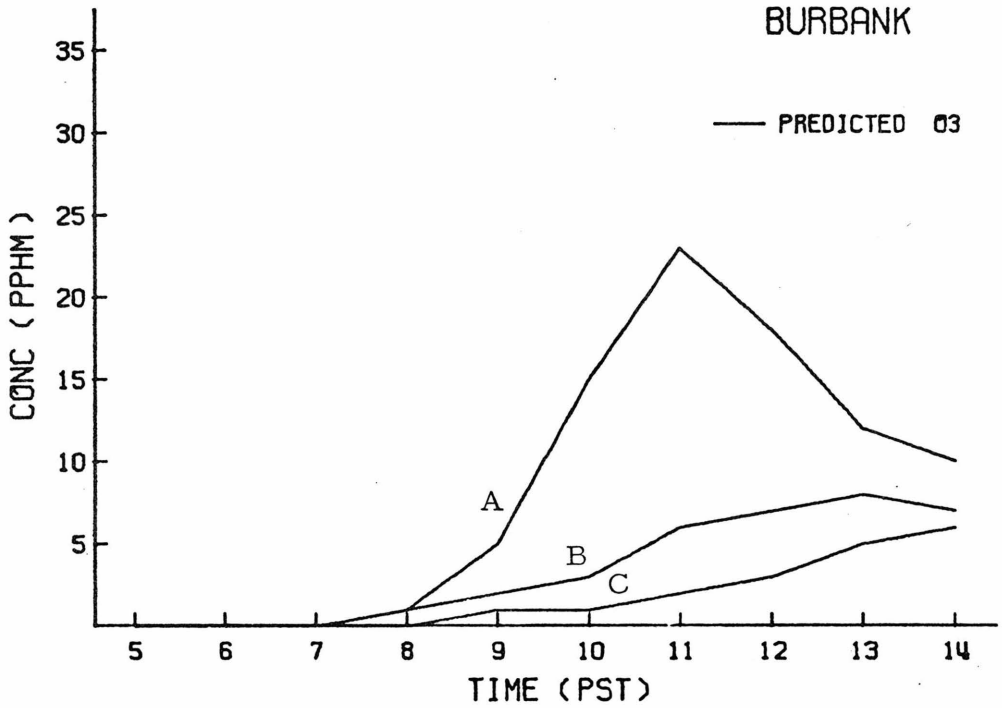
BURBANK
PREDICTED O3
CONC (PPHM)
TIME (PST)
A
B
C
35
30
25
20
15
10
5
5
6
7
8
9
10
11
12
13
14

Figure 5.6b

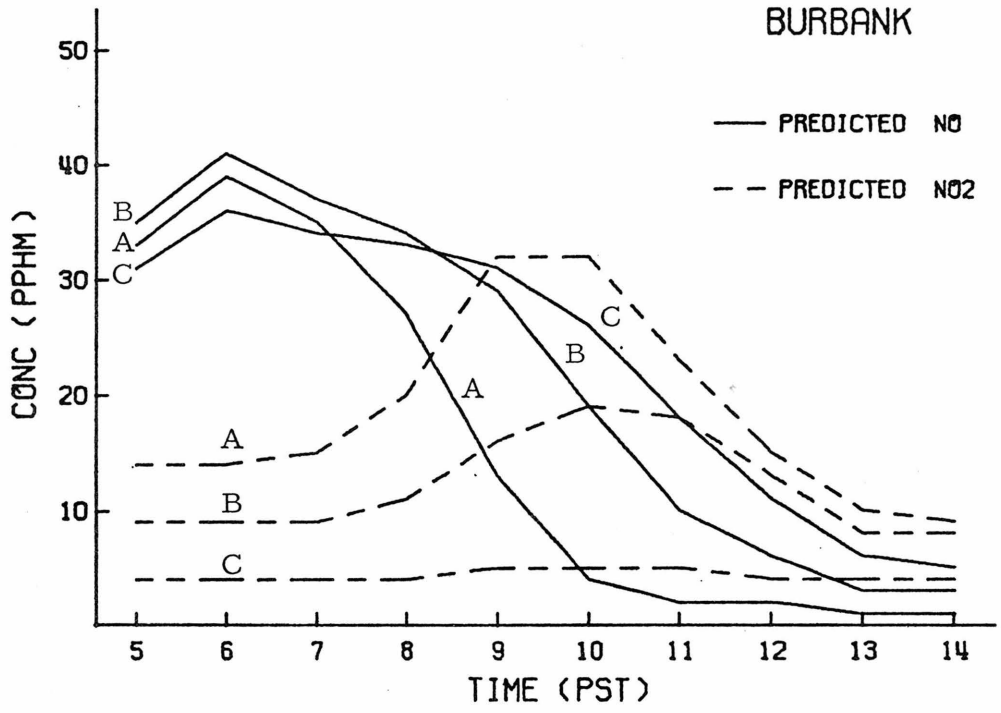
BURBANK
PREDICTED NO
PREDICTED NO2
CONC (PPHM)
TIME (PST)
A
B
C

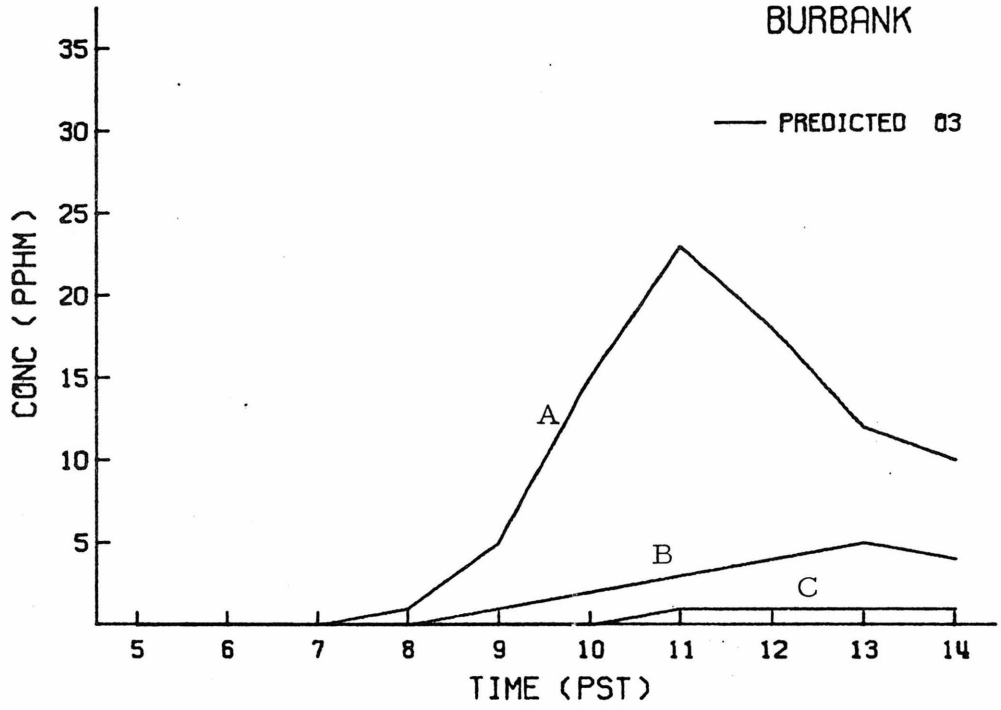
BURBANK
PREDICTED O3
CONC (PPHM)
TIME (PST)
A
B
C

Figure 5.7a

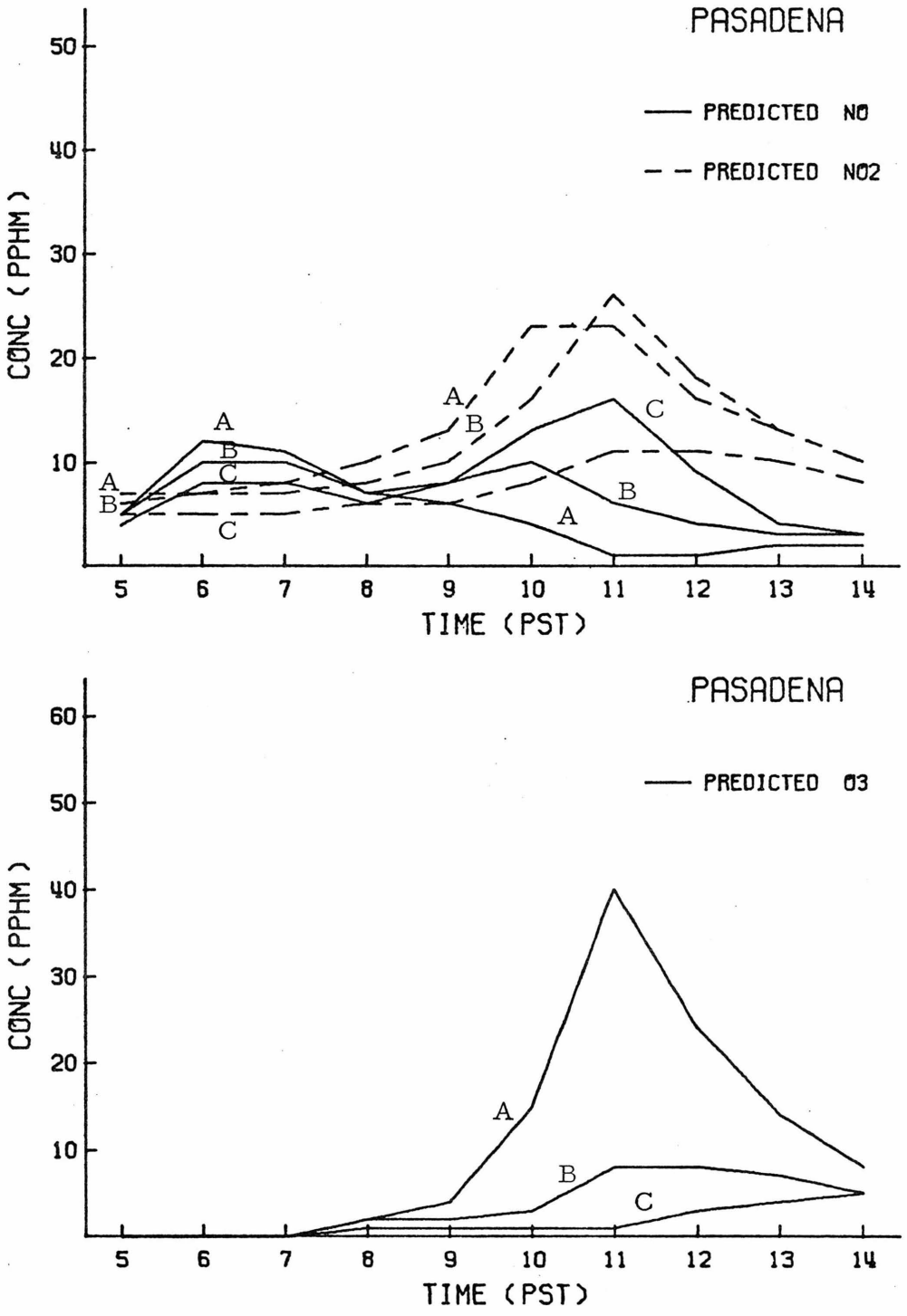
PASADENA
PREDICTED NO
PREDICTED NO2
CONC (PPHM)
TIME (PST)
PASADENA
PREDICTED O3
CONC (PPHM)
TIME (PST)

Figure 5.7b

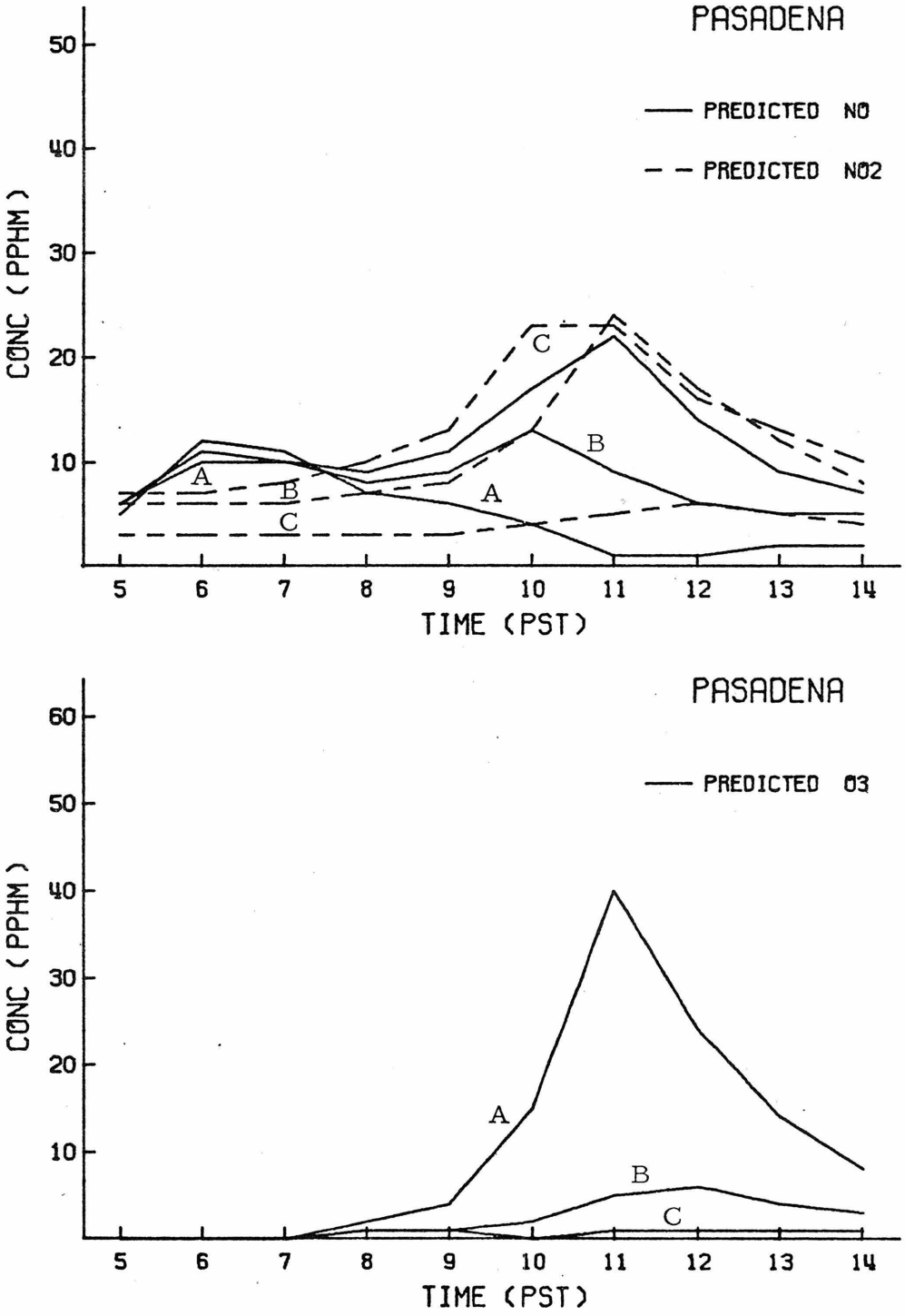
PASADENA
PREDICTED NO
PREDICTED NO2
CONC (PPHM)
TIME (PST)
A
B
C
PASADENA
PREDICTED O3
CONC (PPHM)
TIME (PST)
A
B
C

Figure 5.8a

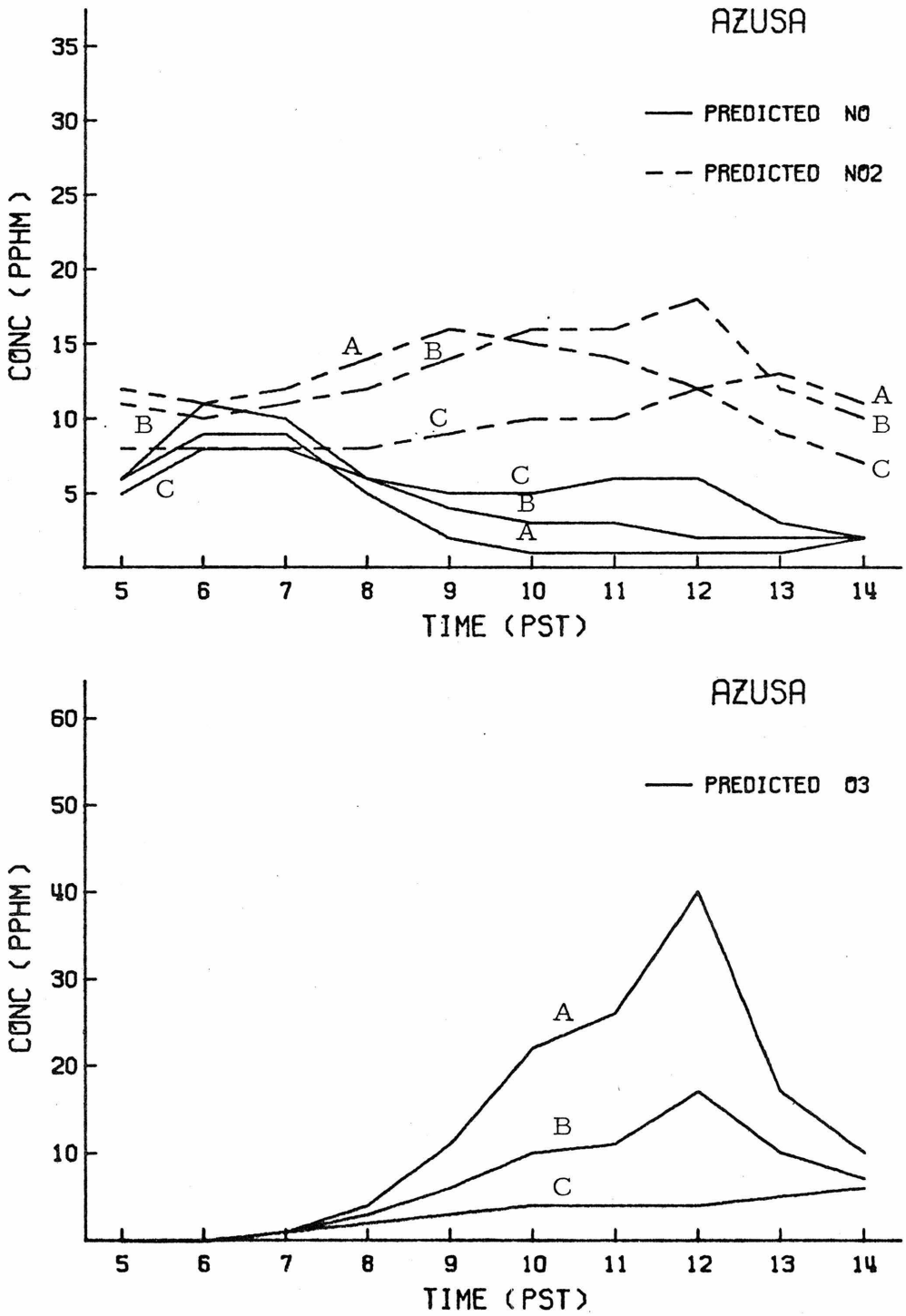
AZUSA
PREDICTED NO
PREDICTED NO2
CONC (PPHM)
TIME (PST)
AZUSA
PREDICTED O3
CONC (PPHM)
TIME (PST)

Figure 5.8b

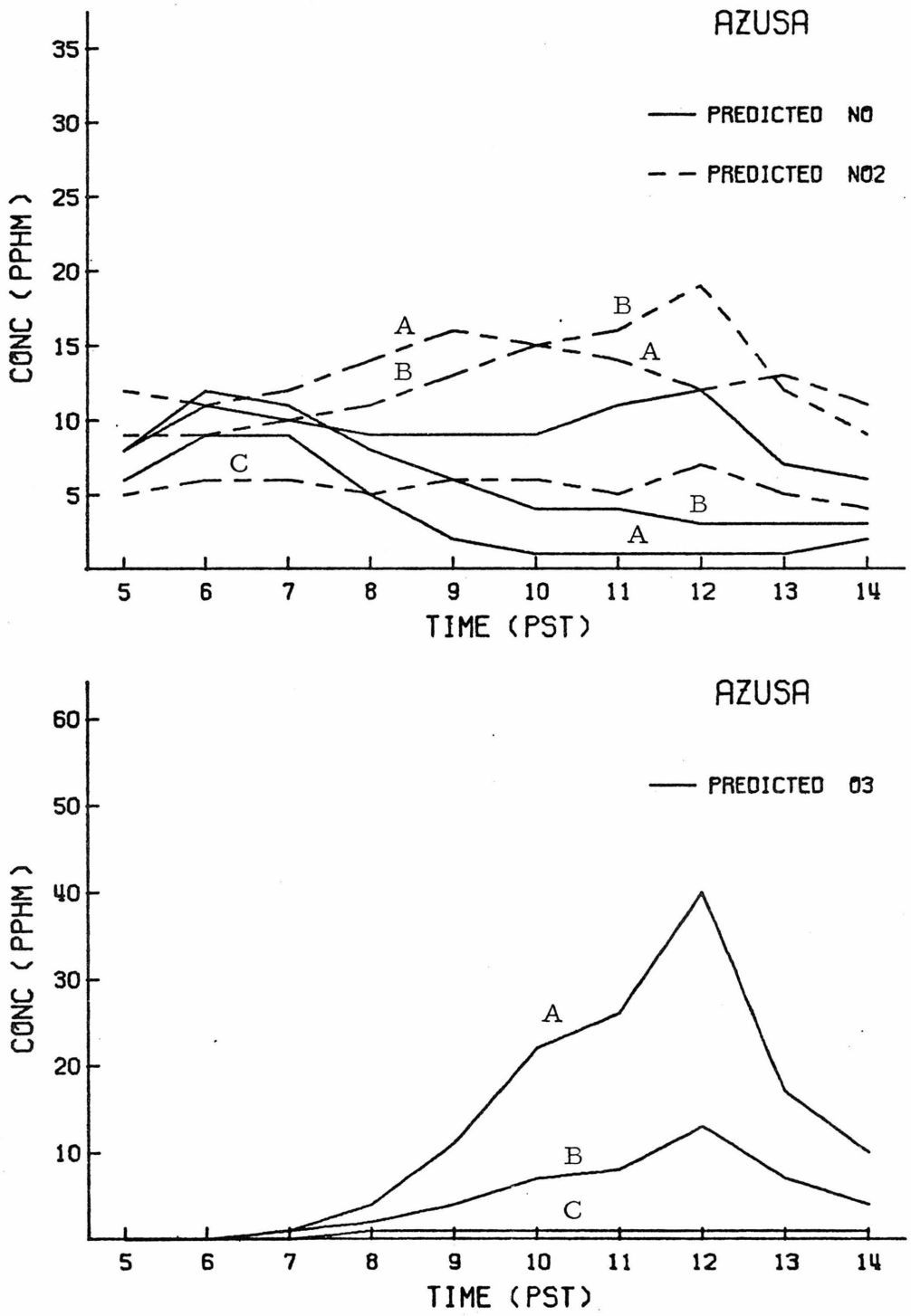
AZUSA
PREDICTED NO
PREDICTED NO2
CONC (PPHM)
TIME (PST)
A
B
C
AZUSA
PREDICTED O3
CONC (PPHM)
TIME (PST)
A
B
C

Figure 5.9a

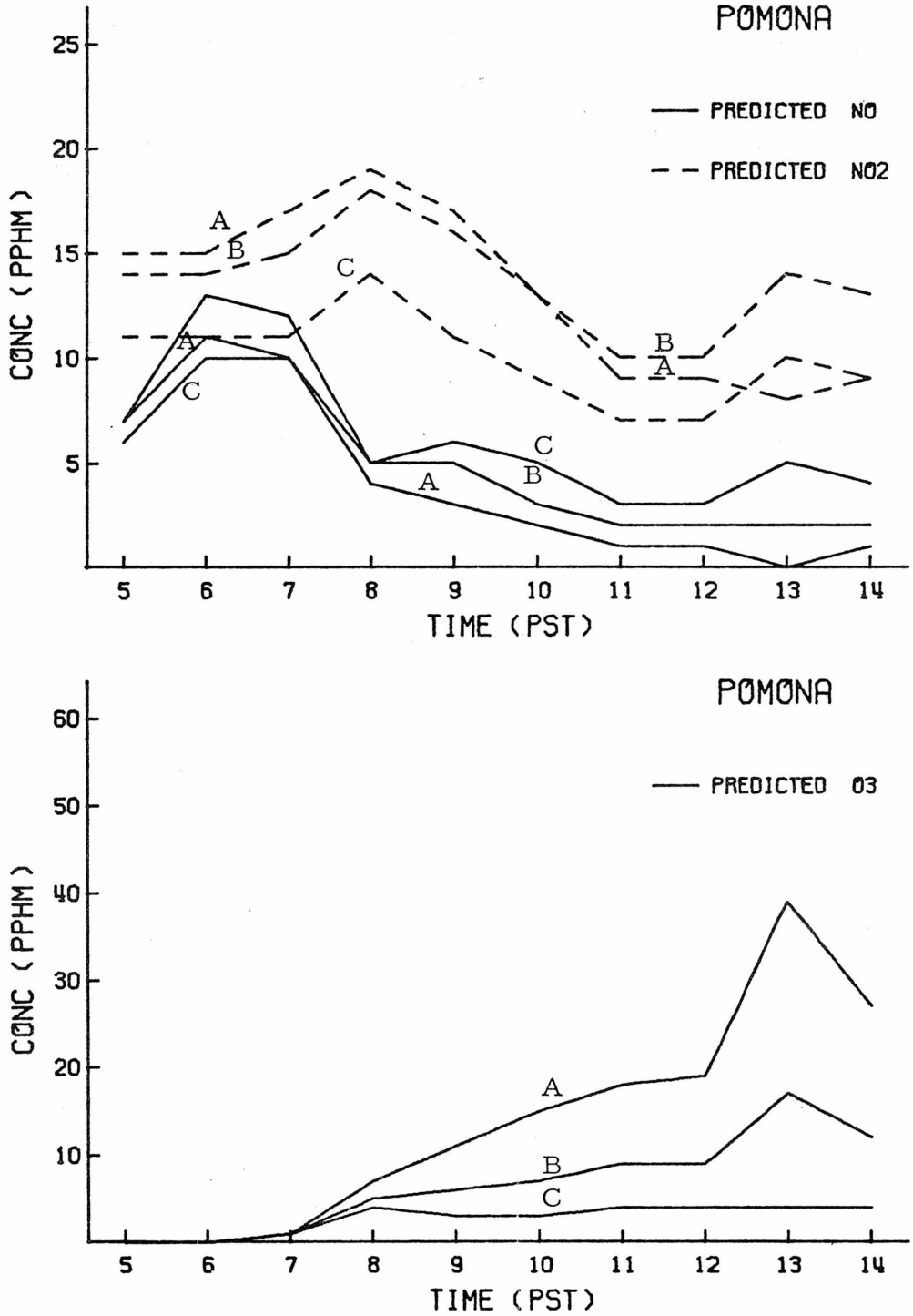
POMONA
PREDICTED NO
PREDICTED NO2
CONC (PPHM)
TIME (PST)
A
B
C
POMONA
PREDICTED O3
CONC (PPHM)
TIME (PST)
A
B
C

Figure 5.9b

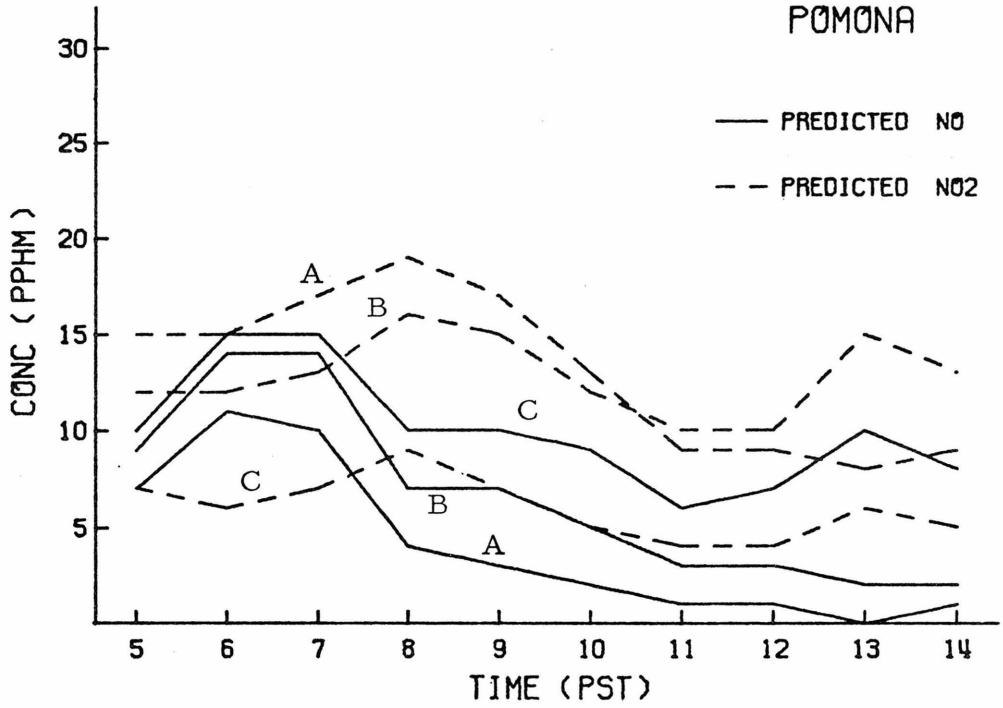
POMONA
PREDICTED NO
PREDICTED NO2
CONC (PPHM)
30
25
20
15
10
5
A
B
C
C
B
A
5
6
7
8
9
10
11
12
13
14
TIME (PST)

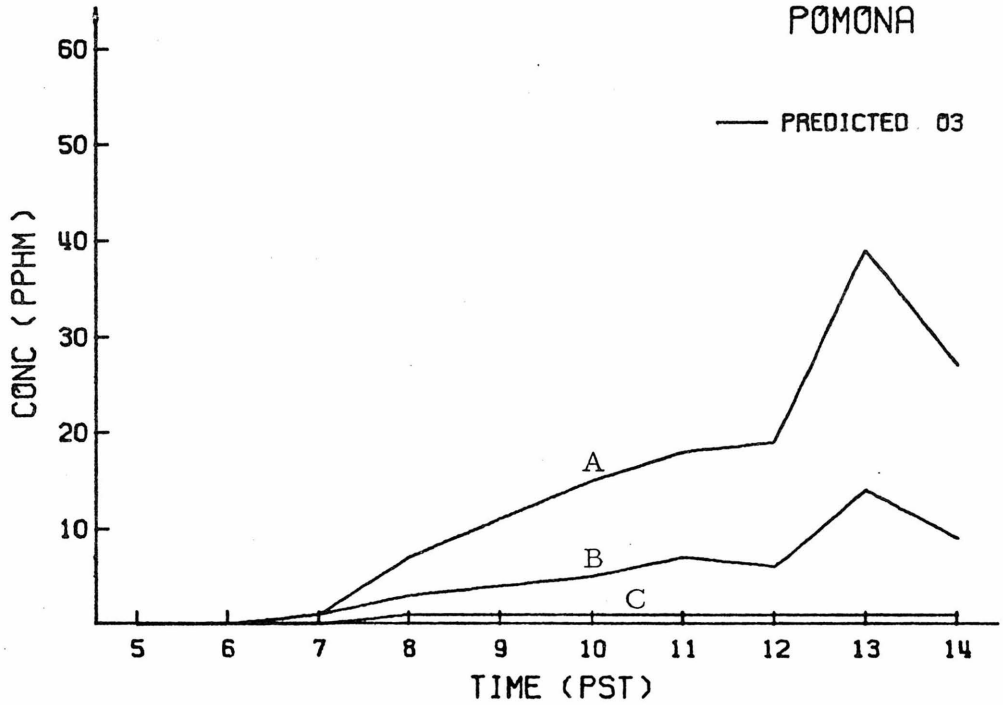
POMONA
PREDICTED O3
CONC (PPHM)
60
50
40
30
20
10
A
B
C
5
6
7
8
9
10
11
12
13
14
TIME (PST)

Figure 5.10a

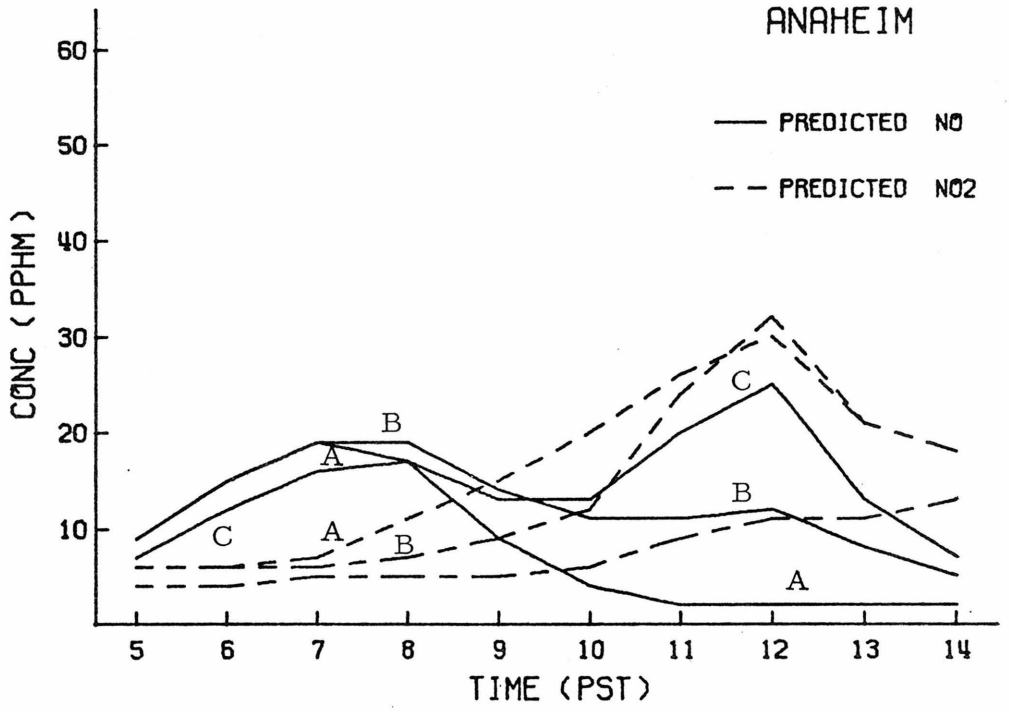
ANAHEIM
PREDICTED NO
PREDICTED NO2
CONC (PPHM)
60
50
40
30
20
10
5
6
7
8
9
10
11
12
13
14
TIME (PST)
A
B
C

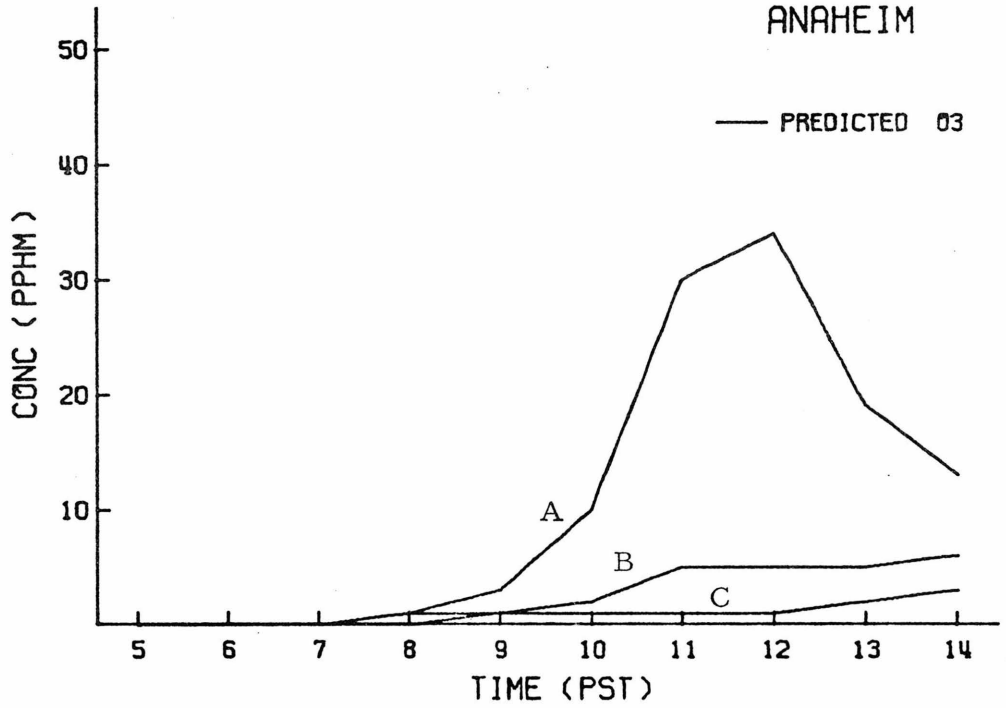
ANAHEIM
PREDICTED O3
CONC (PPHM)
50
40
30
20
10
5
6
7
8
9
10
11
12
13
14
TIME (PST)
A
B
C

Figure 5.10b

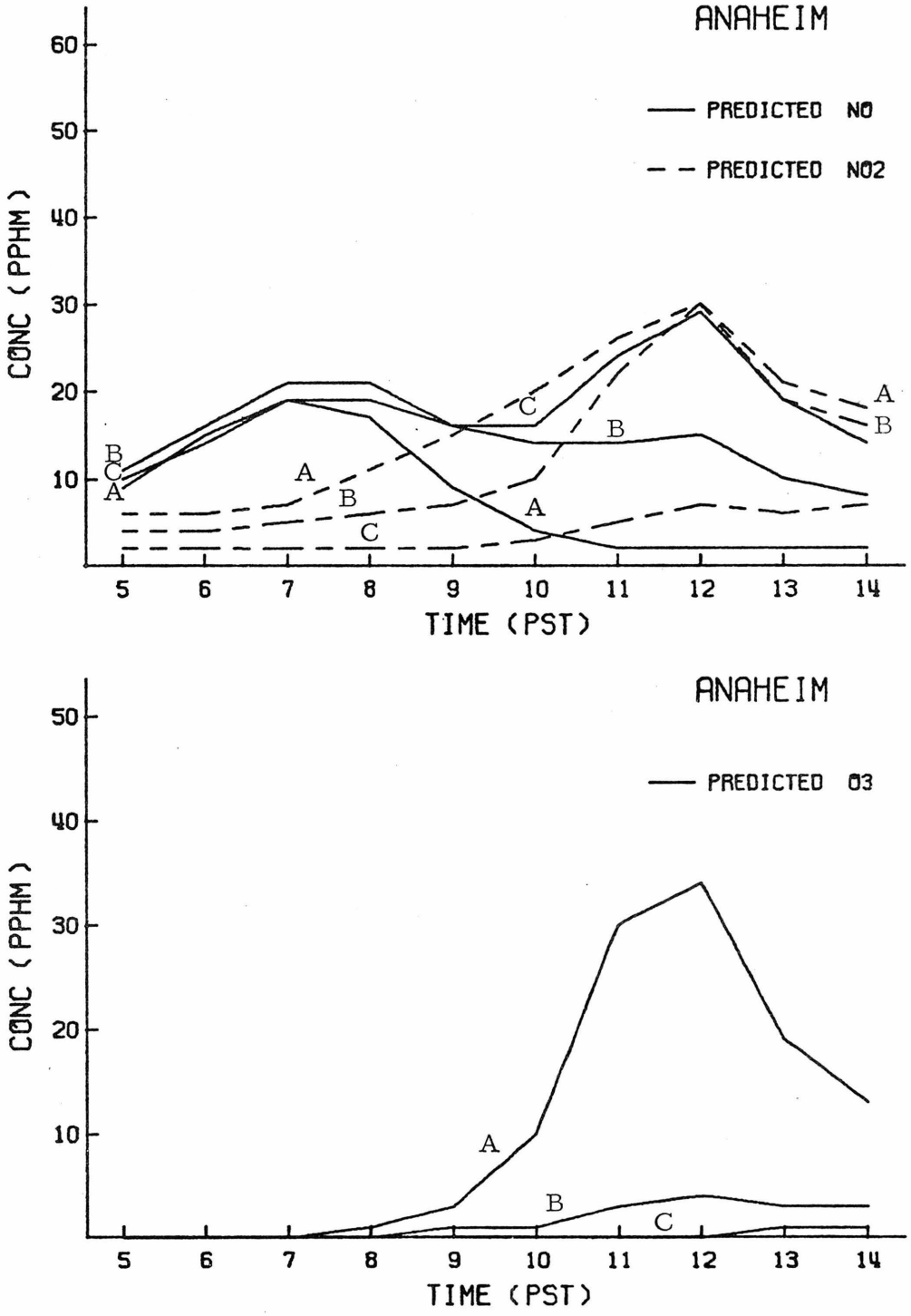
ANAHEIM
PREDICTED NO
PREDICTED NO2
CONC (PPHM)
TIME (PST)
ANAHEIM
PREDICTED O3
CONC (PPHM)
TIME (PST)

Figure 5.11

AVERAGE GROUND LEVEL CONCENTRATIONS (PPHM) OF O3 BETWEEN THE HOURS OF 1200. AND 1300. PST

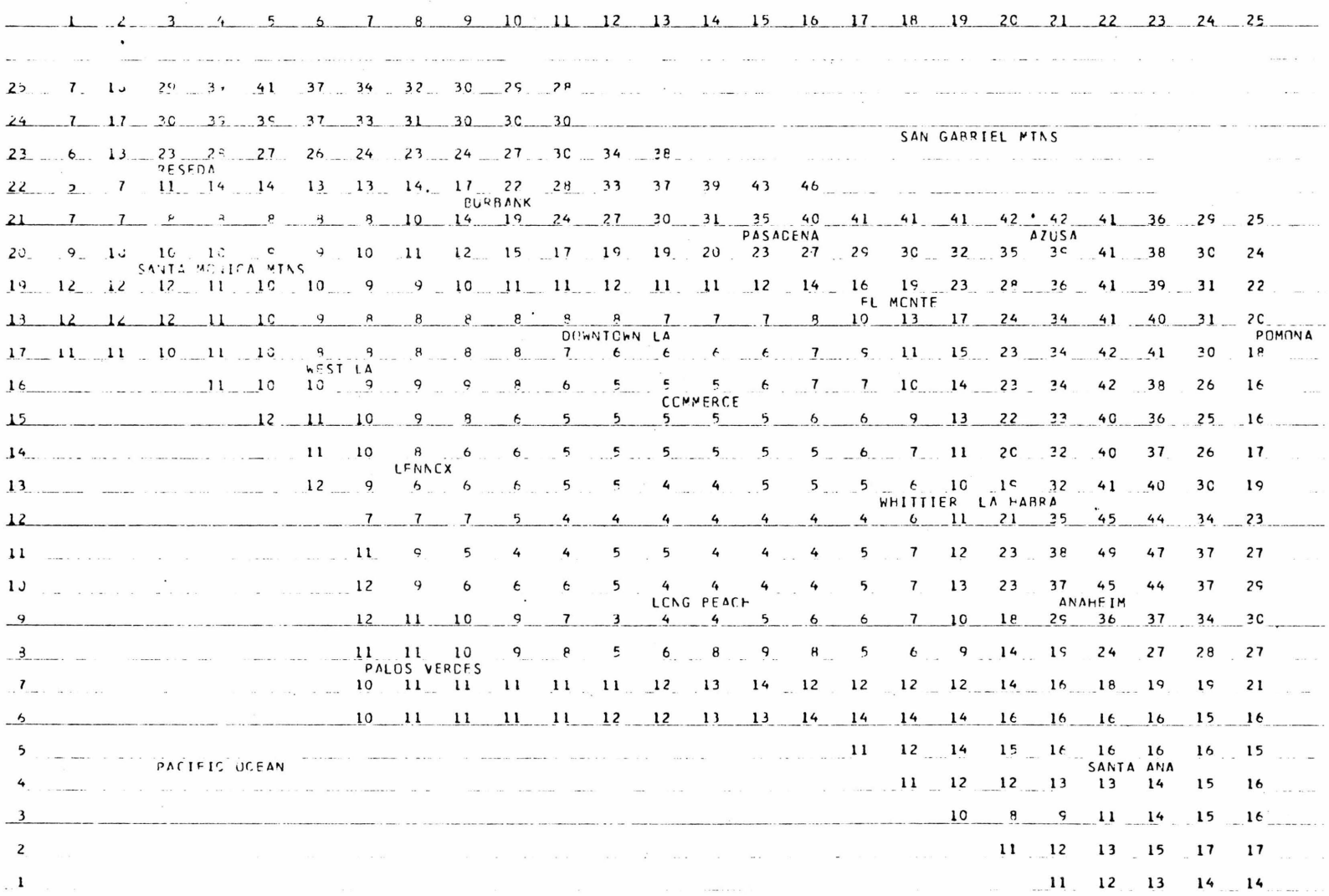

Figure 5.12a

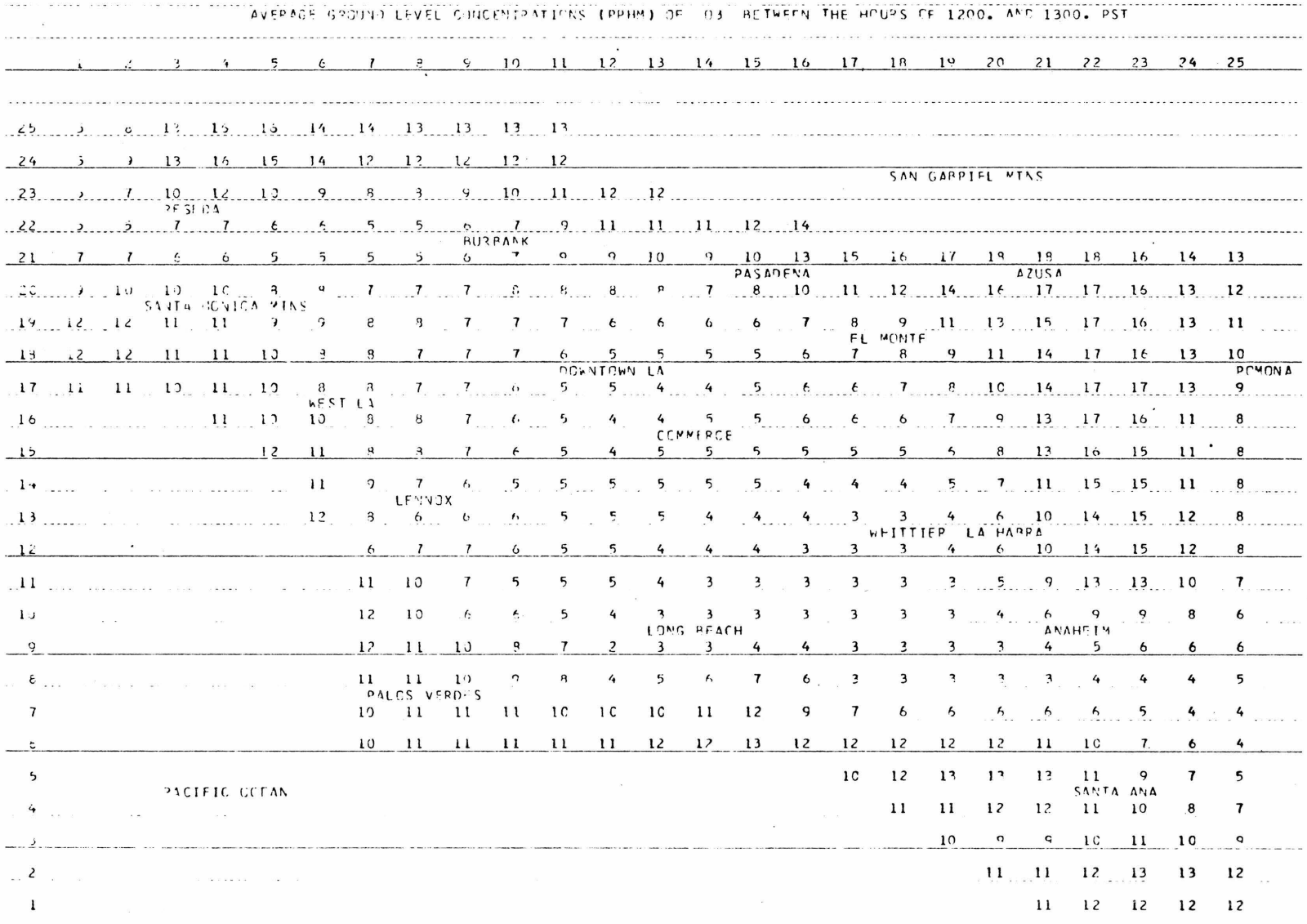
AVERAGE GROUND LEVEL CONCENTRATIONS (PPHM) OF O3 BETWEEN THE HOURS OF 1200. AND 1300. PST
1 2 3 4 5 6 7 8 9 10 11 12 13 14 15 16 17 18 19 20 21 22 23 24 25
25 9 8 13 15 16 14 14 13 13 13 13
24 9 9 13 16 15 14 12 12 12 12 12
23 9 7 10 12 13 9 8 8 9 10 11 12 12
SAN GABRIEL MTNS
22 9 8 7 7 6 6 5 5 6 7 9 11 11 11 12 14
PESIDA
21 7 7 6 6 5 5 5 5 6 7 9 9 10 9 10 13 15 16 17 19 18 16 14 13
BURBANK
20 9 10 10 10 8 9 7 7 7 8 8 8 8 7 8 10 11 12 14 16 17 17 16 13 12
PASADENA
AZUSA
19 12 12 11 11 9 9 8 8 7 7 7 6 6 6 6 7 8 9 11 13 15 17 16 13 11
SANTA MONICA MTNS
18 12 12 11 11 10 9 8 7 7 7 6 5 5 5 5 6 7 8 9 11 14 17 16 13 10
EL MONTE
17 11 11 10 11 10 8 8 7 7 6 5 5 4 4 5 6 6 7 8 10 14 17 17 13 9
DOWNTOWN LA
POMONA
16 11 10 10 8 8 7 6 5 4 4 5 5 6 6 6 7 9 13 17 16 11 8
WEST LA
15 12 11 8 8 7 6 5 4 5 5 5 5 5 6 8 13 16 15 11 8
COMMERCE
14 11 9 7 6 5 5 5 5 5 5 4 4 4 5 7 11 15 15 11 8
13 12 8 6 6 6 5 5 5 4 4 4 3 3 4 6 10 14 15 12 8
LENNOX
12 6 7 7 6 5 5 4 4 4 3 3 3 4 6 10 14 15 12 8
WHITTIER
LA HABRA
11 11 10 7 5 5 5 4 3 3 3 3 3 3 5 9 13 13 10 7
10 12 10 6 6 5 4 3 3 3 3 3 3 3 4 6 9 9 8 6
LONG BEACH
ANAHEIM
9 12 11 10 8 7 2 3 3 4 4 3 3 3 3 4 5 6 6 6
8 11 11 10 9 8 4 5 6 7 6 3 3 3 3 3 4 4 4 5
PALOS VERDES
7 10 11 11 11 10 10 10 11 12 9 7 6 6 6 6 6 5 4 4
6 10 11 11 11 11 11 12 12 13 12 12 12 12 12 11 10 7 6 4
5 10 12 13 13 13 11 9 7 5
PACIFIC OCEAN
SANTA ANA
4 11 11 12 12 11 10 8 7
3 10 9 9 10 11 10 9
2 11 11 12 13 13 12
1 11 12 12 12 12

Figure 5.12b

AVERAGE GROUND LEVEL CONCENTRATIONS (PPHM) OF O3 BETWEEN THE HOURS OF 1200. AND 1300. PST

	1	2	3	4	5	6	7	8	9	10	11	12	13	14	15	16	17	18	19	20	21	22	23	24	25
25	3	6	9	12	12	11	10	9	8	8	8														
24	3	6	10	13	11	10	8	8	8	8	8														
23	3	5	7	8	7	6	5	5	5	6	7	8	8								SAN GABRIEL MTNS				
			RESEDA																						
22	3	3	4	4	4	3	3	3	4	5	6	7	8	8	9	10									
									BURBANK																
21	4	4	4	4	3	3	3	3	4	5	6	6	7	6	7	9	11	12	13	14	14	14	12	10	10
															PASADENA						AZUSA				
20	5	5	6	6	5	5	5	5	4	5	5	5	5	5	5	7	8	9	10	12	13	14	12	10	9
			SANTA MONICA MTNS																						
19	7	7	7	7	6	6	5	5	4	4	4	4	3	3	4	5	5	6	8	9	12	13	12	10	8
																		EL MONTE							
18	7	7	7	7	6	6	4	4	4	4	3	3	3	3	3	3	4	5	6	8	11	13	13	10	7
											DOWNTOWN LA														POMONA
17	7	6	6	6	6	4	4	4	4	3	3	3	2	2	3	3	4	4	5	7	11	14	13	9	6
						WEST LA																			
16				7	6	5	4	4	4	3	3	2	2	3	3	3	3	4	5	7	10	13	12	8	5
													COMMERCE												
15					7	5	4	4	4	3	2	2	3	3	3	3	3	3	4	6	10	12	11	8	5
14						5	5	4	3	3	3	3	3	3	3	2	2	2	3	5	9	12	11	8	5
								LENNOX																	
13						7	4	3	3	3	3	3	3	2	2	2	2	2	3	4	9	11	11	8	5
																		WHITTIER		LA HABRA					
12							3	3	4	3	3	3	2	2	2	2	2	2	2	4	8	11	12	8	5
11							7	6	3	3	3	3	2	2	2	2	2	2	2	4	7	10	10	7	4
10							7	6	3	3	3	2	2	2	2	2	2	2	2	3	5	7	7	5	4
													LONG BEACH									ANAHEIM			
9							7	6	6	5	4	1	2	2	2	2	2	2	2	2	3	4	4	4	4
8							7	6	6	5	4	2	3	3	4	3	2	2	2	2	2	3	3	3	3
							PALOS VERDES																		
7							6	7	7	6	6	6	6	6	7	5	4	3	3	4	4	4	3	3	3
6							6	7	7	6	7	7	7	8	9	8	8	7	7	7	7	6	5	4	3
5																	6	7	8	8	8	7	6	5	4
			PACIFIC OCEAN																			SANTA ANA			
4																		6	7	7	7	6	6	5	4
3																			6	5	5	6	6	6	6
2																				6	7	7	8	8	7
1																					6	7	7	8	7

Figure 5.13a

AVERAGE GROUND LEVEL CONCENTRATIONS (PPHM) OF O3 BETWEEN THE HOURS OF 1200. AND 1300. PST

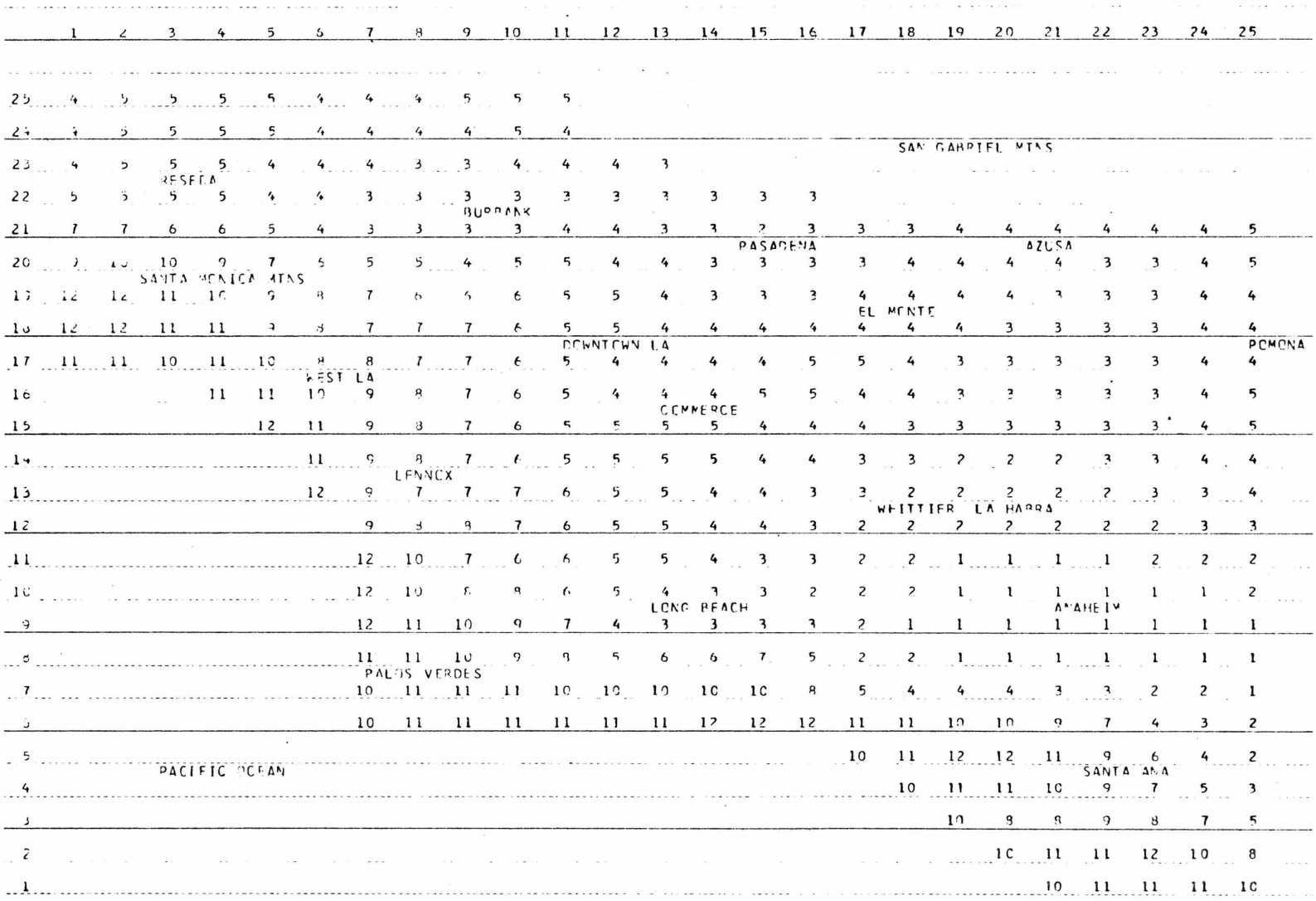

Figure 5.13b

AVERAGE GROUND LEVEL CONCENTRATIONS (PPHM) OF O3 BETWEEN THE HOURS OF 1200. AND 1300. PST

	1	2	3	4	5	6	7	8	9	10	11	12	13	14	15	16	17	18	19	20	21	22	23	24	25
25	1	1	1	1	1	1	1	1	1	1	1														
24	1	1	1	1	1	1	1	1	1	1	1														
23	1	1	1	1	1	1	1	1	1	1	1	1	1												
22	1	1	1	1	1	1	1	1	1	1	1	1	1	1	1	1									
21	2	2	1	1	1	1	1	1	1	1	1	1	1	1	1	1	1	1	1	1	1	1	1	1	1
20	2	2	2	2	2	2	2	1	1	1	1	1	1	1	1	1	1	1	1	1	1	1	1	1	1
19	3	3	3	3	2	2	2	2	1	1	1	1	1	1	1	1	1	1	1	1	1	1	1	1	1
18	3	3	3	3	2	2	2	1	1	1	1	1	1	1	1	1	1	1	1	1	1	1	1	1	1
17	3	3	3	3	2	2	2	1	1	1	1	1	1	1	1	1	1	1	1	1	1	1	1	1	1
16				3	2	2	2	2	1	1	1	1	1	1	1	1	1	1	1	1	1	1	1	1	1
15					3	3	2	1	1	1	1	1	1	1	1	1	1	1	1	1	1	1	1	1	1
14						3	2	1	1	1	1	1	1	1	1	1	1	1	1	1	1	1	1	1	1
13						3	2	1	1	1	1	1	1	1	1	1	1	1	1	1	1	1	1	1	1
12							2	2	2	1	1	1	1	1	1	1	1	1	1	1	1	1	1	1	1
11							3	2	1	1	1	1	1	1	1	1	1	1	1	1	1	1	1	1	1
10							3	2	2	2	1	1	1	1	1	1	1	1	0	0	0	1	1	1	1
9							3	3	2	2	2	1	1	1	1	1	1	1	0	0	0	0	0	0	0
8							3	3	2	2	2	1	1	1	1	1	1	1	0	0	0	0	0	0	0
7							3	3	3	3	2	2	2	2	2	2	1	1	1	1	1	1	1	1	0
6							3	3	3	3	3	3	3	3	3	3	3	3	2	2	2	2	1	1	1
5																	3	3	3	3	2	2	1	1	1
4																		3	3	2	2	2	1	1	1
3																			2	2	2	2	2	2	1
2																				3	3	3	3	3	2
1																					3	3	3	3	3

PACIFIC OCEAN
PESEDA
SANTA MONICA MTNS
BURBANK
WEST LA
DOWNTOWN LA
COMMERCE
LENNOX
PALOS VERDES
LONG BEACH
PASADENA
SAN GABRIEL MTNS
EL MONTE
AZUSA
POMONA
WHITTIER
LA HABRA
ANAHEIM
SANTA ANA

Figure 5.14

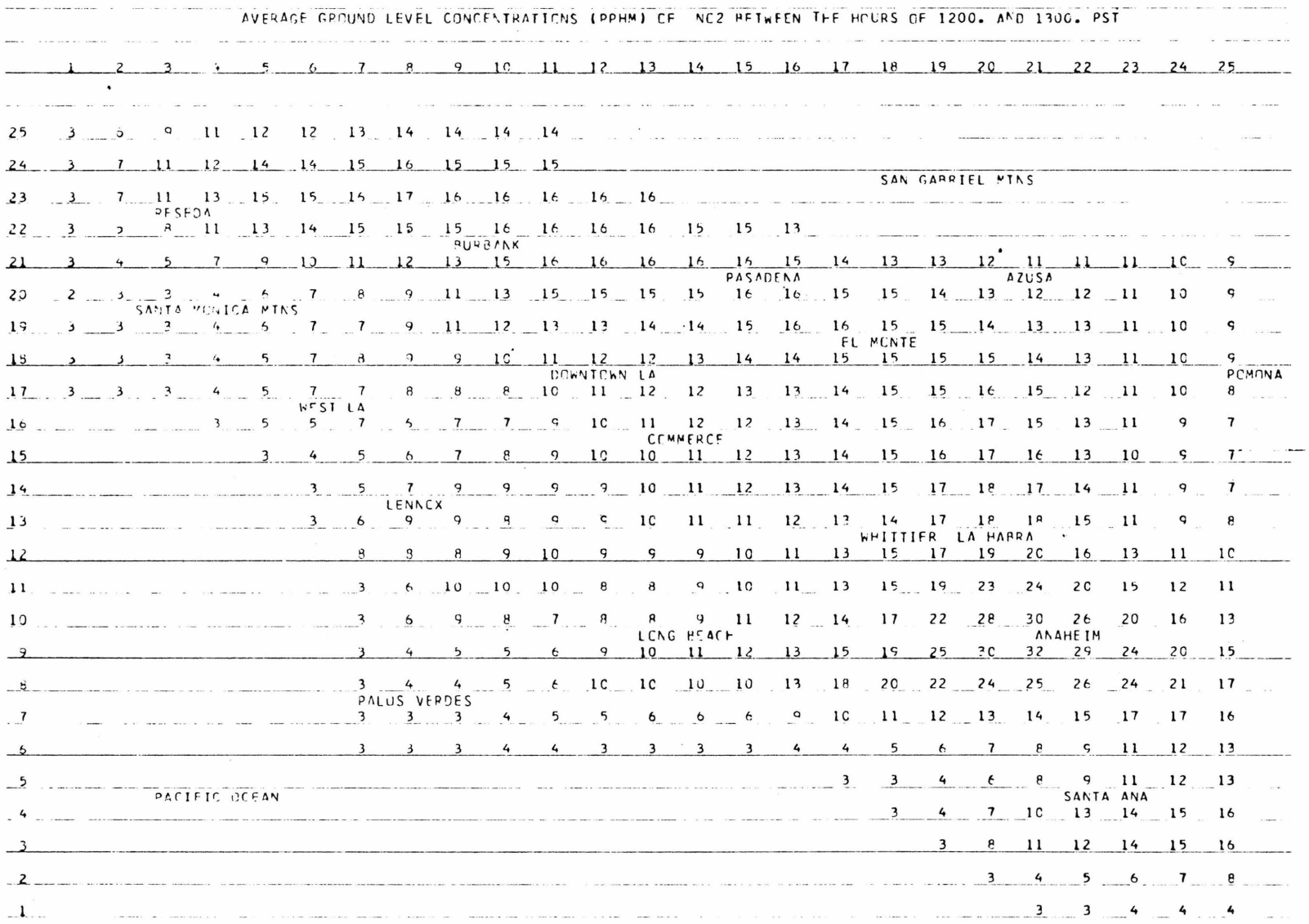
AVERAGE GROUND LEVEL CONCENTRATIONS (PPHM) OF NO2 BETWEEN THE HOURS OF 1200. AND 1300. PST
SAN GABRIEL MTNS
RESEDA
BURBANK
PASADENA
AZUSA
SANTA MONICA MTNS
EL MONTE
DOWNTOWN LA
POMONA
WEST LA
COMMERCE
LENNOX
WHITTIER
LA HABRA
LONG BEACH
ANAHEIM
PALOS VERDES
PACIFIC OCEAN
SANTA ANA

Figure 5.15a

AVERAGE GROUND LEVEL CONCENTRATIONS (PPHM) OF NO2 BETWEEN THE HOURS OF 1200. AND 1300. PST

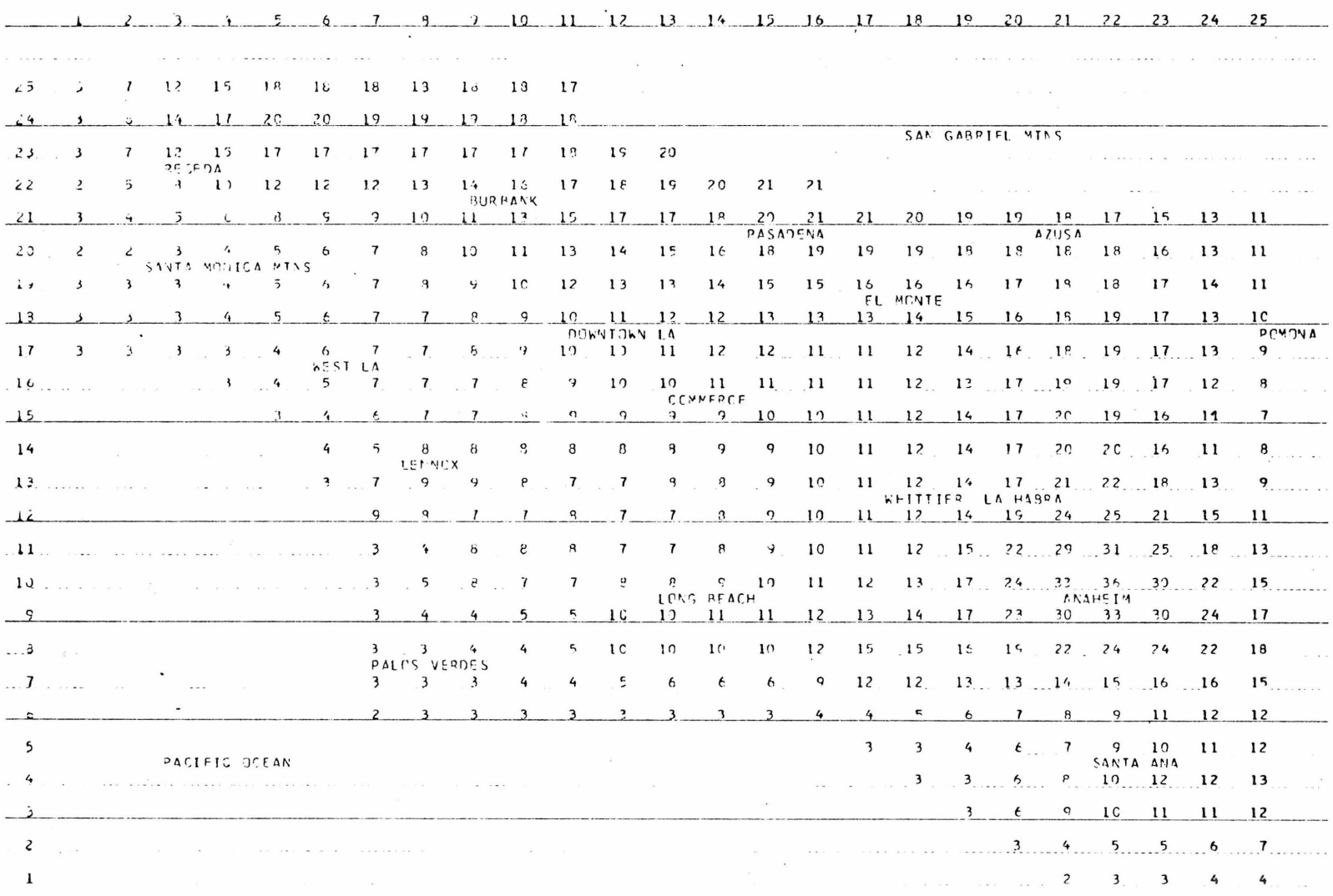

Figure 5.15b

AVERAGE GROUND LEVEL CONCENTRATIONS (PPHM) OF NO2 BETWEEN THE HOURS OF 1200. AND 1300. PST

	1	2	3	4	5	6	7	8	9	10	11	12	13	14	15	16	17	18	19	20	21	22	23	24	25
25	2	5	12	16	19	19	18	18	18	17	17														
24	2	7	14	18	20	20	19	19	18	18	18														
23	2	7	12	15	16	16	16	16	16	17	18	19	19									SAN GABRIEL MTNS			
22	2	6	7	9	10	11	11	11	12	15	16	18	19	19	21	21									
21	2	3	4	6	7	8	8	9	10	12	15	16	17	18	20	21	21	21	20	19	19	17	16	13	11
20	2	2	3	3	5	6	7	8	9	10	12	13	14	15	17	19	19	19	19	19	19	19	17	14	11
19	3	3	3	4	5	6	6	7	8	9	10	11	12	12	13	14	15	15	16	17	18	19	17	14	11
18	3	3	3	3	5	6	6	7	7	8	9	9	10	10	11	12	12	13	14	16	18	19	17	14	10
17	3	3	3	3	4	5	6	6	7	7	8	8	9	10	10	10	10	11	13	16	18	19	17	13	9
16				3	4	4	6	6	6	6	7	8	8	9	9	9	9	10	12	16	19	20	17	12	8
15					3	4	6	6	6	7	7	7	7	8	8	9	9	10	12	16	20	20	16	11	7
14						4	5	6	7	7	7	6	6	7	8	8	9	10	12	16	20	20	17	11	7
13						3	6	7	7	6	6	6	6	7	7	8	9	10	12	16	21	22	18	13	9
12							7	7	6	6	6	6	6	6	7	8	9	10	12	17	23	25	21	15	10
11							3	4	6	7	6	6	6	6	7	8	9	10	13	20	28	31	25	18	12
10							3	4	7	6	6	6	6	7	8	9	10	11	15	23	32	35	29	21	14
9							3	3	6	4	5	7	7	8	9	10	11	12	15	21	28	31	28	22	16
8							3	3	3	4	5	6	8	8	9	10	12	13	14	16	19	22	22	19	16
7							2	3	3	4	4	5	5	6	6	8	10	11	11	12	13	13	14	14	13
6							2	2	3	3	3	3	3	3	3	3	4	4	6	7	8	9	10	10	10
5																	2	3	4	6	7	9	10	10	11
4																		2	3	5	8	10	11	12	12
3																			3	6	8	9	10	11	11
2																				2	3	4	5	6	7
1																					2	3	3	4	4

RESEDA
BURBANK
PASADENA
AZUSA
SANTA MONICA MTNS
EL MONTE
DOWNTOWN LA
POMONA
WEST LA
COMMERCE
LENNOX
WHITTIER
LA HABRA
LONG BEACH
ANAHEIM
PALOS VERDES
PACIFIC OCEAN
SANTA ANA

Figure 5.16a

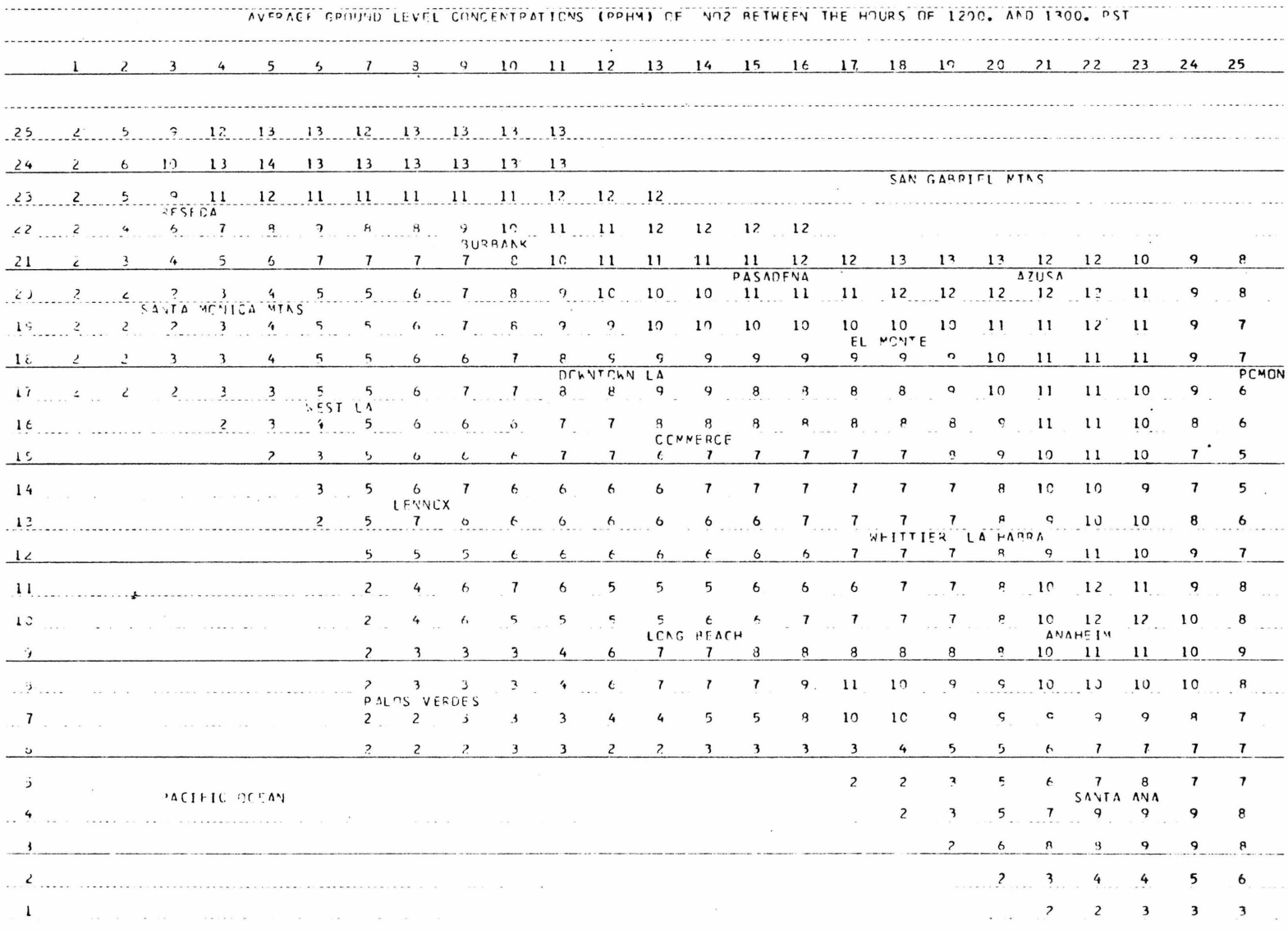
AVERAGE GROUND LEVEL CONCENTRATIONS (PPHM) OF NO2 BETWEEN THE HOURS OF 1200. AND 1300. PST
1 2 3 4 5 6 7 8 9 10 11 12 13 14 15 16 17 18 19 20 21 22 23 24 25
SAN GABRIEL MTNS
JESEDA
BURBANK
PASADENA
AZUSA
SANTA MONICA MTNS
EL MONTE
DOWNTOWN LA
POMON
WEST LA
COMMERCE
LENNOX
WHITTIER
LA HABRA
LONG BEACH
ANAHEIM
PALOS VERDES
PACIFIC OCEAN
SANTA ANA

Figure 5.16b

AVERAGE GROUND LEVEL CONCENTRATIONS (PPHM) OF NO2 BETWEEN THE HOURS OF 1200. AND 1300. PST

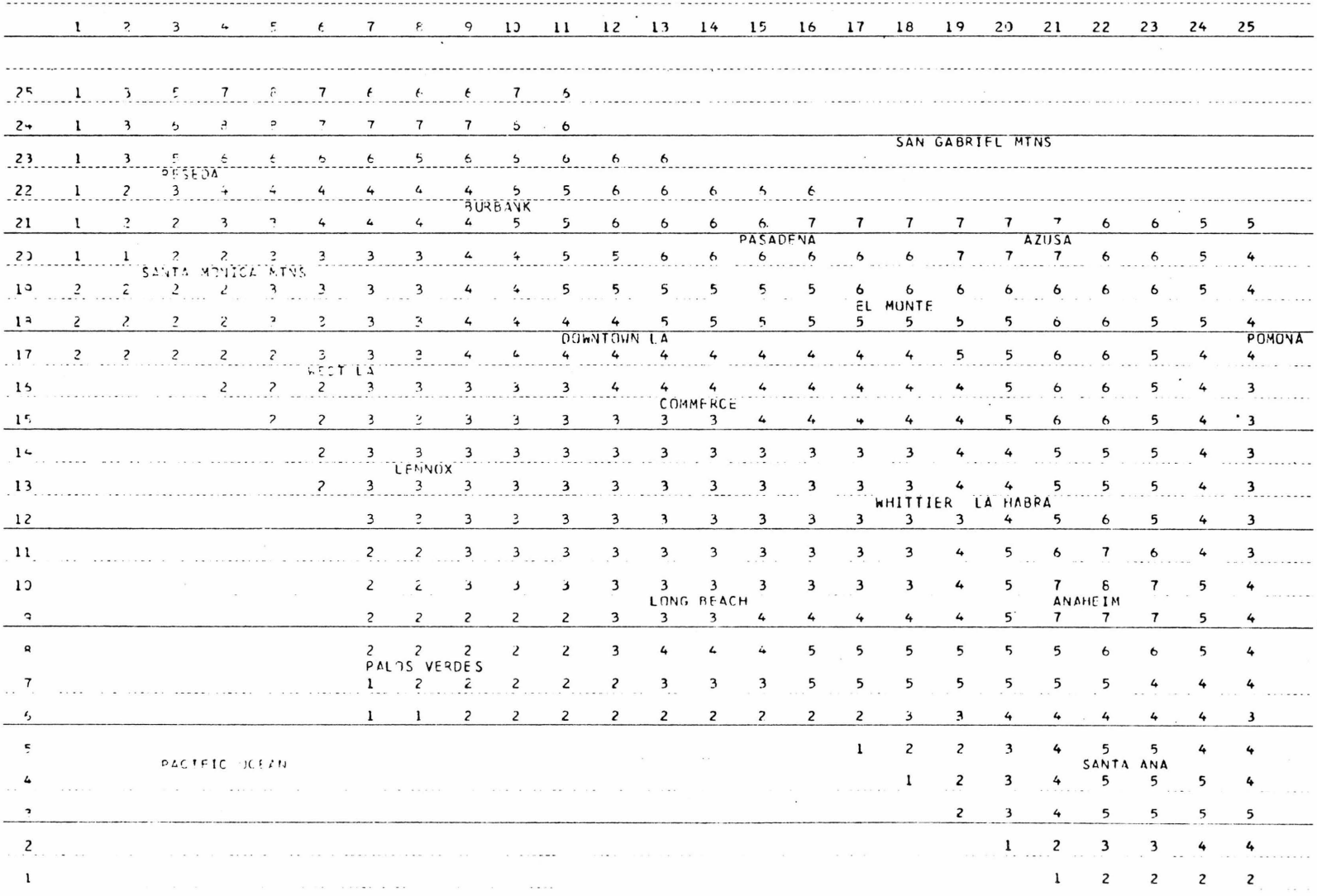

CHAPTER 6

RECOMMENDATIONS FOR FUTURE STUDIES

In the previous five chapters, a detailed discussion has been presented describing the basic components of the photochemical airshed model developed in this study. The model was evaluated by first simulating a ten-hour period on each of six days in 1969 and then comparing the model predictions with actual measurements of pollutant concentrations. To illustrate the utility of the model, the 1977 EPA control strategy proposed for the Los Angeles Basin was examined using the model in order to ascertain the plan's impact on air quality. Throughout the discussion of the development, evaluation, and application of the model, reference has been made to the fact that improvements in several aspects of the model and its usage are needed. In this chapter a number of recommendations are made for future research and development efforts which should both improve the performance and extend the capabilities of the model.

The recommendations to be made will focus on the treatment of meteorological variables, atmospheric chemistry, pollutant emissions, numerical analysis, model validation, and model applications. Suggestions aimed at improving the treatment of meteorological variables are considered first.

Treatment of Meteorological Variables

As mentioned in Chapter 1, the preparation of meteorological inputs, including wind speeds and directions and mixing depths, is a very time-consuming task, especially if the inputs are specified

manually as they were in this study. There is a clear need for the implementation of an automated input routine to facilitate the specification of the meteorological variables at each grid point. The routine should accept the available measurements as inputs, and through use of an interpolation procedure, calculate the required meteorological parameters. In a study carried out by Liu et al. (1973), automated input routines such as those envisioned above have been developed and applied to the calculation of wind speed and direction and mixing depth in the Los Angeles airshed. Although wind fields and mixing depths were only calculated for one day in 1969, the results were encouraging. It is thus recommended that the procedures employed by Liu et al. (1973) be further developed and validated, as needed, so as to provide a convenient means for inputting the necessary meteorological parameters into the airshed model.

Another meteorological parameter in need of further study is the turbulent diffusivity. Note from Chapter 1 that the "plateau" value of the vertical diffusivity is considered only to be a function of wind speed. Employing measured diffusivity data reported by Hosler (1969), Eschenroeder et al. (1972) have found that the vertical diffusivity does not correlate well with wind speed alone. They did find, however, that a reasonable correlation could be achieved between the diffusivity and the vertical temperature gradient. Thus, it is recommended that the treatment of the diffusivity be reformulated to reflect its dependence on the stability of the atmosphere. Ragland (1973) has recently

given several expressions for the height dependence of the vertical diffusivity in the surface layer. Further work will be required, however, to correctly specify the vertical diffusivity in the remaining portion of the planetary boundary layer. While considerable study of the vertical diffusivity has been reported, very few guidelines exist for the estimation of the horizontal diffusivity. The development of an algorithm for the computation of the horizontal diffusivity is needed for inclusion in both the airshed and microscale models.

The Chemical Kinetics Mechanism

One of the most important components of a photochemical airshed model is an accurate, yet concise, kinetic mechanism describing the chemical reactions that take place in the urban atmosphere. One of the shortcomings of the mechanism described in Chapter 1 is the use of generalized stoichiometric coefficients which are determined by trial and error computations involving the use of the mechanism to simulate smog chamber experiments. Hecht and Seinfeld (1973) have recently proposed a mechanism which averts the use of generalized coefficients through the introduction of lumped hydrocarbon species. For example, a hydrocarbon mixture would be segmented into four lumped species -- olefins, aromatics, paraffins, and aldehydes. While such a treatment of the hydrocarbon mixture may be desirable from a chemical viewpoint, it does introduce several problems as far as actual implementation in an airshed model is concerned. First, additional hydrocarbon species must be followed in the airshed model, increasing computation times. Second, detailed hydrocarbon measurements will be needed to specify both

initial and boundary concentrations for each hydrocarbon class, and in addition, emission rates must also be estimated for each lumped species. While practical considerations may limit the desirability of including this new mechanism in the airshed model at the present time, the mechanism should be made as concise as possible and thoroughly validated, especially for hydrocarbon mixtures similar to those found in the urban atmosphere, so that it may be included in the airshed model at a future time when the appropriate measurements and faster computing machines and algorithms become available.

Another aspect of the chemical mechanism worthy of further study is the temperature dependence of the reaction rate constants. In this report, the rate constants were assumed to be invariant with changes in temperature throughout the day. In the Los Angeles airshed, for example, the temperature at points near the coast may be substantially different from that at points in the inland valleys during the day. To ascertain the importance of temperature effects, a series of smog chamber experiments could be performed in which the temperature is allowed to vary from, say, 60° to 100° F (the temperature in any given experiment would be held constant). If temperature effects were found to be important, then the appropriate steps could be taken to determine the temperature dependence of the reaction rate constants in the mechanism.

Pollutant Emissions

The key needs for improved estimation of pollutant emissions are 1) the determination of representative driving cycles for each type of motor vehicle, 2) information with regard to the spatial and

temporal distribution of fixed source emissions, and 3) detailed data on the types and amounts of hydrocarbons emitted from each source. The primary importance of examining the driving characteristics of motorists in a particular urban area is to assess whether or not emission estimates obtained from vehicles tested using the California or Federal Driving Cycles will accurately reflect motor vehicle emissions. If driving patterns in a particular area are found to differ substantially from the CDC or the FDC, then emissions from a representative sample of the vehicle population should be measured using the appropriate driving conditions.

While the determination of the spatial and temporal distribution of fixed source emissions is basically a straightforward process, efforts to compile such an inventory for Los Angeles were hampered by the fact that the appropriate data were not available. However, the Los Angeles County APCD (1973) has recently released a detailed listing of major fixed sources in the county, including estimates of daily hydrocarbon, NO_x and CO emissions. This information and future data to be made available by the APCD will make it feasible to compile a more reliable fixed source inventory for Los Angeles.

Finally, more detailed data are needed with regard to the types and quantities of hydrocarbons emitted from each source, especially for the reactive hydrocarbons. This information is necessary to properly calculate the reactive/unreactive hydrocarbon split. In addition, recent studies in the development of mechanisms to represent the chemical reactions that take place in the atmosphere indicate that several types of reactive hydrocarbons may have to be

followed in order to adequately simulate the photochemical processes. As mentioned in the previous section, one such mechanism would require detailed emission estimates for paraffins, olefins, aromatics, and aldehydes.

Numerical Methods

In view of the fact that the present ratio of simulated to real time for photochemical simulations (on an IBM 370/155) is only 8:1 and, in addition, given the possible need to expand the number of chemical species to be followed, an improved numerical integration method will be required which is significantly faster than that employed in this study, especially if the model is to enjoy widespread usage in evaluating either emission control strategies or regional planning decisions. Another important aspect of the numerical integration procedure is the accuracy of the method. As the parameters in the model are known more accurately, it will be important to have available numerical methods whose accuracy is such that the error in the predicted results is largely due to the errors inherent in the model parameters rather than those attributable to numerical inaccuracies.

Motivated by the desire to find faster and more accurate alternatives to the conventionally employed finite-difference methods, several investigators have either developed new techniques or extended existing methods which are potentially suitable for inclusion in an airshed model (a list of references is given in Chapter 3). In particular, initial studies of the particle-in-cell, finite element, and Galerkin-type methods have given an indication that simulations

employing these techniques may provide more accurate numerical results in less computer time than those using finite-difference methods. However, only the particle-in-cell technique has been completely adapted for use in three-dimensional photochemical calculations. Thus, it is recommended that each method cited in Chapter 3 be thoroughly evaluated with regard to its suitability for solving the governing equations of the model. Then a set of comparative tests should be performed to determine the accuracy and computational speed of each method.

Model Evaluation

While photochemical simulations were carried out in this study for six days in 1969, there is a need to perform further validation simulations. At present it is difficult to ascertain which parameters in the model are responsible for the discrepancies between prediction and measurement, especially when many of the parameters can only be specified with limited accuracy. Thus, to properly assess the validity of the model, a comprehensive set of emissions, meteorological, and air quality measurements are needed with which to test the model.

Until a reasonable set of data becomes available, sensitivity studies should be performed to determine the extent to which each parameter affects the predicted results. For example, it would be of interest to vary each of the emissions, meteorological, and chemical parameters in the model within their range of uncertainty. Future efforts aimed at improving the model could then be limited to those features found to significantly influence the predicted

concentrations. In addition, a sensitivity analysis may also be used to indicate the degree of detail required in each portion of the model. For instance, if wind shear effects were found to be important, then a more sophisticated treatment of the windfield aloft than that employed in the present study would have to be developed.

The final recommendation with regard to model evaluation is that multiday simulations should be performed. Note that model usage has been limited to the simulation of ten-hour daylight periods. Multiday runs will, in the immediate future, serve as an aid in the identification of possible sources of error in the model. Errors incurred in a short term (say, less than 12 hours) simulation will not accumulate to the extent they would over a three or four day period. As an example, suppose the concentrations of total nitrogen oxides were observed to accumulate to much higher values than measured after a simulation of several days. This might suggest that either NO_x emissions are too high, or that sinks of NO_x have not been properly accounted for in the model.

Model Applications

While the present study has primarily focused on the development of an airshed model and aside from the fact that further efforts must be made to improve the model, the most interesting and potentially useful future studies will be those associated with the actual application of the model for use in either performing short range forecasts of ground level concentrations or evaluating emission control strategies for various urban areas. In the former application,

means will have to be developed to forecast the meteorological inputs to the model for up to several days in the future. The latter application will be very important in both the near and distant future. In the near future, there will be a need to examine the control strategy implementation plans proposed for several urban areas in conjunction with the requirements of the Clean Air Act. In the long term, studies can be performed to determine effects of regional planning decisions on air quality in future years such 1990 or 2000.

APPENDIX A

THE CALCULATION OF AVERAGE MOTOR VEHICLE EXHAUST EMISSION RATES FOR LOS ANGELES IN 1977

A.1 Introduction

Since motor vehicles will contribute significantly to the photochemical air pollution problem in the Los Angeles Basin for many years, a comprehensive emissions inventory applicable during this period must include exhaust emissions from these important sources. The two quantities needed to describe the total exhaust emissions injected into the airshed are 1) the rate at which each pollutant is emitted from the "average" motor vehicle (grams/mile), and 2) the number of miles travelled on both surface streets and freeways in each ground-level grid cell (miles/day). Because driving conditions on surface streets and freeways tend to differ, the rate at which pollutants are emitted from a vehicle will depend on the type of roadway on which it is operated. Driving on surface streets involves a full range of idle, cruise, acceleration, and deceleration operating modes, and thus emissions are best quantified by measuring the amount of pollutants emitted while the vehicle is operated on a "driving cycle," such as the California or Federal Driving Cycles. On freeways, however, vehicles may be subjected to somewhat more stable operating conditions (i.e., the driving speed tends to fluctuate less). Emissions may be quantifiified in this instance by measuring the rate at which pollutants are emitted at several cruising speeds and from this data, determining an emissions/driving speed correlation. In this Appendix the discussion will focus on the methodology employed to calculate

the various emission rates cited above for all types of vehicles to be operated in the Los Angeles Basin in 1977.

To compute hot and cold-start emission rates and the emissions/driving speed correlations for use in the 1969 model validation study, several assumptions were made because the appropriate measurements were not available (see Chapter 2). Subsequently, a study of light-duty vehicle emissions was sponsored by EPA and carried out by Automotive Environmental Systems, Inc. (Fegraus et al., 1973; AESi, 1973). In this study, 1000 motor vehicles from six cities, including Denver, Chicago, Houston, St. Louis, Washington, and Los Angeles, were tested for emissions of NO_x, CO, CO_2, and hydrocarbons using the following test procedures:

1. 1972 Federal Test Procedure (FTP),
2. 1975 FTP; and
3. Steady cruise operation at idle, 15, 30, 45, and 60 mph.

Since only 1957-71 model year vehicles were tested by AESi, other means must be developed to estimate emissions from 1972-77 vehicles. The assumptions made and algorithms employed will be discussed later in this Appendix.

Average hot-start, cold-start, or steady cruise emission rates may be obtained by averaging the emissions from each type of motor vehicle using the following equation

$$E_\ell = \frac{\sum_{i=1}^{8} \mu_i \sum_{j=65}^{77} x_{ij} m_{ij} e_{\ell ij}}{\sum_{i=1}^{8} \mu_i \sum_{j=65}^{77} x_{ij} m_{ij}} \qquad \text{(A. 1)}$$

where ℓ, i, and j are indices denoting chemical species, vehicle class, and model year, respectively, and

E_ℓ = average emission rate of species ℓ (grams/mile)

μ_i = fraction of motor vehicles belonging to class i

x_{ij} = fraction of class i vehicles manufactured in model year j

m_{ij} = annual or daily mileage (miles/year or miles/day) for class i, model year j vehicles

$e_{\ell ij}$ = emission rate of species ℓ from class i, model year j vehicles (grams/mile)

The eight classes of motor vehicles considered in this study are listed in Table A.1. Vehicles are further grouped according to model year, designated by the index j, where j = 65, 66, . . . , 77 corresponds to pre-1966, 1966, . . . , 1977 model years, respectively. The appropriate values of $e_{\ell ij}$ to be used in equation (A.1) are either hot-start, cold-start, or steady cruise emissions, the choice depending on the type of average emission factor desired.

Table A.1 Motor Vehicle Class Definitions

Class	Type of Vehicle
1	light-duty domestic automobiles
2	light-duty foreign automobiles
3	light-duty domestic trucks
4	light-duty foreign trucks
5	heavy-duty gasoline trucks
6	heavy-duty diesel trucks
7	two-stroke motorcycles
8	four-stroke motorcycles

Since vehicles produced by various manufacturers may exhibit different emission rates, the value of $e_{\ell ij}$ for a particular class and model year may be determined from the following equation*

$$e_{\ell ij} = \sum_{k=1}^{N^m} \eta_{ijk} \bar{e}_{\ell ijk} \qquad \text{(A.2)}$$

where k is an index denoting the manufacturer, and

N^m = number of different manufacturers

η_{ijk} = fraction of class i, model year j vehicles produced by manufacturer k

$\bar{e}_{\ell ijk}$ = emission rate of species ℓ from the average class i, model year j vehicle produced by manufacturer k (grams/mile)

In this study equation (A.2) is not used directly because reported emission rate data are more appropriately interpreted as yielding values of $e_{\ell ij}$ directly. Although values of $\bar{e}_{\ell ijk}$ for light duty automobiles may be estimated from the AESi (1973) data, these estimates may be subject to considerable error since the number of vehicles tested was necessarily small. For example, only one 1970 Buick was tested in Los Angeles; whether or not the emissions from this vehicle are representative of all 1970 Buicks in the Basin is uncertain. The number and type of vehicles selected for testing in the AESi study were carefully chosen, however, to reflect the nationwide distribution of light-duty automobiles in 1971. By averaging the

---

* Note that use of equations (A.1) and (A.2) assumes that the annual (or daily) mileage of a particular class and model year vehicle is independent of the manufacturer.

test results for a given model year, a reasonable estimate may be obtained for the value of $e_{\ell ij}$ for light-duty vehicles. Since the objective of this study is to examine air quality in Los Angeles, only the Los Angeles test data are used to estimate the emission rates of 1957-71 vehicles.

The remainder of this Appendix is devoted to a discussion of all parameters appearing in equation (A. 1). First, the distribution of vehicles, both with respect to class and model year, is derived in Section A. 2, and in Section A. 3 data pertaining to the annual mileage accumulated by each type of vehicle are presented. Section A. 4 is devoted to a detailed discussion of cold-start, hot-start, and steady cruise emission rates for each class of vehicles considered in this study. Finally, the average emission rates obtained from equation (A. 1) are summarized in Section (A. 5).

A. 2 Distribution of Vehicles by Class and Model Year

Two procedures may be employed to determine the class and model year vehicle distributions. The first, and most sophisticated, involves the use of sales and scrappage models. Basically, the number of vehicles sold (or to be sold) in the region of interest is predicted by the sales model, while the fraction of vehicles of a particular model year still in service in some future year is obtained from the scrappage model. A model of this type for trucks and buses is discussed by Tingley and Johnson (1973). Unfortunately, no such model for the Los Angeles Basin is readily available, and the development of an appropriate model is beyond the scope of this study.

Another approach which may be used involves the determination of the present (or recent) distribution of vehicles in the modeling region. This distribution is then assumed to apply in some future year of interest. For this methodology to be successful, however, sales and scrappage rates must remain at those levels which will cause no future change to occur in the given age and class distributions. To what extent this criterion will be valid in the Basin is unknown. In view of the fact that an alternative method is not available, the second scheme discussed above has been adopted for use in this study. This methodology has also been used by the State of California ARB (Bratton, 1973) and the EPA (EPA, 1973a) for predicting the future distribution of motor vehicles.

The statewide distribution of motor vehicles, by model year, for class 1-6 vehicles on July 1, 1972 was obtained from the State of California ARB (Bratton, 1973). Assuming that these data will also apply on July 1, 1977, and also assuming that the statewide distribution is applicable in the Los Angeles Basin, values of x_{ij} used in equation (A.1) are given in Table A.2. The age distribution of motorcycles is assumed to be uniform since emission data as a function of model year are not available. Thus, $x_{ij} = .0769$ (i.e., 1.0/13) for $7 \leq i \leq 8$.*

* A more detailed age distribution for motorcycles, as of 1971, is given in the 1972 California Statistical Abstract, published by the State of California.

Table A.2 Estimated Distribution of Automobiles and Trucks, by Model Year, on July 1, 1977*

Model Year/Class	1	2	3	4	5 and 6
1977	.0727	.0941	.0757	.1658	.0762
1976	.0750	.1712	.0765	.2414	.0802
1975	.0825	.1229	.0814	.1725	.0812
1974	.0904	.1393	.0853	.1086	.0856
1973	.0880	.0950	.0675	.0591	.0684
1972	.0775	.0802	.0553	.0539	.0571
1971	.0868	.0614	.0637	.0390	.0642
1970	.0934	.0472	.0693	.0268	.0688
1969	.0794	.0395	.0633	.0228	.0623
1968	.0653	.0323	.0522	.0213	.0529
1967	.0513	.0231	.0414	.0112	.0425
1966	.0313	.0197	.0295	.0123	.0309
pre-1966	.1064	.0741	.2390	.0653	.2288

* The data presented in this Table were derived from the California statewide vehicle population on July 1, 1972. Source: State of California ARB (Bratton, 1973).

Having discussed the age distribution for each type of vehicle, attention is now focused on the distribution of vehicles by class, that is, the values of μ_i in equation (A.1). 1972 vehicle registration statistics for Los Angeles and Orange Counties have been published by the County Supervisors Association of California (1972). However, only the total number of automobiles, trucks, and motorcycles are reported. Data on the statewide distribution of automobiles and trucks were obtained from the State of California ARB (Bratton, 1973). Thus, the percentage of the total automobile population in the Basin of domestic origin is assumed to be equal to the corresponding

statewide percentage. The truck population is treated analogously. On a statewide basis in 1972, domestic automobiles represented 81.02% of the total automobile population, while class 3-6 trucks represented 73.99%, 7.90%, 13.72%, and 4.39%, respectively, of the entire truck population. The motorcycle population is assumed to be comprised of 38% two-stroke and 62% four-stroke motorcycles (EPA, 1973b). Employing the percentages cited and the registration statistics for automobiles, trucks, and motorcycles, the distribution of vehicles, by class, may be derived. These values of μ_i are assumed to apply on July 1, 1977 and are summarized in Table A.3.

Table A.3

Estimated Distribution of Vehicles, by Class, on July 1, 1977

Class	Fraction of the Total Vehicle Population
1	.6851
2	.1605
3	.0876
4	.0093
5	.0162
6	.0052
7	.0137
8	.0224

A.3 Annual Mileage

To properly compute an average emission rate, the emissions from each vehicle must be weighted with respect to the annual (or daily) mileage it will accumulate. This weighting is important

because late model year vehicles may be driven over twice the annual mileage as that of older vehicles during a given year. Further, heavy-duty vehicles tend to accumulate more mileage than light-duty vehicles, and thus their contribution to the average emission rate must be weighted accordingly. Annual mileages for automobiles and trucks as a function of vehicle age were obtained from the State of California ARB (Bratton, 1973). These data, adapted for use in 1977, are presented in Table A. 4.

Upon examining the reported annual mileages of heavy-duty diesel trucks, it was found that the average vehicle is driven about 52, 500 miles per year, with new vehicles reported to travel 89, 000 miles annually. Much of this mileage, however, is probably not due to travel in the Basin, but may arise instead from intra and interstate freight shipping. In an effort to determine the average number of miles driven each year by diesel vehicles within Los Angeles County, estimated daily diesel fuel consumption data were obtained from the Los Angeles APCD (MacBeth, 1973). It is estimated that 20, 732 diesel vehicles consumed 185, 000 gallons of fuel per day in Los Angeles County in 1972. Assuming that diesel vehicles obtain 5.1 miles per gallon of fuel (EPA, 1973c), the average yearly mileage may be computed in the following manner:

$$\frac{185,000 \text{ (gal/day)} \times 5.1 \text{ (miles/day)} \times 365 \text{ (days/year)}}{20,732 \text{ vehicles}} \cong 16,600 \frac{\text{miles}}{\text{vehicle year}}$$

Thus, all annual mileage data for diesel vehicles obtained from the State of California ARB were scaled by the ratio of 16,600 miles/year to 52,500 miles/year. The entries for class 6 vehicles in Table A. 4

reflect this scaling of the original ARB data.

Table A. 4

Estimated Annual Mileage to be Accumulated by Motor Vehicles in 1977 (miles/year)*

Model Year/Class	1 and 3	2 and 4	5	6
1977	14, 400	12, 500	19, 600	28, 140
1976	14, 100	12, 500	19, 600	28, 140
1975	12, 900	11, 600	18, 000	25, 800
1974	11, 400	11, 400	18, 000	25, 800
1973	8, 600	10, 300	14, 000	20, 110
1972	6, 800	9, 500	14, 000	20, 110
1971	5, 700	8, 400	11, 000	15, 870
1970	4, 800	5, 900	11, 000	15, 870
1969	4, 000	4, 000	8, 400	12, 140
1968	3, 600	3, 100	8, 400	12, 140
1967	3, 500	2, 400	4, 300	6, 130
1966	3, 500	2, 100	4, 300	6, 130
pre-1966	3, 500	2, 000	4, 300	6, 130

* Source: State of California ARB (Bratton, 1973). Diesel mileages scaled from the original ARB data (see text).

A. 4 Exhaust Emissions

This section is devoted to a discussion of the methodology employed to estimate values of $e_{\ell ij}$ for use in equation (A. 1). An attempt has been made to base all estimates on actual measurements whenever possible, but unfortunately, several emission rates must be determined from computations based on assumptions whose validity cannot be completely verified. The difficulties to be encountered in estimating emissions from vehicles which have yet to be produced are obvious. Very little data are available which may be used to

establish the speed/emissions correlation for either past, present, or future heavy-duty vehicles. As the results of present and future vehicle emission measurement programs are reported, many of the emission estimates given in this section may be subject to revision.

The remainder of this section is divided into three parts in which emissions from light-duty vehicles, heavy-duty vehicles, and motorcycles are discussed separately.

A.4.1 Light-Duty Vehicle Emissions

Four classes of light-duty vehicles are defined in equation (A.1), including domestic and foreign automobiles and trucks. Assuming that the Federal Driving Cycle is a reasonable representation of the driving conditions encountered on surface streets in the Basin, hot and cold-start emission rates for 1957-71 light-duty vehicles may be estimated from the AESi (1973) study. The emissions/driving speed correlation may also be derived from the steady cruise emissions at 15, 30, 45 and 60 mph reported in this study.

Due to the limited number of foreign automobiles tested and the fact that no light-duty trucks were included in the Los Angeles vehicle sample, a single emission factor for each model year is calculated for all class 1-4 vehicles by averaging the available test data for that year. As additional measurements become available for class 2-4 vehicles, then separate emission rates may be determined for each of the four classes. The four classes have been treated distinctly, rather than forming one large class of light-duty vehicles, for two reasons. First, the federal emission standards for post-1974 light-duty trucks are not as strict as the standards for

automobiles, and second, different exhaust control retrofit devices are scheduled for installation on foreign and domestic vehicles. Thus, as a matter of computational convenience, four classes of light-duty vehicles are treated in this study.

Before discussing the emissions data and the various algorithms employed in this study, it is best to first briefly review the 1972 and 1975 FTP. The 1972 FTP is comprised of measuring emissions from a cold-started vehicle operated on a dynamometer to stimulate a "typical" urban trip [i.e., the Federal Driving Cycle (FDC)], of 7.5 miles length and 22 minutes, 52 seconds duration. The pollutants emitted during the initial 505 seconds and the remaining 867 seconds are referred to as the cold-transient and cold-stabilized emissions, respectively. The cold-start emission rate for species ℓ, e_ℓ^c, may be obtained directly from test results based on the 1972 FTP using the following equation*

$$e_\ell^c = \frac{M_\ell^{ct} + M_\ell^{cs}}{7.5 \text{ miles}} \qquad \text{(A. 3)}$$

where M_ℓ^{ct} = mass of pollutant ℓ emitted during the cold-transient portion of the 1972 FTP (grams)

M_ℓ^{cs} = mass of pollutant ℓ emitted during the cold-stabilized portion of the 1972 FTP (grams)

For exhaust emission certification, post-1974 model year light-duty vehicles will be tested according to the 1975 FTP, which is an expanded version of the 1972 FTP. After cold-transient and

* In actual practice, all emissions are collected in a single bag, and the total mass ($M_\ell^{ct} + M_\ell^{cs}$) is reported.

cold-stabilized emissions are collected, the vehicle is allowed to soak for about 10 minutes. Then emissions are measured as the vehicle is operated through the first 505 seconds (or transient portion) of the FDC. Pollutants emitted during this segment of the test are called the hot-transient emissions, where "hot" refers to the fact that the vehicle is hot-started. Cold and hot-transient emissions are combined with the cold-stabilized emissions to yield the following emission factor

$$e_{\ell}^{ch} = \frac{0.43\, M_{\ell}^{ct} + 0.57\, M_{\ell}^{ht} + M_{\ell}^{cs}}{7.5 \text{ miles}} \qquad \text{(A. 4)}$$

where e_{ℓ}^{ch} = rate of emission of pollutant ℓ based on the 1975 FTP (grams/mile)

M_{ℓ}^{ht} = mass of pollutant ℓ emitted during the hot-transient portion of the 1975 FTP (grams).

The hot-start emission rate is obtained by measuring emissions from a hot-started vehicle operated on the FDC in a manner similar to the 1972 FTP. The emission rate is computed from

$$e_{\ell}^{h} = \frac{M_{\ell}^{ht} + M_{\ell}^{hs}}{7.5 \text{ miles}} \qquad \text{(A. 5)}$$

where e_{ℓ}^{h} = hot-start emission rate for species ℓ based on the FDC (grams/mile)

M_{ℓ}^{hs} = mass of pollutant ℓ emitted during the hot-stabilized portion of a hot-start test (grams).

Thus, the measurement or estimation of cold and hot-transient and cold and hot-stabilized emissions is required to establish the cold and hot-start emission factors from equations (A. 3) and (A. 5).

As an aid in presenting exhaust emissions, light-duty vehicles have been segmented into the following three model year groups: pre-1972, 1972-1974, and 1975-1977. Emissions from each group of motor vehicles are discussed below.

A.4.1.1 Pre-1972 Vehicles

As mentioned previously, emissions from pre-1972 vehicles are based on tests of 174* vehicles operated in the Basin. Emissions from each vehicle were determined using both the 1972 and 1975 FTP; steady cruise emissions at 15, 30, 45, and 60 mph were also reported. In addition, 55 vehicles were subjected to a complete hot-start emissions test. Therefore, cold-start emissions are available for each of the 174 vehicles tested, but the hot-start data are incomplete.

In an effort to estimate hot-start emissions from those vehicles which were not subjected to a complete hot-start test, the following assumption is made. If hot-stabilized emissions are not reported for a particular vehicle, then it is assumed that the cold-stabilized emissions may be substituted for the hot-stabilized emissions in equation (A.5). That is, assuming $M_{\ell}^{hs} \cong M_{\ell}^{cs}$, then e_{ℓ}^{h} may be obtained from

$$e_{\ell}^{h} \cong \frac{M_{\ell}^{ht} + M_{\ell}^{cs}}{7.5 \text{ miles}} \qquad \text{(A.6)}$$

Thus, using either equation (A.5) or (A.6), the choice depending on the availability of hot-stabilized emission measurements, values of e_{ℓ}^{h} may be calculated for each vehicle tested by AESi. To justify

* Actually, 175 vehicles were tested in Los Angeles, but vehicle number 53 has been removed from the sample (Sachtschale, 1973).

this assumption, hot-start emission rates were computed using equations (A. 5) and (A. 6) for each of the 55 vehicles for which this was possible. On the average, emissions differed by only 7%. Based on these results, the algorithm cited above seems to provide a reasonable means of estimating hot-start emissions when hot-stabilized emissions are not available for use directly. The cold and hot-start emission rates for HC, CO, and NO_x calculated from a computer generated summary of all AESi data taken in Los Angeles (Sachtschale, 1973) are summarized in Table A. 5. Steady-cruise emissions at 15, 30, 45, and 60 mph may be found in the AESi (1973) report.

Exhaust control device deterioration must be considered for HC and CO emissions from post-1965 vehicles and NO_x emissions from post-1969 model year vehicles. Deterioration factors for each model year as a function of the age of the vehicle have been compiled by EPA (1973b). However, these factors are for use with low-mileage emissions. Since most vehicles tested by AESi were not at low-mileage, the EPA deterioration factors must be modified to account for the deterioration present at the time of the AESi study. The appropriate deterioration factors, $d_{\ell j}$, which must be multiplied by the emissions in Table A. 5 to yield the final values of $e_{\ell ij}$ for use in equation (A. 1) are given by

$$d_{\ell j} = \frac{d_{\ell j}(1977)}{d_{\ell j}(1972)}$$

where $d_{\ell j}(1977)$ = deterioration factor for model year j vehicles on July 1, 1977.

Table A.5

Estimated Cold and Hot-Start Emission Rates for Light-Duty Vehicles in Los Angeles in 1977 (Grams/Mile)[†]

Model Year	Cold-Start HC	Cold-Start CO	Cold-Start NO_x	Hot-Start HC	Hot-Start CO	Hot-Start NO_x
1977*	.42	3.4	.31	.08	.59	.31
1977**	2.17	18.6	1.49	.73	5.4	1.49
1976*	.42	3.4	.60	.08	.59	.60
1976**	2.17	18.6	1.49	.73	5.4	1.49
1975*	.73	5.3	1.49	.14	.91	1.49
1975**	2.17	18.6	1.49	.73	5.4	1.49
1974	2.17	18.6	1.49	.73	5.4	1.49
1973	2.17	18.6	1.90	1.03	7.7	1.90
1972	2.43	22.9	2.31	1.48	12.2	2.31
1971	3.51	51.9	3.82	2.65	35.0	3.89
1970	5.22	62.6	4.51	3.77	41.6	4.68
1969	5.87	87.1	5.45	4.26	53.3	5.39
1968‡	5.36	75.3	3.90	3.84	46.2	4.13
1967	6.22	81.4	3.30	4.60	55.2	3.50
1966	8.73	78.1	3.24	7.10	54.2	3.40
pre-1966	11.81	106.3	2.94	10.02	87.5	2.91

† Emissions for 1972-1977 vehicles are at low-mileage. All other emissions were obtained from AESi (1973) and a computer-generated listing summarizing all exhaust emission measurements made by AESi in Los Angeles (Sachtschale, 1973). Thus, pre-1972 emissions are not at low mileage. HC and CO emissions from 1966-1977 vehicles and NO_x emissions from 1970-1977 vehicles are subject to exhaust control device deterioration (see text).

‡ Emissions from vehicle number 53 in the AESi (1973) data base are not included.

* Emissions for automobiles

** Emissions for trucks

$d_{\ell j}(1972)$ = deterioration factor for model year j vehicles at the time of the AESi study.

Calculated values of $d_{\ell j}$ for pre-1972 light-duty vehicles applicable on July 1, 1977 are summarized in Table A.6.

Table A.6

Deterioration Factors for Pre-1972 Light-Duty Vehicles in 1977*

Model Year	HC	CO	NO_x
1971	1.16	1.30	1.14
1970	1.13	1.17	1.00
1969	1.10	1.14	1.00
1968	1.10	1.18	1.00
1967	1.05	1.16	1.00
1966	1.04	1.04	1.00
pre-1966	1.00	1.00	1.00

* These deterioration factors are only suitable to use with the emission rates given in Table A.5.

A.4.1.2 1972-1974 Vehicles

Since studies of emissions from in-use 1972-74 vehicles in Los Angeles have not been reported, other means must be developed to estimate emissions from these vehicles. Cold-start emissions for 1973 vehicles may be estimated from the certification test results published by EPA (1973d). As certification emissions are obtained by multiplying low-mileage emissions by the degradation factor at 50,000 miles, the low-mileage emission rates for 1973 appearing in Table A.5 were estimated in the following manner. First, representative HC, CO, and NO_x emissions were determined from an examination of the data for Ford, Chrysler, General Motors,

and Volkswagon motor vehicles. These certification emissions, when divided by the degradation factors for four year old 1973 vehicles given by EPA (1973b), yield an estimate for 1973 low-mileage emissions.* Emissions for 1972 and 1974 vehicles, calculated in an analogous manner, are assumed to be somewhat greater than and equal to, respectively, 1973 emissions.

Since emission standards for 1972-74 vehicles are based on the 1972 FTP, it is not possible to use the standards directly to estimate hot-start emissions. In addition, there is evidence indicating that the cold-start will contribute a substantial portion of the HC and CO emissions from 1972-1977 vehicles (Wendell et al., 1973; NAS, 1973). Estimates of the percentage of the total CO cold-start emissions that are emitted during the first two minutes of vehicle operation are given by Wendell et al. (1973). These data are employed in this study to provide a "conservative" estimate of the ratio of cold-transient emissions to the total cold-start emissions, γ_j, for model year j. Thus, for $1 \leq i \leq 4$, $72 \leq j \leq 74$, and ℓ corresponding to HC and CO,

$$\gamma_j = \frac{M_{\ell ij}^{ct}}{M_{\ell ij}^{ct} + M_{\ell ij}^{cs}} \qquad \text{(A. 7)}$$

where values of γ_j are given in Table A. 7. By further assuming that the ratio of hot-transient emissions to hot-stabilized emissions for 1972-74 vehicles is unchanged from the corresponding ratio for 1971

* From vehicle age and mileage accumulation data obtained from the ARB (Bratton, 1973), vehicles in California accumulate 50, 000 miles in about 4 years.

vehicles, and also assuming that $M_{\ell ij}^{cs} \cong M_{\ell ij}^{hs}$, the hot-start emission factors for 1972-74 vehicles may be estimated from

$$e_{\ell ij}^{h} = (1+\delta_{\ell})(1-\gamma_{j})\, e_{\ell ij}^{c} \qquad \text{(A. 8)}$$

where $e_{\ell ij}^{c}$ = low-mileage cold-start emissions

δ_{ℓ} = ratio of hot-transient emissions to hot-stabilized emissions for species ℓ from 1971 vehicles (obtained from the AESi data); values of δ_{ℓ} for HC and CO are found to be 0.97 and 0.72, respectively.

The calculated values of $e_{\ell ij}^{h}$ obtained from equation (A. 8) are presented in Table A. 5.

As a partial check of the assumptions leading to equation (A. 8), hot-start emissions were calculated for 1971 vehicles using equation (A. 8) and then compared with the actual measured hot-start emissions as given in Table A. 5. Computed hot-start emissions for HC and CO were found to be 2.65 and 33.9 grams per mile, respectively, which are in reasonable agreement with the measured values given in Table A. 5. Although this test is far from definitive, the results are encouraging. Of course, the computed hot-start emission rates should be replaced by actual measured emissions as new test data become available.

Hot-start NO_x emissions from 1972-74 vehicles are assumed to be equal to the corresponding cold-start values given in Table A. 5. This assumption is based on the observation that hot and cold-start emissions from 1971 vehicles are approximately equal (see Table A. 5).

Table A. 7

Ratio of Cold-Transient Emissions to Total Cold-Start Emissions*

Model Year (j)	γ_j
1971	0.62
72	0.69
73	0,76
74	0.83
75	0.90
76	0.90
77	0.90

* Adapted from Wendell et al. (1973)

Steady cruise emissions at 15, 30, 45, and 60 mph for 1972-74 vehicles are estimated by assuming that the ratio of hot-start emissions to steady cruise emissions at a particular speed for 1971 vehicles remains unchanged for 1972-74 model year vehicles. Thus, steady cruise emissions are calculated using the following relationship:

$$e_{\ell ij}(v) = e^{h}_{\ell ij} \frac{e_{\ell i71}(v)}{e^{h}_{\ell i71}} \qquad \text{(A. 9)}$$

where $e_{\ell ij}(v)$ = steady cruise emissions at driving speed v (grams/mile)

Exhaust control device deterioration factors, obtained from EPA (1973b) must be multiplied times the emission rates discussed in this section. This completes the specification of emission rates for 1972-74 light-duty vehicles.

A.4.1.3 1975-77 Model Year Vehicles

Hot and cold-start emissions from 1975-77 vehicles are difficult to estimate for several reasons. First, the standards are based on the 1975 FTP, a test which involves both hot and cold-start emissions. Second, the Administrator of EPA has waived the strict 1975 standards for HC and CO and the 1976 standards for NO_x (EPA, 1973e; EPA, 1973f). However, interim standards have been established for all vehicles to be sold in California so as to require automobile manufacturers to equip these vehicles with catalytic devices. Thus, California will serve as the initial "proving grounds" for the devices to be installed on all vehicles on a nationwide basis one year later. Since catalyst technology is changing rapidly and only a few emission tests have been reported for prototype 1975-76 vehicles (Martinez et al., 1971; NAS, 1973), emission rates based on any test procedure will certainly be subject to revision when mass produced vehicles and devices become available for testing. It will also be important to test in-use vehicles because actual driving conditions may lead to faster deterioration of the control devices than is indicated by the 1975 FTP certification results.

Since emission standards are based on the 1975 FTP, it is convenient to begin by estimating low-mileage emissions based on this test. To convert HC and CO estimates to hot and cold-start emissions, a number of assumptions must be made. First, assuming $M_{\ell ij}^{cs} \cong M_{\ell ij}^{hs}$ (i.e., stabilized emissions are independent of the type of start), equation (A.3) may be written in the following form

$$e^{ch}_{\ell ij} \cong \frac{0.43\, M^{ct}_{\ell ij} + 0.57\, M^{ht}_{\ell ij} + M^{s}_{\ell ij}}{7.5 \text{ miles}} \qquad (A.10)$$

where $M^{s}_{\ell ij}$ is the mass of pollutant emitted during the stabilized portion of the FDC. Using the data presented by Wendell et al. (1973) to relate cold-transient emissions to stabilized emissions (see Section A.4.1.2), the following expression may be written:

$$M^{ct}_{\ell ij} = M^{s}_{\ell ij} \frac{\gamma_j}{1-\gamma_j} \qquad (A.11)$$

where values of γ_j are given in Table A.7. By further assuming that the ratio of hot-transient emissions to stabilized emissions for 1975-77 vehicles will be equal to the corresponding ratio for 1971 vehicles, then

$$\frac{M^{ht}_{\ell ij}}{M^{s}_{\ell ij}} = \delta_{\ell} \qquad (A.12)$$

where δ_{ℓ} is equal to 0.97 and 0.72 for HC and CO, respectively, as determined from the AESi (1973) emissions tests. Given values of $e^{ch}_{\ell ij}$, γ_j, and δ_{ℓ}, equations (A.10)-(A.12) yield the following expressions for the mass of pollutant emitted during each part of the 1975 FTP

$$M^{ct}_{\ell ij} = \frac{(7.5 \text{ miles}) \times e^{ch}_{\ell ij}\, \gamma_j}{.43\,\gamma_j + (1-\gamma_j)(1+0.57\,\delta_{\ell})} \qquad (A.13)$$

$$M^{s}_{\ell ij} = \frac{M^{ct}_{\ell ij}\,(1-\gamma_j)}{\gamma_j} \qquad (A.14)$$

$$M^{ht}_{\ell ij} = M^{s}_{\ell ij}\,\delta_{\ell} \qquad (A.15)$$

The values of $e^{ch}_{\ell ij}$ used in equation (A. 13) are given in Table A. 8.

Table A. 8

Estimated Low-Mileage HC and CO Emission Rates for 1975-77 Light-Duty Vehicles Based on the 1975 FTP

Model Year	Emissions (grams/mile) HC	CO	Source
1977	0.23	1.8	EPA (1973b)
76	0.23	1.8	EPA (1973b)
75	0.40	2.8	NAS (1973)

Cold or hot-start emission rates are obtained by adding the cold or hot-transient emissions to the stabilized emissions and dividing the sum by 7.5 miles, as in equations (A. 3) and (A. 4).

As a partial test of the algorithm given above hot and cold-start emission rates were calculated for 1971 vehicles and compared with the actual measured emissions given in Table A. 3. The comparisons are illustrated in Table A. 9. Based on the reasonable comparisons achieved, the algorithm described above has been used in this study to provide interim estimates of hot and cold-start emission rates for 1975-77 light-duty vehicles.

Since data pertaining to NO_x emissions from 1971 vehicles show little dependence on the type of start, it is assumed that hot and cold-start NO_x emissions from 1975-77 vehicles will be equal. To what extent this assumption will hold for post-1975 vehicles using catalysts to control NO_x emissions is unknown. Under these conditions, emission estimates based on the 1975 FTP may be used directly to specify the hot and cold-start NO_x emission rates.

Steady-cruise emissions at 15, 30, 45, and 60 mph were calculated employing the same procedure discussed in Section A.4.1.2 for 1972-74 light-duty vehicles.

Table A.9

Comparison of Calculated and Measured Emissions for 1971 Vehicles

Test	Pollutant	Calculated	Measured
		grams/mile	
Cold-Start	HC	3.53	3.51
Cold-Start	CO	52.6	51.9
Hot-Start	HC	2.64	2.65
Hot-Start	CO	34.4	35.0

A.4.2 Heavy-Duty Vehicle Emissions

Two classes of heavy-duty vehicles are considered in this study, including both gasoline and diesel fueled trucks. Emissions for gasoline trucks have been estimated by EPA (1973b), but no attempt has been made to distinguish between hot and cold-start truck emissions. Thus, the hot and cold-start gasoline truck emissions used in this study are both equal to the emission rates given in the report cited above. In addition, the appropriate degradation factors are also included in the EPA report.

Since emissions for diesel vehicles as a function of model year are not given in the EPA (1973b) report, values of these parameters were obtained from the State of California ARB (Bratton, 1973). The estimated emissions, including degradation, as of July 1, 1977, are presented in Table A.10. As with gasoline trucks, the entries in Table A.10 are used in both hot and cold-start emission calculations.

Table A.10

Estimated Heavy-Duty Diesel Truck Emissions on July 1, 1977*

Model Year	HC	CO	NO_x
		(grams/mile)	
pre-1973	4.4	26.0	43.0
73	2.4	15.0	46.0
74	2.8	15.0	45.0
75	1.2	12.0	15.0
76	1.0	11.0	15.0
77	0.8	9.0	13.0

*Source: State of California ARB (Bratton, 1973)

Unfortunately, very little information is available to serve as a guide for estimating the steady-cruise emissions at 15, 30, 45, and 60 mph. Thus, the following algorithm has been devised for the calculation of interim emission estimates. The basic assumption made in this study is that the ratio of hot-start emissions to steady-cruise emissions at a particular speed is the same for both light and heavy-duty vehicles. This relationship may be expressed in the following manner

$$e_{\ell ij}(v) = e^{h}_{\ell ij} \frac{e_{\ell 3j}(v)}{e^{h}_{\ell 3j}} \qquad \text{(A.16)}$$

for $5 \leq i \leq 6$ and any driving speed v. This assumption is especially difficult to justify in view of the fact that the driving cycles for light and heavy-duty vehicles are not identical. Thus, steady-cruise emissions obtained from equation (A.16) will certainly be subject to revision when the appropriate data become available.

A. 4. 3 Motorcycle Emissions

Emissions from two and four-stroke motorcycles are summarized in the EPA (1973b) report. Since emissions are not given as a function of model year, it is assumed that all motorcycles of a particular type emit pollutants at the same rate.

A. 5 Emissions Summary

By employing equation (A. 1) and the data either presented or alluded to in Sections (A. 2)-(A. 4), average hot and cold-start emission rates, as well as steady-cruise emissions, have been calculated for Los Angeles as of July 1, 1977, and are presented in Table A. 11.

Table A. 11

Estimated Average Emission Rates for Motor Vehicles in Los Angeles as of July 1, 1977

Test	(grams/mile) HC	CO	NO_x
cold-start	3.20	35.0	2.58
hot-start	2.14	21.5	2.60
15 mph	1.66	24.0	0.32
30 mph	1.14	9.9	1.13
45 mph	1.04	7.0	2.64
60 mph	0.95	7.9	3.83

Steady-cruise emissions are related to the vehicle speed through use of the following correlation

$$E_\ell(v) = a_\ell (v)^{b_\ell}$$

where $E_\ell(v)$ = emission rate of species ℓ at speed v (grams/mile)

v = driving speed (mph)

and a_ℓ and b_ℓ are constants to be determined from the values of $E_\ell(v)$ given in Table A.11. If the above correlation is reasonable, then a log-log plot of emissions vs. driving speed should yield a straight line. As illustrated in Figure A.1, NO_x emissions are correlated well over the entire driving speed range. HC and CO emissions, however, exhibit marked deviation from linear behavior at 15 and 60 mph data points, respectively. While emissions for these species generally lie on a line for three consecutive speeds, the correlation does not seem to hold over the entire driving speed range. In an effort to minimize the discrepancy between the correlation function and the predicted emissions, two sets of "constants" are given for HC and CO, where the particular set to be used in a particular situation will depend on the driving speed. The straight lines from which a_ℓ and b_ℓ were derived are illustrated in Figure A.1; the computed values of a_ℓ and b_ℓ are given in Table A.12.

Table A.12
Emissions/Driving Speed Correlation Parameters
for Motor Vehicles in Los Angeles in 1977

Species	Driving Speed Range (mph)	a_ℓ	b_ℓ
HC	15-30	7.253	-.544
HC	30-60	2.746	-.259
CO	15-45	4.288×10^2	-1.080
CO	45-60	1.498	.406
NO_x	15-60	2.094	1.846

Figure A.1 Emissions Vs. Driving Speed for the Average Motor Vehicle in Los Angeles in 1977

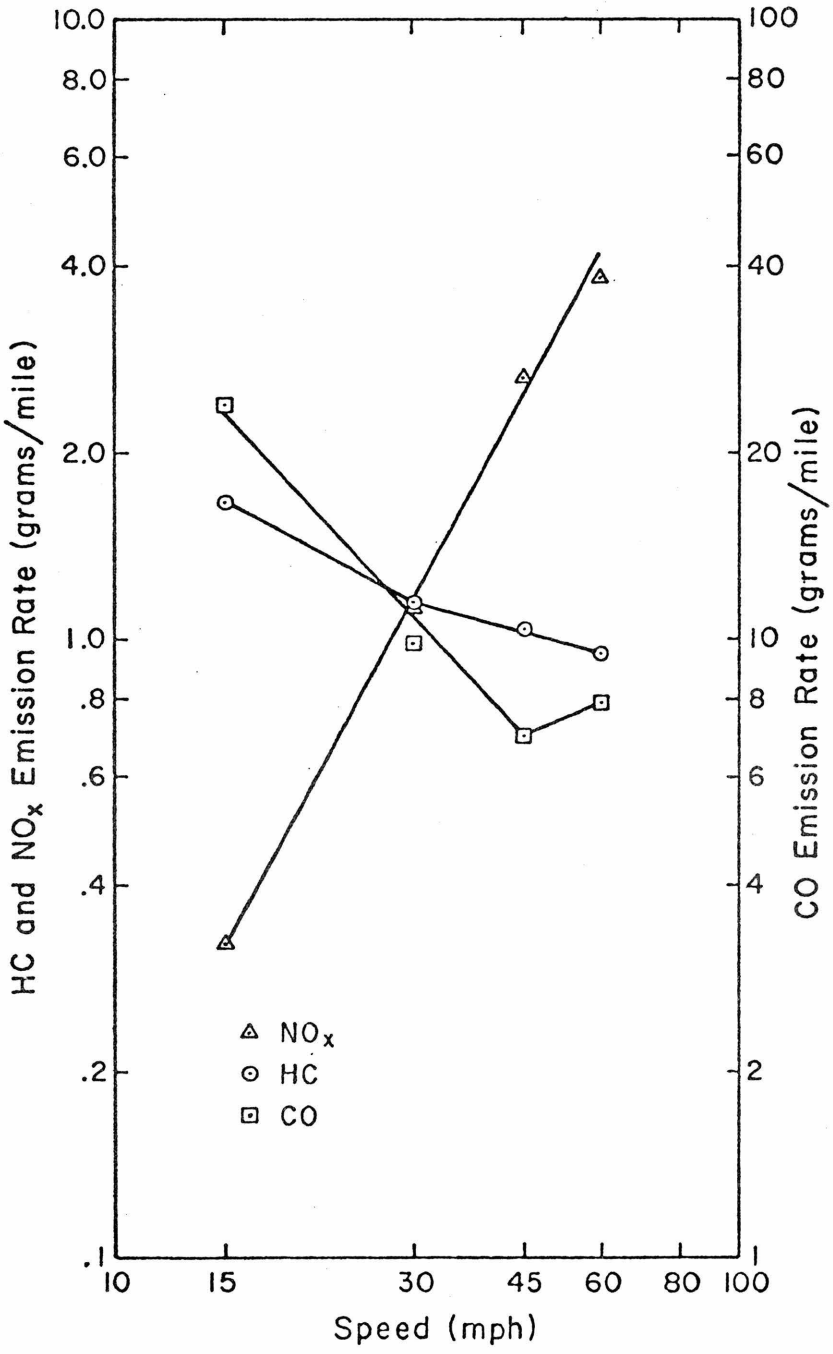

APPENDIX B

METEOROLOGICAL DATA FOR SEPTEMBER 29, 1969

This Appendix is devoted to a listing of all wind speed, wind direction, and mixing depth inputs used in the validation study for September 29, 1969. The wind speeds given in Figures B.1-B.11 are hourly averages (averaged from the half-hour to the half-hour), have the units of mph, and are multiplied by a factor of 10. Wind directions illustrated in Figures B.12-B.22 are also hourly averages (averaged from the half-hour to the half-hour), have the units of degrees, and represent the direction, measured clockwise from north, in which the pollutants are advected. Values of the mixing depths, in feet, at each hour are given in Figures B.23-B.33.

Figure B.1

WIND SPEED ON 9/29/69 AT 500.0 PST

	1	2	3	4	5	6	7	8	9	10	11	12	13	14	15	16	17	18	19	20	21	22	23	24	25
25	45	50	60	65	70	65	65	60	60	50	40	30	30	30	30	30	30	30	30	30	30	30	30	30	30
24	40	40	50	60	60	60	65	60	65	50	40	30	30	30	30	30	30	30	30	30	30	30	30	30	30
23	35	35	40	50	50	50	55	55	50	50	40	30	30	30	30	30	30	30	30	30	30	30	30	30	30
22	30	35	35	40	40	40	40	40	40	40	40	30	30	30	30	30	30	30	30	30	35	30	30	25	25
21	20	30	30	30	30	30	30	30	30	30	40	40	30	25	25	25	30	30	30	30	35	30	25	25	25
20	20	20	20	20	20	20	20	20	10	20	30	40	40	30	20	25	30	30	30	40	40	30	25	20	20
19	10	10	10	10	10	10	10	10	10	20	35	45	45	35	25	25	30	30	25	30	30	25	20	20	20
18	10	10	10	10	10	10	10	20	20	30	40	50	50	40	30	20	20	20	20	20	20	20	20	20	20
17	20	20	20	10	10	10	30	35	40	40	50	50	50	40	30	20	20	10	10	10	10	10	10	10	10
16	40	40	40	40	40	30	50	55	55	55	55	50	50	40	30	30	20	10	0	10	10	10	10	10	10
15	50	60	70	70	70	65	60	60	55	55	55	55	50	50	45	40	30	20	10	20	20	20	20	20	20
14	70	70	70	60	60	65	60	55	55	55	55	50	50	45	40	40	35	30	20	30	30	30	30	30	25
13	60	60	60	50	50	50	50	50	50	50	50	45	45	40	40	40	40	40	30	30	30	30	30	30	30
12	50	50	45	45	40	40	40	40	40	40	40	50	50	40	40	40	30	35	30	30	30	30	30	30	25
11	40	40	40	40	30	30	30	30	40	40	50	40	30	30	30	30	30	30	30	30	25	25	25	25	25
10	35	35	35	30	25	30	30	30	30	30	40	30	30	25	25	25	25	25	25	25	25	25	25	20	20
9	30	30	30	25	25	25	25	25	25	25	30	20	20	20	20	20	25	25	25	25	20	20	20	20	20
8	25	25	25	25	25	25	25	25	20	20	20	20	20	20	20	20	20	20	20	20	20	20	20	25	25
7	25	25	25	25	20	20	20	20	20	20	20	20	20	20	20	20	20	20	20	20	25	25	25	25	25
6	25	25	20	20	20	20	20	20	20	20	20	20	20	20	20	20	20	20	20	25	25	25	25	30	30
5	20	20	20	20	20	20	20	20	20	20	20	20	20	20	20	20	20	25	25	25	25	30	30	30	30
4	20	20	20	20	20	20	20	20	20	20	20	20	20	20	20	25	25	25	25	25	30	30	30	30	30
3	20	20	20	20	20	20	20	20	20	20	20	20	20	25	25	25	25	25	25	30	30	30	30	30	30
2	20	20	20	20	20	20	20	20	20	20	20	25	25	25	25	25	25	25	25	30	30	30	30	30	30
1	20	20	20	20	20	20	20	20	20	20	25	25	25	25	25	25	25	25	30	30	30	30	30	30	30

Figure B.2

WIND SPEED ON 9/29/69 AT 600.0 PST

	1	2	3	4	5	6	7	8	9	10	11	12	13	14	15	16	17	18	19	20	21	22	23	24	25
25	10	10	15	20	30	40	30	30	25	25	25	20	20	20	20	20	25	25	30	30	30	35	35	40	40
24	10	10	15	20	25	30	30	30	25	25	25	20	20	20	20	20	25	25	25	30	30	35	35	40	40
23	10	10	15	20	20	30	30	30	25	20	20	20	20	20	20	20	25	30	30	30	35	35	40	40	40
22	10	10	20	20	20	30	30	30	20	20	20	20	20	20	20	20	25	30	30	35	35	35	40	40	40
21	10	15	20	30	30	30	30	20	20	20	20	20	25	20	20	25	30	35	35	35	40	40	40	40	40
20	10	15	15	20	20	20	20	10	10	20	20	25	25	20	20	30	40	40	35	40	40	40	40	40	40
19	10	10	10	10	10	10	10	10	20	20	25	25	25	30	30	40	50	50	45	40	40	40	40	40	40
18	10	10	10	10	10	10	10	20	20	25	30	30	30	40	40	40	50	50	45	45	40	40	40	40	40
17	15	15	15	15	15	10	15	20	25	30	35	40	40	45	45	50	50	45	45	40	40	40	30	30	30
16	20	20	20	20	20	20	20	30	30	40	40	40	50	50	50	50	50	45	40	40	30	30	25	25	25
15	30	30	30	30	30	30	30	30	40	40	45	45	50	50	50	50	45	40	40	30	30	25	25	25	25
14	30	30	30	30	30	30	30	40	45	45	45	50	55	50	50	50	40	40	30	30	25	25	25	25	25
13	25	25	25	25	25	25	30	40	45	50	50	60	60	60	50	50	40	30	30	20	20	25	25	20	20
12	25	25	25	25	25	25	25	30	40	50	60	70	70	60	60	50	50	40	40	30	20	20	20	20	20
11	20	20	20	20	20	20	20	20	30	40	50	50	50	50	50	50	50	50	40	30	20	20	20	20	20
10	20	20	20	20	20	20	20	20	30	30	40	30	30	40	40	40	40	40	30	25	20	20	20	20	20
9	20	20	20	20	20	20	20	20	25	25	30	30	30	30	30	30	30	30	25	25	20	20	20	20	20
8	20	20	20	20	20	20	20	20	20	20	25	25	30	30	30	30	25	25	20	20	20	20	20	20	20
7	20	20	20	20	20	20	20	20	20	20	20	25	25	25	25	25	20	20	20	20	20	20	20	20	20
6	20	20	20	20	20	20	20	20	20	20	20	20	25	20	20	20	20	20	20	20	20	20	20	20	20
5	20	20	20	20	20	20	20	20	20	20	20	20	20	20	20	20	20	20	20	20	20	20	20	20	20
4	20	20	20	20	20	20	20	20	20	20	20	20	20	20	20	20	20	20	20	20	20	20	20	20	20
3	20	20	20	20	20	20	20	20	20	20	20	20	20	20	20	20	20	20	20	20	20	20	20	20	20
2	20	20	20	20	20	20	20	20	20	20	20	20	20	20	20	20	20	20	20	20	20	20	20	20	20
1	20	20	20	20	20	20	20	20	20	20	20	20	20	20	20	20	20	20	20	20	20	20	20	20	20

Figure B. 3

WIND SPEED ON 9/29/69 AT 7JJ.J PST

	1	2	3	4	5	6	7	8	9	10	11	12	13	14	15	16	17	18	19	20	21	22	23	24	25
25	10	10	10	10	10	10	15	15	15	20	20	20	20	20	20	20	20	20	20	20	20	20	20	20	20
24	10	10	10	10	10	10	15	15	15	20	20	20	20	20	20	20	20	20	20	20	20	20	20	20	20
23	10	10	10	10	10	15	15	15	15	20	20	20	20	20	20	20	20	20	20	20	20	20	20	20	20
22	10	10	10	15	15	15	15	15	20	20	20	20	20	20	20	20	20	20	20	20	20	20	20	20	20
21	10	10	15	20	20	20	15	15	15	20	20	20	20	20	20	25	25	25	25	25	20	20	20	15	15
20	10	10	10	15	15	15	10	10	10	15	20	20	20	25	25	25	25	30	25	25	20	20	15	15	10
19	10	10	10	10	10	10	10	10	15	20	25	25	25	25	25	30	30	30	30	25	20	15	15	10	10
18	10	10	10	10	10	10	10	15	20	25	25	30	25	30	30	30	30	30	30	25	20	15	15	10	10
17	10	10	10	10	10	10	15	20	20	25	30	30	30	30	30	30	30	30	25	20	15	15	10	10	10
16	10	10	10	10	10	15	15	20	25	25	30	30	30	30	30	30	30	30	20	20	15	10	10	10	10
15	10	10	10	10	10	15	20	25	25	30	30	30	30	30	30	30	30	35	20	15	10	10	10	10	10
14	15	15	15	15	15	20	25	25	25	30	30	30	30	30	30	30	30	35	25	15	10	10	10	10	10
13	25	25	20	20	20	25	25	25	30	30	30	30	30	30	30	25	30	40	25	15	10	10	10	10	10
12	20	20	20	20	25	25	30	30	30	30	30	30	30	25	25	25	20	30	20	10	10	10	10	10	10
11	20	20	25	25	25	30	30	30	30	30	30	30	25	25	20	20	20	20	15	10	10	10	10	10	10
10	25	25	25	25	30	30	30	30	30	30	30	25	20	20	20	20	15	15	15	10	10	10	10	10	10
9	25	25	30	30	30	30	30	25	25	25	25	20	20	20	15	15	15	10	10	10	10	10	10	10	10
8	30	30	30	30	30	25	25	25	25	25	20	20	15	15	15	15	10	10	10	10	10	10	10	10	10
7	30	30	30	30	25	25	25	25	25	20	20	15	15	15	15	10	10	10	10	10	10	10	10	10	10
6	30	30	30	25	25	25	25	25	20	20	15	15	15	15	10	10	10	10	10	10	10	10	10	10	10
5	30	25	25	25	25	25	25	20	20	15	15	15	15	10	10	10	10	10	10	10	10	10	10	10	10
4	25	25	25	25	25	20	20	15	15	15	15	15	10	10	10	10	10	10	10	10	10	10	10	10	10
3	25	25	25	25	20	20	15	15	15	15	15	10	10	10	10	10	10	10	10	10	10	10	10	10	10
2	25	25	25	20	20	15	15	15	15	15	10	10	10	10	10	10	10	10	10	10	10	10	10	10	10
1	20	20	20	20	15	15	15	15	10	10	10	10	10	10	10	10	10	10	10	10	10	10	10	10	10

Figure B.4

WIND SPEED ON 9/29/69 AT 800.0 PST

	1	2	3	4	5	6	7	8	9	10	11	12	13	14	15	16	17	18	19	20	21	22	23	24	25
25	10	10	10	10	10	10	10	10	10	10	10	10	10	10	10	10	10	10	10	10	10	10	15	15	20
24	15	15	15	15	15	10	10	10	10	10	10	10	10	10	10	10	10	10	10	10	10	15	15	20	20
23	15	15	15	15	15	15	10	10	10	10	10	10	10	10	10	10	10	10	10	15	15	15	20	20	20
22	20	20	20	20	20	20	15	15	10	10	10	10	10	10	10	10	10	10	15	15	20	20	20	20	20
21	20	20	20	25	20	20	15	15	10	10	10	10	10	10	10	10	10	15	15	20	20	20	20	20	20
20	15	15	15	20	15	15	15	10	10	10	10	10	10	10	10	10	15	20	20	20	20	20	20	20	20
19	15	15	15	15	15	10	10	10	10	10	20	20	20	20	20	20	20	20	20	20	20	20	20	20	20
18	10	10	10	10	10	10	10	10	10	20	30	30	30	25	25	25	20	20	20	20	20	20	20	20	20
17	10	10	10	10	10	10	10	10	10	20	30	30	30	30	30	30	20	20	15	15	15	15	15	15	15
16	15	15	15	15	15	10	10	10	15	25	30	30	30	30	30	30	25	20	15	10	10	10	10	10	10
15	20	20	20	20	20	20	25	25	25	25	30	30	30	30	30	30	20	10	0	0	0	0	0	0	0
14	30	30	30	20	20	20	25	25	25	30	30	30	30	30	30	30	20	15	10	5	5	5	5	5	5
13	30	30	30	30	30	30	30	30	30	30	30	30	30	25	25	20	20	20	15	10	10	10	10	10	10
12	30	30	30	30	30	30	30	30	30	30	30	30	30	25	20	20	15	15	10	10	10	10	10	10	10
11	30	30	30	30	30	30	30	30	30	30	30	30	30	20	20	15	15	10	10	10	10	10	10	10	10
10	30	30	30	30	30	30	30	30	30	30	30	30	30	30	25	20	20	15	10	10	10	10	10	10	10
9	30	30	30	30	30	30	30	30	30	30	30	30	30	30	30	30	25	20	15	10	10	10	10	10	10
8	30	30	30	30	30	30	30	30	30	30	30	30	30	30	30	30	30	25	15	10	10	10	10	10	10
7	30	30	30	30	30	30	30	30	30	30	30	30	30	30	30	30	30	20	15	10	10	10	10	10	10
6	30	30	30	30	30	30	30	30	30	30	30	30	30	30	30	30	30	20	15	10	10	10	10	10	10
5	30	30	30	30	30	30	30	30	30	30	30	30	30	30	30	30	30	30	20	15	15	10	10	10	10
4	30	30	30	30	30	30	30	30	30	30	30	30	30	30	30	30	30	30	20	15	15	10	10	10	10
3	30	30	30	30	30	30	30	30	30	30	30	30	30	30	30	30	30	30	30	20	15	15	10	10	10
2	30	30	30	30	30	30	30	30	30	30	30	30	30	30	30	30	30	30	30	20	15	15	10	10	10
1	30	30	30	30	30	30	30	30	30	30	30	30	30	30	30	30	30	30	30	20	15	15	10	10	10

Figure B.5

WIND SPEED ON 9/29/69 AT 900.0 PST

	1	2	3	4	5	6	7	8	9	10	11	12	13	14	15	16	17	18	19	20	21	22	23	24	25
25	10	10	10	10	10	10	10	10	10	10	10	10	10	10	10	10	15	20	20	20	20	20	20	20	20
24	10	10	10	10	10	10	10	10	10	10	10	10	10	10	10	10	15	20	20	20	20	20	20	20	20
23	15	15	15	15	15	10	10	10	10	10	10	10	10	10	20	20	20	20	20	20	20	20	20	20	20
22	15	20	20	20	20	15	10	10	10	10	10	15	20	20	30	30	25	20	20	20	20	20	20	20	20
21	20	20	30	30	30	20	15	10	10	10	15	20	30	35	35	30	30	25	20	20	20	20	20	20	20
20	15	15	20	20	20	15	10	10	10	15	20	30	35	40	40	35	35	30	25	25	20	20	20	20	20
19	15	15	15	15	15	10	10	10	15	20	30	35	35	40	40	35	30	30	30	25	20	20	20	20	20
18	10	10	10	10	10	10	10	15	20	30	35	35	40	40	40	35	30	30	30	25	20	20	20	20	20
17	10	10	10	10	10	10	10	20	30	35	40	40	40	35	35	30	30	30	25	20	20	20	20	20	20
16	20	20	20	30	30	30	25	30	40	40	40	40	30	30	30	30	30	25	25	20	20	20	20	20	20
15	30	30	30	50	50	40	40	40	40	40	40	40	30	30	30	30	30	25	25	20	20	20	20	20	20
14	40	40	50	50	50	45	45	40	40	40	40	40	35	30	30	30	30	20	20	20	20	20	20	20	20
13	50	50	50	50	45	45	45	40	40	40	40	40	35	30	30	25	20	20	20	20	20	20	20	20	20
12	50	50	45	45	45	40	40	40	40	40	40	40	35	30	25	20	15	15	10	15	15	20	20	20	20
11	45	45	45	45	40	40	40	40	40	40	40	40	40	35	30	30	20	10	10	10	10	15	20	20	20
10	45	45	40	40	40	40	40	40	40	40	40	40	40	40	35	30	20	15	10	10	10	10	15	20	20
9	45	45	40	40	40	40	40	40	40	40	40	40	40	40	35	30	25	20	15	10	10	10	15	20	20
8	40	40	40	40	40	40	40	40	40	40	40	40	40	40	35	25	25	20	15	10	10	10	15	20	20
7	40	40	40	40	40	40	40	40	40	40	40	40	40	40	35	30	30	25	20	15	15	15	20	20	20
6	40	40	40	40	40	40	40	40	40	40	40	40	40	40	35	30	30	25	25	20	20	20	20	20	20
5	40	40	40	40	40	40	40	40	40	40	40	40	40	40	35	35	30	30	25	25	20	20	20	20	20
4	40	40	40	40	40	40	40	40	40	40	40	40	40	40	35	35	30	30	30	25	25	20	20	20	20
3	40	40	40	40	40	40	40	40	40	40	40	40	40	40	40	35	35	30	30	30	25	25	20	20	20
2	40	40	40	40	40	40	40	40	40	40	40	40	40	40	40	35	35	30	30	30	25	25	20	20	20
1	40	40	40	40	40	40	40	40	40	40	40	40	40	40	40	35	35	30	30	30	25	25	20	20	20

Figure B.6

WIND SPEED ON 9/29/69 AT 1000.0 PST

	1	2	3	4	5	6	7	8	9	10	11	12	13	14	15	16	17	18	19	20	21	22	23	24	25
25	10	10	10	10	10	10	10	15	15	15	15	15	15	10	10	10	10	10	10	10	10	10	10	10	10
24	15	15	15	15	10	10	10	15	15	15	15	15	15	15	10	10	10	10	10	10	10	10	10	10	10
23	15	15	20	20	15	10	10	10	10	15	20	20	20	20	15	15	10	10	10	10	10	10	10	10	10
22	15	20	25	25	25	15	15	10	10	15	20	20	20	20	20	15	15	15	10	10	10	10	10	10	10
21	20	25	30	30	30	25	20	15	10	10	20	25	25	20	20	20	15	15	15	10	10	10	10	15	15
20	15	15	20	20	20	15	15	10	10	10	20	30	30	30	20	20	20	15	15	15	10	15	15	15	15
19	15	15	15	15	15	15	10	10	15	20	30	40	40	30	30	20	20	20	20	15	15	15	15	20	20
18	10	10	10	10	10	10	15	20	20	30	40	50	50	40	35	30	20	20	20	20	20	20	20	20	20
17	15	15	15	20	20	20	25	30	30	40	50	60	55	50	40	35	30	20	20	20	20	20	20	20	20
16	20	20	20	30	30	30	40	40	45	50	60	60	60	60	50	40	30	20	20	20	20	20	20	20	20
15	25	25	25	30	30	30	40	40	50	55	60	60	60	50	45	40	30	25	25	20	20	20	20	15	15
14	30	30	30	30	30	30	35	40	50	60	65	70	60	50	45	40	35	30	25	25	25	15	15	10	10
13	30	30	30	30	30	30	30	40	50	60	70	80	70	60	50	40	30	20	25	30	25	20	15	10	10
12	30	30	30	30	30	30	30	40	50	70	80	90	80	60	50	40	30	20	20	25	20	20	20	15	15
11	30	30	30	30	30	30	30	40	50	60	70	80	70	60	50	40	30	20	20	20	20	20	20	20	20
10	30	30	30	30	30	30	30	30	40	50	60	70	70	60	50	40	30	20	20	20	20	20	20	20	20
9	30	30	30	30	30	30	30	30	40	50	60	70	70	60	50	40	30	25	20	20	20	20	20	20	20
8	30	30	30	30	30	30	30	30	35	40	50	60	60	50	45	40	30	25	20	20	20	20	20	20	20
7	30	30	30	30	30	30	30	30	30	35	40	50	50	45	40	35	30	30	25	25	25	20	20	20	20
6	30	30	30	30	30	30	30	30	30	30	35	40	40	40	35	30	30	30	30	30	25	25	25	20	20
5	30	30	30	30	30	30	30	30	30	30	30	35	35	35	35	30	30	30	30	30	30	30	30	25	25
4	30	30	30	30	30	30	30	30	30	30	30	30	35	35	35	35	30	30	30	30	30	30	30	30	30
3	30	30	30	30	30	30	30	30	30	30	30	30	30	35	35	35	30	30	30	30	30	30	30	30	30
2	30	30	30	30	30	30	30	30	30	30	30	30	30	30	35	35	30	30	30	30	30	30	30	30	30
1	30	30	30	30	30	30	30	30	30	30	30	30	30	30	35	35	30	30	30	30	30	30	30	30	30

Figure B.7

WIND SPEED ON 9/29/69 AT 1100.0 PST

	1	2	3	4	5	6	7	8	9	10	11	12	13	14	15	16	17	18	19	20	21	22	23	24	25
25	10	10	10	10	10	20	20	25	20	30	35	35	40	40	40	45	45	50	50	50	50	50	50	50	50
24	10	10	10	10	10	20	20	25	30	35	35	35	40	40	40	45	50	50	50	50	50	50	50	50	50
23	10	10	10	10	10	20	20	25	30	35	35	40	40	40	40	40	40	45	50	50	50	50	50	50	50
22	10	10	20	20	20	20	20	25	30	35	35	40	40	40	30	30	35	40	50	50	50	50	50	50	50
21	20	20	30	30	30	30	30	30	30	35	40	45	40	30	20	25	30	40	50	50	50	50	50	50	50
20	30	30	30	30	30	30	30	30	30	35	40	45	35	25	20	25	30	35	40	45	50	50	50	50	45
19	30	30	30	30	30	30	30	35	35	45	50	50	45	35	30	40	45	45	50	50	50	50	50	45	40
18	30	30	30	30	30	35	35	40	40	50	60	60	55	60	50	55	60	60	60	55	55	50	50	45	40
17	30	30	30	40	40	40	40	50	50	60	70	70	70	70	65	65	60	55	50	50	50	45	45	40	40
16	40	40	40	40	50	50	50	60	60	65	65	70	70	70	70	65	60	55	50	50	45	40	40	40	40
15	40	40	50	50	60	60	60	60	65	65	70	70	70	70	60	60	55	50	50	45	40	35	35	35	35
14	50	50	60	60	60	60	60	60	65	70	70	70	70	60	50	50	50	50	45	40	40	35	35	30	30
13	60	60	60	60	55	55	55	55	60	70	75	75	75	65	55	50	50	50	45	40	40	35	30	30	30
12	60	60	55	55	55	55	55	55	60	70	75	80	75	70	60	50	50	45	45	40	35	30	30	30	30
11	55	55	55	55	55	50	50	50	60	65	70	70	65	60	55	50	45	40	40	35	30	30	30	30	30
10	55	55	55	50	50	50	50	50	55	60	60	60	60	50	50	45	40	40	35	30	30	30	30	30	30
9	50	50	50	50	50	50	50	50	55	55	55	55	50	50	45	45	40	40	35	30	30	30	30	30	30
8	50	50	50	50	50	50	50	50	50	50	50	50	50	45	45	40	40	40	40	35	35	30	30	30	30
7	50	50	50	50	50	50	50	50	50	50	45	45	45	45	40	40	40	40	40	40	35	35	35	35	30
6	50	50	50	50	50	50	50	50	50	45	45	45	40	40	40	40	40	40	40	40	40	40	40	35	35
5	50	50	50	50	50	50	50	45	45	45	45	40	40	40	40	40	40	40	40	40	40	40	40	40	40
4	50	50	50	50	45	45	45	45	45	45	40	40	40	40	40	40	40	40	40	40	40	40	40	40	40
3	50	50	45	45	45	40	40	40	40	40	40	40	40	40	40	40	40	40	40	40	40	40	40	40	40
2	45	45	45	40	40	40	40	40	40	40	40	40	40	40	40	40	40	40	40	40	40	40	40	40	40
1	45	40	40	40	40	40	40	40	40	40	40	40	40	40	40	40	40	40	40	40	40	40	40	40	40

Figure B.8

WIND SPEED ON 9/29/69 AT 1200.0 PST

	1	2	3	4	5	6	7	8	9	10	11	12	13	14	15	16	17	18	19	20	21	22	23	24	25
25	20	20	20	20	20	20	25	30	35	40	50	50	60	60	55	50	50	50	50	50	50	50	50	50	50
24	20	20	20	20	20	20	25	30	35	40	50	60	60	55	55	50	50	50	50	50	50	50	50	50	50
23	20	20	20	20	25	25	30	35	35	40	50	60	60	55	55	50	50	50	50	50	50	50	50	50	50
22	30	30	30	30	30	30	35	35	40	40	50	50	55	50	50	50	50	50	50	60	60	55	55	50	50
21	40	40	40	40	40	40	40	40	50	50	50	50	50	45	40	40	50	60	60	70	70	65	65	60	50
20	45	45	45	45	45	45	50	50	60	60	60	60	50	40	30	40	50	70	70	75	70	70	60	50	40
19	50	50	50	50	50	50	60	60	70	70	70	70	60	50	40	50	60	80	80	75	75	70	60	50	40
18	50	50	50	55	55	55	70	70	80	80	80	80	70	65	60	60	70	80	75	75	70	60	50	45	40
17	55	55	55	55	60	60	80	90	90	95	90	90	90	90	85	85	75	75	75	70	60	50	45	40	40
16	60	60	60	60	80	80	90	95	95	95	95	90	90	90	85	80	70	70	70	65	60	50	40	30	30
15	70	80	90	80	100	100	100	95	95	90	90	95	90	80	80	70	65	65	65	60	50	40	30	30	30
14	80	90	100	100	95	95	95	90	90	90	95	95	90	80	70	65	60	60	60	50	45	40	30	30	30
13	90	100	100	95	90	90	90	90	90	90	95	100	90	80	70	50	60	60	60	50	45	40	30	30	30
12	100	95	95	90	85	85	85	85	85	90	100	100	90	80	70	60	60	60	50	50	40	40	30	30	30
11	95	90	90	85	85	85	80	80	85	85	90	100	90	80	70	60	60	55	50	45	40	30	30	30	30
10	90	85	85	85	85	80	80	80	80	85	85	90	90	80	70	60	60	50	45	40	40	30	30	35	35
9	85	85	85	85	80	80	80	80	80	80	80	80	80	70	70	65	60	50	45	40	30	30	35	40	35
8	85	85	80	90	80	80	90	70	70	80	80	80	80	75	70	65	60	50	50	40	40	40	40	40	40
7	85	80	80	80	80	80	70	70	70	70	70	75	75	70	70	65	60	60	50	50	45	40	40	45	45
6	80	80	80	80	80	80	80	80	70	70	70	70	70	70	70	65	60	60	50	50	50	45	45	50	50
5	80	80	80	80	80	80	80	75	75	70	70	70	70	70	65	65	60	60	50	50	50	50	50	50	50
4	80	80	80	80	80	80	75	75	70	70	70	70	65	65	65	60	60	55	55	50	50	50	50	50	50
3	80	80	80	80	80	75	75	70	70	70	70	65	65	65	65	60	55	55	55	50	50	50	50	50	50
2	80	80	80	80	75	75	70	70	70	70	65	65	65	65	60	60	55	55	50	50	50	50	50	50	50
1	80	80	80	75	75	70	70	70	70	65	65	65	60	60	60	60	55	55	50	50	50	50	50	50	50

Figure B. 9

WIND SPEED ON 9/29/69 AT 1300.0 PST

	1	2	3	4	5	6	7	8	9	10	11	12	13	14	15	16	17	18	19	20	21	22	23	24	25
25	20	20	20	20	30	30	40	40	50	50	60	60	60	60	60	60	60	60	60	60	60	60	60	60	60
24	20	20	20	20	30	30	40	40	50	50	55	60	60	60	60	60	60	60	60	60	60	50	60	60	60
23	20	20	20	30	30	35	40	40	40	50	55	60	60	60	60	60	60	60	60	60	60	60	60	60	60
22	30	30	30	30	30	40	50	50	40	50	60	60	60	60	50	50	55	60	60	65	65	65	60	60	60
21	40	40	40	40	40	40	40	50	50	50	60	60	55	50	40	40	55	60	70	70	70	65	60	60	60
20	45	45	45	45	45	45	45	50	50	60	65	65	55	40	30	40	55	65	70	70	70	65	60	60	50
19	45	45	45	45	45	50	50	50	60	70	70	70	60	40	40	55	75	90	80	80	70	60	60	50	45
18	50	50	50	50	50	50	50	60	70	80	80	80	80	70	70	80	100	100	90	80	70	60	50	45	40
17	50	50	50	50	50	50	50	70	80	90	90	90	90	100	100	100	95	90	80	70	60	50	45	45	40
16	70	70	70	70	70	70	70	90	90	90	90	100	100	110	100	80	90	80	70	60	50	50	50	40	40
15	80	80	80	90	90	90	90	90	90	90	100	110	110	110	100	90	85	80	70	55	55	55	50	40	40
14	90	90	90	90	90	90	90	90	90	100	110	120	120	110	100	90	80	70	60	60	50	50	40	40	40
13	90	90	85	85	80	80	90	90	90	100	110	120	120	110	95	80	70	60	60	60	50	40	40	40	40
12	85	85	80	80	80	80	80	80	90	105	120	130	120	110	95	80	70	70	60	55	50	40	40	40	40
11	80	80	80	80	75	75	70	75	80	90	100	110	110	100	95	90	80	80	70	60	50	40	40	40	40
10	80	80	75	75	75	70	70	70	70	80	90	100	100	100	95	90	80	70	60	50	40	40	40	40	40
9	75	75	70	70	70	70	70	70	70	70	80	90	100	95	90	80	70	65	60	50	40	50	50	50	50
8	70	70	70	70	70	65	65	65	70	70	70	80	90	85	80	70	65	60	55	50	50	50	50	55	55
7	70	70	70	65	65	65	65	65	65	70	70	70	80	75	70	65	60	60	60	55	55	55	55	55	55
6	65	65	65	65	65	65	65	65	65	65	70	70	70	65	60	60	60	60	60	60	60	55	55	60	60
5	65	65	65	65	65	65	65	65	65	60	60	60	60	60	60	60	60	60	60	60	60	60	60	60	60
4	65	65	65	65	65	65	65	60	60	60	60	50	60	60	60	60	60	60	60	60	60	60	60	60	60
3	65	65	65	65	60	60	60	60	60	60	60	60	60	60	60	60	60	60	60	60	60	60	60	60	60
2	65	65	60	60	60	60	60	60	60	60	60	60	60	60	60	60	60	60	60	60	60	60	60	60	60
1	60	60	60	60	60	60	60	60	60	60	60	60	60	60	60	60	60	60	60	60	60	60	60	60	60

Figure B.10

WIND SPEED ON 9/29/69 AT 1400.0 PST

	1	2	3	4	5	6	7	8	9	10	11	12	13	14	15	16	17	18	19	20	21	22	23	24	25
25	40	40	40	40	40	40	40	40	40	40	45	45	45	45	50	50	50	50	50	60	70	80	85	90	90
24	40	40	40	40	40	40	40	45	45	45	45	45	50	50	50	50	50	50	60	70	80	85	90	90	90
23	40	40	40	40	40	45	45	50	50	50	50	50	50	50	50	50	50	60	70	80	85	90	90	90	80
22	50	50	50	50	50	50	50	50	50	50	50	50	50	50	50	50	60	70	80	85	90	90	90	80	80
21	50	55	60	60	60	50	50	50	50	50	50	50	50	50	50	50	65	80	90	90	90	90	80	80	70
20	50	50	50	50	50	50	50	50	50	50	50	50	50	50	40	50	75	100	95	90	90	90	80	70	70
19	50	50	50	50	50	50	50	50	50	50	55	55	70	70	65	80	100	110	100	90	90	80	70	70	60
18	50	50	50	50	50	50	50	50	60	60	70	70	90	90	90	100	110	110	100	90	90	80	70	60	60
17	50	50	50	50	50	50	60	70	70	70	90	90	100	100	100	110	110	100	90	90	80	70	60	60	50
16	70	70	70	70	70	70	70	90	90	90	100	100	110	120	110	100	100	90	90	80	70	60	50	50	50
15	80	80	80	80	90	90	90	90	95	100	110	110	120	110	100	100	90	90	80	70	60	50	50	50	40
14	90	90	90	90	90	90	90	90	95	100	110	110	120	110	100	90	90	80	70	60	50	50	50	40	40
13	90	90	90	90	90	85	85	90	95	100	110	120	120	110	100	90	80	70	60	50	50	50	40	40	40
12	90	90	90	90	85	85	85	90	95	110	120	130	120	110	100	90	90	80	70	60	50	50	40	40	40
11	85	85	85	85	85	85	85	90	90	100	100	110	110	100	100	90	90	90	70	60	50	40	40	40	40
10	85	85	85	85	85	80	80	80	90	90	90	100	100	100	90	70	80	80	70	60	50	40	40	40	40
9	80	80	80	80	80	80	80	75	80	80	85	90	100	90	80	80	70	70	60	50	40	40	40	40	40
8	80	80	80	75	75	75	75	70	70	70	80	80	90	80	70	70	60	60	55	50	45	45	40	40	40
7	80	80	75	75	75	75	70	70	60	60	70	70	80	70	60	60	55	55	50	50	45	45	45	45	45
6	75	75	70	70	70	70	70	65	60	60	60	60	70	60	55	55	55	50	50	50	50	50	45	45	45
5	70	70	70	70	65	65	65	65	60	60	60	60	60	55	55	55	50	50	50	50	50	50	50	50	50
4	70	70	65	65	65	60	60	60	60	55	55	55	55	50	50	50	50	50	50	50	50	50	50	50	50
3	65	65	65	65	60	60	55	55	55	50	50	50	50	50	50	50	50	50	50	50	50	50	50	50	50
2	65	60	60	60	60	55	50	50	50	50	50	50	50	50	50	50	50	50	50	50	50	50	50	50	50
1	60	60	60	55	55	50	50	50	50	50	50	50	50	50	50	50	50	50	50	50	50	50	50	50	50

Figure B.11

WIND SPEED ON 9/29/69 AT 1500.0 PST

	1	2	3	4	5	6	7	8	9	10	11	12	13	14	15	16	17	18	19	20	21	22	23	24	25
25	60	60	60	60	60	60	60	60	50	40	40	40	45	45	50	50	55	60	60	70	80	90	90	90	90
24	60	60	60	60	60	60	60	60	50	50	40	40	40	40	50	55	60	60	70	80	90	90	90	90	90
23	60	60	60	60	60	60	60	60	50	50	50	40	40	50	50	60	70	70	80	90	90	90	60	90	90
22	60	60	60	60	60	60	60	60	55	50	50	50	50	60	60	70	80	80	90	90	90	90	90	90	80
21	55	60	60	60	60	60	60	55	50	50	50	50	60	70	70	80	90	90	100	100	100	100	90	80	80
20	50	55	55	55	55	55	55	50	50	50	50	60	70	80	80	90	100	100	110	110	100	90	80	70	70
19	50	50	50	50	50	50	50	50	50	50	60	70	80	90	100	100	110	120	110	100	90	80	70	70	60
18	50	50	50	50	50	50	50	50	60	60	70	80	90	100	110	110	120	120	100	90	80	80	70	70	60
17	50	50	50	50	50	50	50	60	70	70	80	90	90	100	120	120	110	100	90	80	50	70	60	60	60
16	50	50	70	70	70	70	70	80	80	80	90	100	100	120	110	100	100	90	80	70	70	60	60	50	50
15	70	70	80	80	90	90	90	80	90	90	100	110	120	110	100	90	90	90	70	70	60	50	50	50	50
14	80	80	90	90	90	90	90	90	100	100	110	120	110	100	90	80	80	70	60	60	50	50	50	50	50
13	90	90	90	90	90	90	90	90	100	110	120	130	110	100	90	80	80	70	70	60	50	50	50	50	40
12	90	90	90	85	85	85	90	90	100	110	130	150	130	110	100	90	80	80	70	65	60	50	50	40	40
11	85	85	85	80	80	80	80	90	100	110	120	140	130	110	100	100	90	90	80	70	60	50	40	40	40
10	85	80	80	80	80	80	80	80	90	100	120	130	130	110	100	90	90	80	70	60	50	40	40	40	40
9	80	80	80	80	80	80	80	85	90	100	110	120	130	110	100	90	80	70	60	50	40	40	40	40	40
8	80	80	80	80	80	80	80	80	85	90	90	100	110	100	90	80	70	60	55	55	45	40	40	40	40
7	80	80	80	80	80	80	80	80	85	85	85	90	100	90	80	70	60	55	55	50	50	45	45	40	40
6	80	80	80	80	80	80	80	80	80	80	85	85	90	80	70	60	55	55	50	50	50	50	45	45	45
5	80	80	80	80	80	80	80	80	80	80	80	90	80	70	60	55	50	50	50	50	50	50	50	45	45
4	80	80	80	80	80	80	80	75	70	70	70	70	70	60	55	50	50	50	50	50	50	50	50	50	45
3	80	80	80	80	80	75	75	70	60	60	60	60	60	55	50	50	50	50	50	50	50	50	50	50	50
2	80	80	80	75	75	70	70	60	60	50	50	50	50	50	50	50	50	50	50	50	50	50	50	50	50
1	80	80	75	75	70	70	60	60	50	50	50	50	50	50	50	50	50	50	50	50	50	50	50	50	50

Figure B.12

WIND DIRECTION ON 9/29/69 AT 5JJ.J PST

	1	2	3	4	5	6	7	8	9	10	11	12	13	14	15	16	17	18	19	20	21	22	23	24	25
25	106	111	116	121	127	131	135	139	143	147	151	158	165	171	177	184	191	198	203	208	213	218	222	227	231
24	100	103	107	111	117	126	130	135	139	144	148	155	162	170	178	186	193	201	209	217	225	227	229	231	235
23	90	94	98	102	106	110	125	130	135	140	146	152	158	164	173	182	191	201	211	222	227	232	240	242	244
22	80	85	92	97	100	105	116	124	130	136	142	148	155	162	171	180	189	203	216	220	225	232	239	246	253
21	70	77	83	90	95	100	108	115	121	124	132	140	147	153	161	174	187	204	218	234	242	246	252	256	260
20	82	84	86	88	90	95	100	105	112	118	124	132	140	150	162	174	185	210	225	248	254	261	265	267	267
19	92	92	93	93	93	93	95	95	95	100	102	108	124	140	156	169	182	203	228	248	254	261	265	267	267
18	94	94	93	94	94	94	95	97	98	99	102	115	104	132	147	162	180	206	235	260	264	264	264	265	265
17	89	91	90	91	90	90	92	93	93	93	95	96	104	109	120	130	170	200	230	260	264	264	264	265	265
16	82	82	82	82	82	83	86	86	87	87	90	90	92	95	98	101	106	132	160	88	88	88	88	88	88
15	80	80	81	82	81	84	85	85	85	87	85	87	92	95	95	97	96	85	85	86	87	89	89	89	89
14	80	81	81	82	84	84	87	86	88	89	99	89	89	89	89	84	86	85	85	85	86	86	86	86	86
13	78	82	80	85	85	83	84	82	78	77	80	83	81	80	80	81	80	81	83	85	85	85	85	85	85
12	75	73	75	75	75	75	75	75	75	77	77	77	80	88	79	80	83	83	83	83	84	84	87	87	87
11	72	72	72	71	74	74	72	72	74	75	76	79	79	75	75	75	75	78	78	78	80	80	83	83	83
10	70	72	71	71	72	69	72	72	75	76	75	70	65	70	72	74	75	76	80	82	85	87	89	90	90
9	70	70	71	71	70	70	72	72	70	70	70	68	70	71	72	70	71	75	73	73	78	82	82	85	85
8	70	70	70	70	69	67	67	65	65	69	68	69	70	65	65	68	70	70	73	75	77	78	75	75	75
7	69	70	69	64	63	63	64	65	65	66	67	62	62	62	62	66	70	72	72	68	68	68	68	68	68
6	66	66	63	62	62	62	63	65	65	65	62	60	60	60	62	65	60	64	64	64	64	65	65	55	55
5	61	64	62	62	61	62	62	61	60	58	57	58	60	60	64	60	61	63	63	63	55	50	50	50	50
4	61	60	60	61	61	62	62	55	55	55	56	57	59	59	54	54	56	56	59	57	51	43	43	45	45
3	62	60	60	60	60	59	56	54	54	55	56	56	57	53	52	53	55	54	53	43	40	40	44	44	44
2	60	60	59	55	55	54	54	53	53	54	55	55	52	52	52	53	56	50	45	39	39	42	42	42	42
1	60	59	57	54	54	51	52	53	52	54	53	52	51	50	50	52	54	44	35	35	39	40	40	40	40

Figure B.13

WIND DIRECTION ON 9/29/69 AT 600.0 PST

	1	2	3	4	5	6	7	8	9	10	11	12	13	14	15	16	17	18	19	20	21	22	23	24	25
25	98	103	108	113	118	123	123	136	141	146	148	149	150	150	150	150	151	151	151	150	150	150	150	150	150
24	89	93	97	106	115	121	127	132	137	142	147	148	148	149	148	146	144	144	144	142	142	142	142	140	140
23	80	85	91	98	112	119	126	132	138	145	147	148	147	146	146	145	143	140	136	136	131	120	120	120	120
22	75	79	84	96	110	118	125	132	139	147	147	148	147	146	142	138	135	132	129	125	120	117	115	113	110
21	76	80	85	95	108	115	121	128	135	142	146	147	147	142	138	135	130	125	120	115	110	107	105	103	100
20	77	81	85	94	105	112	117	124	131	138	146	145	144	139	135	133	128	123	117	110	95	93	92	91	90
19	77	81	86	93	102	109	114	120	126	133	138	142	141	136	133	130	125	120	110	100	95	93	92	91	90
18	78	82	86	92	99	105	110	116	122	129	131	137	135	133	130	127	119	113	106	100	95	93	92	91	90
17	79	83	87	91	97	102	106	111	117	125	126	130	129	130	128	123	115	110	105	98	95	93	92	91	90
16	79	83	87	91	95	99	103	107	112	119	120	123	123	128	126	120	113	108	105	100	95	93	92	91	91
15	80	84	88	92	96	100	104	107	110	113	115	117	117	118	118	117	112	107	104	100	95	95	93	91	91
14	81	84	88	91	94	97	100	103	106	100	113	116	117	118	117	116	111	107	107	101	96	92	90	90	90
13	82	84	87	90	92	94	96	99	102	107	111	115	117	118	118	116	114	105	106	101	97	93	90	90	90
12	83	85	87	89	90	91	93	95	99	105	109	114	117	120	122	122	122	105	102	100	95	93	93	93	93
11	84	85	86	88	88	89	90	91	96	103	108	113	117	120	123	125	125	125	125	105	96	92	92	92	92
10	84	85	85	87	88	89	90	90	96	103	108	113	117	119	123	126	120	122	116	107	98	95	92	91	91
9	85	86	87	88	89	90	92	93	98	103	107	111	115	118	123	126	121	115	111	108	101	99	96	92	92
8	87	88	88	89	91	92	94	96	99	103	107	110	113	116	124	128	130	130	126	100	96	96	92	90	90
7	88	89	90	91	92	94	96	98	100	104	106	109	111	117	124	128	130	130	120	115	110	100	95	91	90
6	90	91	92	93	94	96	98	100	102	104	106	108	110	110	125	125	127	124	113	104	98	93	90	90	90
5	90	91	92	93	94	96	98	100	102	104	106	108	110	111	112	115	119	120	116	109	103	96	92	90	90
4	90	91	92	93	94	96	98	100	102	104	106	108	110	110	110	112	111	111	109	104	104	100	92	90	90
3	90	91	92	93	94	96	98	100	102	104	106	106	110	110	110	110	110	108	106	100	107	92	90	90	90
2	90	91	92	93	94	96	98	100	102	104	106	108	110	110	109	109	111	111	111	105	100	92	90	90	90
1	90	91	92	93	94	96	98	100	102	104	106	108	110	110	109	109	111	111	111	105	100	92	90	90	90

Figure B.14

WIND DIRECTION ON 9/29/69 AT 700.0 PST

	1	2	3	4	5	6	7	8	9	10	11	12	13	14	15	16	17	18	19	20	21	22	23	24	25
25	270	268	266	263	260	255	250	240	210	180	173	166	160	148	137	134	131	128	125	122	119	116	113	110	108
24	269	267	265	262	259	254	249	240	211	179	173	169	163	152	142	137	134	130	128	122	119	116	112	109	106
23	268	266	264	261	257	253	248	241	213	178	173	171	166	155	147	140	137	132	131	123	119	115	111	108	104
22	266	264	262	259	255	251	247	242	215	176	173	173	169	159	152	144	140	134	134	124	119	115	110	106	102
21	263	261	259	252	250	247	240	220	198	174	173	173	170	163	156	149	142	135	129	124	119	114	109	104	100
20	259	257	255	245	230	220	210	188	180	172	172	176	175	170	165	161	157	139	127	117	107	97	94	91	89
19	254	252	250	230	195	180	180	160	168	170	171	178	178	180	173	177	169	154	140	129	118	107	100	94	90
18	180	180	180	180	150	151	153	155	160	165	170	180	190	191	192	194	180	168	154	140	129	117	107	98	90
17	90	92	100	110	125	140	145	150	156	162	170	182	192	190	193	195	177	167	154	143	133	123	115	107	93
16	94	96	104	112	125	138	142	147	153	159	169	181	189	190	194	196	174	166	155	146	137	129	121	116	104
15	98	100	107	114	125	136	140	144	150	157	166	181	187	193	190	191	171	164	155	148	141	135	128	124	115
14	102	104	110	116	125	134	138	142	147	155	164	180	184	186	183	180	168	162	156	150	145	141	136	132	128
13	106	108	113	118	125	131	135	139	144	153	165	180	182	180	175	170	165	160	156	152	149	146	143	140	138
12	110	112	116	120	125	129	132	136	140	150	165	180	180	178	170	165	161	157	154	150	148	146	143	140	140
11	114	116	119	122	125	127	130	133	137	148	155	162	162	156	165	160	157	154	152	148	147	145	143	141	141
10	117	120	122	125	128	129	132	135	138	144	153	158	158	153	160	155	153	151	150	147	146	145	144	142	142
9	121	123	125	128	130	131	134	136	139	145	150	154	155	150	154	151	149	148	148	146	145	144	144	142	143
8	125	127	128	130	132	133	135	137	140	144	147	150	149	148	148	147	147	146	146	145	145	144	144	143	143
7	129	131	132	133	134	135	137	139	141	143	145	147	149	148	148	147	147	146	146	145	145	144	144	143	143
6	129	131	132	133	134	135	137	139	141	143	145	147	149	148	148	147	147	146	146	145	145	144	144	143	143
5	129	131	132	133	134	135	137	139	141	143	145	147	149	148	148	147	147	146	146	145	145	144	144	143	143
4	129	131	132	133	134	135	137	139	141	143	145	147	149	148	148	147	147	146	146	145	145	144	144	143	143
3	129	131	132	133	134	135	137	139	141	143	145	147	149	148	148	147	147	146	146	145	145	144	144	143	143
2	129	131	132	133	134	135	137	139	141	143	145	147	149	148	148	147	147	146	146	145	145	144	144	143	143
1	129	131	132	133	134	135	137	139	141	143	145	147	149	148	148	147	147	146	146	145	145	144	144	143	143

Figure B.15

WIND DIRECTION ON 9/29/69 AT 800.0 PST

	1	2	3	4	5	6	7	8	9	10	11	12	13	14	15	16	17	18	19	20	21	22	23	24	25
25	266	266	265	264	263	262	261	260	259	258	257	256	255	251	247	243	239	235	231	227	223	221	219	217	215
24	267	267	266	265	264	263	262	261	260	259	258	257	256	251	247	242	236	232	227	225	223	223	222	225	232
23	258	263	267	266	265	264	263	262	261	260	259	258	257	251	246	238	233	226	223	223	223	225	228	235	245
22	269	269	268	267	266	265	264	263	262	261	260	259	258	252	246	235	230	223	220	221	226	232	249	250	256
21	270	270	269	268	267	266	265	264	263	262	261	260	259	252	246	232	226	221	216	220	230	245	270	270	270
20	260	260	260	260	260	280	235	232	277	272	268	263	259	243	236	229	224	220	215	240	250	270	265	264	263
19	250	250	200	200	200	220	220	288	283	280	270	265	259	234	230	226	222	218	213	215	218	224	234	244	255
18	170	170	150	150	155	160	160	220	220	288	280	270	260	227	217	208	206	201	195	191	193	197	209	217	230
17	90	91	92	93	95	97	99	160	160	220	220	275	280	221	201	191	190	183	178	174	171	170	184	189	189
16	90	91	92	94	95	98	100	104	105	160	160	220	310	215	185	175	170	165	161	157	154	153	156	155	150
15	90	92	93	95	97	99	101	104	106	107	130	160	165	160	170	155	150	147	144	141	139	136	134	132	130
14	90	92	94	96	98	100	102	104	106	108	110	112	115	125	150	150	148	144	141	138	136	134	132	130	127
13	93	94	96	98	100	102	104	106	108	112	114	117	100	126	135	143	142	139	136	134	132	130	129	127	125
12	95	96	98	100	102	104	106	108	111	114	117	121	125	127	130	136	135	133	131	130	128	127	126	125	123
11	95	96	98	100	102	104	106	108	111	114	117	121	125	125	126	129	128	127	126	126	125	124	123	123	121
10	95	96	98	100	102	104	106	108	111	114	117	121	125	122	122	122	122	121	121	121	121	121	120	120	120
9	95	96	98	100	102	104	106	108	111	114	117	121	125	124	124	124	124	123	123	123	123	123	122	122	122
8	95	96	98	100	102	104	106	108	111	114	117	121	125	126	126	126	126	125	125	125	125	125	124	124	124
7	95	96	98	100	102	104	106	108	111	114	117	121	125	128	128	128	128	127	127	127	127	127	127	127	127
6	95	96	98	100	102	104	106	108	111	114	117	121	125	130	130	130	130	130	130	130	130	130	130	130	130
5	95	96	98	100	102	104	106	108	111	114	117	121	125	130	130	130	130	130	130	130	130	130	130	130	130
4	95	96	98	100	102	104	106	108	111	114	117	121	125	130	130	130	130	130	130	130	130	130	130	130	130
3	95	96	98	100	102	104	106	108	111	114	117	121	125	130	130	130	130	130	130	130	130	130	130	130	130
2	95	96	98	100	102	104	106	108	111	114	117	121	125	130	130	130	130	130	130	130	130	130	130	130	130
1	95	96	98	100	102	104	106	108	111	114	117	121	125	130	130	130	130	130	130	130	130	130	130	130	130

Figure B.16

WIND DIRECTION ON 9/29/69 AT 900.0 PST

	1	2	3	4	5	6	7	8	9	10	11	12	13	14	15	16	17	18	19	20	21	22	23	24	25
25	330	330	325	325	320	320	315	310	300	300	300	300	300	294	294	294	294	298	310	320	330	340	350	355	0
24	330	330	325	325	320	320	315	310	300	300	300	300	300	300	300	296	296	304	311	322	335	345	355	0	5
23	340	335	335	330	325	320	320	315	310	310	300	300	300	300	300	296	296	300	309	313	313	350	0	5	10
22	340	335	335	335	330	325	320	315	315	305	300	300	300	300	300	309	312	308	305	322	340	350	0	5	10
21	340	340	335	335	335	335	330	325	320	310	310	310	310	310	310	313	320	320	320	332	355	0	0	5	10
20	355	0	0	0	0	0	0	0	0	0	0	0	0	0	355	345	345	340	338	338	0	0	5	11	11
19	30	40	40	40	40	40	40	40	40	68	67	65	60	50	35	50	355	340	340	333	3	0	5	12	12
18	50	73	73	72	72	70	70	70	69	69	65	65	65	65	45	20	10	8	5	5	5	5	5	13	13
17	72	72	72	71	70	70	68	68	68	68	65	65	65	65	45	25	22	20	15	10	12	10	11	14	14
16	72	72	72	72	71	70	68	68	68	68	65	65	65	65	35	32	31	27	25	25	20	17	15	15	15
15	72	72	72	70	70	70	70	70	70	69	69	69	67	42	39	39	32	31	31	28	25	18	18	17	17
14	72	72	70	70	72	72	70	70	69	66	65	61	60	46	46	42	42	35	35	32	32	25	21	19	19
13	72	72	72	70	70	70	70	70	65	60	60	59	52	53	53	47	44	42	40	35	25	20	20	20	20
12	72	72	70	70	70	65	65	65	60	60	60	60	60	53	50	45	46	45	42	30	26	29	26	22	22
11	74	74	74	73	73	70	69	69	66	66	66	66	66	60	50	46	52	50	47	44	36	31	31	26	26
10	75	75	75	72	71	70	70	70	69	69	65	60	55	52	54	52	49	45	37	37	37	32	27	20	20
9	75	75	73	73	72	72	72	70	66	63	60	56	57	55	55	52	45	40	35	40	39	34	27	25	25
8	75	75	75	75	70	70	70	65	60	60	60	57	56	56	55	50	42	42	42	40	40	38	32	32	32
7	75	75	75	72	70	67	60	62	62	62	60	60	60	55	55	50	46	46	45	45	40	35	30	30	30
6	75	73	70	65	65	65	60	62	62	62	60	60	55	50	48	47	49	47	45	42	40	35	33	32	32
5	74	74	74	74	77	77	77	77	80	82	82	85	85	85	87	88	90	91	92	93	95	96	96	96	96
4	75	75	75	76	76	78	80	81	81	81	82	82	83	83	83	84	86	88	89	92	95	95	99	99	99
3	75	75	75	76	78	78	78	78	78	79	80	80	82	82	85	86	86	86	87	91	94	96	97	97	97
2	75	75	75	75	75	75	75	78	80	80	81	81	82	83	84	85	85	87	88	92	93	96	97	97	97
1	75	75	75	75	77	77	80	80	83	84	81	81	83	83	85	86	87	88	90	90	90	94	97	97	97

Figure B.17

WIND DIRECTION ON 9/29/69 AT 1000.0 PST

	1	2	3	4	5	6	7	8	9	10	11	12	13	14	15	16	17	18	19	20	21	22	23	24	25
25	320	320	325	325	325	330	330	340	345	350	355	0	0	5	15	20	30	35	36	36	36	32	30	28	28
24	330	330	330	330	330	335	340	345	345	355	0	5	5	10	20	25	35	35	38	37	37	34	32	31	31
23	340	340	340	340	340	340	345	345	350	0	5	10	10	15	25	30	35	35	39	38	38	36	35	34	34
22	350	350	350	350	350	350	350	350	355	0	10	20	20	25	30	35	35	35	35	39	39	38	37	37	37
21	355	355	355	355	355	355	355	355	355	0	15	25	25	30	35	40	40	40	40	40	40	40	40	40	40
20	0	0	0	0	0	0	0	0	10	15	30	30	30	30	30	35	36	36	36	40	41	42	42	43	43
19	60	60	55	55	50	50	45	40	40	35	35	30	30	30	30	35	39	40	40	40	43	44	45	46	47
18	65	65	60	60	55	55	50	45	40	40	38	40	40	42	42	42	42	45	50	50	44	45	47	49	51
17	68	67	65	65	60	55	50	40	45	44	45	42	42	42	44	44	45	45	50	48	47	47	50	52	55
16	69	65	64	61	60	55	53	53	53	50	50	45	45	50	45	45	45	50	55	55	55	57	60	60	60
15	69	64	64	60	60	61	56	56	55	50	50	56	56	56	55	55	60	62	62	65	65	67	70	67	65
14	68	67	67	67	67	67	67	62	60	60	60	60	55	55	55	58	59	61	64	65	70	72	75	72	70
13	69	68	68	68	65	63	63	63	63	63	62	62	62	62	62	65	65	65	65	70	75	77	80	77	75
12	70	70	70	68	63	69	69	68	68	67	67	67	57	67	67	65	60	60	75	85	85	87	89	90	80
11	70	71	71	71	71	71	71	72	72	71	70	68	69	66	70	75	85	87	89	90	91	92	92	92	85
10	71	72	73	73	73	73	73	73	73	72	72	75	79	84	84	85	86	88	90	91	92	93	93	93	90
9	72	72	73	74	74	74	74	75	77	77	79	80	81	83	85	85	87	89	90	92	92	94	94	94	94
8	74	74	74	74	74	73	73	75	75	77	80	82	82	84	85	85	85	88	90	91	92	93	93	93	93
7	74	74	74	74	74	74	76	77	77	77	80	81	83	84	85	85	89	89	90	91	92	93	93	93	93
6	74	74	74	74	74	75	75	75	77	79	79	80	84	84	85	85	85	88	90	91	92	94	95	95	95
5	75	75	75	75	75	77	77	79	80	80	81	91	82	85	85	85	85	87	89	92	93	93	95	95	95
4	75	75	75	75	75	78	78	80	80	80	81	81	82	82	84	85	87	88	90	91	92	95	96	96	96
3	75	75	75	75	76	78	78	77	80	81	81	81	81	82	84	85	87	89	90	91	94	95	96	96	96
2	75	75	75	75	76	78	78	77	80	81	82	82	82	82	85	86	87	89	91	91	94	96	97	97	97
1	75	75	75	75	76	78	78	77	80	81	82	82	82	82	85	86	87	89	91	91	94	96	97	97	97

Figure B.18

WIND DIRECTION ON 9/29/69 AT 1100.0 PST

	1	2	3	4	5	6	7	8	9	10	11	12	13	14	15	16	17	18	19	20	21	22	23	24	25
25	67	67	67	66	66	65	63	61	59	57	55	53	45	37	35	35	35	36	36	37	38	42	45	47	47
24	72	72	71	70	68	66	65	62	60	58	56	50	43	37	37	40	39	39	39	35	37	42	45	47	47
23	76	75	74	73	70	67	67	63	62	58	53	47	41	42	45	45	40	39	39	35	37	40	45	50	50
22	80	78	77	75	72	68	69.	65	60	56	50	46	42	41	45	45	42	42	41	40	45	50	51	54	55
21	83	81	79	77	74	70	67	63	58	53	47	45	42	40	40	40	40	40	40	42	47	50	53	55	55
20	84	80	76	74	72	67	64	60	55	50	47	45	43	45	40	40	40	44	44	45	45	52	57	57	57
19	81	78	73	71	68	64	61	57	52	51	49	47	47	43	45	49	46	50	52	54	54	59	62	62	60
18	77	74	70	68	65	61	58	54	53	52	52	52	52	51	51	50	55	57	57	58	60	64	65	65	65
17	74	71	68	65	62	58	56	54	55	55	55	55	55	55	57	60	60	60	60	65	67	67	67	67	70
16	69	68	66	64	60	57	54	56	56	57	57	58	57	55	55	58	59	59	60	62	66	67	68	74	75
15	66	65	64	62	60	58	58	58	59	62	62	62	59	60	63	65	65	66	66	66	67	68	69	80	83
14	63	63	63	62	60	58	58	59	60	63	62	58	62	65	65	66	66	68	68	68	70	75	80	85	85
13	63	63	62	60	60	60	61	62	62	62	65	65	65	65	69	69	67	75	77	83	85	87	87	87	87
12	63	60	59	59	59	60	62	62	64	64	66	66	66	66	68	68	70	75	80	85	87	89	89	89	89
11	59	59	59	59	60	62	63	63	63	63	64	65	70	72	76	76	78	80	81	82	82	86	87	87	87
10	59	59	60	60	60	60	60	60	62	65	66	68	69	71	74	77	80	84	86	86	86	86	86	86	86
9	59	60	60	60	58	58	59	62	63	65	66	67	70	75	75	76	77	80	82	85	86	86	86	86	86
8	59	57	57	57	57	58	60	62	63	64	66	68	70	75	76	79	82	82	82	82	86	88	90	90	90
7	59	55	55	55	59	60	62	62	64	65	70	72	75	76	76	76	77	80	82	85	87	87	88	88	88
6	55	55	55	57	58	60	61	62	63	66	70	72	72	73	75	78	80	83	85	86	88	90	92	94	95
5	55	56	59	60	62	63	65	71	71	72	72	72	76	77	81	83	84	84	86	87	91	94	94	96	96
4	57	60	60	62	70	70	72	72	74	75	77	80	80	81	81	83	84	85	87	90	92	93	94	95	95
3	65	70	71	71	71	72	75	77	79	79	79	79	80	81	81	83	83	85	86	89	91	92	94	95	95
2	72	74	73	79	79	79	79	79	79	80	78	77	80	81	82	82	83	85	86	89	92	94	96	97	97
1	80	80	80	80	80	80	80	80	80	80	80	80	81	82	82	84	85	85	87	90	91	92	93	95	95

Figure B.19

WIND DIRECTION ON 9/29/69 AT 1200.0 PST

	1	2	3	4	5	6	7	8	9	10	11	12	13	14	15	16	17	18	19	20	21	22	23	24	25
25	68	65	62	59	56	53	50	48	46	44	42	40	38	36	34	32	30	30	30	32	35	39	40	40	40
24	72	70	67	64	61	57	54	51	49	47	45	43	42	39	37	35	33	32	35	37	37	37	40	40	40
23	77	75	72	69	66	62	59	55	52	50	48	46	44	42	40	38	38	38	38	39	39	39	40	40	40
22	81	80	77	74	71	67	63	59	55	53	49	47	46	45	45	44	44	43	43	43	43	43	43	43	43
21	86	84	82	79	75	72	68	63	58	55	53	51	49	48	47	46	45	45	45	45	45	45	45	45	45
20	83	79	76	73	70	67	62	58	60	56	54	54	51	51	50	50	50	50	49	49	47	47	47	47	47
19	78	74	70	69	69	62	62	61	61	58	57	57	55	54	54	54	54	54	54	52	52	52	52	52	52
18	73	70	66	65	64	62	62	62	62	60	59	60	58	55	56	56	55	55	56	56	56	56	56	56	56
17	67	66	65	64	63	62	62	62	62	63	62	61	61	60	62	62	62	61	60	60	60	60	60	58	58
16	65	65	64	63	62	62	62	63	64	65	65	65	64	64	62	62	60	60	60	60	60	60	60	60	60
15	63	63	62	62	62	62	62	62	62	62	63	64	64	65	63	61	61	59	59	59	60	60	60	61	63
14	61	61	61	61	61	61	62	62	62	62	63	63	64	65	65	62	62	60	60	60	60	60	62	63	65
13	59	59	59	61	61	61	63	64	65	65	65	70	71	69	66	65	61	61	61	60	60	61	63	65	67
12	57	57	57	59	59	61	63	65	65	69	70	72	72	70	69	67	66	70	70	70	70	70	70	70	70
11	55	55	57	57	59	61	63	65	69	69	75	73	73	80	75	70	73	75	75	75	75	73	73	70	70
10	53	53	55	57	59	61	65	69	69	70	75	75	75	75	75	75	75	77	75	72	72	67	66	64	64
9	52	53	55	56	58	61	66	68	69	75	75	75	76	77	77	80	79	78	76	72	67	67	67	67	70
8	52	52	54	56	58	61	64	67	69	73	75	76	77	80	80	80	79	78	76	73	72	73	73	75	79
7	51	52	54	56	58	61	67	67	69	72	75	77	77	80	80	80	79	78	76	73	73	73	75	78	83
6	50	52	54	56	58	61	64	67	69	73	75	77	77	80	80	80	78	78	77	75	73	73	75	79	84
5	50	52	54	56	58	61	64	67	69	72	74	75	76	77	77	77	78	79	78	77	80	81	82	83	84
4	50	52	54	56	58	61	64	67	69	72	74	75	76	75	75	75	78	79	79	80	81	81	82	83	84
3	50	52	54	56	58	61	64	67	69	72	74	75	76	70	72	75	78	79	79	80	81	81	82	83	84
2	50	52	54	56	58	61	64	67	69	72	74	75	76	70	72	75	78	79	79	80	81	81	82	83	84
1	50	52	54	56	58	61	64	67	69	72	74	75	76	70	72	75	78	79	79	80	81	81	82	83	84

Figure B.20

WIND DIRECTION ON 9/29/69 AT 1300.0 PST

	1	2	3	4	5	6	7	8	9	10	11	12	13	14	15	16	17	18	19	20	21	22	23	24	25
25	10	10	15	15	15	15	20	20	20	20	20	20	25	25	30	30	30	30	32	35	40	40	40	40	40
24	15	15	15	15	15	20	20	20	20	20	20	25	31	31	33	33	33	33	35	37	40	40	40	40	45
23	20	20	20	20	20	25	25	25	25	25	25	25	32	35	35	35	35	35	35	40	40	40	40	45	45
22	25	25	25	25	25	30	30	30	30	30	30	34	35	35	37	37	37	37	37	43	45	45	45	45	45
21	30	30	30	30	30	35	35	35	35	35	35	36	37	37	40	40	40	40	40	43	45	45	45	45	50
20	35	35	35	35	40	40	40	40	40	40	40	40	40	40	43	45	45	45	45	45	50	50	50	50	50
19	35	35	40	40	45	45	45	45	45	45	45	45	45	45	45	47	45	47	50	55	55	55	55	55	50
18	45	45	45	45	50	50	50	50	50	50	50	50	50	50	47	47	47	50	55	60	55	55	55	55	50
17	50	50	50	50	55	55	55	55	55	55	55	55	53	51	50	50	50	55	55	65	60	55	55	55	55
16	55	55	55	55	55	56	56	56	56	58	58	58	54	53	53	53	55	55	55	62	60	60	55	55	55
15	60	60	60	62	61	60	60	60	60	59	59	60	60	55	55	55	60	60	60	60	60	60	55	55	55
14	65	63	63	63	63	63	64	64	65	65	63	60	60	57	57	60	60	60	60	60	60	60	55	55	55
13	65	65	65	65	65	65	66	64	65	65	63	60	60	60	60	60	55	55	55	55	55	55	55	55	55
12	65	65	67	68	68	68	63	65	65	65	65	65	60	60	60	63	60	55	55	55	55	55	55	55	55
11	67	67	67	68	68	68	67	65	65	65	67	65	63	63	63	63	60	55	55	55	55	55	55	55	55
10	69	69	68	68	68	68	67	65	67	67	67	66	65	65	65	65	60	60	60	55	55	55	55	55	55
9	69	69	69	70	70	70	68	65	65	70	69	67	65	65	65	65	63	60	60	55	55	55	55	55	55
8	70	70	70	70	70	70	68	68	68	70	70	69	67	66	65	65	63	60	60	55	55	54	54	54	54
7	71	73	75	73	70	70	70	69	69	70	70	69	68	68	65	65	63	60	60	55	55	56	56	56	56
6	75	75	77	75	75	75	73	70	70	70	70	70	69	69	65	65	63	63	60	60	60	56	56	56	56
5	79	79	79	78	75	75	74	72	72	71	70	70	70	70	67	65	65	64	62	62	58	56	56	56	56
4	79	78	78	78	75	75	75	72	74	72	70	70	70	70	67	66	66	65	60	60	57	56	56	56	56
3	75	75	75	75	75	75	75	73	74	72	71	71	70	69	68	63	63	63	56	56	56	56	56	56	56
2	75	75	75	75	75	75	75	75	73	72	72	72	70	65	65	60	60	60	56	56	56	56	56	56	56
1	73	73	75	75	75	75	75	75	72	72	72	72	65	60	60	56	56	56	56	56	56	56	56	56	56

Figure B.21

WIND DIRECTION ON 9/29/69 AT 1400.0 PST

	1	2	3	4	5	6	7	8	9	10	11	12	13	14	15	16	17	18	19	20	21	22	23	24	25
25	102	100	98	96	94	89	84	80	76	71	65	60	50	45	40	42	42	42	42	42	42	42	42	42	42
24	102	100	98	96	94	89	84	80	76	72	67	62	53	47	44	44	44	43	43	43	42	41	41	42	43
23	103	103	100	96	94	89	84	81	76	73	68	64	55	49	48	47	46	45	45	44	43	41	40	41	40
22	106	105	101	96	95	90	85	82	77	74	70	65	57	50	50	50	49	47	45	43	40	40	40	40	40
21	100	100	98	96	95	91	86	83	78	75	65	62	50	52	51	50	50	50	50	45	40	41	41	40	40
20	90	90	90	88	30	85	77	77	68	68	64	61	53	53	52	52	52	50	50	48	45	45	44	42	40
19	88	88	85	80	75	74	72	71	70	65	63	60	54	54	53	53	53	53	50	50	47	47	47	46	45
18	91	86	78	76	75	70	70	70	70	63	62	57	55	55	55	55	55	54	53	50	47	55	52	51	45
17	88	75	75	73	70	69	68	68	63	62	60	59	59	59	57	57	56	55	60	58	55	55	55	55	55
16	82	75	70	70	67	64	63	63	63	63	62	60	60	60	59	58	57	60	60	58	56	56	56	56	60
15	75	75	68	68	67	67	65	65	65	65	64	63	63	63	60	57	57	60	64	62	60	59	57	60	60
14	68	68	68	70	70	70	69	68	68	68	64	64	64	64	63	60	60	63	65	65	65	60	57	60	60
13	73	72	72	72	73	70	70	70	70	70	64	64	64	64	64	64	63	65	68	70	70	65	60	60	60
12	75	75	75	75	75	73	72	71	70	69	65	65	65	65	65	66	68	70	73	75	75	70	60	63	65
11	75	75	75	75	75	72	71	70	70	68	65	65	65	65	68	68	68	75	75	76	79	80	70	70	70
10	75	75	75	75	75	71	70	69	69	68	70	70	70	72	73	80	80	81	82	82	83	84	76	75	75
9	76	76	76	75	75	70	72	72	72	70	76	76	76	76	77	79	79	83	82	81	82	82	82	82	80
8	76	76	76	75	75	73	73	73	74	74	76	76	78	77	77	78	79	85	83	80	80	82	85	85	85
7	76	76	76	76	75	75	75	75	74	74	75	75	80	78	76	77	78	80	80	79	79	81	84	85	86
6	75	76	76	76	75	75	75	75	74	74	75	75	78	78	76	76	77	78	78	78	79	80	83	85	88
5	76	75	75	75	75	75	75	75	74	74	74	74	76	77	76	76	76	76	77	78	79	79	80	84	87
4	76	75	75	75	75	75	75	75	74	74	74	74	74	74	74	76	76	76	76	77	78	79	80	83	86
3	76	75	74	74	74	74	74	74	74	74	74	74	74	74	74	75	75	75	76	77	78	79	80	83	85
2	76	75	74	74	74	74	74	74	74	74	74	74	74	74	74	75	75	75	76	77	78	79	80	86	85
1	76	75	74	74	74	74	74	74	74	74	74	74	74	74	75	75	75	75	76	77	78	79	80	83	85

Figure B.22

WIND DIRECTION ON 9/29/69 AT 1500.0 PST

	1	2	3	4	5	6	7	8	9	10	11	12	13	14	15	16	17	18	19	20	21	22	23	24	25
25	125	115	106	105	99	95	90	85	78	70	65	63	50	35	36	36	35	35	35	35	35	34	32	30	30
24	131	125	110	107	98	94	90	85	78	70	65	60	37	35	36	36	36	36	36	36	35	34	31	30	30
23	126	126	112	110	99	95	90	83	83	65	60	47	38	36	36	36	37	37	37	37	36	33	30	30	30
22	116	116	116	110	100	95	90	80	77	63	55	50	41	40	40	40	40	39	38	38	36	33	30	30	30
21	110	110	110	110	103	95	90	79	73	63	50	48	41	40	43	44	45	39	37	37	37	36	35	35	43
20	90	90	90	90	91	88	87	83	68	55	46	46	48	49	49	49	49	45	45	43	40	40	43	45	50
19	80	80	80	78	78	76	75	70	60	60	46	49	50	53	50	50	50	50	50	44	44	44	45	53	58
18	82	82	80	78	77	75	75	70	53	50	50	50	55	54	53	52	51	50	50	50	50	60	62	65	68
17	80	80	80	75	70	68	60	57	58	58	59	59	57	55	56	56	54	52	58	60	65	65	72	72	73
16	75	75	75	70	63	62	60	60	60	63	60	59	59	58	58	56	56	60	63	65	67	70	72	72	73
15	72	72	70	65	63	65	66	65	64	64	63	62	60	60	59	59	60	63	63	65	65	67	72	72	73
14	70	69	66	65	65	66	66	66	65	65	64	62	62	61	60	60	60	63	63	65	65	70	72	73	73
13	70	69	66	66	66	67	67	66	66	65	64	62	62	62	62	62	62	66	66	68	68	72	73	74	74
12	69	66	66	69	69	68	68	66	66	64	63	62	62	62	64	64	64	68	68	70	70	74	75	75	75
11	70	69	69	70	71	69	68	66	65	64	62	62	62	64	66	68	68	70	72	72	73	74	75	75	75
10	71	71	72	72	70	68	67	66	64	64	62	64	70	66	68	72	72	72	72	72	73	74	75	75	75
9	72	72	72	70	70	68	66	64	64	66	66	66	73	72	72	72	72	72	72	72	73	74	75	75	76
8	72	72	72	72	69	68	63	68	68	70	71	72	72	72	72	72	72	72	73	73	74	74	76	76	76
7	73	73	73	73	72	70	70	70	70	73	72	72	72	72	72	73	73	73	73	73	75	75	76	76	76
6	73	73	73	74	73	73	73	73	73	73	73	73	73	73	73	73	73	73	73	73	76	76	77	77	78
5	74	74	74	75	75	73	73	73	73	73	73	73	73	73	73	73	73	73	73	74	74	77	77	79	79	80
4	76	75	75	75	75	73	73	73	73	73	73	73	73	73	73	73	73	73	75	77	79	82	83	83	83
3	76	75	75	74	74	73	73	73	73	73	73	73	73	73	73	73	73	73	75	77	79	82	83	83	83
2	75	74	74	73	73	73	73	73	73	73	73	73	73	73	73	73	73	73	75	77	79	82	83	83	83
1	75	74	74	73	73	73	73	73	73	73	73	73	73	73	73	73	73	73	75	77	79	82	83	83	83

Figure B.23

MIXING DEPTHS ON 9/29/69 AT 500.0 PST

	1	2	3	4	5	6	7	8	9	10	11	12	13	14	15	16	17	18	19	20	21	22	23	24	25
25	100	100	100	100	100	100	100	150	150	200	200	200	200	200	200	200	200	200	200	200	200	200	500	200	200
24	100	100	100	100	100	100	100	100	100	150	200	200	200	200	200	200	200	200	200	200	200	200	200	200	200
23	100	100	100	100	100	100	100	100	100	100	150	150	150	200	200	200	200	200	200	200	200	200	200	200	200
22	100	100	100	100	100	100	100	100	100	100	100	100	100	150	150	200	200	200	200	200	200	200	200	200	200
21	100	100	100	100	100	100	100	100	100	100	100	100	100	100	100	100	100	100	100	100	100	175	200	200	200
20	100	100	100	100	100	100	150	150	150	150	100	100	100	100	100	100	100	100	100	100	100	125	150	150	150
19	200	200	200	200	200	200	200	200	200	200	150	140	120	100	100	100	100	100	100	100	100	100	100	100	150
18	300	300	300	300	300	275	250	250	250	225	200	170	150	125	100	100	100	100	100	100	100	100	100	100	100
17	400	400	400	400	375	325	300	300	275	250	225	200	175	150	125	100	100	100	100	100	100	100	100	120	150
16	500	500	500	480	450	410	350	325	300	275	250	225	200	175	150	125	100	100	100	100	100	125	140	160	150
15	500	500	500	500	495	460	410	350	325	300	275	250	225	200	175	150	125	100	100	100	100	125	150	150	150
14	500	500	500	500	500	470	425	375	350	325	300	275	250	225	200	175	150	125	125	125	125	150	200	200	200
13	500	500	500	500	500	480	450	400	375	350	325	300	275	250	230	225	200	150	150	150	150	175	200	200	200
12	500	500	500	500	500	500	490	450	400	375	350	325	300	300	280	270	225	200	175	175	175	200	200	200	200
11	500	500	500	500	500	500	470	460	430	400	375	350	350	350	340	330	250	250	200	200	200	225	225	225	250
10	500	500	500	500	500	500	495	450	450	400	400	400	400	400	400	375	300	300	250	225	225	250	250	250	200
9	500	500	500	500	500	500	500	480	480	400	425	430	450	450	450	400	350	330	300	275	250	250	250	275	200
8	500	500	500	500	500	500	400	350	350	400	450	450	480	475	470	450	400	370	350	325	300	300	300	300	250
7	500	500	500	500	500	500	400	350	350	350	480	495	495	490	485	475	450	400	400	375	350	325	325	325	325
6	500	500	500	500	500	500	500	500	400	350	485	500	500	500	500	500	480	450	450	425	400	375	350	350	350
5	500	500	500	500	500	500	500	500	500	500	500	500	500	500	500	500	495	490	480	450	425	400	375	375	350
4	500	500	500	500	500	500	500	500	500	500	500	500	500	500	500	500	500	490	495	480	460	425	400	400	400
3	500	500	500	500	500	500	500	500	500	500	500	500	500	500	500	500	500	500	500	500	480	450	425	400	400
2	500	500	500	500	500	500	500	500	500	500	500	500	500	500	500	500	500	500	500	500	500	480	400	350	350
1	500	500	500	500	500	500	500	500	500	500	500	500	500	500	500	500	500	500	500	500	500	500	400	350	300

Figure B.24

MIXING DEPTHS ON 9/29/69 AT 600.0 PST

	1	2	3	4	5	6	7	8	9	10	11	12	13	14	15	16	17	18	19	20	21	22	23	24	25
25	100	100	100	100	100	100	100	150	150	200	200	200	200	200	200	200	200	200	200	200	200	200	500	200	200
24	100	100	100	100	100	100	100	100	100	150	200	200	200	200	200	200	200	200	200	200	200	200	200	200	200
23	100	100	100	100	100	100	100	100	100	100	150	150	150	200	200	200	200	200	200	200	200	200	200	200	200
22	100	100	100	100	100	100	100	100	100	100	100	100	100	150	220	200	200	200	200	200	200	200	200	200	200
21	100	100	100	100	100	100	100	100	100	100	100	100	100	100	100	100	100	100	100	100	100	175	200	200	200
20	100	100	100	100	100	100	150	150	150	150	100	100	100	100	100	100	100	100	100	100	100	125	150	150	150
19	200	200	200	200	200	200	200	200	200	200	150	140	120	100	100	100	100	100	100	100	100	100	100	100	150
18	300	300	300	300	300	275	250	250	250	225	200	170	150	125	100	100	100	100	100	100	100	100	100	100	100
17	400	400	400	400	375	325	300	300	275	250	225	200	175	150	125	100	100	100	100	100	100	100	100	120	150
16	500	500	500	490	450	420	350	325	300	275	250	225	200	175	150	125	100	100	100	100	100	125	140	160	150
15	500	500	500	500	485	460	410	350	325	300	275	250	225	200	175	150	125	100	100	100	100	125	150	150	150
14	500	500	500	500	500	470	425	375	350	325	300	275	250	225	200	175	150	125	125	125	125	150	200	200	200
13	500	500	500	500	500	480	450	400	375	350	325	300	275	250	230	225	200	150	150	150	150	175	200	200	200
12	500	500	500	500	500	500	490	450	400	375	350	325	300	300	280	270	225	200	175	175	175	200	200	200	200
11	500	500	500	500	500	500	470	460	430	400	375	350	350	350	340	330	250	250	200	200	200	225	225	225	250
10	500	500	500	500	500	500	495	450	450	400	400	400	400	400	400	375	300	300	250	225	225	250	250	250	200
9	500	500	500	500	500	500	500	480	430	400	425	430	450	450	450	400	350	330	300	275	250	250	250	275	200
8	500	500	500	500	500	500	400	350	350	400	450	450	480	475	470	450	400	370	350	325	300	300	300	300	250
7	500	500	500	500	500	500	400	350	350	350	480	495	495	490	485	475	450	400	400	375	350	325	325	325	325
6	500	500	500	500	500	500	500	500	400	350	485	500	500	500	500	500	480	450	450	425	400	375	350	350	350
5	500	500	500	500	500	500	500	500	500	500	500	500	500	500	500	500	495	490	480	450	425	400	375	375	350
4	500	500	500	500	500	500	500	500	500	500	500	500	500	500	500	500	500	490	495	480	460	425	400	400	400
3	500	500	500	500	500	500	500	500	500	500	500	500	500	500	500	500	500	500	500	500	480	450	425	400	400
2	500	500	500	500	500	500	500	500	500	500	500	500	500	500	500	500	500	500	500	500	500	480	400	350	350
1	500	500	500	500	500	500	500	500	500	500	500	500	500	500	500	500	500	500	500	500	500	500	400	350	300

Figure B.25

MIXING DEPTHS ON 9/29/69 AT 700.0 PST

	1	2	3	4	5	6	7	8	9	10	11	12	13	14	15	16	17	18	19	20	21	22	23	24	25
25	200	200	200	200	200	200	200	200	200	200	200	200	200	200	200	200	200	200	200	200	200	200	200	200	200
24	125	125	125	125	125	125	125	125	150	175	200	200	200	200	200	200	200	200	200	200	200	200	200	200	200
23	125	125	125	125	125	125	125	125	125	150	200	200	200	200	200	200	200	200	200	200	200	200	200	200	200
22	125	125	125	125	125	125	125	125	125	125	150	150	150	190	200	200	200	200	200	200	200	200	200	200	200
21	150	150	150	150	150	150	150	150	150	150	125	125	125	150	150	150	150	150	150	150	150	200	200	200	200
20	200	200	200	200	200	200	175	175	175	175	150	150	150	125	125	125	125	125	125	125	125	150	190	200	200
19	250	250	250	250	250	250	250	250	250	250	225	200	200	175	150	150	125	125	125	125	125	150	150	150	180
18	350	350	350	350	350	300	275	275	275	250	250	225	200	175	175	160	150	150	150	125	125	150	200	200	200
17	450	450	450	450	400	350	325	325	300	275	250	250	225	200	200	175	175	175	175	150	150	150	200	200	200
16	500	500	500	490	450	400	375	350	325	300	275	275	250	230	225	200	200	200	200	175	175	175	200	200	200
15	500	500	500	500	495	470	425	375	350	325	300	300	275	260	250	225	225	225	220	200	200	175	150	150	200
14	500	500	500	500	500	480	450	400	375	350	325	325	300	290	275	250	250	250	240	225	225	200	175	175	150
13	500	500	500	500	500	480	470	425	400	400	375	350	325	320	300	275	275	275	270	250	250	225	200	175	175
12	500	500	500	500	500	500	500	450	450	425	375	375	350	330	325	300	300	300	290	275	275	250	225	200	175
11	500	500	500	500	500	500	490	480	450	420	400	375	375	360	350	330	325	325	320	300	300	275	250	225	200
10	500	500	500	500	500	500	495	480	460	430	420	410	400	380	375	360	350	350	340	325	325	300	275	250	225
9	500	500	500	500	500	500	500	480	460	440	440	440	440	420	400	390	375	375	370	350	350	325	300	275	250
8	500	500	500	500	500	500	450	400	400	450	450	480	480	470	430	420	400	400	400	375	375	350	325	300	275
7	500	500	500	500	500	500	450	400	400	400	500	495	495	490	470	460	430	425	420	400	400	375	350	325	300
6	500	500	500	500	500	500	500	500	400	350	485	500	500	500	500	500	470	450	440	425	425	400	375	350	325
5	500	500	500	500	500	500	500	500	500	500	500	500	500	500	500	500	495	470	460	450	450	430	400	375	350
4	500	500	500	500	500	500	500	500	500	500	500	500	500	500	500	500	500	490	480	470	460	440	420	400	380
3	500	500	500	500	500	500	500	500	500	500	500	500	500	500	500	500	500	500	500	495	470	460	440	420	400
2	500	500	500	500	500	500	500	500	500	500	500	500	500	500	500	500	500	500	500	500	480	470	450	400	400
1	500	500	500	500	500	500	500	500	500	500	500	500	500	500	500	500	500	500	500	500	500	500	470	400	350

Figure B.26

MIXING DEPTHS ON 9/29/69 AT 800.0 PST

	1	2	3	4	5	6	7	8	9	10	11	12	13	14	15	16	17	18	19	20	21	22	23	24	25
25	300	300	300	300	300	300	300	300	300	300	350	350	350	350	350	350	350	350	350	350	350	350	350	350	350
24	200	200	200	200	200	200	200	200	200	250	350	350	350	350	350	350	350	350	350	350	350	350	350	350	350
23	200	200	200	200	200	200	200	200	200	250	300	300	300	300	350	350	350	350	350	350	350	350	350	350	350
22	200	200	200	200	200	200	200	200	250	200	250	250	250	250	300	300	300	300	300	300	300	350	350	350	350
21	300	300	300	300	300	300	300	300	275	250	200	200	200	200	250	250	250	250	250	250	250	300	300	300	300
20	350	350	350	350	350	350	325	325	300	300	275	250	225	225	200	200	200	200	200	200	200	250	240	250	250
19	400	400	400	400	375	375	350	350	325	300	300	275	250	250	225	225	200	200	200	200	200	200	200	220	230
18	450	450	450	450	425	400	375	375	350	325	300	275	250	250	225	225	225	200	200	200	200	200	250	250	250
17	500	500	500	500	450	425	400	375	375	350	325	300	275	275	250	225	225	225	200	200	200	200	250	270	250
16	500	500	500	500	475	450	425	400	375	350	325	325	300	300	275	250	250	225	225	225	200	200	200	250	250
15	500	500	500	500	495	475	450	425	400	375	350	325	325	300	275	250	250	250	225	225	225	200	200	250	250
14	500	500	500	500	500	500	475	450	425	400	375	350	350	325	300	275	275	250	250	250	225	225	200	200	200
13	500	500	500	500	500	480	475	450	425	400	375	350	350	350	325	300	300	275	250	250	250	225	225	200	200
12	500	500	500	500	500	500	480	450	450	425	400	375	400	375	350	325	325	300	275	250	250	250	225	225	225
11	500	500	500	500	500	500	490	475	450	425	425	400	425	400	375	350	350	325	300	275	275	275	250	250	225
10	500	500	500	500	500	500	495	475	450	425	425	425	450	425	400	375	375	350	325	300	275	300	275	250	250
9	500	500	500	500	500	500	500	475	425	425	450	450	475	450	430	400	400	375	350	325	300	325	300	275	250
8	500	500	500	500	500	500	500	450	450	450	500	500	500	480	470	440	430	400	375	350	325	350	325	300	275
7	500	500	500	500	500	500	450	400	400	400	500	495	500	500	500	480	460	430	400	375	350	375	350	325	300
6	500	500	500	500	500	500	500	500	400	400	485	500	500	500	500	500	480	460	430	400	375	400	375	350	325
5	500	500	500	500	500	500	500	500	500	500	500	500	500	500	500	500	495	490	460	430	400	425	400	375	350
4	500	500	500	500	500	500	500	500	500	500	500	500	500	500	500	500	500	500	490	460	430	450	440	400	375
3	500	500	500	500	500	500	500	500	500	500	500	500	500	500	500	500	500	500	500	490	460	475	470	450	400
2	500	500	500	500	500	500	500	500	500	500	500	500	500	500	500	500	500	500	500	500	500	500	470	425	425
1	500	500	500	500	500	500	500	500	500	500	500	500	500	500	500	500	500	500	500	500	500	500	475	450	250

Figure B.27

MIXING DEPTHS ON 9/23/69 AT 900.0 PST

	1	2	3	4	5	6	7	8	9	10	11	12	13	14	15	16	17	18	19	20	21	22	23	24	25
25	500	500	500	500	500	500	500	500	500	500	500	500	500	500	500	500	500	500	500	500	500	500	500	500	500
24	400	400	400	400	400	400	400	400	400	450	500	500	500	500	500	500	500	500	500	500	500	500	500	500	500
23	400	400	400	400	400	400	400	400	400	450	500	500	500	500	500	500	500	500	500	500	500	500	500	500	500
22	400	400	400	400	400	400	400	400	400	400	500	500	500	500	500	500	500	500	500	500	500	500	500	500	500
21	425	425	425	425	425	425	425	425	425	425	450	450	450	450	450	450	450	450	450	450	450	500	500	500	500
20	450	450	450	450	450	450	450	450	450	450	475	475	450	425	400	400	400	400	400	400	400	450	450	450	450
19	475	475	475	475	475	475	475	475	475	475	500	500	500	450	420	400	400	400	400	400	400	400	400	420	430
18	500	500	500	500	500	500	500	500	500	500	515	515	510	495	480	465	450	400	400	400	400	400	450	450	450
17	550	550	550	550	550	550	550	540	540	540	530	530	530	520	520	520	490	480	450	450	400	400	450	450	450
16	550	550	550	550	550	550	550	560	560	570	570	570	580	590	580	550	520	500	470	470	450	450	450	450	450
15	550	550	550	550	550	550	560	560	570	580	590	600	610	640	620	590	550	530	500	500	475	450	450	450	450
14	550	550	550	550	550	550	560	570	580	590	600	610	630	630	610	600	580	560	530	520	500	475	470	470	465
13	550	550	550	550	550	550	550	550	570	590	610	620	615	620	610	610	590	570	560	540	520	500	490	490	490
12	550	550	550	550	550	550	550	565	580	595	610	610	600	600	600	610	600	590	580	560	540	520	510	500	495
11	550	550	550	550	550	550	550	570	570	600	580	595	590	590	590	600	610	600	600	580	560	540	530	510	510
10	550	550	550	550	550	550	550	570	570	575	560	580	580	580	580	590	600	610	610	600	580	560	550	530	525
9	550	550	550	550	550	550	550	570	550	550	540	565	570	570	570	590	590	600	600	610	600	580	570	550	540
8	550	550	550	550	550	550	550	500	500	500	520	550	560	560	560	570	580	590	590	600	610	600	590	570	555
7	550	550	550	550	550	550	500	450	450	450	500	550	550	550	550	560	570	580	580	590	600	610	600	590	570
6	550	550	550	550	550	550	550	550	500	500	550	550	550	550	550	550	560	570	570	580	590	600	610	600	585
5	550	550	550	550	550	550	550	550	550	550	550	550	550	550	550	550	550	560	560	570	580	590	600	610	600
4	550	550	550	550	550	550	550	550	550	550	550	550	550	550	550	550	550	550	550	560	570	580	575	570	570
3	550	550	550	550	550	550	550	550	550	550	550	550	550	550	550	550	550	550	550	550	560	570	550	530	520
2	550	550	550	550	550	550	550	550	550	550	550	550	550	550	550	550	550	550	550	550	550	560	525	490	450
1	550	550	550	550	550	550	550	550	550	550	550	550	550	550	550	550	550	550	550	550	550	550	500	450	300

Figure B.28

MIXING DEPTHS ON 9/29/69 AT 1000.0 PST

	1	2	3	4	5	6	7	8	9	10	11	12	13	14	15	16	17	18	19	20	21	22	23	24	25
25	750	750	750	750	750	750	750	750	700	700	700	700	700	700	700	700	700	700	700	700	700	700	700	700	700
24	650	650	650	650	650	650	650	650	670	700	700	700	700	700	700	700	700	700	700	700	700	700	700	700	700
23	640	640	640	640	640	640	640	650	650	700	700	700	700	700	700	700	700	700	700	700	700	700	700	700	700
22	640	640	640	640	640	640	640	650	660	680	700	700	700	700	700	700	700	700	700	700	700	700	700	700	700
21	630	630	630	630	630	635	640	650	650	680	670	690	700	700	680	700	700	670	650	650	650	650	650	650	650
20	620	620	620	620	630	640	650	660	670	680	660	680	700	700	630	650	650	650	650	600	600	600	600	600	600
19	610	615	620	635	640	650	660	670	680	690	700	700	690	690	680	670	660	650	650	630	630	630	620	620	620
18	650	650	650	650	650	660	670	680	690	690	700	700	690	690	680	670	660	650	650	650	630	650	650	650	650
17	575	575	575	575	600	600	630	670	670	670	690	700	710	710	700	700	680	700	680	630	650	650	650	650	650
16	550	550	550	550	550	560	600	650	680	680	700	720	740	770	760	760	760	750	730	700	670	650	650	650	650
15	550	550	550	550	550	570	625	650	690	710	730	750	770	790	780	800	780	760	720	710	700	670	650	650	650
14	550	550	550	550	550	570	625	670	680	700	730	750	765	780	770	780	770	760	720	710	700	680	660	660	660
13	550	550	550	550	550	550	600	650	675	700	730	750	750	770	760	770	760	750	730	700	700	680	670	670	670
12	550	550	550	550	550	550	550	660	675	700	730	750	750	750	750	760	750	750	730	700	700	690	670	670	670
11	550	550	550	550	550	550	550	660	660	700	700	710	730	740	735	740	740	740	740	700	700	650	630	670	660
10	550	550	550	550	550	550	550	610	620	650	660	675	710	720	715	720	730	740	740	710	715	700	690	670	650
9	550	550	550	550	550	550	550	580	590	600	610	650	680	690	700	700	720	740	740	720	725	700	700	680	650
8	550	550	550	550	550	550	550	500	500	500	550	600	650	660	670	690	710	740	740	730	720	710	700	630	650
7	550	550	550	550	550	550	500	500	500	500	550	580	610	610	620	630	650	680	680	680	680	670	660	650	640
6	550	550	550	550	550	550	550	550	500	500	550	550	550	550	550	590	600	620	620	630	640	635	630	630	630
5	550	550	550	550	550	550	550	550	550	550	550	550	550	550	550	550	550	570	570	580	590	600	600	600	620
4	550	550	550	550	550	550	550	550	550	550	550	550	550	550	550	550	550	550	550	565	570	570	570	570	580
3	550	550	550	550	550	550	550	550	550	550	550	550	550	550	550	550	550	550	550	550	565	575	560	550	530
2	550	550	550	550	550	550	550	550	550	550	550	550	550	550	550	550	550	550	550	550	550	550	550	500	475
1	550	550	550	550	550	550	550	550	550	550	550	550	550	550	550	550	550	550	550	550	550	550	525	475	325

Figure B.29

MIXING DEPTHS ON 9/29/69 AT 1100.0 PST

	1	2	3	4	5	6	7	8	9	10	11	12	13	14	15	16	17	18	19	20	21	22	23	24	25
25	1250	1250	1200	1200	1200	1200	1200	1200	1200	1100	1000	900	800	800	800	800	800	800	800	800	800	800	800	800	800
24	1000	1000	1000	1000	1000	1000	1000	1000	1000	1050	1000	900	850	850	850	850	850	850	850	800	800	800	800	800	800
23	1000	1000	1000	1000	1000	1000	1000	1000	1000	1000	1000	900	800	800	800	800	800	800	800	800	800	800	800	800	800
22	1000	1000	1000	1000	1000	1000	1000	1000	1000	1000	1000	900	850	800	800	800	800	800	800	800	800	800	800	800	800
21	950	950	950	950	950	950	950	950	950	1000	1000	1000	900	900	900	900	900	900	900	900	900	900	900	900	900
20	900	900	900	900	900	900	900	900	900	950	950	950	900	1000	1000	1000	1000	1000	1000	1000	1000	1000	950	950	950
19	800	800	800	800	800	800	800	825	850	875	900	925	950	975	1000	1000	1000	1000	1000	1000	1000	1000	1000	1000	1000
18	700	700	700	700	700	725	750	775	800	825	850	875	900	925	950	975	1000	1000	1000	1000	1000	1000	1000	1000	1000
17	600	600	600	600	630	660	700	730	760	790	820	850	880	910	945	980	1000	1000	1000	1000	1000	1000	1000	1000	1000
16	550	550	550	570	600	630	670	710	750	785	820	855	890	925	960	970	960	1000	1000	1000	1000	1000	1000	1000	1000
15	550	550	550	550	570	600	640	690	740	780	820	860	900	940	910	910	930	960	960	1000	1000	1000	1000	1000	1000
14	550	550	550	550	550	580	620	665	715	760	800	840	880	900	870	870	900	930	930	960	975	960	960	960	970
13	550	550	550	550	550	550	600	640	690	740	780	820	840	860	830	830	870	900	900	930	950	920	930	930	940
12	550	550	550	550	550	550	580	620	670	720	760	750	800	810	790	790	830	870	870	900	925	890	900	900	910
11	550	550	550	550	550	550	570	600	650	700	700	720	750	760	750	750	790	830	830	870	900	860	870	870	880
10	550	550	550	550	550	550	560	590	640	660	650	680	700	710	710	710	750	790	790	830	860	830	840	840	850
9	550	550	550	550	550	550	550	580	590	600	600	640	650	660	670	670	720	750	750	790	820	800	810	810	820
8	550	550	550	550	550	550	550	540	540	545	550	600	600	610	630	640	680	720	720	750	780	770	780	780	790
7	550	550	550	550	550	550	550	500	500	500	500	550	560	570	590	610	640	680	680	720	740	740	750	750	760
6	550	550	550	550	550	550	550	550	500	500	500	550	550	550	550	570	600	640	640	680	700	710	720	720	730
5	550	550	550	550	550	550	550	550	550	550	550	550	550	550	550	550	570	600	600	640	670	680	690	690	700
4	550	550	550	550	550	550	550	550	550	550	550	550	550	550	550	550	550	570	570	600	640	650	660	660	670
3	550	550	550	550	550	550	550	550	550	550	550	550	550	550	550	550	550	550	550	570	600	620	630	630	640
2	550	550	550	550	550	550	550	550	550	550	550	550	550	550	550	550	550	550	550	550	570	590	600	600	600
1	550	550	550	550	550	550	550	550	550	550	550	550	550	550	550	550	550	550	550	550	550	550	570	550	500

Figure B. 30

MIXING DEPTHS IN 9/29/69 AT 1200.0 PST

	1	2	3	4	5	6	7	8	9	10	11	12	13	14	15	16	17	18	19	20	21	22	23	24	25
25	1750	1750	1750	1750	1750	1750	1750	1500	1300	1200	1100	1000	1000	1000	1000	1000	1000	1000	1000	1000	1000	1000	1000	1000	1000
24	1500	1500	1500	1500	1500	1500	1500	1300	1200	1150	1100	1000	1000	1000	1000	1000	1000	1000	1000	1000	1000	1000	1000	1000	1000
23	1500	1500	1500	1500	1500	1500	1500	1300	1200	1150	1100	1000	1000	1000	1000	1000	1000	1000	1000	1000	1000	1000	1000	1000	1000
22	1500	1500	1500	1500	1500	1500	1500	1300	1200	1150	1050	1000	1000	1000	1000	1000	1000	1000	1000	1000	1000	1000	1000	1000	1000
21	1300	1300	1300	1300	1300	1300	1300	1250	1200	1150	1050	1025	1000	1000	1000	1000	1000	1100	1100	1100	1100	1100	1100	1100	1100
20	1100	1100	1100	1100	1150	1200	1200	1225	1200	1150	1050	1050	1050	1050	1080	1130	1200	1250	1250	1250	1250	1250	1250	1250	1250
19	950	900	900	900	950	1000	1000	1025	1050	1050	1050	1050	1050	1050	1130	1200	1250	1350	1350	1350	1350	1300	1300	1300	1300
18	750	750	750	750	950	875	1000	1000	1000	1050	1050	1050	1075	1100	1180	1280	1350	1350	1350	1350	1350	1300	1300	1300	1300
17	600	600	600	600	650	670	800	850	900	950	1000	1050	1080	1090	1150	1230	1300	1300	1300	1300	1300	1300	1300	1300	1300
16	550	550	550	550	575	620	725	750	800	850	900	950	1040	1090	1100	1280	1250	1250	1250	1250	1250	1250	1250	1250	1250
15	550	550	550	550	550	600	650	675	750	800	850	900	1000	1050	1080	1200	1200	1200	1200	1200	1200	1200	1200	1200	1250
14	550	550	550	550	550	550	600	625	700	750	800	850	950	1030	1050	1100	1100	1150	1170	1175	1175	1175	1200	1200	1200
13	550	550	550	550	550	550	550	600	650	700	750	800	900	990	980	1000	1000	1020	1050	1075	1100	1125	1150	1175	1200
12	550	550	550	550	550	550	550	580	640	675	725	750	850	950	930	930	930	950	980	1000	1030	1060	1100	1125	1150
11	550	550	550	550	550	550	550	580	620	650	675	700	800	890	900	900	900	925	950	950	975	1000	1000	1025	1050
10	550	550	550	550	550	550	550	570	600	625	650	675	725	810	820	825	850	850	900	875	900	900	900	925	950
9	550	550	550	550	550	550	550	550	575	600	625	625	650	730	740	750	775	800	825	825	850	800	825	825	850
8	550	550	550	550	550	550	550	550	550	575	600	600	610	650	660	675	700	750	750	775	700	725	750	775	800
7	550	550	550	550	550	550	550	500	500	550	580	550	570	580	590	610	650	700	700	700	700	700	725	760	770
6	550	550	550	550	550	550	550	550	550	550	550	550	550	550	550	550	600	650	650	700	700	700	700	700	700
5	550	550	550	550	550	550	550	550	550	550	550	550	550	550	550	550	550	600	600	650	650	625	625	600	600
4	550	550	550	550	550	550	550	550	550	550	550	550	550	550	550	550	550	550	570	600	575	550	525	500	500
3	550	550	550	550	550	550	550	550	550	550	550	550	550	550	550	550	550	550	570	600	575	550	525	500	500
2	550	550	550	550	550	550	550	550	550	550	550	550	550	550	550	550	550	550	550	550	550	550	525	500	475
1	550	550	550	550	550	550	550	550	550	550	550	550	550	550	550	550	550	550	550	550	550	550	525	500	450

Figure B. 31

MIXING DEPTHS JN 9/29/69 AT 1300.0 PST

	1	2	3	4	5	6	7	8	9	10	11	12	13	14	15	16	17	18	19	20	21	22	23	24	25
25	2500	2500	2500	2500	2500	2400	2400	2300	2200	2100	2000	1800	1600	1400	1200	1200	1200	1200	1200	1200	1200	1200	1200	1200	1200
24	2500	2500	2500	2500	2500	2500	2500	2400	2300	2200	2200	2000	1800	1600	1500	1500	1500	1500	1500	1500	1500	1500	1500	1500	1500
23	2500	2500	2500	2500	2500	2500	2500	2500	2400	2300	2300	2100	2000	1800	1800	1800	1800	1800	1800	1800	1800	1800	1800	1800	1800
22	2500	2500	2500	2500	2500	2500	2500	2500	2500	2400	2400	2300	2250	2200	2200	2200	2200	2200	2200	2200	2200	2200	2200	2200	2200
21	2000	2000	2000	2000	2000	2100	2200	2300	2400	2500	2500	2500	2500	2500	2500	2500	2500	2500	2500	2500	2500	2500	2500	2500	2500
20	1650	1650	1650	1700	1800	1900	2000	2100	2200	2350	2500	2500	2500	2500	2500	2500	2500	2500	2500	2500	2500	2500	2500	2500	2500
19	1300	1300	1300	1350	1400	1450	1500	1650	1700	2100	2300	2500	2500	2500	2500	2500	2500	2500	2500	2500	2500	2500	2500	2500	2500
18	950	950	950	950	950	950	1000	1200	1400	1600	1800	2000	2100	2200	2300	2400	2500	2500	2500	2500	2500	2500	2500	2500	2500
17	600	600	600	640	700	800	850	900	1000	1100	1200	1600	1650	1750	1850	1950	2050	2100	2250	2300	2250	2200	2200	2200	2300
16	550	550	550	580	640	700	740	780	850	900	1000	1200	1200	1300	1400	1500	1600	1700	2000	2100	2000	1900	2000	2000	2100
15	550	550	550	550	580	600	630	660	690	720	750	780	810	840	860	1000	1100	1400	1700	1800	1750	1700	1800	1800	2000
14	550	550	550	550	550	590	610	640	670	700	735	760	790	800	830	840	900	1000	1400	1500	1500	1500	1600	1600	1800
13	550	550	550	550	550	580	600	625	650	690	720	740	760	770	790	810	830	860	1000	1100	1200	1300	1400	1400	1600
12	550	550	550	550	550	550	580	610	640	670	700	715	730	740	750	770	790	810	830	860	1000	1100	1200	1300	1400
11	550	550	550	550	550	550	580	600	620	660	680	690	700	710	720	730	750	770	790	810	830	860	1100	1200	1200
10	550	550	550	550	550	550	570	590	610	620	640	655	670	680	690	700	720	740	760	780	800	820	840	1000	1100
9	550	550	550	550	550	550	550	570	575	590	610	625	630	640	650	670	690	710	735	740	770	790	810	820	830
8	550	550	550	550	550	550	550	530	540	560	580	600	600	610	610	630	660	680	710	710	740	755	765	785	795
7	550	550	550	550	550	550	550	500	500	500	530	570	570	580	570	600	630	650	680	690	710	720	730	750	760
6	550	550	550	550	550	550	550	550	550	500	535	550	550	550	550	570	600	620	650	660	670	690	700	720	730
5	550	550	550	550	550	550	550	550	550	550	550	550	550	550	550	550	570	590	620	630	640	660	670	690	700
4	550	550	550	550	550	550	550	550	550	550	550	550	550	550	550	550	560	590	600	610	630	640	660	670	
3	550	550	550	550	550	550	550	550	550	550	550	550	550	550	550	550	550	550	550	570	580	600	610	630	640
2	550	550	550	550	550	550	550	550	550	550	550	550	550	550	550	550	550	550	550	550	560	570	580	600	600
1	550	550	550	550	550	550	550	550	550	550	550	550	550	550	550	550	550	550	550	550	550	550	550	500	500

Figure B. 32

MIXING DEPTHS ON 9/29/69 AT 1400.0 PST

	1	2	3	4	5	6	7	8	9	10	11	12	13	14	15	16	17	18	19	20	21	22	23	24	25
25	2500	2500	2500	2500	2500	2500	2400	2300	2200	2100	1800	1500	1200	1200	1200	1200	1200	1200	1200	1200	1200	1200	1200	1200	1200
24	2500	2500	2500	2500	2500	2500	2400	2350	2200	2100	1900	1800	1500	1500	1500	1500	1500	1500	1500	1500	1500	1500	1500	1500	1500
23	2500	2500	2500	2500	2500	2500	2350	2350	2250	2150	2100	2000	1800	1900	1900	1800	1800	1800	1800	1800	1800	1800	1800	1800	1800
22	2500	2500	2500	2500	2500	2350	2250	2250	2250	2200	2200	2200	2100	2200	2200	2200	2200	2200	2200	2200	2200	2200	2200	2200	2200
21	2500	2500	2500	2500	2500	2450	2300	2250	2200	2250	2300	2350	2400	2450	2500	2500	2500	2500	2500	2500	2500	2500	2500	2500	2500
20	1500	1500	1500	1500	1500	1550	1650	1700	1800	1900	2050	2150	2200	2200	2200	2200	2500	2500	2500	2500	2300	2300	2300	2300	2300
19	1200	1200	1200	1200	1200	1250	1350	1400	1650	1750	1800	1850	1900	1900	1900	2000	2500	2500	2500	2500	2300	2200	2200	2200	2200
18	900	900	900	900	900	950	1050	1050	1300	1350	1400	1450	1500	1500	1500	1800	2200	2500	2500	2500	2300	2200	2100	2100	2100
17	600	600	600	600	625	650	750	750	900	1000	1000	1050	1100	1100	1100	1500	2000	2250	2500	2500	2300	2200	2100	2000	2000
16	550	550	550	550	500	650	700	700	725	750	750	750	800	850	850	1200	1600	1800	2000	2300	2200	2100	2000	1900	1900
15	550	550	550	550	550	600	625	650	660	680	700	730	760	790	825	1000	1300	1600	1800	2000	1950	1900	1800	1700	1700
14	550	550	550	550	550	580	600	630	650	660	680	700	750	780	800	950	1200	1500	1700	1850	1750	1700	1700	1650	1650
13	550	550	550	550	550	550	600	610	630	640	660	690	725	750	780	800	1000	1200	1500	1600	1500	1500	1500	1400	1400
12	550	550	550	550	550	550	550	600	620	630	650	680	700	710	725	750	900	950	1150	1300	1250	1250	1250	1200	1200
11	550	550	550	550	550	550	550	600	610	620	630	660	670	675	700	700	800	900	1000	1050	1000	1000	1000	1000	1000
10	550	550	550	550	550	550	550	600	600	600	620	640	640	650	650	650	700	750	800	850	850	900	900	900	900
9	550	550	550	550	550	550	550	550	550	570	610	620	620	620	620	625	625	650	650	700	700	750	775	800	850
8	550	550	550	550	550	550	550	500	500	550	600	600	600	600	600	600	600	625	650	650	675	700	750	775	800
7	550	550	550	550	550	550	550	500	500	500	550	550	550	550	550	600	600	600	625	625	650	675	700	725	750
6	550	550	550	550	550	550	550	550	550	550	550	550	550	550	550	550	550	600	600	600	625	650	675	700	700
5	550	550	550	550	550	550	550	550	550	550	550	550	550	550	550	550	550	550	575	575	600	625	650	650	650
4	550	550	550	550	550	550	550	550	550	550	550	550	550	550	550	550	550	550	550	550	600	600	600	600	600
3	550	550	550	550	550	550	550	550	550	550	550	550	550	550	550	550	550	550	550	550	600	600	550	550	550
2	550	550	550	550	550	550	550	550	550	550	550	550	550	550	550	550	550	550	550	550	550	550	500	500	500
1	550	550	550	550	550	550	550	550	550	550	550	550	550	550	550	550	550	550	550	550	550	550	525	500	500

Figure B. 33

MIXING DEPTHS ON 9/29/69 AT 1500.0 PST

	1	2	3	4	5	6	7	8	9	10	11	12	13	14	15	16	17	18	19	20	21	22	23	24	25
25	2500	2500	2500	2500	2500	2500	2400	2300	2200	2000	1800	1500	1200	1200	1200	1200	1200	1200	1200	1200	1200	1200	1200	1200	1200
24	2500	2500	2500	2500	2500	2500	2400	2300	2200	2000	1900	1700	1500	1500	1500	1500	1500	1500	1500	1500	1500	1500	1500	1500	1500
23	2500	2500	2500	2500	2500	2300	2200	2200	2200	2000	1900	1800	1800	1800	1800	1800	1800	1800	1800	1800	1800	1800	1800	1800	1800
22	2400	2400	2400	2400	2400	2200	2100	2100	2200	2000	1900	1900	1900	2000	2100	2200	2200	2200	2200	2200	2200	2200	2200	2200	2200
21	2000	2000	2000	2000	2000	2000	2000	2000	2200	2000	1800	1800	1800	2000	2300	2300	2300	2300	2300	2300	2300	2300	2300	2300	2300
20	1500	1500	1500	1500	1500	1500	1500	1500	1800	1700	1500	1500	1500	1800	2000	2300	2500	2500	2500	2500	2500	2500	2500	2500	2500
19	1200	1200	1200	1200	1200	1200	1200	1200	1500	1400	1300	1300	1300	1500	1700	2000	2300	2500	2500	2500	2300	2300	2300	2300	2300
18	900	900	900	900	900	900	900	900	1000	1000	1100	1100	1100	1200	1400	1700	2000	2500	2500	2300	2200	2200	2200	2200	2200
17	600	600	600	600	600	600	600	600	800	900	950	950	950	950	1000	1400	2000	2200	2300	2200	2200	2200	2200	2200	2200
16	550	550	550	550	550	575	600	600	650	675	700	725	750	775	825	1200	1500	1800	2000	2000	2000	2000	2000	2000	2000
15	550	550	550	550	550	550	575	600	630	650	680	700	720	740	800	1200	1400	1600	1800	1800	1800	1800	1800	1800	1800
14	550	550	550	550	550	550	600	600	600	630	660	690	700	800	900	1100	1300	1500	1500	1500	1500	1600	1600	1600	1600
13	550	550	550	550	550	550	550	575	600	630	650	700	700	700	800	1000	1100	1300	1300	1300	1300	1400	1400	1400	1400
12	550	550	550	550	550	550	550	575	600	630	650	700	750	800	850	900	1000	1100	1100	1100	1100	1200	1200	1200	1200
11	550	550	550	550	550	550	550	575	575	610	650	670	700	750	775	800	850	950	1000	1000	1000	1100	1100	1100	1100
10	550	550	550	550	550	550	550	575	575	600	625	640	650	700	700	700	750	900	900	900	900	1000	1000	1000	1000
9	550	550	550	550	550	550	550	550	550	575	600	600	600	625	625	650	650	800	800	800	800	850	850	850	850
8	550	550	550	550	550	550	550	500	500	575	575	575	575	575	575	600	600	700	750	750	750	750	750	750	750
7	550	550	550	550	550	550	550	500	500	550	550	550	550	550	550	575	600	600	650	675	675	675	675	675	675
6	550	550	550	550	550	550	550	500	500	550	550	550	550	550	550	550	575	600	600	600	600	600	600	600	600
5	550	550	550	550	550	550	550	550	550	550	550	550	550	550	550	550	550	575	575	575	575	575	575	575	575
4	550	550	550	550	550	550	550	550	550	550	550	550	550	550	550	550	550	550	550	550	550	550	550	550	550
3	550	550	550	550	550	550	550	550	550	550	550	550	550	550	550	550	550	550	550	550	550	525	500	500	500
2	550	550	550	550	550	550	550	550	550	550	550	550	550	550	550	550	550	550	550	550	550	525	500	500	450
1	550	550	550	550	550	550	550	550	550	550	550	550	550	550	550	550	550	550	550	550	550	525	500	450	

APPENDIX C

DISTRIBUTION AND SPEED OF TRAFFIC ON LOS ANGELES FREEWAYS IN 1969

In this Appendix, figures are given illustrating the speed of traffic flow in both the slow and fast freeway directions at hourly intervals between 6 A.M. and 9 A.M.. A speed of 60 mph is assumed to apply on all freeways in both directions before 6 A.M. and between 9 A.M. and 3 P.M. Linear interpolation, in time, may be employed to estimate the speed in a particular grid cell at times other than those designated on the figures. The ratio of the mileage driven in the slow direction to that driven in the fast direction is given in Figures C.9 - C.12 . These values are assumed constant over the time interval given on each figure. Figures C.1 - C.12 are derived from the work reported in Appendix A of Reynolds et al. (1973).

Figure C.1 Average Vehicle Speed in "Slow" Direction ($\overline{v}_s$)

at 6:00 A.M.

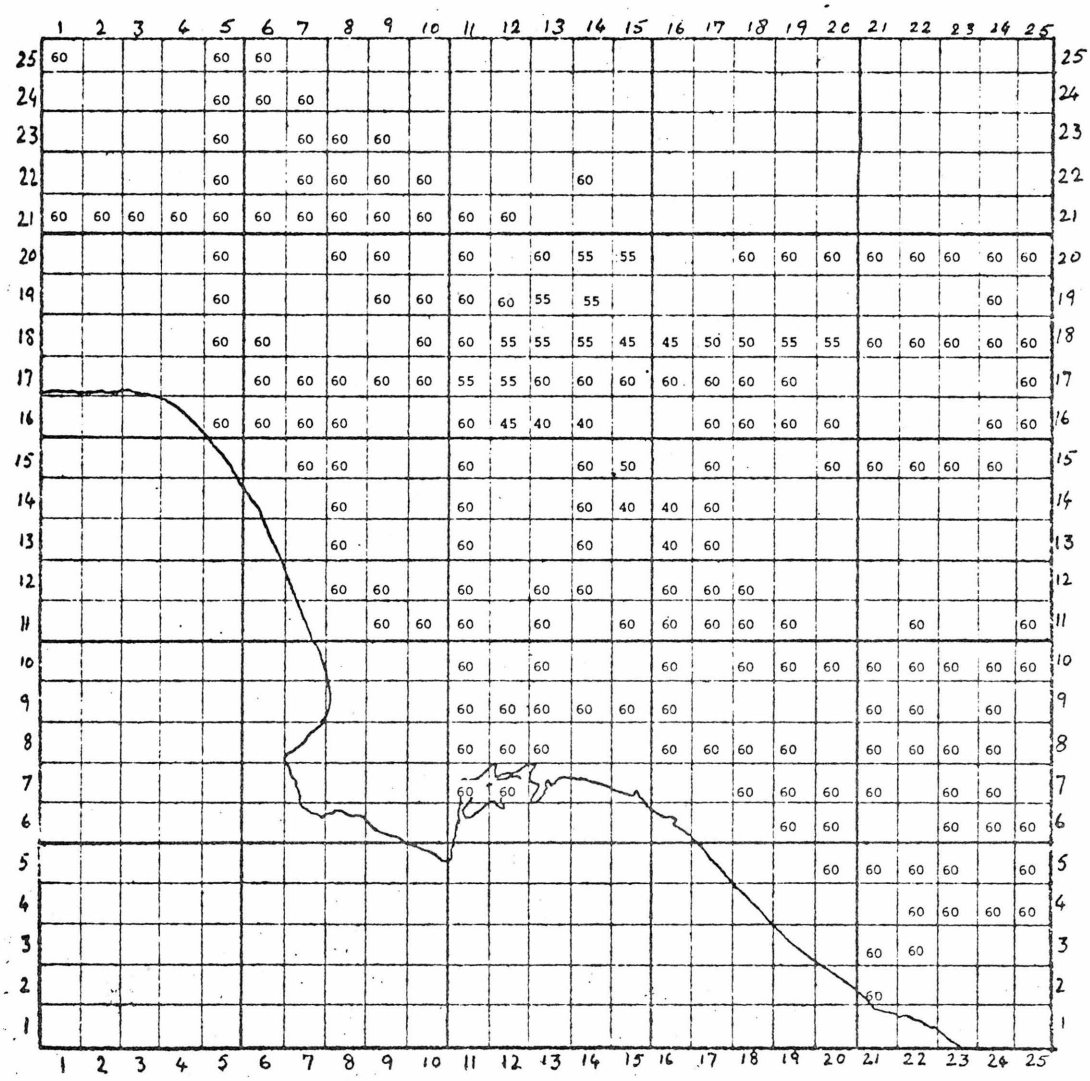

Figure C.2 Average Vehicle Speed in "Slow" Direction ($\bar{v}_s$) at 7:00 A.M.

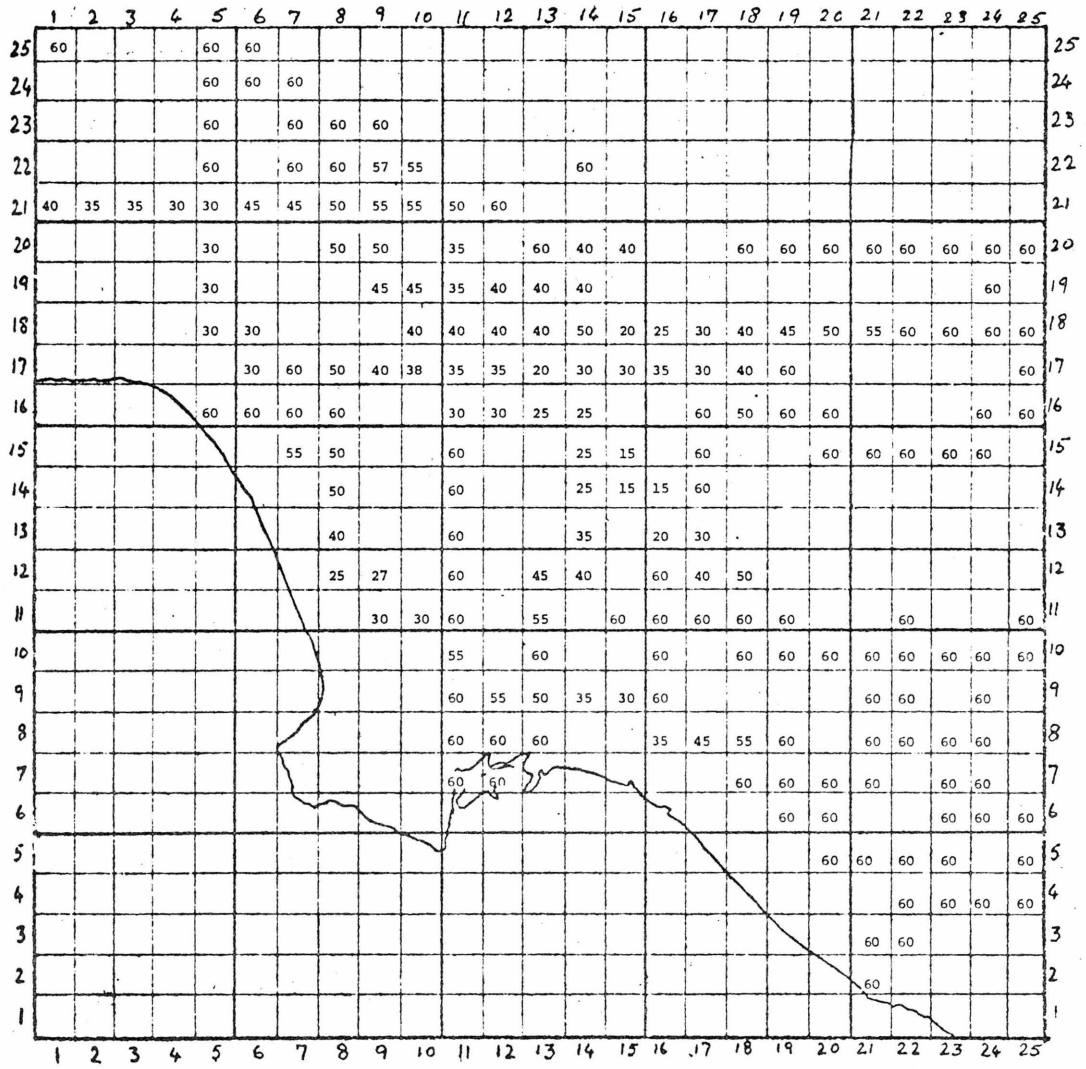

Figure C.3 Average Vehicle Speed in "Slow" Direction ($\bar{v}_s$) at 8:00 A.M.

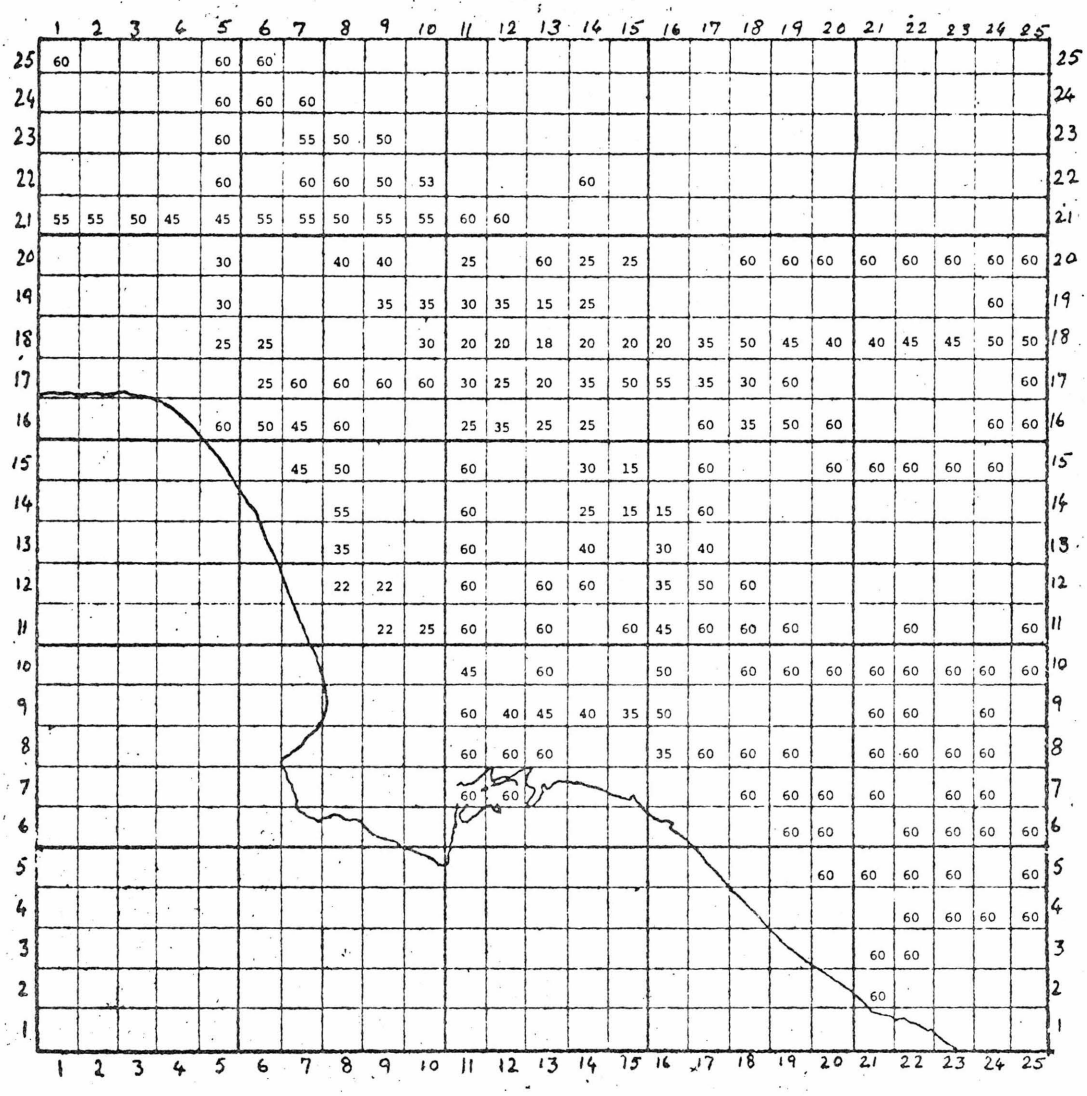

Figure C.4 Average Vehicle Speed in "Slow" Direction ($\bar{v}_s$) at 9:00 A.M.

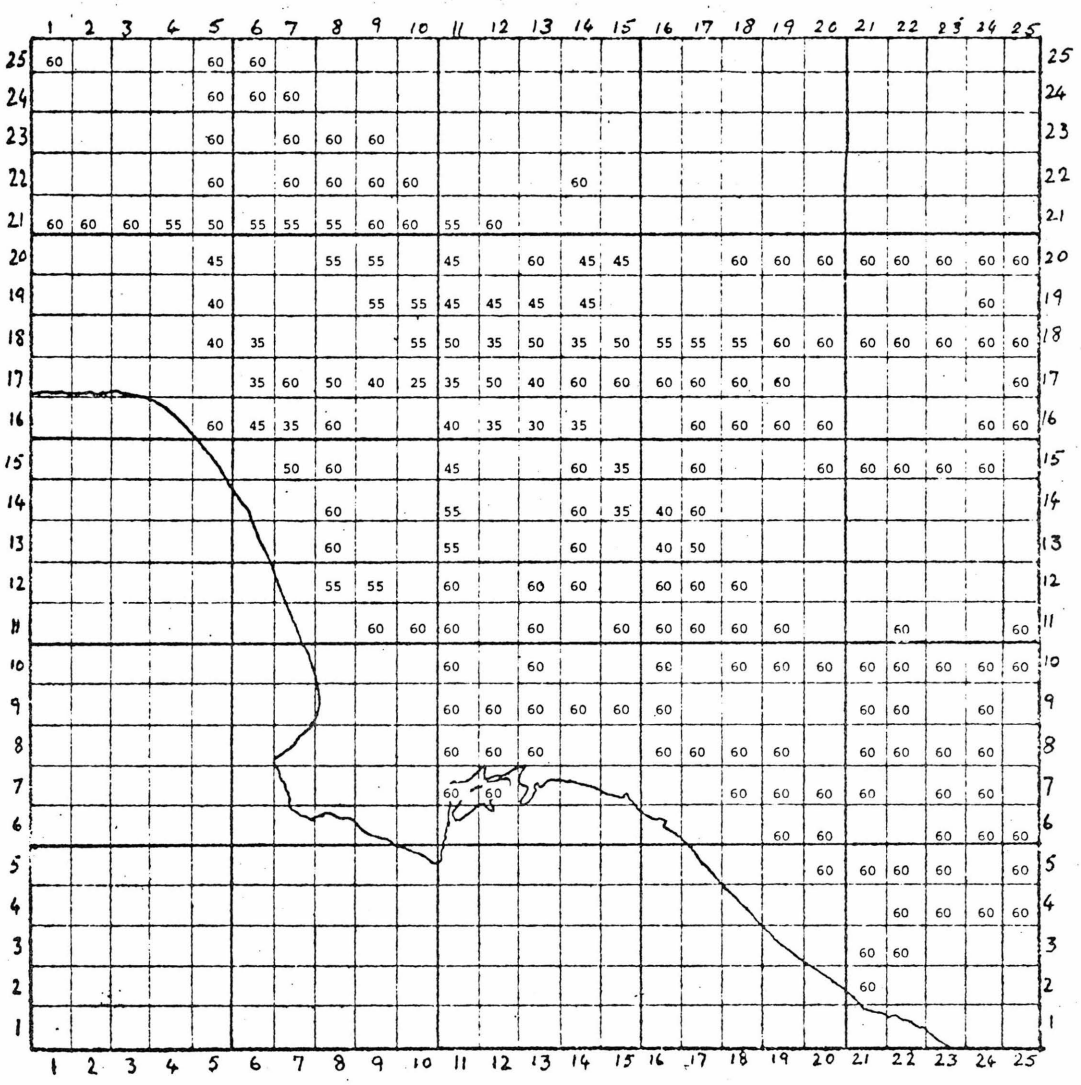

Figure C.5 Average Vehicle Speed in "Fast" Direction ($\overline{v}_f$)

at 6:00 A.M.

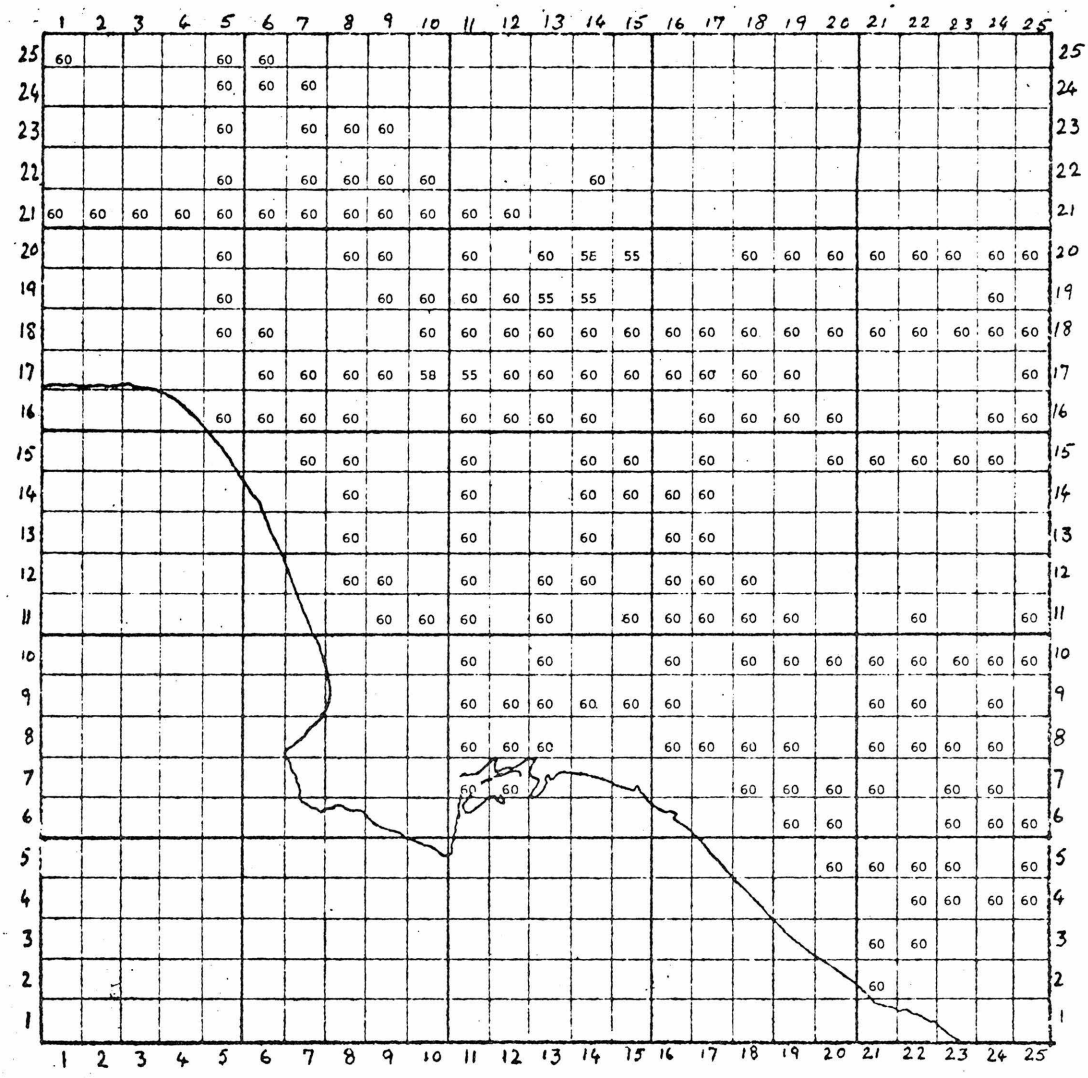

Figure C.6 Average Vehicle Speed in "Fast" Direction ($\overline{v}_f$) at 7:00 A.M.

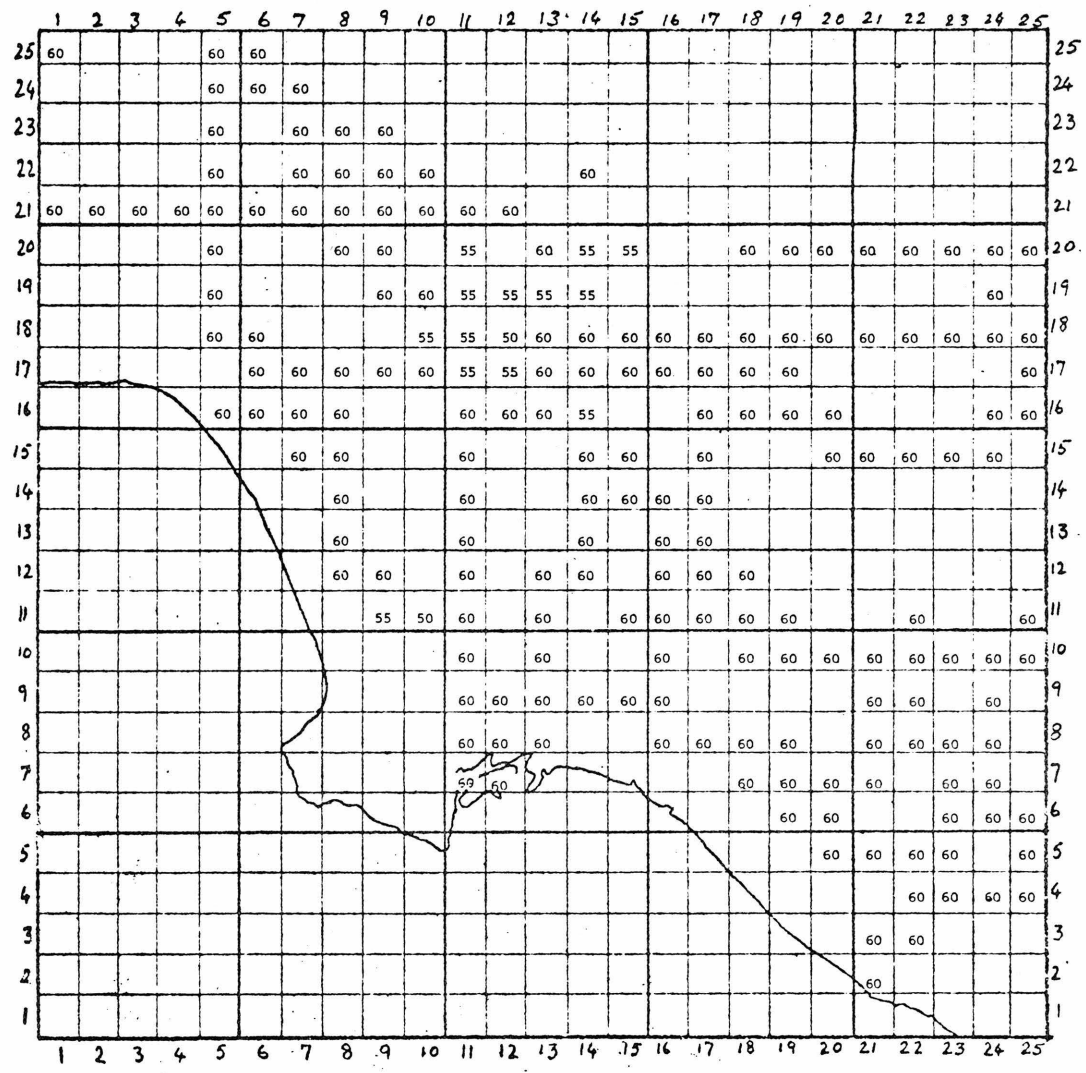

Figure C. 7 Average Vehicle Speed in "Fast" Direction ($\overline{v}_f$)

at 8:00 A. M.

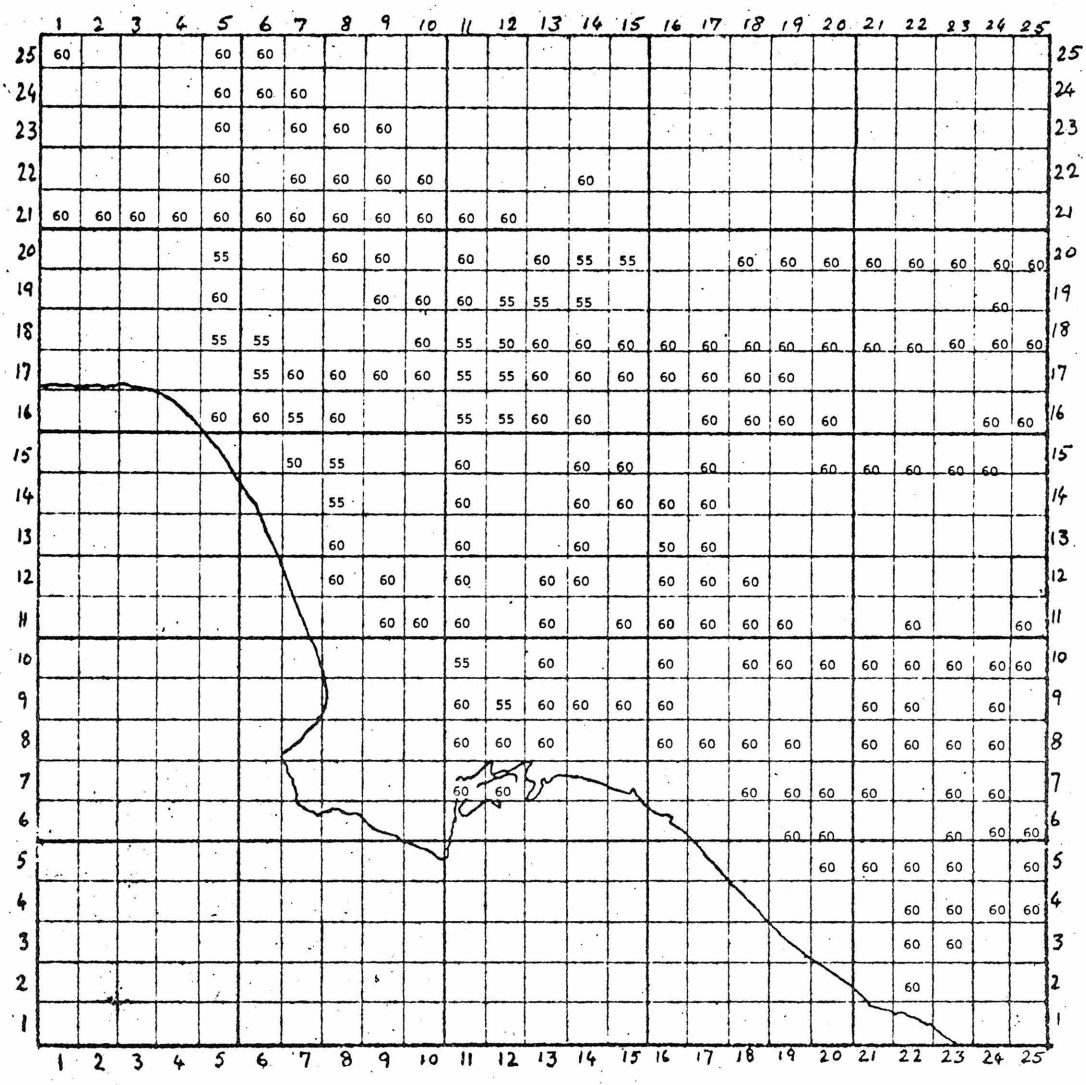

Figure C.8 Average Vehicle Speed in "Fast" Direction ($\overline{v}_f$)

at 9:00 A.M.

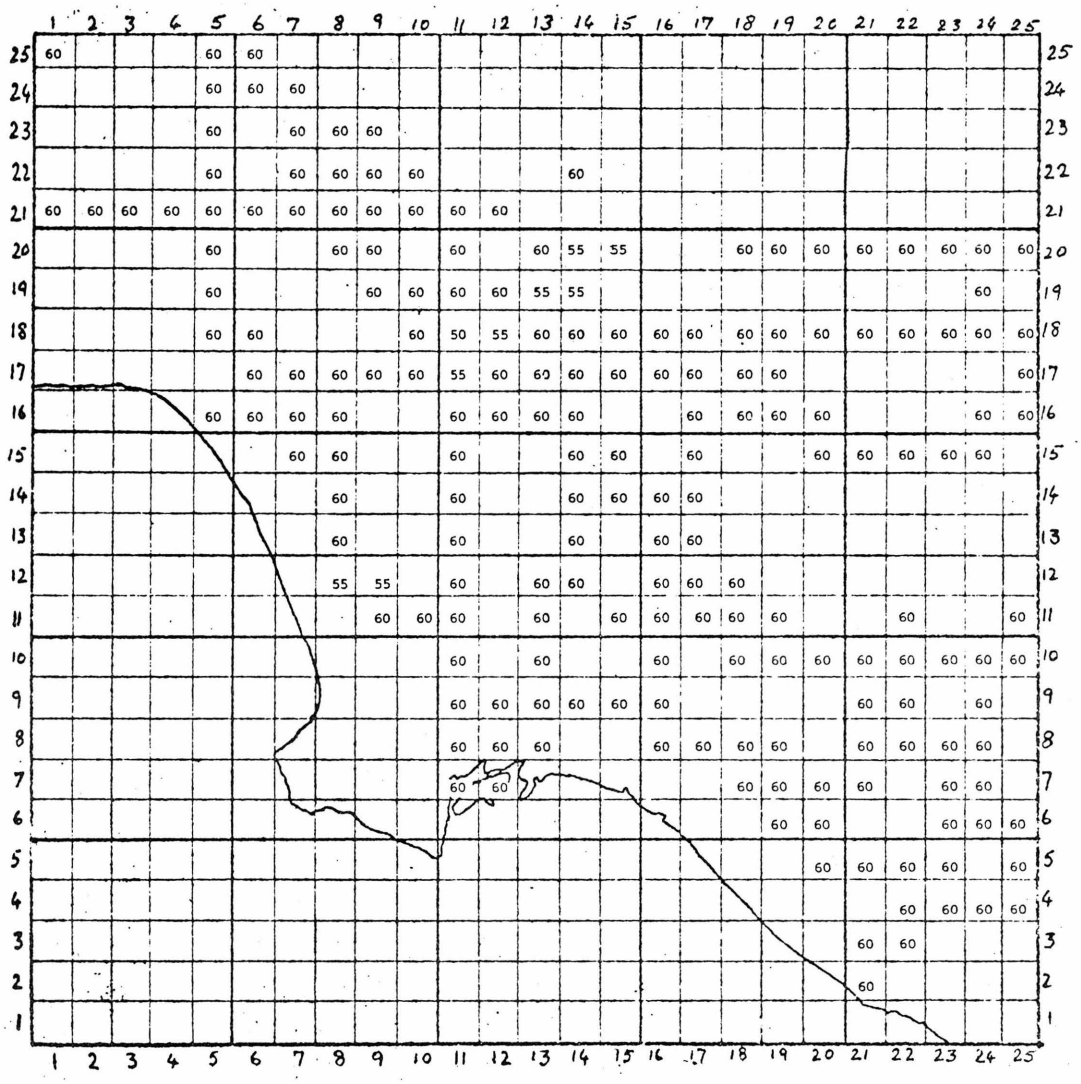

Figure C. 9 Ratio of Number of Vehicles Traveling in "Slow" Direction to the Number Traveling in "Fast" Direction, x, at 6:00 A. M.

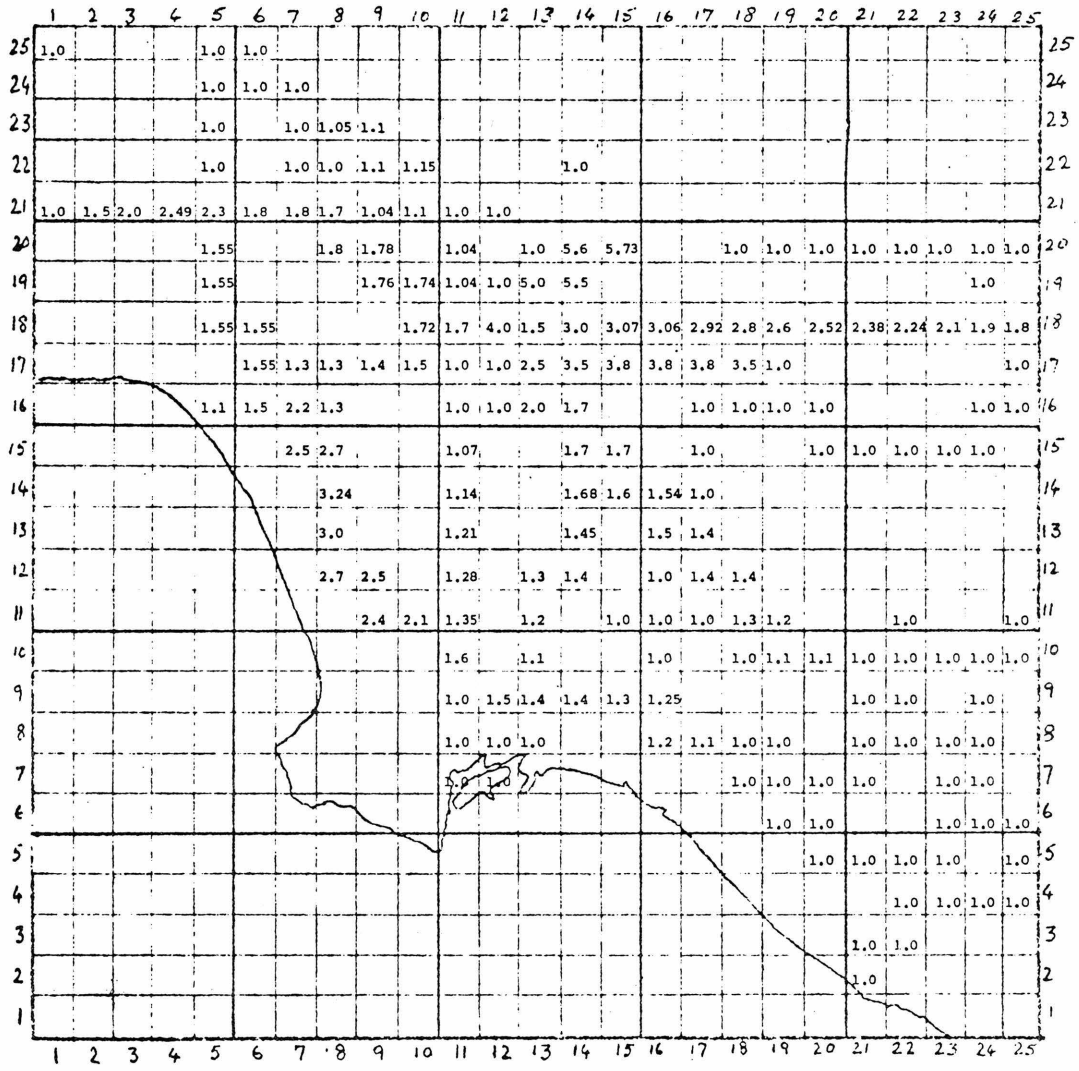

Figure C.10 Ratio of Number of Vehicles Traveling in "Slow" Direction to the Number Traveling in "Fast" Direction, x, at 7:00 A.M.

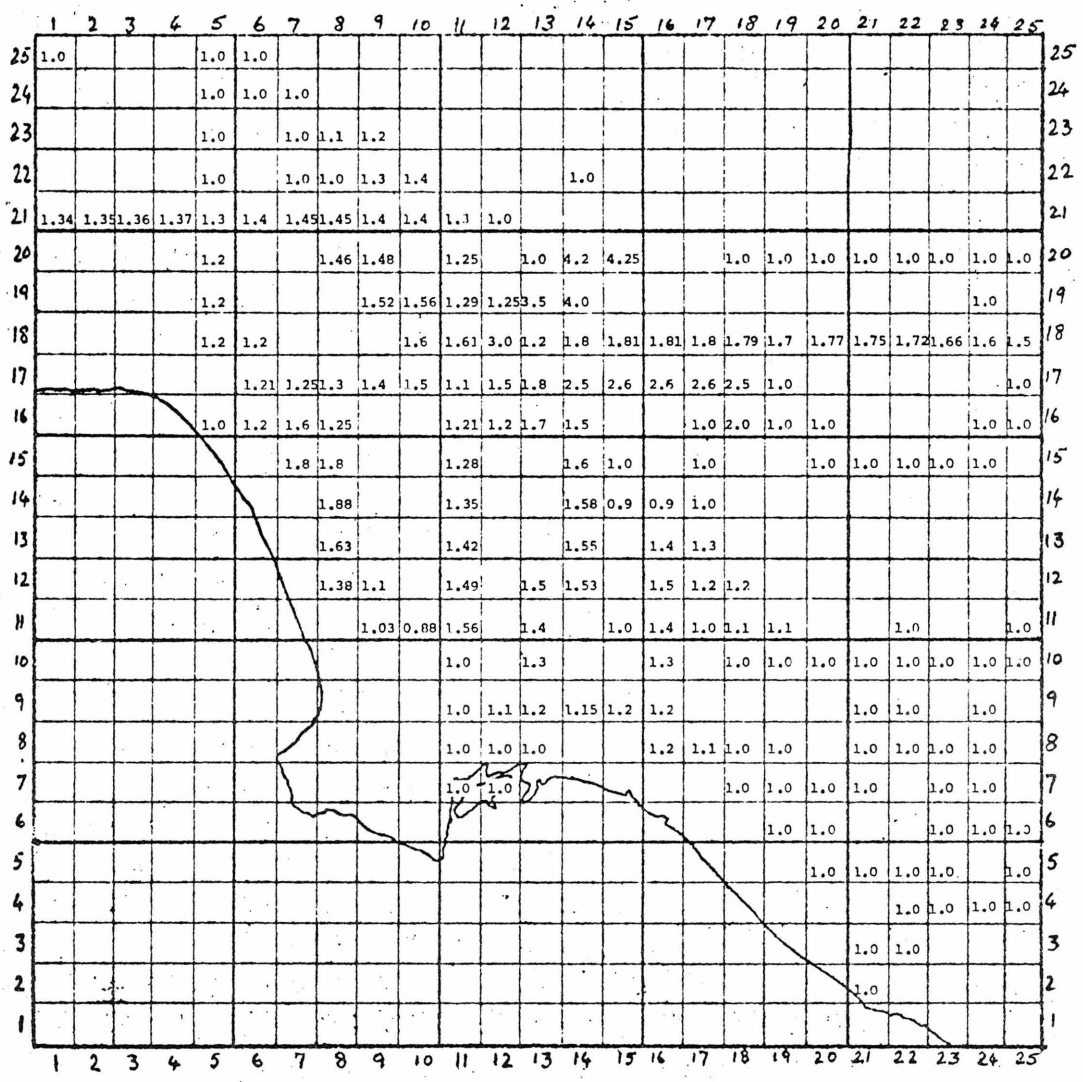

Figure C.11 Ratio of Number of Vehicles Traveling in "Slow" Direction to the Number Traveling in "Fast" Direction, x, at 8:00 A.M.

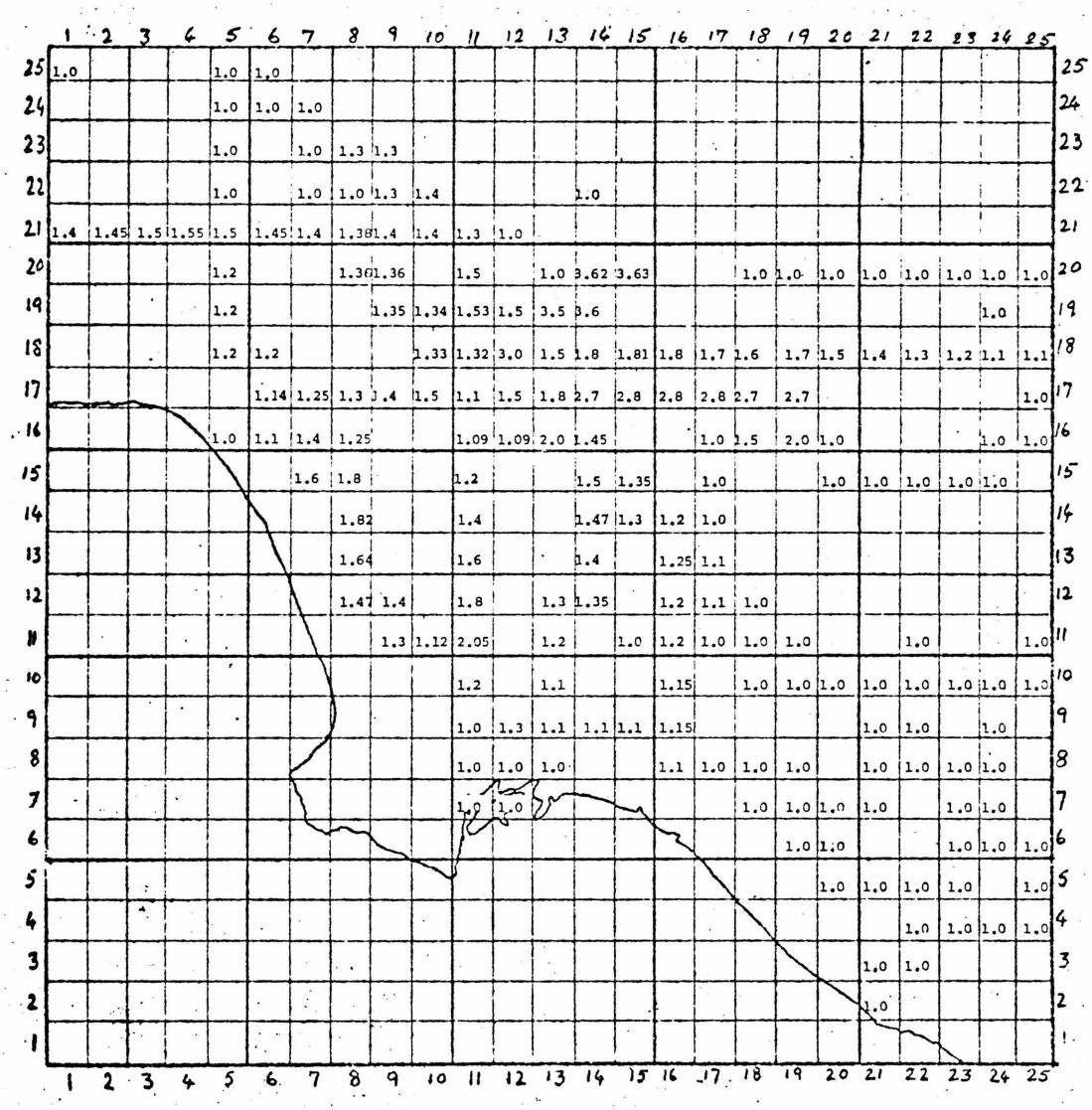

Figure C. 12 Ratio of Number of Vehicles Traveling in "Slow" Direction to the Number Traveling in "Fast" Direction, x, at 9:00 A. M.

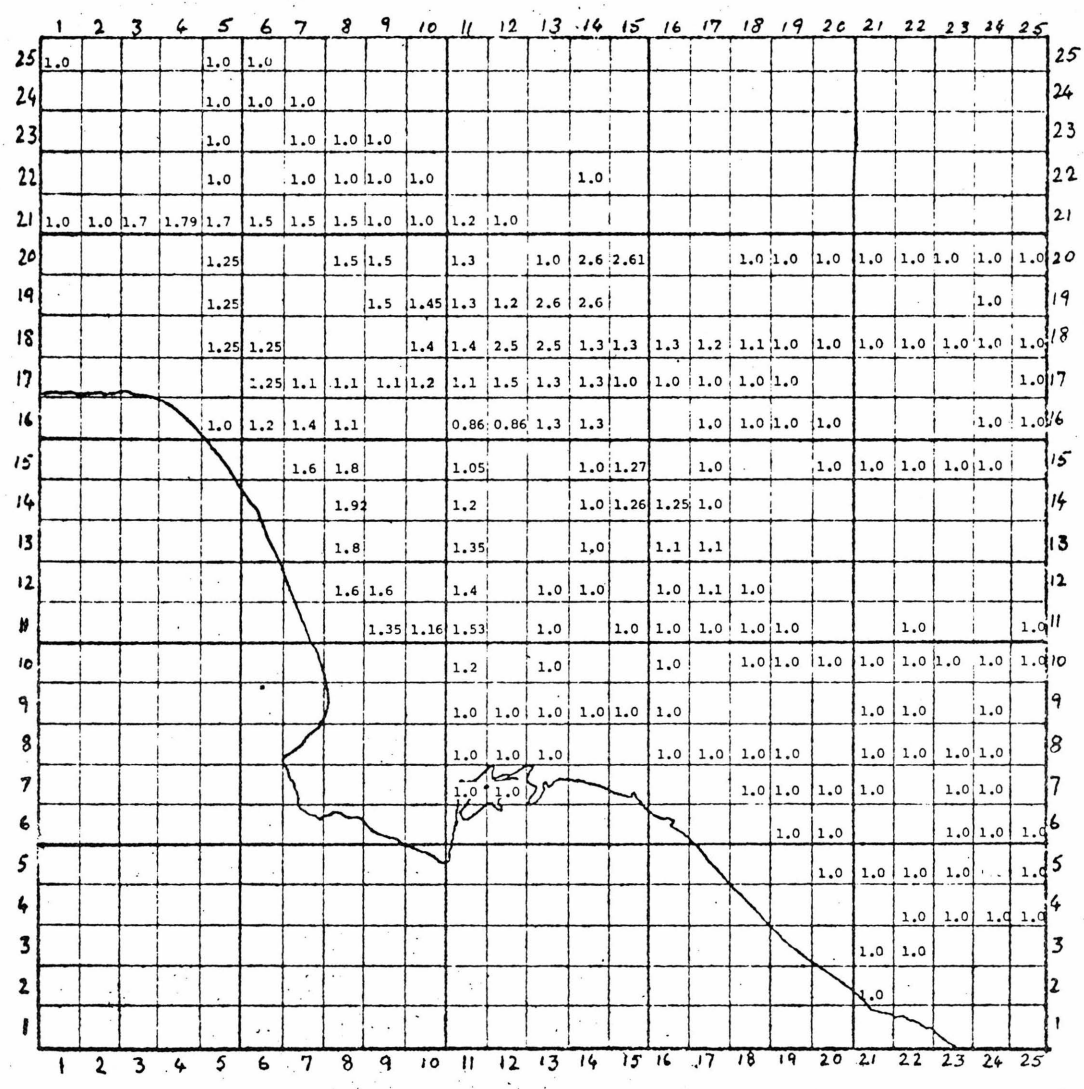

APPENDIX D

CALCULATION OF $\beta_\ell(t)$

The relationship for $\beta_\ell(t)$, the correction for the nonuniform distribution of trip starts, is derived in the following manner: let

t = time of day

T = length of FDC (minutes)

$c(t)$ = distribution of vehicle trip-start times, such that the number of vehicles started between times t and t + dt equals $c(t)dt$

τ = time elapsed after vehicle startup (minutes)

$\epsilon^c_\ell(\tau)$ = emissions from a vehicle at time τ after a cold-start (grams/mile)

$\epsilon^h_\ell(\tau)$ = emissions from a vehicle at time τ after a hot-start (grams/mile)

$y(t)$ = ratio of cold-starts to total starts during time interval dt

The number of vehicles started between time $t-\tau-d\tau$ and $t-\tau$ is given by $c(t-\tau)d\tau$. The emissions rate of species ℓ from a vehicle at time t, cold-started at the time $t-\tau$, is $\epsilon^c_\ell(\tau)$. Assuming that the average trip length for all vehicles is T, the total emissions rate of species ℓ at time t is given by

$$\int_0^T [y(t-\tau)\epsilon^c_\ell(\tau) + (1-y(t-\tau))\epsilon^h_\ell(\tau)]c(t-\tau)d\tau$$

and the average emissions rate from each vehicle by

$$E_{\ell}^{s}(t) = \frac{\int_{o}^{T} [y(t-\tau)\epsilon_{\ell}^{c}(\tau) + (1-y(t-\tau))\epsilon_{\ell}^{h}(\tau)]c(t-\tau)d\tau}{\int_{o}^{T} c(t-\tau)d\tau} \quad (D.1)$$

The correction factor is then defined as

$$\beta_{\ell}(t) = \frac{E_{\ell}^{s}(t)}{Q_{\ell}^{s}(t)} \quad (D.2)$$

where $Q_{\ell}^{s}(t)$ is given in equation 2.7.

In order to integrate equation (D.1), it is necessary to establish a functional form for ϵ_{ℓ}^{c} and $\epsilon_{\ell}^{h}(\tau)$. Recent data obtained from the EPA (Sigworth, 1972) show that engine operating temperatures reach steady-state levels about 8.5 minutes after a "cold-start." Based on this information, it is assumed that a simple relationship exists between $\epsilon_{\ell}^{c}(\tau)$ and time, as shown in Figure 2.3. A linear decrease in the emissions rate is postulated during the first 8.5 minutes of operation, after which the emissions rate is assumed constant. This constant rate is equal to $\epsilon_{\ell}^{h}(\tau)$, and, being constant over time is also equal to Q_{ℓ}^{h}. The slope of the $\epsilon_{\ell}^{c}(\tau)$ curve during the warmup period is calculated by equating the area under the solid line to the area under the dashed line in Figure 2.3.

In order to calculate $\beta_{\ell}(t)$ for carbon monoxide and hydrocarbons using equations (D.1) and (D.2), the temporal dependence of c(t) must be determined. Kearin et al. (1971) recently carried out a survey of average driving patterns for six urban areas in the United States. In their survey, based on a sample of 946 drivers (169 drivers

in the Los Angeles area),* they were able to estimate for each area average trip distances, trip elapsed times, average speed, elapsed time between trips, number of trips per day, and other pertinent variables. Of particular interest is their estimated distribution of weekday trip-starts for the Los Angeles area, which is reproduced in Figure 2.5.

The calculation of $\beta_{\ell}(t)$ is carried out as follows. Let the total number of trips started in the fifteen minute interval, denoted by n, be equal to c_n. Assuming the trip-start rate to be uniform during each fifteen minute interval, the integrals in equation (D.1) can be approximated by:

$$E^s_{\ell}(t_n) = \frac{\frac{c_{n-2}}{30}\,\epsilon^h_{\ell} + c_{n-1}\{(1-y_{n-1})\epsilon^h_{\ell} + y_{n-1}\bar{\epsilon}_{\ell}\} + \frac{c_n}{2}\{(1-y_n)\epsilon^h_{\ell} + y_n\tilde{\epsilon}_{\ell}\}}{\frac{c_{n-2}}{30} + c_{n-1} + \frac{c_n}{2}} \qquad \text{(D.3)}$$

where

n = denotes a fifteen minute time interval

$E^s_{\ell}(t_n)$ = Average emissions rate of species ℓ evaluated at the midpoint of time interval n.

$\bar{\epsilon}_{\ell}$ = Average emissions rate of species ℓ from an automobile over the time period between 7.5 and 22.5 minutes after a cold-start.

---

* Kearin et al. note that "...when one considers the number of automobile trips made daily in even the smallest of the cities sampled, it becomes clear that our sample sizes are puny...." Thus, while the statistics employed in this analysis are the most useful available, their reliability is clearly subject to question, and they must be used with caution.

$\tilde{\epsilon}_\ell$ = Average emissions rate of species ℓ from an automobile over the time period between zero and 7.5 minutes after a cold-start.

Using the emissions factors given earlier, $\bar{\epsilon}_\ell$ and $\tilde{\epsilon}_\ell$ are estimated to be:

Species	$\bar{\epsilon}_\ell$ (grams/mile)	$\tilde{\epsilon}_\ell$ (grams/mile)
CO	69.1	136.2
HC	10.82	13.52

In using the results of Kearin et al., the weekday is segmented into eight time periods, as suggested by the slope of the curve in Figure 2.5. A constant value of y, the ratio of cold-starts to total starts, is assigned to each period. These values of y given in Table D.1, the values of $Q_\ell^s(t)$ given in the same table, the emissions curve of Figure 2.4, and the distribution of vehicle startups c_n shown in Figure 2.5 form the basis for evaluating equation (D.3) to obtain $\beta_{CO}(t)$ and $\beta_{HC}(t)$. The results of these integrations are given in Figure 2.4. Note, again, that $\beta_{NO_x}(t) = 1$, as $Q^h_{NO_x} = Q^c_{NO_x}$.

Table D.1 Temporal Distribution of Cold-Starts

n	Time Period	c_n* % of daily trips started	y_n fraction of cold-starts to total starts	Q_ℓ** emissions rate (grams/mile) CO	HC
1	0:00 - 5:59	2.0	0.90	88.8	11.61
2	6:00 - 8:59	21.0	0.85	87.6	11.57
3	9:00 - 11:29	6.9	0.25	74.2	11.03
4	11:30 - 13:29	10.7	0.30	75.3	11.07
5	13:30 - 16:29	12.1	0.20	73.1	10.98
6	16:30 - 18:29	24.7	0.50	79.8	11.25
7	18:30 - 20:59	16.1	0.15	72.0	10.94
8	21:00 - 23:59	6.5	0.20	73.1	10.98

Note: Kearin et al. (1971) have estimated that a vehicle in Los Angeles makes an average of 4.66 trips per weekday. Of these 4.66 trips it is estimated that 2 are cold-started and 2.66 are hot-started. Thus:

$$\sum_{n=1}^{8} y_n c_n = 42.92, \text{ and } \sum_{n=1}^{8} (1-y_n)c_n = 57.08$$

Using the figures from the above table:

$$\sum_{n=1}^{8} y_n c_n \approx 43\%, \text{ and } \sum_{n=1}^{8} (1-y_n)c_n \approx 57\%$$

---

* Estimated from Figure 2.5.

** These entries should be multiplied by $\beta_\ell(t)$ (Figure 2.4) to obtain the surface street emissions factors, $E^s_\ell(t)$. ($\beta_\ell(t) = 1$, except for the period 6:00 - 9:23 A.M.)

APPENDIX E

SUMMARY OF 1969 VALIDATION RESULTS

The figures in this Appendix represent a complete summary of all comparisons of predicted and measured concentrations for those monitoring sites operating on the six validation days. The results for each day are grouped together, as indicated in the following table.

Validation Day	Figures
September 9, 1969	E.1 - E.7
September 29, 1969	E.8 - E.14
September 30, 1969	E.15 - E.21
October 29, 1969	E.22 - E.28
October 30, 1969	E.29 - E.35
November 4, 1969	E.36 - E.42

Those pollutants measured at monitoring stations operated in the modeling region by the Los Angeles and Orange County Air Pollution Control Districts and Scott Research Laboratories (1970) are summarized in Table E.1.

Table E.1

Pollutants Measured at Air Quality Monitoring Stations
Operative in the Los Angeles Basin in 1969

Station	CO	NO	NO_2	Oxidant	Total Hydrocarbon	Methane
Reseda	X	X	X	X		
Burbank	X	X	X	X		
Pasadena	X	X	X	X	X	X
Azusa	X	X	X	X	X	X
El Monte	X	X	X	X	X	
Downtown LA	X	X	X	X	X	X
Pomona	X	X	X	X		
West LA	X	X	X	X		
Commerce	X	X	X	X	X	
Lennox	X	X	X	X		
Whittier	X	X	X	X		
La Habra		X	X	X		
Long Beach	X	X	X	X		
Anaheim	X	X	X	X	X	
Santa Ana				X		

Figure E.1

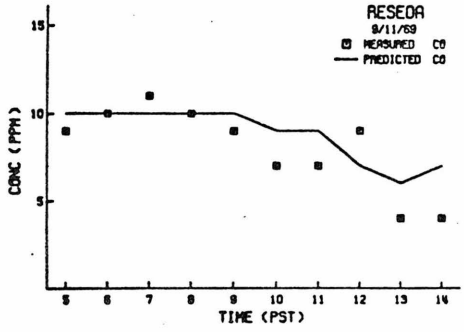
RESEDA
9/11/69
MEASURED CO
PREDICTED CO
CONC (PPM)
TIME (PST)

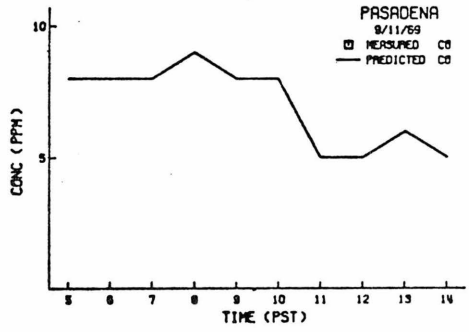
PASADENA
9/11/69
MEASURED CO
PREDICTED CO
CONC (PPM)
TIME (PST)

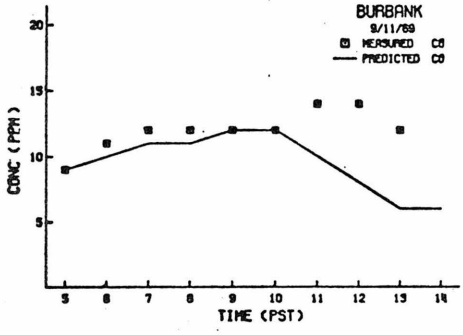
BURBANK
9/11/69
MEASURED CO
PREDICTED CO
CONC (PPM)
TIME (PST)

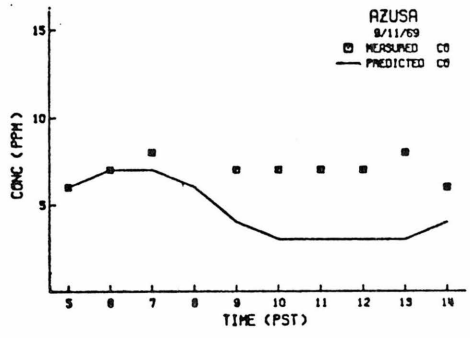
AZUSA
9/11/69
MEASURED CO
PREDICTED CO
CONC (PPM)
TIME (PST)

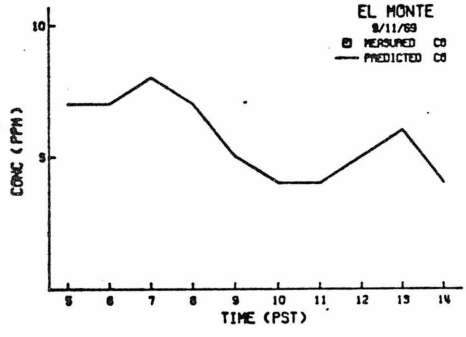
EL MONTE
9/11/69
MEASURED CO
PREDICTED CO
CONC (PPM)
TIME (PST)

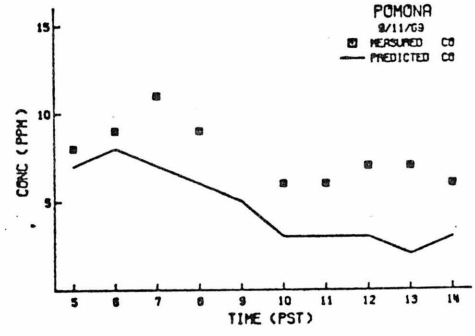
POMONA
9/11/69
MEASURED CO
PREDICTED CO
CONC (PPM)
TIME (PST)

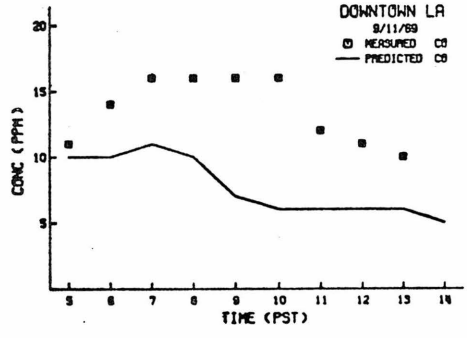
DOWNTOWN LA
9/11/69
MEASURED CO
PREDICTED CO
CONC (PPM)
TIME (PST)

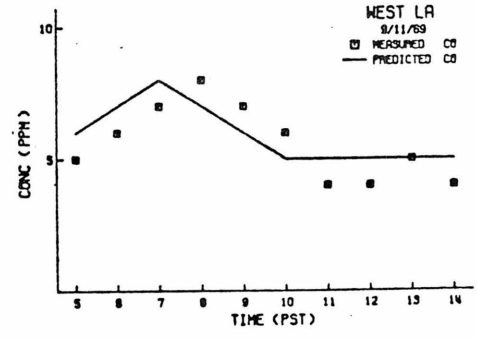
WEST LA
9/11/69
MEASURED CO
PREDICTED CO
CONC (PPM)
TIME (PST)

Figure E.2

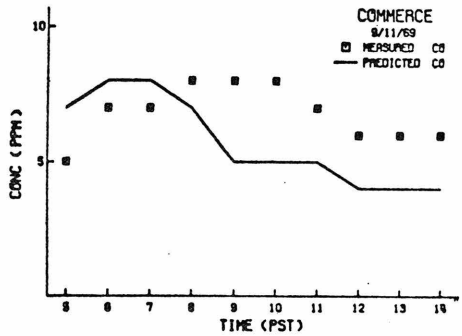
COMMERCE
9/11/69
MEASURED CO
PREDICTED CO
CONC (PPM)
TIME (PST)

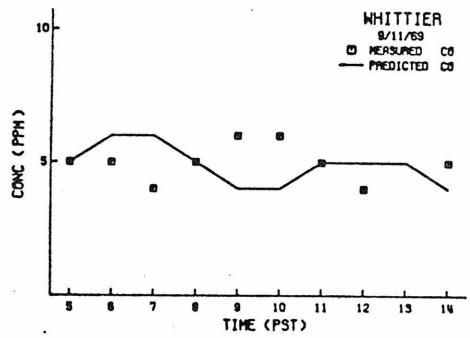
WHITTIER
9/11/69
MEASURED CO
PREDICTED CO
CONC (PPM)
TIME (PST)

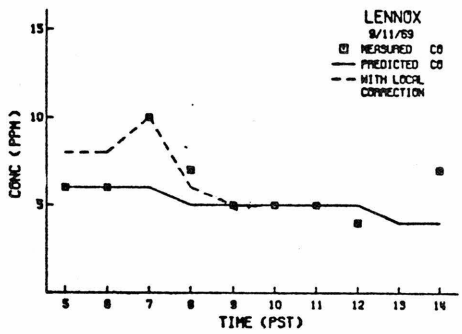
LENNOX
9/11/69
MEASURED CO
PREDICTED CO
WITH LOCAL CORRECTION
CONC (PPM)
TIME (PST)

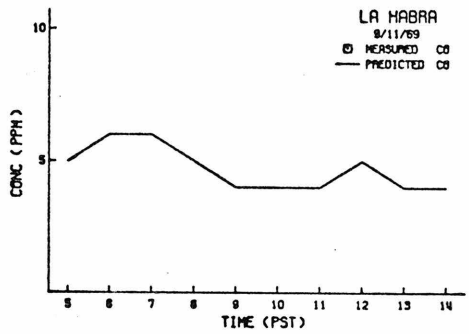
LA HABRA
9/11/69
MEASURED CO
PREDICTED CO
CONC (PPM)
TIME (PST)

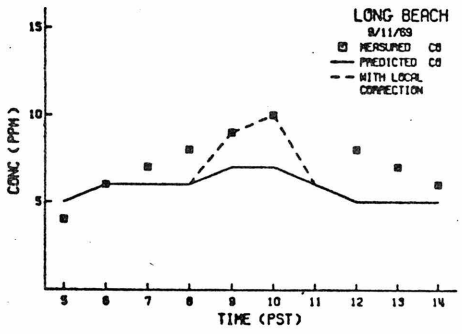
LONG BEACH
9/11/69
MEASURED CO
PREDICTED CO
WITH LOCAL CORRECTION
CONC (PPM)
TIME (PST)

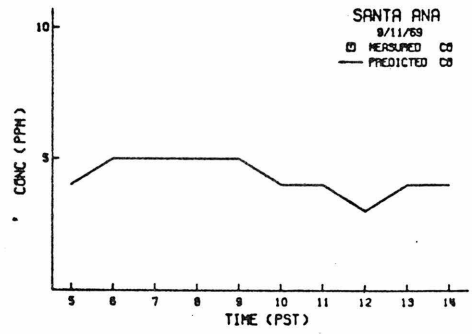
SANTA ANA
9/11/69
MEASURED CO
PREDICTED CO
CONC (PPM)
TIME (PST)

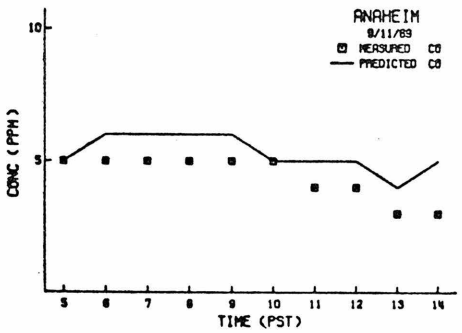
ANAHEIM
9/11/69
MEASURED CO
PREDICTED CO
CONC (PPM)
TIME (PST)

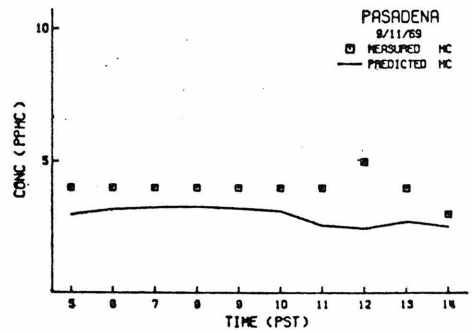
PASADENA
9/11/69
MEASURED HC
PREDICTED HC
CONC (PPMC)
TIME (PST)

Figure E.3

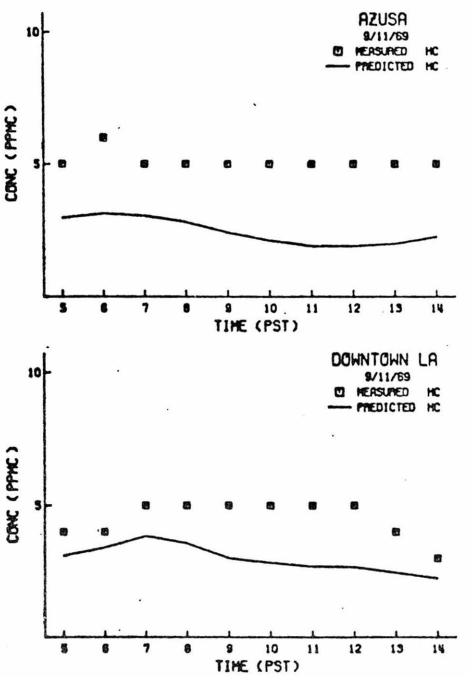
AZUSA
9/11/69
MEASURED HC
PREDICTED HC
CONC (PPMC)
10
5
5 6 7 8 9 10 11 12 13 14
TIME (PST)
DOWNTOWN LA
9/11/69
MEASURED HC
PREDICTED HC
CONC (PPMC)
10
5
5 6 7 8 9 10 11 12 13 14
TIME (PST)

Figure E.4

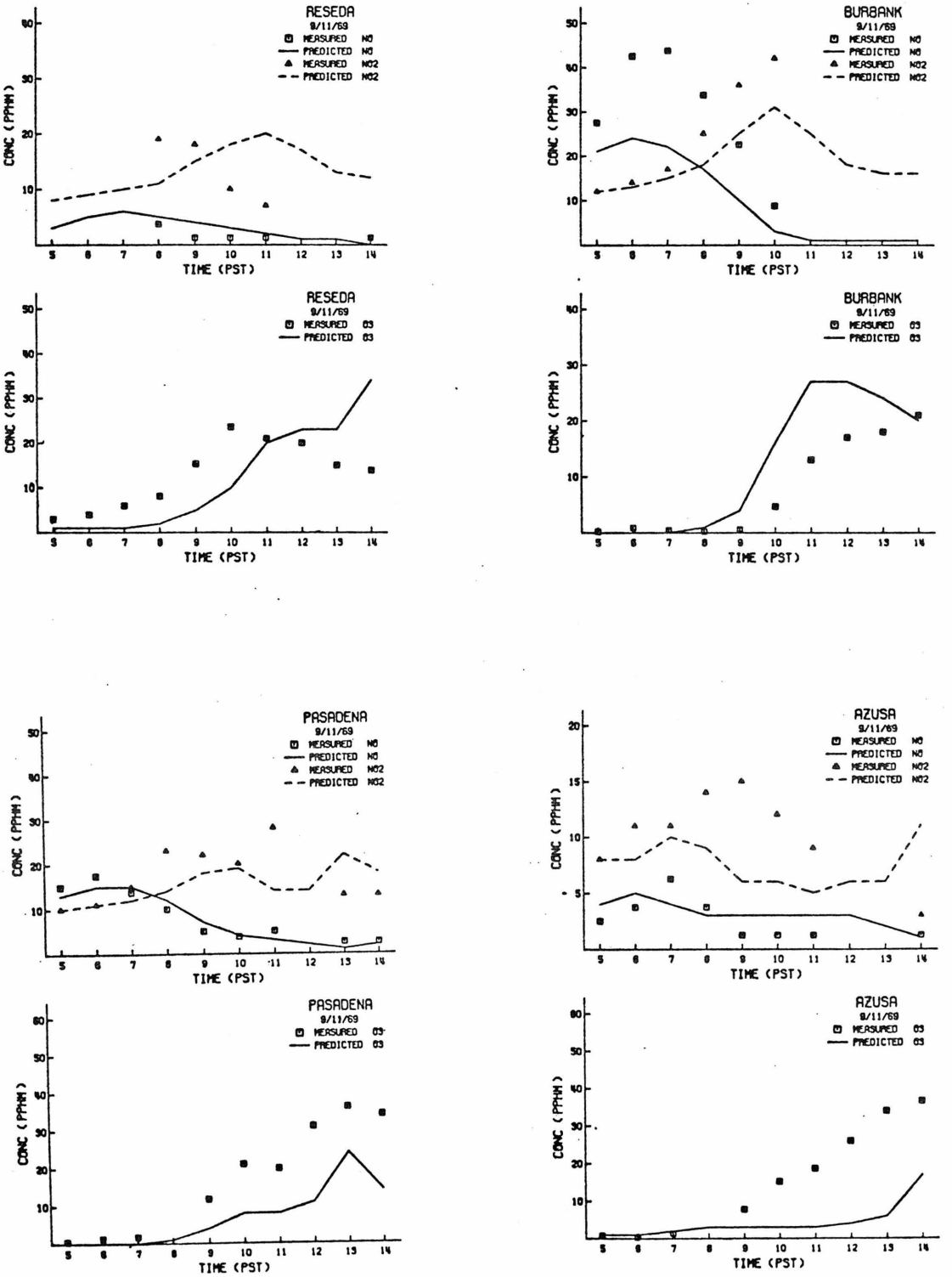
RESEDA
9/11/69
MEASURED NO
PREDICTED NO
MEASURED NO2
PREDICTED NO2
CONC (PPHM)
TIME (PST)
RESEDA
9/11/69
MEASURED O3
PREDICTED O3
CONC (PPHM)
TIME (PST)
BURBANK
9/11/69
MEASURED NO
PREDICTED NO
MEASURED NO2
PREDICTED NO2
CONC (PPHM)
TIME (PST)
BURBANK
9/11/69
MEASURED O3
PREDICTED O3
CONC (PPHM)
TIME (PST)
PASADENA
9/11/69
MEASURED NO
PREDICTED NO
MEASURED NO2
PREDICTED NO2
CONC (PPHM)
TIME (PST)
PASADENA
9/11/69
MEASURED O3
PREDICTED O3
CONC (PPHM)
TIME (PST)
AZUSA
9/11/69
MEASURED NO
PREDICTED NO
MEASURED NO2
PREDICTED NO2
CONC (PPHM)
TIME (PST)
AZUSA
9/11/69
MEASURED O3
PREDICTED O3
CONC (PPHM)
TIME (PST)

Figure E, 5

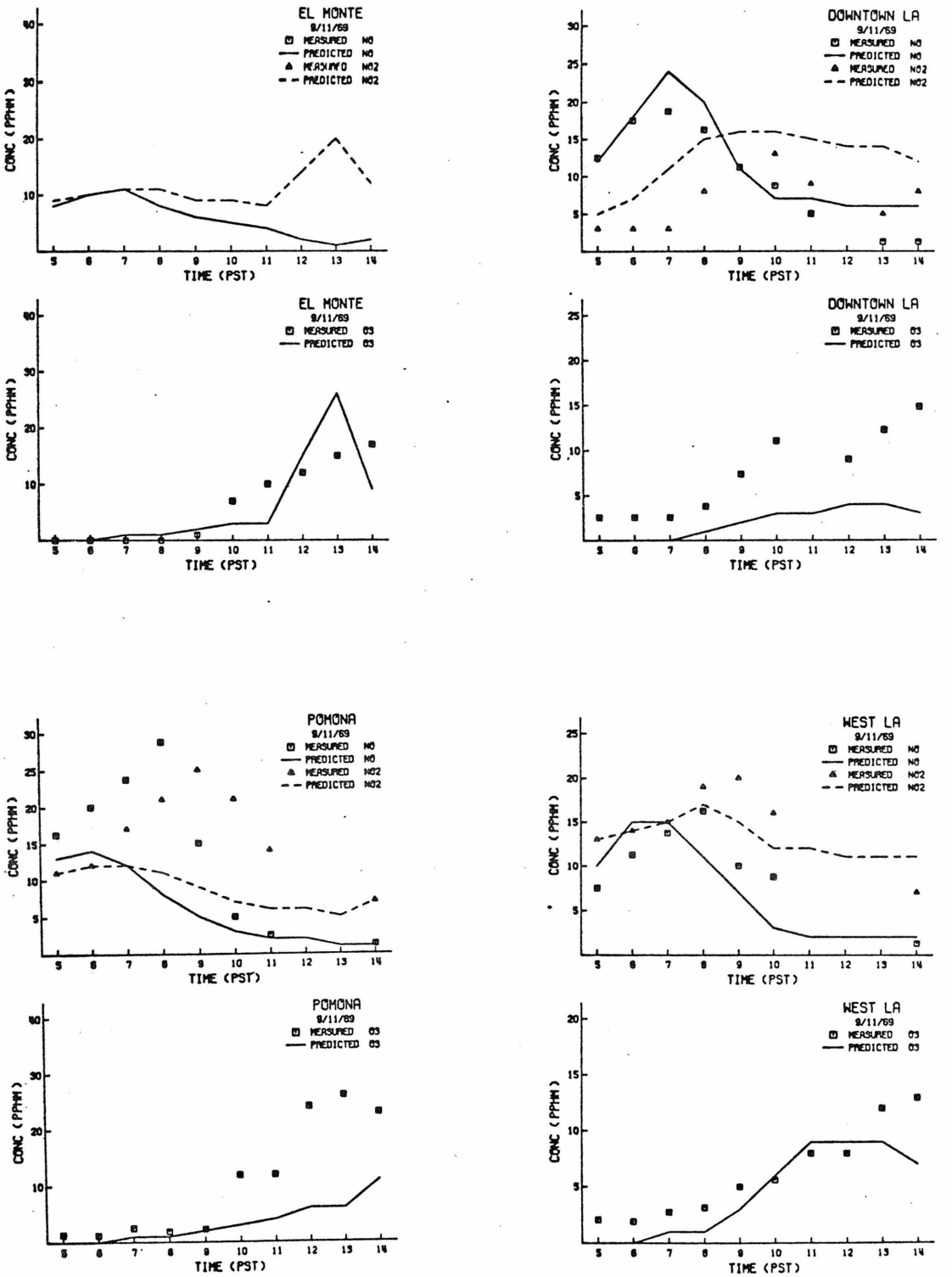
EL MONTE
9/11/69
MEASURED NO
PREDICTED NO
MEASURED NO2
PREDICTED NO2
CONC (PPHM)
TIME (PST)
EL MONTE
9/11/69
MEASURED O3
PREDICTED O3
CONC (PPHM)
TIME (PST)
DOWNTOWN LA
9/11/69
MEASURED NO
PREDICTED NO
MEASURED NO2
PREDICTED NO2
CONC (PPHM)
TIME (PST)
DOWNTOWN LA
9/11/69
MEASURED O3
PREDICTED O3
CONC (PPHM)
TIME (PST)
POMONA
9/11/69
MEASURED NO
PREDICTED NO
MEASURED NO2
PREDICTED NO2
CONC (PPHM)
TIME (PST)
POMONA
9/11/69
MEASURED O3
PREDICTED O3
CONC (PPHM)
TIME (PST)
WEST LA
9/11/69
MEASURED NO
PREDICTED NO
MEASURED NO2
PREDICTED NO2
CONC (PPHM)
TIME (PST)
WEST LA
9/11/69
MEASURED O3
PREDICTED O3
CONC (PPHM)
TIME (PST)

Figure E.6

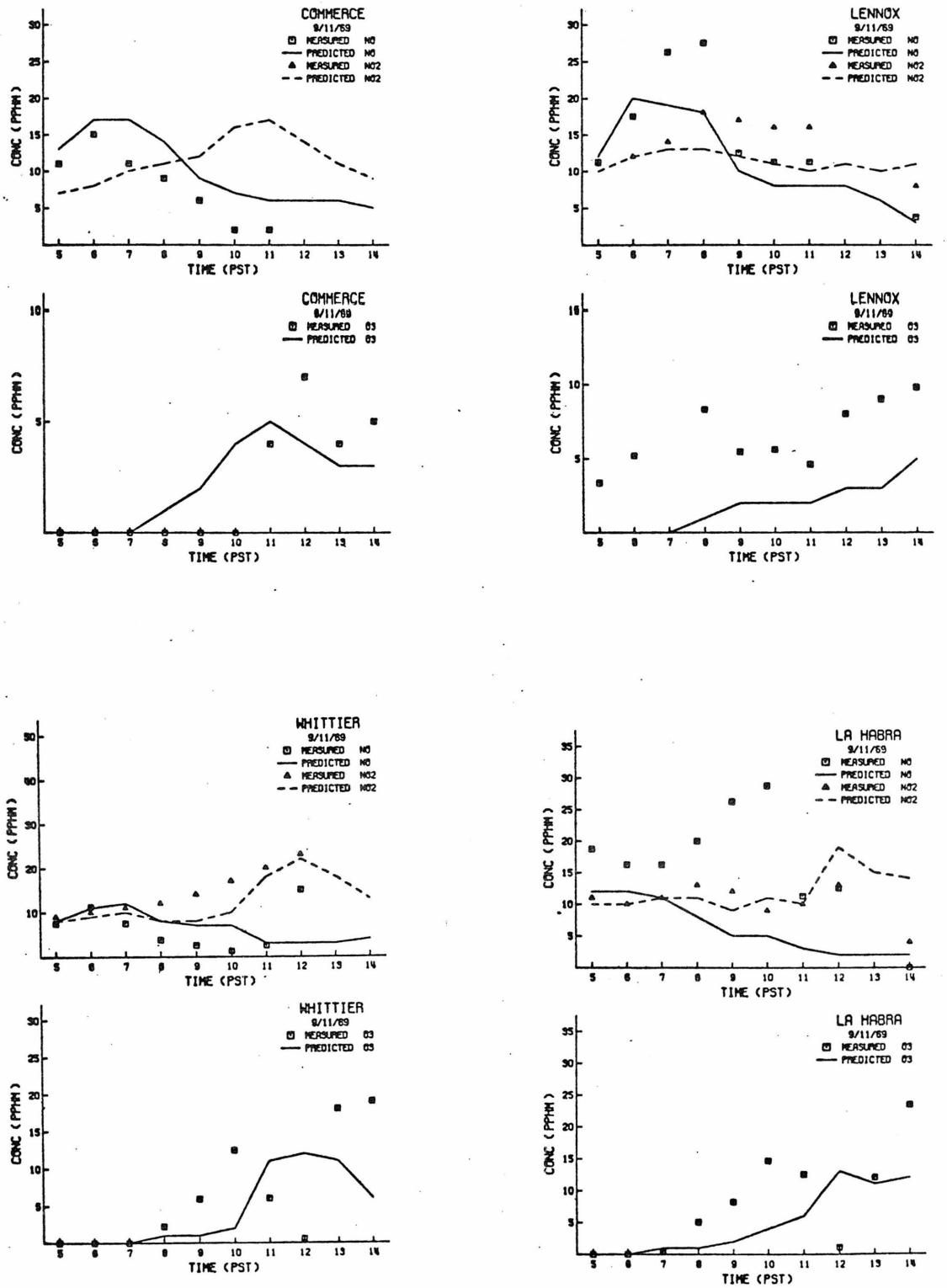
COMMERCE
9/11/69
MEASURED NO
PREDICTED NO
MEASURED NO2
PREDICTED NO2
CONC (PPHM)
TIME (PST)
LENNOX
9/11/69
MEASURED NO
PREDICTED NO
MEASURED NO2
PREDICTED NO2
CONC (PPHM)
TIME (PST)
COMMERCE
9/11/69
MEASURED O3
PREDICTED O3
CONC (PPHM)
TIME (PST)
LENNOX
9/11/69
MEASURED O3
PREDICTED O3
CONC (PPHM)
TIME (PST)
WHITTIER
9/11/69
MEASURED NO
PREDICTED NO
MEASURED NO2
PREDICTED NO2
CONC (PPHM)
TIME (PST)
LA HABRA
9/11/69
MEASURED NO
PREDICTED NO
MEASURED NO2
PREDICTED NO2
CONC (PPHM)
TIME (PST)
WHITTIER
9/11/69
MEASURED O3
PREDICTED O3
CONC (PPHM)
TIME (PST)
LA HABRA
9/11/69
MEASURED O3
PREDICTED O3
CONC (PPHM)
TIME (PST)

Figure E.7

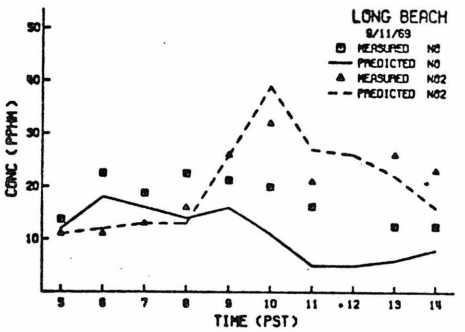
LONG BEACH
9/11/69
MEASURED NO
PREDICTED NO
MEASURED NO2
PREDICTED NO2
CONC (PPM)
TIME (PST)

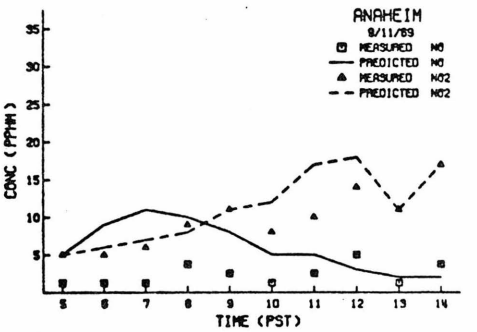
ANAHEIM
9/11/69
MEASURED NO
PREDICTED NO
MEASURED NO2
PREDICTED NO2
CONC (PPM)
TIME (PST)

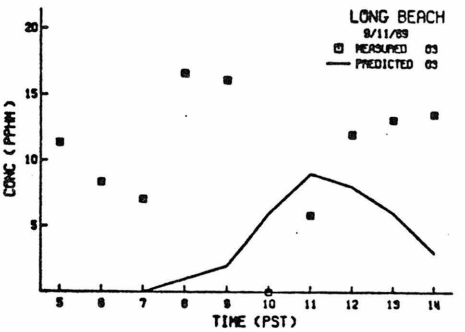
LONG BEACH
9/11/69
MEASURED O3
PREDICTED O3
CONC (PPM)
TIME (PST)

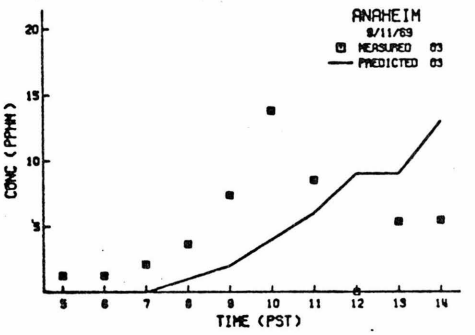
ANAHEIM
9/11/69
MEASURED O3
PREDICTED O3
CONC (PPM)
TIME (PST)

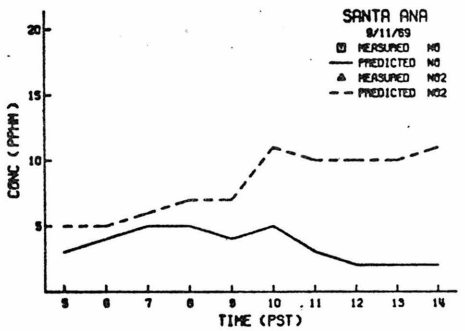
SANTA ANA
9/11/69
MEASURED NO
PREDICTED NO
MEASURED NO2
PREDICTED NO2
CONC (PPM)
TIME (PST)

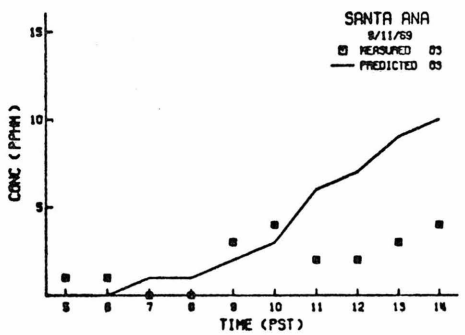
SANTA ANA
9/11/69
MEASURED O3
PREDICTED O3
CONC (PPM)
TIME (PST)

Figure E.8

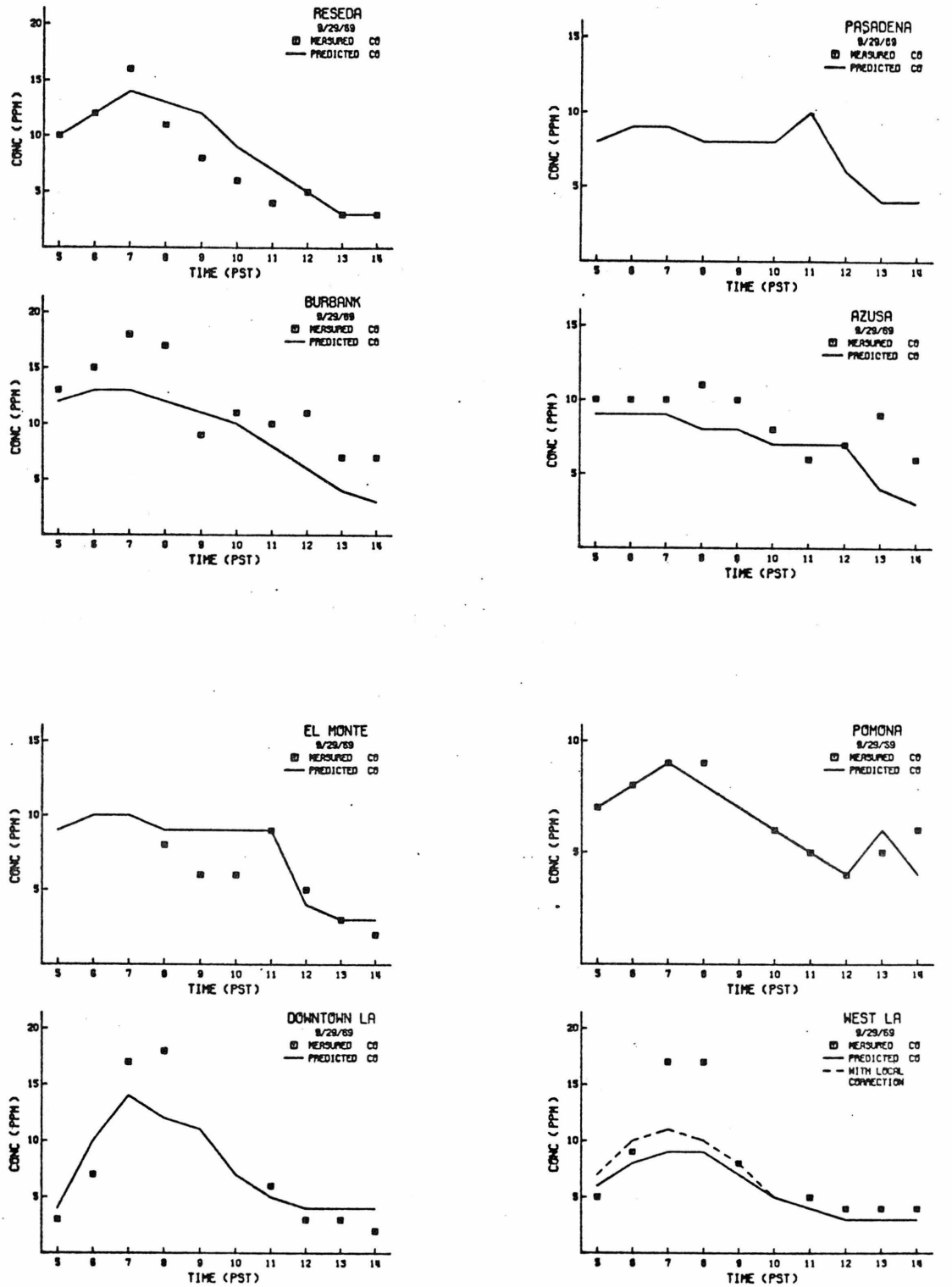
RESEDA
9/29/69
MEASURED CO
PREDICTED CO
CONC (PPM)
TIME (PST)
PASADENA
9/29/69
MEASURED CO
PREDICTED CO
CONC (PPM)
TIME (PST)
BURBANK
9/29/69
MEASURED CO
PREDICTED CO
CONC (PPM)
TIME (PST)
AZUSA
9/29/69
MEASURED CO
PREDICTED CO
CONC (PPM)
TIME (PST)
EL MONTE
9/29/69
MEASURED CO
PREDICTED CO
CONC (PPM)
TIME (PST)
POMONA
9/29/69
MEASURED CO
PREDICTED CO
CONC (PPM)
TIME (PST)
DOWNTOWN LA
9/29/69
MEASURED CO
PREDICTED CO
CONC (PPM)
TIME (PST)
WEST LA
9/29/69
MEASURED CO
PREDICTED CO
WITH LOCAL CONNECTION
CONC (PPM)
TIME (PST)

Figure E.9

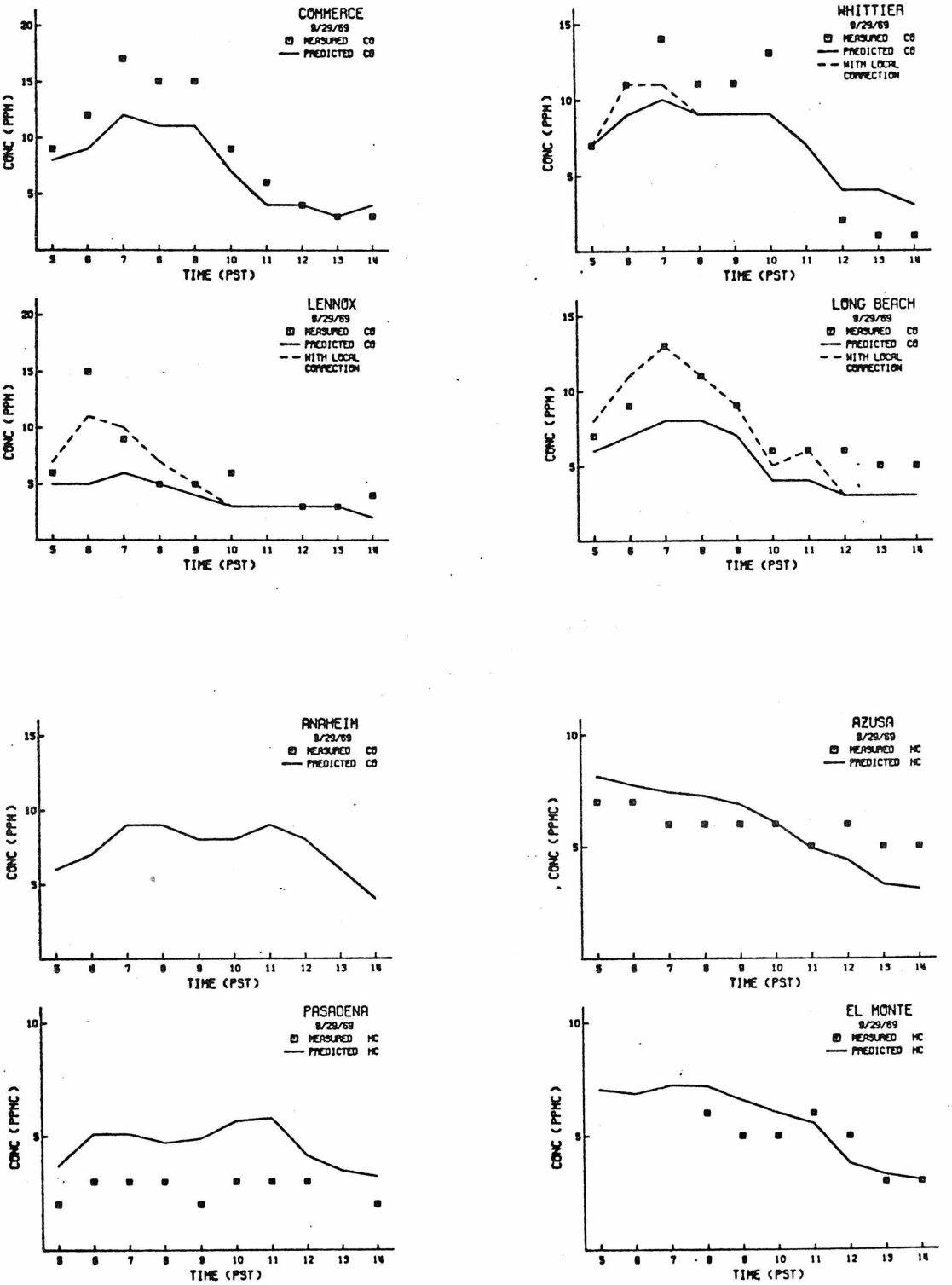
COMMERCE
9/29/69
MEASURED CO
PREDICTED CO
CONC (PPM)
TIME (PST)
WHITTIER
9/29/69
MEASURED CO
PREDICTED CO
WITH LOCAL CORRECTION
CONC (PPM)
TIME (PST)
LENNOX
9/29/69
MEASURED CO
PREDICTED CO
WITH LOCAL CORRECTION
CONC (PPM)
TIME (PST)
LONG BEACH
9/29/69
MEASURED CO
PREDICTED CO
WITH LOCAL CORRECTION
CONC (PPM)
TIME (PST)
ANAHEIM
9/29/69
MEASURED CO
PREDICTED CO
CONC (PPM)
TIME (PST)
AZUSA
9/29/69
MEASURED HC
PREDICTED HC
CONC (PPMC)
TIME (PST)
PASADENA
9/29/69
MEASURED HC
PREDICTED HC
CONC (PPMC)
TIME (PST)
EL MONTE
9/29/69
MEASURED HC
PREDICTED HC
CONC (PPMC)
TIME (PST)

Figure E.10

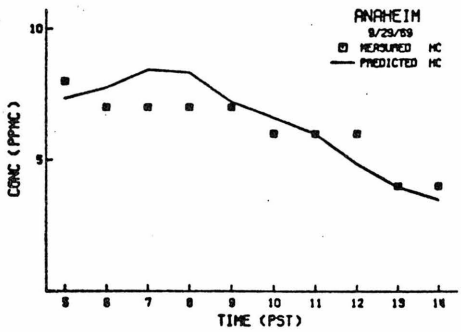
ANAHEIM
9/29/69
MEASURED HC
PREDICTED HC
CONC (PPMC)
TIME (PST)

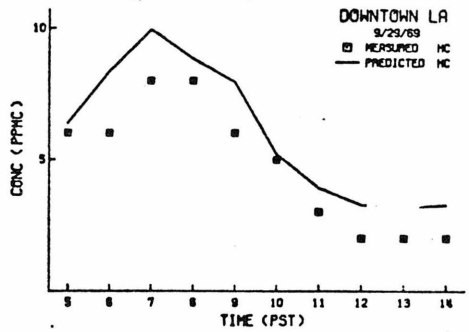
DOWNTOWN LA
9/29/69
MEASURED HC
PREDICTED HC
CONC (PPMC)
TIME (PST)

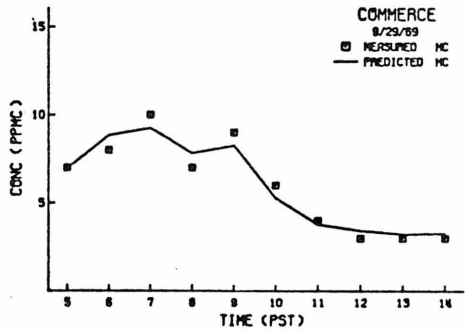
COMMERCE
9/29/69
MEASURED HC
PREDICTED HC
CONC (PPMC)
TIME (PST)

Figure E. 11

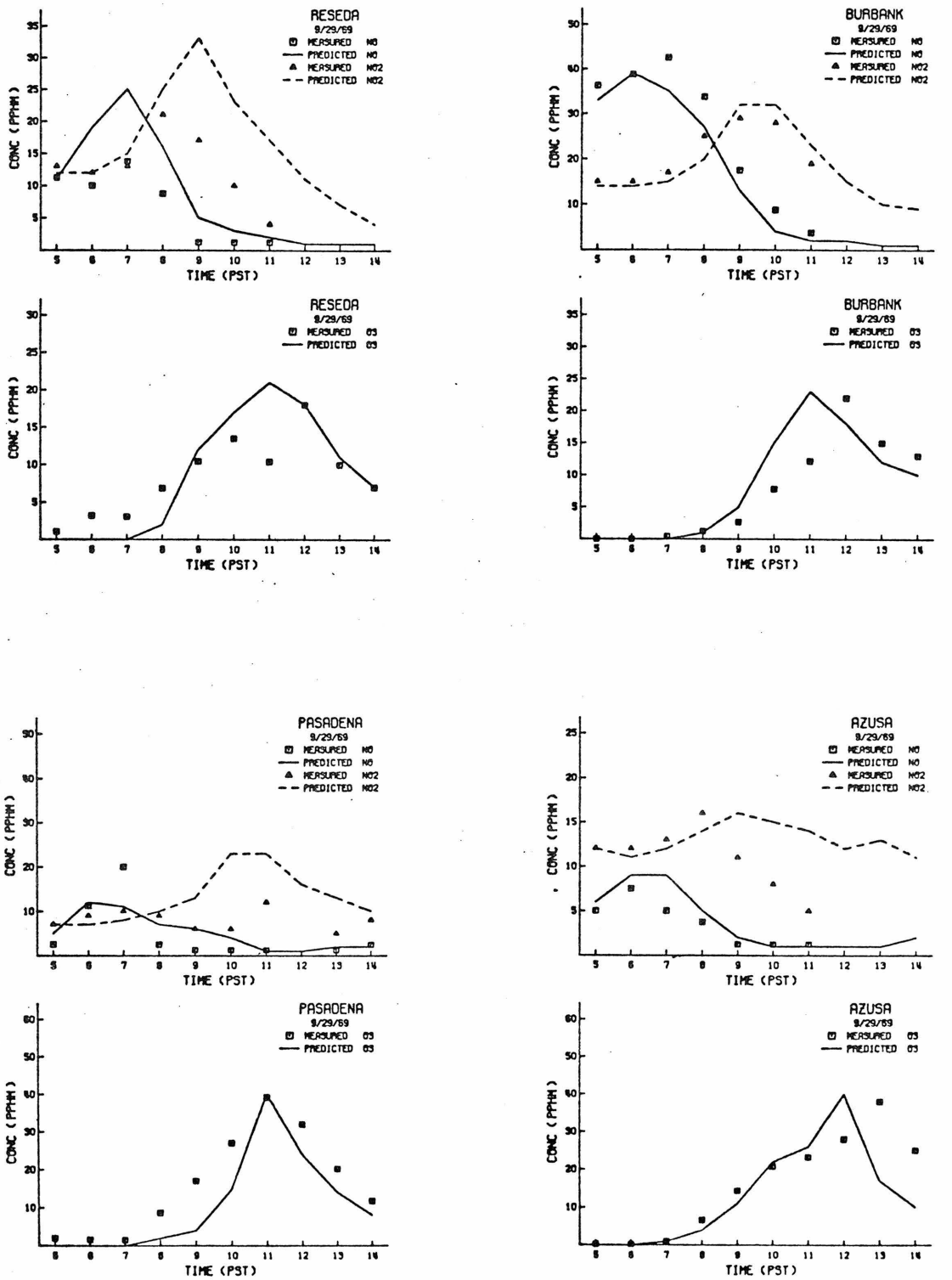
RESEDA
9/29/69
MEASURED NO
PREDICTED NO
MEASURED NO2
PREDICTED NO2
CONC (PPHM)
TIME (PST)
BURBANK
9/29/69
MEASURED NO
PREDICTED NO
MEASURED NO2
PREDICTED NO2
CONC (PPHM)
TIME (PST)
RESEDA
9/29/69
MEASURED O3
PREDICTED O3
CONC (PPHM)
TIME (PST)
BURBANK
9/29/69
MEASURED O3
PREDICTED O3
CONC (PPHM)
TIME (PST)
PASADENA
9/29/69
MEASURED NO
PREDICTED NO
MEASURED NO2
PREDICTED NO2
CONC (PPHM)
TIME (PST)
AZUSA
9/29/69
MEASURED NO
PREDICTED NO
MEASURED NO2
PREDICTED NO2
CONC (PPHM)
TIME (PST)
PASADENA
9/29/69
MEASURED O3
PREDICTED O3
CONC (PPHM)
TIME (PST)
AZUSA
9/29/69
MEASURED O3
PREDICTED O3
CONC (PPHM)
TIME (PST)

Figure E.12

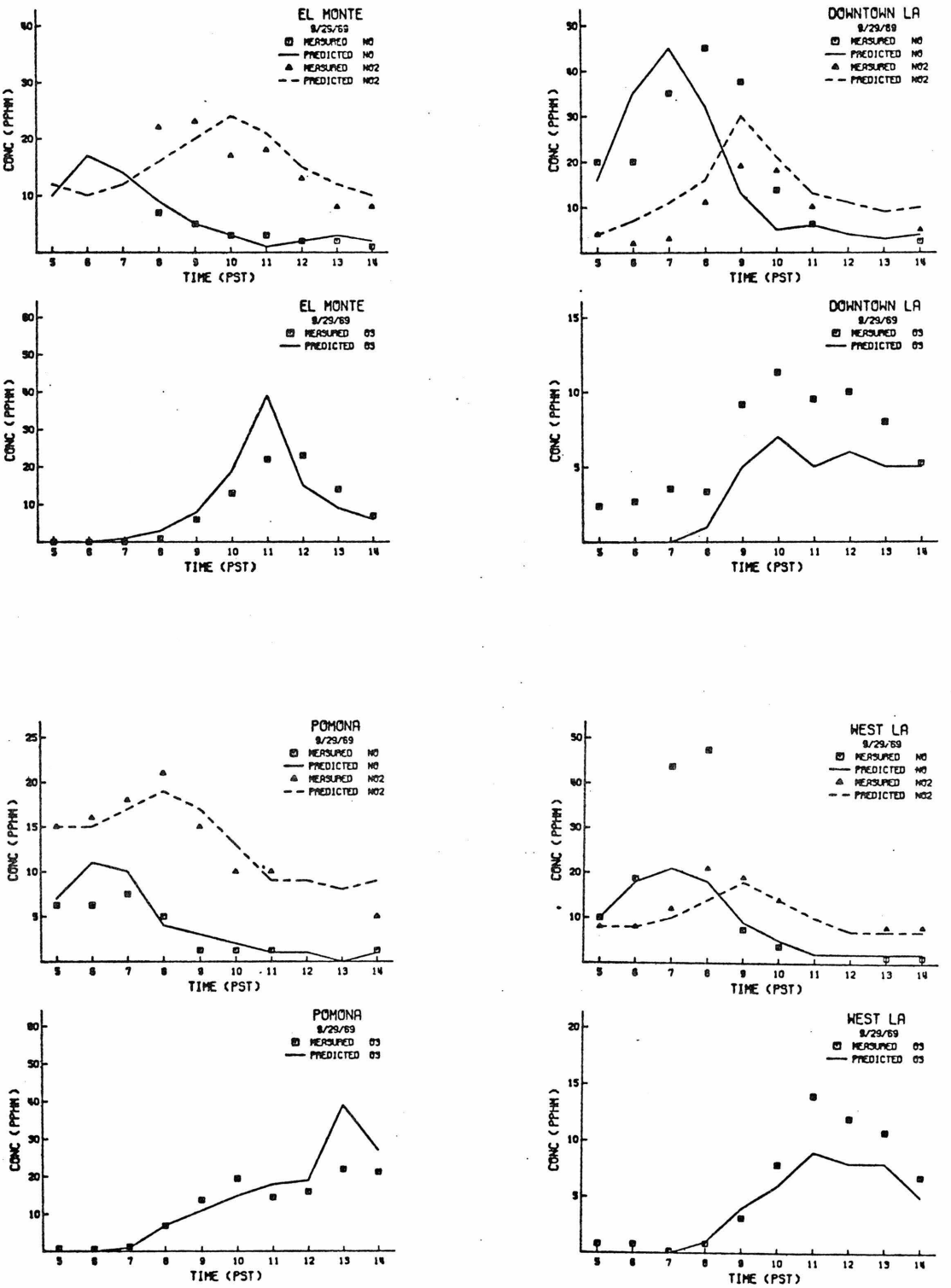
EL MONTE
9/29/69
MEASURED NO
PREDICTED NO
MEASURED NO2
PREDICTED NO2
CONC (PPHM)
TIME (PST)
DOWNTOWN LA
9/29/69
MEASURED NO
PREDICTED NO
MEASURED NO2
PREDICTED NO2
CONC (PPHM)
TIME (PST)
EL MONTE
9/29/69
MEASURED O3
PREDICTED O3
CONC (PPHM)
TIME (PST)
DOWNTOWN LA
9/29/69
MEASURED O3
PREDICTED O3
CONC (PPHM)
TIME (PST)
POMONA
9/29/69
MEASURED NO
PREDICTED NO
MEASURED NO2
PREDICTED NO2
CONC (PPHM)
TIME (PST)
WEST LA
9/29/69
MEASURED NO
PREDICTED NO
MEASURED NO2
PREDICTED NO2
CONC (PPHM)
TIME (PST)
POMONA
9/29/69
MEASURED O3
PREDICTED O3
CONC (PPHM)
TIME (PST)
WEST LA
9/29/69
MEASURED O3
PREDICTED O3
CONC (PPHM)
TIME (PST)

Figure E.13

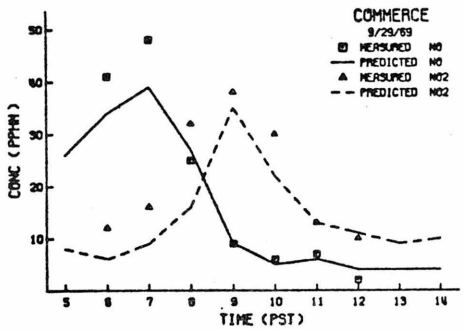
COMMERCE
9/29/69
MEASURED NO
PREDICTED NO
MEASURED NO2
PREDICTED NO2
CONC (PPHM)
TIME (PST)

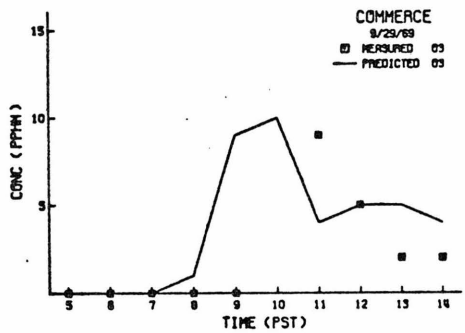
COMMERCE
9/29/69
MEASURED O3
PREDICTED O3
CONC (PPHM)
TIME (PST)

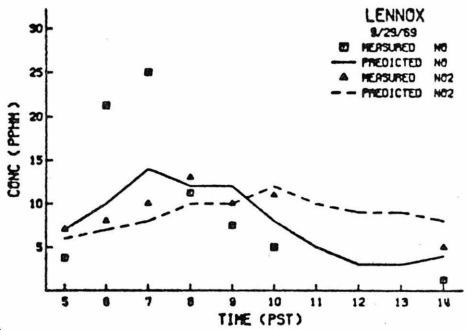
LENNOX
9/29/69
MEASURED NO
PREDICTED NO
MEASURED NO2
PREDICTED NO2
CONC (PPHM)
TIME (PST)

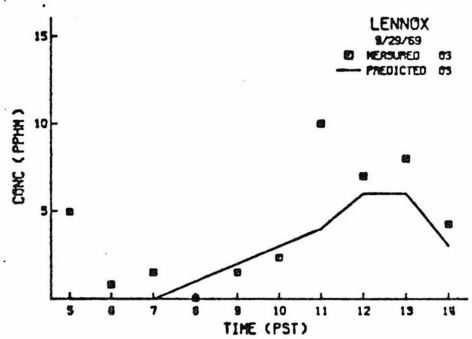
LENNOX
9/29/69
MEASURED O3
PREDICTED O3
CONC (PPHM)
TIME (PST)

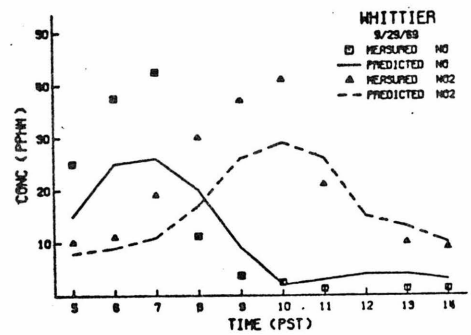
WHITTIER
9/29/69
MEASURED NO
PREDICTED NO
MEASURED NO2
PREDICTED NO2
CONC (PPHM)
TIME (PST)

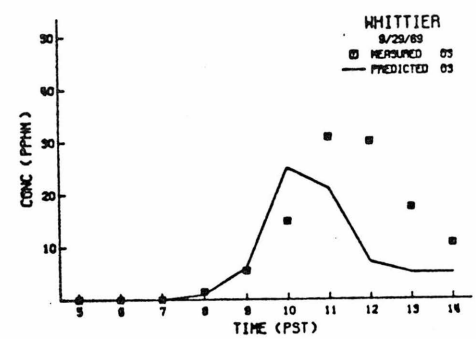
WHITTIER
9/29/69
MEASURED O3
PREDICTED O3
CONC (PPHM)
TIME (PST)

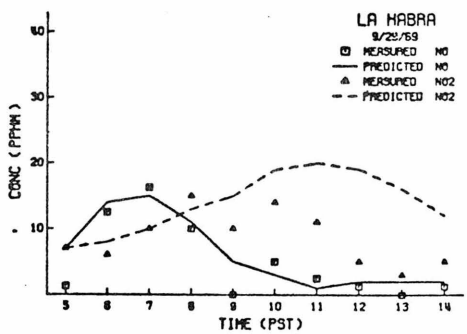
LA HABRA
9/29/69
MEASURED NO
PREDICTED NO
MEASURED NO2
PREDICTED NO2
CONC (PPHM)
TIME (PST)

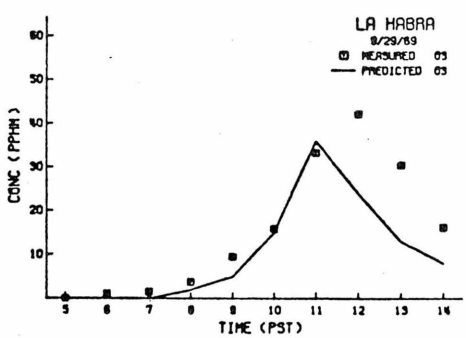
LA HABRA
9/29/69
MEASURED O3
PREDICTED O3
CONC (PPHM)
TIME (PST)

Figure E.14

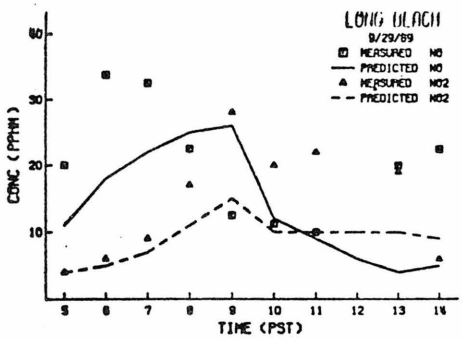
LONG BEACH
9/29/69
MEASURED NO
PREDICTED NO
MEASURED NO2
PREDICTED NO2
CONC (PPHM)
TIME (PST)

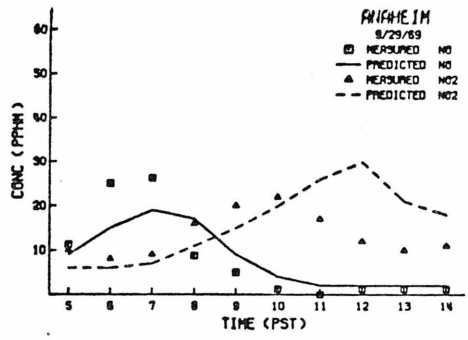
ANAHEIM
9/29/69
MEASURED NO
PREDICTED NO
MEASURED NO2
PREDICTED NO2
CONC (PPHM)
TIME (PST)

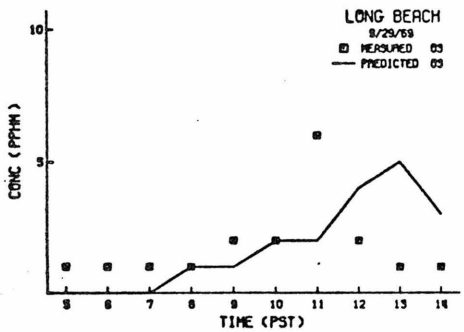
LONG BEACH
9/29/69
MEASURED O3
PREDICTED O3
CONC (PPHM)
TIME (PST)

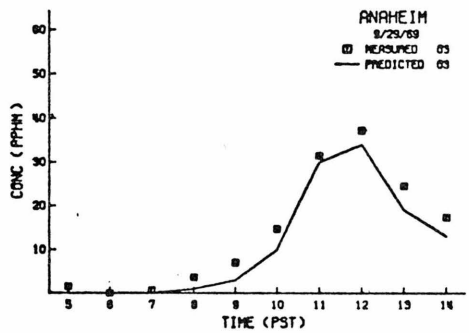
ANAHEIM
9/29/69
MEASURED O3
PREDICTED O3
CONC (PPHM)
TIME (PST)

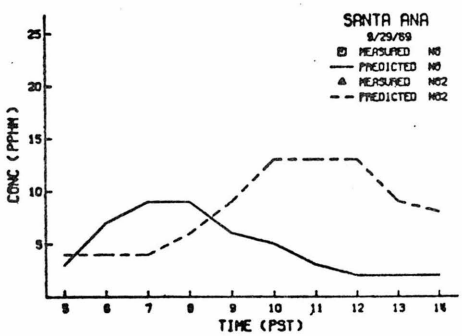
SANTA ANA
9/29/69
MEASURED NO
PREDICTED NO
MEASURED NO2
PREDICTED NO2
CONC (PPHM)
TIME (PST)

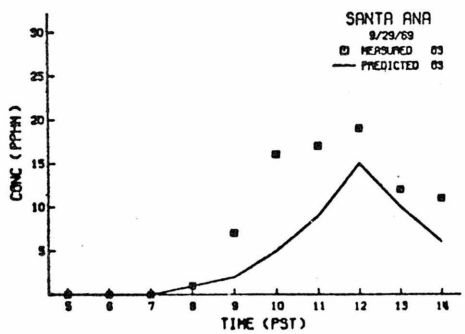
SANTA ANA
9/29/69
MEASURED O3
PREDICTED O3
CONC (PPHM)
TIME (PST)

Figure E.15

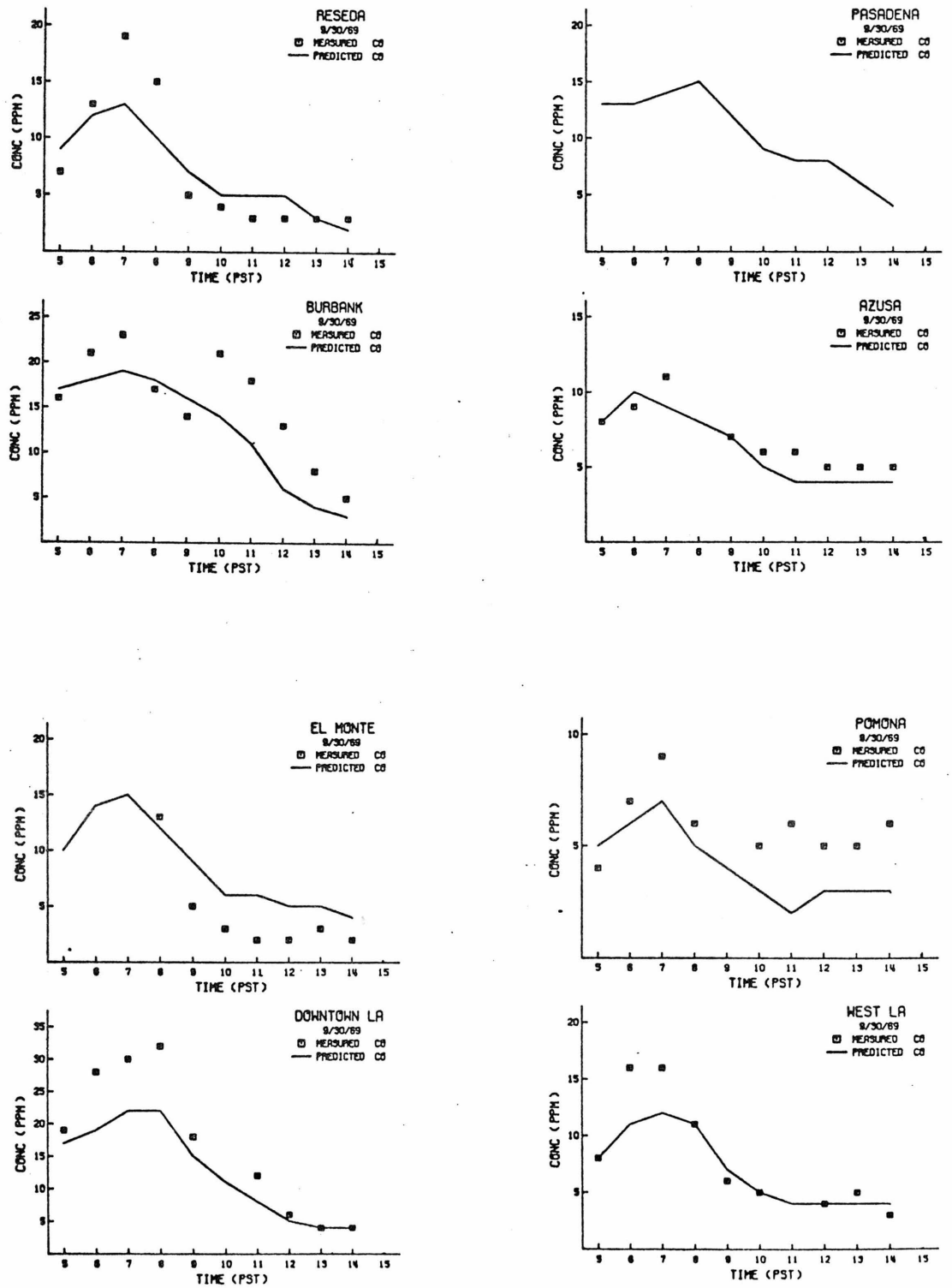
RESEDA
9/30/69
MEASURED CO
PREDICTED CO
CONC (PPM)
TIME (PST)
PASADENA
9/30/69
MEASURED CO
PREDICTED CO
CONC (PPM)
TIME (PST)
BURBANK
9/30/69
MEASURED CO
PREDICTED CO
CONC (PPM)
TIME (PST)
AZUSA
9/30/69
MEASURED CO
PREDICTED CO
CONC (PPM)
TIME (PST)
EL MONTE
9/30/69
MEASURED CO
PREDICTED CO
CONC (PPM)
TIME (PST)
POMONA
9/30/69
MEASURED CO
PREDICTED CO
CONC (PPM)
TIME (PST)
DOWNTOWN LA
9/30/69
MEASURED CO
PREDICTED CO
CONC (PPM)
TIME (PST)
WEST LA
9/30/69
MEASURED CO
PREDICTED CO
CONC (PPM)
TIME (PST)

Figure E.16

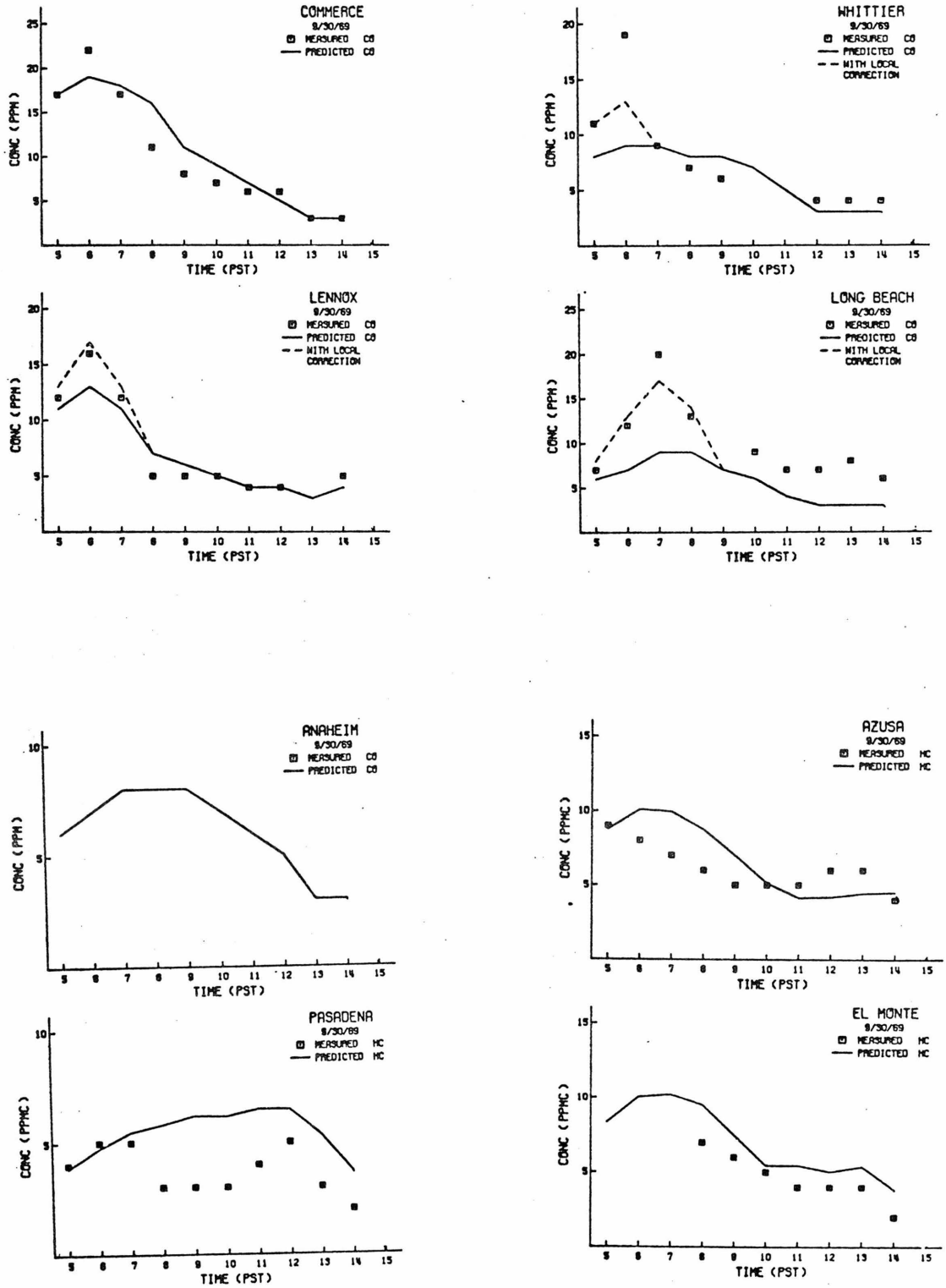
COMMERCE
9/30/69
MEASURED CO
PREDICTED CO
CONC (PPM)
TIME (PST)
WHITTIER
9/30/69
MEASURED CO
PREDICTED CO
WITH LOCAL CORRECTION
CONC (PPM)
TIME (PST)
LENNOX
9/30/69
MEASURED CO
PREDICTED CO
WITH LOCAL CORRECTION
CONC (PPM)
TIME (PST)
LONG BEACH
9/30/69
MEASURED CO
PREDICTED CO
WITH LOCAL CORRECTION
CONC (PPM)
TIME (PST)
ANAHEIM
9/30/69
MEASURED CO
PREDICTED CO
CONC (PPM)
TIME (PST)
AZUSA
9/30/69
MEASURED HC
PREDICTED HC
CONC (PPMC)
TIME (PST)
PASADENA
9/30/69
MEASURED HC
PREDICTED HC
CONC (PPMC)
TIME (PST)
EL MONTE
9/30/69
MEASURED HC
PREDICTED HC
CONC (PPMC)
TIME (PST)

Figure E.17

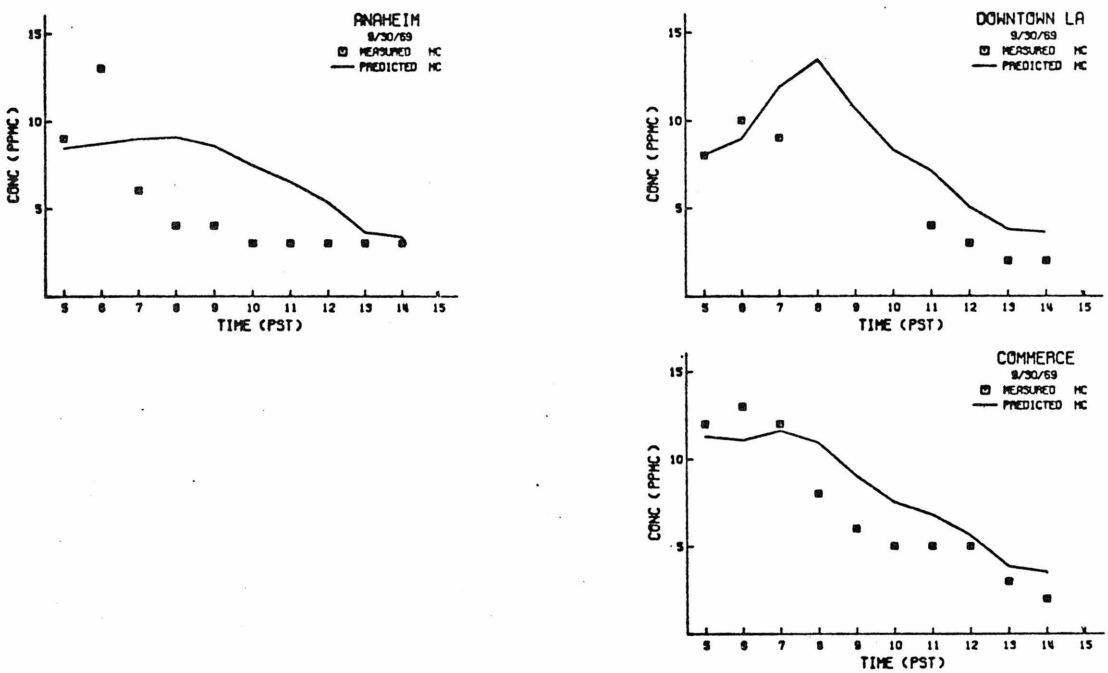
ANAHEIM
9/30/69
MEASURED HC
PREDICTED HC
CONC (PPMC)
TIME (PST)
DOWNTOWN LA
9/30/69
MEASURED HC
PREDICTED HC
CONC (PPMC)
TIME (PST)
COMMERCE
9/30/69
MEASURED HC
PREDICTED HC
CONC (PPMC)
TIME (PST)

Figure E.18

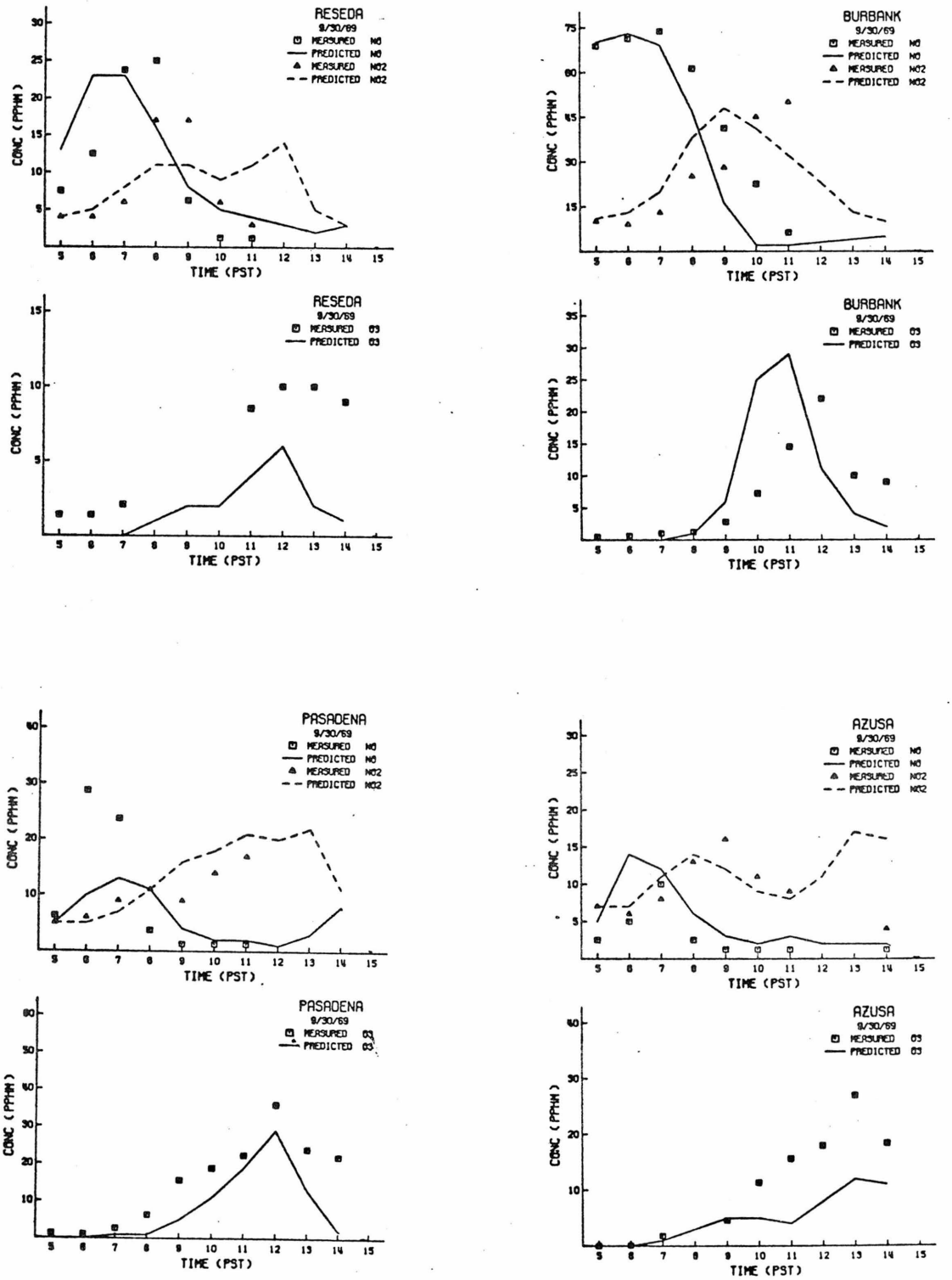
RESEDA
9/30/69
MEASURED NO
PREDICTED NO
MEASURED NO2
PREDICTED NO2
CONC (PPHM)
TIME (PST)
RESEDA
9/30/69
MEASURED O3
PREDICTED O3
CONC (PPHM)
TIME (PST)
BURBANK
9/30/69
MEASURED NO
PREDICTED NO
MEASURED NO2
PREDICTED NO2
CONC (PPHM)
TIME (PST)
BURBANK
9/30/69
MEASURED O3
PREDICTED O3
CONC (PPHM)
TIME (PST)
PASADENA
9/30/69
MEASURED NO
PREDICTED NO
MEASURED NO2
PREDICTED NO2
CONC (PPHM)
TIME (PST)
PASADENA
9/30/69
MEASURED O3
PREDICTED O3
CONC (PPHM)
TIME (PST)
AZUSA
9/30/69
MEASURED NO
PREDICTED NO
MEASURED NO2
PREDICTED NO2
CONC (PPHM)
TIME (PST)
AZUSA
9/30/69
MEASURED O3
PREDICTED O3
CONC (PPHM)
TIME (PST)

Figure E.19

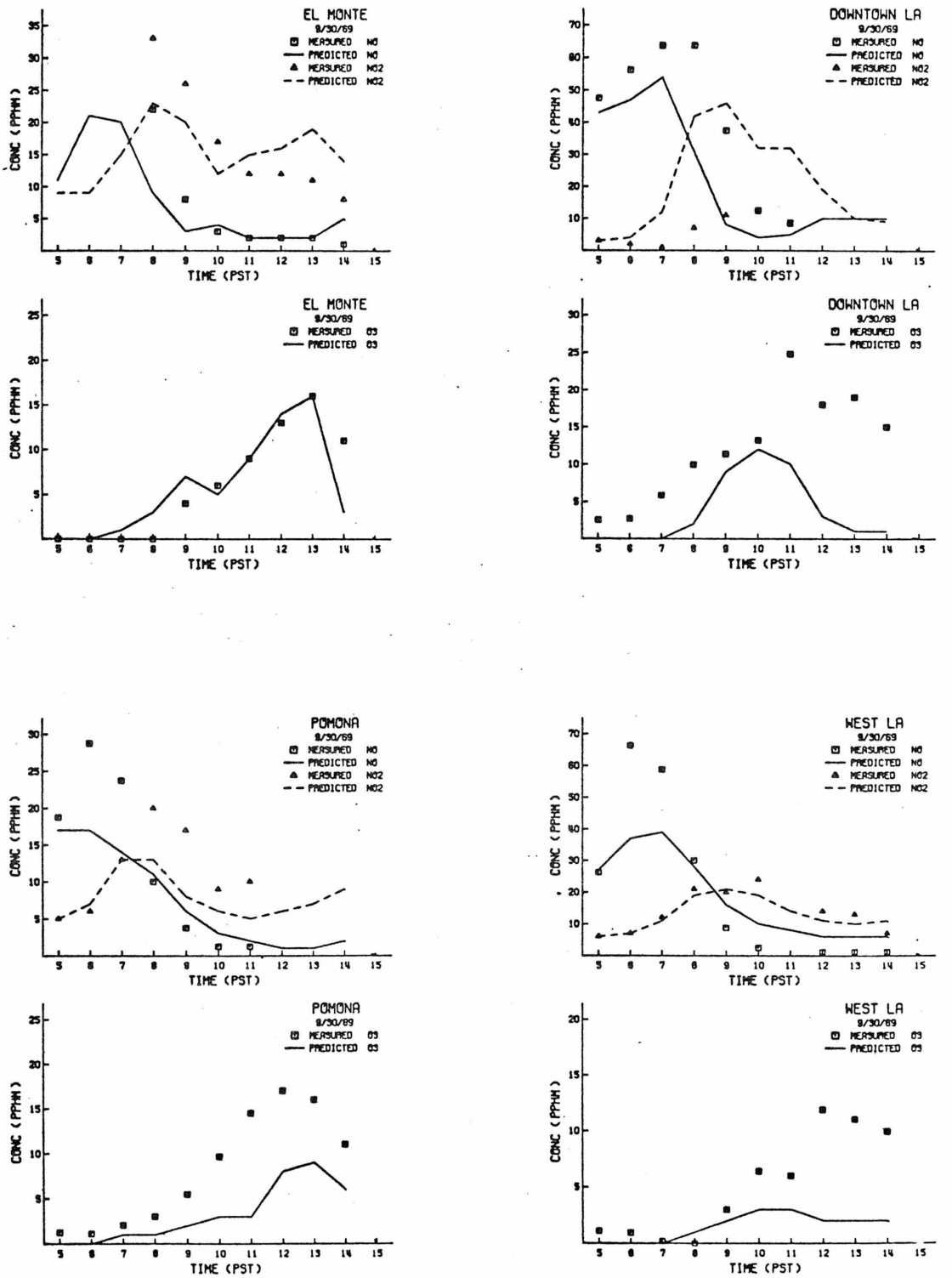
EL MONTE
9/30/69
MEASURED NO
PREDICTED NO
MEASURED NO2
PREDICTED NO2
CONC (PPHM)
TIME (PST)
EL MONTE
9/30/69
MEASURED O3
PREDICTED O3
CONC (PPHM)
TIME (PST)
DOWNTOWN LA
9/30/69
MEASURED NO
PREDICTED NO
MEASURED NO2
PREDICTED NO2
CONC (PPHM)
TIME (PST)
DOWNTOWN LA
9/30/69
MEASURED O3
PREDICTED O3
CONC (PPHM)
TIME (PST)
POMONA
9/30/69
MEASURED NO
PREDICTED NO
MEASURED NO2
PREDICTED NO2
CONC (PPHM)
TIME (PST)
POMONA
9/30/69
MEASURED O3
PREDICTED O3
CONC (PPHM)
TIME (PST)
WEST LA
9/30/69
MEASURED NO
PREDICTED NO
MEASURED NO2
PREDICTED NO2
CONC (PPHM)
TIME (PST)
WEST LA
9/30/69
MEASURED O3
PREDICTED O3
CONC (PPHM)
TIME (PST)

Figure E.20

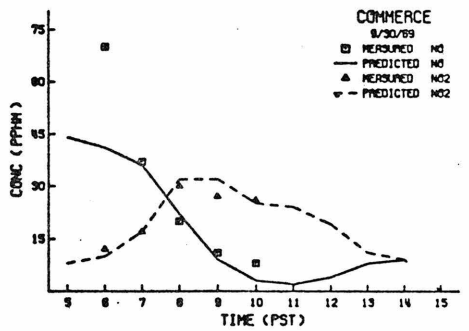
COMMERCE
9/30/69
MEASURED NO
PREDICTED NO
MEASURED NO2
PREDICTED NO2
CONC (PPHM)
TIME (PST)

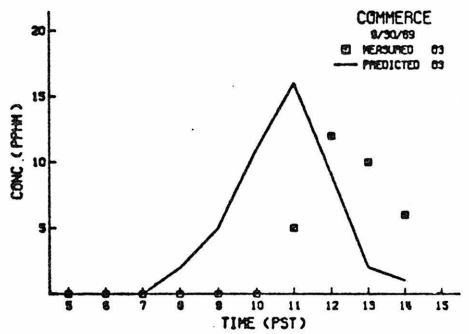
COMMERCE
9/30/69
MEASURED O3
PREDICTED O3
CONC (PPHM)
TIME (PST)

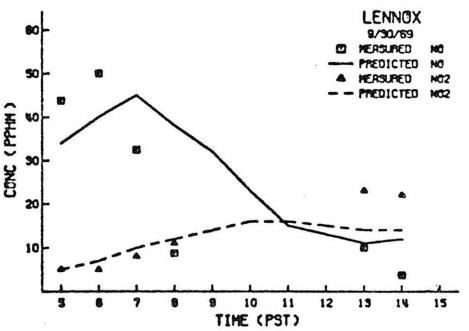
LENNOX
9/30/69
MEASURED NO
PREDICTED NO
MEASURED NO2
PREDICTED NO2
CONC (PPHM)
TIME (PST)

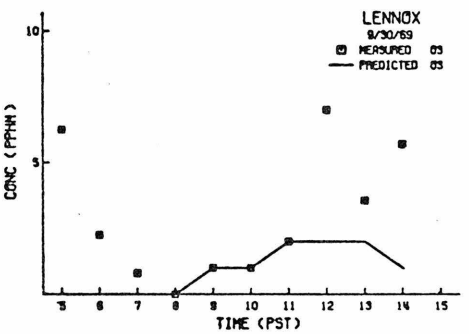
LENNOX
9/30/69
MEASURED O3
PREDICTED O3
CONC (PPHM)
TIME (PST)

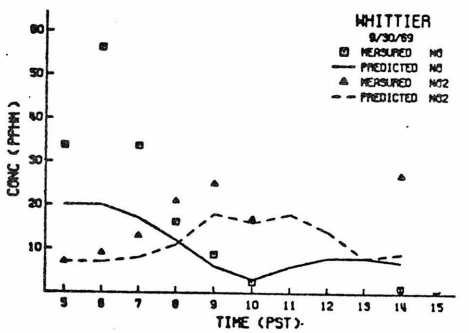
WHITTIER
9/30/69
MEASURED NO
PREDICTED NO
MEASURED NO2
PREDICTED NO2
CONC (PPHM)
TIME (PST)

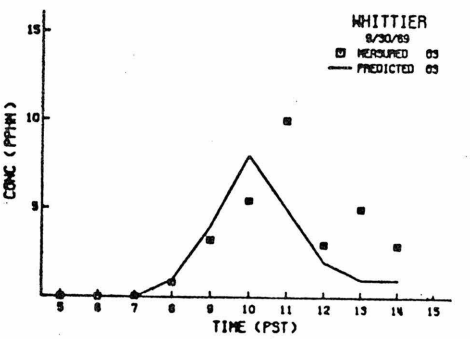
WHITTIER
9/30/69
MEASURED O3
PREDICTED O3
CONC (PPHM)
TIME (PST)

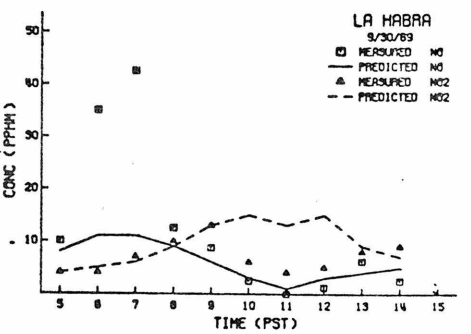
LA HABRA
9/30/69
MEASURED NO
PREDICTED NO
MEASURED NO2
PREDICTED NO2
CONC (PPHM)
TIME (PST)

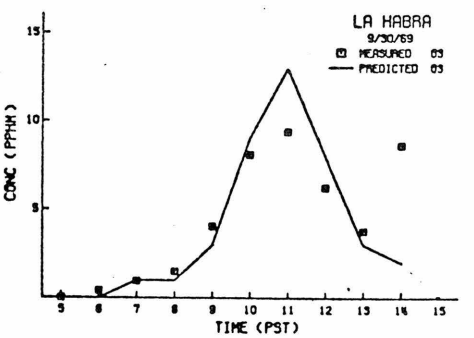
LA HABRA
9/30/69
MEASURED O3
PREDICTED O3
CONC (PPHM)
TIME (PST)

Figure E.21

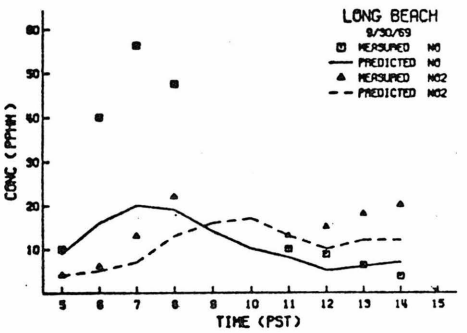
LONG BEACH
9/30/69
MEASURED NO
PREDICTED NO
MEASURED NO2
PREDICTED NO2
CONC (PPHM)
TIME (PST)

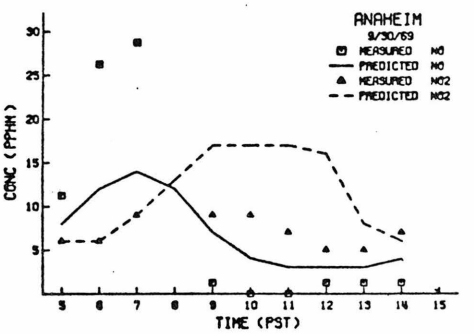
ANAHEIM
9/30/69
MEASURED NO
PREDICTED NO
MEASURED NO2
PREDICTED NO2
CONC (PPHM)
TIME (PST)

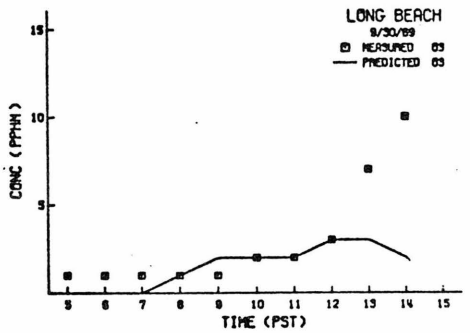
LONG BEACH
9/30/69
MEASURED O3
PREDICTED O3
CONC (PPHM)
TIME (PST)

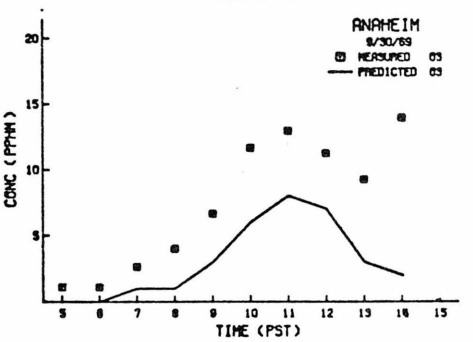
ANAHEIM
9/30/69
MEASURED O3
PREDICTED O3
CONC (PPHM)
TIME (PST)

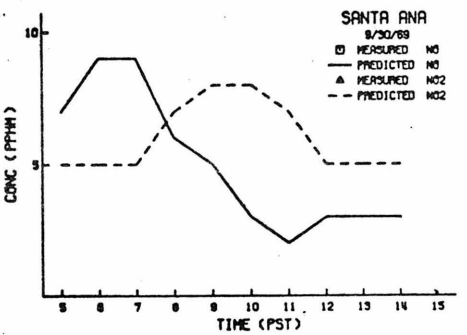
SANTA ANA
9/30/69
MEASURED NO
PREDICTED NO
MEASURED NO2
PREDICTED NO2
CONC (PPHM)
TIME (PST)

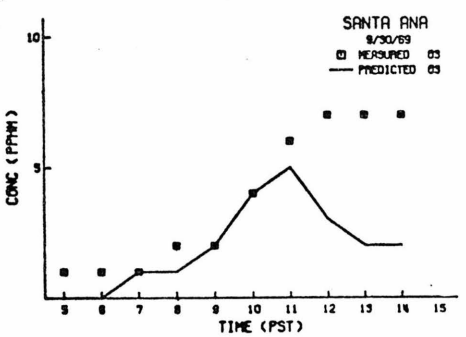
SANTA ANA
9/30/69
MEASURED O3
PREDICTED O3
CONC (PPHM)
TIME (PST)

Figure E.22

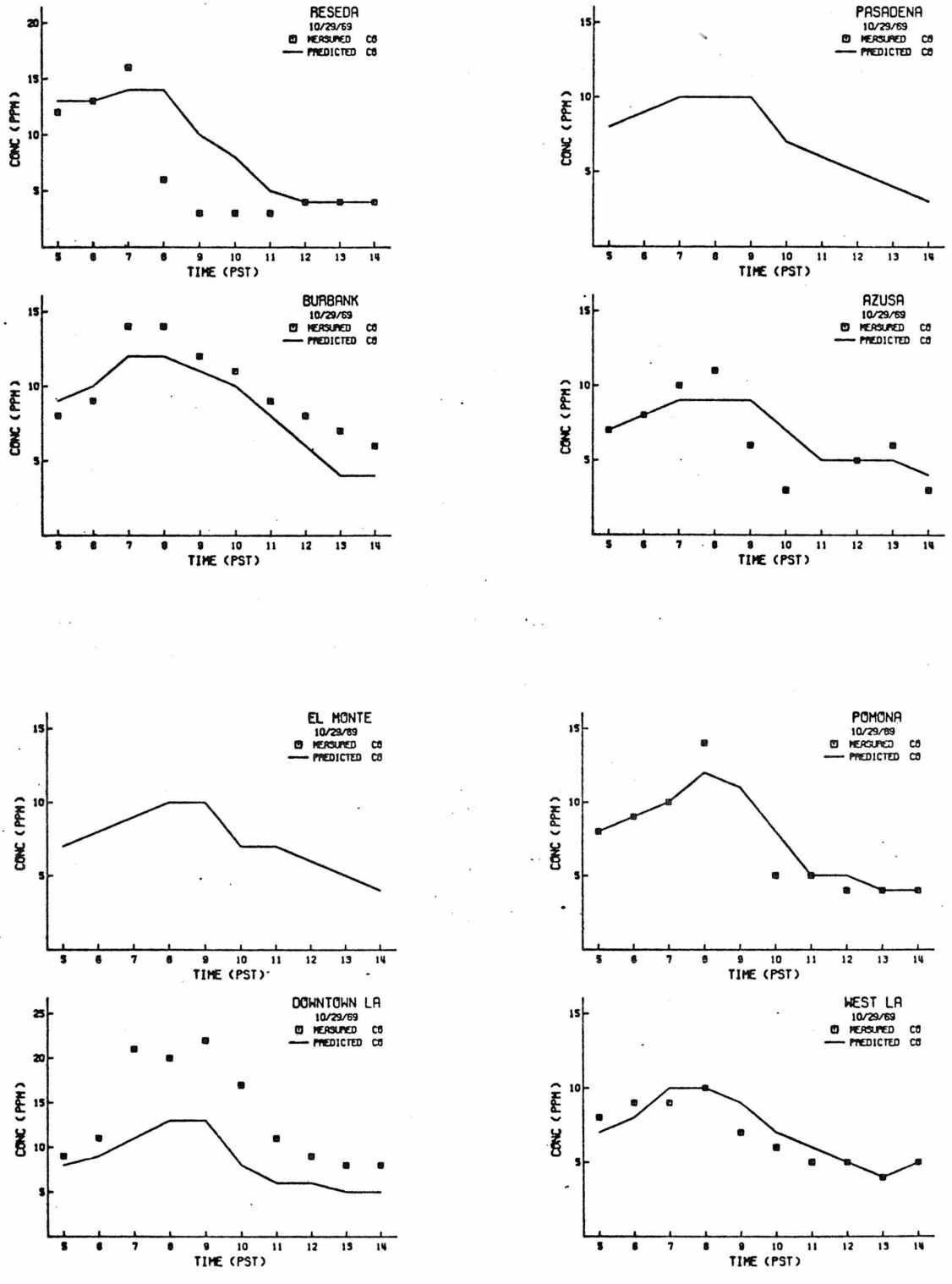
RESEDA
10/29/69
MEASURED CO
PREDICTED CO
CONC (PPM)
TIME (PST)
PASADENA
10/29/69
MEASURED CO
PREDICTED CO
CONC (PPM)
TIME (PST)
BURBANK
10/29/69
MEASURED CO
PREDICTED CO
CONC (PPM)
TIME (PST)
AZUSA
10/29/69
MEASURED CO
PREDICTED CO
CONC (PPM)
TIME (PST)
EL MONTE
10/29/69
MEASURED CO
PREDICTED CO
CONC (PPM)
TIME (PST)
POMONA
10/29/69
MEASURED CO
PREDICTED CO
CONC (PPM)
TIME (PST)
DOWNTOWN LA
10/29/69
MEASURED CO
PREDICTED CO
CONC (PPM)
TIME (PST)
WEST LA
10/29/69
MEASURED CO
PREDICTED CO
CONC (PPM)
TIME (PST)

Figure E.23

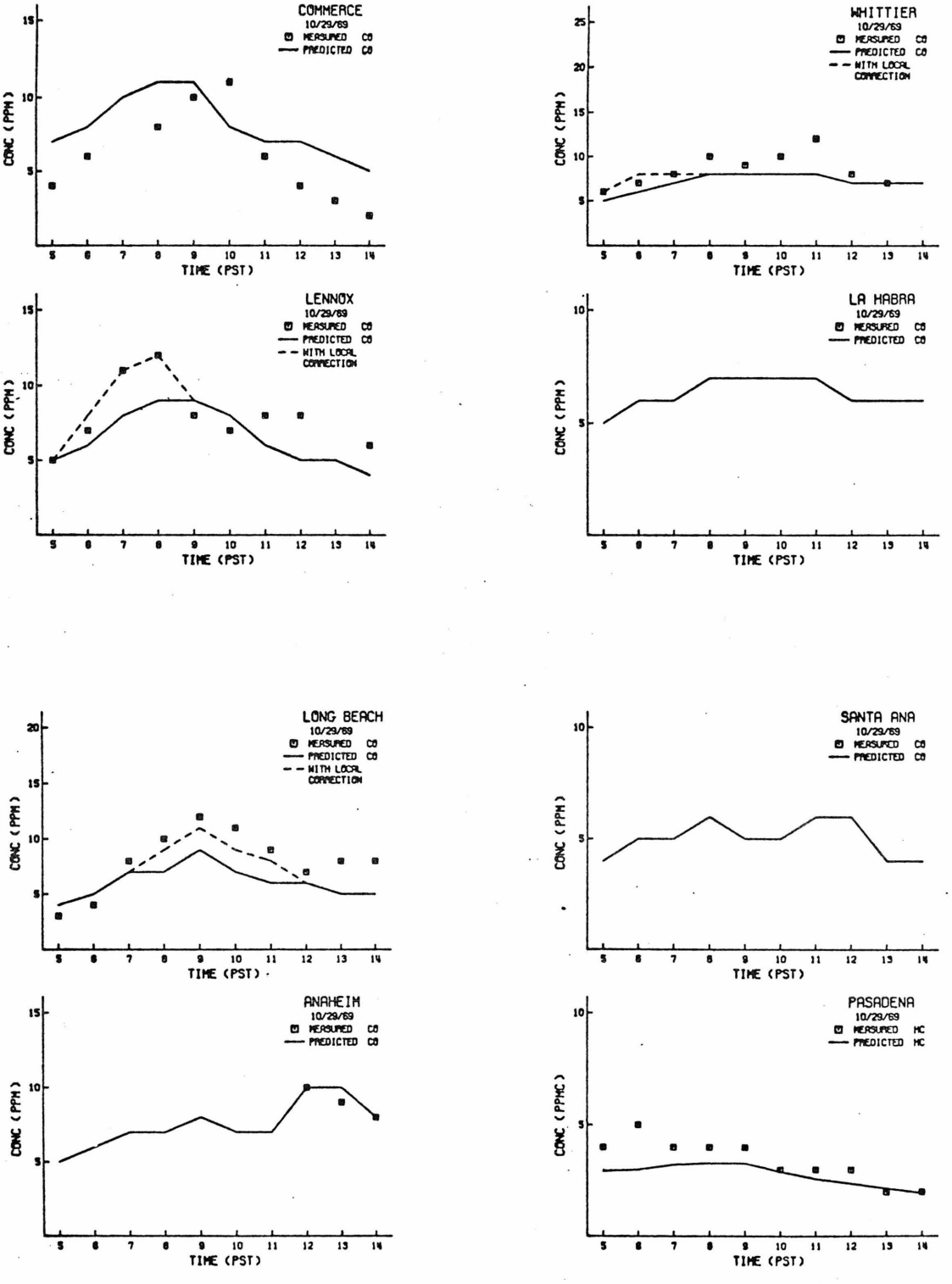
COMMERCE
10/29/69
MEASURED CO
PREDICTED CO
CONC (PPM)
TIME (PST)
WHITTIER
10/29/69
MEASURED CO
PREDICTED CO
WITH LOCAL CORRECTION
CONC (PPM)
TIME (PST)
LENNOX
10/29/69
MEASURED CO
PREDICTED CO
WITH LOCAL CORRECTION
CONC (PPM)
TIME (PST)
LA HABRA
10/29/69
MEASURED CO
PREDICTED CO
CONC (PPM)
TIME (PST)
LONG BEACH
10/29/69
MEASURED CO
PREDICTED CO
WITH LOCAL CORRECTION
CONC (PPM)
TIME (PST)
SANTA ANA
10/29/69
MEASURED CO
PREDICTED CO
CONC (PPM)
TIME (PST)
ANAHEIM
10/29/69
MEASURED CO
PREDICTED CO
CONC (PPM)
TIME (PST)
PASADENA
10/29/69
MEASURED HC
PREDICTED HC
CONC (PPMC)
TIME (PST)

Figure E.24

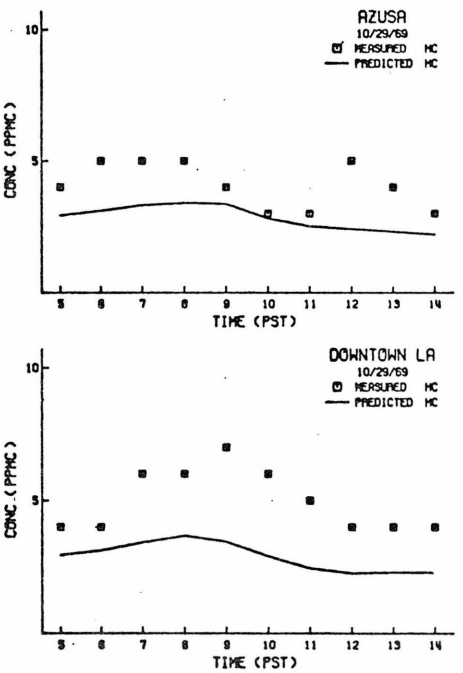
AZUSA
10/29/69
MEASURED HC
PREDICTED HC
CONC (PPMC)
10
5
5 6 7 8 9 10 11 12 13 14
TIME (PST)
DOWNTOWN LA
10/29/69
MEASURED HC
PREDICTED HC
CONC.(PPMC)
10
5
5 6 7 8 9 10 11 12 13 14
TIME (PST)

Figure E.25

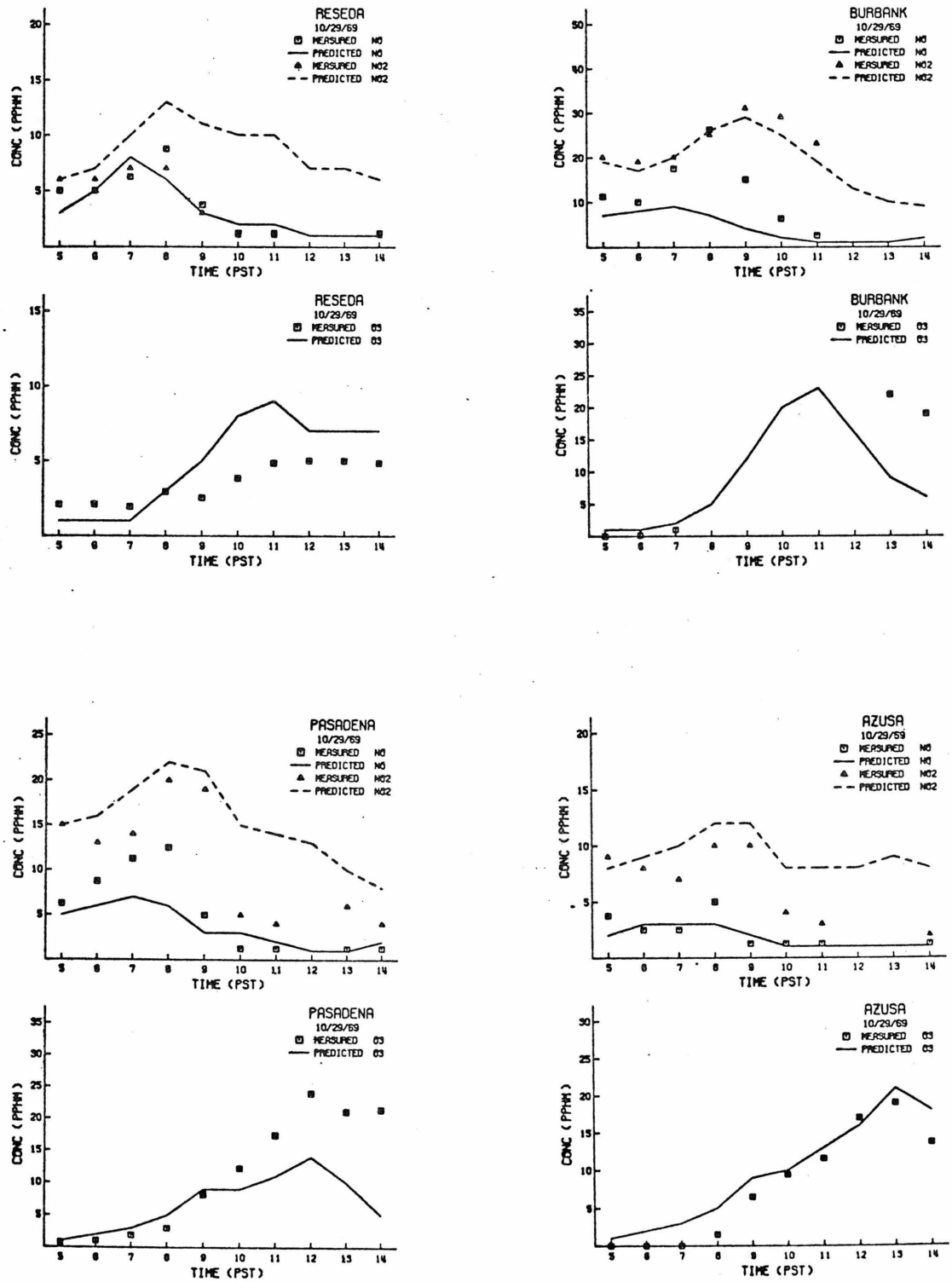
RESEDA
10/29/69
MEASURED NO
PREDICTED NO
MEASURED NO2
PREDICTED NO2
CONC (PPHM)
TIME (PST)
RESEDA
10/29/69
MEASURED O3
PREDICTED O3
CONC (PPHM)
TIME (PST)
BURBANK
10/29/69
MEASURED NO
PREDICTED NO
MEASURED NO2
PREDICTED NO2
CONC (PPHM)
TIME (PST)
BURBANK
10/29/69
MEASURED O3
PREDICTED O3
CONC (PPHM)
TIME (PST)
PASADENA
10/29/69
MEASURED NO
PREDICTED NO
MEASURED NO2
PREDICTED NO2
CONC (PPHM)
TIME (PST)
PASADENA
10/29/69
MEASURED O3
PREDICTED O3
CONC (PPHM)
TIME (PST)
AZUSA
10/29/69
MEASURED NO
PREDICTED NO
MEASURED NO2
PREDICTED NO2
CONC (PPHM)
TIME (PST)
AZUSA
10/29/69
MEASURED O3
PREDICTED O3
CONC (PPHM)
TIME (PST)

Figure 4.26

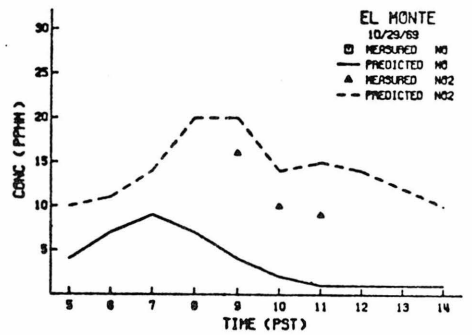
EL MONTE
10/29/69
MEASURED NO
PREDICTED NO
MEASURED NO2
PREDICTED NO2
CONC (PPHM)
TIME (PST)

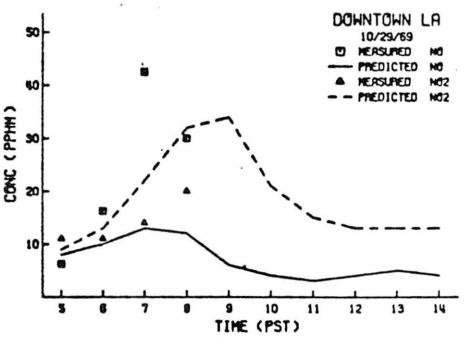
DOWNTOWN LA
10/29/69
MEASURED NO
PREDICTED NO
MEASURED NO2
PREDICTED NO2
CONC (PPHM)
TIME (PST)

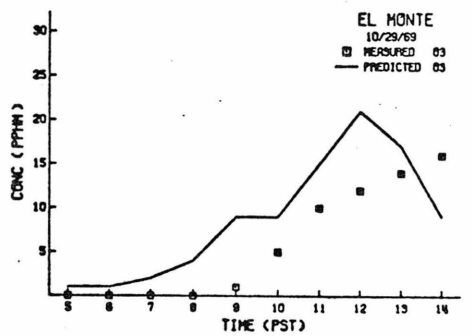
EL MONTE
10/29/69
MEASURED O3
PREDICTED O3
CONC (PPHM)
TIME (PST)

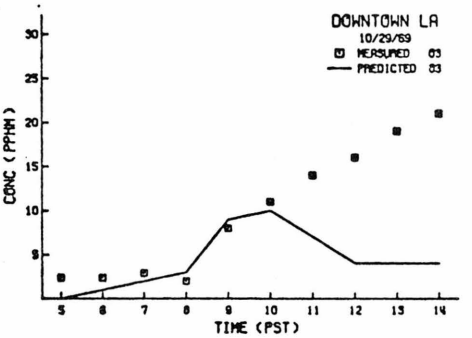
DOWNTOWN LA
10/29/69
MEASURED O3
PREDICTED O3
CONC (PPHM)
TIME (PST)

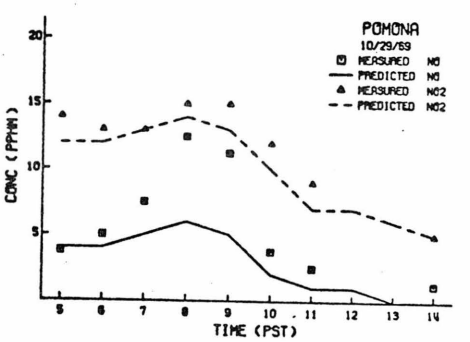
POMONA
10/29/69
MEASURED NO
PREDICTED NO
MEASURED NO2
PREDICTED NO2
CONC (PPHM)
TIME (PST)

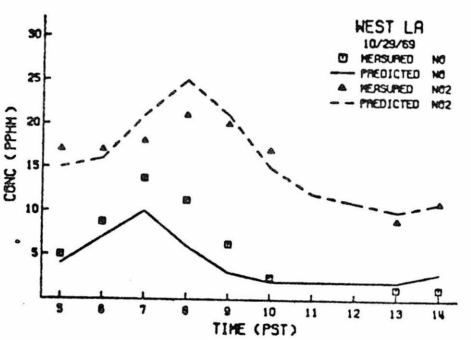
WEST LA
10/29/69
MEASURED NO
PREDICTED NO
MEASURED NO2
PREDICTED NO2
CONC (PPHM)
TIME (PST)

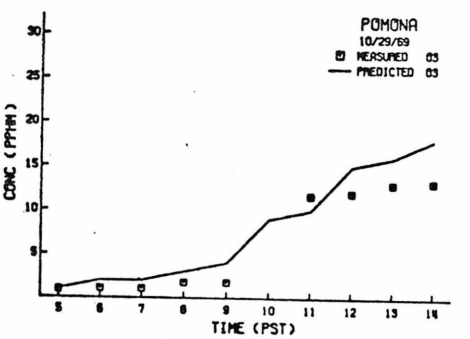
POMONA
10/29/69
MEASURED O3
PREDICTED O3
CONC (PPHM)
TIME (PST)

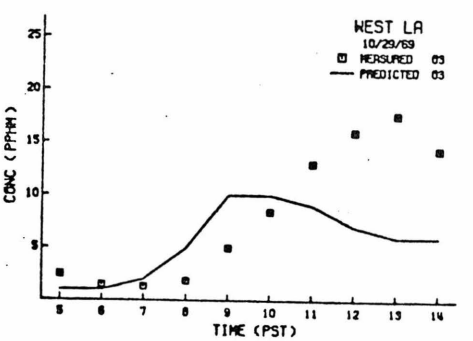
WEST LA
10/29/69
MEASURED O3
PREDICTED O3
CONC (PPHM)
TIME (PST)

Figure E.27

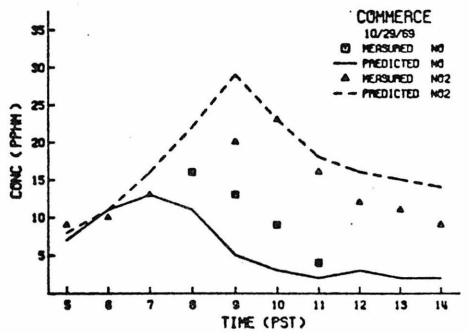
COMMERCE
10/29/69
MEASURED NO
PREDICTED NO
MEASURED NO2
PREDICTED NO2
CONC (PPHM)
TIME (PST)

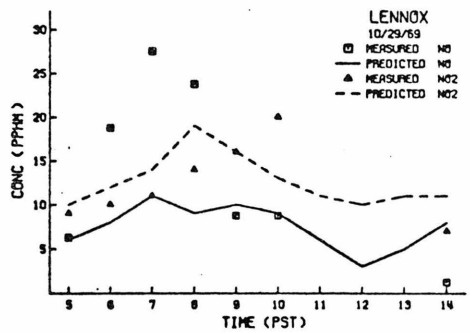
LENNOX
10/29/69
MEASURED NO
PREDICTED NO
MEASURED NO2
PREDICTED NO2
CONC (PPHM)
TIME (PST)

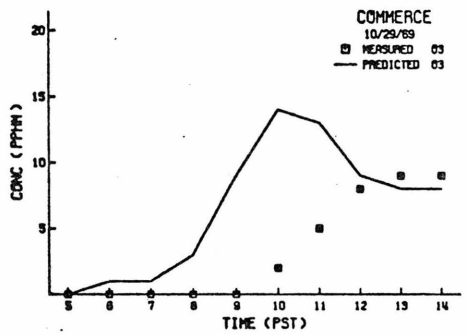
COMMERCE
10/29/69
MEASURED O3
PREDICTED O3
CONC (PPHM)
TIME (PST)

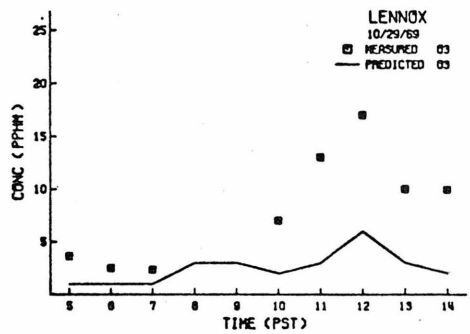
LENNOX
10/29/69
MEASURED O3
PREDICTED O3
CONC (PPHM)
TIME (PST)

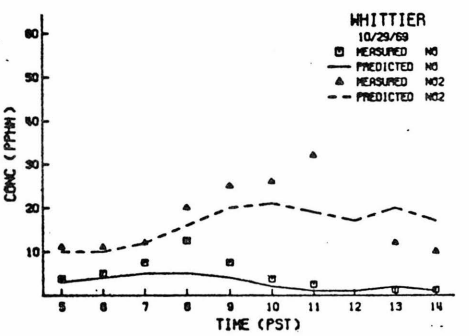
WHITTIER
10/29/69
MEASURED NO
PREDICTED NO
MEASURED NO2
PREDICTED NO2
CONC (PPHM)
TIME (PST)

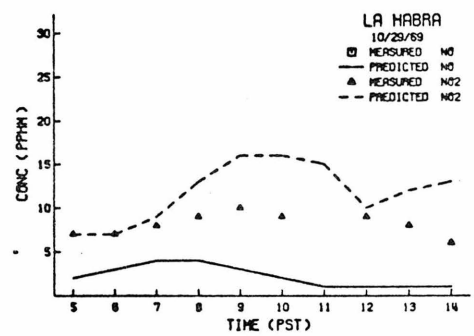
LA HABRA
10/29/69
MEASURED NO
PREDICTED NO
MEASURED NO2
PREDICTED NO2
CONC (PPHM)
TIME (PST)

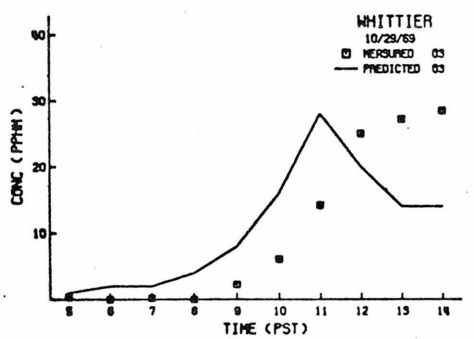
WHITTIER
10/29/69
MEASURED O3
PREDICTED O3
CONC (PPHM)
TIME (PST)

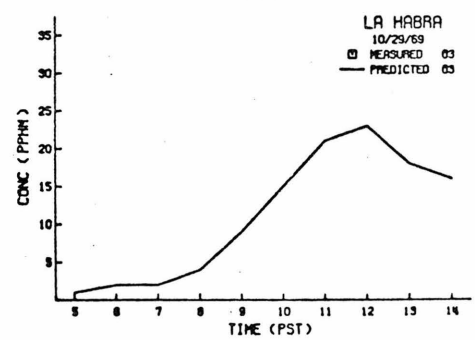
LA HABRA
10/29/69
MEASURED O3
PREDICTED O3
CONC (PPHM)
TIME (PST)

Figure E.28

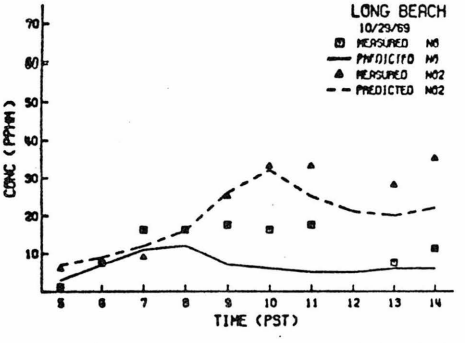
LONG BEACH
10/29/69
MEASURED NO
PREDICTED NO
MEASURED NO2
PREDICTED NO2
CONC (PPHM)
TIME (PST)

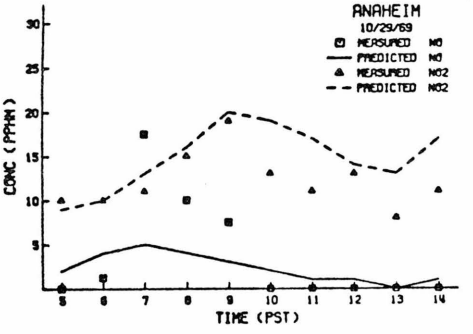
ANAHEIM
10/29/69
MEASURED NO
PREDICTED NO
MEASURED NO2
PREDICTED NO2
CONC (PPHM)
TIME (PST)

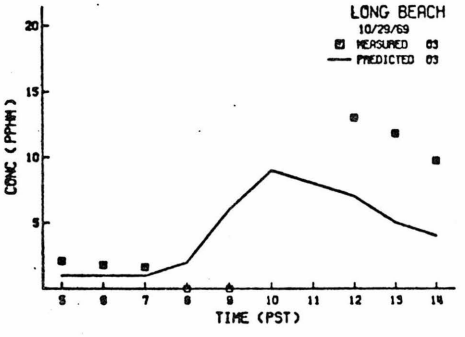
LONG BEACH
10/29/69
MEASURED O3
PREDICTED O3
CONC (PPHM)
TIME (PST)

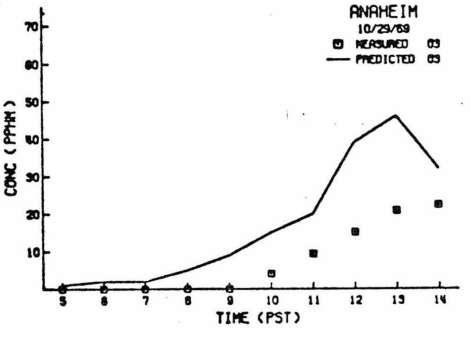
ANAHEIM
10/29/69
MEASURED O3
PREDICTED O3
CONC (PPHM)
TIME (PST)

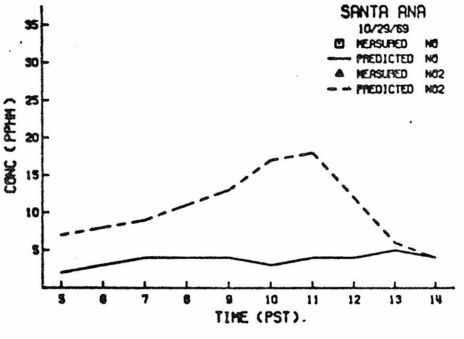
SANTA ANA
10/29/69
MEASURED NO
PREDICTED NO
MEASURED NO2
PREDICTED NO2
CONC (PPHM)
TIME (PST)

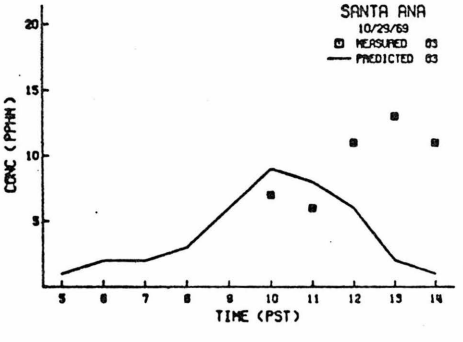
SANTA ANA
10/29/69
MEASURED O3
PREDICTED O3
CONC (PPHM)
TIME (PST)

Figure E.29

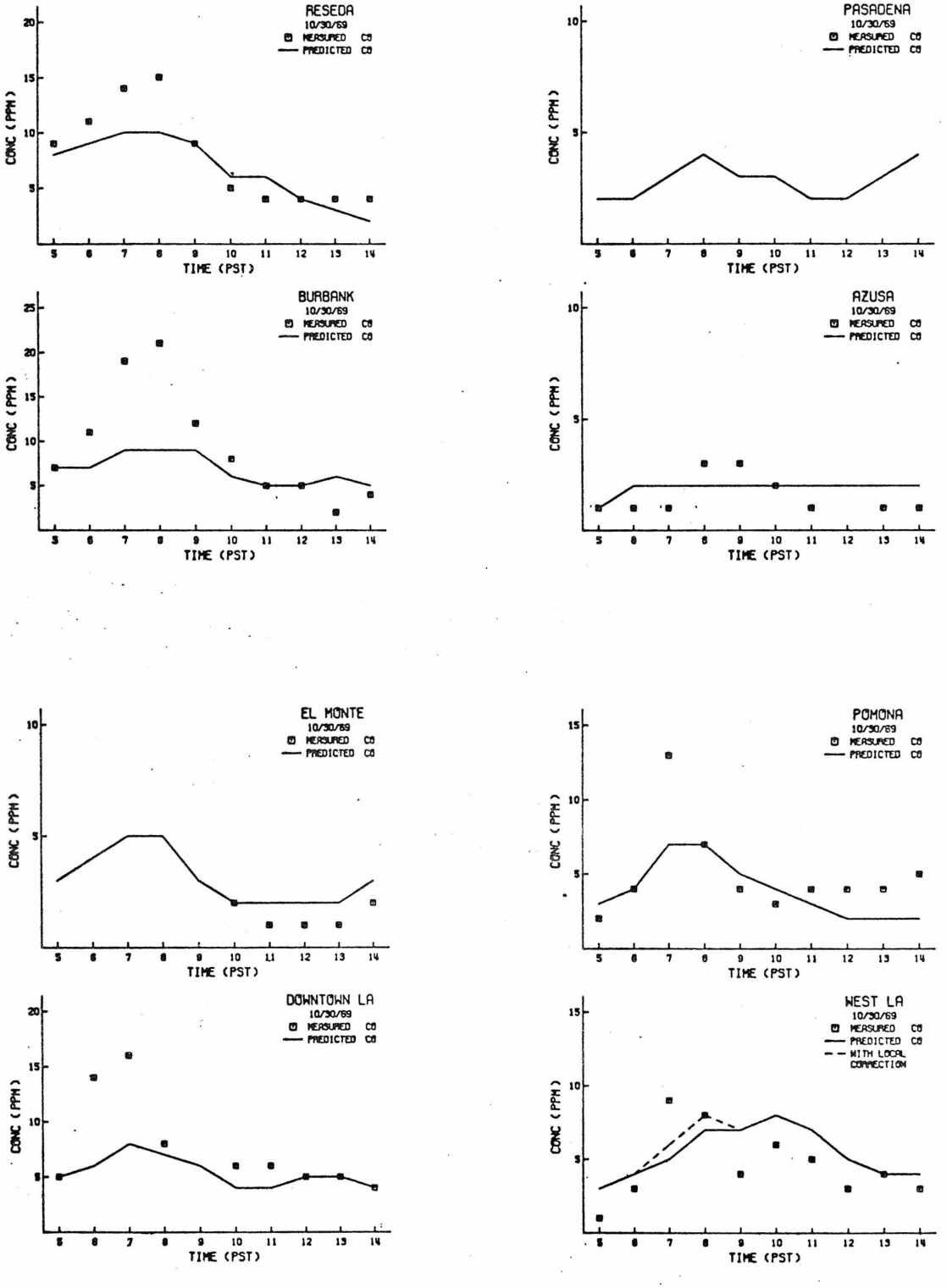
RESEDA
10/30/69
MEASURED CO
PREDICTED CO
CONC (PPM)
TIME (PST)
PASADENA
10/30/69
MEASURED CO
PREDICTED CO
CONC (PPM)
TIME (PST)
BURBANK
10/30/69
MEASURED CO
PREDICTED CO
CONC (PPM)
TIME (PST)
AZUSA
10/30/69
MEASURED CO
PREDICTED CO
CONC (PPM)
TIME (PST)
EL MONTE
10/30/69
MEASURED CO
PREDICTED CO
CONC (PPM)
TIME (PST)
POMONA
10/30/69
MEASURED CO
PREDICTED CO
CONC (PPM)
TIME (PST)
DOWNTOWN LA
10/30/69
MEASURED CO
PREDICTED CO
CONC (PPM)
TIME (PST)
WEST LA
10/30/69
MEASURED CO
PREDICTED CO
WITH LOCAL CORRECTION
CONC (PPM)
TIME (PST)

Figure E. 30

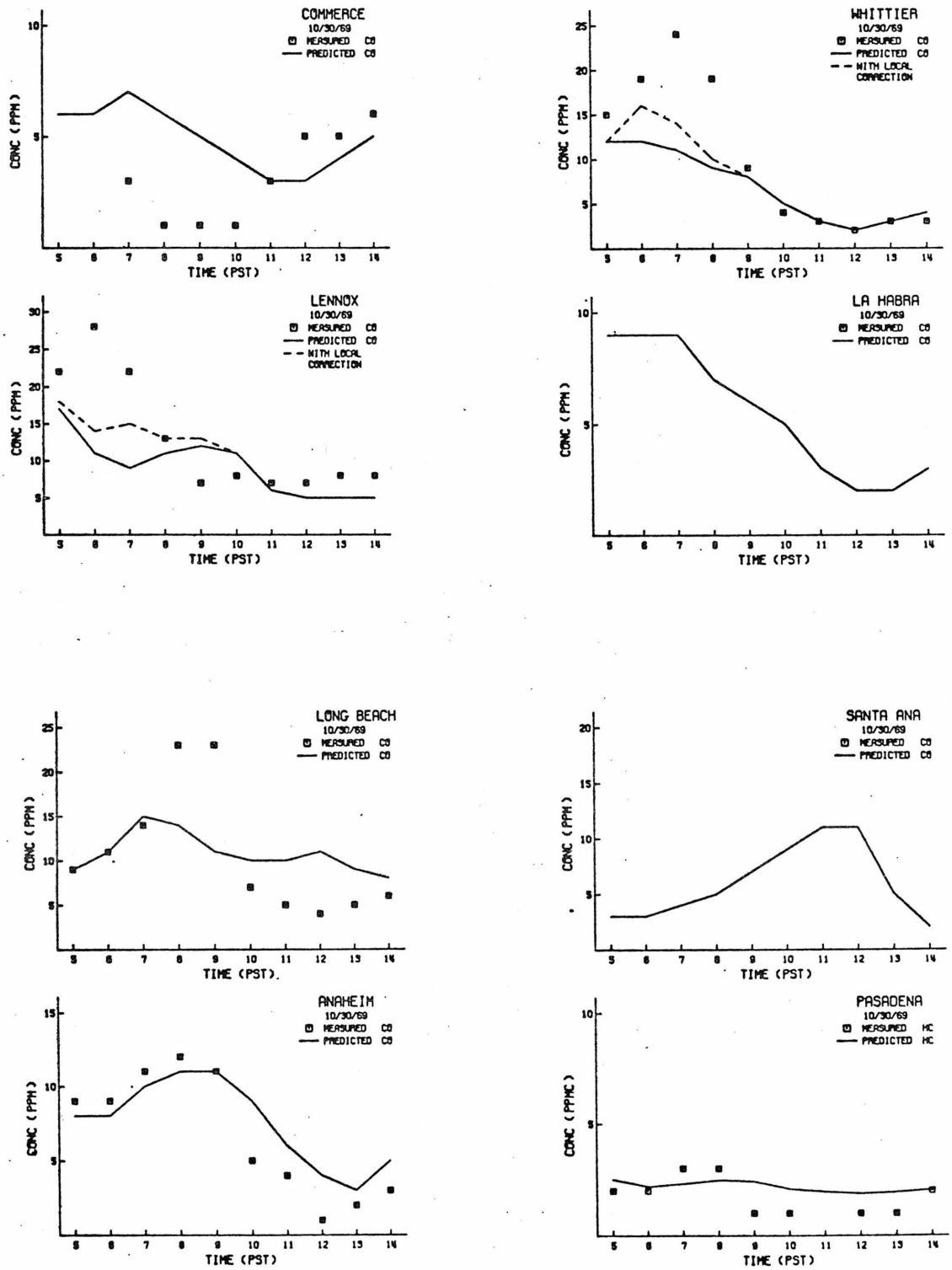
COMMERCE
10/30/69
MEASURED CO
PREDICTED CO
CONC (PPM)
TIME (PST)
WHITTIER
10/30/69
MEASURED CO
PREDICTED CO
WITH LOCAL CORRECTION
CONC (PPM)
TIME (PST)
LENNOX
10/30/69
MEASURED CO
PREDICTED CO
WITH LOCAL CORRECTION
CONC (PPM)
TIME (PST)
LA HABRA
10/30/69
MEASURED CO
PREDICTED CO
CONC (PPM)
TIME (PST)
LONG BEACH
10/30/69
MEASURED CO
PREDICTED CO
CONC (PPM)
TIME (PST)
SANTA ANA
10/30/69
MEASURED CO
PREDICTED CO
CONC (PPM)
TIME (PST)
ANAHEIM
10/30/69
MEASURED CO
PREDICTED CO
CONC (PPM)
TIME (PST)
PASADENA
10/30/69
MEASURED HC
PREDICTED HC
CONC (PPMC)
TIME (PST)

Figure E.31

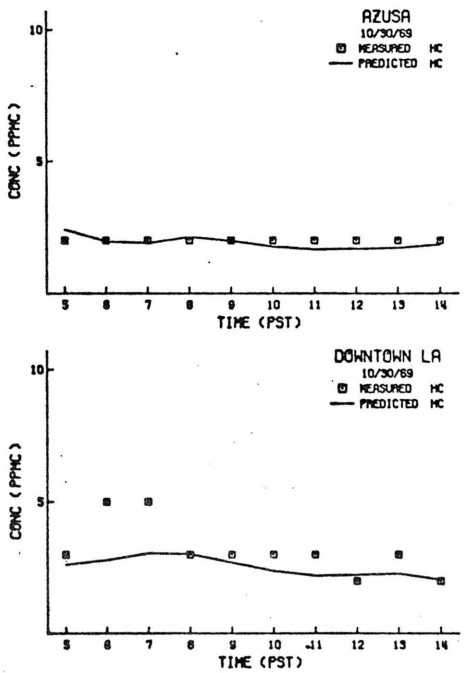
AZUSA
10/30/69
MEASURED HC
PREDICTED HC
CONC (PPMC)
10
5
5 6 7 8 9 10 11 12 13 14
TIME (PST)
DOWNTOWN LA
10/30/69
MEASURED HC
PREDICTED HC
CONC (PPMC)
10
5
5 6 7 8 9 10 11 12 13 14
TIME (PST)

Figure E. 32

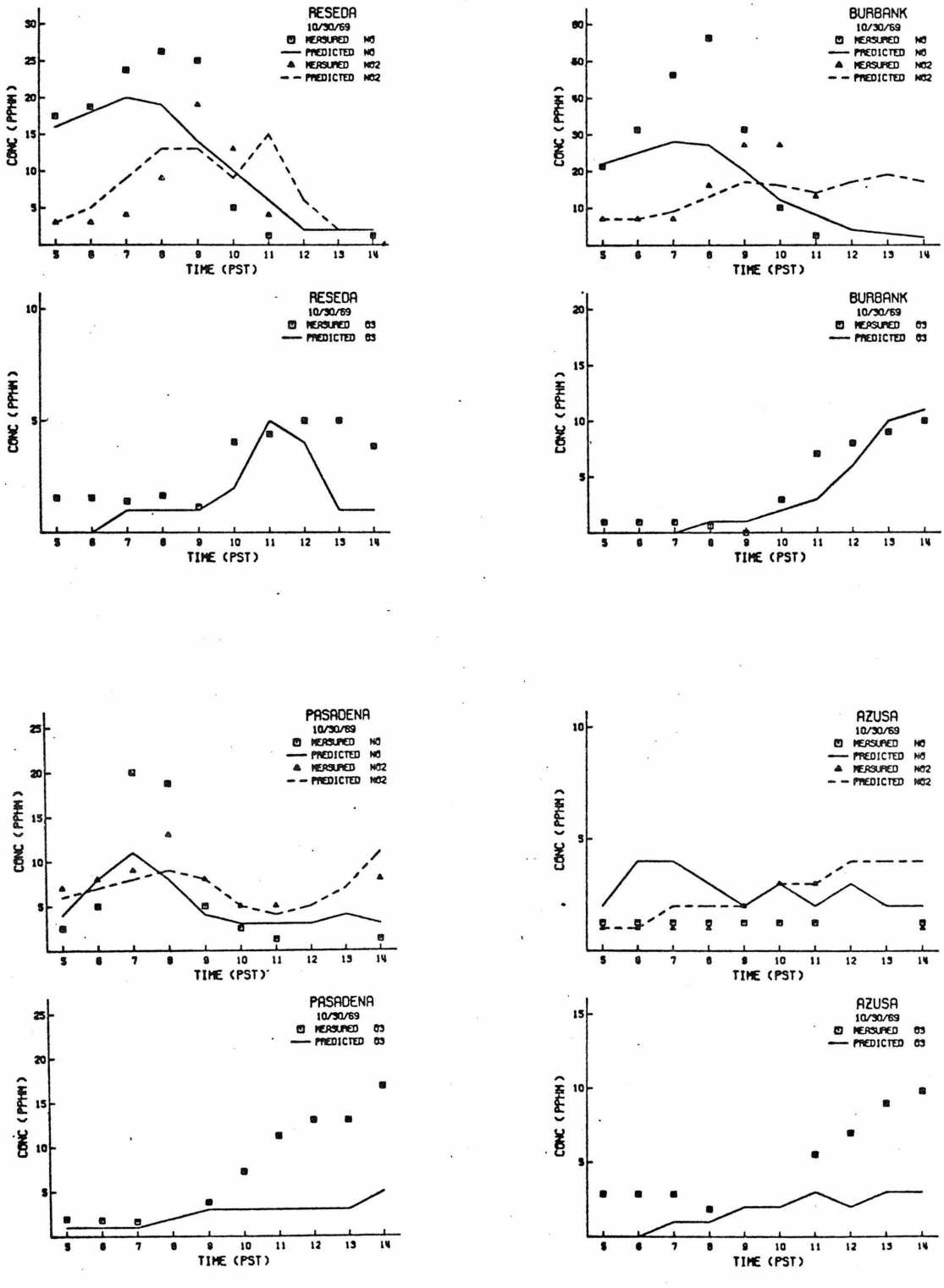
RESEDA
10/30/69
MEASURED NO
PREDICTED NO
MEASURED NO2
PREDICTED NO2
CONC (PPHM)
TIME (PST)
BURBANK
10/30/69
MEASURED NO
PREDICTED NO
MEASURED NO2
PREDICTED NO2
CONC (PPHM)
TIME (PST)
RESEDA
10/30/69
MEASURED O3
PREDICTED O3
CONC (PPHM)
TIME (PST)
BURBANK
10/30/69
MEASURED O3
PREDICTED O3
CONC (PPHM)
TIME (PST)
PASADENA
10/30/69
MEASURED NO
PREDICTED NO
MEASURED NO2
PREDICTED NO2
CONC (PPHM)
TIME (PST)
AZUSA
10/30/69
MEASURED NO
PREDICTED NO
MEASURED NO2
PREDICTED NO2
CONC (PPHM)
TIME (PST)
PASADENA
10/30/69
MEASURED O3
PREDICTED O3
CONC (PPHM)
TIME (PST)
AZUSA
10/30/69
MEASURED O3
PREDICTED O3
CONC (PPHM)
TIME (PST)

Figure E.33

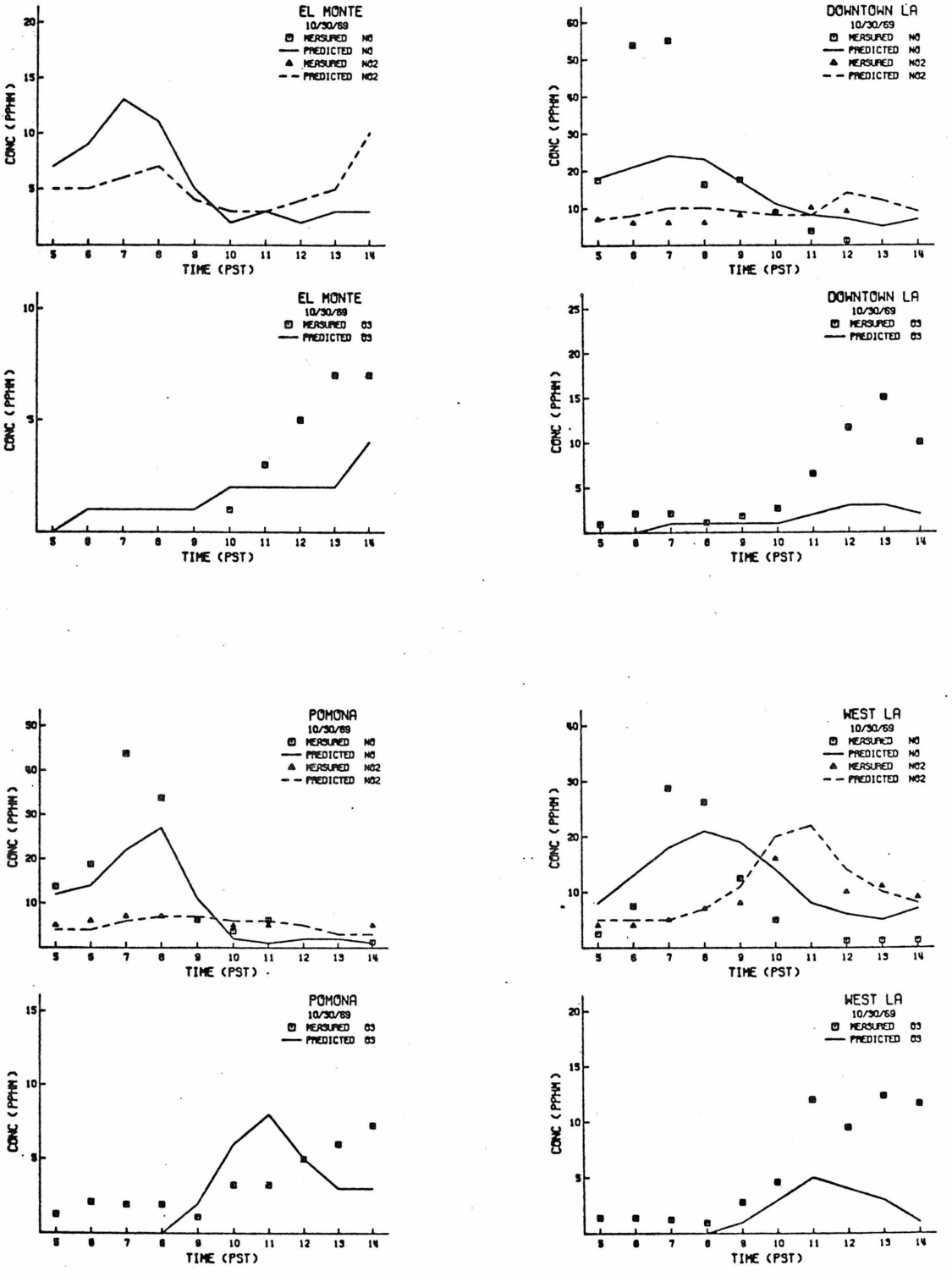
EL MONTE
10/30/69
MEASURED NO
PREDICTED NO
MEASURED NO2
PREDICTED NO2
CONC (PPHM)
TIME (PST)
EL MONTE
10/30/69
MEASURED O3
PREDICTED O3
CONC (PPHM)
TIME (PST)
DOWNTOWN LA
10/30/69
MEASURED NO
PREDICTED NO
MEASURED NO2
PREDICTED NO2
CONC (PPHM)
TIME (PST)
DOWNTOWN LA
10/30/69
MEASURED O3
PREDICTED O3
CONC (PPHM)
TIME (PST)
POMONA
10/30/69
MEASURED NO
PREDICTED NO
MEASURED NO2
PREDICTED NO2
CONC (PPHM)
TIME (PST)
POMONA
10/30/69
MEASURED O3
PREDICTED O3
CONC (PPHM)
TIME (PST)
WEST LA
10/30/69
MEASURED NO
PREDICTED NO
MEASURED NO2
PREDICTED NO2
CONC (PPHM)
TIME (PST)
WEST LA
10/30/69
MEASURED O3
PREDICTED O3
CONC (PPHM)
TIME (PST)

Figure E. 34

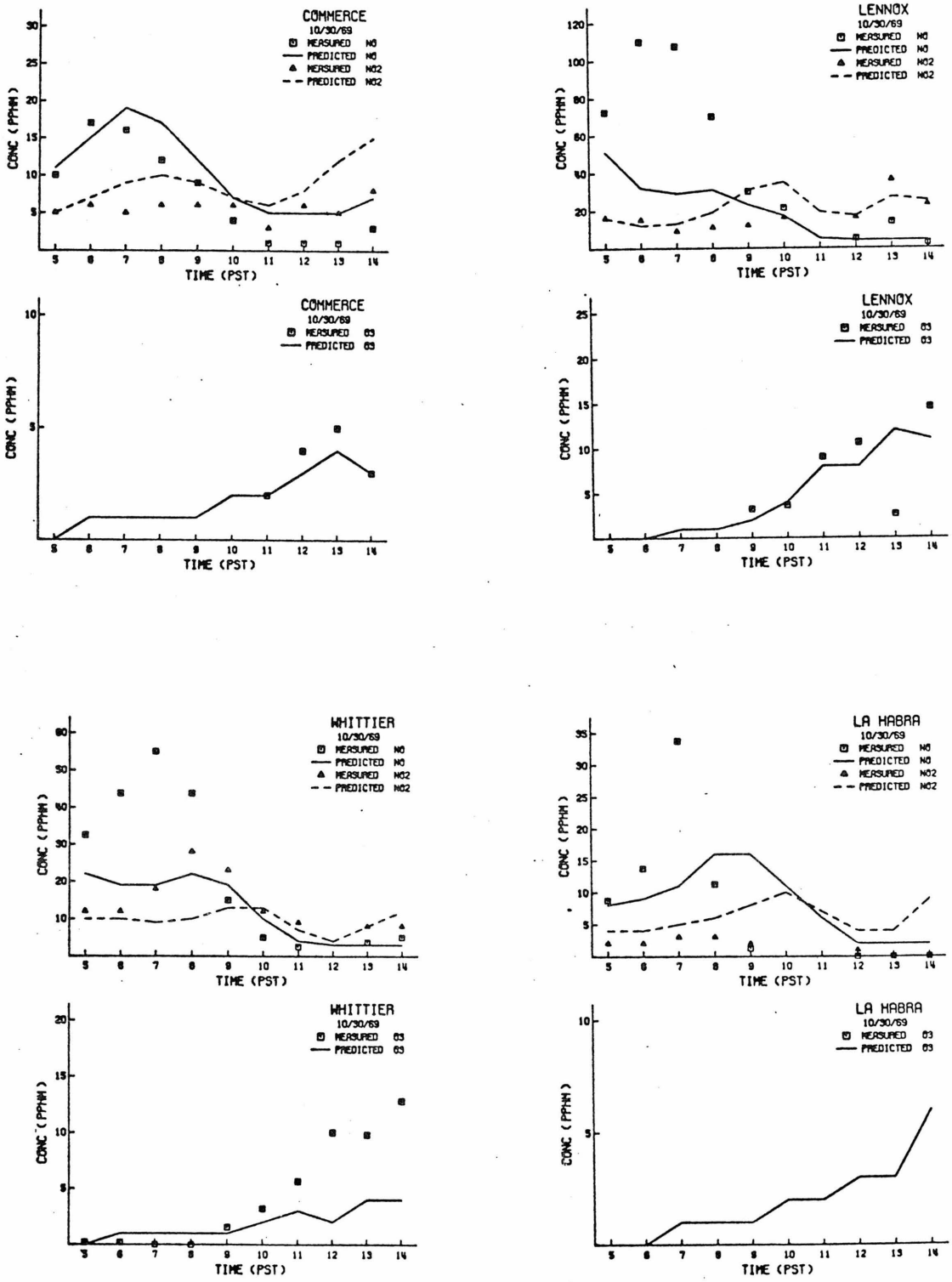
COMMERCE
10/30/69
MEASURED NO
PREDICTED NO
MEASURED NO2
PREDICTED NO2
CONC (PPHM)
TIME (PST)
LENNOX
10/30/69
MEASURED NO
PREDICTED NO
MEASURED NO2
PREDICTED NO2
CONC (PPHM)
TIME (PST)
COMMERCE
10/30/69
MEASURED O3
PREDICTED O3
CONC (PPHM)
TIME (PST)
LENNOX
10/30/69
MEASURED O3
PREDICTED O3
CONC (PPHM)
TIME (PST)
WHITTIER
10/30/69
MEASURED NO
PREDICTED NO
MEASURED NO2
PREDICTED NO2
CONC (PPHM)
TIME (PST)
LA HABRA
10/30/69
MEASURED NO
PREDICTED NO
MEASURED NO2
PREDICTED NO2
CONC (PPHM)
TIME (PST)
WHITTIER
10/30/69
MEASURED O3
PREDICTED O3
CONC (PPHM)
TIME (PST)
LA HABRA
10/30/69
MEASURED O3
PREDICTED O3
CONC (PPHM)
TIME (PST)

Figure E.35

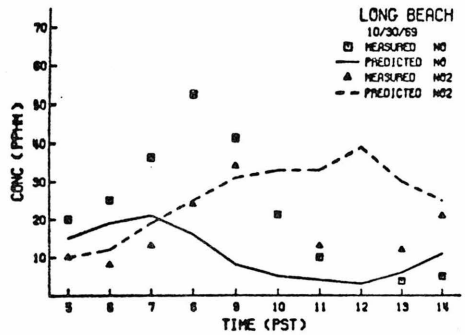
LONG BEACH
10/30/69
MEASURED NO
PREDICTED NO
MEASURED NO2
PREDICTED NO2
CONC (PPHM)
TIME (PST)

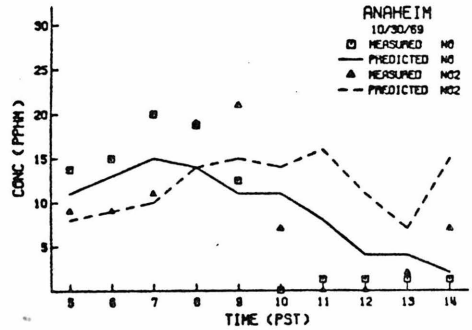
ANAHEIM
10/30/69
MEASURED NO
PREDICTED NO
MEASURED NO2
PREDICTED NO2
CONC (PPHM)
TIME (PST)

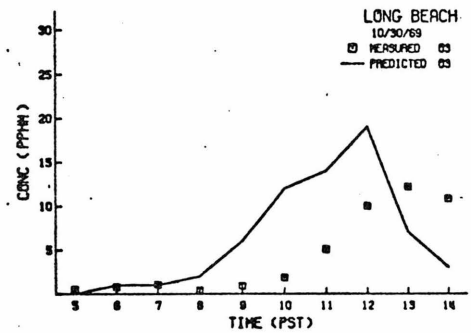
LONG BEACH
10/30/69
MEASURED O3
PREDICTED O3
CONC (PPHM)
TIME (PST)

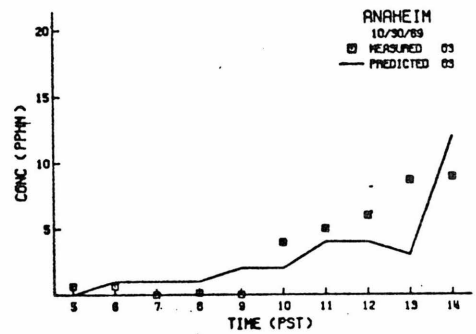
ANAHEIM
10/30/69
MEASURED O3
PREDICTED O3
CONC (PPHM)
TIME (PST)

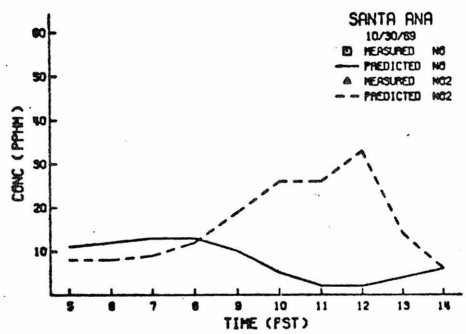
SANTA ANA
10/30/69
MEASURED NO
PREDICTED NO
MEASURED NO2
PREDICTED NO2
CONC (PPHM)
TIME (PST)

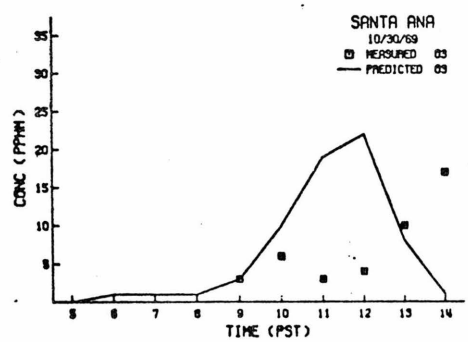
SANTA ANA
10/30/69
MEASURED O3
PREDICTED O3
CONC (PPHM)
TIME (PST)

Figure E.36

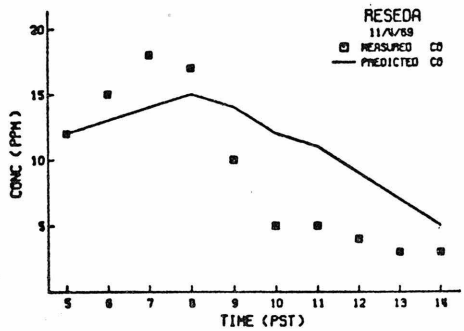
RESEDA
11/4/69
MEASURED CO
PREDICTED CO
CONC (PPM)
TIME (PST)

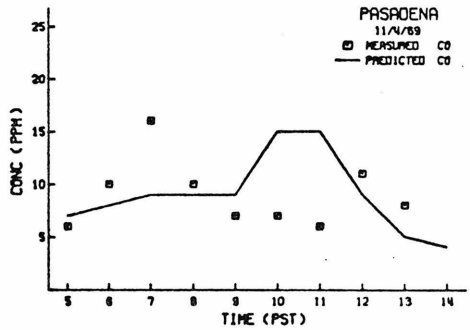
PASADENA
11/4/69
MEASURED CO
PREDICTED CO
CONC (PPM)
TIME (PST)

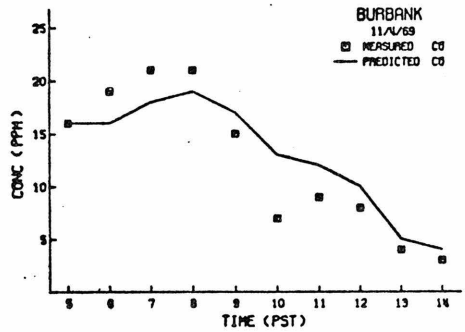
BURBANK
11/4/69
MEASURED CO
PREDICTED CO
CONC (PPM)
TIME (PST)

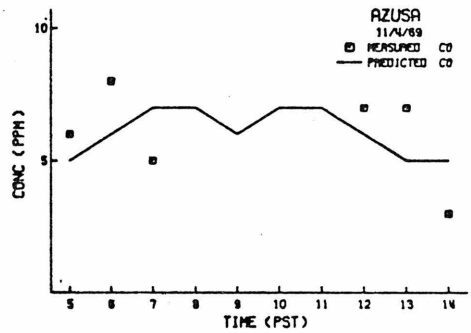
AZUSA
11/4/69
MEASURED CO
PREDICTED CO
CONC (PPM)
TIME (PST)

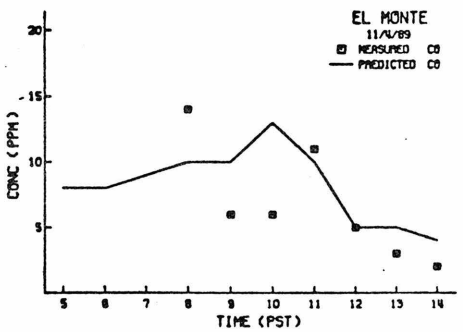
EL MONTE
11/4/69
MEASURED CO
PREDICTED CO
CONC (PPM)
TIME (PST)

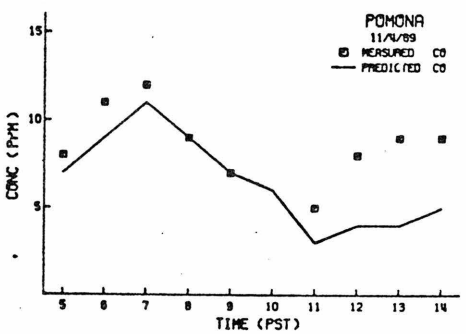
POMONA
11/4/69
MEASURED CO
PREDICTED CO
CONC (PPM)
TIME (PST)

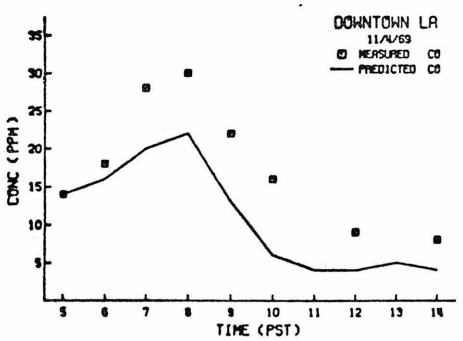
DOWNTOWN LA
11/4/69
MEASURED CO
PREDICTED CO
CONC (PPM)
TIME (PST)

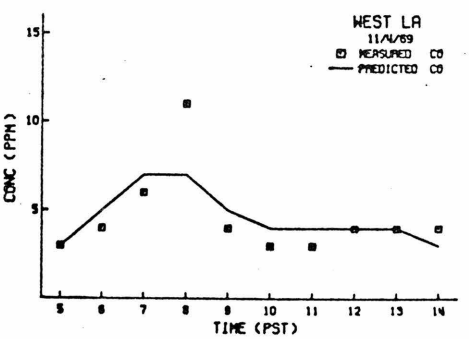
WEST LA
11/4/69
MEASURED CO
PREDICTED CO
CONC (PPM)
TIME (PST)

Figure E.37

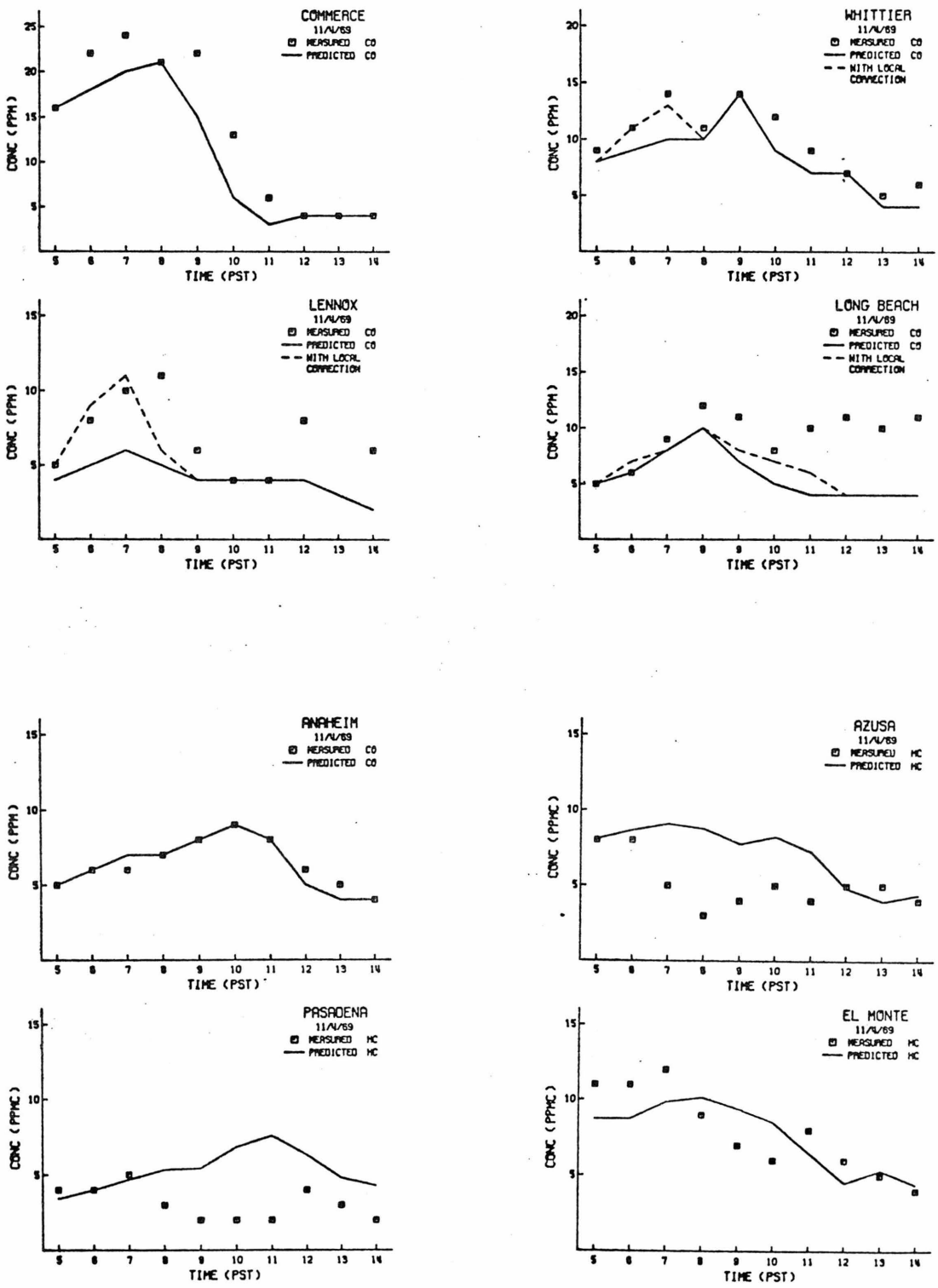
COMMERCE
11/1/69
MEASURED CO
PREDICTED CO
CONC (PPM)
TIME (PST)
WHITTIER
11/1/69
MEASURED CO
PREDICTED CO
WITH LOCAL CORRECTION
CONC (PPM)
TIME (PST)
LENNOX
11/1/69
MEASURED CO
PREDICTED CO
WITH LOCAL CORRECTION
CONC (PPM)
TIME (PST)
LONG BEACH
11/1/69
MEASURED CO
PREDICTED CO
WITH LOCAL CORRECTION
CONC (PPM)
TIME (PST)
ANAHEIM
11/1/69
MEASURED CO
PREDICTED CO
CONC (PPM)
TIME (PST)
AZUSA
11/1/69
MEASURED HC
PREDICTED HC
CONC (PPMC)
TIME (PST)
PASADENA
11/1/69
MEASURED HC
PREDICTED HC
CONC (PPMC)
TIME (PST)
EL MONTE
11/1/69
MEASURED HC
PREDICTED HC
CONC (PPMC)
TIME (PST)

Figure E.38

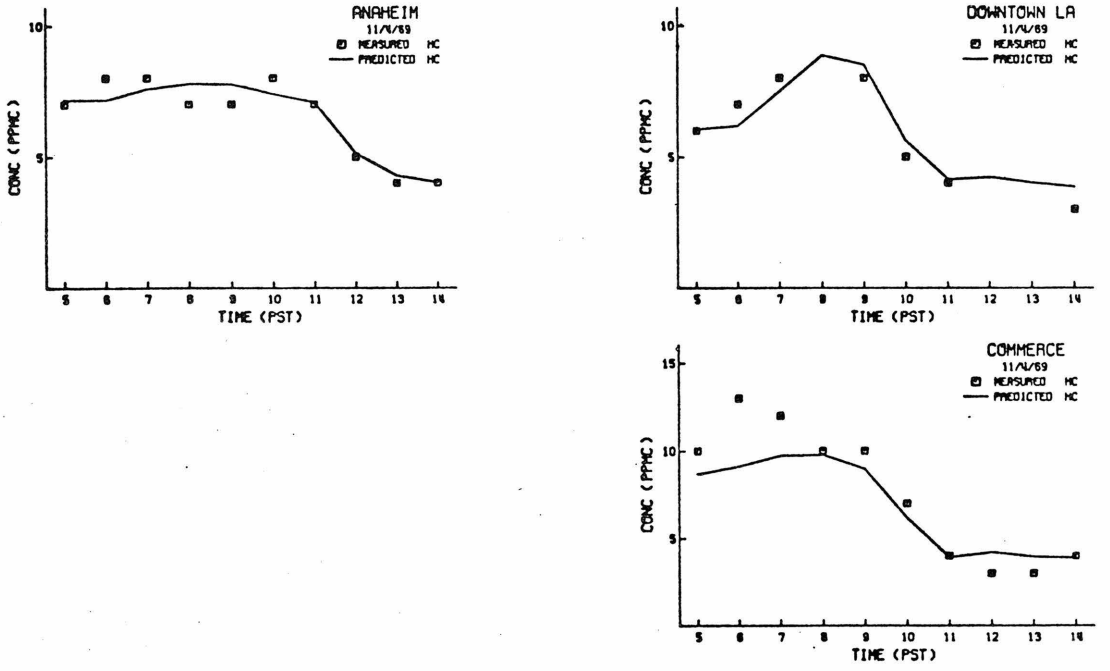
ANAHEIM
11/1/69
MEASURED HC
PREDICTED HC
CONC (PPMC)
TIME (PST)
DOWNTOWN LA
11/1/69
MEASURED HC
PREDICTED HC
CONC (PPMC)
TIME (PST)
COMMERCE
11/1/69
MEASURED HC
PREDICTED HC
CONC (PPMC)
TIME (PST)

Figure E.39

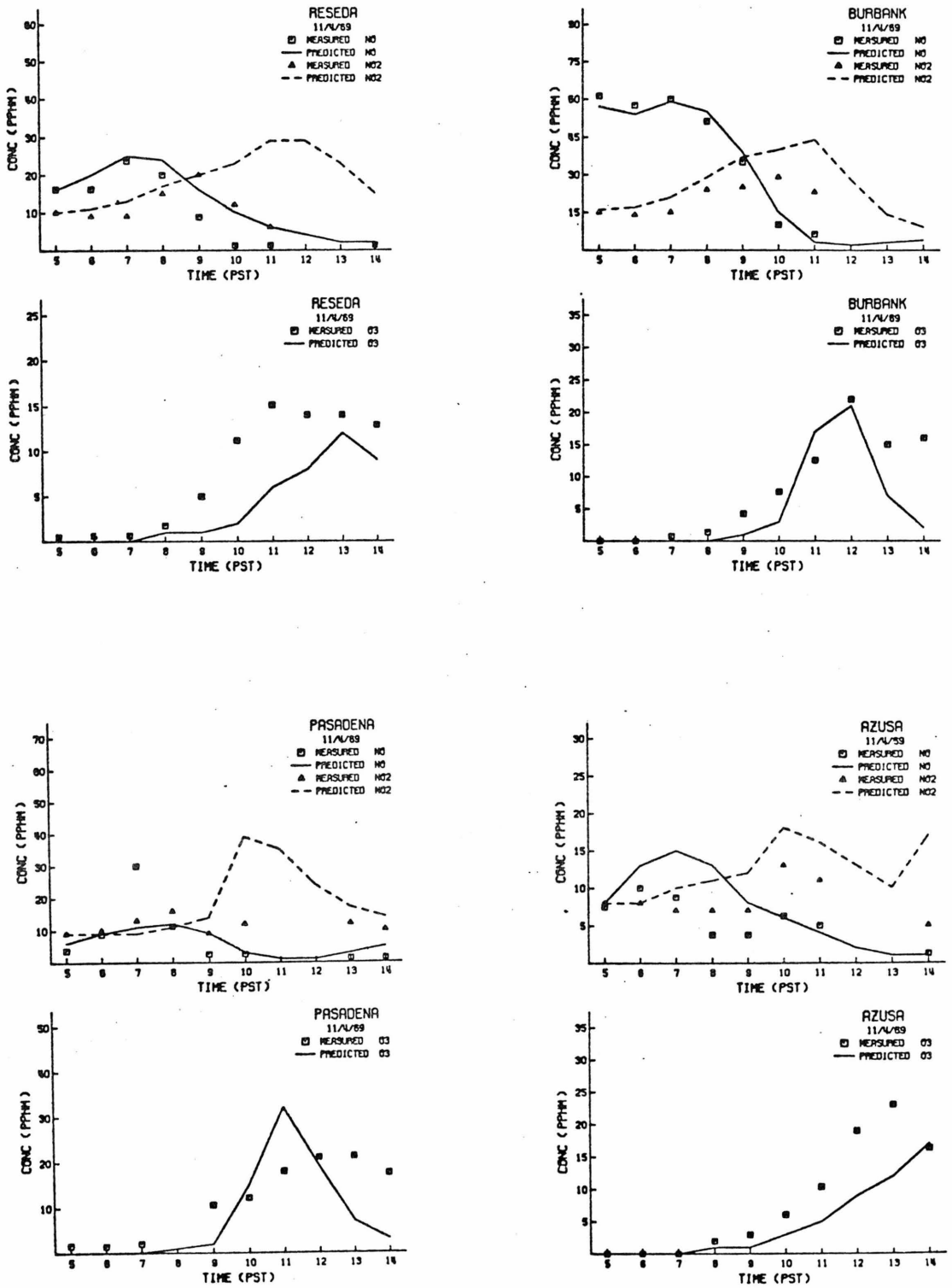
RESEDA
11/4/69
MEASURED NO
PREDICTED NO
MEASURED NO2
PREDICTED NO2
CONC (PPHM)
TIME (PST)
RESEDA
11/4/69
MEASURED O3
PREDICTED O3
CONC (PPHM)
TIME (PST)
BURBANK
11/4/69
MEASURED NO
PREDICTED NO
MEASURED NO2
PREDICTED NO2
CONC (PPHM)
TIME (PST)
BURBANK
11/4/69
MEASURED O3
PREDICTED O3
CONC (PPHM)
TIME (PST)
PASADENA
11/4/69
MEASURED NO
PREDICTED NO
MEASURED NO2
PREDICTED NO2
CONC (PPHM)
TIME (PST)
PASADENA
11/4/69
MEASURED O3
PREDICTED O3
CONC (PPHM)
TIME (PST)
AZUSA
11/4/69
MEASURED NO
PREDICTED NO
MEASURED NO2
PREDICTED NO2
CONC (PPHM)
TIME (PST)
AZUSA
11/4/69
MEASURED O3
PREDICTED O3
CONC (PPHM)
TIME (PST)

Figure 4.40

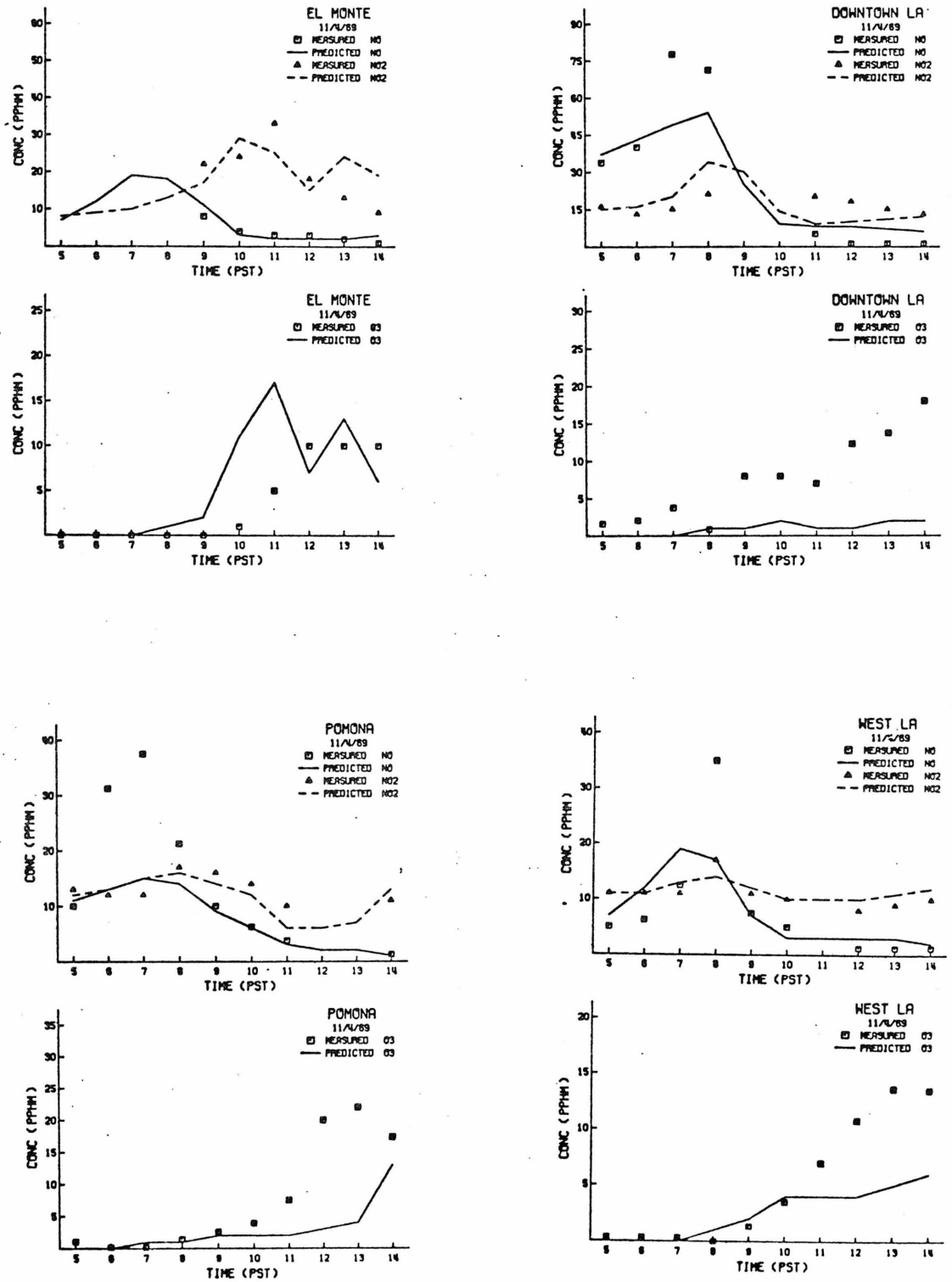
EL MONTE
11/6/69
MEASURED NO
PREDICTED NO
MEASURED NO2
PREDICTED NO2
CONC (PPHM)
TIME (PST)
EL MONTE
11/6/69
MEASURED O3
PREDICTED O3
CONC (PPHM)
TIME (PST)
DOWNTOWN LA
11/6/69
MEASURED NO
PREDICTED NO
MEASURED NO2
PREDICTED NO2
CONC (PPHM)
TIME (PST)
DOWNTOWN LA
11/6/69
MEASURED O3
PREDICTED O3
CONC (PPHM)
TIME (PST)
POMONA
11/6/69
MEASURED NO
PREDICTED NO
MEASURED NO2
PREDICTED NO2
CONC (PPHM)
TIME (PST)
POMONA
11/6/69
MEASURED O3
PREDICTED O3
CONC (PPHM)
TIME (PST)
WEST LA
11/6/69
MEASURED NO
PREDICTED NO
MEASURED NO2
PREDICTED NO2
CONC (PPHM)
TIME (PST)
WEST LA
11/6/69
MEASURED O3
PREDICTED O3
CONC (PPHM)
TIME (PST)

Figure E.41

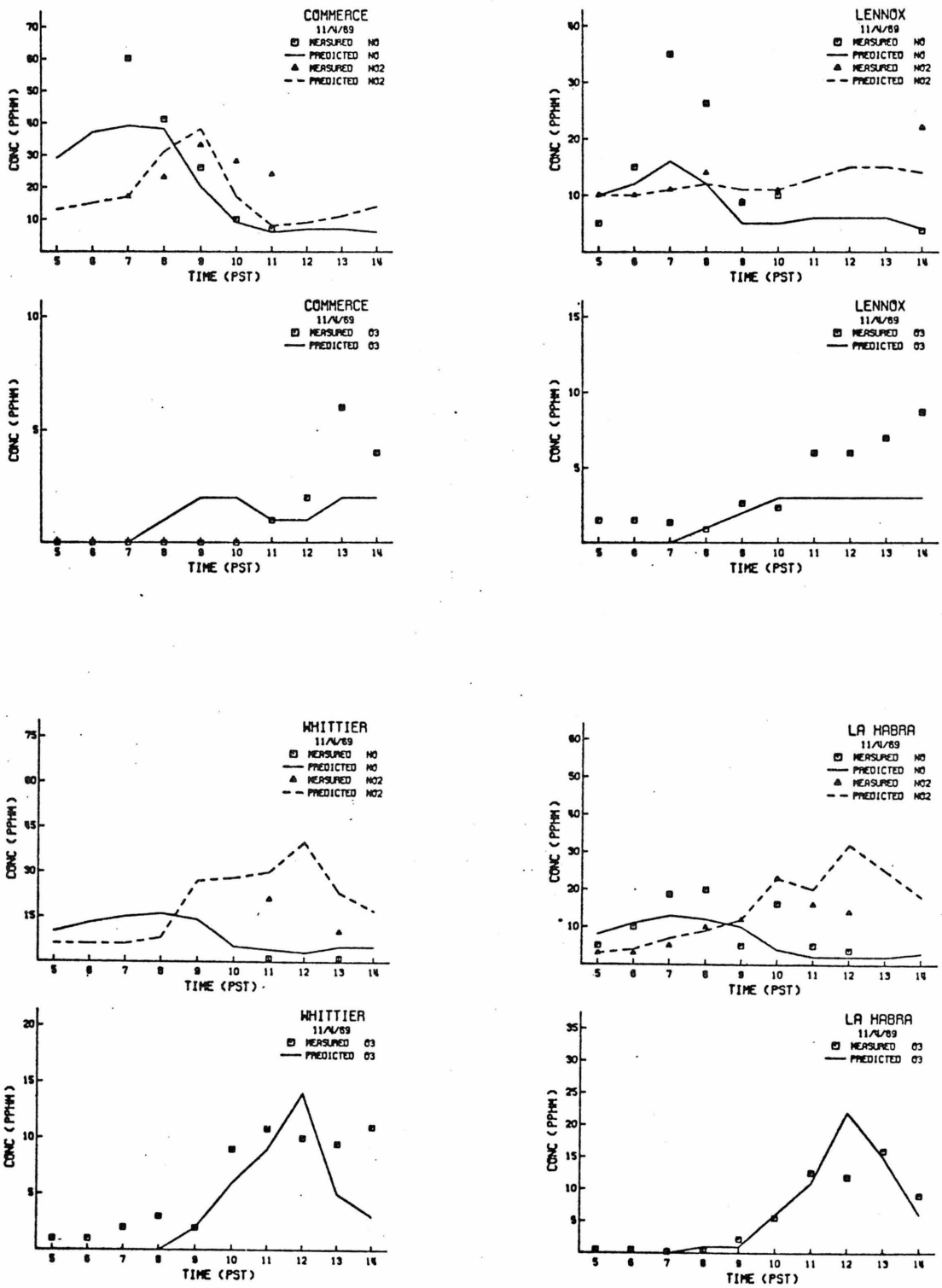
COMMERCE
11/A/69
MEASURED NO
PREDICTED NO
MEASURED NO2
PREDICTED NO2
CONC (PPHM)
TIME (PST)
LENNOX
11/A/69
MEASURED NO
PREDICTED NO
MEASURED NO2
PREDICTED NO2
CONC (PPHM)
TIME (PST)
COMMERCE
11/A/69
MEASURED O3
PREDICTED O3
CONC (PPHM)
TIME (PST)
LENNOX
11/A/69
MEASURED O3
PREDICTED O3
CONC (PPHM)
TIME (PST)
WHITTIER
11/A/69
MEASURED NO
PREDICTED NO
MEASURED NO2
PREDICTED NO2
CONC (PPHM)
TIME (PST)
LA HABRA
11/A/69
MEASURED NO
PREDICTED NO
MEASURED NO2
PREDICTED NO2
CONC (PPHM)
TIME (PST)
WHITTIER
11/A/69
MEASURED O3
PREDICTED O3
CONC (PPHM)
TIME (PST)
LA HABRA
11/A/69
MEASURED O3
PREDICTED O3
CONC (PPHM)
TIME (PST)

Figure E.42

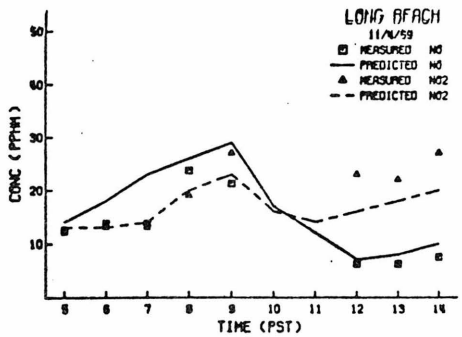
LONG BEACH
11/4/69
MEASURED NO
PREDICTED NO
MEASURED NO2
PREDICTED NO2
CONC (PPHM)
TIME (PST)

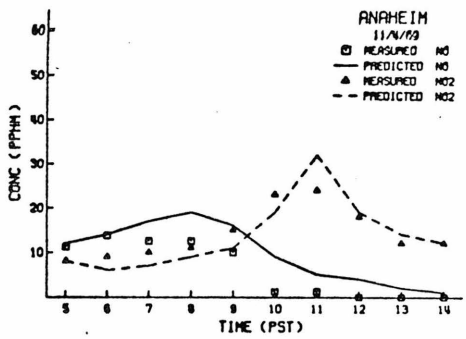
ANAHEIM
11/4/69
MEASURED NO
PREDICTED NO
MEASURED NO2
PREDICTED NO2
CONC (PPHM)
TIME (PST)

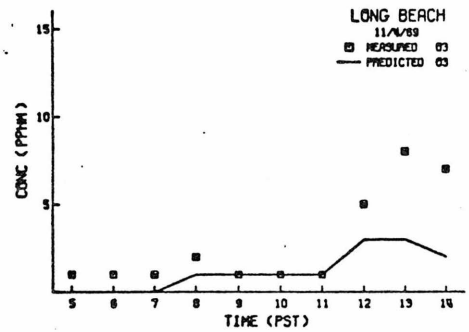
LONG BEACH
11/4/69
MEASURED O3
PREDICTED O3
CONC (PPHM)
TIME (PST)

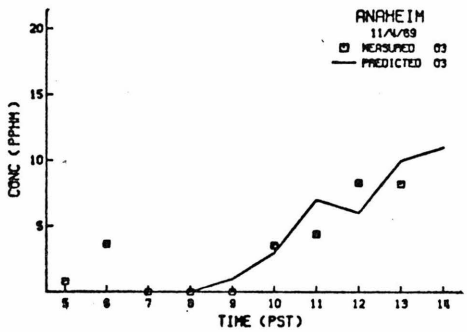
ANAHEIM
11/4/69
MEASURED O3
PREDICTED O3
CONC (PPHM)
TIME (PST)

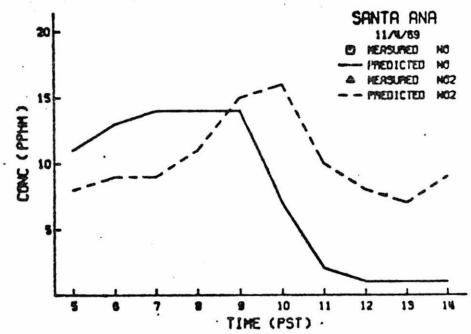
SANTA ANA
11/4/69
MEASURED NO
PREDICTED NO
MEASURED NO2
PREDICTED NO2
CONC (PPHM)
TIME (PST)

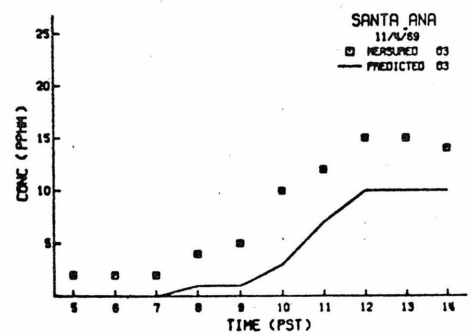
SANTA ANA
11/4/69
MEASURED O3
PREDICTED O3
CONC (PPHM)
TIME (PST)

References

Altshuller, A. P., Kopczynski, S. L., Lonneman, W. A., Becker, T. L., and Slater, R. (1967a), Chemical Aspects of the Photo-oxidation of the Propylene-Nitrogen Oxide System. Environ. Sci. Technol., 1, 899.

Altshuller, A. P., Kopczynski, S. L., Lonneman, W. A. and Wilson, D. L. (1967b). Photochemical Reactivities of Exhausts from 1966 Model Automobiles to Reduce Hydrocarbon Emissions. Jour. Air Poll. Control Assoc., 17, 734.

Altshuller, A. P., Kopczynski, S. L., Wilson, D. L., Lonneman, W. A., and Sutterfield, F. D. (1969). Photochemical Reactivities of Paraffinic Hydrocarbon-Nitrogen Oxide Mixtures Upon Addition of Propylene or Toluene. Jour. Air Poll. Control Assoc., 19, 791.

Altshuller, A. P., Kopczynski, S. L., Lonneman, W. A., Sutterfield, F. D., and Wilson, D. L. (1970). Photochemical Reactivities of Aromatic Hydrocarbon-Nitrogen Oxide and Related Systems, Environ. Sci. Technol., 4, 44.

Angell, J. K., Pack, D. H., Machta, L., Dickson, C. R. and Hoecker, W. H. (1972). Three-dimensional air trajectories determined from tetroon flights in the planetary boundary layer of the Los Angeles Basin. J. Appl. Meteorol., 11, 451.

Arcineaux, J. (1971). Private communication. State of California Division of Highways.

Automotive Environmental Systems (1973). A study of emissions from light duty vehicles in six cities. U. S. Environmental Protection Agency Report APTD-1497, Westminster, California.

Barth, D. S. (1970). Federal motor vehicle emission goals for CO, HC and NO_x based on desired air quality levels. Jour. Air Poll. Control Assoc., 20, 519.

Bastress, E. K. and Fletcher, R. S. (1969). Aircraft Engine Exhaust Emissions. Presented at the American Society of Mechanical Engineers Annual Winter Meeting, November 16-20, Los Angeles, California.

Bell, G. B. (1959). A study of pollutant transport due to surface winds in Los Angeles, Orange, Riverside and San Bernardino Counties. State of California, Department of Public Health.

Bella, D. A. and Grenney, W. J. (1970). Finite-difference convection errors. Journ. Sanitary Eng. Div., A.S.C.E., 96, 1361.

Bratton, D. (1973). Private communication. State of California Air Resources Board, Sacramento, California.

Brief, R. S., Jones, A. R., and Yoder, J. D. (1960). Lead, Carbon Monoxide, and Traffic. Jour. Air Poll. Control Assoc., 10, 384.

Calder, K. (1949). Eddy diffusion and evaporation in flow over aerodynamically smooth and rough surfaces: a treatment based on laboratory laws of turbulent flow with special reference to conditions in the lower atmosphere. Quart. J. Mech. Appl. Math., 2, 153.

Calder, K. L. (1965). On the equation of atmospheric diffusion. Quart. J. Roy. Meteorol. Soc., 91, 514.

Chang, P. C., Wang, P. N., and Lin, A. (1971). Turbulent Diffusion in a City Street. Air Pollution, Turbulence and Diffusion Symposium, Las Cruces, New Mexico.

Conte, S. D. (1965). Elementary Numerical Analysis. McGraw-Hill, New York.

Corrsin, S. (1958). Statistical behavior of a reacting mixture in isotropic turbulence, Phys. Fluid, 1, 42.

County of Orange Air Pollution Control District (1970). Emissions Inventory 1969.

County Supervisors Association of California (1972). California County Fact Book, Sacramento, California.

Crowley, W. P. (1968). Numerical advection experiments. Monthly Weather Review, 96, 1.

Culham, W. E. and Varga, R. S. (1971). Numerical methods for time-dependent, nonlinear boundary value problems. Soc. Petroleum Eng. Journal, 11, 374.

Djuric, D. and Thomas, J. (1971). A Numerical Study of Convective Transport of a Gaseous Air Pollutant in the Vicinity of Tall Buildings. Air Pollution, Turbulence and Diffusion Symposium, Las Cruces, New Mexico.

Dodge, M. C. and Bufalini, J. J. (1972). The Role of Carbon Monoxide in Polluted Atmospheres. Adv. in Chem., 113, 232.

Donaldson, C. DuP. and Hilst, G. R. (1972). Effect of inhomogeneous mixing on atmospheric photochemical reactions. Environ. Sci. Technol., 6, 812.

Douglas, J., Jr. and DuPont, T. (1970). Galerkin methods for parabolic equations. SIAM J. Numer. Anal., 7, 575.

Edinger, J. G. (1959). Changes in the depth of the marine layer over the Los Angeles Basin. J. Meteorol., 16, 219.

Egan, B. A. and Mahoney, J. R. (1972). Numerical modeling of advection and diffusion of urban area source pollutants. J. Appl. Meteor., 11, 312.

Environmental Protection Agency (1971). National primary and secondary ambient air quality standards. Federal Register, 36, 8186.

Environmental Protection Agency (1973a). Technical support document for the metropolitan Los Angeles Intrastate Air Quality Control Region. San Francisco, California.

Environmental Protection Agency (1973b). Compilation of air pollutant emission factors (second edition). Report AP-42, Office of Air and Water Programs, Research Triangle Park, N. C.

Environmental Protection Agency (1973c). Guide for compiling a comprehensive emission inventory. Report APTD-1135, Office of Air and Water Programs, Research Triangle Park, N. C.

Environmental Protection Agency (1973d). Federal certification test results for 1973 model year. Federal Register, 38, 10868.

Environmental Protection Agency (1973e). 1975 motor vehicle exhaust emission standards. Federal Register, 38, 20365.

Environmental Protection Agency (1973f). Interim standards for 1976 model year light duty vehicles. Federal Register, 38, 22474.

Environmental Protection Agency (1973g). California air quality control--approval and promulgation of implementation plans. Federal Register, 38, 17683.

Environmental Protection Agency (1973h). California air quality standards--approval and promulgation of implementation plans. Federal Register, 38, 2194.

Eschenroeder, A. Q. and Martinez, J. R. (1969). Mathematical modeling of photochemical smog. Report No. IMR 1210, General Research Corp., Santa Barbara, Calif.

Eschenroeder, A. Q. and J. R. Martinez (1970). Analysis of Los Angeles Atmospheric Reaction Data from 1968 and 1969. General Research Corporation, Santa Barbara, Calif.

Eschenroeder, A. Q., Martinez, J. R., and Nordsieck, R. A. (1972). Evaluation of a diffusion model for photochemical smog simulation. Report No. CR-1-273, General Research Corp., Santa Barbara, California.

Fegraus, C. E., Domke, C. J., and Marzen, J. (1973). Contribution of the motor vehicle population to atmospheric pollution. Society of Automotive Engineers Paper No. 730530, Presented at the May 14-18 Automotive Engineers Meeting, Detroit, Michigan.

Felgar, D. N. (1973). Private communication. Southern California Edison Company, Rosemead, California.

Fromm, J. C. (1969). Practical investigation of convective difference approximations of reduced dispersion. Phys. Fluids Supp. II, 12, II-3.

Gear, C. W. (1971). The automatic integration of ordinary differential equations. ACM, 14, 176.

Georgii, H. W., Busch, E., and Weber, E. (1967). Investigation of the Temporal and Spatial Distribution of the Emission Concentration of Carbon Monoxide in Frankfurt/Main. Report No. 11 of the Institute for Meteorology and Geophysics, University of Frankfurt/Main.

Georgii, H. W. (1969). The Effects of Air Pollution on Urban Climates. Bull. of the World Health Org., 40, 4, 624.

Guymon, G. L. (1970). A finite element solution of the one-dimensional diffusion-convection equation. Water Res. Research, 6, 204.

Guymon, G. L., Scott, V. H., and Herrmann, L. R. (1970). A general numerical solution of the two-dimensional diffusion-convection equation by the finite element method. Water Res. Research, 6, 1611.

Hay, J. S. and Pasquill, F. (1959). Diffusion from a continuous source in relation to the spectrum and scale of turbulence. Advances in Geophysics, Vol. 6, F. N. Frenkiel and P. A. Sheppard, editors, Academic Press, New York.

Hecht, T. A. and Seinfeld, J. H. (1972). Development and Validation of a Generalized Mechanism for Photochemical Smog. Environ. Sci. Technol., 6, 47.

Hecht, T. A. and Seinfeld, J. H. (1973). Further Development of a Generalized Kinetic Mechanism for Photochemical Smog. Environ. Sci. Tech., submitted for publication.

Hochheiser, S. and Lozano, E. R. (1968). Air Pollution Emissions from Jet Aircraft Operating in the New York Metropolitan Area. Presented at the Air Transportation Meeting, April 29-May 2, New York.

Holmes, J., Horowitz, J., Reid, R., and Stolpman, P. (1973). The Clean Air Act and transportation controls--an EPA White Paper. U. S. Environmental Protection Agency, Office of Air and Water Programs, Washington, D. C.

Horowitz, J. (1973a). Inspection and maintenance for reducing automobile emissions. Journal Air Poll. Control Assoc., 23, 273.

Horowitz, J. (1973b). The effectiveness and cost of retrofit for reducing automotile emissions. Journal Air Poll. Control Assoc., 23, 395.

Hosler, C. R. (1969). Vertical diffusivity from Radon profiles. Jour. Geophys. Res., 74, 7018.

Hotchkiss, R. S. (1971). The Numerical Calculation of Three Dimensional Flows of Air and Particulates About Structures. Turbulence and Diffusion Symposium, Las Cruces, New Mexico.

Hubert, R. (1973). Private communication. Federal Aviation Administration, Los Angeles, California.

Hurn, R. W. (1968). Air Pollution (A. Stern, Ed.), Vol. III, Academic Press, Second edition.

Isaacson, E. and Keller, H. B. (1966). Analysis of Numerical Methods. John Wiley and Sons, New York.

Jehn, K. H. and Gerhardt, J. R. (1950). A Preliminary Study of the Transfer of Heat near the Earth's Surface. Electronics Engineering Laboratory Report No. 37.

Johnston, H. S., Pitts, J. N., Jr., Lewis, J., Zafonte, L., and Mottershead, T. (1970). Atmospheric Chemistry and Physics. Project Clean Air, Vol. 4, University of California.

Johnson, W. B., Ludwig, F. L., Dabberdt, W. F. and Allen, R. J. (1971). Development and Initial Evaluation of an Urban Diffusion Model for Carbon Monoxide, Sixty-fourth Annual Meeting Amer. Inst. of Chem. Engineers, Paper 25B, San Francisco, Calif.

Kearin, D. H., Lamoureux, R. L., and Goodwin, B. C. (1971). A survey of Average Driving Patterns in Six Urban Areas of the United States: Summary Report. Report TM-(L)-4119 Vol. 7, Systems Development Corporation, Santa Monica, Calif.

Kircher, D. (1972). Private communication, Environmental Protection Agency, Research Triangle Park, North Carolina.

Kraichnan, R. H. (1962). The closure problem of turbulence theory. Proc. of Symposia in Appl. Math., 13, 199.

Kyan, C. P. and Seinfeld, J. H. (1973). Real-time control of air pollution. A.I.Ch.E. Journ., 19, 579.

Lamb, R. G. (1968). An Air Pollution Model of Los Angeles. Masters Thesis, University of California, Los Angeles, Calif.

Lamb, R. G. and Neiburger, M. (1970). Mathematical model of the diffusion and reactions of pollutants emitted over an urban area. Project Clean Air. Research Reports, Vol. 4, University of California, Berkeley.

Lamb, R. G. (1973). Note on the application of K-theory to diffusion problems involving nonlinear chemical reaction. Atmos. Environ., 7, 257.

Lamb, R. G. and Seinfeld, J. H. (1973). Mathematical modeling of urban air pollution-general theory. Environ. Sci. Technol. 7, 3, 253.

Lantz, R. B. (1971). Quantitative evaluation of numerical diffusion (truncation error). Soc. Petroleum Engr. Journ., 11, 315.

Larson, G. P., et al. (1955). Distribution and Effects of Automotive Exhaust Gases in Los Angeles. S.A.E. Technical Progress Series, Vol. 6.

Lee, J. (1966). Isotropic turbulent mixing under a second-order chemical reaction. Phys. Fluids, 9, 1753.

Lee, R. E., Jr., Patterson, R. K., Crider, W. L. and Wagman, J. (1971). Concentration and Particle Size Distribution of Particulate Emissions in Automobile Exhaust. Atmos. Environ., 5, 225.

Lees, L., et al. (1972). Smog--A Report to the People. Environmental Quality Laboratory, California Institute of Technology, Pasadena, California.

Lemke, E. E., Shaffer, N. R., and Verssen, J. A. (1965). Air Pollution from Aircraft in Los Angeles County. Report of the Los Angeles County Air Pollution Control District.

Levaggi, D. (1973). Private communication. Bay Area Air Pollution Control District, San Francisco, California.

Liu, M. K. (1973). Private communication. Systems Applications, Inc., Beverly Hills, California.

Liu, M. K., Whitney, D. C., Reynolds, S. D., Roth, P. M. (1973). Automation of meteorological and air quality data for the SAI urban airshed model. Report R73-SAI-32, Systems Applications, Inc., Beverly Hills, California.

Los Angeles County Air Pollution Control District (1969). Profile of Air Pollution Control in Los Angeles County. Los Angeles, Calif.

Los Angeles County Air Pollution Control District (1971). Profile of air pollution control. Los Angeles, California.

Los Angeles County Air Pollution Control District (1971). Study of jet aircraft emissions and air quality in the vicinity of the Los Angeles International Airport. Los Angeles, California.

Los Angeles County Air Pollution Control District (1973). Major point sources of air pollution in Los Angeles County-April 1973. Los Angeles, California.

Lozano, E. R., Melvin, Jr., W. W., and Hochheiser, S. (1968). Air Pollution Emissions from Jet Engines. Jour. Air Poll. Control Assoc., 18, 392.

Lumley, J. L. and Panofsky, H. A. (1964). The Structure of Atmospheric Turbulence. Interscience, New York.

MacBeth, W. G. (1973). Private communication. Los Angeles County Air Pollution Control District, Los Angeles, California.

Martinez, J. R., Nordsieck, R. A., and Eschenroeder, A. Q., (1971). Morning Vehicle-Start Effects on Photochemical Smog. Report CR-2-191, General Research Corporation, Santa Barbara, Calif.

McCormick, R. A. and Xintaras, C. (1962). Variation of Carbon Monoxide Concentrations as Related to Sampling Interval, Traffic and Meteorological Factors. Jour. Air Poll. Control Assoc., 17, 46.

Molenkamp, C. R. (1968). Accuracy of finite-difference methods applied to the advection equation. J. Appl. Meteor., 7, 160.

Monin, A. S. and Yaglom, A. M. (1971). Statistical Fluid Mechanics. MIT Press, Cambridge, Mass.

National Academy of Sciences (1973). Report by the Committee on Motor Vehicle Emissions. Washington, D. C.

Neiburger, M., and Edinger, J. G. (1954). Meteorology of the Los Angeles Basin. Air Pollution Foundation, Report No. 1, Los Angeles, California.

Neiburger, M., Renzetti, N. A. and Tice, R. (1956). Wind trajectory studies of the movement of polluted air in the Los Angeles Basin. Air Pollution Foundation, Report No. 13, Los Angeles, California.

Nevitt, J. S. (1973). Private communication. Los Angeles Air Pollution Control District, Los Angeles, California.

Northern Research and Engineering Corporation (1968). Nature and Control of Aircraft Engine Exhaust Emissions. CFSTI # PB 187771.

O'Brien, E. E. (1966). Closure approximations applied to stochastically distributed second-order reactants. Phys. Fluids, 9, 1561.

O'Brien, E. E. (1968a). Closure for stochastically distributed second-order reactants. Phys. Fluids, 11, 1883.

O'Brien, E. E. (1968b). Lagrangian history direct interaction equations for isotropic turbulent mixing under a second-order chemical reaction. Phys. Fluids, 11, 2328.

O'Brien, E. E. (1969). Postulate of statistical independence for decaying reactants in homogeneous turbulence. Phys. Fluids, 12, 1999.

O'Brien, E. E. (1971). Turbulent mixing of two rapidly reacting chemical species. Phys. Fluids, 14, 1326.

Ott, W., (1971). An Urban Survey Technique for Measuring the Spatial Variation of Carbon Monoxide Concentrations in Cities. Ph.D. Thesis, Stanford University.

Ozolins, G. and Smith, R. (1966). Rapid Survey Technique for Estimating Community Air Pollution Emissions. Public Health Service Pub. No. 999-AP-29.

Papa, L. J. (1967). Gas Chromatography-Measuring Exhaust Hydrocarbons Down to Parts Per Billion. Mid Year Meeting of the Society of Automotive Engineers, No. 670494, Chicago, Illinois.

Pasquill, F. (1962). Atmospheric Diffusion. van Nostrand, London.

Price, H. S., Varga, R. S., and Warren, J. E. (1966). Application of oscillation matrices to diffusion-convection equations. J. Math. Phys., 45, 301.

Price, H. S., Cavendish, J. C. and Varga, R. S. (1968). Numerical methods of higher-order accuracy for diffusion-convection equations. Soc. Petroleum Eng. Journal, 8, 293.

Ragland, K. W. (1973). Multiple box model for dispersion of air pollutants from area sources. Journ. Air Poll. Control Assoc., 7, 1017.

Rehmann, C. R. (1968). Motor Vehicle Exhaust-Emissions--Gary, Indiana. Public Health Service, National Center for Air Pollution Control Publication APTD-68-5, CFSTI #PB 195156.

Reynolds, S. D. (1973). User's guide and description of the computer programs. Report R73-18, Systems Applications, Inc., Beverly Hills, California.

Reynolds, S. D., Liu, M., Roth, P. M., Hecht, T. A. and Seinfeld, J. H. (1973). Evaluation of a Simulation Model for Estimating Ground Level Concentrations of Photochemical Pollutants. Systems Applications, Inc., Beverly Hills, Calif.

Richtmyer, R. D. and Morton, K. W. (1967). Difference Methods for Initial-Value Problems. Wiley-Interscience, New York.

Roberts, K. V. and Weiss, N. O. (1966). Convective difference schemes. Math. of Comp., 20, 272.

Rose, Jr., A. H., Smith, R., McMichael, W. F., and Kruse, R. E. (1965). Comparison of Auto Exhaust Emissions from Two Major Cities. Jour. Air Poll. Control Assoc., 15, 362.

Roth, P. M., Reynolds, S. D., Roberts, P.J.W., and Seinfeld, J. H. (1971). Development of a simulation model for estimating ground-level concentrations of photochemical pollutants. Final Report and Six Appendices. Systems Applications, Inc., Beverly Hills, California.

Sachtschale, J. R. (1973). Private communication. Automotive Environmental Systems, Inc., Westminster, California.

Saffman, P. G. (1969). Application of the Wiener-Hermite expansion to the diffusion of a passive scalar in a homogeneous turbulent flow. Phys. Fluids, 12, 1786.

Sawyer, R. (1972). Private communication. University of California, Berkeley.

Schnelle, K. B., Ziegler, F. G., and Krenkel, P. A. (1969). A Study of the Vertical Distribution of Carbon Monoxide and Temperature Above an Urban Intersection. Air Poll. Control Assoc. Paper No. 69-152.

Scott Research Laboratories (1970). Program design and methodology data summary and discussion. 1969 Atmospheric Reaction Studies in the Los Angeles Basin. Final report.

Scott Research Laboratories (1970). A Study of Exhaust Emissions from Reciprocating Aircraft Power Plants. Contract No. CPA 22-69-129.

Shir, C. C. and Shieh, L. J. (1973). A generalized urban air pollution model and its application to the study of SO_2 distributions in the St. Louis metropolitan area. Report RJ 1227, IBM Research Laboratory, San Jose, California.

Shum, Y. M. (1971). Use of finite-element method in the solution of diffusion-convection equations. Soc. Petroleum Eng. Journal, 11, 139.

Sigworth, H. W. (1971). Private communication. Air Pollution Control Office, Environmental Protection Agency.

Sigworth, H. W. (1972). Private communication. Air Pollution Control Office, Environmental Protection Agency.

Sklarew, R. C., Fabrick, A. J. and Prager, J. E. (1971). A particle-in-cell method for numerical solution of the atmospheric diffusion equation, and applications to air pollution problems. Report No. 3SR-844, Systems, Science and Software, La Jolla, Calif.

Smith, M. and Manos, M. J. (1972). Determination and Evaluation of Urban Vehicle Operating Patterns, Presented at the 65th Annual Meeting of the Air Pollution Control Assoc., Miami Beach, Florida, June 18-22.

Sonderling, H. (1973). Private communication. Los Angeles Department of Water and Power, Los Angeles, California.

Springer, K. J. (1969). An Investigation of Emissions from Trucks Above 6000 lb-GVW Powered by Spark-Ignited Engines. Final Report Prepared for U. S. Public Health Service, under Contract No. PH 86-67-72, Southwest Research Institute.

Staley, D. O. (1956). The Diurnal Temperature Wave for Bounded Eddy Conductivity. Jour. Meteorology, 13, 13.

State of California (1972). California Statistical Abstract 1972. Sacramento, California.

State of California Air Resources Board (1968). California Exhaust Emissions Standards for Test Procedures for Gasoline-Powered Motor Vehicles.

State of California Air Resources Board (1972). The State of California implementation plan for achieving and maintaining the National Ambient Air Quality Standards. Sacramento, California.

State of California Air Resources Board (1973). STP Corporation application and accreditation of a modified NO_x control device for certain 1966-70 model-year vehicles with engines in class (a) and in classes (b) through (f). Staff Report No. 73-10-2, Sacramento, California.

Tingley, D. S. and Johnson, J. H. (1973). The development of a computer model for prediction of the U. S. truck and bus population, fuel usage, and air pollution contribution. Paper presented at the Fourth Annual Pittsburg Conference on Modeling and Simulation, April 23-24, 1973, School of Engineering, University of Pittsburg.

Trijonis, J. C. (1972). An economic air pollution control model-application: photochemical smog in Los Angeles County in 1975. Ph.D. Thesis, California Institute of Technology, Pasadena, California.

TRW (1973). Transportation control strategy development for the metropolitan Los Angeles region. Report APTD-1372, Redondo Beach, California.

Turner, D. B. (1969). Workbook of Atmospheric Dispersion Estimates. U. S. Department of Health, Education and Welfare, Public Health Service, Pub. No. 999-AP-26.

Walters, T. S. (1969). The Importance of Diffusion Along the Mean Wind Direction for a Ground-Level Crosswind Line Source. Atmos. Environ., 3, 461.

Wehner, J. F. and Wilhelm, R. H. (1956). Boundary conditions of flow reactor. Chem. Eng. Sci., 6, 89.

Wendell, R. E., Norco, J. E., and Croke, K. G. (1973). Emission prediction and control strategy: evaluation of pollution from transportation systems. Journ. Air Poll. Control Assoc., 23, 91.

Wilson, W. E., Jr. (1972). Personal communication.

Yanenko, N. N. (1971). The Method of Fractional Steps. Springer-Verlag, New York.

PROPOSITION

Convective Difference Approximations and Their Upstream Counterparts

Abstract

A convective difference approximation may be combined with its upstream counterpart to yield a more accurate difference scheme. A method for determining the best combination of such approximations is proposed based on a truncation error analysis.

Much current work in numerical analysis is devoted to developing new methods and determining the potential of existing methods. This proposition falls into the latter category. Fromm (1968) has demonstrated that it is possible to combine a convective difference approximation with its upstream counterpart to reduce phase errors. Taking Fromm's basic idea, it will be shown that numerical errors can be reduced further.

The focus of this study is finite-difference approximations to hyperbolic partial differential equations. A typical example of such an equation is the Helmholz vorticity equation for an ideal fluid:

$$\frac{\partial \omega}{\partial t} + u \frac{\partial \omega}{\partial x} + v \frac{\partial \omega}{\partial y} = 0 \qquad (1)$$

where $\omega \equiv \frac{\partial v}{\partial x} - \frac{\partial u}{\partial y}$ = vorticity

u = x component of velocity

v = y component of velocity

The velocities are related to the stream function ψ by the following relationships:

$$u = \frac{\partial \psi}{\partial y} \qquad v = -\frac{\partial \psi}{\partial x} \qquad (2)$$

Substitution of (2) into the definition of vorticity gives:

$$-\omega = \frac{\partial^2 \psi}{\partial x^2} + \frac{\partial^2 \psi}{\partial y^2} \qquad (3)$$

Equations (1) and (3) are a complete set of coupled equations which can be used in numerical fluid flow calculations. We shall restrict our attention, however, to the numerical treatment of equations similar to (1).

We shall first examine the one-dimensional analog of equation (1), that is:

$$\frac{\partial \omega}{\partial t} + u \frac{\partial \omega}{\partial x} = 0 \tag{4}$$

where u is taken to be a constant.

Introducing the following finite-difference notation

$$\omega_{\ell}^{n} = \omega(\ell \Delta x, n\Delta t)$$

consider the following advection characteristic diagram:

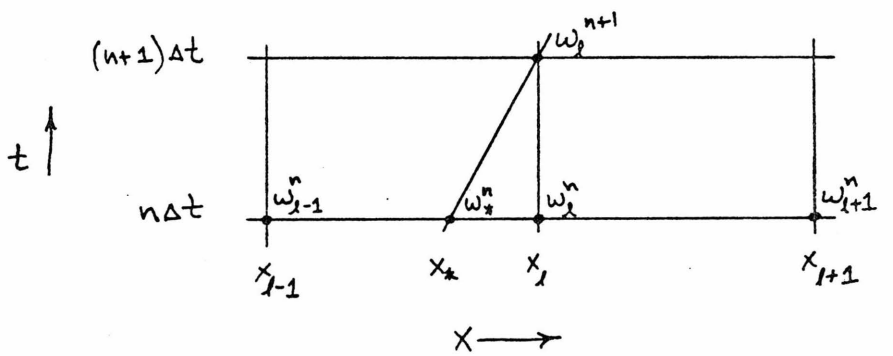

The value of ω_{ℓ}^{n+1} is found by following the characteristic back to the $n\Delta t$ time level. Thus,

$$\omega_{\ell}^{n+1} = \omega_{*}^{n}$$

where $$x_{*} = x_{\ell} - u\Delta t$$

Because ω_{*}^{n} is usually not located at a mesh point, a Taylor series is used to obtain:

$$\omega_{\ell}^{n+1} = \omega_{*}^{n} \approx \omega_{\ell}^{n} + (x_{*}-x_{\ell}) \frac{\partial \omega}{\partial x}\bigg|_{x_{\ell},n\Delta t} + \frac{(x_{*}-x_{\ell})^{2}}{2} \frac{\partial^{2} \omega}{\partial x^{2}}\bigg|_{x_{\ell},n\Delta t} \tag{5}$$

Since $x_\ell - x_* = u\Delta t$, equation (5) can be written as

$$\omega_\ell^{n+1} \approx \omega_\ell^n - u\Delta t \left.\frac{\partial \omega}{\partial x}\right|_{x_\ell, n\Delta t} + \frac{u^2\Delta t^2}{2} \left.\frac{\partial^2 \omega}{\partial x^2}\right|_{x_\ell, n\Delta t}$$

We approximate the spatial derivatives by centered differences yielding the Lax-Wendroff scheme:

$$\omega_\ell^{n+1} = \omega_\ell^n + \frac{\alpha}{2}\left(\omega_{\ell-1}^n - \omega_{\ell+1}^n\right) + \frac{\alpha^2}{2}\left(\omega_{\ell-1}^n - 2\omega_\ell^n + \omega_{\ell+1}^n\right) \qquad (6)$$

where $$\alpha = \frac{u\Delta t}{\Delta x}$$

Upon substituting a Fourier component solution

$$\omega_\ell^n = A r^n \exp(ik_x \ell \Delta x)$$

into equation (6), we obtain:

$$r = 1 - i\alpha \,\mathrm{Sin}(k_x \Delta x) + \alpha^2 \,(\mathrm{Cos}(k_x \Delta x) - 1)$$

For stability the magnitude of r must be less than or equal to one, that is:

$$r\,\bar{r} \leq 1$$

for all k_x, where $\bar{r}$ is the complex conjugate of r. The condition for stability can be shown to be:

$$|\alpha| \leq 1$$

Although advection should not change the amplitude of the function $\exp(ik_x \ell \Delta x)$, the Lax-Wendroff method decreases it by a factor of $|r|$ each time step. This type of error is known as damping. Since $\omega(x, t) = \exp(ik_x(x-ut))$ is a solution of (4), the

true phase shift, ϕ_o, after a time interval Δt is given by the following expression:

$$\phi_o = -k_x u \Delta t$$

The phase shift in the numerical solution, ϕ_1, is given by:

$$\phi_1 = \tan^{-1} \frac{Im(r)}{Re(r)}$$

Thus the phase error $\Delta\Phi$ introduced by the numerical method may be represented as follows:

$$\Delta\Phi = \phi_o - \phi_1$$

It can be shown that the Lax-Wendroff method has a lagging phase error. Fromm(1968) made the observation that if an advanced time solution were known, then one could calculate a solution from it, and the phase error would appear as a leading phase error. Consider the following advection characteristic diagram:

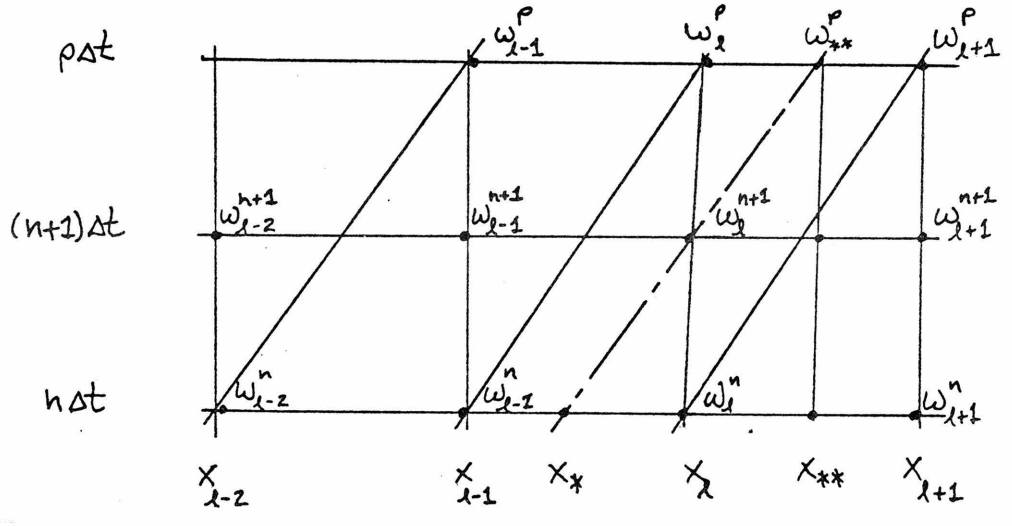

The advanced time solution corresponds to the solution at the $p\Delta t = n\Delta t + \frac{\Delta x}{u}$ time level, which is easily determined. Thus, we write:

$$\omega_{\ell}^{n+1} = \omega_{**}^{p} \approx \omega_{\ell}^{p} + (x_{**}-x_{\ell}) \frac{\partial \omega}{\partial x}\Big|_{x_{\ell}, p\Delta t} + \frac{(x_{**}-x_{\ell})^2}{2} \frac{\partial^2 \omega}{\partial x^2}\Big|_{x_{\ell}, p\Delta t} \tag{7}$$

Note that

$$\omega_{\ell}^{p} = \omega_{\ell-1}^{n}$$

$$x_{**}-x_{\ell} = \Delta x - u\Delta t$$

$$\frac{\partial \omega}{\partial x}\Big|_{x_{\ell}, p\Delta t} = \frac{\partial \omega}{\partial x}\Big|_{x_{\ell-1}, n\Delta t}$$

Writing equation (7) in finite-difference form yields:

$$\omega_{\ell}^{n+1} = \omega_{\ell-1}^{n} + \frac{(\alpha-1)}{2}\left(\omega_{\ell-2}^{n} - \omega_{\ell}^{n}\right) + \frac{(\alpha-1)^2}{2}\left(\omega_{\ell-2}^{n} - 2\omega_{\ell-1}^{n} + \omega_{\ell}^{n}\right) \tag{8}$$

The difference scheme in equation (8) has a leading phase error. Since equations (6) and (8) have opposite phase characteristics, we take a linear combination of both estimates of ω_{ℓ}^{n+1}, resulting in the following equation for ω_{ℓ}^{n+1}:

$$\begin{aligned} \omega_{\ell}^{n+1} = (1-a)\left\{\omega_{\ell}^{n} + \frac{\alpha}{2}\left(\omega_{\ell-1}^{n} - \omega_{\ell+1}^{n}\right) + \frac{\alpha^2}{2}\left(\omega_{\ell-1}^{n} - 2\omega_{\ell}^{n} + \omega_{\ell+1}^{n}\right)\right\} \\ + a\left\{\omega_{\ell-1}^{n} + \frac{\alpha-1}{2}\left(\omega_{\ell-2}^{n} - \omega_{\ell}^{n}\right) + \frac{(\alpha-1)^2}{2}\left(\omega_{\ell-2}^{n} - 2\omega_{\ell-1}^{n} + \omega_{\ell}^{n}\right)\right\} \end{aligned} \tag{9}$$

where $0 \le a \le 1$. In studies with $a = 0.5$, Fromm (1968) has demonstrated that (9) introduces much smaller phase errors than the Lax-Wendroff scheme. If the phase errors of (6) and (8) were directly proportional to Δt, then we would choose a equal to α, as proposed by Fromm (1969). At this point it is of interest to examine the phase and damping properties of (9) with respect to the choice of a. In a computational situation, we are given a value of α at a mesh point.

We seek a functional dependence of a on α that will minimize the numerical error of the integration.

Substituting a Fourier component solution into (9) yields

$$r = 1 - i\alpha \mathrm{Sin}\,\theta_x (1-a) - a\alpha i \mathrm{Sin}\,\theta_x (\mathrm{Cos}\,\theta_x - i\,\mathrm{Sin}\,\theta_x)$$

$$+ (1-a)\alpha^2 (\mathrm{Cos}\,\theta_x - 1) + a(\alpha^2 - 2\alpha)(\mathrm{Cos}\,\theta_x - 1)(\mathrm{Cos}\,\theta_x - i\mathrm{Sin}\,\theta_x)$$

where $\theta_x = k_x \Delta x$. We next expand each term on the right hand side of equation (9) in a Taylor series about the point ω_ℓ^n:

$$\omega_\ell^{n+1} = \omega_\ell^n - \alpha \Delta x \left.\frac{\partial \omega}{\partial x}\right|_{x_\ell,\, n\Delta t} + \frac{\alpha^2 \Delta x^2}{2} \left.\frac{\partial^2 \omega}{\partial x^2}\right|_{x_\ell, n\Delta t} - \frac{\{\alpha - 3a\alpha + 3a\alpha^2\}\Delta x^3}{6} \left.\frac{\partial^3 \omega}{\partial x^3}\right|_{x_\ell, n\Delta t}$$

We thus choose a such that:

$$\alpha - 3a\alpha + 3a\alpha^2 = \alpha^3$$

Solving this equation for a yields the desired relationship:

$$a = \frac{1+\alpha}{3} \tag{10}$$

We now examine the phase and damping properties of (9) using two previously suggested methods for determining a, Fromm (1968) and Fromm (1969), and the relationship proposed in equation (10). The three methods are summarized below:

$$a = 0.5 \qquad \text{Fromm (1968)} \tag{11a}$$

$$a = \alpha \qquad \text{Fromm (1969)} \tag{11b}$$

$$a = \frac{1+\alpha}{3} \qquad \text{equation (10)} \tag{11c}$$

Figure 1 is a plot of $|r|^2$ vs. α for $k_x\Delta x = \pi/4$. Note that the damping error is symmetric about $\alpha = 0.5$. We observe that (11b) has the best damping characteristics, which was also found for values of $k_x\Delta x$ equal to $2\pi/3$, $\pi/2$, $\pi/3$, and $\pi/5$. Scheme (11c) has better damping properties than (11a) for all values of $k_x\Delta x$ given above. Thus from a damping point of view, the schemes must be ranked in the following order:

(11b) best

(11c)

(11a)

Figure 2 is a plot of the phase error vs. α for $k_x\Delta x = \pi/4$. The phase error is anti-symmetric about $\alpha = 0.5$, and also note that (11a) has a leading phase error for this Fourier component. Examination of the phase characteristics for the five values of $k_x\Delta x$ cited above yields the following rankings:

$k_x\Delta x = 2\pi/3,\ \pi/2,\ \pi/3$

(11a) best

(11c)

(11b)

$k_x\Delta x = \pi/4,\ \pi/5$

(11c) best

(11a)

(11b)

Note that a switch in the rankings takes place between $\pi/3$ and $\pi/4$. Equation (11c) is found to have the best phase characteristics for the long wave length components.

At this point we see that (11b) has the best damping properties and the poorest phase properties. To determine which scheme is to be preferred, we examine the combined damping and phase errors. In particular, consider the difference between the correct treatment of the Fourier component and the numerical treatment, E, given by the following equation:

$$E = \left| e^{-iu\Delta t k_x} - r \right|$$

Figure 3 is a plot of the combined error vs. α for $k_x \Delta x = \pi/4$. We note that (11c) has the best combined error characteristics. This was also found for values of $k_x \Delta x$ equal to $2\pi/3$, $\pi/2$, $\pi/3$, and $\pi/5$. It is thus recommended that (11c) be used to determine the value of a in equation (9).

We now turn our attention to the two-dimensional problem given by equation (1). We shall use the method of fractional time steps (Marchuk, 1964) to obtain the numerical solution. Introducing the following notation

$$\omega^{n}_{\ell, m} = \omega(\ell\Delta x, m\Delta y, n\Delta t)$$

The computational scheme proceeds in the following two steps:

$$\begin{aligned}\tilde{\omega}_{\ell, m} = (1-a)\Big\{\omega_{\ell, n} &+ \frac{\alpha^{n}_{\ell,m}}{2}\left(\omega^{n}_{\ell-1, m} - \omega^{n}_{\ell+1, m}\right) \\ &+ \frac{(\alpha^{n}_{\ell,m})^2}{2}\left(\omega^{n}_{\ell-1, m} - 2\omega^{n}_{\ell, m} + \omega^{n}_{\ell+1, m}\right)\Big\} + a\Big\{\omega^{n}_{\ell-1, m} \\ &+ \frac{(\alpha^{n}_{\ell, m}-1)}{2}\left(\omega^{n}_{\ell-2, m} - \omega^{n}_{\ell, m}\right) + \frac{(\alpha^{n}_{\ell, m}-1)^2}{2}\left(\omega^{n}_{\ell-2, m} - 2\omega^{n}_{\ell-1, m} + \omega^{n}_{\ell, m}\right)\Big\}\end{aligned} \tag{12}$$

$$\omega_{\ell,m}^{n+1} = (1-b)\left\{\tilde{\omega}_{\ell,m} + \frac{\beta_{\ell,m}^{n}}{2}\left(\tilde{\omega}_{\ell,m-1} - \tilde{\omega}_{\ell,m+1}\right) + \frac{(\beta_{\ell,m}^{n})^2}{2}\left(\tilde{\omega}_{\ell,m-1} - 2\tilde{\omega}_{\ell,m} + \tilde{\omega}_{\ell,m+1}\right)\right\} + b\left\{\tilde{\omega}_{\ell,m-1} + \frac{(\beta_{\ell,m}^{n}-1)}{2} \times \left(\tilde{\omega}_{\ell,m-2} - \tilde{\omega}_{\ell,m}\right) + \frac{(\beta_{\ell,m}^{n}-1)^2}{2}\left(\tilde{\omega}_{\ell,m-2} - 2\tilde{\omega}_{\ell,m-1} + \tilde{\omega}_{\ell,m}\right)\right\} \quad (13)$$

where

$$\alpha_{\ell,m}^{n} = \frac{u_{\ell,m}^{n}\,\Delta t}{\Delta x} \qquad 0 \le a \le 1$$

$$\beta_{\ell,m}^{n} = \frac{v_{\ell,m}^{n}\,\Delta t}{\Delta y} \qquad 0 \le b \le 1$$

Consider the following two-dimensional analogs of equations (11a-11c) for choosing a and b:

$$a = b = 0.5 \quad (14a)$$

$$a = \alpha, \quad b = \beta \quad (14b)$$

$$a = \frac{1+\alpha}{3}, \quad b = \frac{1+\beta}{3} \quad (14c)$$

The Fourier component solution now takes the form:

$$\omega_{\ell,m}^{n} = A r^{n} \exp[i(k_x \ell \Delta x + k_y m \Delta y)] \quad (15)$$

Substitution of (15) into (12) and (13) yields:

$$r = \left\{1 - i\alpha \mathrm{Sin}\,\theta_x (1-a) - a\alpha i \mathrm{Sin}\theta_x (\mathrm{Cos}\theta_x - i\mathrm{Sin}\theta_x) + (1-a)\alpha^2 (\mathrm{Cos}\theta_x - 1) + a(\alpha^2 - 2\alpha)(\mathrm{Cos}\theta_x - 1)\right.$$
$$\left.(\mathrm{Cos}\theta_x - i\mathrm{Sin}\theta_x)\right\} \cdot \left\{1 - i\beta \mathrm{Sin}\theta_y (1-b) - b\,\beta i \mathrm{Sin}\theta_y (\mathrm{Cos}\theta_y - i\mathrm{Sin}\theta_y) + (1-b)\beta^2 (\mathrm{Cos}\theta_y - 1)\right.$$
$$\left. + b(\beta^2 - 2\beta)(\mathrm{Cos}\theta_y - 1)(\mathrm{Cos}\theta_y - i\mathrm{Sin}\theta_y)\right\}$$

where $\theta_x = k_x \Delta x$

$\theta_y = k_y \Delta y$

Stability is achieved if $|\alpha| \leq 1$ and $|\beta| \leq 1$. The true phase shift is given by:

$$\phi_o = - k_x u \Delta t - k_y v \Delta t$$

while the phase shift in the numerical solution can be represented as:

$$\phi_1 = \tan^{-1} \frac{\mathrm{Im}(r)}{\mathrm{Re}(r)}$$

The method also introduces damping as before. For convenience, we set $\theta_x = \theta_y$ in equation (16) and examine the phase and damping properties for values of α and β such that

$$0 \leq \alpha \leq 1, \qquad 0 \leq \beta \leq 1$$

Scheme (14b) is found to have the best damping properties, as it did in the one dimensional case. We also observe that schemes (14a) and (14c) have the best phase characteristics. Thus, we must examine the combined phase and damping error. Upon examination of the combined error for $\theta_x = \theta_y = 2\pi/3$, $\pi/2$, $\pi/3$, $\pi/4$ and $\pi/5$, the following algorithm for choosing a and b is recommended:

if $\alpha < \frac{1}{2}, \ \beta < \frac{1}{2}$ or $\alpha > \frac{1}{2}, \ \beta > \frac{1}{2}$ } use (14c)

if $\alpha > \frac{1}{2}, \ \beta < \frac{1}{2}$ or $\alpha < \frac{1}{2}, \ \beta > \frac{1}{2}$ } use (14b)

This algorithm is pictured in the diagram below:

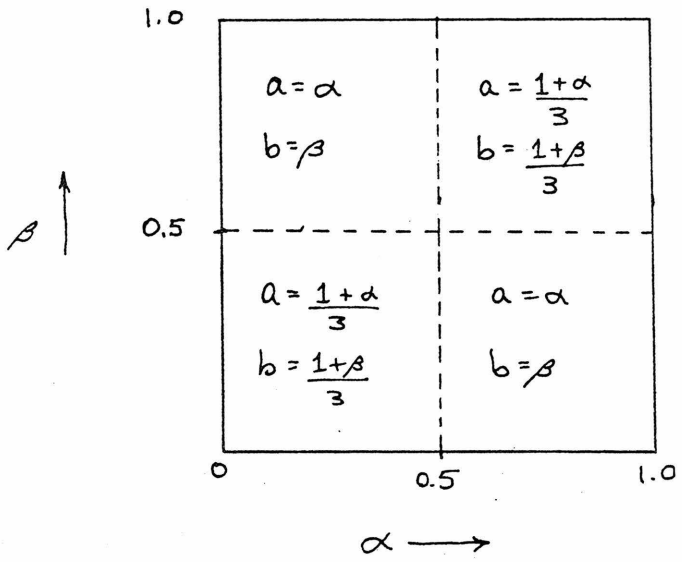

The better damping properties of (14b) outweigh the phase advantages of (14c) in the upper left and lower right quadrants. There are no phase errors on the line $\alpha + \beta = 1$ for any of the three schemes. Thus the scheme with the least damping will be the most accurate on this line.

A method for choosing the linear combination of a difference approximation and its upstream counterpart based on a truncation error analysis is proposed. The method should give better results in one space dimension than other proposed methods. An extension to two space dimensions is given with recommendations for choosing the manner in which the linear combination should be formed.

FIGURE 1

Damping Properties

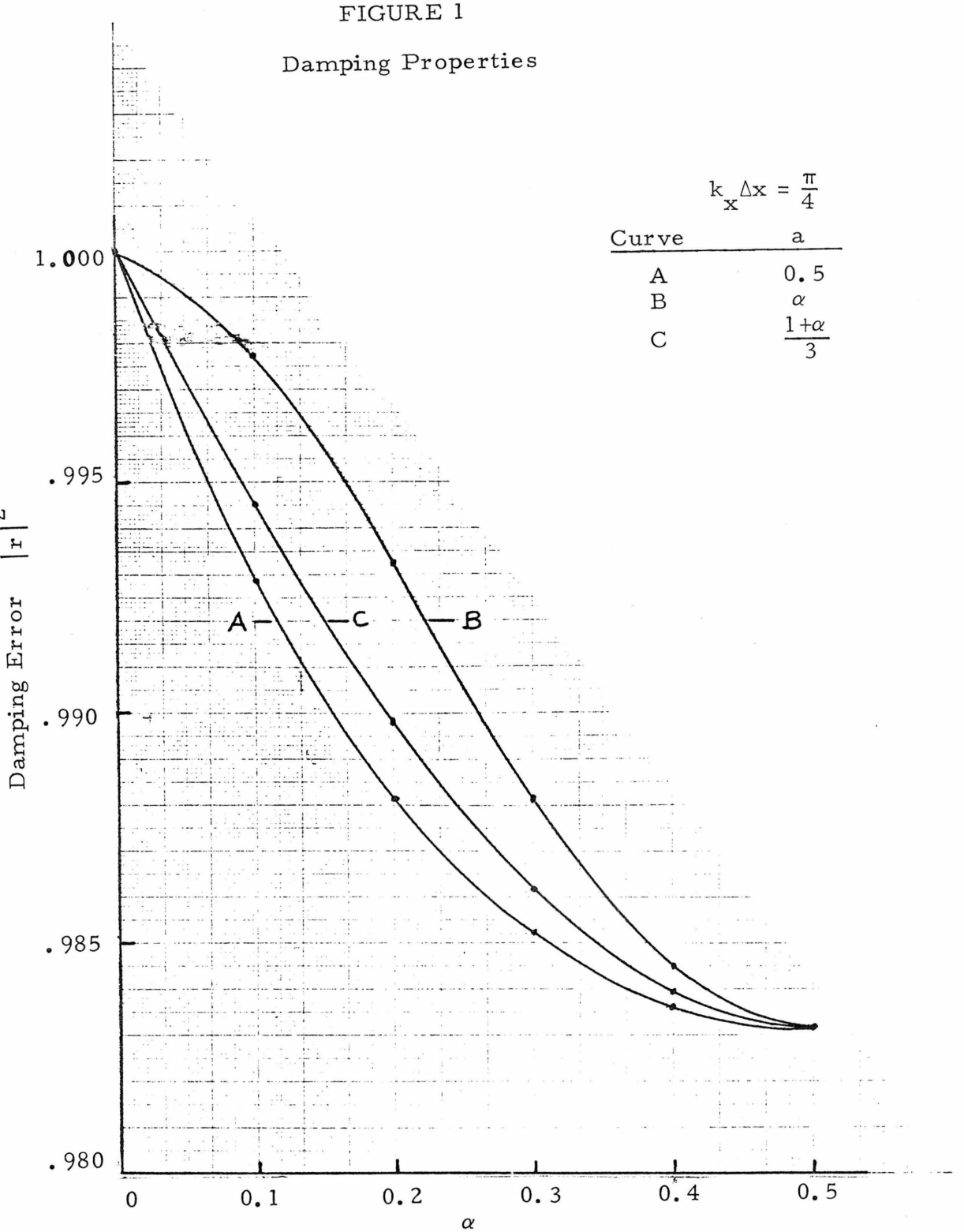

FIGURE 2

Phase Properties

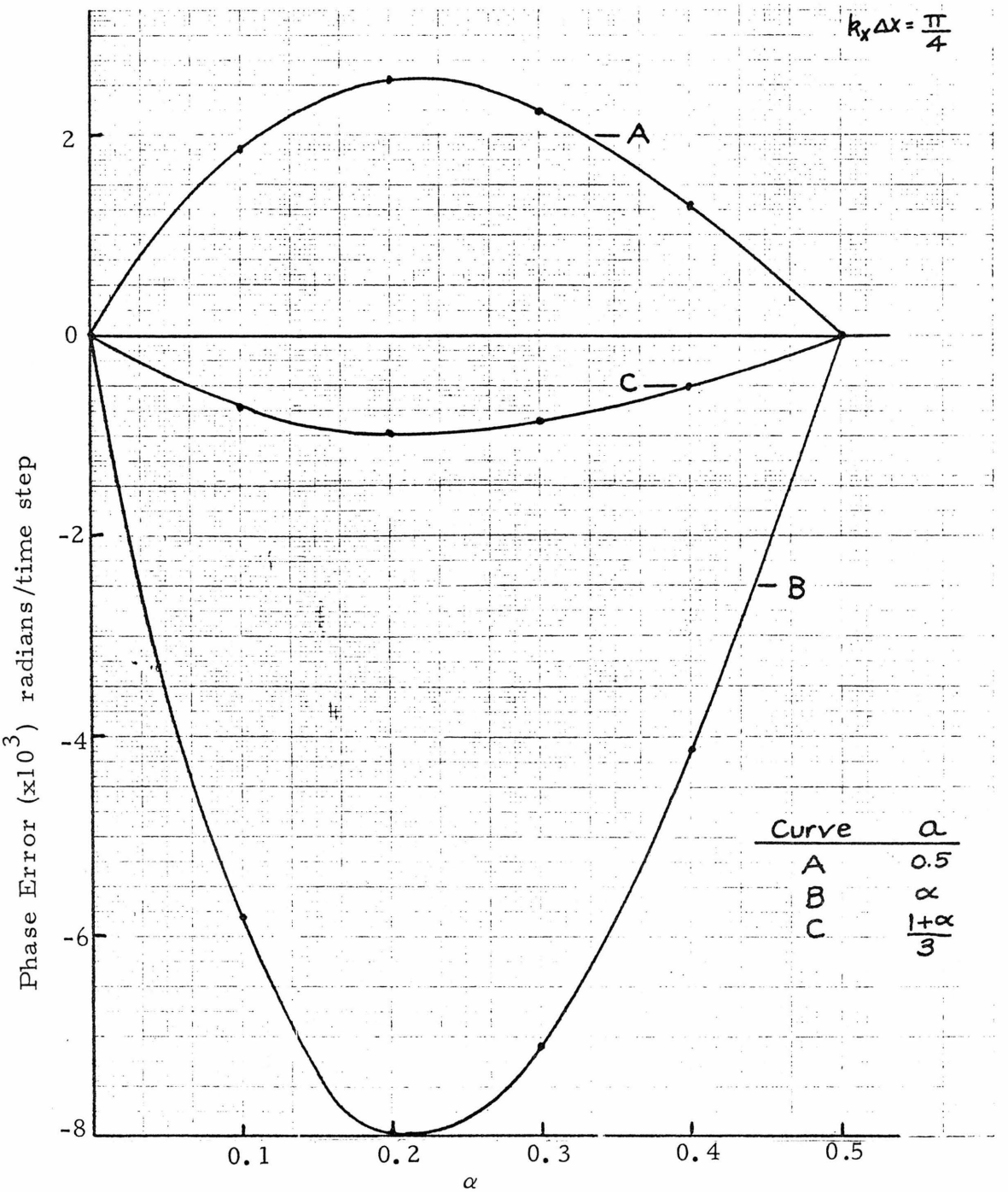

FIGURE 3

Combined Phase and Damping

Properties

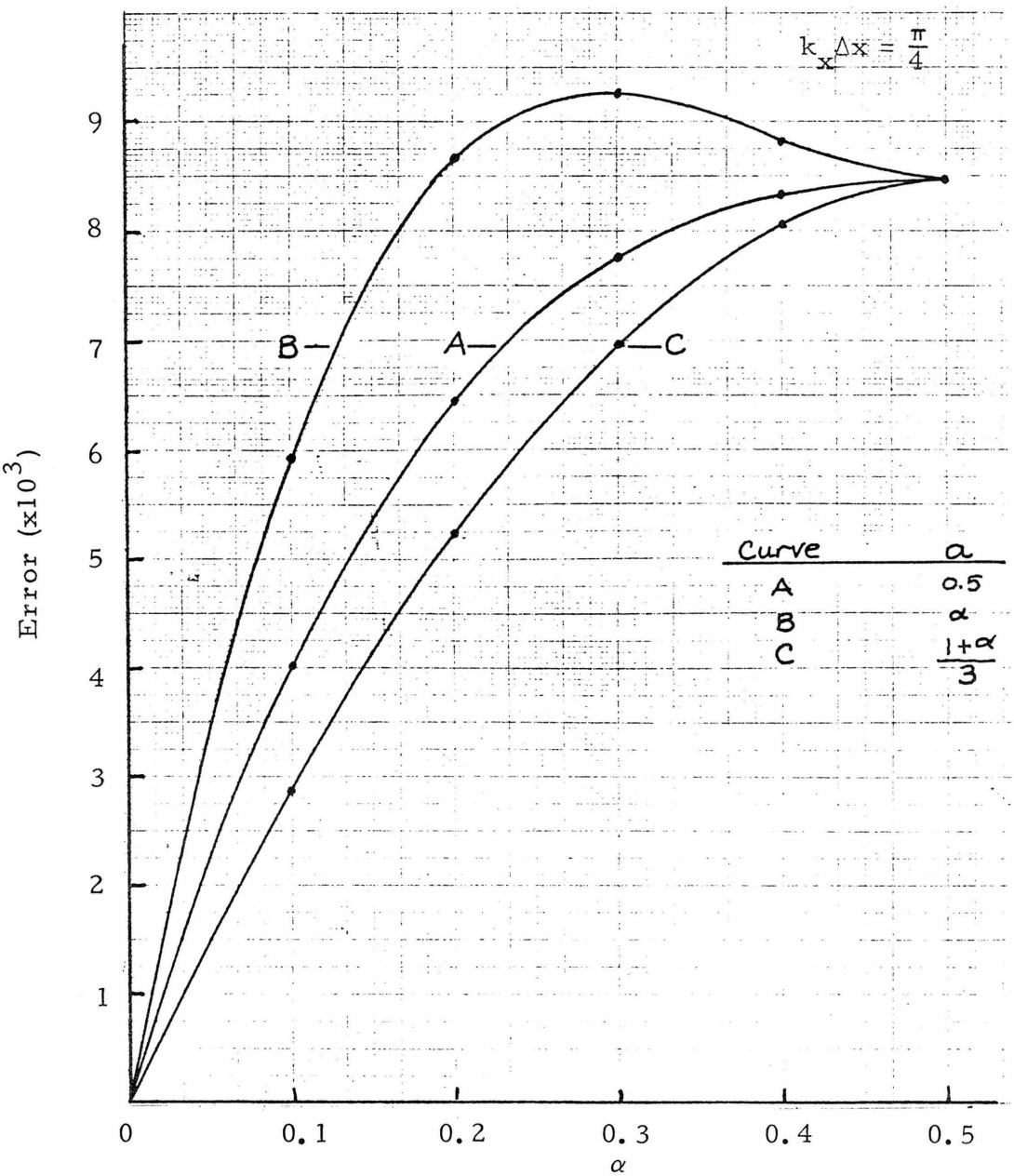

References

Fromm, J. E. (1968). Jour. Comp. Physics, 3, 176.

Fromm, J. E. (1969). Phys. Fluids Supp. II, 12, II-3.

Marchuk, G. I. (1964). Dokl. Akad. Nauk SSSR, 155, 1065

PROPOSITION

On Predicting Spatial and Temporal Characteristics of the Base Height of an Elevated Temperature Inversion

Abstract

A relatively simple means for predicting the dynamic behavior of the depth of a planetary boundary layer capped by an elevated stable inversion layer is presented. The depth of the mixed layer, as a function of x, y, and t, is obtained from the solution of two coupled partial differential equations. The effect of penetrative convection at the interface between the stable and unstable layers is also considered in the formulation.

The objective of this study is to develop a means for predicting the height of the base of an elevated temperature inversion situated over an urban area throughout the course of a day. In the proposed formulation, consideration is given to both temporal and spatial variations in the base height. To facilitate implementation of the method, assumptions consistent with planetary boundary layer observations are imposed, although an attempt has been made to represent the important phenomena believed to be responsible for the development of the mixed layer.

Several alternative approaches have been proposed for predicting mixing depths. The first, and most sophisticated, is that involving the numerical solution of the mass, momentum, and energy equations written for the planetary boundary layer. This approach, which is being developed, for example, by Deardorff (1973), requires extensive amounts of computing time and is presently primarily a research tool rather than a practical, easily implemented methodology. In contrast, other investigators have simplified the problem by noting the characteristics of the vertical temperature structure of the mixed layer.

Typically, during daylight hours a superadiabatic temperature gradient exists in the surface layer within the first few tens of meters of the atmosphere. In the region between the top of the surface layer and the base of the elevated inversion, the temperature gradient can usually be closely approximated by the adiabatic lapse rate, although near the inversion base the gradient may tend to be slightly stable.

Air in the capping inversion layer is, of course, characterized by a stable temperature gradient. In Figure 1 we illustrate an idealized vertical temperature profile. Between the mixed and stable layers is a transition zone, called the interfacial entrainment layer (Carson, 1973). Since the thickness of this layer is relatively thin (a few tens of meters; see Stull, 1973), it is convenient to represent the change in temperature going from the mixed layer to the undisturbed stable layer above by a step discontinuity in the vertical temperature profile. This treatment of the interfacial layer has been employed in several recent studies (Lilly, 1968; Carson, 1973; Tennekes, 1973).

Figure 1. Idealized Vertical Temperature Profile

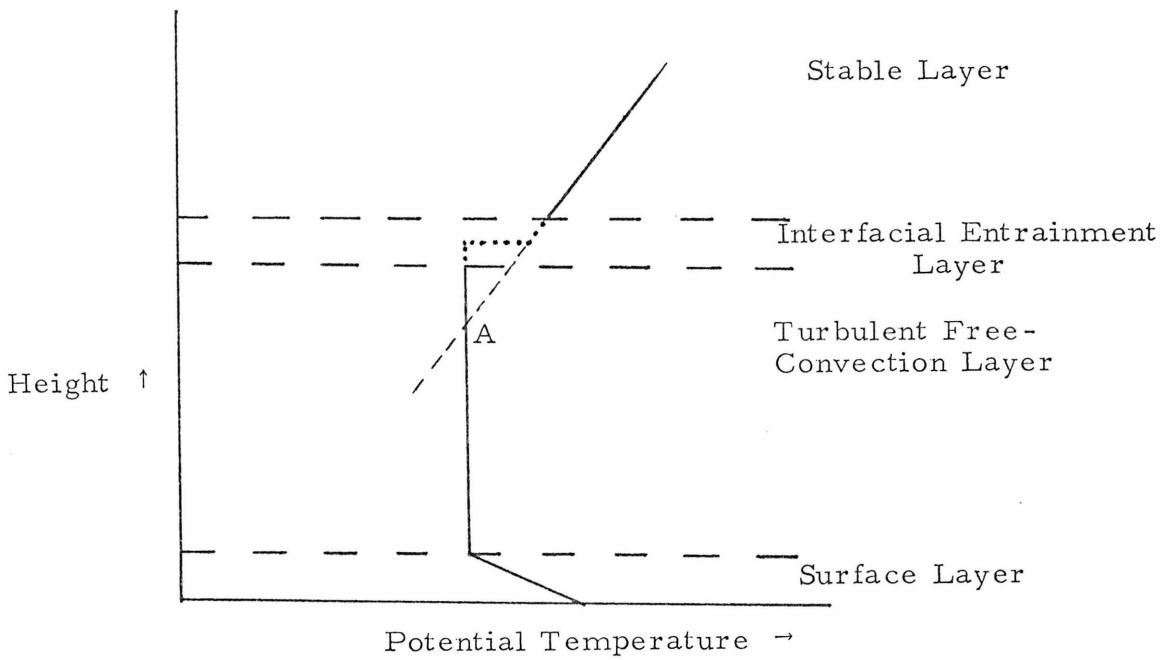

Anderson (1972) and Kokin et al. (1973) have utilized the fact that the adiabatic lapse rate generally represents the vertical temperature gradient throughout most of the mixed layer and have employed the following algorithm to estimate the height of the inversion base. Data from vertical temperature soundings are used to characterize the thermal structure of the "undisturbed" stable layer. To calculate the mixing depth at any location in the region, one first obtains an estimate of the "surface" temperature at the point of interest (for example, through interpolation of reported meteorological monitoring station data). Then the adiabat passing through the "surface" temperature at the observation level is examined, and the point (elevation) at which this adiabat intersects the "undisturbed" temperature profile of the stable layer is used as the height of the inversion base.

The advantages of this approach are that it is easy to implement and does not require the solution of differential equations. In addition, the elevation of the inversion base may be determined at only those places of particular interest, rather than at each point on a horizontal grid encompassing the entire urban area. However, there are several drawbacks to this technique. First, it is necessary to estimate a value for the "surface" temperature. While reasonable approximations can conceivably be obtained for particular days in the "past" by interpolation of recorded meteorological data, greater difficulties will be encountered in attempting to use the methodology in a "future" predictive sense. That is, rather sophisticated techniques will be required to estimate "surface" temperatures one or

more days in advance. Another aspect of this approach worthy of note is that the height at which the "surface" temperature is measured should be greater than the thickness of the surface layer. This is necessary to properly estimate the vertical temperature profile in the free-convection layer. Even if appropriate measurements are available, we note from Figure 1 that the inversion height in this instance would be estimated to be at the point A. Thus, there may be a tendency to underestimate mixing depths. Using results obtained by Carson (1973), the error involved may range from 10 to 25 percent of the actual height of the inversion base.

We have reviewed two approaches which may be used to estimate mixing depths and have found that both possess certain drawbacks which, atpresent, will limit their usefulness in actual practical application. It is proposed here that an approach of somewhat less sophistication than a complete planetary boundary layer simulation model be developed to calculate the dynamics of the inversion base.

In this study we shall consider the lowest few kilometers of the atmosphere to be segmented into two regions. The lower, or mixed, layer is assumed to be bounded below by the ground and aloft by the base of a stable inversion layer. The upper, or stable, layer is that region above the inversion base extending to a height of several kilometers. To facilitate this presentation, it will be assumed that the thermal structure of the stable layer is only a function of z (the height above the ground) and t (time), and that this dependence is determined from direct measurements or other means. A second issue of concern is the treatment of the wind field in the boundary

layer. Again to restrict the scope of this effort, it will be assumed that the wind velocity, as a function of space and time, is known (for example, from measurements or the results of a simulation model).

To estimate the depth of the boundary layer, we will need to know the temperature field in the boundary layer is a function of space and time. The appropriate starting point for this calculation is the following form of the heat equation:

$$\left(\frac{\partial \overline{\theta}}{\partial t} + \underset{\sim}{\overline{V}} \cdot \underset{\sim}{\nabla} \overline{\theta}\right) = - \frac{\partial}{\partial z} \left(\overline{w'\theta'}\right) + \overline{S}_R \qquad (1)$$

where $\overline{\theta}$ = potential temperature

$\underset{\sim}{\overline{V}}$ = wind velocity vector,

$\overline{w'\theta'}$ = turbulent flux of potential temperature in the z direction,

$\overline{S}_R$ = radiative heating (or cooling) term, and the overbar denotes spatial averaging (see Deardorff, 1973).

In writing equation (1) we have assumed:

- atmospheric flow is incompressible,
- horizontal turbulent fluxes of potential temperature may be neglected compared to horizontal advective fluxes,
- molecular diffusion of potential temperature is small compared to turbulent diffusion.

Furthermore, the air will be assumed to be dry; the presence of appreciable amounts of water vapor can be accounted for by employing the virtual potential temperature (Tennekes, 1973; Deardorff, 1973).

Finally, treatment of the radiation term, $\overline{S}_R$, is discussed by Bergstrom and Viskanta (1973).

As we have noted earlier, the vertical temperature gradient throughout most of the boundary layer (with the exception of the surface layer) is approximately equal to the adiabatic lapse rate. Thus, we shall consider $\overline{\theta}$ to only be a function of x, y, and t, thereby significantly reducing the effort that will be required to solve equation (1). Consistent with this treatment of $\overline{\theta}$, we also assume that the horizontal components of $\underset{\sim}{\overline{V}}$ are not functions of Z. It is suggested that vertically averaged values of the horizontal components be employed. Imposing the assumptions cited above, equation (1) reduces to:

$$\frac{\partial \overline{\theta}}{\partial t} + \overline{u}\frac{\partial \overline{\theta}}{\partial x} + \overline{v}\frac{\partial \overline{\theta}}{\partial y} = -\frac{(\overline{w'\theta'})_h - (\overline{w'\theta'})_o}{h} + \overline{S}_R \qquad (2)$$

$\overline{u}, \overline{v}$ = vertically averaged wind components in the x and y directions, respectively,

$(\overline{w'\theta'})_o$ = turbulent flux at the ground,

$(\overline{w'\theta'})_h$ = turbulent flux at the base of the stable layer.

We also note that $\overline{S}_R$ now represents the vertically averaged contribution from radiative heating. Means for specifying the turbulent flux terms will be discussed shortly. Having derived an equation for estimating θ, we need another relationship for h.

To derive an additional equation involving h, we shall now treat $\overline{\theta}$ as a generalized function of x, y, z, t and integrate equation

(1) across the interface from h-ε to h+ε Thus, we can write the following equation:

$$\int_{h-\varepsilon}^{h+\varepsilon} \left[\frac{\partial \overline{\theta}}{\partial t} + \nabla . \underset{\sim}{\overline{V}}\, \overline{\theta} + \frac{\partial}{\partial z} (\overline{w'\theta'}) - \overline{S}_R \right] dz = 0$$

which, upon invoking the Leibnitz rule and taking the limit as $\varepsilon \to 0$, reduces to

$$\frac{\partial h}{\partial t} + \overline{u} \frac{\partial h}{\partial x} + \overline{v} \frac{\partial h}{\partial y} = \overline{w} - \frac{(\overline{w'\theta'})_{h-}}{\Delta \overline{\theta}} \qquad (3)$$

where

$$(\overline{w'\theta'})_{h-} = \underset{\varepsilon \to 0}{\text{limit}} \; (\overline{w'\theta'})_{h-\varepsilon}$$

and $\Delta \overline{\theta} = \overline{\theta}_s(h, t) - \overline{\theta}_t(x, y, t)$,

$\theta_s(z, t)$ = potential temperature in the stable layer,

$\overline{\theta}_t(x, y, t)$ = potential temperature in the boundary layer (i.e. $\overline{\theta}$ in equation (2))

In deriving equation (3), it is assumed that turbulence is suppressed in the stable layer so that

$$(\overline{w'\theta'})_{h+\varepsilon} \approx 0 = \underset{\varepsilon \to 0}{\text{limit}} \; (\overline{w'\theta'})_{h-\varepsilon} \quad .$$

The term $(\overline{w'\theta'})_{h-}$ in equation (3) corresponds to the term $(\overline{w'\theta'})_h$ in equation (2). Once values of $(\overline{w'\theta'})_o$ and $(\overline{w'\theta'})_h$ have been specified, equations (2) and (3) may be solved numerically for $\overline{\theta}(x, y, t)$ and $h(x, y, t)$.

At this point it is appropriate to discuss, in a general manner, the initial and boundary conditions for equations (2) and (3). First, the

initial conditions are that $\overline{\theta}(x, y, t_o)$ and $h(x, y, t_o)$ be specified, where t_o is the time at which the integration is to start. For boundary conditions, one should specify the potential temperature and mixing depth at any point on the horizontal boundary where the wind flows into the modeling region. No boundary condition is required at a point of horizontal flow out of the region.

We now turn our attention to the treatment of the turbulent fluxes $(\overline{w'\theta'})_o$ and $(\overline{w'\theta'})_h$. A technique for estimating $(\overline{w'\theta'})_o$ based on an energy balance at the earth-air interface is given by Leahey and Friend (1971). Several investigators (Ball, 1960; Lilly, 1968; Carson, 1973; Tennekes, 1973) have argued that the turbulent flux at h is proportional to the flux at the ground, that is

$$(\overline{w'\theta'})_h = -A(\overline{w'\theta'})_o$$

where cited values of A range between 0 and 1. Tennekes (1973) suggests that A probably lies between 0.1 and 0.2, while results presented by Carson (1973) indicate that A may be a function of time ranging from 0 to 0.5. Unfortunately, a definitive means for estimating A is presently not available. It is recommended here that an "interim" value of 0.2 be employed until better information becomes available (see Tennekes, 1973).

In closing, it is recommended that the method for predicting mixing depths proposed in equations (2) and (3) undergo further validation and evaluation. The validation procedure may be carried out in three stages:

- validation for conditions in which the boundary layer is homogeneous in the horizontal plane,
- validation for the conditions along an air trajectory over land, and
- full validation for a large urban area, such as the San Francisco Bay, Los Angeles, or San Diego areas.

It is of interest to note that equations (2) and (3) are a more general form of those employed by Carson (1973) to estimate mixing depths under horizontally homogeneous conditions. In simulations of the temporal behavior of the inversion at O'Neill in 1953, Carson was able to achieve reasonably close agreement with available measurements. With these encouraging results, it is suggested that equations (2) and (3) be employed to estimate mixing depths for urban areas in which significant spatial variations of inversion height occur, such as major West Coase metropolitan areas. For computational convenience, these calculations may first be performed along a trajectory. Vertical temperature measurements reported by Scott Research Laboratories (1970) and Blumenthal et al. (1973) for the Los Angeles area may be of value in validation efforts. If the mixing depths along trajectories can be estimated accurately, then regional-scale simulation of the temporal and spatial behavior of the depth of the mixed layer may be undertaken.

References

Anderson, G. E. (1972). A mesoscale windfield analysis of the Los Angeles Basin. The Center for the Environment and Man, Inc., Hartford, Connecticut.

Ball, F. K. (1960). Control of inversion height by surface heating. Quart. Jour. Roy. Meteor. Soc., 86, 483.

Bergstrom, R. W., Jr. and Viskanta, R. (1973). Modeling of the effects of gaseous and particulate pollutants in the urban atmosphere. Part I: Therman structure. Jour. Applied Meteor., 12, 901

Blumenthal, D. L., et al. (1973). Three dimensional pollutant gradient study--1972 program. Report MRI 73 FR-1084, Meteorological Research, Inc., Altadena, Calif.

Carson, D. J. (1973). The development of a dry inversion-capped convectively unstable boundary layer. Quart. J. Roy. Met. Soc., 99, 450.

Deardorff, J. W. (1973). Three-dimensional numerical modeling of the planetary boundary layer. In Workshop in Micrometeorology, Edited by D. A. Haugen, American Meteorological Society.

Kokin, A., Wayne, L. G., and Weisburd, M. (1973). Controlled evaluation of the reactive environmental simulation model (REM) - Volume II: User's Guide. Pacific Environmental Services, Inc., Santa Monica, California

Leahey, D. M. and Friend, J. P. (1971). A model for predicting the depth of the mixed layer over an urban heat island with applications to New York City. Jour. Applied Meteor. 10, 1162.

Lilly, D. K. (1968). Models of cloud-topped mixed layers under a strong inversion. Quart. J. Roy. Meteor. Soc., 94, 292.

Scott Research Laboratories (1970). 1969 Atmospheric reaction studies in the Los Angeles Basin - Volume IV: Airborne data and ESSA cooperative data. Scott Research Laboratories, Plumsteadville, Pa.

Stull, R. G. (1973). Inversion rise model based on penetrative convection. Jour. Atm. Sciences, 30, 1092.

Tennekes, H. (1973). A model for the dynamics of the inversion above a convective boundary layer. Jour. Atm. Sciences, 30, 558.

PROPOSITION

Relating Air Quality Measurements to Populace Exposure

Abstract

Primary air quality standards pertain to populace exposure to air pollutants. It is suggested that current air monitoring practice may not necessarily provide accurate indices of this exposure. A simple means for relation air quality measurements to populace exposure is developed, and implementation of the technique is discussed.

Under provisions of the Clean Air Act, national primary and secondary air quality standards have been established by the Environmental Protection Agency (EPA). The primary standards reflect contaminant dosage levels which, if not exceeded, would protect the public health with an adequate margin of safety from any known or anticipated adverse effects of a pollutant (EPA, 1971a). Secondary standards, on the other hand, are designed to protect the public welfare (i.e., vegetation, materials, animals, visibility, personal comfort, and well being) from the harmful effects of a pollutant. Compliance with the standards is ascertained from the measurements taken at air quality monitoring stations. It is contended here that current air monitoring practice does not provide accurate indices against which to determine compliance with air quality standards. To substantiate this claim, we first need to briefly review how standards are determined and where monitoring stations are "sited." Since public health is of paramount importance, we shall restrict the focus of this study to consideration of primary standards only.

Primary air quality standards are derived from the results of toxicological and epidemiological studies. For example, the CO standard is based on studies of the decrement of human performance at various carboxyhemoglobin levels in the bloodstream, and the NO_2 standard is derived from an epidemiological study involving school children in Chattanooga, Tennessee. While the actual numerical values of the standards adopted are somewhat controversial (see Heuss et al. (1971) and Barth et al. (1971) for a further discussion of some of the issues and additional references for health-effects

studies), one fact is clear. That is, the primary air quality standards reflect population dosage levels. Thus, compliance with primary air quality standards should be judged on the basis of populace exposure.

At the present time, air quality data collected at pollutant monitoring stations is used to ascertain compliance with federal standards. However, it is interesting to note that there are several objectives of monitoring air quality. Guidelines issued by EPA (1971b) state that regional air quality surveillance must provide information which may be used to:

1. judge compliance with and/or progress toward meeting ambient air quality standards,
2. activate emergency control measures to prevent air pollution episodes,
3. observe pollution trends throughout the region including the nonurban areas,
4. provide a data base for development and evaluation of urban, land use, and transportation planning studies, abatement strategies, and diffusion model validation studies.

Considering the four objectives cited, the EPA report suggests monitoring stations be situated in the following locations:

1. the area of highest pollutant concentrations,
2. densely populated areas,
3. around the periphery of the region (to assess air quality entering the area),
4. areas of projected population growth,
5. strategic areas where the impact of control measures may be ascertained.

A further discussion of the practical problems associated with planning a monitoring network is presented by Hamburg (1971). Because of the multiplicity of air surveillance objectives and due to the usual problem of limited funding, monitoring stations cannot always be situated in the best location for measuring populace exposure. In Allegheny County, Pennsylvania, for example, it was decided by County officials that sites should be selected primarily to monitor emissions from large industrial sources (Stockton, 1970). Locating stations to accurately represent exposure levels does not appear to have been of much concern in this instance.

Even when a monitoring station is intended primarily to measure exposure levels, there will always be some difficulty in finding an appropriate site. This difficulty arises because pollutant concentrations vary substantially over relatively small spatial scales (say, a few miles). Of particular concern is the fact that people frequent numerous characteristic areas, or microenvironments, throughout the course of a day. For example, typical microenvironments include the inside of a home, car, school, office or store, the sidewalk adjacent to a street, and the outdoors, associated either with work or leisure. Thus, different people living or working in the general vicinity of the same monitoring station may be exposed to significantly different pollutant levels. As an example, consider the potential differences in CO exposure that may exist between a housewife situated in a residential area as opposed to a cab driver or traffic policeman working for long periods of time near a street.

Quantitative evidence supporting the above contentions is provided in a study of the distribution of CO concentrations in San Jose, California, reported by Ott (1971) and Ott and Eliassen (1973). In this work, CO concentrations were measured in the downtown area as well as surrounding residential and industrial locations. It was found that CO samples taken at normal breathing height while walking along the sidewalk in the downtown shopping area were, on the average, 60% higher than the corresponding monitoring station measurements. Further examination of the data indicated that pedestrian exposure on downtown streets could exceed the federal standard, while the reported monitoring station data was significantly below the standard. Other measurements taken at randomly selected sites not near major streets were only one-half as large as the reported monitoring data. It would be difficult to conclude that air quality data collected in San Jose is truly reflective of actual populace exposure. Similar problems exist in Los Angeles County where several stations are located on heavily-travelled streets. Consequently, the measurements reported at these sites are often only representative of concentrations in the local environs.

Another issue of concern is that "ambient air" is defined as "that portion of the atmosphere, external to buildings, to which the general public has access" (EPA, 1971a). As far as exposure to pollutants is concerned, it really does not matter whether a person is inside or outside of a building. In view of the fact that many people spend in excess of 80% of their time indoors (Benson et al., 1972), to

properly quantify populace exposure, means must be developed to relate outdoor air quality to that found indoors. Generally, indoor pollutant concentrations are controlled by outdoor levels and by other factors, such as interior activities, atmospheric conditions, time, location, type of building, and air conditioning and filtration systems (Benson et al., 1972; General Electric, 1972; Derham et al., 1974). Based on a review of available data, Benson et al. suggest that indoor concentrations of CO, particulates, and other nonreactive gases can be assumed equal to outdoor concentrations, although indoor levels may be somewhat lower than outdoor concentrations when outdoor levels are high. The ratio of indoor to outdoor SO_2 concentrations, however, may be as low as 0.2 (Neese, 1970), which is accounted for by the fact that wall coverings tend to sorb the pollutant. Data reported by Derham et al. (1974) indicate that indoor NO concentrations are approximately equal to outdoor levels. We should expect, however, that concentrations in buildings in the immediate vicinity of heavily-travelled streets or large point sources will be substantially higher than those situated farther away from major sources. Thus, significant spatial variations in indoor concentrations may exist throughout a particular area.

To summarize the previous discussion, we have noted that:

1. primary air quality standards relate to populace exposure,
2. monitoring stations are not necessarily sited for the purpose of determining exposure, and

3. significant variations in pollutant concentrations may exist throughout particular areas.

The impact of points 2 and 3 is that current air monitoring practice does not necessarily provide accurate estimates of exposure. In particular, no definitive information is available with regard to the mean, range, and distribution of populace exposure for any urban area. Until information of this type is obtained on a regular basis, it will be difficult to determine whether or not acceptable air quality exists in an area. The remainder of this report is devoted to a discussion of a possible methodology for relating air quality measurements to populace exposure.

We begin by noting that the estimation of pollutant dosage for any individual in a community would be extremely difficult, requiring detailed knowledge of pollutant concentrations virtually everywhere (both indoors and outdoors) in the area. In this instance, an individual's exposure would best be determined through use of a dosiometer, a small badge-like pollutant dosage detector. Unfortunately, such devices are not readily available at this time for all pollutants. In order to obtain a reasonable estimate of current populace dosage levels, and perhaps some insight into what previous levels have been, we first segment the population of an area surrounding a monitoring station into various vocational groupings, such as:

. housewives/shoppers
. school children
. office workers
. construction workers
. factory workers
. traffic policemen
. cab and truck drivers

In addition, we segment the region of interest into a number of micro-environments which are characteristic of those places inhabited by the members of the various vocational groups cited above. Micro-environments in typical urban areas might include:

- inside/outside residential areas
- inside/outside schools
- inside office buildings
- on the sidewalk in business areas
- inside a motor vehicle
- inside/outside factories

The exact list of vocational groupings and microenvironments would, of course, depend on the particular community. The objective now will be to estimate the average dosage for each vocational group. The desired relationship for the average exposure to pollutant p over the time interval from t_o to t_1 is given by:

$$d_p(t_o, t_1) = \sum_{i,m} \mu_i \int_{t_o}^{t_1} \alpha_{im}(t) \bar{c}_{pm}(t)\, dt$$

where the subscripts i, m, and p refer to the vocational group, microenvironment, and pollutant, respectively, and

d_p = average populace exposure,

μ_i = fraction of the population belonging to vocational group i,

$\alpha_{im}(t)$ = fraction of group i in microenvironment m at time t,

$\bar{c}_{pm}(t)$ = characteristic concentration of pollutant p in microenvironment m at time t.

In order to evaluate the above expression for d_p, data for u_i should be available from either the Department of Labor or the local Chamber of Commerce. To estimate $\alpha_{im}(t)$, it is recommended

that a survey of several members of each vocational group be undertaken in each community to determine which microenvironments are frequented by each group throughout the day. Finally, the most difficult parameter to estimate will be the concentration in each microenvironment. Ideally, we seek a functional relationship between this concentration and that reported at the monitoring station. An experimental study similar to that performed by Ott (1971) in San Jose would be appropriate for determining an average correlational relationship between the two measures. Another alternative would be to use local physical models to calculate the elevation in pollutant concentrations above the area-wide average concentrations caused by strong, nearby sources. For example, a street canyon model could be employed to calculate the concentration along a heavily-travelled street.

The simple model discussed above involving a single community may be extended to treat larger urban areas. In this case, it will be important to characterize daily population movements. For example, office workers may live in one community and commute to and work in another. This factor will be important for estimating relatively long term exposure (say over a 24 hour period) but will be of somewhat lesser significance in computing the dosage over a 1 hour time span.

Because of the dearth of actual exposure data, there is an immediate need to carry out a measurement study to ascertain the magnitude of the discrepancies that may exist between actual populace exposure and that calculated from monitoring station data. In particular, exposure profiles should be prepared for various vocational

groups, which would make it possible to examine both the mean and the range of populace exposure. To facilitate implementation of the study, a relatively small, self-contained community should be chosen in order to minimize the effort and associated cost of the program. If significant differences are found in actual and calculated dosage levels, then similar studies should be carried out in other urban areas.

REFERENCES

Barth, D.S., Romanovsky, J.C., Knelson, J.H., Altshuller, A.P., Horton, R.J.M. (1971) Jour. Air Poll. Cont. Assoc., Vol. 21, p. 544.

Benson, F.B., Henderson, J.J., Caldwell, D.E. (1972), Indoor-Outdoor Air Pollution, Relationships: A Literature Review, U. S. Environmental Protection Agency Publication, No. AP-112, Research Triangle Park, N.C.

Derham, R.L., Peterson, G., Sabersky, R.H., Shair, F.H. (1974), Jour. Air Poll. Cont. Assoc., Vol. 24, p. 158.

Environmental Protection Agency (1971a), Federal Register, Vol. 36, p. 8186.

Environmental Protection Agency (1971b), Guidelines: Air Quality Surveillance Networks. Publication No. AP-98. Research Triangle Park, N.C.

General Electric Co. (1972), Indoor-Outdoor Carbon Monoxide Pollution Study. Report EPA R4 73 020, Philadelphia, Pa.

Hamburg, F.C. (1971), Jour. Air Poll. Cont. Assoc., Vol. 21, p. 609.

Heuss, J.M., Nebel, G.J., and Colucci, J.M. (1971), Jour. Air Poll. Cont. Assoc., Vol. 21, p. 535.

Ott, W. (1971), An Urban Survey Technique for Measuring the Spatial Variation of Carbon Monoxide Concentrations in Cities. Ph. D. Thesis, Stanford University, Stanford, California.

Ott, W. and Eliassen, R. (1973), Jour. Air Poll. Cont. Assoc., Vol. 23, p. 685.

Reese, K.M., (1970), Chem. and Eng. News, Vol. 48, (35), p.52.

Stockton, E.L. (1970), Jour. Air Poll. Cont. Assoc., Vol. 20, p. 456.